

From Research to Applied Geotechnics

**Invited Lectures of the XVI Pan-American
Conference on Soil Mechanics and
Geotechnical Engineering (XVI PCSMGE),
17-20 November 2019, Cancun, Mexico**



EDITED BY

Norma Patricia López-Acosta
Eduardo Martínez-Hernández
Alejandra Liliana Espinosa-Santiago
Alexandra Ossa López



**IOS
Press**

Millpress

From Research to Applied Geotechnics

Invited Lectures of the XVI Pan-American Conference on Soil Mechanics and Geotechnical Engineering (XVI PCSMGE), 17-20 November 2019, Cancun, Mexico

The first Pan-American Conference on Soil Mechanics and Geotechnical Engineering (PCSMGE) was held in Mexico in 1959. Every 4 years since then, PCSMGE has brought together the geotechnical engineering community from all over the world to discuss the problems, solutions and future challenges facing this engineering sector. Sixty years after the first conference, the 2019 edition returns to Mexico.

The XVI PCSMGE 2019 conference was held in Cancun, Mexico, from 17 – 20 November 2019. This book presents the plenary lectures from the conference, delivered by distinguished geotechnical engineers of international renown. Experience and youth combine in this special publication, which includes the 9th Arthur Casagrande lecture, the plenary lecture of the ISSMGE President, 3 Bright Spark lectures, and the manuscripts of the 13 invited lecturers of practically all the technical sessions at the XVI PCSMGE 2019. Topics cover both research and applied geotechnics, including recent developments in geotechnical engineering.

Representing a valuable reference for engineering practitioners and graduate students, and helping to identify new issues and shape future directions for research, the book will be of interest to all those working in the field, involved in soil mechanics and geotechnical engineering.

ISBN 978-1-64368-032-3 (print)
ISBN 978-1-64368-033-0 (online)



9 781643 680323 >

IOS
Press Millpress

Millpress is an imprint of IOS Press

FROM RESEARCH TO APPLIED GEOTECHNICS

Advances in Soil Mechanics and Geotechnical Engineering

Advances in Soil Mechanics and Geotechnical Engineering (ASMGE) is a peer-reviewed book series covering the developments in the key application areas of geotechnical engineering. ASMGE will focus on theoretical, experimental and case history-based research, and its application in engineering practice. The series will include proceedings and edited volumes of interest to researchers in academia, as well as industry. The series is published by IOS Press under the imprint Millpress.

Volume 7

Recently published in this series

- Vol. 6. V.A. Rinaldi, M.E. Zeballos and J.J. Clariá (Eds.), Deformation Characteristics of Geomaterials – Proceedings of the 6th International Symposium on Deformation Characteristics of Geomaterials, IS-Buenos Aires 2015, 15–18 November 2015, Buenos Aires, Argentina
- Vol. 5. A.O. Sfriso, D. Manzanal and R.J. Rocca (Eds.), Geotechnical Synergy in Buenos Aires 2015 – Invited Lectures of the 15th Pan-American Conference on Soil Mechanics and Geotechnical Engineering and the 8th South American Congress on Rock Mechanics, 15–18 November 2015, Buenos Aires, Argentina
- Vol. 4. V.M. Ulitsky, Michael B. Lisyuk and Alexey G. Shashkin (Eds.), Soil-Structure Interaction, Underground Structures and Retaining Walls – Proceedings of the ISSMGE Technical Committee 207 International Conference on Geotechnical Engineering
- Vol. 3. D.G. Toll, H. Zhu, A. Osman, W. Coombs, X. Li and M. Rouainia (Eds.), Information Technology in Geo-Engineering – Proceedings of the 2nd International Conference (ICITG), Durham, UK
- Vol. 2. Y.-J. Cui, F. Emeriault, F. Cuira, S. Ghabezloo, J.-M. Pereira, M. Reboul, H. Ravel and A.M. Tang (Eds.), Proceedings of the 5th International Young Geotechnical Engineers' Conference – 5th iYGEC 2013
- Vol. 1. P. Arnold, G.A. Fenton, M.A. Hicks, T. Schreckendiek and B. Simpson (Eds.), Modern Geotechnical Design Codes of Practice – Implementation, Application and Development

ISSN 2212-781X (print)
ISSN 2212-7828 (online)

From Research to Applied Geotechnics

Invited Lectures of the XVI Pan-American Conference on
Soil Mechanics and Geotechnical Engineering (XVI PCSMGE),
17–20 November 2019, Cancun, Mexico

Edited by

Norma Patricia López-Acosta

Instituto de Ingeniería UNAM, Mexico

Eduardo Martínez-Hernández

Instituto de Ingeniería UNAM, Mexico

Alejandra Liliana Espinosa-Santiago

Instituto de Ingeniería UNAM, Mexico

Alexandra Ossa López

Instituto de Ingeniería UNAM, Mexico

IOS
Press

Amsterdam • Berlin • Washington, DC

© 2019 The authors and IOS Press.

This book is published online with Open Access and distributed under the terms of the Creative Commons Attribution Non-Commercial License 4.0 (CC BY-NC 4.0).

ISBN 978-1-64368-032-3 (print)

ISBN 978-1-64368-033-0 (online)

Library of Congress Control Number: 2019953227

doi: 10.3233/ASMGE7

Publisher

IOS Press BV

Nieuwe Hemweg 6B

1013 BG Amsterdam

Netherlands

fax: +31 20 687 0019

e-mail: order@iospress.nl

For book sales in the USA and Canada:

IOS Press, Inc.

6751 Tepper Drive

Clifton, VA 20124

USA

Tel.: +1 703 830 6300

Fax: +1 703 830 2300

sales@iospress.com

LEGAL NOTICE

The publisher is not responsible for the use which might be made of the following information.

PRINTED IN THE NETHERLANDS

Preface

This book constitutes the imprint of the Plenary Conferences delivered by distinguished geotechnical engineers of renowned international quality in the XVI Pan-American Conference on Soil Mechanics and Geotechnical Engineering (XVI PCSMGE), which was held from November 17 to 20, 2019 in Cancun, Mexico.

Experience and youth are combined in this special volume that includes the 9th Arthur Casagrande Lecture, the Plenary Conference of ISSMGE President, three Bright Spark Lectures, and thirteen manuscripts of the Invited Lecturers of practically all the technical sessions of the XVI PCSMGE 2019, among them *Analytical and physical modelling in Geotechnics, Unsaturated soils, Soft soils, Foundations and retaining structures, Excavations and tunnels, Offshore Geotechnics, Transportation in Geotechnics, Natural hazards, Preservation of historic sites, Rock mechanics, Education and Energy Geotechnics*.

This special volume covers both the research and the applied Geotechnics, including the recent developments in geotechnical engineering. Besides, it provides valuable references for engineering practitioners and graduate students and helps to identify new issues and to shape future directions for research. We are very pleased to disseminate all these contributions among the scientific community.

We would like to express our thanks to all the Invited Lecturers for their high quality and valuable contributions. In addition, we are especially grateful to Eduardo Martínez, Alejandra Liliana Espinosa and José Alfredo Promotor for their assistance with the preparation of this Invited Lectures Volume.

Norma Patricia López Acosta, Chairwoman, Editorial Committee

Alexandra Ossa López, Chairwoman, Technical Committee

Walter I. Paniagua Zavala, Chairman, Organizing Committee

Cancun, Mexico, November 17 to 20, 2019

This page intentionally left blank

Conference Organization

Organizing Committee XVI PCSMGE, Cancun, Mexico 2019

Chairman: Walter I. Paniagua Zavala

Secretary: Juan Paulín Aguirre

Treasurer: Juan de Dios Alemán Velásquez

Technical Committee

Chairwoman: Alexandra Ossa López

Committee

- Carlos Roberto Torres Álvarez
- Enrique Ibarra Razo
- José Luis Rangel Núñez
- Juan Félix Rodríguez
- Marcela González Blandón
- Miguel Ángel Figueras Corte
- Moisés Juárez Camarena
- Ricardo Ortiz Hermosillo
- Rigoberto Rivera Constantino

Editorial Committee

Chairwoman: Norma Patricia López Acosta

Committee

- Eduardo Martínez Hernández
- Alejandra Liliana Espinosa Santiago
- Víctor Manuel Pineda Núñez
- José Alfredo Mendoza Promotor
- Diana Margarita Portillo Arreguín

Local Committee

- Rodolfo Ramírez
- Zenón Medina Pacheco

Local Advisory Committee

- Gabriel Auvinet Guichard
- Gabriel Moreno Pecero
- Guillermo Springall Caram

Public Relations and Sponsorship Committee

- Gabriel Martínez
- Raúl López Roldán

Technical Session Co-Chairs**S1. Laboratory and in situ testing**

- Heraldo Luiz Giacheti (Brazil)
- Iván Rivera (Canada)
- Osvaldo Flores (Mexico)

S2. Analytical and physical modelling in geotechnics

- Alejandro Martínez Vela (USA)
- Celestino Valle Molina (Mexico)
- Marcio de Souza Soares de Almeida (Brazil)
- Marcos Orozco Calderón (Mexico)

S3. Numerical modelling in geotechnics

- Alejo Sfriso (Argentina)
- José Luis Rangel Núñez (Mexico)
- Richard Wan (Canada)

S4. Unsaturated soils

- Alfredo Zepeda Garrido (Mexico)
- Eduardo Rojas González (Mexico)
- John McCartney (USA)
- Laureano R. Hoyos (USA/Colombia)

S5. Soft soils

- Jorge Alberto Rodríguez (Colombia)
- Manuel J. Mendoza López (Mexico)

S6. Foundations and retaining structures

- Jarbas Militizky (Brazil)
- Mary Ellen Large (USA)
- Walter I. Paniagua Zavala (Mexico)

S7. Excavations and tunnels

- Andrés Marulanda Escobar (Colombia)
- Juan Jacobo Schmitter Martín del Campo (Mexico)
- Luiz Guilherme de Mello (Brazil)

S8. Offshore Geotechnics

- Diego Cruz Roque (Mexico)
- José Parra (Venezuela)
- Rachel Guerreiro Basilio Costa Genzani (Brazil)
- Víctor M. Taboada Urtuzuástegui (USA)

S9. Transportation in geotechnics

- Alexandra Ossa López (Mexico)
- Gloria Beltrán Calvo (Colombia)
- Luis Guillermo Loria Salazar (Costa Rica)
- Paul Garnica Anguas (Mexico)

S10. Natural hazards

- Hernán Eduardo Martínez Carvajal (Colombia)
- Juan Félix Rodríguez (Brazil)
- Renato Pinto da Cunha (Brazil)
- Roberto Terzariol (Argentina)

S11. Embankments and tailings dams

- Juan de Dios Alemán Velásquez (Mexico)
- Ramón Verdugo (Chile)
- Rolando Vega Beirute (Costa Rica)

S12. Soils dynamics and earthquake engineering

- Adrián Rodríguez Marek (USA)
- Gonzalo Montalva (Chile)
- Raúl Aguilar Becerril (Mexico)

S13. Ground improvement

- Eduardo Villa Corta Lucchesi (Peru)
- Hubert Guimont (Canada)
- Rémi Chatte (Mexico)

S14. Sustainability and geoenvironment

- Elizabeth Burton (USA)
- Gonzalo Zambrano Narváez (Canada)
- Moisés Dávila (Mexico)

S15. Preservation of historic sites

- Damien Tamagnan (Mexico)
- Efraín Ovando Shelley (Mexico)

S16. Forensics engineering

- Luis Bernardo Rodríguez (Mexico)
- Paul W. Mayne (USA)
- Edgar E. Rodríguez Granados (Colombia)

S17. Rock mechanics

- Carlos Carranza Torres (USA)
- Sergio Fontoura (Brazil)
- Valentín Castellanos Pedroza (Mexico)

S18. Education

- Emir José Macari (USA)
- Jorge E. Alva Hurtado (Peru)
- Miguel Ángel Figueiras (Mexico)
- Rigoberto Rivera Constantino (Mexico)

S19. Energy geotechnics

- Marcelo Sánchez (USA)
- Norma Patricia López Acosta (Mexico)

Contents

Preface <i>Norma Patricia López Acosta, Alexandra Ossa López and Walter I. Paniagua Zavala</i>	v
Conference Organization	vii
Invited Lectures of the XVI Pan-American Conference on Soil Mechanics and Geotechnical Engineering (XVI PCSMGE)	
The 9th Arthur Casagrande Lecture	
Biographical Data of Gabriel Y. Auvinet	6
Table of Contents, List of Tables, List of Figures	7
The 9th Casagrande Lecture. Presentation and Biographical Sketch of Professor Gabriel Auvinet Guichard <i>Efrain Ovando Shelley</i>	10
Geotechnical Engineering in Spatially Variable Soft Soils. The Case of Mexico City. The 9th Arthur Casagrande Lecture <i>Gabriel Y. Auvinet</i>	13
Plenary Lecture ISSMGE President	
Biographical Data of C.W.W. Ng	111
Interplay Between Ecology and Unsaturated Soil Mechanics for Bioengineered Landfill Covers and Slopes <i>C.W.W. Ng, J.J. Ni and C. Zhou</i>	112
Keynote Lectures	
Technical Session #2: “Analytical and Physical Modelling in Geotechnics” Biographical Data of Jorge Zornberg	127
Centrifuge Technology for Characterization of Expansive Clays <i>Jorge Zornberg</i>	128
Technical Session #4: “Unsaturated Soils” Biographical Data of Eduardo Rojas	149
A General Fully Coupled Model for Unsaturated Soils <i>Eduardo Rojas</i>	150
Technical Session #5: “Soft Soils” Biographical Data of Marcio S.S. Almeida	165

Field Studies of Stone Columns and Geosynthetic-Encased Columns <i>Marcio S.S. Almeida, Iman Hosseinpour and Bruno Lima</i>	166
Technical Session #6: “Foundations and Retaining Structures” Biographical Data of Anne Lemnitzer	181
Laterally Loaded Pile Behavior at Soil-Rock-Impedance Contrast <i>Anne Lemnitzer, Carter Cox, Rabie Farrag and Benjamin Turner</i>	182
Technical Session #7: “Excavations and Tunnels” Biographical Data of Werner Bilfinger	193
Tunneling Through the Rock-Soil Interface <i>Werner Bilfinger</i>	194
Technical Session #8: “Offshore Geotechnics” Biographical Data of Per Sparrevik	215
Offshore Wind Turbine Foundations State of the Art <i>Per Sparrevik</i>	216
Technical Session #8: “Offshore Geotechnics” Biographical Data of Phil Watson	239
Foundation Design in Offshore Carbonate Sediments – Building on Knowledge to Address Future Challenges <i>Phil Watson, Fraser Bransby, Zine Labidine Delimi, Carl Erbrich, Ian Finnie, Henry Krisdani, Chris Meecham, Michael O'Neill, Mark Randolph, Mike Rattley, Marcelo Silva, Bob Stevens, Stephen Thomas and Zack Westgate</i>	240
Technical Session #9: “Transportation in Geotechnics” Biographical Data of Erol Tutumluer	275
Sustainable Pavement Foundations with Chemically Stabilized Quarry By-Products <i>Erol Tutumluer, Issam Qamhia and Hasan Ozer</i>	276
Technical Session #10: “Natural Hazards” Biographical Data of Murray D. Fredlund	291
Developments in Landslide Analysis Methodologies <i>Murray D. Fredlund, Delwyn G. Fredlund and Gilson de F.N. Gitirana Jr.</i>	292
Technical Session #15: “Preservation of historic sites” Biographical Data of Carlo Viggiani	327
The Behaviour of an Ancient Tower Through History and Monitoring <i>Carlo Viggiani</i>	328
Technical Session #17: “Rock Mechanics” Biographical Data of C. Carranza-Torres	341
Analytical and Numerical Study of the Stability of Shallow Circular Cavities in Weak Rocks <i>C. Carranza-Torres</i>	342

Technical Session #18: “Education” Biographical Data of Jorge E. Alva Hurtado	347
Advances in the Teaching of Geotechnical Engineering in Peru <i>Jorge E. Alva Hurtado</i>	348
Technical Session #19: “Energy Geotechnics” Biographical Data of Lyesse Laloui	355
Experimental Analyses on the Multiphysical Phenomena Governing Energy Pile Behavior <i>Lyesse Laloui and Melis Sutman</i>	356
Bright Spark Lectures	
Biographical Data of Tugce Baser	373
Thermal Energy Storage in Borehole Arrays Installed in Unsaturated Soils <i>Tugce Baser, John S. McCartney and Ayse Ozdogan-Dolcek</i>	374
Biographical Data of Carlos Omar Vargas	391
Analysis and Seismic Design of Tailings Dams and Liquefaction Assessment <i>Carlos Omar Vargas</i>	392
Biographical Data of Marlísio Oliveira Cecílio Junior	417
Personal Account on Reliability Analyses, from a Young Geotechnical Engineer <i>Marlísio Oliveira Cecílio Junior</i>	418
Subject Index	439
Author Index	441

This page intentionally left blank

**Invited Lectures of the XVI Pan-American
Conference on Soil Mechanics and
Geotechnical Engineering (XVI PCSMGE)**

This page intentionally left blank

The 9th Arthur Casagrande Lecture

This page intentionally left blank

Geotechnical Engineering in Spatially Variable Soft Soils. *The Case of Mexico City.* The 9th Arthur Casagrande Lecture

Ingeniería geotécnica en suelos blandos con
variación espacial.
El caso de la Ciudad de México.
La 9.^a Conferencia Arthur Casagrande

by

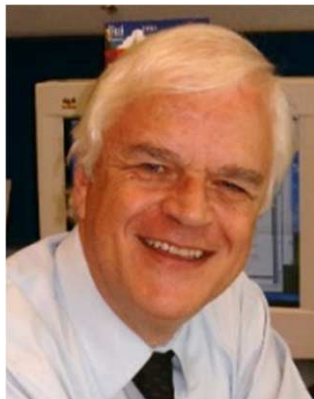
Gabriel Y. AUVINET

*Professor, Instituto de Ingeniería,
Universidad Nacional Autónoma de México,
Mexico City, Mexico
GAuvinetG@iingen.unam.mx*

prepared for

XVI Pan-American Conference on Soil Mechanics and Geotechnical Engineering
Cancún, Mexico
November, 2019

The 9th Arthur Casagrande Lecture



Gabriel Y. AUVINET

Gabriel Auvinet obtained a Doctor degree in Engineering from UNAM, Mexico in 1986. He is a Researcher at Instituto de Ingeniería (Institute of Engineering), UNAM (National University of Mexico) and Faculty member of UNAM Postgraduate program. He was a guest Professor in the French Universities of Grenoble (1986), Nancy (1993-1994) and Clermont (2003-2004). He has directed a large number of professional, master and doctoral theses and is author of 367 papers in Journals and National and International Conferences and 248 research reports. He is presently Head of the Geotechnical Computing Laboratory of Institute of Engineering, UNAM. He has dedicated his research work to Soil Mechanics with emphasis on special foundations and tunnels in consolidating soft soils. Simultaneously, he has developed new techniques for application of probabilistic and geostatistical methods in Civil Engineering. He has been involved as a consultant in many large projects in Mexico, Central and South America and Europe. He performed geostatistical and geomechanical analyses for the design of award-winning Rion-Antirion bridge foundation in Greece. Professor Auvinet has been President of the Mexican Society for Soil Mechanics (SMIG, 1992-1993) and Vice President for North America of International Society for Soil Mechanics and Geotechnical Engineering (ISSMGE, 2009-2013). He has received a number of teaching and research awards in Mexico, France and South America. From 2001 to 2009 he chaired ISSMGE's Technical Committee TC36: "Foundation Engineering in difficult soft soils conditions". In 2002 he delivered the Sixteenth "Nabor Carrillo" Lecture: "Uncertainty in Geotechnical Engineering". He is a member of the Mexican Science Academy, and National Engineering Academy of Mexico. In 2015, He received a Doctor Honoris Causa degree from Universidad Nacional de Córdoba, Argentina. He is author of the updated version (2017) of the internationally known book "The subsoil of Mexico City".

Table of contents

List of Tables

List of Figures

Presentation and Biographical Sketch of Professor Gabriel Auvinet Guichard

Abstract/Resumen

1. Introduction

2. Soft soils

- 2.1. Classification of soft soils
- 2.2. Typical soft soil deposits
- 2.3. The lacustrine clays of Mexico City

3. Soft soils characterization

- 3.1. Soil stratigraphy, ground water conditions and mechanical parameters
- 3.2. Practice of soft soil characterization in Mexico City

4. Spatial variations

- 4.1. Factors contributing to soft soils spatial variations
- 4.2. Spatial variations within the lacustrine zone of Mexico City

5. Modeling spatial variations of soft soils

- 5.1. Deterministic models
- 5.2. Statistical and probabilistic models
- 5.3. Reduction of variance in soils
- 5.4. Modeling spatial variations of the subsoil of Mexico City

6. Geotechnical analysis considering soft soils spatial variations

- 6.1. Available methods
- 6.2. Dealing with spatial variability in Mexico City clays
 - 6.2.1. Friction pile
 - 6.2.2. Footing
 - 6.2.3. Slope stability

7. Geotechnical solutions for mitigating the effects of spatial variations of soft soils

- 7.1. Available techniques
- 7.2. Mitigating the effects of soil spatial variations in Mexico City clays by preloading.

8. Conclusions

Acknowledgments

List of Symbols

References

Appendix I. Considerations about some physical properties of soft soils

Appendix II. Random fields and Geotechnical engineering

Appendix III. Reduction of variance in a 1D random field with exponential autocorrelation coefficient

List of Tables

- Table 1.** Geotechnical borings performed from 2013 to 2016 (NAICM).
Table 2. Laboratory tests (NAICM).
Table 3. Typical values of index properties in the Lake Zone (Borehole Pc 28, Marsal, 1975 [58]).
Table 4. Statistical analysis of water content and void ratio for the 5 to 15m deep layer of Figure 8b

Appendix I

- Table 1.** Comparison of average and true values of void ratio and water content.

List of Figures

- Figure 1.** Relation between Liquid limit and Plasticity index for typical soils (Casagrande, 1948 [2]).
Figure 2. Urban area of Mexico City and surroundings neighborhoods.
Figure 3. Plasticity chart based on water content w' defined by Eq. (2).
Figure 4. Initial yielding surface for typical Mexico City clay.
Figure 5. Geotechnical zoning of Mexico City and surrounding areas (GCDMX, 2017a [59]).
Figure 6. Typical soil profile for the different geotechnical zones.
Figure 7. Variations of water content w (Eq. (1)) in a cross-section of a Mexico City clay sample.
Figure 8. (a) Typical soil profile, San Juan de Aragón site, Lake Zone, (b) Zoom on water content of the 5 to 15m deep layer
Figure 9. Water content profiles in a Lake Zone site established using different definitions of water content (a) Eq. (1), (b) Eq. (2), (c) Eq. (3) and corresponding histograms.
Figure 10. Geotechnical anomalies within the lacustrine clays of Mexico City.
Figure 11. Subsidence rate in Mexico City lacustrine area.
Figure 12. Variation of CPT profile with time, SCT site, Lake Zone, 1985, 2000, 2011.
Figure 13. Soil fissuring around Santa Catarina range due to regional subsidence.
Figure 14. Soil fractures induced by (a) regional subsidence (b) hydraulic fracturing in flooding zones.
Figure 15. Statistical correlation between coefficient of compressibility, α_v , in preconsolidation interval, and water content, w , (Eq. (1)), Marsal and Mazari (2017 [33]).
Figure 16. Shear strength c (s_u) vs water content w (Eq. (1)) for Mexico City clays.
Figure 17. Correlation between coefficient of volumetric compressibility m_v and water content defined by (a) Eq. (1) and (b) Eq. (2).
Figure 18. Correlations between shear wave velocity, V_s , and water content defined by: (a) Eq. (1), (b) Eq. (2), (c) Eq. (3).
Figure 19. Geostatistical estimation of water content contours in a cross-section of a Mexico City clay sample for different definitions of water content; (a) Eq. (1), (b) Eq. (2) and (c) Eq. (3).
Figure 20. Typical water content profile (w , Eq. (1)), in the upper clay formation of the Lake Zone. (a) Original field (b) Residual stationary field.
Figure 21. Vertical correlograms for water content profiles of Figure 20.
Figure 22. Original V_s (a) and w (Eq. (1)) (b) profiles and improved V_s profile (c) obtained by cokriging, using water content as a secondary random field.
Figure 23. Vertical autocorrelograms of V_s and w and cross-correlogram V_s-w obtained from profiles of Figure 22.
Figure 24. Original V_s (a) and w' (Eq. (2)) (b) profiles and improved V_s profile (c) obtained by cokriging, using water content w' as a secondary random field.
Figure 25. Vertical auto-correlograms of V_s and w' (Eq. (2)) and vertical cross-correlogram V_s-w' for profiles of Figure 24.
Figure 26. Improved V_s profile obtained by kriging (c) and cokriging (d), using CPT tip resistance q_c (b) as a secondary random field.
Figure 27. Empirical correlation between shear wave velocity V_s and CPT tip resistance, q_c . ($1/t/m^2 = 10\text{kPa}$).

- Figure 28.** Location of *Deep Deposits* depth data.
- Figure 29.** Contour map of estimated *Deep Deposits* depth within the Lake Zone in Mexico City.
- Figure 30.** Typical horizontal correlogram for water content field in Mexico City Lake Zone.
- Figure 31.** Longitudinal profile of estimated water content defined by (a) Eq. (1), (b) Eq. (2) and (c) Eq. (3) (Runway 6, NAICM).
- Figure 32.** Longitudinal profile of simulated water content defined by Eq. (1) (Runway 6, NAICM).
- Figure 33.** Longitudinal profiles of simulated water content w' defined by Eq. (2) (Runway 6, NAICM).
- Figure 34.** Longitudinal profile of: (a) estimated water content w (Eq. (1)) and (b) CPT tip resistance q_c . (Terminal building area, NAICM).
- Figure 35.** Longitudinal profiles of estimated soil properties: (a) Shear wave velocity V_s (kriging), (b) CPT tip resistance q_c (kriging), (c) Shear wave velocity V_s improved by cokriging with q_c (Terminal building, east side).
- Figure 36.** Spatial distribution of estimated water content along the 12 lines of Mexico City subway system.
- Figure 37.** “Light” brought about by boreholes improving knowledge of soil characteristics (a) before borehole SPT1 was performed and (b) after it was performed.
- Figure 38.** Friction pile in soft soil with undrained shear strength considered as a 1D random field.
- Figure 39.** Reduction of coefficient of variation of friction pile bearing capacity, Q , as a function of ratio between pile length L and vertical correlation distance $\delta = 2a$.
- Figure 40.** Uncertainty on displacements of a footing on a random material as a function of correlation distance.
- Figure 41.** Uncertainty on differential displacements between points A and B for a footing built on a random material as a function of correlation distance.
- Figure 42.** Cross-section of slope and potential slip surface.
- Figure 43.** Forces acting on base of a single column.
- Figure 44.** Semi planar failure mechanism.
- Figure 45.** Slope of a trial excavation in Mexico City clay.
- Figure 46.** Semi planar failure mechanism of a trial excavation slope (Courtesy, W.I. Paniagua).
- Figure 47.** Preloading system.
- Figure 48.** Principle of preloading with surcharge.
- Figure 49.** Target final condition.
- Figure 50.** Variations of yield stress σ'_p along embankment longitudinal axis. (Runway 2, NAICM).
- Figure 51.** Conditional simulation of the σ'_p field along embankment longitudinal axis (Runway 2, NAICM).
- Figure 52.** Typical pore pressure depletion within Mexico City subsoil.
- Figure 53.** Settlement induced by seepage forces between tip of PVD drains and first hard permeable layer (CD).
- Appendix I*
- Figure 1.** Compressibility curves expressed in term of (a) void ratio e and (b) porosity n .
- Figure 2.** Variations of water contents w (Eq. (9)) and w' (Eq. (10)) as a function of w'' (Eq. (12))
- Appendix II*
- Figure 1.** Bivariate Gaussian copula density plots for different correlation coefficients.

The 9th Casagrande Lecture

Presentation and Biographical Sketch of Professor Gabriel Auvinet Guichard

Efraín OVANDO SHELLEY^{a,1}

^aResearch Professor, Instituto de Ingeniería, Universidad Nacional Autónoma de México, Mexico

Today we meet again to honour the memory of Professor Arthur Casagrande, as we did on eight previous occasions. We pride ourselves that the memory of Casagrande is honoured like this in Mexico, a country that Casagrande knew as a geotechnician, a country where he unselfishly displayed his wit and knowledge, a place that profited from that display. In previous Panamerican conferences the lecture bearing his name has always been of the highest quality, given by colleagues of the highest level. Our lecturer today is by no means the exception.

Professor Gabriel Auvinet obtained the title of civil engineer from the *Ecole Spéciale des Travaux Publics de Paris*. Later, he got a diploma as a specialist in prestressed concrete from the *Centre des Hautes Etudes de la Construction*, also in Paris. He has been living in Mexico since 1968. He joined the Graduate School of Engineering at UNAM where he got his master's and doctoral degrees. The totality of his career as a research engineer has taken place at the *Instituto de Ingeniería* of UNAM, which he joined formally in 1970. There, he benefited from the influence of Raúl J. Marsal, Daniel Reséndiz, Jesús Alberro and Emilio Rosenblueth who backed him at the beginning of his career. He has been the Coordinator of the Geotechnics Section and Sub-Director at the Institute, as well as head of the Civil Engineering Department at the Graduate School of Engineering at UNAM.

In his study of granular media, Gabriel Auvinet put forth an original description of discrete media with which a continuous link between the granular scale and the scale of continua can be established by means of the concept of the *geometric scale effect*, expressed in terms of probabilities. This allowed him, for example, to provide an answer to the problem of Soritos, posed by the ancient Greeks, i. e. “*How many particles in a group of grains are required to have a mass of sand?*” In developing these concepts, he pondered on their practical implications in Geotechnics, such as the definition of soil mixtures having the minimum possible porosity, the design of filters and the selection and control of materials for earth structures, the evaluation of the hydraulic conductivity of porous media and the mechanical behaviour of discrete media. His algorithms have also been used by specialists of other fields, especially in connection to the interpretation of the mechanical behaviour of metallic dusts.

His most important contributions in the field of numerical and analytical modelling are related to the analysis of deep foundations in Mexico City's difficult soil conditions. Early in his career, he developed graphical, numerical and analytical elasticity-based solutions relevant for the analysis of foundations. Later he developed an interest in the analysis of piled foundations in soils undergoing a consolidation process, as in Mexico

¹ Research Professor, Instituto de Ingeniería, UNAM. Email: EOvandoS@iingen.unam.mx

City. Using load cells of his own and novel design, he measured the development of negative friction on point bearing and friction piles in Lake Texcoco. With analytical and numerical models, he interpreted the behaviour of those piles and was able to elucidate the complex interaction mechanism between piles, substructure and soil in deep foundations. After the 1985 earthquakes, he performed and published meticulous interpretations of the behaviour of foundations during that event. He participated in the project for the correction of differential settlements in Mexico City's Metropolitan Cathedral putting forth an original method for analysing a system of rigid inclusions to control soil settlements. In view of his contributions in this field, he coordinated the team responsible for drafting the new regulations for the design of foundations in Mexico City.

Auvinet has actively promoted the application of the probabilistic approach to geotechnical engineering. Using it, he has made significant contributions to the development of new methods to consider uncertainty in soil mechanics analyses. Combined with Geographical Information Systems, he has continuously been using these tools for more nearly three decades to improve on the geotechnical description of the subsoil in the Basin of Mexico. This knowledge has allowed him to develop a geotechnical zoning map present in the city's building code.

On the other hand, Gabriel Auvinet has also come up with a rational interpretation of the fissures that so often appear in Mexico City's lacustrine clays. Using field observations and fracture mechanics, he proposed crack generation and propagation criteria that have been used after the 19 September 2017 earthquake. These criteria are presently being applied under Auvinet's supervision in the southern portion of the Basin of Mexico, to define confinement and reinforcement techniques with which such a problematic phenomenon can be mitigated or even avoided.

He has also pioneered the development and application of the *stochastic finite element method* with which uncertainties related to the mechanical parameters of soils can be accounted for. He has developed simple, time efficient and innovative techniques for solving three dimensional seepage problems using the Monte Carlo Method, as well as new methods for the assessment of geotechnical risks that can also be used to estimate the reliability of foundations, dams, slopes, trenches, retaining walls and culverts.

He developed the geostatistic model of the foundation soil of the Rion-Antirion bridge on the Gulf of Corinth, in Greece, one of the largest of the world, collaborating with such specialists as Professors Ralph B. Peck, Ricardo Dobry and Alain Pecker. His contributions in this field have been recognized by his peers in the international geotechnical community. Recently, application of geostatistics in the project of the new airport for Mexico City in Texcoco proved to be a most useful tool for developing a comprehensive stratigraphical model at that site. His contributions in that project were also paramount in analysing the behaviour of airport infrastructure in the short and long terms.

Dr. Auvinet's knowledge and research into earth and rockfill dams led him to participate as a consultant in the design, construction and behaviour assessments of many such works not only in Mexico but also in France, Central and South America. He co-authored the seminal book in Spanish on this subject, "*Presas de tierra y enrocamientos*" edited by R. J. Marsal and D. Reséndiz which was awarded the Javier Barros Sierra prize by the *Colegio de Ingenieros Civiles de México*. He was awarded that prize again as a co-author of a manual for Geotechnical construction published by the Mexican Society for Geotechnical Engineering (SMIG).

Professor Auvinet has been President of the Mexican Society for Soil Mechanics (SMIG, 1992-1993) and Vice President for North America of ISSMGE (2009-2013). He

has received a number of teaching and research awards in Mexico, France and South America. From 2001 to 2009, he chaired ISSMGE's Technical Committee TC36: "Foundation Engineering in difficult soft soils conditions". In 2002, he delivered the Sixteenth "Nabor Carrillo" Lecture: "Uncertainty in Geotechnical Engineering". He is a member of the Mexican Science Academy, and National Engineering Academy of Mexico. In 2015, he received a Doctor Honoris Causa degree from *Universidad Nacional de Córdoba. Argentina*. He is author of the updated version (2017) of the internationally known book "The subsoil of Mexico City".

Direct beneficiaries of his research work at the Instituto de Ingeniería and in French universities are the 172 students that have up to now received their bachelors, masters, and doctoral degrees under his tutorship. The rest of us have profited from his publications, lectures, informal talks and his humour.

Gabriel Auvinet's broader interests overlap Geotechnical Engineering. He is also a historian, a profound connoisseur and also a joyful one, of a large part of Mexican History and of the history of Mexico City. His incursions into historical research are known only by a few and it is only needed that more get to know them to be more recognized in this field, as in Geotechnics. He is also an art lover and appreciates good food at least as much as History or Soil Mechanics. In that I declare and confess that I have been his occasional accomplice.

It is not enough goodness, nor fine manners, nor the appreciation for the good things of life, nor historiographic rigour, nor the love for his adoptive country to justify his designation as the ninth Casagrande Lecturer. My words, those of a friend, are of little use to argue on his behalf, in attention to objectivity, which in this case I can't pretend to have, nor do I wish to have. His career as a researcher and a teacher says very much more, at times as a field engineer and on other occasions as a mender of geotechnical misdemeanours, as a rigorous practitioner of Soil Mechanics, an art that, without science, ceases to be in art, as shown by the richness of our lecturer's work.

Geotechnical Engineering in Spatially Variable Soft Soils.

The Case of Mexico City.

The 9th Arthur Casagrande Lecture

Ingeniería geotécnica en suelos blandos con variación espacial.

El caso de la Ciudad de México.

La 9.^a Conferencia Arthur Casagrande

Gabriel Y. AUVINET^{a,2}

^aProfessor, Instituto de Ingeniería, Universidad Nacional Autónoma de México,
Mexico

Abstract. Many large cities such as Tokyo, Bangkok, Río de Janeiro, Recife, Bogota and, of course, Mexico City, to name only a few, were built and are still being developed on soft soils. In many cases, these cities also experience regional subsidence induced by pumping of groundwater from deep local aquifers. Among the sources of uncertainty prevailing in the geotechnical characterization of these sites, soil properties spatial variability is one of the most difficult to deal with since the associated uncertainty cannot be eliminated only by improving laboratory and field-testing techniques. For an accurate evaluation of the subsoil conditions, spatial variations of the soil profile and mechanical properties together with the groundwater conditions must be assessed by performing a sufficient number of soil explorations, processing a generally large amount of data and developing either deterministic or probabilistic models of these variations. The techniques available to develop such models and some difficulties encountered to implement them are examined in this lecture. Some geotechnical analysis and design methods that take into account soft soils spatial variations are also reviewed together with constructions techniques aimed at mitigating consequences of soil variability.

The above considerations are illustrated with reference to Mexico City's highly compressible volcanic lacustrine clays. Models of the spatial variability of these materials developed over the years for different projects using traditional and geostatistical techniques are presented. Some of the geotechnical analysis and construction methods used by geotechnical engineers to deal with soil spatial variability in this megacity once called by Terzaghi "the paradise of soil mechanics", are also discussed.

² Dr. Gabriel Y. Auvinet, Laboratorio de Geoinformática, Instituto de Ingeniería, Universidad Nacional Autónoma de México, Torre de Ingeniería, 2º nivel, Ciudad Universitaria, 04510, Ciudad de México, Mexico; e-mail: GAuvinetG@iingen.unam.mx

Keywords. Soft soils, geotechnical characterization, spatial variations, deterministic models, probabilistic models, geostatistics, analysis, design, reliability.

Resumen. Un gran número de ciudades tales como Tokio, Bangkok, Río de Janeiro, Recife, Bogotá y, por supuesto, la Ciudad de México, para nombrar solamente algunas, han sido construidas y siguen desarrollándose sobre suelos blandos. En muchos casos estos sitios están también afectados por subsidencia regional inducida por el bombeo de agua desde acuíferos profundos locales. Entre las fuentes principales de incertidumbre para la caracterización geotécnica de estos sitios, la variación espacial de las propiedades del suelo es una de las más difíciles de tomar en cuenta porque no puede eliminarse simplemente mejorando la calidad de los ensayos de campo y de laboratorio. Para una satisfactoria evaluación de las condiciones del subsuelo, las variaciones espaciales de la estratigrafía y de las propiedades mecánicas del subsuelo y de las condiciones piezométricas deben ser determinadas mediante un número suficiente de exploraciones, procesando grandes cantidades de datos y desarrollando modelos deterministas o probabilistas que representen estas variaciones. En esta conferencia se examinan las diferentes técnicas existentes para desarrollar tales modelos y las dificultades que comúnmente se encuentran para implementarlas. Se discuten asimismo algunos métodos de análisis y diseño geotécnico y técnicas constructivas que permiten mitigar las consecuencias de las variaciones espaciales del suelo.

Las consideraciones anteriores se ilustran tomando como referencia principal el caso de las arcillas volcánicas altamente compresibles de la ciudad de México. Se presentan algunos modelos que han sido desarrollados para representar las variaciones espaciales de estos materiales recurriendo a técnicas tradicionales y geoestadísticas. Se presentan asimismo algunos métodos de análisis y diseño empleados por los ingenieros geotecnistas para tomar en cuenta la variación espacial del suelo en esta ciudad que fue alguna vez llamada por Terzaghi “el paraíso de la mecánica de suelos”.

Palabras clave. Suelos blandos, caracterización geotécnica, variaciones espaciales, modelos deterministas, modelos probabilistas, geoestadística, análisis, diseño, confiabilidad.

1. Introduction

Throughout the world, many large cities have been built and are still being developed on soft ground. Large projects are being developed on sites that were previously considered as unfit for construction due to the high compressibility and low shear strength of the soft subsoil. This constitutes a serious challenge for geotechnical engineers.

Foundations of constructions on soft materials must be designed taking into account that they should not be loaded significantly beyond their yielding stress. This is a condition particularly difficult to achieve when the soil characteristics present spatial variations due to their formation process and to local anomalies due to geological or anthropic factors.

Spatial variations of the soil must be assessed by performing a sufficient number of soil explorations, processing a generally large amount of data and developing deterministic or probabilistic models of these variations that can be introduced in geotechnical analyses.

A wide variety of models can be developed, depending on the available information and the problem to be solved. As asserted in the famous sentence attributed to Einstein these models should be “as simple as possible but not more simple”. These models can be deterministic or probabilistic.

In this lecture, the techniques available to develop appropriate models and some difficulties encountered to implement them in practice are examined. Geotechnical analysis and design methods that take into account soft soils spatial variations are also reviewed together with some construction techniques aimed at mitigating consequences of soil variability.

The above considerations are illustrated with reference to the Mexico City's highly compressible volcanic lacustrine clays. Models of the spatial variability of these materials developed over the years for different projects using traditional and geostatistical techniques are presented. Some of the geotechnical analysis and construction methods used by local geotechnical engineers to deal with soil spatial variability in this megacity, which was called by Terzaghi "the paradise of soil mechanics", are also discussed.

2. Soft soils

2.1. Classification of soft soils

As asserted by Ladd and DeGroot in a previous Casagrande lecture (2003 [1]), and according to the Unified Soil Classification System (USCS), soft soils are generally clays (CL and CH), silts (ML and MH) and organic soils (OL and OH) that were deposited in an alluvial, lacustrine or marine environment and are essentially saturated.

The Unified Soil Classification System (USCS), an outgrowth of the Airfield Classification system developed by Casagrande (1948 [2]), has remained along the years as the main reference frame for soft soils classification for geotechnical purposes.

Resiliency of USCS is in fact somewhat surprising if it is considered that, as far as soft soils are concerned, this system was probably not based on the best physical and index properties available.

Consider for example soil gravimetric water content, w , defined since the early stages of soil mechanics as:

$$w = \frac{W_w}{W_s} \quad (1)$$

where W_w = weight of water in sample, and W_s = weight of solids in sample.

The original argument for using definition of Eq. (1) was apparently that it allowed describing in a simple way the variations of water content and volumetric changes of soils for a given (constant) amount of solids (Spangler and Handy, 1982 [3]). This advantage becomes however a drawback when dealing with soft soil spatial variability. It can in fact be argued that this was a poorly chosen descriptive property, especially for heterogeneous soft soils with high water content. As shown in Appendix I, the parameter defined by Eq. (1) is very unstable for small samples and for high water content soils. Strictly speaking, it cannot be averaged on a volume. Averaging local water contents introduces a bias and overestimates the actual water content of the whole sample (Appendix I). Water content as defined by Eq. (1) can thus be considered as ill-fitted for statistical analyses. Note that Atterberg's limits w_L (liquid limit) and w_p (plasticity limit) are also gravimetric water contents based on Eq. (1).

To avoid these difficulties, water content can be defined differently switching for example to another gravimetric definition adopted in most fields of science:

$$w' = \frac{W_w}{W_T} \quad (2)$$

where W_T = total weight of sample ($= W_w + W_s$).

A volumetric definition of water content can also be adopted:

$$w'' = \frac{V_w}{V_T} \quad (3)$$

where V_w = volume of water in sample, and V_T = total volume of sample.

The merits of these alternative definitions are evaluated in Appendix I.

Some objections to the plasticity chart introduced by Casagrande as a central element of USCS (Figure 1) have also been presented (Gutiérrez García, 2006 [4]).

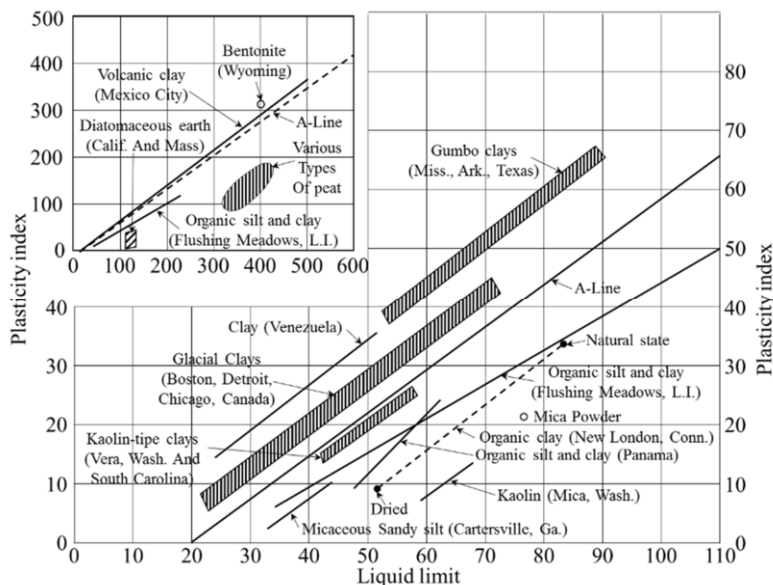


Figure 1. Relation between Liquid limit and Plasticity index for typical soils (Casagrande, 1948 [2]).

In this chart, the same variable w_L , is present on both the abscissae (Liquid limit, w_L) and ordinates (Plasticity Index, $PI = w_L - w_P$) axes. This condition introduces a spurious correlation between PI and w_L that explains to some degree why Casagrande observed that all the soils he had studied could be represented along straight lines practically parallel to the A-Line. This objection is not so serious since, apparently, Casagrande was not trying to establish linear correlations between PI and w_L for different soils. He was only looking for a practical way to define a partition of the Atterberg's limits space into disjoint subsets where different types of soils could be classified without ambiguity.

Some proposals have also been published to modify clays classification (Moreno-Maroto and Alonso-Azcárate, 2018 [5]). The advantages of these new concepts have yet to be assessed.

The original USCS system did had to be modified to provide a more detailed classification of organic soils based on Atterberg limits after oven drying (ASTM D2487-85, D2488-84, 1989 [6]). Other modifications based on Von Post humidification tests reflecting the state of the fiber structure of the organic matter have also been proposed (Perrin, 1974 [7]; Magnan, 1980 [8]).

Notwithstanding the above observations, Casagrande's USCS has proven to be a very robust system that has been extremely useful worldwide to myriads of geotechnical engineers during the last 71 years.

2.2. Typical soft soil deposits

A large number of soft soil deposits have been described in the technical literature and the difficulties encountered to deal with them from a geotechnical engineering point of view have been exposed.

Akagi (2004 [9]) refers to the soft clayey ground of Tokyo Bay where most underground structures are constructed. Large settlements of the soft ground around the tunnels were observed due to consolidation originating from excess pore water pressure induced by reclaimed soil and other construction works such as pumping of underground water. 3-D finite element simulations of the interaction between soil and tunnels with flexible joints were performed.

According to Phien-wej *et al.* (2009 [10]), the city of Bangkok is founded on a soft marine clay, 12 to 18m in thickness, followed by thin layers of medium and stiff clay of the same origin overlying a sand layer typically found at a depth of 20 to 22m. Land subsidence due to deep well pumping has affected the area reaching a rate as high as 12cm/year in the early 1980's. In spite of measures that were exerted to mitigate the phenomenon, ground surface in some parts of the city has sunk below the mean sea level, which makes flood drainage more difficult and costly.

Kempfert and Raithel (2005 [11]) presented experiences on dike foundations and landfills on very soft soils for the extension of an airplane dockyard in Hamburg, Germany. These and other experiences were the basis for the preparation of an excellent monograph on excavations and foundations in soft soils (Kempfert, 2006 [12]).

As far as the Americas are concerned, Mitchell and Coutinho (1991 [13]) presented a general overview of "Occurrence, geotechnical properties and special problems of some soil in America" that included many soft soil sites in the U.S. and Canada but also in Mexico, Ecuador and Brazil.

Coutinho and Oliveira (2005 [14]) described the soft clay and organic soil deposits that can be found in about fifty percent of the lowland of the urban area of the city of Recife on the Northeastern coast of Brazil. Comprehensive program of laboratory and in situ tests have been performed in two research sites. Databases have been developed to support foundation design and as a pedagogical tool.

Almeida *et al.* (2004 [15]) also discussed the geotechnical properties and behavior of ten deposits of soft to medium clays situated in industrialized and residential areas of Rio de Janeiro City and Río de Janeiro State. A summary describing index properties, compressibility, stress history and undrained and drained strengths was presented.

As exposed by Martínez (1991 [16]) and Caicedo *et al.* (2018 [17]), the city of Bogotá (Colombia) is located on a high plateau of the Andes Mountains at 2550 m above

sea level. More than 60% of the area of this city with 9 million of inhabitants is located on soft soil deposits. At some sites of the plateau, the depth of the lacustrine deposit can reach 586m. Shallow deposits of soil from 5 m to 10 m deep are overconsolidated, but in deeper layers, the soil can reach extreme values for some geotechnical properties: consistency index lower than 0.5, water content higher than 200%, liquid limit up to 400%, void ratio as high as 5, and high diatomaceous percentage.

It is noteworthy to observe that in the presentation of most of these different soft soil sites, scant attention was given to the description of spatial variations of the soil properties in statistical or probabilistic terms. This reflects the still prevalent reluctance of many geotechnical engineers to using these tools in spite of the wide diffusion they have received (Whitman, 1996 [18]; Lacasse and Nadim, 1996 [19]; Fenton, 1997 [20]; Phoon and Kulhawy, 1999 [21]; Auvinet, 2001 [22], 2002 [23]; Baecher and Christian, 2003 [24]; Huber, 2013 [25]).

2.3. The lacustrine clays of Mexico City

Geologically, the so-called valley of Mexico is actually a closed basin located in the highest part and southern end of the Mexican plateau. It is located between parallels 19°00' and 20°12' north and meridians 98°10' and 99°33' west. It is bounded on the north by the mountains of Tepozotlan, Tezontlalpan and Pachuca, east by the plains of Apan and the Sierra Nevada, south by the mountains of Chichinautzin and Ajusco and west by Sierras de Las Cruces, Monte Alto and Monte Bajo. Its surface is about 9600 km², of which only 30% is flat. The geology of the Valley of Mexico has been the subject of many studies, from the first surveys of Del Castillo and Ordoñez (1893 [26]) to those presented more recently by Mooser *et al.* (1978 [27]; 1996 [28], 2018 [29]) and other geologists. Physiographically, the Basin of Mexico belongs to the Neovolcanic belt, an awesome volcanic range that crosses the Mexican territory from east to west.

The metropolitan area of Mexico City (Figure 2, Auvinet *et al.*, 2017 [30]) is limited by large topographic elevations. Two major volcanic units dominate the East part of the valley: Popocatepetl and Iztaccihuatl. Within the valley, some isolated volcanic domes such as Peñon de los Baños, Peñon del Marqués, Cerro de la Estrella and those forming Sierra de Santa Catarina protrude from the lacustrine area. The Valley of Mexico is mainly formed by volcanic and pyroclastic materials interspersed with alluvial deposits covered in the center of the valley by lacustrine clays. According to Mooser (1978 [27]), before the Pleistocene, the basin drained south to the Amacuzac River by two deep ravines passing through Cuautla and Cuernavaca. During the late Pliocene, fractures occurred predominantly in the WE direction in the area of Puebla and south of Toluca, and large outpourings of basalt formed the Sierra de Chichinautzin in the Quaternary. According to paleomagnetic measurements, massive eruptions occurred during the last 700.000 years. These events transformed the valley into a closed basin. The Sierra de Chichinautzin, lying between Sierra de Zempoala in the West and Popocatepetl in the East, and resting in the center on the Tepozteco massif formed a huge natural barrier that dammed the valley of Mexico.

Until the end of the XVIIIth century, the valley of Mexico remained a closed basin, with a number of shallow lakes. Mexico City (then Tenochtitlán) was founded in a small island of the Texcoco Lake. The valley became an open basin when the Nochistongo cut was completed in 1789. During the XXth century, the lakes were drained through the Tequisquiac tunnel, completed in 1900, and the Deep Drainage tunnel (Emisor Central), built in 1967. A new drainage tunnel (Túnel Emisor Oriente), 7m in diameter and 62 km

long is expected to be finished by the date of the present lecture. Today, with the exception of small remaining bodies of water, the lakes have practically disappeared.

A large part of the city was thus built on lacustrine sediments in the lower part of the basin with a surface of some 2050km². These are highly compressible soft clays interbedded with layers of silt, sand and sandy gravels of alluvial origin. With a growing population now exceeding 20 million inhabitants, the metropolitan area of Mexico Valley is one of the largest urban conglomerates in the world.

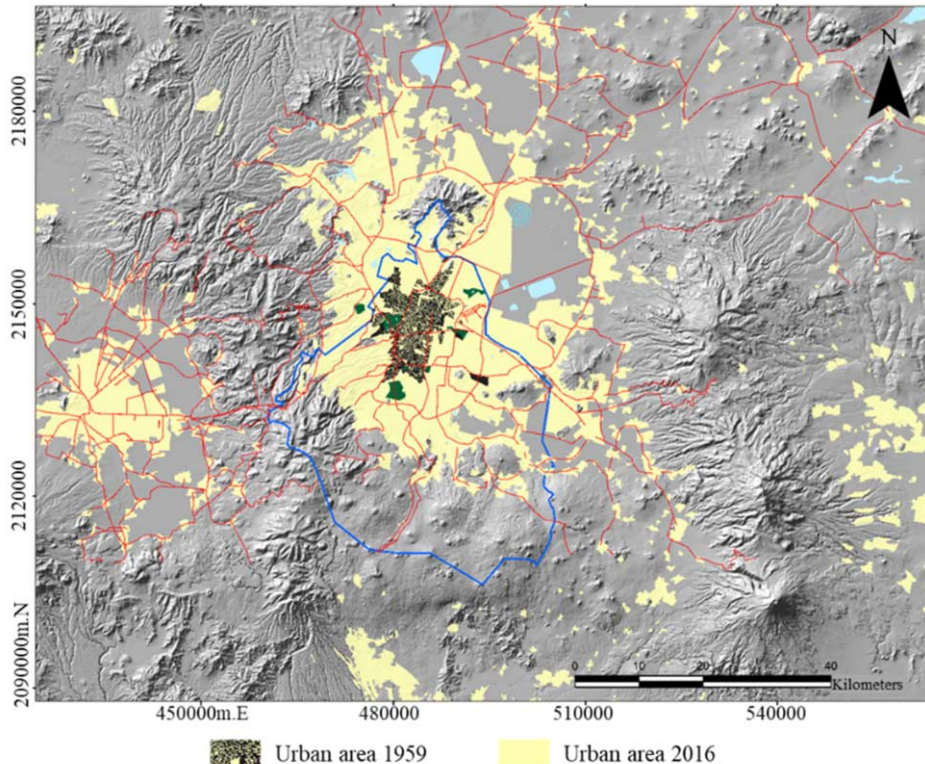


Figure 2. Urban area of Mexico City and surroundings neighborhoods.

3. Soft soils characterization

3.1. Soil stratigraphy, ground water conditions and mechanical parameters

For identification of the soil type of successive layers, a number of rapidly evolving field techniques have become available. Semi continuous penetration tests such as CPT (Cone Penetration Test), CPTu (Cone Penetration Test with pore pressure measurement, also called piezocone test) or DMT (Marchetti Dilatometer test) are now generally preferred to SPT (Standard Penetration Test) (Robertson, 2009 [31]; 2012 [32]).

The SPT approach has the advantage of providing split spoon samples for visual classification and obtaining index properties such as water content that are very useful to assess spatial variations. On the other hand, CPTu tests can readily differentiate between

free draining lenses and the soft soil matrix, and it is often considered that piezocone soundings provide the most rapid and detailed approach for soil profiling. The continuous nature of the CPTu results provides valuable information about soil variability that is difficult to match with sampling and laboratory testing, because the CPT obtains more channels of data (typically 3) at more frequent intervals (typically every 20 to 50 mm). Performing a well-balanced combination of SPT and CPTu tests seems the best way to go, although simple direct-push samplers can also be used to obtain small (typically 25 to 50 mm in diameter) disturbed soil samples of similar size to that obtained from SPT. Charts are used for definition of soil type descriptions derived from CPTu data. Note that the zones in these charts are imprecise compared to the Unified Soil Classification System (USCS) and thus it is highly advisable that the site investigation include sampling for final classification of soft cohesive strata. As recommended by Ladd and De Groot (2003 [1]), the final developed soil profile should always include the USCS designation for each soil type.

When performing CPT tests, shear strength is estimated in terms of the net tip resistance as:

$$s_u = \frac{q_c - \sigma_0}{N_k} \quad (4)$$

where s_u = undrained shear strength, q_c = tip resistance in CPT test, σ_0 = total vertical stress at the level of the measurement, and N_k = cone factor.

A large number of increasingly sophisticated relationships between CPT results and parameters such as the Over Consolidation Ratio (*OCR*), yield stress σ'_p , shear wave velocity V_s , small strain shear modulus G_0 as well as coefficient of volumetric compressibility m_v have also been established (Robertson, 2012 [32]).

Geotechnical practitioners are sometimes puzzled by the refinements introduced in the coefficients or exponents of the proposed relationships between CPT tests results and soil properties, some of them with no evident physical meaning. In all cases, formal statistical analyses indicating clearly the soil population to which they are applicable and showing the scattering of the data around the established relationships should always be presented.

Ground water conditions assessment through piezometric measurements is also an important part of the characterization of any soft soil deposit, since the original effective state of stress within the medium can only be known when a full knowledge of water table location (and variations) has been achieved and possible drawdown conditions due to deep pumping have been evaluated.

Laboratory tests on high quality samples laboratory tests must also be performed. Consolidation tests will provide compression index, C_v and swelling index, C_s as well as yield stress σ'_p . Triaxial shear tests will furnish value of undrained shear strength, s_u . Using advanced soft soil constitutive laws in geotechnical analyses, many based on the modified Cam-clay model implicit in most modern geotechnical software, may require assessing additional parameters.

In seismic areas, dynamic parameters such as shear modulus, damping ratio and seismic wave velocity will also be required in order to evaluate seismic site effects and performing dynamic soil-structure analyses. Some of this information can be obtained through CPT tests but performing geophysical field tests and cyclic laboratory tests may also be required.

3.2. Practice of soft soil characterization in Mexico City

The main reference regarding geotechnical characterization of Mexico City clays is still “The Subsoil of Mexico City” by Marsal and Mazari (2017 [33]), an encyclopedic work initially published in 1959, that presents an impressive number of laboratory and field tests results. Casagrande used to refer to this book as “The Bible”. This publication was recently updated with a third volume summarizing more recent works on this topic (Auvinet *et al.*, 2017 [30]). Valuable information is also found in Zeevaert (1972 [34]). Additional laboratory and field tests results have been presented by Santoyo *et al.* (2005 [35]) and Ovando (2011 [36]).

The unique properties of Mexico City clay have been evaluated in a number of studies performed to assess their mineral composition and structure (Zeevaert, 1952 [37]; Marsal and Mazari, 1959 [33]; Leonards and Girault, 1961 [38]; Girault, 1964 [39]; Lo, 1962 [40]; Mesri, Rokhsar and Bohor, 1975 [41]; Peralta y Fabi, 1973 [42]; Diaz-Rodriguez *et al.*, 2003 [43]). Most of these studies are inconclusive. This heterogeneous volcanic lacustrine clay appears to be a complex mixture of clayey and non-clayey minerals with microorganisms, dissolved salts and organic components. The presence of microfossils such as ostracods and diatoms could explain some of the properties of the material including its high water content.

Note that when the plasticity chart of USCS was established (Casagrande, 1948 [2]), Mexico City clay was “expelled” together with various types of peat and Wyoming bentonite, from the main chart due to their high water content (and liquid limit) (Figure 1). This was in fact a consequence of the definition adopted for water content (Eq. (1)). Figure 3 shows a plasticity chart in which a more conventional definition of water content (w' , Eq. (2)) was adopted. In this chart, Mexico City clay is reunited with the large family of fine-grained soils.

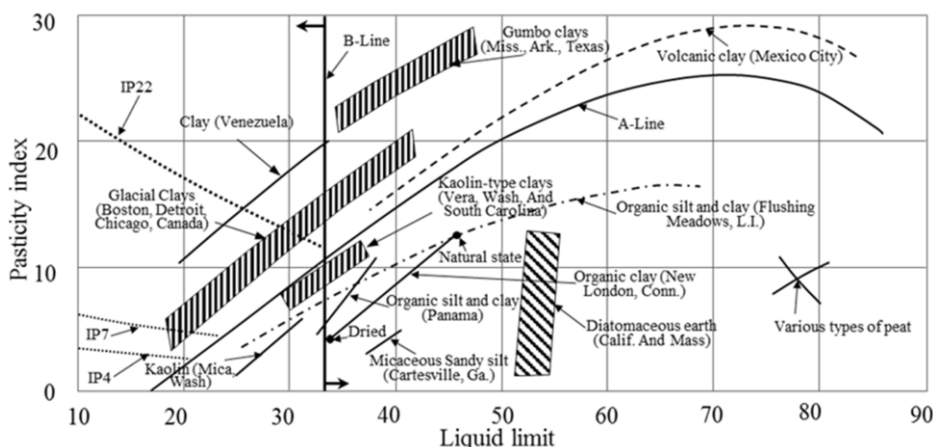


Figure 3. Plasticity chart based on water content w' defined by Eq. (2).

A discussion has been going on regarding whether Mexico City clay should be classified as a “highly organic material” as suggested by some authors (Mesri *et al.*, 1975 [41]). This opinion has been reinforced by the fact that when CPT tests are performed, the behavior of Mexico City clay seems typical of organic materials (Cruz and Mayne,

2006 [44]; Mayne, 2019 [45]). This should be clarified since Marsal and Mazari (1959 [33]) carried out measurements of the organic content of the fine soils of Mexico City based on the carbonate content, that indicate that these soils have a medium to low percentage (5% percent as an average) of organic components. The highest percentages correspond to the upper part of the clayey series (between 5 and 15m deep). In a recent study (Rangel *et al.*, 2019 [46]), the organic content has been determined using the Walkley and Black method (1934 [47]). All soils samples tested presented a low organic content. The same authors are currently performing additional tests on materials obtained from the former Texcoco Lake (water with high salt content) and Xochimilco Lake (fresh water).

Materials from the clayey deposits of Mexico City subsoil are characterized by their extraordinary compressibility. Coefficient of compressibility a_v , defined as the quotient between the decrement of void ratio and the respective increment of applied pressure may reach values as high as $6 \text{ cm}^2/\text{kg}$ ($0.06 \text{ m}^2/\text{kN}$). The clay shear strength is higher than what could be expected taking into account the exceptionally high water content of this material, showing that it is highly structured. However, average values of 40 kN/m^2 are not uncommon, with extreme values as low as 15 kN/m^2 .

Mexico City clay is commonly described as an elasto-plastic material. The initial yielding surface of typical Mexico City clay samples was defined performing a number of triaxial tests following distinct different stress paths (Díaz-Rodríguez *et al.* 1992 [48]). Wheeler (2003 [49]) adjusted the model presented in Figure 4 to these results.

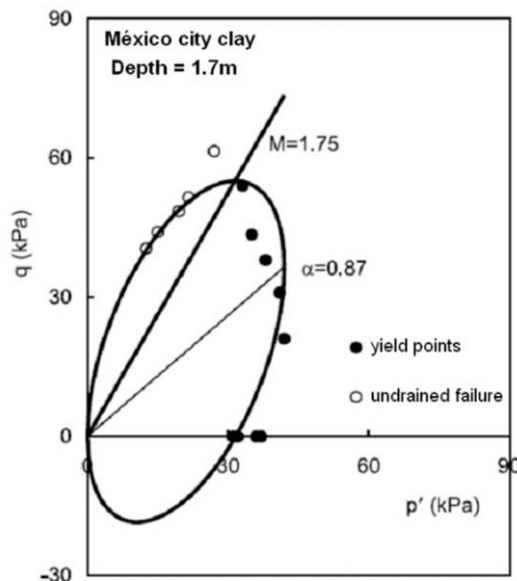


Figure 4. Initial yielding surface for typical Mexico City clay.

Field-tests techniques commonly used for Mexico City soft soil characterization have been extensively described by Santoyo (2010 [50]). To illustrate the present Mexican practice, reconnaissance and laboratory tests that were performed recently on a site considered at some point for developing a new airport in Mexico City (NAICM) are presented in Tables 1 and 2 (Mendoza *et al.*, 2018 [51]).

Table 1. Geotechnical borings performed from 2013 to 2016 (NAICM).

Type	Preliminary exploration (2013)	Test embankments (2014a)	Terminal Building area (2014b)	Terminal Building and Control Tower area (2015)	Runways, platforms and taxiways (2016)	Test embankments (2016)	Total
Test pits (PCA)		19	10		261		290
Dynamic cone penetrometer (PND)		72			323		395
Standard Penetration Test (SPT)	3		7		90		100
Mixed boring (SM)	66			20	90	7	183
Continuous sampling (SC)		12	1		2		15
Selective sampling (SS)	14	6	3		54		77
Cone penetration test (CPT)		11	7		13		31
Cone penetration test with pore pressure measurement (CPTu)			3	30	177	7	217
Suspension PS logging (Sds)		6		6			12
Dilatometer (DMT)				2	20		22
Seismic dilatometer (SDMT)				1			1
Vane shear test (VST)					30		30
Total	83	126	34	56	1060	14	1373

Table 2. Laboratory tests (NAICM).

Type	Preliminary reconnaissance (2013)	Test embankments	Terminal Building and Control Tower area.	Runways, platforms and taxiways	Total
Water content	1512	1190	4504	34961	42167
Atterberg limits		208	131	855	1194
% of fines		208	136	850	1194
Specific gravity of solids		25	118	744	887
Triaxial UU	21	31	60	308	420
Triaxial CU			46	274	320
Consolidation	41	12	69	363	485
Total	1574	1674	5064	38355	46667

In this project, the portable dynamic cone penetrometer (Panda) was useful to assess the thickness and mechanical characteristics of the crust of desiccated soils topping the clay deposits. Standard Penetration Tests (SPT) were performed mainly to obtain representative samples for soil classification and water content determination. Undisturbed samples were obtained using Shelby type or special samplers for laboratory tests. A large number of Cone Penetration Tests (CPT and CPTu) and a limited number of Vane Shear Tests (VST), formerly a much more popular test, were also performed. To assess shear wave velocity, the suspension PS logging technique was preferred to other geophysical methods. In the lakebed area soft clay deposits, shear wave velocity ranges from 40 to 90 m/s. Silt and sand lenses interspersed in the clay as well as the hard crust and the superficial fills topping the clay may however present a much higher velocity.

Regarding characterization of Mexico City clay shear strength from CPT tests, an empirical relation has proven to provide better estimates than the classic Eq. (4). This relation is considered to be of general applicability for the Basin of Mexico clays (Santoyo *et al.*, 1989 [52]):

$$s_u = \frac{q_c}{N_k} \quad (5)$$

where s_u = undrained shear strength, q_c = tip resistance in CPT test, and N_k = cone factor.

A large number of field and laboratory determinations showed that a very good agreement between shear strength estimated with Eq. (5) and actual laboratory measurements (UU tests) is obtained when $N_k = 13$ (Alanís, 2003 [53]). However, evidences suggesting a significant influence of Over Consolidation Ratio (OCR) on the cone factor have also been presented (Montañez, 1983 [54]).

For modelling of deep foundations, tunnels, and other geotechnical structures in Mexico City clay, the Soft-Soil model (Plaxis software) has been extensively used in Mexico City with satisfactory results (Rodríguez, 2011 [55]). The Hardening soil model is however generally preferred for modelling excavations where the soil is submitted to unloading. To take into account the anisotropic behavior apparent in Figure 3, models such as the S-Clay1 are preferred. Visco-elastic behavior of Mexico City clay has also been assessed and the results are being incorporated into new constitutive models (Ossa, 2004 [56]).

Experimental investigations have shown that the dynamic response of Mexico City clays strongly depends on the strain level induced. At low deformations, the response is relatively linear, the clay has low capacity to dissipate energy and degradation with the number of stress cycle applications is negligible. For large deformations, the response is strongly non-linear, damping increases notably and stiffness degradation may be important. The threshold shear strain between linear and non-linear behavior of clays depends on clay characteristics. It has been shown that of all factors that affect the degree of non-linearity of clay behavior, the most important appears to be the plasticity index, PI. The upper bound seems to be given by the highly plastic clays of Mexico City ($PI > 200\%$). The behavior of these clays remains practically elastic with low damping up to an angular strain level of the order of 0.5%. This contributes to explain the large site effects registered in the lake zone of Mexico City during earthquakes (Romo and Auvinet, 1992 [57]). For large amplitude cyclic strains, the clay structure degrades continuously causing pore water pressure variations and reductions in stiffness and strength.

4. Spatial variations

4.1. Factors contributing to soft soils spatial variations

Spatial variations of soft soils properties can be induced by many factors. The formation process of soft soils, especially lacustrine soils, generally leads to a stratified structure with strong vertical variations and smooth horizontal differences. Many natural anomalies can however be present in soft soil deposits due to interference with other

geological formations and to anthropic factors, including the land use and loading history of the area that affect significantly the properties of the subsoil, especially in urban areas.

To detect topographical anomalies suggesting local variations of soil characteristics and to assess subsidence, new remote sensing techniques such as LiDAR (light detection and ranging, or laser radar; GPS based), InSAR (Interferometric Synthetic Aperture Radar) or DinSAR (Differential Synthetic Aperture Radar Interferometry) techniques have proven to be extremely useful (Auvinet *et al.*, 2017 [30]).

4.2. Spatial variations within the lacustrine zone of Mexico City

In Mexico City, large spatial variations of the subsoil are observed at different scales.

The urban area of Mexico Valley is usually divided in three main geotechnical zones (Marsal, 1975 [58]): Foothills (Zone I), Transition (Zone II) and Lake (Zone III). Figure 5 shows the three zones as defined in the present building code (GCDMX, 2017a [59]). In the foothills, very compact but heterogeneous volcanic soils and lava are found. These materials contrast with the highly compressible soft soils of the Lake Zone. Generally, in between, a Transition Zone is found where clayey layers of lacustrine origin alternate with sandy alluvial deposits.

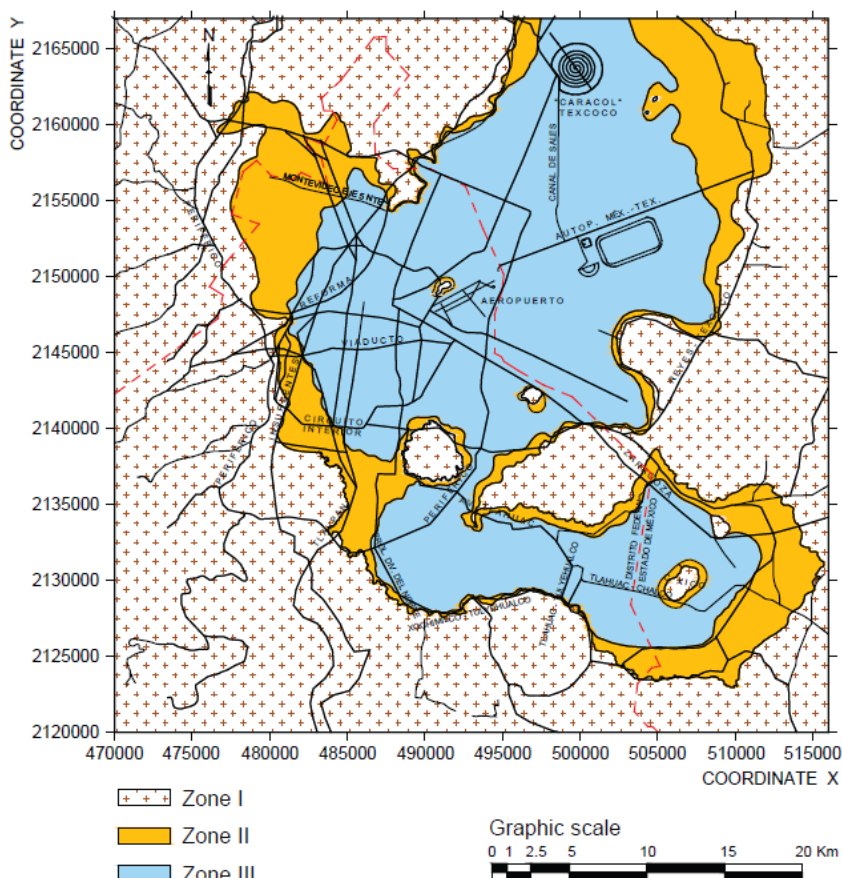


Figure 5. Geotechnical zoning of Mexico City and surrounding areas (GCDMX, 2017a [59]).

In Figure 6, typical soil profiles are presented (Marsal, 1975 [58]). Borehole Pc-28 corresponds to the Lake Zone. The water table is close to the surface. Three clayey layers are to be distinguished, denominated upper clay formation (Formación Arcillosa Superior, FAS), lower clay formation (Formación Arcillosa Inferior, FAI) and deep deposits (Depósitos Profundos, DP). The clays of FAS are separated from FAI by a hard layer (Capa Dura, CD), a sandy clayey stratum, generally less than 3m thick, found at a typical depth of 30 to 35m. In most sites, FAS is topped by a desiccated crust and/or artificial fills several meters thick.

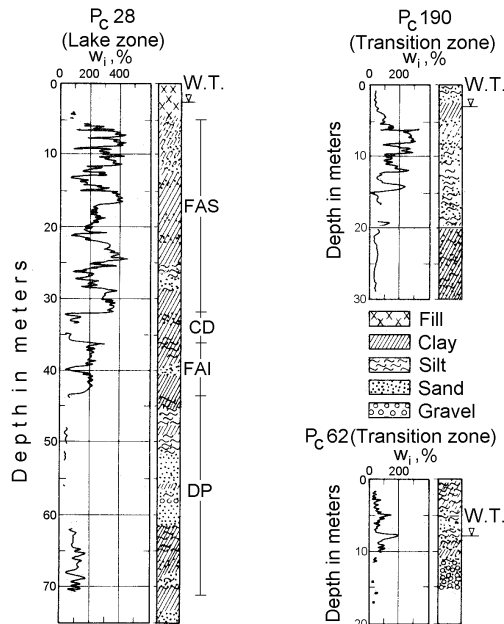


Figure 6. Typical soil profile for the different geotechnical zones.

Typical values of index properties for borehole P_c 28 are presented in Table 3. In some areas of the lacustrine zone, the water content of this exceptional material can indeed be higher than the value indicated in Table 3. The highest water contents in the city lake area are found in the upper part of the upper clay formation, down to a depth of about 20m.

Table 3. Typical values of index properties in the Lake Zone (Borehole P_c 28, Marsal, 1975 [58]).

Property	FAS	CD	FAI
Water content, % (Eq.(1))	270	58	191
Liquid limit w_L , %	300	59	288
Plastic limit, w_p , %	86	45	68
Density of solids, G_s	2.30	2.58	2.31
Initial void ratio, e_0	6.17	1.36	4.53
Unconfined compressive strength, q_u , kN/m ²	85	24	160

At a small scale, spatial water content variations within the soft soil deposits are also observed. Marsal (1959, [33]) determined the water content of Mexico City clays at different points of horizontal cross-sections of samples obtained using a thin wall Shelby sampler (Figure 7)

The scattering of the values obtained locally looks surprisingly high and raises the question of what the true water content of the sample really is. Most of the scattering is however due to the definition of water content w given by Eq. (1). The standard deviation of the w data presented in Figure 7 is 28.5% and the coefficient of variation is 7%. Switching to the definition of Eq. (2), the standard deviation of w' is 1.1 % and the coefficient of variation is only 1.4%. Finally, using definition of Eq. (3) the standard deviation of w'' is 1.6% and the coefficient of variation decreases further to .6%.

As can be expected in lacustrine materials, horizontal variations of the material are in fact hardly significant.

As mentioned earlier in this lecture, averaging the local values as suggested by Marsal in Figure 7 overestimates the true water content of the whole sample. The magnitude of the overestimation can be obtained as described in Appendix I. A simple calculation shows that in this case the true global value of water content w' (Eq. (1)) for the whole sample is of the order of 404.8%, only slightly inferior to the average value indicated in Figure 7. The variations of water content observed in Figure 7 will be examined further in this lecture (Figure 19).

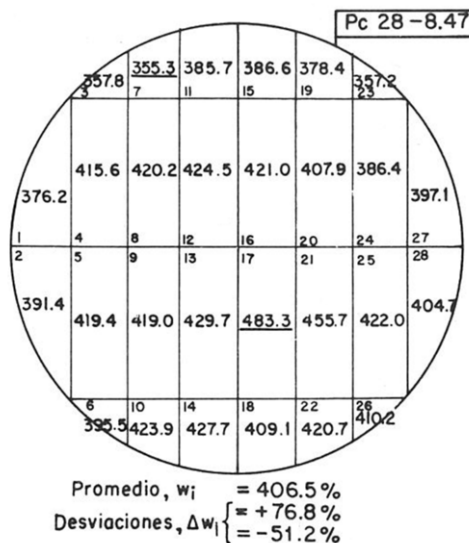


Figure 7. Variations of water content w (Eq. (1)) in a cross-section of a Mexico City clay sample.

In some areas of Mexico valley and especially in former Texcoco Lake (eastern part of the lacustrine area) the salinity of the soil is particularly high. In its central and northern zones, it can reach 54,000 mg/l in the first 60 m. It decreases gradually with depth and diminishes towards the edge of the former lake area and towards the south. Maximum concentrations of salt in former Texcoco Lake may be as large as 18%, according to data provided by Murillo and Morales (1991 [60]). Presence of salt leads to

a significantly smaller apparent water content that can be corrected to account for the presence of dissolved minerals following Marsal and Graue (1969 [61]):

$$w = \frac{w_{ap}}{1 - cw_{ap}} \quad (6)$$

where c = salt concentration in %, w_{ap} = apparent water content (including salt in solids, Eq. (1)), and w = actual water content.

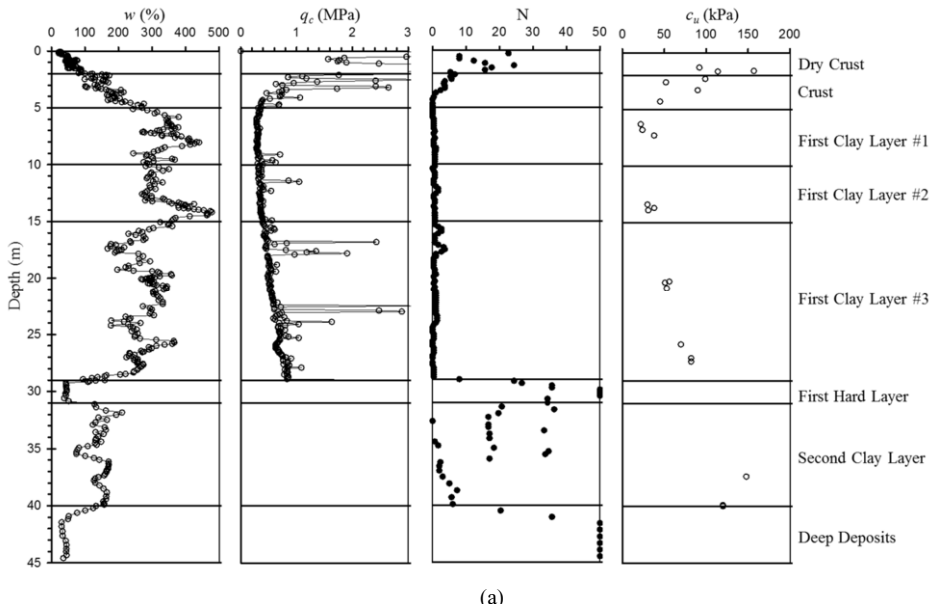
Differences between the apparent and true water content are significant. This is mainly due to the definition of water content given in Eq. (1). When definition of Eq. (2) is adopted, differences are much smaller. In that case, the actual water content w' can be obtained as:

$$w' = \frac{w_{ap}'}{1 + (1 - c) w_{ap}'} \quad (7)$$

where w'_{ap} = apparent water content (including salt in solids, Eq. (2)).

When using definition of Eq. (3), no correction is needed.

At a larger scale, Figure 7 presents a typical soil profile for the Lake Zone clays that includes water content, CPT tip resistance, SPT blow count number and undrained shear strength (Rodríguez, 2011 [55]).



(a)

Figure 8. (a) Typical soil profile, San Juan de Aragón site, Lake Zone, (b) Zoom on water content of the 5 to 15m deep layer.

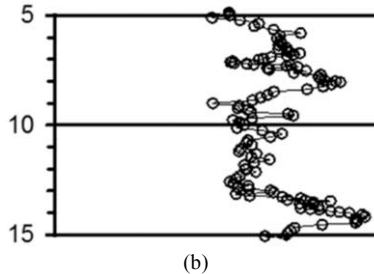


Figure 8. (continued) (a) Typical soil profile, San Juan de Aragón site, Lake Zone, (b) Zoom on water content of the 5 to 15m deep layer.

As observed on the soil profiles of Figures 6 and 8, in the Lake Zone, the water content of the clays presents wild variations on short vertical distances. This is generally attributed to a complex history of successive volcanic eruptions as well as to flooding and drying episodes.

It can however be observed that water content variations are not matched by equivalent variations of the CPT tip resistance q_c , except at the elevation of sand lenses interspersed within the clay. A large part of the apparently strong variations of the water content within the clay layers observed in Figures 6 and 8 should in fact be traced to the definition of water content itself.

Focusing the analysis on the water content measured in the 5 to 15m deep layer (Figure 8b), the statistical results presented on Table 4 are obtained.

Table 4. Statistical analysis of water content and void ratio for the 5 to 15m deep layer of Figure 8b.

	w , %	w' , %	w'' , %	e
Average	366.1	77.1	89.3	9.15
STD	240.9	5.5	2.7	6.02
CV, %	65.8	7.1	3.0	65.8
True value	333.8	76.9	89.3	8.34
Bias	32.3	0.2	0	0.81

The scattering of the values of water content w is high. The standard deviation of the w data in this layer is 240.5% and the coefficient of variation is 65.8%. Most of the scattering is however due to the definition of water content w given by Eq. (1). Switching to the definition of Eq. (2), the standard deviation of w' is 5.5 % and the coefficient of variation is only 7.1%. Finally, using definition of Eq. (3) the standard deviation of w'' is 2.7% and the coefficient of variation decreases further to 3%.

As mentioned earlier in this paper, averaging the local values overestimates the true water content of the whole population. The magnitude of the overestimation can be obtained as described in Appendix I. A simple calculation shows that the true value of water content w' (Eq. (1)) for the whole population is of the order of 333.8%, clearly inferior to the average value of 366.1%.

In the same way, it can be observed that the scattering of the void ratio is very high. The average value of the e data in this layer is 9.15, the standard deviation is 6.02 and the coefficient of variation is 65.8%. However, this is basically due to the definition of void ratio adopted in geotechnical engineering. Switching to porosity (in this case equal

to w'') the coefficient of variation is only 3%. Note also that averaging the void ratio local values leads to a value of 9.15 when the true global value is 8.34. Characterizing a layer by the average values of void ratio, e , and water content, w , can be a source of significant errors for this type of soil, in particular for settlements computations.

Figure 9 shows three water content profiles corresponding to the same site (Runway 6, NAICM) and presented using the alternative definitions of water content corresponding to Eqs. (1) to (3). With the gravimetric definition referred to the total weight of the sample (Eq. (2)) (centre of Figure 9), differences between water contents at distinct elevations within the upper clay formation are no longer so conspicuous, especially at depth between 0 and 20m. The profile is even smoother when the volumetric definition of water content (Eq. (3)) is used (right hand side of Figure 9). It can then be concluded that different definitions of water content provide quite different descriptions of the soil. Profiles based on water content defined by Eq. (1) suggest that large variations in the composition the soil occur when in fact these variations correspond to small changes in the amount of water and solids in the soil. This is due to the high non-linearity of the relation between w and weight of solids W_s in Eq. (1) (Appendix I).

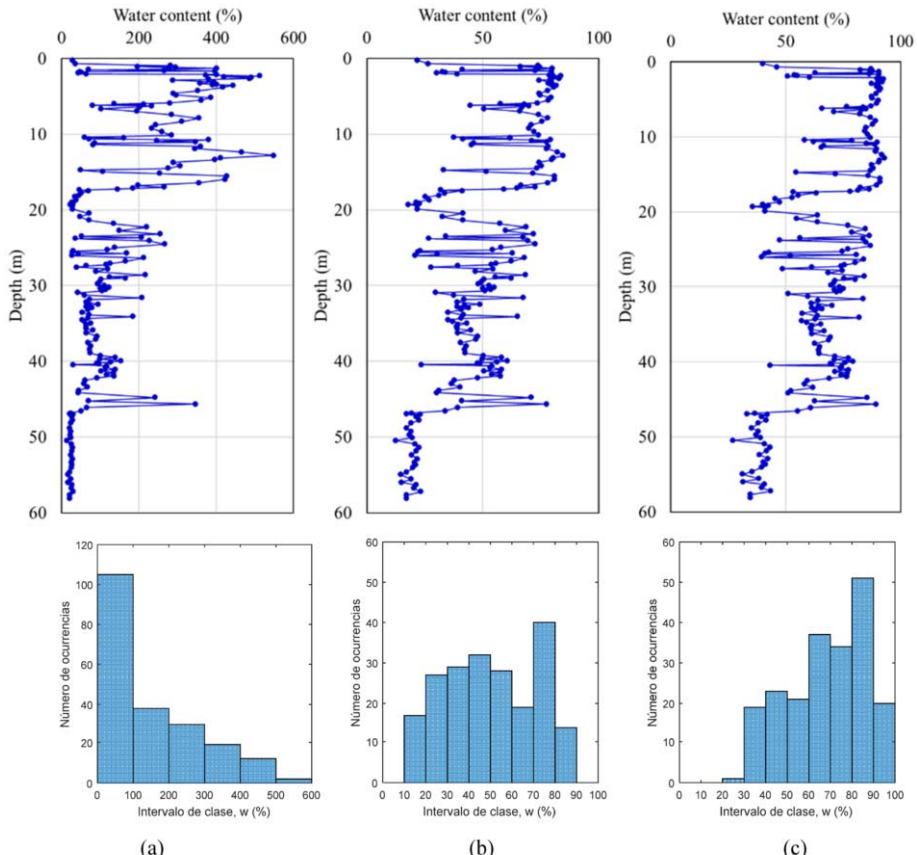


Figure 9. Water content profiles in a Lake Zone site established using different definitions of water content (a) Eq. (1), (b) Eq. (2), (c) Eq. (3) and corresponding histograms.

The shape of the water content histograms corresponding to different definitions of water content is extremely variable. The histogram corresponding to the second definition (Eq. (2)) of water content is slightly bimodal but approximately Gaussian, a condition favorable for geostatistical analyses (Appendix II). The other histograms are strongly skewed respectively to the left (Eq. (1)) and to the right (Eq. (3)). In all cases, geostatistical analyses would benefit from a transformation by *anamorphosis* of the corresponding random field of water content to a Gaussian field (Appendix II).

Local variations are only one aspect of the heterogeneity of the Lake Zone soft clay deposits. Zone III (Figure 5) is far from being homogeneous. Many natural and anthropomorphic anomalies leading to geotechnical variations have been encountered in the valley as shown on Figure 10 (Méndez *et al.*, 2010 [62]; Auvinet *et al.*, 2017 [30]).

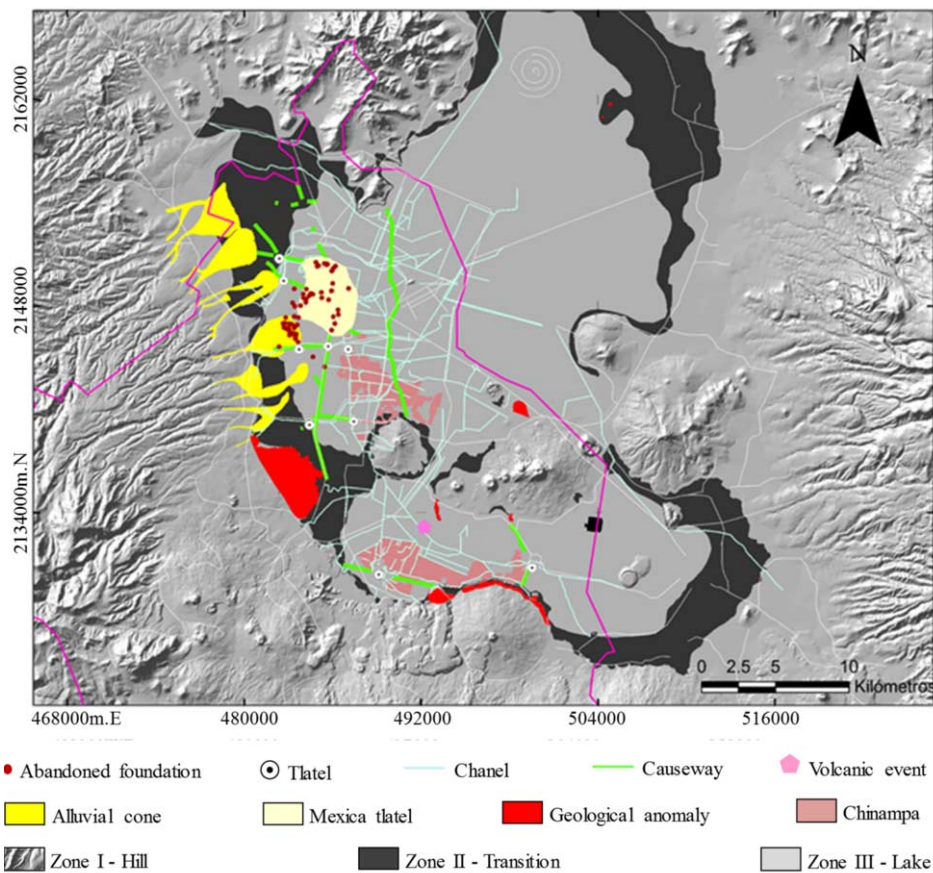


Figure 10. Geotechnical anomalies within the lacustrine clays of Mexico City.

Natural anomalies due to interference between the soft soil deposits and other contiguous geological formations are conspicuous, especially in the perimeter of the Lake zone.

Water content in Mexico City clays varies considerably, depending on the location of individual sites. Sites in the built area, having been subjected to external overburdens

contain less pore water than the so-called virgin clays that are typical of the less or newly urbanized areas.

In general, soils towards the edges of the former lake are less humid than in the central part, a situation that is favored by the existence of sands and sandy silts interspersed with the upper clays in the so-called transition zone (Ovando, 2011 [36]). On the east side of the former lake, alluvial fans shown in Figure 10 originate very complex and heterogeneous local soil conditions including the presence of coarse granular materials and boulders. In other areas, volcanic materials produced by recent eruptions such as volcanic tuffs or basaltic lava, are occasionally found interspersed within the lacustrine materials, especially in the contact with the Santa Catarina and the Chichinautzin ranges, in the south part of the lacustrine zone.

The shallow lakes of Mexico City basin have been, for many centuries, the site of intense human activity. Artificial islands (*Tlalteles*), many of them topped by religious monuments (*Teocalli*), as well as causeways were built with sandy and silty fills brought from the surrounding hills with a thickness varying from a few meters to 15m. Later, as the lakes were recessing as a result of the drainage works, canals were constructed to conduct the water to the still inundated lower part of the valley in Texcoco. These canals were subsequently filled with the surficial material of the dry crust layer or with transported sandy and silty materials. Agriculture techniques adapted to the environment were developed in the south of the lacustrine area since the pre-Columbian era. In the *chinampas* or “floating gardens” a large amount of organic matter was piled upon the soil surface for agricultural purposes. During reconnaissance surveys, geotechnical engineers should thus not be surprised to encounter down to a significant depth some materials with properties quite different from those of the typical lacustrine clays.

The regional subsidence of the Lake and Transition Zones due to pumping of underground water from the deep aquifers also contributes to the subsoil heterogeneity and evolution of its properties with time. Carrillo (1948 [63]) was the first to establish a clear correlation between subsidence and piezometric drawdown induced by pumping. The settlement accumulated since 1862 has reached 14.5m in some areas (Auvinet *et al.*, 2017 [30]). Figure 11 presents an updated evaluation of the subsidence rate. Groundwater pumping from the deep aquifer system underneath the city is now about $52 \text{ m}^3/\text{s}$, representing 72% of potable water provided to the city dwellers and cannot be stopped without serious social consequences. This phenomenon damages drainage and transport systems as well as other services of the city and generates severe foundation behavior problems (Auvinet *et al.*, 2017 [30]).

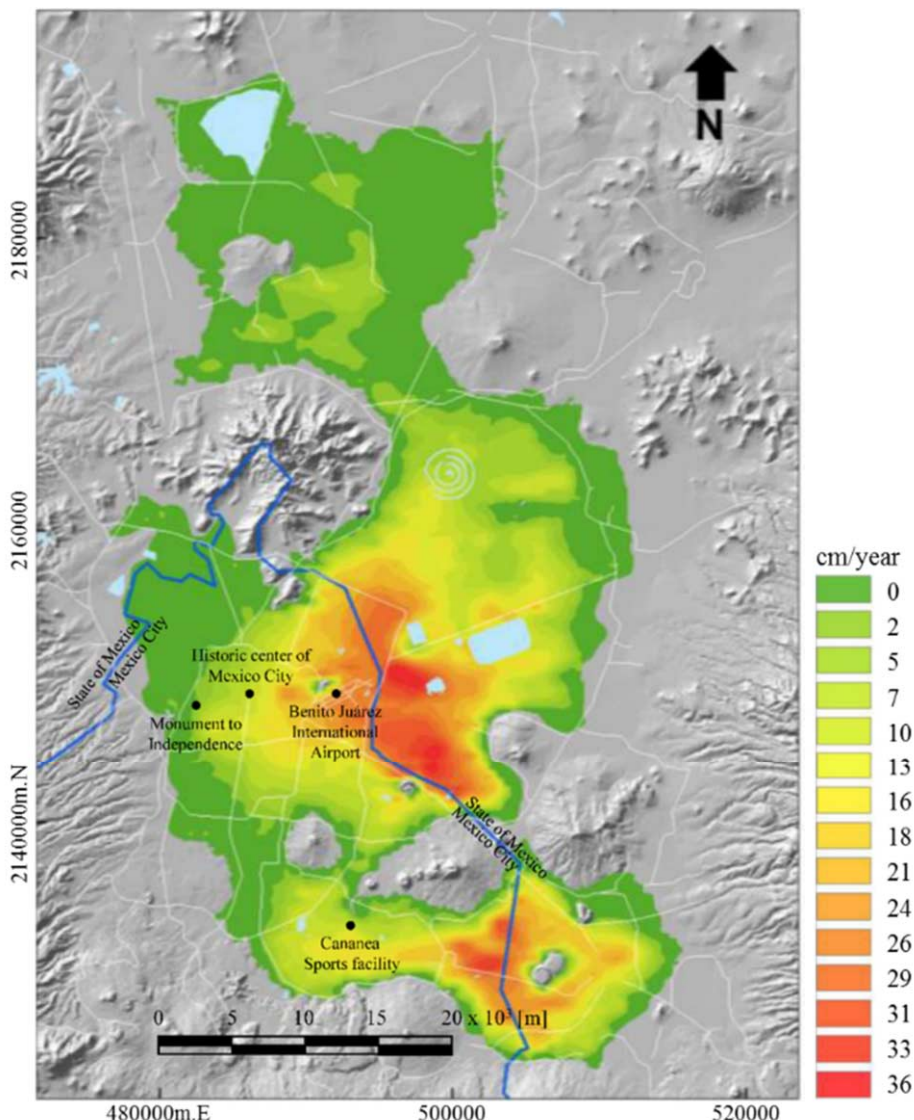


Figure 11. Subsidence rate in Mexico City lacustrine area.

Static and dynamic properties of the subsoil are progressively affected by the ongoing regional consolidation process and are expected to present drastic variations in the future (Ovando *et al.*, 2007 [64]; Jaime and Méndez, 2010 [65]); Figure 12 shows the evolution of CPT results obtained at the Secretaría de Comunicaciones y Transportes (SCT) site in 1985, 2000, and 2011 (González, 2012 [66]).

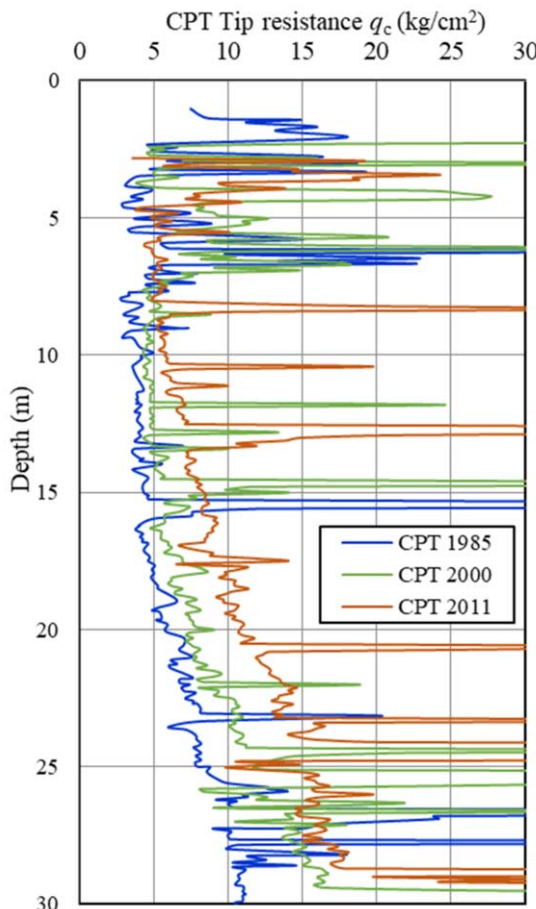


Figure 12. Variation of CPT profile with time, SCT site, Lake Zone, 1985, 2000, 2011.

Implications of the evolution of Mexico City subsoil properties due to water pumping and in particular the effects of future regional subsidence on the seismic response have been evaluated and shown to be very significant (Ovando *et al.*, 2003 [67]; 2007 [64]). It has been recognized that in the future it will be necessary to adapt the Building code seismic requirements to this evolution.

The subsidence phenomenon also has severe consequences in some abrupt transition zones, especially in the contact of the soft materials of the Lake Zone with the Santa Catarina and Chichinautzin ranges (Figure 13). Large fissures due to differential settlements with steps that can exceed 50cm have developed progressively and created a critical geotechnical environment (Auvinet *et al.*, 2011 [68]; 2017 [30]). These fissures affect street pavement, public services and constructions. They are reactivated during large earthquakes as happened on September 19th, 2017 (Figure 14a).

Other fissures are induced in the Lake zone by hydraulic fracturing of the clay formation in flooding areas (Figure 14b).

Special solutions for mitigating the consequences of this phenomenon have been developed (Auvinet *et al.*, 2019 [69]).

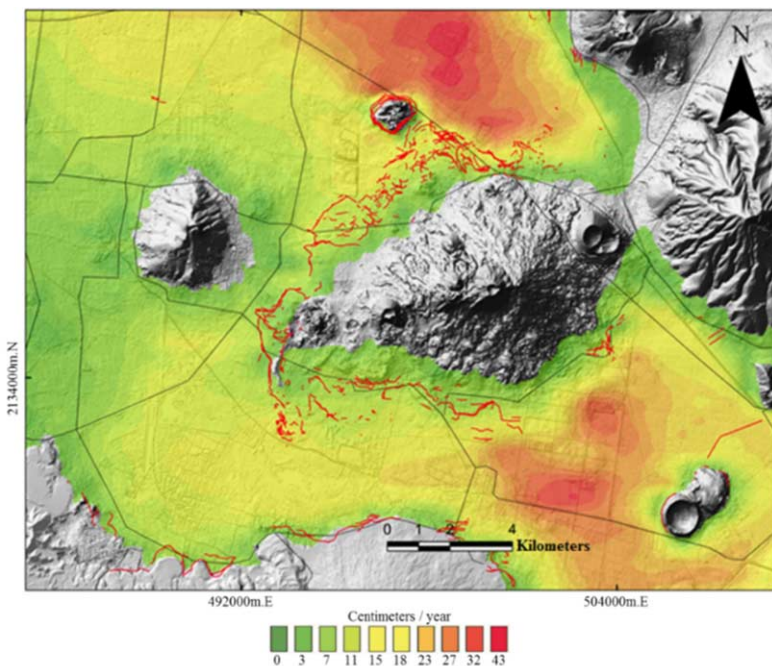


Figure 13. Soil fissuring around Santa Catarina range due to regional subsidence.



Figure 14. Soil fractures induced by (a) regional subsidence (b) hydraulic fracturing in flooding zones.

5. Modeling spatial variations of soft soils

5.1. Deterministic models

During the early years of Geotechnical Engineering, a soft soil deposit was frequently pictured as a simple half space medium with homogeneous properties. This was

equivalent to ignoring spatial soil variability. To take into account the existence of contrasting horizontal layers, approximate methods were considered acceptable (Steinbrenner, 1934 [70]; Button, 1953 [71]). This simple model was also accepted and is in fact still used for dynamic soil-structure interaction analyses based on the half space theory (Richart *et al.*, 1970 [72]).

Subsequently, simple variations models, generally linear, were used to describe spatial variations of properties presenting a tendency to increase with depth.

Ladd and Foote (1974 [73]) formalized a system to present and characterize the variation of undrained shear strength within soft soil masses. This system, known as SHANSEP (Stress History and Normalized Soil Engineering Properties) was based on the observation that the shear strength of many soils can be normalized with respect to the vertical consolidation pressure. When stress strain curves measured in consolidated-undrained (CU) triaxial tests are plotted, a normalized plot can be drawn in which the strain axis is unchanged and the stress axis is normalized by dividing the axial stress difference by the vertical consolidation pressure. For many soft soils, unique curves are obtained for each value of overconsolidation ratio OCR . As the overconsolidation ratio increases from 1 to higher values, the strain at peak stress decreases. The general idea behind the SHANSEP method is thus to perform a series of laboratory tests with a careful control of the stress conditions during consolidation and of the stress path during undrained shear. These tests can be performed over a range of stress histories and stress paths. The in situ stress history of the soil is then evaluated, and the stress path to which the soil will be imposed is determined. Then, strengths from the laboratory tests, which most closely replicate the field conditions, are used to predict the field behavior (Bay *et al.*, 2005 [74]). Based on SHANSEP concepts, Ladd and Foote (1974 [73]) empirically developed the following relationship:

$$\frac{s_u}{\sigma'_0} = S(OCR)^m \quad (8)$$

where: s_u = undrained shear strength, OCR = overconsolidation ratio, σ'_0 = effective vertical stress at the considered elevation, m = exponent that usually falls between 0.75 and 1.0 and is established by curve fitting, and S = normally consolidated ratio (s_u/σ'_{vo})_{nc}.

Term S varies as a function of the failure mode (testing method, strain rate). Ladd and De Groot (2003 [1]) recommended $S = 0.25$ with a standard deviation of 0.05 (for simple shear loading) and $m = 0.8$ for most soils (Robertson, 2012 [32]). The above equation is also supported by Critical State Soil Mechanics (CSSM) where $S = (1/2) \sin \varphi'$ in direct simple shear (DSS) loading, and, $m = 1 - C_s/C_c$, where C_s is the swelling index and C_c is the compression index (Robertson, 2012 [32]).

A critical analysis of the SHANSEP methodology was presented by Almeida (2004 [15]). According to this author, destructuration and loss of anisotropy can occur when the method is used in natural clays.

5.2. Statistical and probabilistic models

Variations of soft soil properties within a geotechnical medium can be represented resorting to descriptive statistics and tools such as tables or histograms (Figure 9).

Expanding the scope of this approach, it is possible to develop probabilistic models of the spatial variation of the properties of interest by considering them as random variables and fitting a probability density model to histograms obtained from sampling results in order to describe the random behavior of these variables. It becomes then possible to resort to statistical inference, i.e. to the estimation of the general characteristics of the population (a zone within the earth mass) based on a limited number of samples resorting to point estimates or confidence intervals.

Representing spatial variation of soil properties by means of random variables has however, the inconvenience of neither taking into account the specific position of the samples within the medium nor the existing dependence among them. There is no doubt that the properties of two soil samples tend in general to present a closer similarity when they are obtained at contiguous rather than distant locations. A spatial correlation structure, generally strongly anisotropic, exists in most geotechnical media and especially in soft soils.

To take into account spatial correlation, a more advanced formalism based on the concept of spatial random functions or random *field* has been introduced (Vanmarcke, 1983 [75]; 2010 [76]; Auvinet, 2002 [23]). It is then considered that, at each point X of the medium, the property of interest is a random variable $V(X)$. To describe such a field, the following parameters and functions are introduced (Appendix II):

- Expected value:

$$\mu_v(X) = E\{V(X)\} \quad (9)$$

- Variance:

$$\sigma_v^2(X) = \text{Var}[V(X)] \quad (10)$$

- Autocovariance function:

$$C_v(X_1, X_2) = \text{Cov}[V(X_1), V(X_2)] = E\{[V(X_1) - \mu_v(X_1)][V(X_2) - \mu_v(X_2)]\} \quad (11)$$

The function known as *autocovariance*, is used to describe the spatial linear correlation among the variables in two different points. In the simplest models it is accepted that the field is wide-sense stationary (constant expected value and autocovariance depending only on the distance between the two points considered), at least locally, or present wide-sense stationary increments. The field parameters are obtained from experimental data assuming that the field is ergodic and using statistical estimators. Developing random field models has proven particularly useful in geotechnical media of lacustrine or alluvial origin, where a conspicuous horizontal continuity exists.

In some instances, a trend in the data can be observed suggesting a deterministic variation of the property with depth. This trend can be removed from the data in order to define a stationary residual random field. The trend is commonly assumed to be linear and defined by linear regression. Note however that, for some properties such as shear strength, the trend can also be defined using deterministic considerations such as those implicit in the SHANSEP model (5.1).

When a general random field model has been established, it becomes possible to define a conditional field with respect to actually measured values. This field is no longer stationary since it presents a smaller uncertainty close to the sampling points. As exposed

in Appendix II, conditional expected values of the properties of interest at points in which no measurements were performed can be obtained (point estimation) using the linear estimation technique (Auvinet, 2002 [23]; Appendix II) or any of its variants such as the kriging technique (Krige, 1962 [77]; Matheron, 1965 [78]; Juárez, 2015 [79]).

Note that this type of estimation assumes that the estimated values can be expressed as a linear combination of the contiguous measured values. As explained in Appendix I, this is not rigorously the case for properties such as the water content w defined by Eq. (1). Using the linear estimation technique in this case can then be only considered as a first approximation, especially for high water contents.

By combining a large number of estimation points, according to a regular mesh, virtual borings and cross-sections of the subsoil and maps of the depth and thickness of the different layers can be obtained. These graphs represent the conditional expected value of the physical or geometrical property of interest. This, incidentally, leads to a smoothing effect characteristic of this type of estimation. An important advantage of this method on some other approaches based for example on artificial intelligence is that it is coherent: estimations performed at the points where measurements were made does coincide with the measured values.

It is also possible to estimate the average value of the same properties in a certain domain, for example, a finite element or a potentially unsafe failure surface (global estimation).

In all cases, it is convenient to calculate and represent the estimation variance in complementary graphs (Appendix II), in order to detect the areas where information is scarce and additional exploration is in order. To optimize the location of new sampling sites, the concept of *gain* (Azzouz et Bacconnet, 1988 [80]) is particularly useful. This approach contributes to eliminating part of the subjectivity currently existing in the design and interpretation of reconnaissance surveys.

These techniques provide tools that supplement, but does not substitute, traditional interpolation criteria based on geological evidences and in particular on geomorphology and sedimentology. The technique lends to computer programming and therefore to the simultaneous handling of large amounts of data that could be hardly evaluated with the traditional approach; it requires a careful reviewing and systematic organization of the data. The validity of the results obtained depends on the characteristics of the field. It is more likely to provide useful results in fields with an approximate Gaussian-type behavior (Appendix II). It is also better applied to structured media such as lacustrine or alluvial deposits rather than to chaotic media such as conglomerates, breccia or colluvium deposits.

“Plausible” rather than “expected” configurations of the spatial variation of the properties can be obtained by simulation (Appendix II). These simulations provide “realistic” virtual borings, cross-sections or maps, with no smoothing effect. Generating a large number of these images facilitates the evaluation of the possibility (and if desired, the probability) of reaching or exceeding locally some extreme conditions that could be critical for the project under study. The simulation is called unconditional if it is only compatible with the field parameters and conditional if the location and the characteristics of the available samples are also taken into account.

The estimation techniques can also be used when data from several random fields corresponding to different soil parameters are available. This is of foremost importance in Geotechnical engineering since it allows estimating critical (primary) properties such as mechanical parameters from (secondary) variables more easily determined such as physical or index properties, taking advantage of correlations between both types of

properties. This strategy is commonly known as multivariate approach (Wackernagel, 2003 [81]) or “cokriging” (Appendix II). In the context of this lecture, it will be called “multifield” approach.

Note that, alternatively, spatial variability of geotechnical variables can be modeled by means of random functions known as *copulas* (Nelsen, 2006 [82]; Phoon and Ching, 2015 [83]; Vázquez and Auvinet, 2014 [84]). Copulas express spatial dependence without the influence of the first-order distribution functions (Appendix II). Thus, more realistic spatial variability descriptions can be attained.

It should also be observed that in soils submitted to consolidation, the evolution of static and dynamic parameters of the deforming deposit (Figure 12) occurs within a context of pronounced uncertainty. Therefore, introducing a spatio-temporal random field $V(X, t)$ may be helpful to increase the degree of realism of long-term predictions made with geomechanical models and should be considered (Vázquez and Auvinet, 2015 [85]).

5.3. Reduction of variance in soils

When a soil property is represented by a random field, the “scale effect” or “variance reduction” concept acquires an outstanding importance. Consider the average value V_Ω of a certain property represented by a stationary random field $V(X)$, in a subdomain Ω (segment, surface or volume) of R^p ($p = 1, 2$ or 3):

$$V_\Omega = \frac{1}{\Omega} \int_{\Omega} V(X) dX \quad (12)$$

According to Eqs. (21) and (25) of Appendix II:

$$E\{V_\Omega\} = E\left\{ \frac{1}{\Omega} \int_{\Omega} V(X) dX \right\} = E\{V(X)\} \quad (13)$$

$$\text{Var}[V_\Omega] = \frac{\text{Var}[V(X)]}{\Omega^2} \iint_{\Omega \Omega} \rho_V(X_1, X_2) dX_1 dX_2 \quad (14)$$

where $\rho_V(X_1, X_2)$ is the autocorrelation coefficient or normalized autocovariance of the field (Appendix II).

As exposed in Appendix II, since the autocorrelation coefficient is smaller than or equal in absolute value to unity, the variance of the average value of a stationary random property in a subdomain Ω tends to decrease when the dimensions of such subdomain increase (except in the trivial case of perfect correlation). This is the so-called reduction of variance or scale effect phenomenon, analogous to the well-known law of large numbers. This phenomenon has important consequences in geomechanics:

- a) At a small scale, index properties such as porosity, void ratio, unit weight and water content are some sort of average values involving random amount of voids, solids and water. These properties can only be defined unambiguously for samples with a size sufficiently large to guarantee that the associated variance is small. The problem of the convergence of these averages towards stable values was already a

concern for the ancient Greeks philosophers who called it the *Soritos* problem (“How many grains are necessary for an assembly of particles to be considered as a sand?”). Auvinet *et al.* (1984 [86]; 1986 [87]) have proposed a probabilistic solution to this problem for granular media.

- b) At a larger scale, the above averages are commonly considered in geotechnical engineering as punctual values. These values generally also present random variations due to a complex geological formation process or other factors leading to random fields $V(X)$ such as those considered in this lecture (Appendix II). Depending on the volume of soil affected by field tests or geotechnical structures, averages of these punctual values are affected by a significant variance reduction effect.
- c) This variance reduction effect makes it strictly necessary clarifying the size of the samples tested in laboratory or the dimensions of the zone affected by a given field test. The scattering of the results is strongly dependent on these geometrical parameters (Eq. (14)).
- d) Variance of the average value of punctual soil properties along a vertical axis (for example along a borehole, Appendix III), a surface (for example failure surface) or within a given volume (for example fine element) is generally much smaller than the variance of punctual values. This should be taken into account in any geotechnical reliability analysis.
- e) Accuracy of geotechnical engineering predictions owes much to the variance reduction or scale effect, since the safety of most geotechnical structures does not depends on the uncertainty on local shear strength parameters but on the much lower uncertainty on average properties in large subdomains of the geotechnical mass.

5.4. Modeling spatial variations of the subsoil of Mexico City.

Not so long ago, the upper clay formation in Mexico City lake zone used to be idealized as a simple half space medium with homogeneous properties. As an example, immediate displacements due to excavations were successfully modelled assuming the medium to be elastic with a small strain undrained modulus obtained from geophysical measurements (Auvinet, 1969 [88]). Considering the subsoil as a homogeneous or horizontally stratified half space medium is still implicit in the techniques proposed in Mexico City building code for dynamic soil-structure interaction analysis (GCDMX, 2018b [89]).

A statistical approach was used by Marsal and Mazari (2017 [33]) to describe spatial variations of Mexico City clays, from a large number of experiments performed during the late 50's and early 60's of the last century on samples retrieved at different locations in the lacustrine zone in the central part of the city. Assuming that large sub-zones of this part of the city subsoil were “statistically homogeneous”, those authors prepared tables and histograms for each sub-zone and established correlations between index and mechanical properties that have been extremely valuable for several generations of geotechnical engineers. To illustrate the above, Figure 15 presents a correlation between coefficient of compressibility, a_v , in the preconsolidation interval, and water content, w (Eq. (1)).

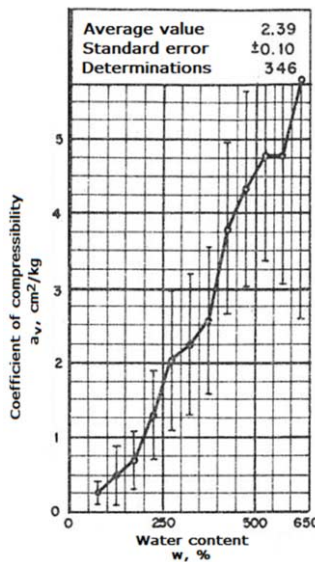


Figure 15. Statistical correlation between coefficient of compressibility, a_v , in preconsolidation interval, and water content, w , (Eq. (1)), Marsal and Mazari (2017 [33]).

Water content has also been related to undrained shear strength from UU tests (Mazari, 1996 [90]). Dispersion is large and only allows for the identification of a general trend with a rather wide range of variability (Figure 16). Similar correlations between undrained shear strength obtained from CPT tests and water contents have been established for the Texcoco Lake (Alanis, 2003 [53]).

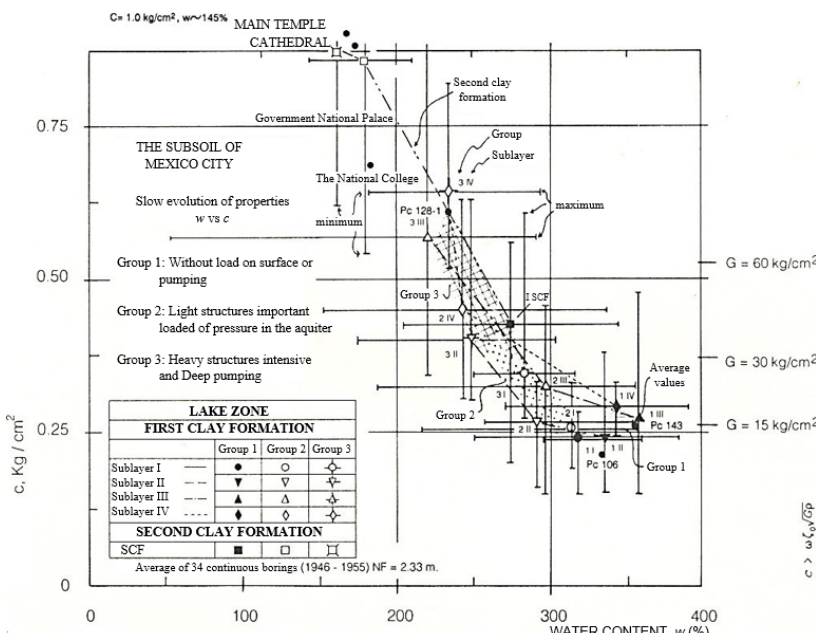


Figure 16. Shear strength c (s_u) vs water content w (Eq. (1)) for Mexico City clays.

The correlations proposed by Marsal and Mazari are strongly affected by the definition of water content that was adopted in the statistical analyses (Eq. (1)). As an example, a correlation between coefficient of volumetric compressibility, m_v , and water content w deduced from Figure 15 is presented in Figure 17 (left hand side). This correlation suggests that, unexpectedly, coefficient m_v remains practically constant for values of w exceeding 400 %. In fact, the non-linear relationship implicit in Eq. (1) causes a distortion of the correlation graph that is no longer observed when w (Eq. (1)) is substituted by w' (Eq. (2)) (Figure 12, right hand side).

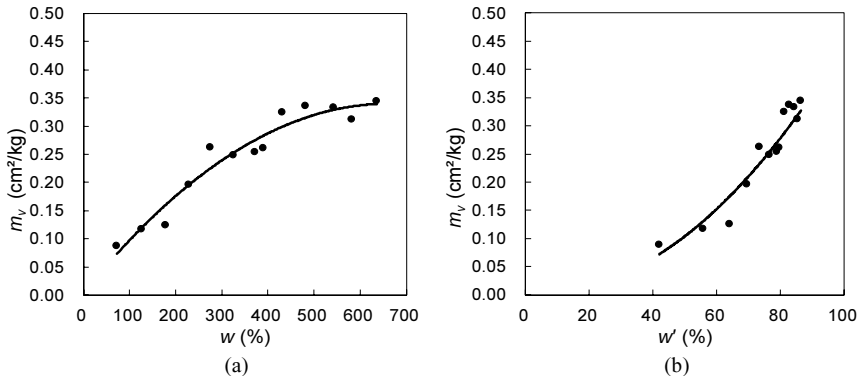


Figure 17. Correlation between coefficient of volumetric compressibility m_v and water content defined by (a) Eq. (1) and (b) Eq. (2).

Modifying the definition of water content generally improves the correlation of this parameter with other properties. Figure 18 shows how correlation between shear wave velocity V_s and water content improves when switching from definition of Eq. (1) to definitions of Eq. (2) or Eq. (3). When applied to the correlation of Figure 16, or to the correlations proposed by Alanis (2003, [53]) this transformation has similar consequences.

Figure 17 and 18 suggest that water contents w' (Eq. (2)) and w'' (Eq. (3)) provide a better insight into mechanical properties of soft soils than the classical parameter w (Eq. (1)).

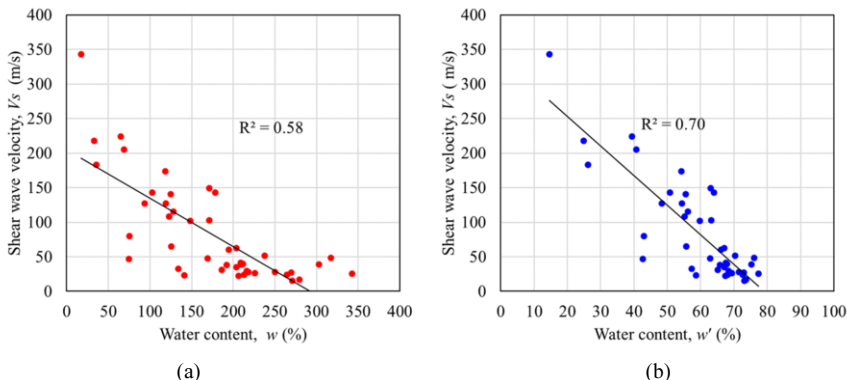


Figure 18. Correlations between shear wave velocity, V_s , and water content defined by: (a) Eq. (1), (b) Eq. (2), (c) Eq. (3).

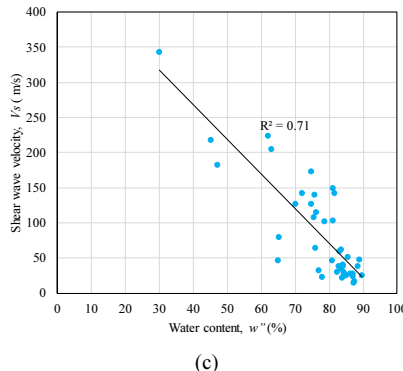


Figure 18. (continued) Correlations between shear wave velocity, V_s , and water content defined by: (a) Eq. (1), (b) Eq. (2), (c) Eq. (3).

Reséndiz and Herrera (1969 [91]) were probably the first to suggest using random fields to describe the variations of Mexico City clays properties. They assumed that all variations in compressibility occurring in a horizontal direction are random and they showed that, within a given natural soil stratum, coefficient of volume compressibility m_v behaves as a Gaussian 2D random field with Dirac delta correlation coefficient (white noise). Based on these considerations they were able to assess the probability of differential settlements of a rectangular foundation exceeding any given tolerable value.

In the last decades, random field models have become particularly useful to describe the clay deposits of the Valley of Mexico (Auvinet *et al.*, 2001 [92]; 2002 [93]; 2005 [94]). They have been used for describing spatial variations at different scales.

a) Small scale

The variations of water content in the horizontal cross-section of a clay sample shown on Figure 7 can be considered as local fluctuations of a 2D random field. Parameters of this field can be roughly estimated using common statistics from the scarce data available. The estimation techniques described in Appendix II, can then provide a dense set of punctual values and contours of estimated water content can be established (Figure 19a). Results obtained in the same way but accepting the definitions of Eq. (2) and Eq. (3) for water content are shown respectively on Figures 19b and 19c.

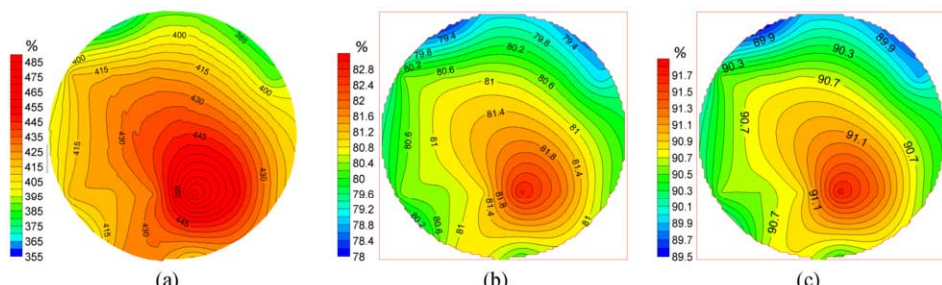


Figure 19. Geostatistical estimation of water content contours in a cross-section of a Mexico City clay sample for different definitions of water content; (a) Eq. (1), (b) Eq. (2) and (c) Eq. (3).

The apparent degree of homogeneity of the sample varies significantly depending on the definition of water content adopted. Definition of Eq. (1) tends to exacerbate the differences between the different zones of the sample.

b) Soil profiles 1D geostatistical estimations.

Variations with depth of soil properties of the upper clay formation of the Lake Zone of Mexico City can be described by a 1D random field.

In the case of the water content profile obtained within the upper clay formation shown in Figure 20a, a trend suggesting reduction of water content with depth is observed. This trend can be removed from the data in order to define a stationary residual random field (Figure 20b). Figure 21 shows vertical correlograms for the original (Figure 21a) and residual (Figure 21b) fields.

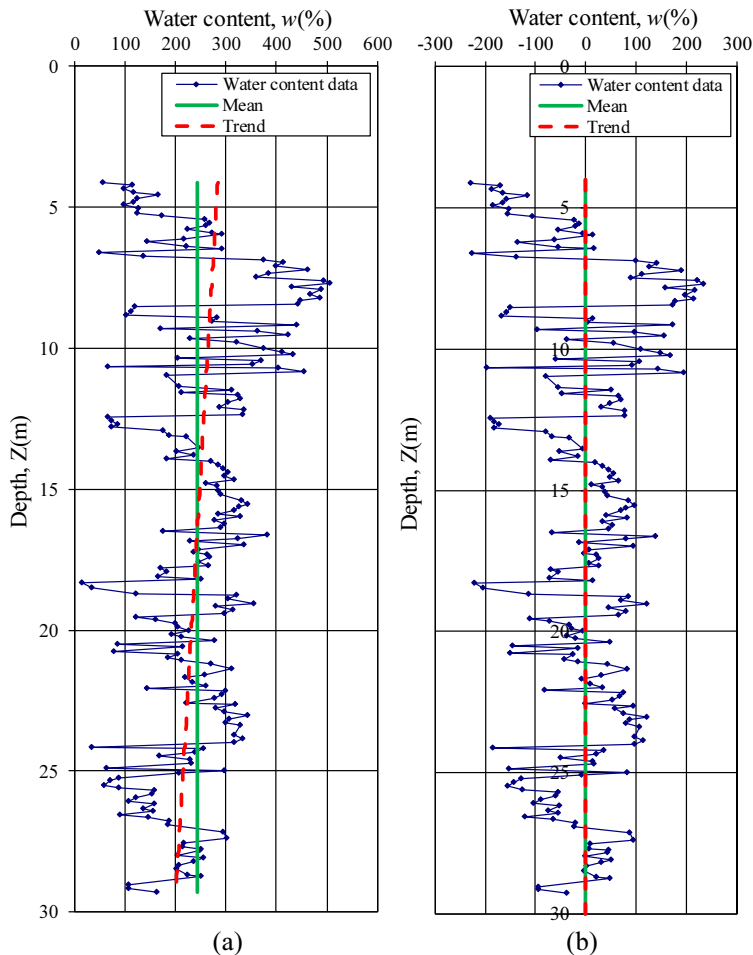


Figure 20. Typical water content profile (w , Eq. (1)), in the upper clay formation of the Lake Zone. (a) Original field (b) Residual stationary field.

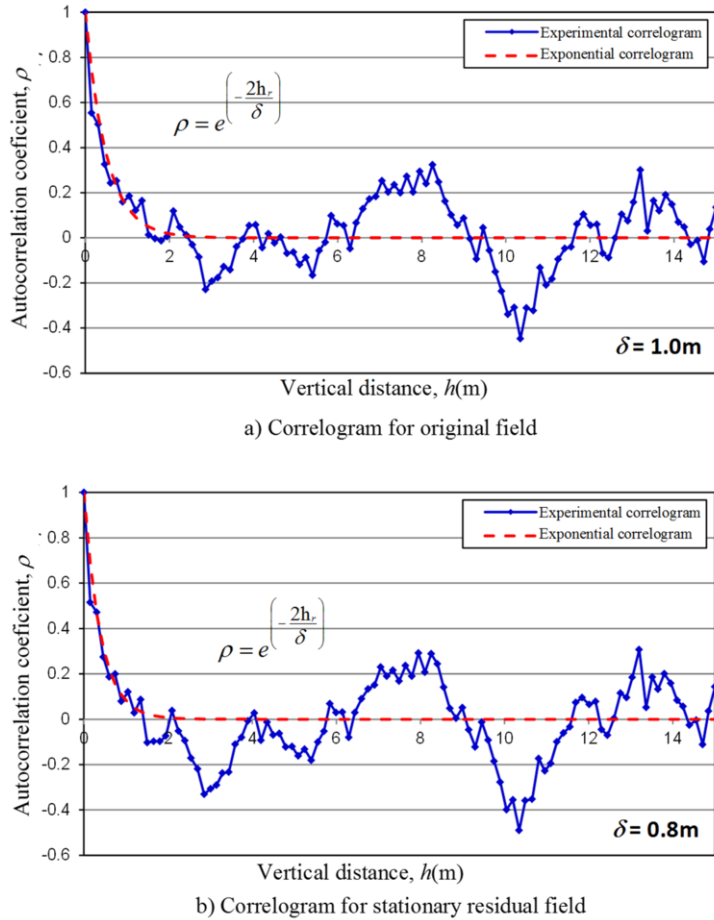


Figure 21. Vertical correlograms for water content profiles of Figure 20.

In both cases, the correlograms exhibit a harmonic behaviour suggesting that the variation of the characteristics of the soil with depth present some periodicity. In practice, this is generally ignored and an exponential function is adjusted to the first stretch of the correlogram to take advantage of the higher correlations corresponding to short vertical distances. Note that the correlation distance δ of the residual field is slightly shorter than the correlation distance of the original field. Both types of correlogramas can be used to obtain more detailed water content profiles, interpolating vertically between measurement points using the estimation techniques presented in Appendix II.

On the other hand, water content profiles can be used as a support for estimating other properties resorting to “multifield” analysis or “cokriging”, (Wackernagel, H., 2003 [81]; Delgado Muñiz, 2017 [95]; Appendix II). Figure 22 shows how a shear wave velocity profile (Figure 22a) can be improved (Figure 22c) by cokriging using water content w (Eq. (1)) as a supporting secondary field (Figure 22b).

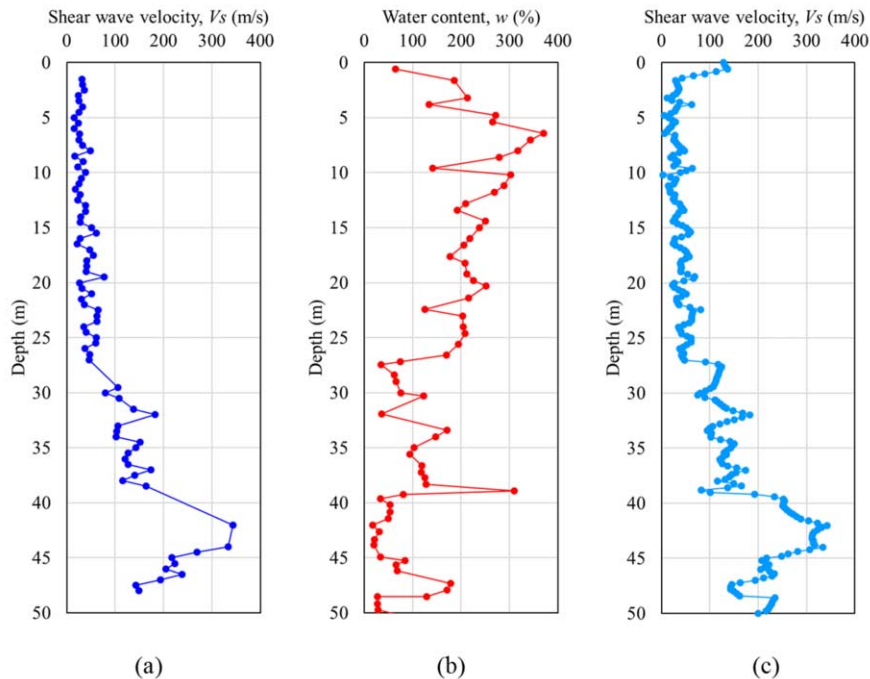


Figure 22. Original V_s (a) and w (Eq. (1)) (b) profiles and improved V_s profile (c) obtained by cokriging, using water content as a secondary random field.

The respective auto-correlograms of V_s and w and the cross-correlogram of V_s and w deduced from the profiles of Figure 22 and used in the cokriging estimation are shown on Figure 23.

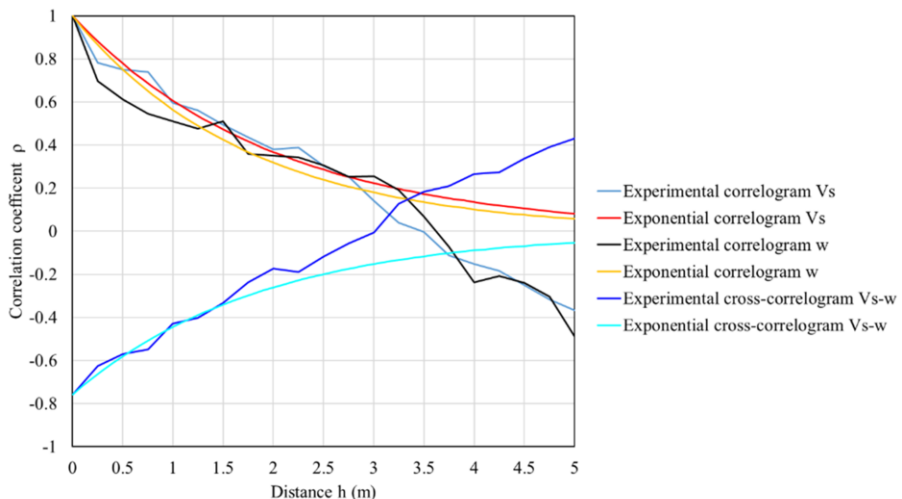


Figure 23. Vertical autocorrelograms of V_s and w and cross-correlogram V_s-w obtained from profiles of Figure 22.

Figure 22c shows that the improved shear wave velocity profile reflects some features of the water content profile that were not present in the original V_s profile, especially close to the surface and at depth where shear wave velocity measurements were scarce (i.e. from 27 to 30m, from 38 to 44m and beyond 48m).

The above cokriging estimation was repeated with better behaved variable w' (Eq. (2)). Figure 24 shows how the shear wave velocity profile (Figure 24a) was also improved (Figure 24c) by cokriging using water content w' (Eq. (2)) as a secondary field (Figure 24b).

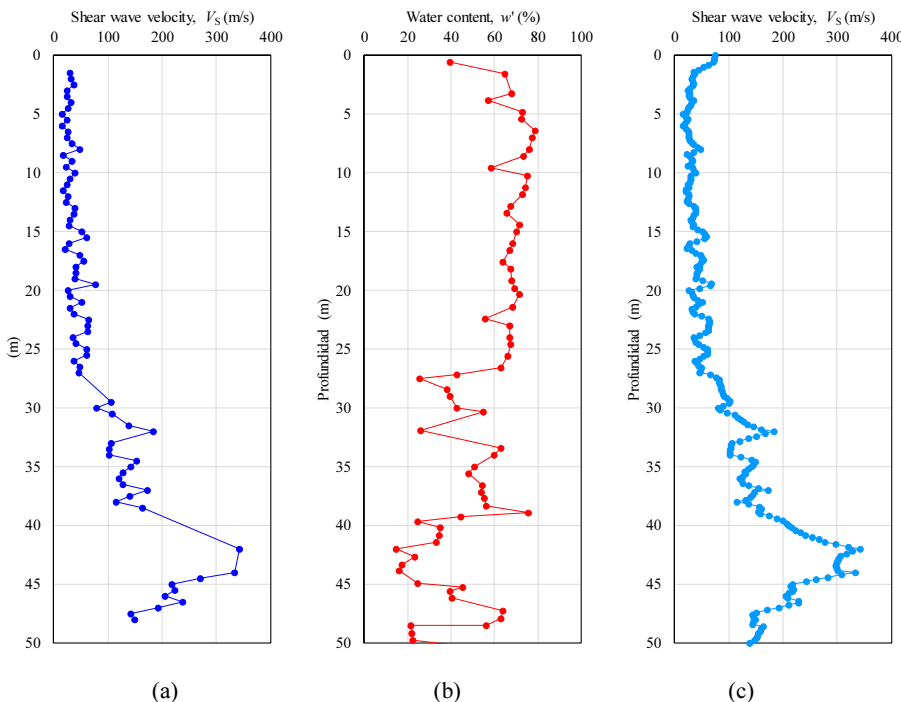


Figure 24. Original V_s (a) and w' (Eq. (2)) (b) profiles and improved V_s profile (c) obtained by cokriging, using water content w' as a secondary random field.

The auto-correlograms of V_s and w' and the cross-correlogram of V_s and w' that were deduced from the profiles of Figure 24 and used in the cokriging estimation are shown on Figure 25.

Figure 24c shows again how the improved shear wave velocity profile reflects features of the water content profile that were not present in the original V_s profile. The influence of the secondary field w' is however less significant than in the case of Figure 22c, suggesting that using definition of Eq. (1) for water content may exaggerate spatial variations of other variables when used in cokriging estimations.

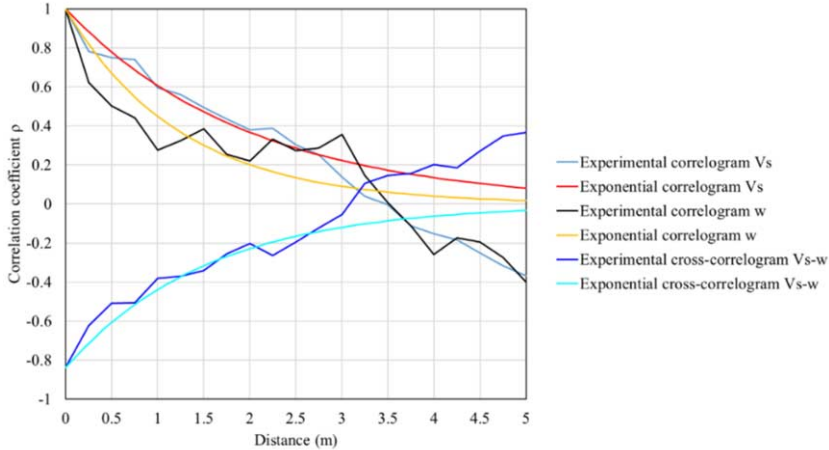


Figure 25. Vertical auto-correlograms of V_s and w' (Eq. (2)) and vertical cross-correlogram V_s-w' for profiles of Figure 24.

On Figure 26, vertical profiles of shear wave velocity V_s (Figure 26a) and CPT tip resistance q_c (Figure 26b) are presented. The shear wave velocity profile was improved interpolating vertically between measurements using the estimation techniques of Appendix II (kriging, Figure 26c).

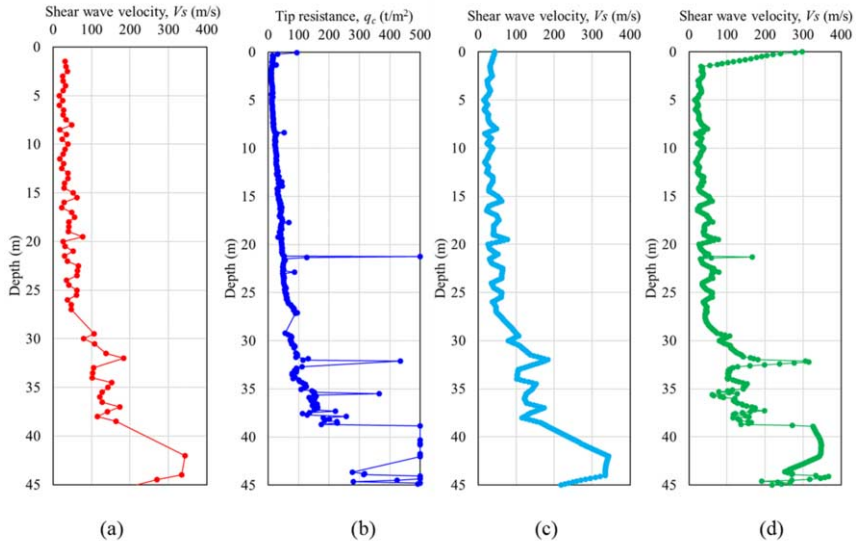


Figure 26. Improved V_s profile obtained by kriging (c) and cokriging (d), using CPT tip resistance q_c (b) as a secondary random field.

It was also taken advantage of the correlation between shear wave velocity V_s and CPT tip resistance q_c (Figure 27) to improve further the estimated shear wave velocity profile using q_c as a secondary field for cokriging (Figure 26d). The improved profile

reflects some features of the CPT tip resistance profile that were not present in the original V_s profile, especially the effect of sand or silt lenses at different elevations.

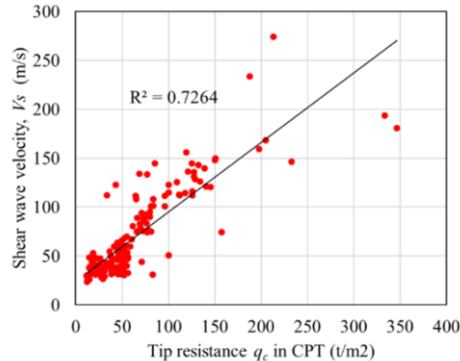


Figure 27. Empirical correlation between shear wave velocity V_s and CPT tip resistance, q_c . ($1\text{t}/\text{m}^2 = 10\text{kPa}$).

c) 2D geostatistical estimations

Since 1992, approximately 10,000 boring logs obtained in the basin of Mexico City have been collected and a Geographic Information System focused on the geotechnical properties of the subsoil has been developed (Auvinet *et al.*, 2017 [30]). This system constitutes a valuable database that can be used to perform geostatistical analyses.

As an example, it has been possible (Juárez *et al.*, 2016 [96]) to assess the depth of the *deep deposits* (DP) below the clay formations in the Lake Zone of Mexico City. This depth was represented by a 2D random field defined in the Lake Zone area. Figure 28 shows the location of the main data used in the analysis.

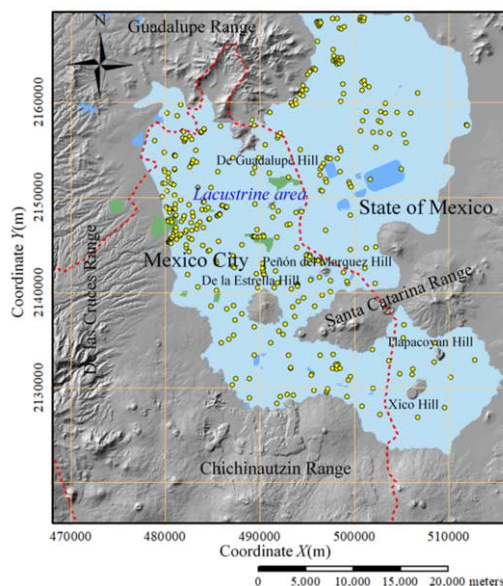


Figure 28. Location of *Deep Deposits* depth data.

Using the techniques described in Appendix II and appropriate correlation models; it was possible to establish a contour map of the estimated depth of Deep Deposits (Figure 29). This map is valuable since these deposits constitute the inferior boundary of most analytical or numerical models, including seismic site effects models. It can also be useful for preliminary design of deep foundations.

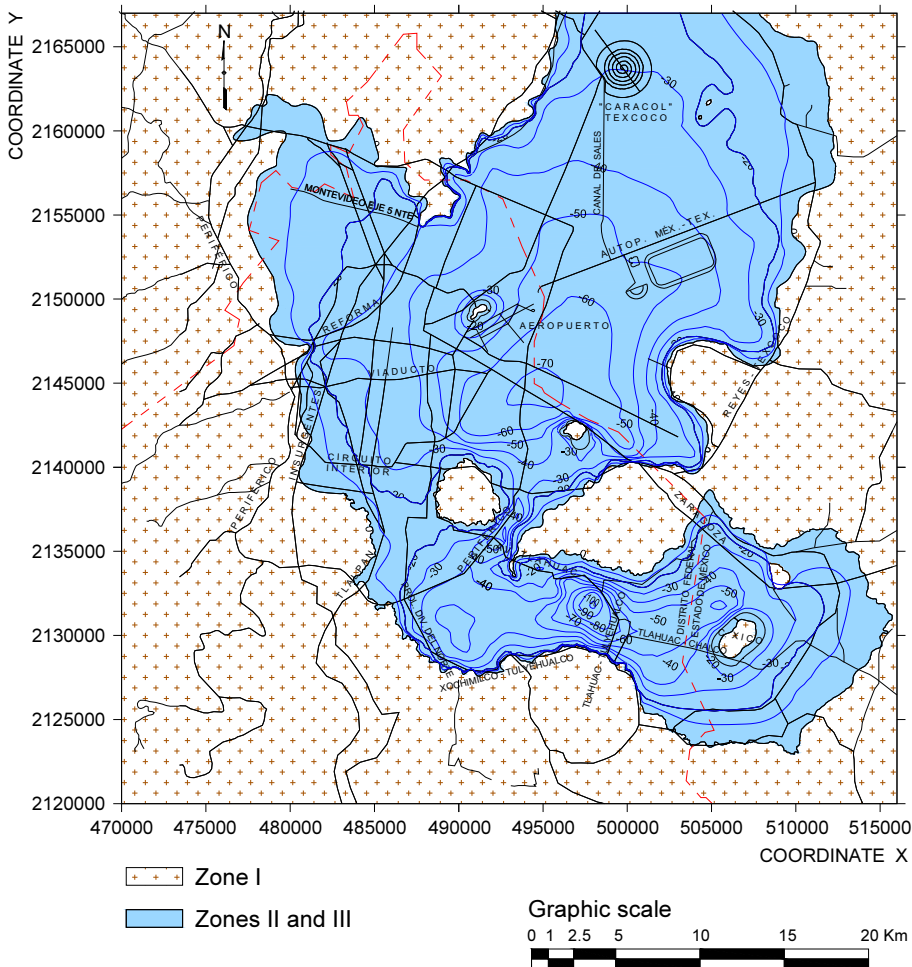


Figure 29. Contour map of estimated *Deep Deposits* depth within the Lake Zone in Mexico City.

d) 3D geostatistical estimations

The database on Mexico City subsoil mentioned in the previous section has been useful to improve the current knowledge on the subsoil of different zones of the Valley of Mexico. A large number of theses related to specific zones of the lacustrine area were presented (Flores Tapia, 2000 [97]; Aguilar, 2001 [98]; Pantoja, 2002 [99], Morales, 2004 [100]; Valencia, 2007 [101]; Jiménez, 2007 [102]; Pérez, 2009 [104]; Rodríguez,

2010 [105]; Hinojosa, 2010 [106]; Tenorio, 2013 [103]; Hernández Vizcarra, 2013 [107]; Juárez, 2015 [79]; Barranco Eyssautier, 2016 [108]; Delgado Muñiz, 2017 [95]).

Virtual subsoil cross-sections at different sites of the lacustrine zone have been established. These 2D or 3D models representing the water content or other estimated geotechnical parameters, have provided a valuable overview of the subsoil conditions in Mexico City (Auvinet *et al.*, 2017 [30]).

The autocorrelation function commonly used in these models is of the exponential type:

$$\rho_v(r, z) = \exp \left\{ -2 \left(\frac{r}{\delta_r} + \frac{z}{\delta_z} \right) \right\} \quad (15)$$

where parameters δ_r and δ_z are, respectively, the horizontal and vertical correlation distances and $r = \sqrt{(x_i - x_j)^2 + (y_i - y_j)^2}$ and $z = |z_i - z_j|$ are respectively the horizontal and vertical distances between two different points of the soil mass with respective coordinates (x_i, y_i, z_i) and (x_j, y_j, z_j) .

The correlation structure of the materials of the lacustrine zone of Mexico City is highly anisotropic. In Figures 21, 23 and 25 it was shown that the vertical correlation distance of the water content is of the order a few meters. Figure 30 shows that the horizontal correlation distance in unlimited domains can attain several kilometres.

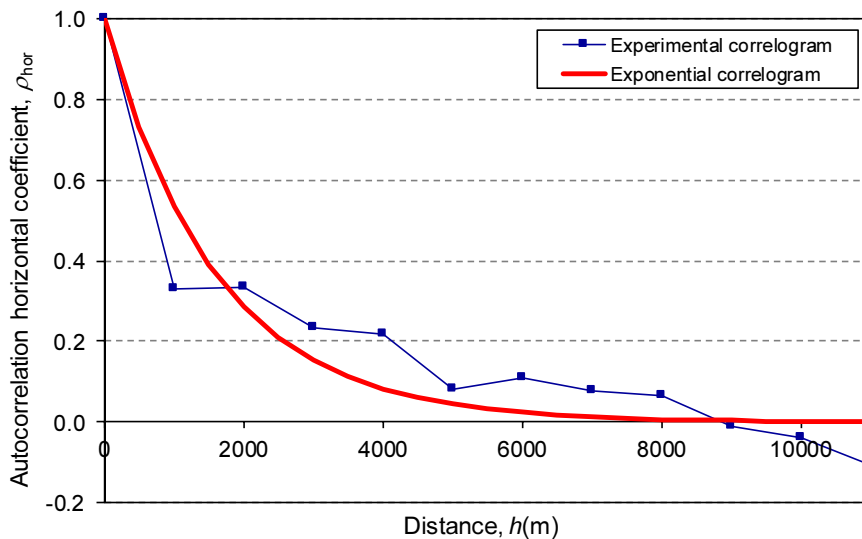


Figure 30. Typical horizontal correlogram for water content field in Mexico City Lake Zone.

Figure 31 shows a longitudinal profile of the estimated water content of the subsoil below an embankment used for the preloading of an area where a runway was being built (Mendoza *et al.*, 2018 [51]).

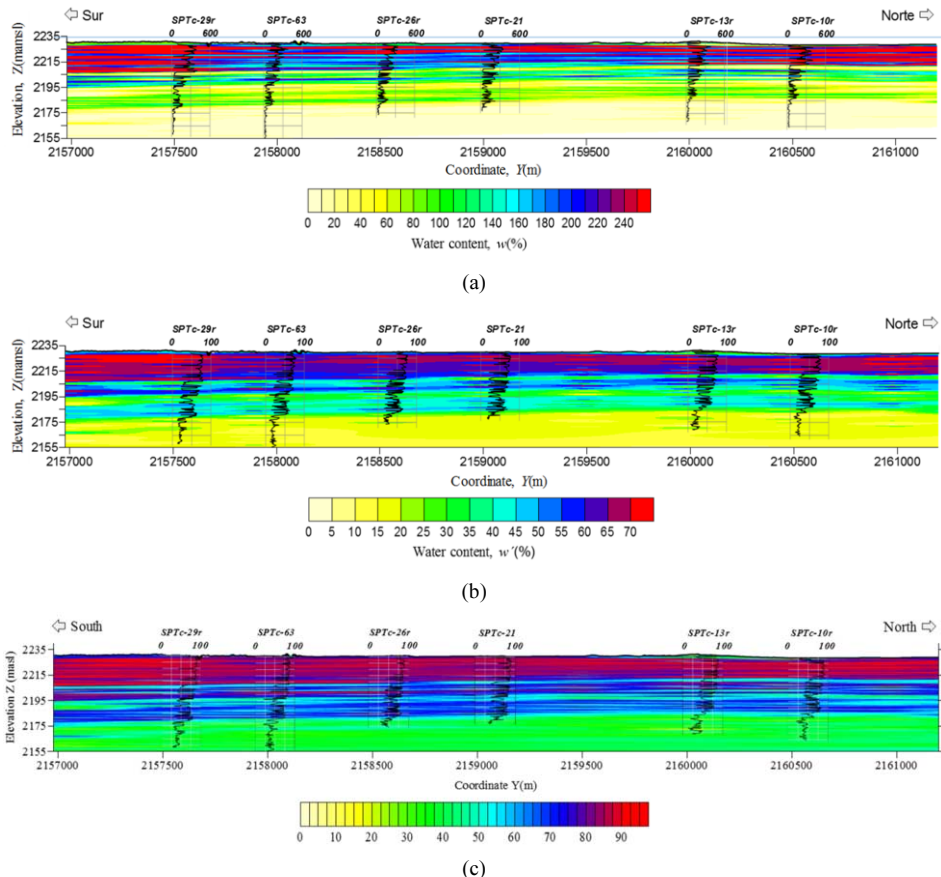


Figure 31. Longitudinal profile of estimated water content defined by (a) Eq. (1), (b) Eq. (2) and (c) Eq. (3) (Runway 6, NAICM).

To dispose of more realistic synthetic pictures of the longitudinal profile of water content in the subsoil, simulated profiles were obtained using the techniques described in Appendix II. Profile presented in Figure 32 corresponds to a simulation performed with the Eq. (1) definition of water content.

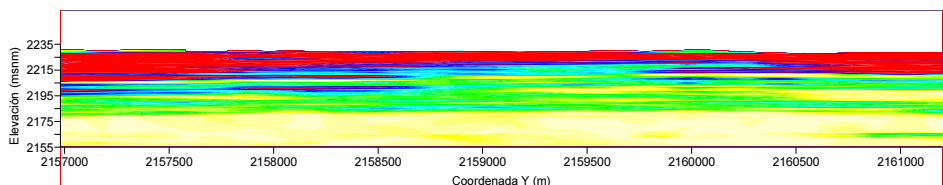


Figure 32. Longitudinal profile of simulated water content defined by Eq. (1) (Runway 6, NAICM).

The five profiles of Figure 33 were established with the definition of water content given by Eq. (2). The same differences are observed as in the case of estimations (Figure 31). As could be expected, the simulated profiles are less homogeneous than the estimated profiles.

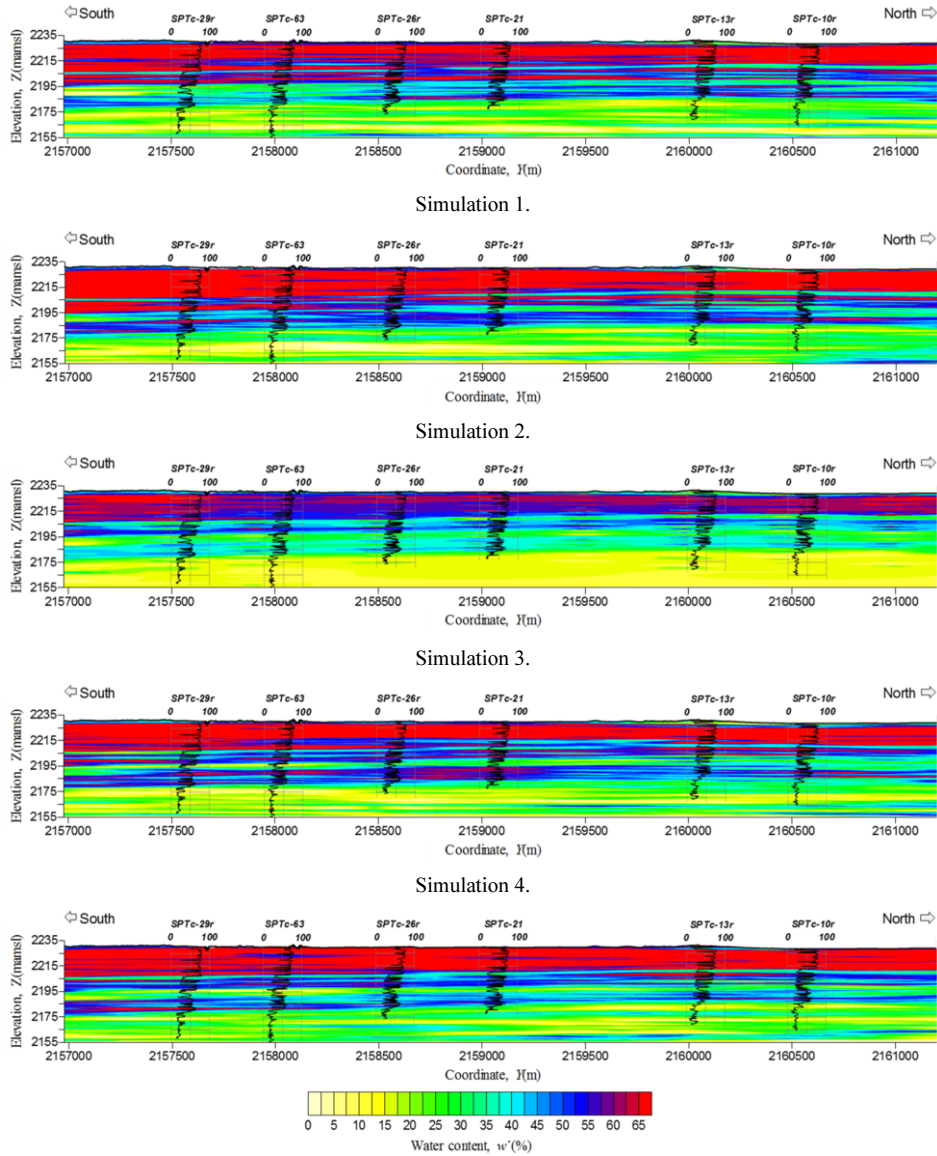


Figure 33. Longitudinal profiles of simulated water content w' defined by Eq. (2) (Runway 6, NAICM).

It can be verified that the average of several simulations such as those presented in Figure 33 tends to coincide with the estimated profile (Figure 31b) as the number of simulations increases.

Figure 34 shows geostatistical 3D models of soil profile (water content w (Eq. (1)) and CPT tip resistance q_c) for the X shaped Terminal Building of NAICM. These two models provide complementary visions of the subsoil of the area.

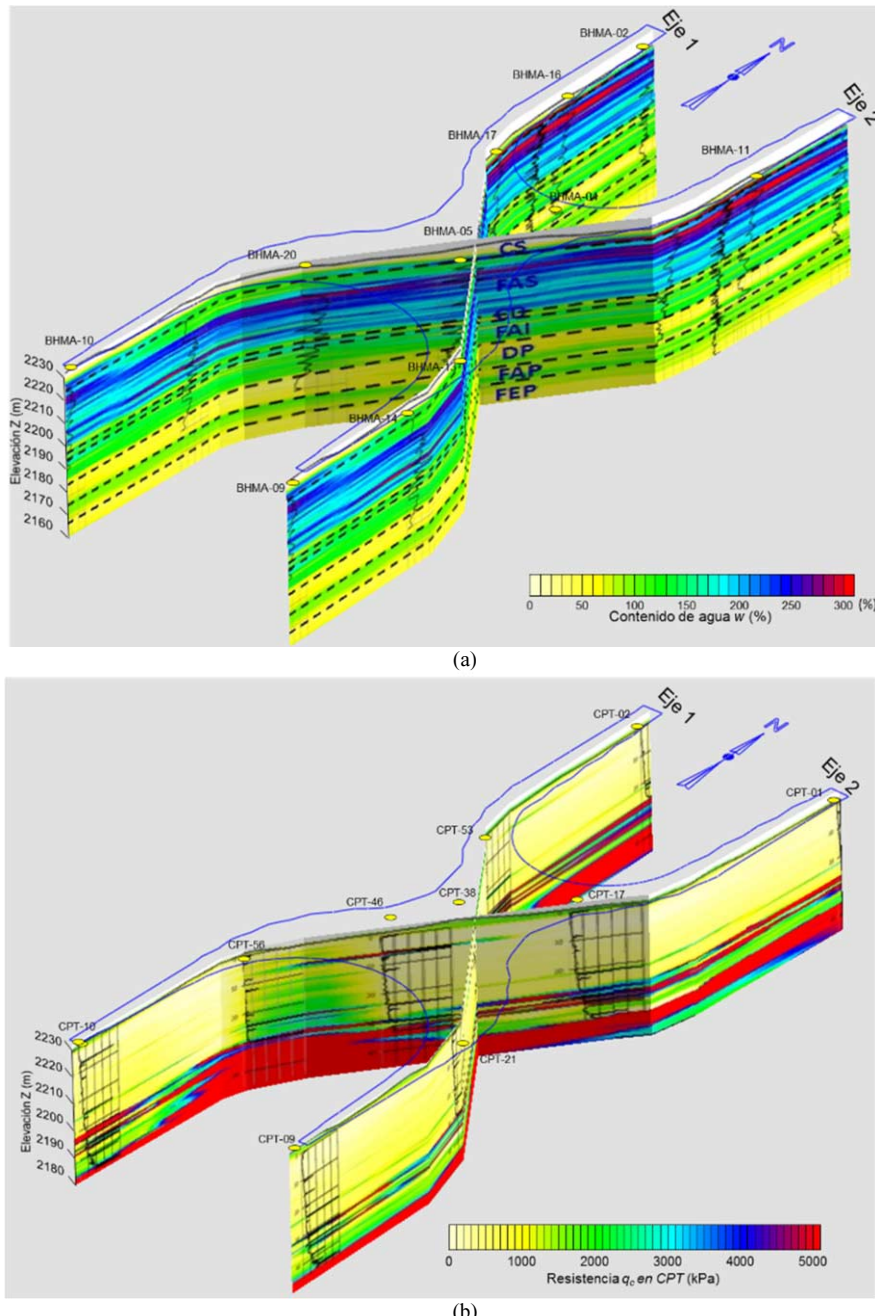


Figure 34. Longitudinal profile of: (a) estimated water content w (Eq. (1)) and (b) CPT tip resistance q_c . (Terminal building area, NAICM).

Figure 35 shows longitudinal profiles of estimated shear wave velocity V_s (kriging), (a) and CPT tip resistance q_c (b) for the east side of the Terminal building of NAICM. A Shear wave velocity V_s profile (c) improved by cokriging with q_c is also presented.

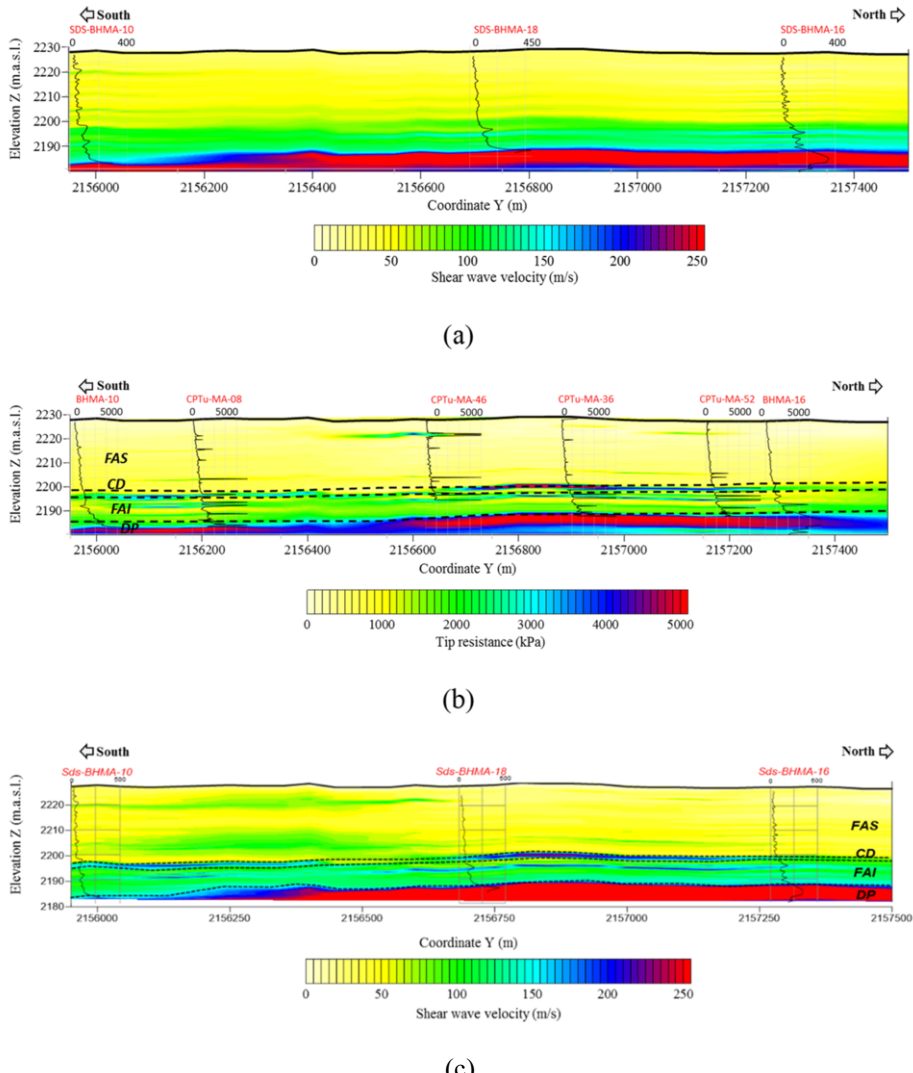


Figure 35. Longitudinal profiles of estimated soil properties: (a) Shear wave velocity V_s (kriging), (b) CPT tip resistance q_c (kriging), (c) Shear wave velocity V_s improved by cokriging with q_c (Terminal building, east side).

Figure 36 shows the estimated profiles of water content w (Eq. (1)) along the 12 lines of the subway system of Mexico City (Auvinet *et al.*, 2017 [30]). An obvious advantage of this type of representation is that it can be easily updated when new boreholes results become available.

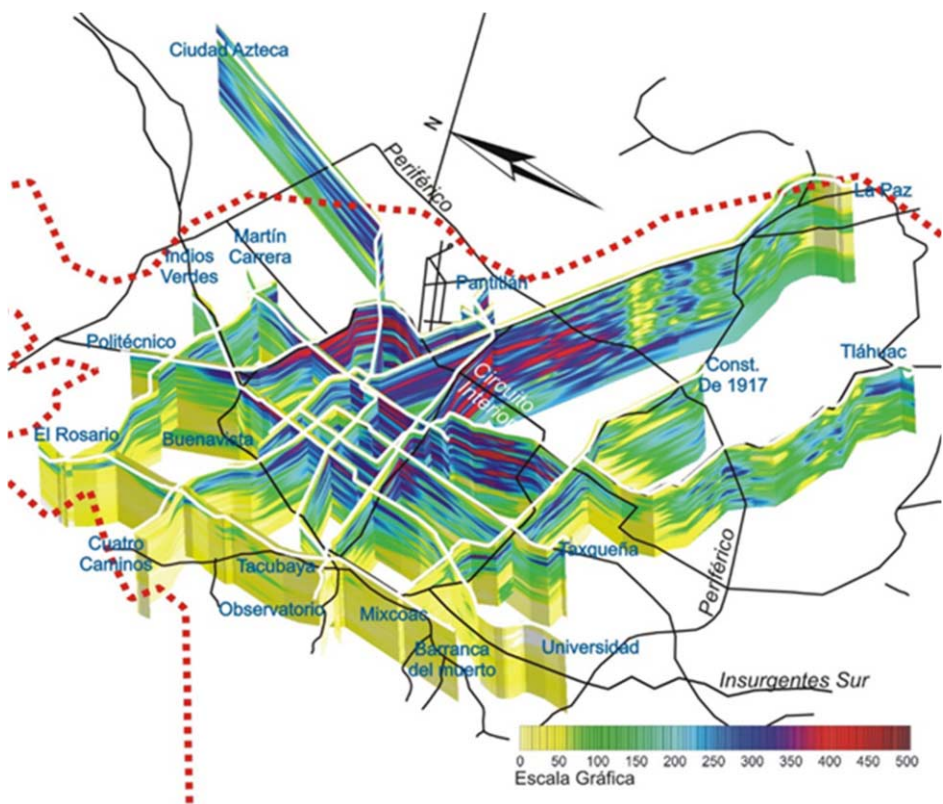
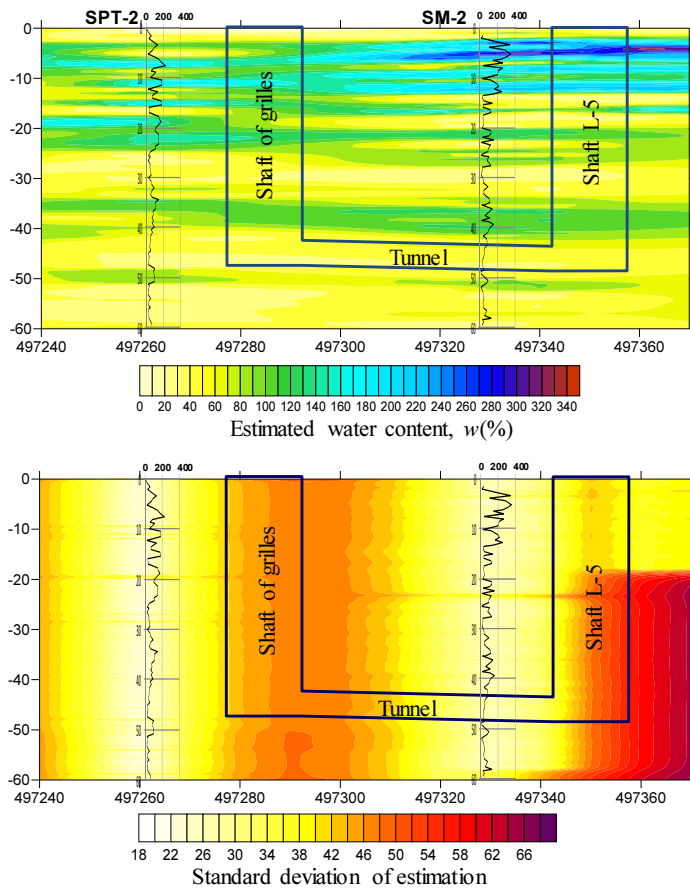
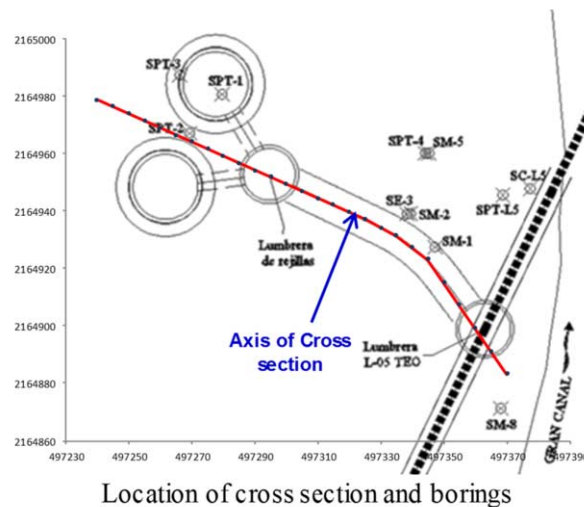


Figure 36. Spatial distribution of estimated water content along the 12 lines of Mexico City subway system.

Together with the estimated properties profiles, geostatistical analyses provide profiles of the estimation error (standard deviation of the estimation, Appendix II). These profiles can be used to define an optimum position for additional boreholes in an exploration program.

As seen in Figure 37, for a tunnel exploration program, adding a new borehole (SM1) (b) changes significantly the original estimation error profile (a). One should look *a priori* for the position of new boreholes that bring more “light” to the existing knowledge of subsoil characteristics,



(a)

Figure 37. “Light” brought about by boreholes improving knowledge of soil characteristics (a) before borehole SPT1 was performed and (b) after it was performed.

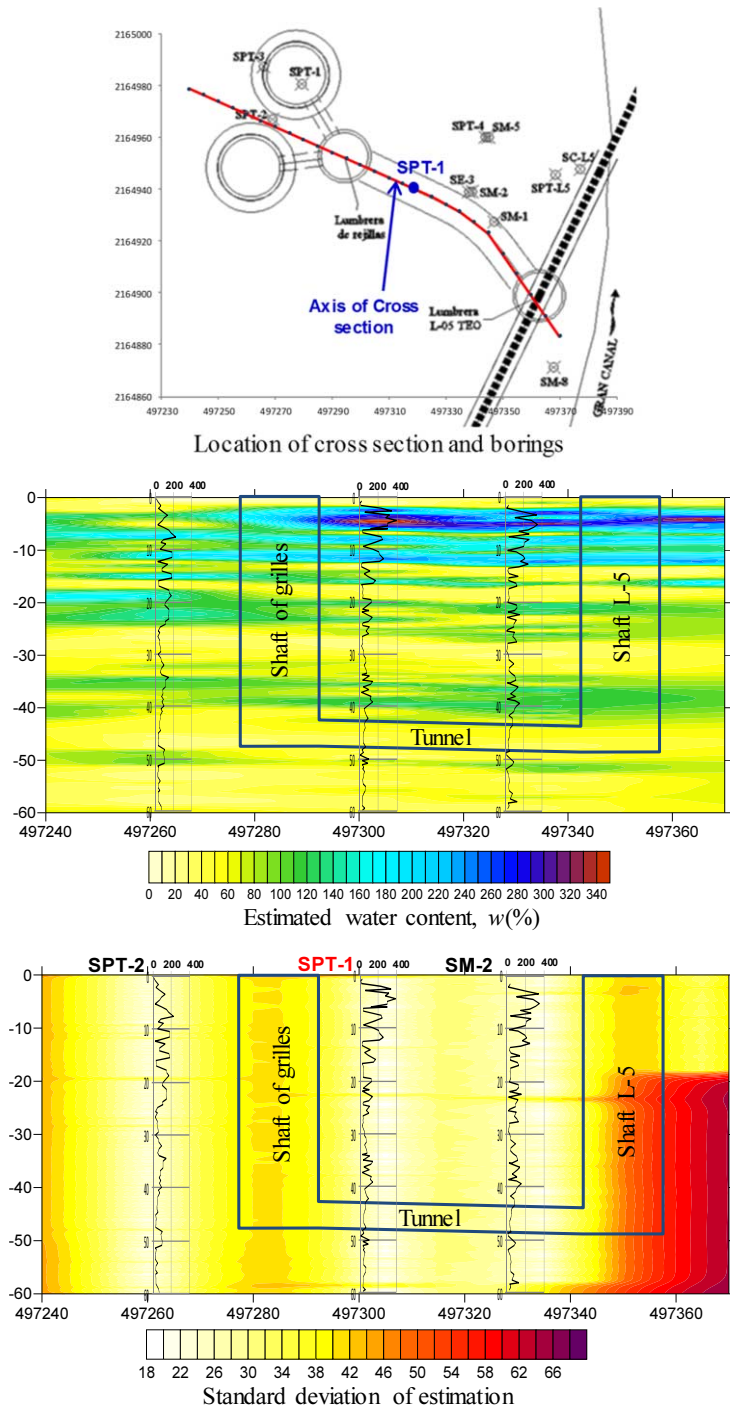


Figure 37. (continued) “Light” brought about by boreholes improving knowledge of soil characteristics (a) before borehole SPT1 was performed and (b) after it was performed.

6. Geotechnical analysis considering soft soils spatial variations

6.1. Available methods

Geotechnical analyses can take into account spatial variations of soft soils resorting to probabilistic techniques.

Many analyses are found in the literature in which soil properties are considered as random variables (Magnan and Boureahoua, 2001 [109]). Most of these studies attempt to take into account uncertainty due to lack of knowledge of soil parameters but few of them take into account explicitly the spatial variability of these parameters.

The uncertainty on the results of a geotechnical analysis for a structure built on a soil mass represented by a random field can be obtained in some instances by analytical methods. However, in most cases it is necessary to resort to numerical methods. In this context, the stochastic finite element method (SFEM) is a particularly useful technique. Auvinet *et al.* (1996 [110]; 2000 [111]; 2002 [23]) exposed the theoretical bases of this method. SFEM generally resorts to the method of perturbations (Mathews and Walker, 1964 [112]), to a punctual approximation (Rosenblueth, 1975 [113]) or to the Monte Carlo technique based on a series of simulations of the random field. Another SFEM technique: the “Spectral approach” (Ghanem and Spanos, 1991 [114]; Pineda, 2015 [115]) has also proven to be useful for application in geotechnical engineering.

Stochastic geotechnical analyses can be brought a step forward and be used for evaluating the probability of failure (or of exceedance of a critical limit) or its complement to unity, reliability. This ambitious objective can seldom be reached but, frequently, it is at least possible to obtain a representative value of the so-called “index of reliability”. The precepts of modern risk and reliability theory first appeared in fundamental papers by Freudenthal (Freudenthal *et al.*, 1964 [116]). This work was followed by contributions of a generation of researchers in structural engineering, including Ang, Cornell, Ditlevsen, Hasofer, Lind, Rackwitz. Rosenblueth and Esteva. Auvinet (2002 [23]) presented a summary of the main concepts of the reliability theory.

6.2. Dealing with spatial variability in Mexico City clays

To show how the stochastic approach can be used in geotechnical analyses performed in soft soils such as those of Mexico City, some very simple examples will be presented.

6.2.1. Friction pile

Friction piles are commonly used in the lacustrine clays of Mexico City in order to reduce the settlements of superficial or compensated foundations (design in terms of settlements) or as the main foundation system (design in terms of bearing capacity). These are generally prefabricated piles with tip located about three meters above the first hard layer.

The bearing capacity of a friction pile installed in a soft soil medium modelled as a 1D stationary (vertical) random field can be estimated together with the corresponding uncertainty.

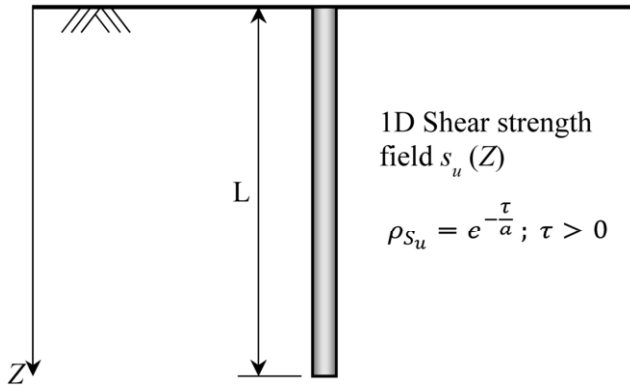


Figure 38. Friction pile in soft soil with undrained shear strength considered as a 1D random field.

Considering a typical case in Mexico City (Figure 38) where shear strength $s_u(Z)$ is assumed to be a stationary 1D random field with expected value $E\{s_u\}$, variance $\text{Var}[s_u]$ and coefficient of autocorrelation function of the exponential type:

$$\rho_{s_u} = e^{-\frac{\tau}{a}} ; \tau > 0 \quad (16)$$

where $\delta = 2a$ is the correlation distance and $\tau = Z_1 - Z_2$.

The friction bearing capacity Q along a pile of length L and perimeter P can be estimated as:

$$Q = s_{uL} PL \quad (17)$$

where S_{uL} is the average shear strength:

$$S_{uL} = \frac{1}{L} \int_0^L s_u(Z) dZ \quad (18)$$

Then (Appendix III):

$$E\{Q\} = E\{s_{uL}\} PL = E\{s_u\} PL \quad (19)$$

and:

$$\text{Var}[Q] = \text{Var}[s_{uL}] (P^2 L^2) = \frac{2a^2}{L^2} \text{Var}[s_u] \left[\frac{L}{a} + e^{\frac{-L}{a}} - 1 \right] (P^2 L^2) \quad (20)$$

The coefficient of variation of random variable Q is:

$$CV[\mathcal{Q}] = \frac{\sqrt{\text{Var}[\mathcal{Q}]}}{E\{\mathcal{Q}\}} \quad (21)$$

When the L/δ ratio increases, this coefficient decreases by a factor R represented in Figure 39. For a typical 30m long friction pile in Mexico City clays where vertical correlation distance δ is of the order of 2.5m, this factor presents a value of 35%.

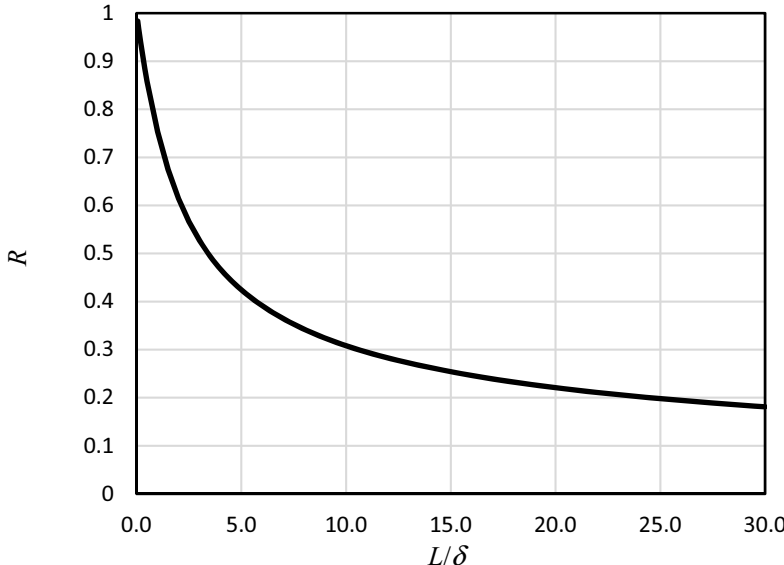


Figure 39. Reduction of coefficient of variation of friction pile bearing capacity, \mathcal{Q} , as a function of ratio between pile length L and vertical correlation distance $\delta = 2a$.

This illustrates the fact, already mentioned in this lecture, that in most cases, the stability of geotechnical structures does not depend on the uncertainty on local shear strength parameters but on the much lower uncertainty prevailing on average properties in large subdomains within the geotechnical medium (in this case along the pile shaft).

The same example could have been developed for a passive horizontal anchor of the type sometimes used in excavations as part of retaining systems. In this case, the correlation distance would be much longer (Figure 30) and the reduction of the variance of the limit capacity of this anchor as a function of length would be hardly significant. Reliability of this type of reinforcement elements within anisotropic random fields is thus strongly dependent on their orientation in space.

6.2.2. Footing

As an illustration of the application of the spectral approach in stochastic analyses, the uncertainty (standard deviation) on the vertical settlement of a flexible superficial footing is evaluated. The footing is 6m wide and transmits a uniform pressure $p = 50$ kPa to a

20m thick clay layer that could correspond to the transition zone of Mexico City (Figure 38). To assess the uncertainty on the settlements of points A and B indicated in the figure due to soil spatial variations, a simplified 2D stochastic finite element analysis was carried out although a 3D analysis would in fact be more realistic. The soil is considered to be an elastic medium with a drained Young modulus represented by a stationary isotropic random field $E'(X)$ with expected value 4,000 kPa and coefficient of variation of 25%. Poisson's ratio ν' is considered as deterministic and equal to 0.3. The expected vertical settlement evaluated by a deterministic analysis is of the order of 25cm at the centre of the footing.

The uncertainty on the vertical settlements of points A and B, respectively δ_A and δ_B , is highly dependent on the horizontal correlation distance of the random field. For a very short correlation distance (white noise material), the medium is an extremely heterogeneous medium that behaves as a deterministic material due to the reduction of variance effect. For very large correlation distances, the material behaves as a strictly homogeneous but random material. This can be appreciated in Figure 40 where the standard deviation of vertical displacements δ_A and δ_B is represented as a function of the correlation distance.

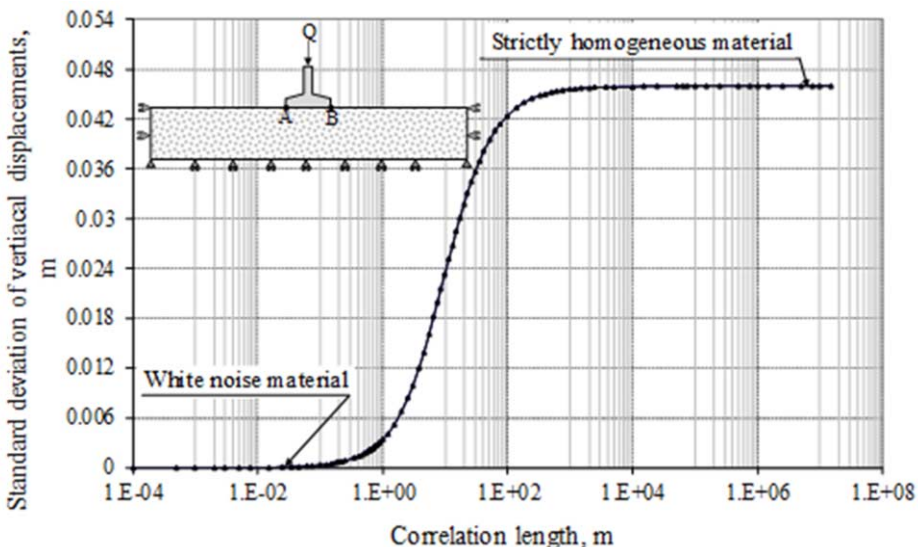


Figure 40. Uncertainty on displacements of a footing on a random material as a function of correlation distance.

The variance of the differential settlement between points A and B can be expressed as:

$$\text{Var}[\delta_A - \delta_B] = \text{Var}[\delta_A] + \text{Var}[\delta_B] - 2\text{Cov}[\delta_A, \delta_B] \quad (22)$$

The corresponding standard deviation of this differential settlement between points A and B is presented on Figure 41.

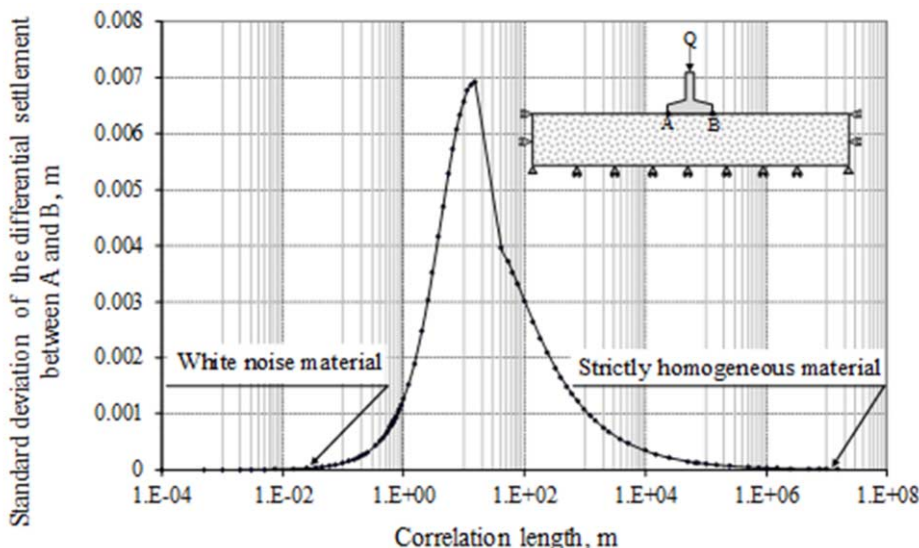


Figure 41. Uncertainty on differential displacements between points A and B for a footing built on a random material as a function of correlation distance.

It can be seen that the standard deviation of the differential settlement between points A and B is nil for the white noise material, then reaches a maximum value when the correlation length is about twice the horizontal dimension of the footing and finally decreases again towards zero for the strictly homogeneous material.

This example illustrates the paramount influence on the behavior of a geotechnical structure of the relation between the dimensions of this structure and the correlation length of the soil (stochastic field) on which it is built.

6.2.3. Slope stability

When assessing the stability of slopes such as those created when constructing unsupported excavations, spatial variations of the soil can be taken into account (Auvinet and González, 2000 [117]).

Contrary to what is commonly found in the technical literature, this type of problem can only be addressed resorting to a 3D analysis. Assuming that a plain strain condition prevails, as assumed in standard 2D equilibrium analyses, is equivalent to accepting that no spatial variation of the soil properties exists along the direction normal to the slope cross-section considered, an obviously unacceptable consideration when assessing the influence of soil properties spatial variations.

A 3D limit equilibrium analysis may thus be performed. Among the available 3D stability analysis methods, the algorithm proposed by Hungr (1987 [118]) presents, among other advantages, some flexibility regarding the type of slip surface that can be considered. In this model, based on a generalization of simplified Bishop's method, the potential sliding mass is divided into an orthogonal assembly of vertical columns. For rotational surfaces, the safety factor, SF , is derived iteratively from the sum of moments around a common horizontal axis. For cohesive soils:

$$SF = \frac{MR}{MM} = \frac{\sum_{i=1}^n s_{ui} a_i R_i}{\sum_{i=1}^n W_i x_i + Ed} \quad (23)$$

where MR and MM are respectively the moments of resisting and driving forces; s_{ui} is the shear strength at base of column i ; a_i is the area of base of column i , R_i is the moment arm of resisting force i ; W_i is the total weight of the column and x_i is the distance from the reference axis to the center of the column. E is the resultant of all horizontal components of applied point loads, if any, with a moment arm d , and n is the total number of active columns (Figure 42).

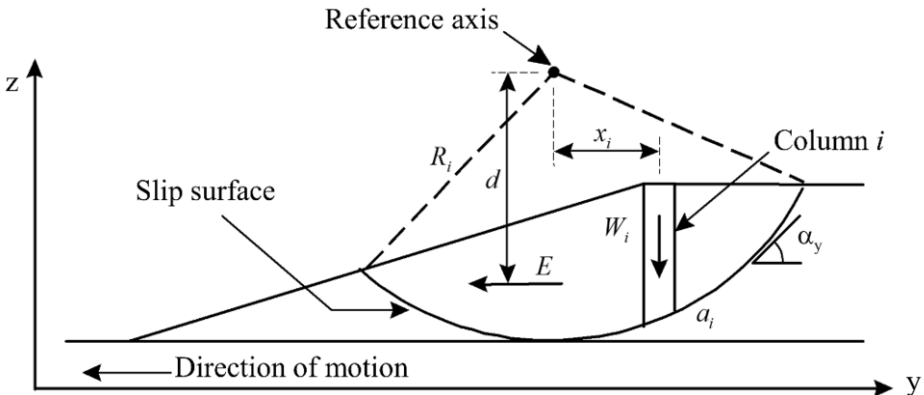


Figure 42. Cross-section of slope and potential slip surface.

In the case of non-rotational surfaces, it is possible to derive the factor of safety from the horizontal forces equilibrium in the direction of the motion (Figure 42):

$$SF = \frac{FR}{FM} = \frac{\sum_{i=1}^n s_{ui} a_i \cos \alpha_y}{\sum_{i=1}^n N_i \cos \gamma_z \tan \alpha_y + E} \quad (24)$$

where FR and FM are respectively the resisting and driving forces and γ_z and α_y are defined on Figure 43. N_i is the total normal force acting on the column base derived from the vertical force equilibrium.

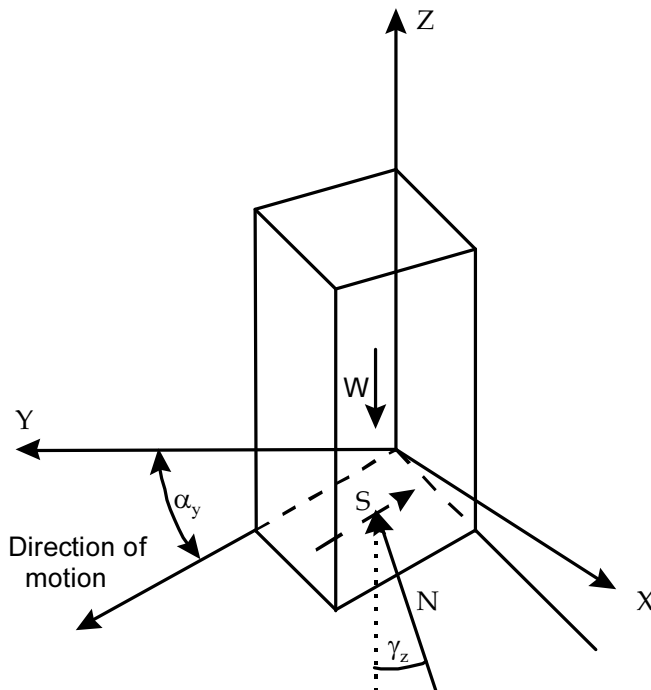


Figure 43. Forces acting on base of a single column.

When the mechanical properties of a soil mass are affected by uncertainty due to spatial variations, variables MR and MM of Eq. (23) (respectively FR and FM in the case of non-rotational mechanisms) must be considered as random variables. The probability of failure associated to a particular slip surface can then be defined as $P_f = P[SF < 1]$ where SF is the safety factor. Reliability is the complement to unity of probability of failure. An equivalent formulation can be introduced defining safety margin, $SM = MR - MM$ (respectively, $FR - FM$). Probability of failure is then defined as $P_f = P[SM < 0]$. Reliability can be expressed in term of a reliability index β defined as:

$$\beta = \frac{E\{SM\}}{\sigma_{SM}} \quad (25)$$

where:

$$\sigma_{SM} = \sqrt{\sigma_{MR}^2 + \sigma_{MM}^2 - 2\text{Cov}[MR, MM]} \quad (26)$$

The short-term resisting forces along the potential slip surface depend on the undrained shear strength s_u along this surface. On the other hand, the driving forces depend on the specific weight of the soil. In most cases, uncertainty on specific weight can be neglected and $\sigma_{SM} = \sigma_{MR}$. Eq. (25) can then be written:

$$\beta = \frac{E\{SM\}}{\sigma_{MR}} \quad (27)$$

A first order approximation of the expected value of the safety margin can be evaluated performing a deterministic stability analysis with the expected value of the shear strength:

$$E\{SM\} \cong E\{MR\} \left(1 - \frac{1}{E\{SF\}} \right) \quad (28)$$

On the other hand, as shown below, standard deviation σ_{MR} of the resisting moment can be defined in terms of the parameters of the shear strength random field $s_u(X)$. For sliding mass divided in vertical columns as in Hungr's model, variance of the moment of resisting forces can be calculated as:

$$\text{Var}[MR] = \text{Var}[s_u] \left[\sum_{i=1}^n (a_i R_i)^2 + 2 \sum_{i=1}^n \sum_{j=i+1}^n a_i R_i a_j R_j \rho_{s_u}(X_i, X_j) \right] \quad (29)$$

where n is the number of columns.

In this expression, the variance of average shear strength at the base of each column is considered to coincide with the point variance of the field (mid-point method). In the same way, the correlation between the average shear strength at the base of different columns is considered equal to the correlation between point values of this property in X_i and X_j , at base of columns i and j . This approximation can be considered as acceptable when the number of columns considered in the analysis is large.

In the case of non-rotational slip surfaces, a similar procedure can be used substituting MR by FR in Eq. (28), and writing:

$$\text{Var}[FR] = \text{Var}[s_u] \left[\sum_{i=1}^n a_i^2 \cos^2 \alpha_{y_i} + 2 \sum_{i=1}^n \sum_{j=i+1}^n a_i \cos \alpha_{y_i} a_j \cos \alpha_{y_j} \rho_{s_u}(X_i, X_j) \right] \quad (30)$$

These expressions make it possible to estimate the reliability index associated to three-dimensional failure mechanisms.

Algorithms to perform the corresponding computations have been developed (Auvinet and González, 2000 [117]). In these algorithms, autocorrelations functions of the type indicated in Eq. (15) are used.

If the shear strength random field can be considered as Gaussian, SM is also Gaussian and the probability of failure can be expressed as:

$$P[SM \leq 0] = \Phi \left(\frac{0 - E\{SM\}}{\sigma_{SM}} \right) = \Phi(-\beta) \quad (31)$$

where Φ is the normalized Gaussian probability distribution function.

The above considerations refer to the reliability associated to a particular slip surface. It must be emphasized that the global failure probability of a slope is the probability that one of the many possible failure mechanisms develops. This probability is difficult to assess; however, taking into account that a significant correlation generally exists between soil properties along close critical slip surfaces, the highest probability of failure found for particular critical surfaces can generally be considered as a useful lower limit of the global probability of failure.

For soils with highly anisotropic autocorrelation function like Mexico City clays, the reliability associated to specific slope failure surfaces is strongly dependent on their shape. Mechanisms with long horizontal planar sections (Figure 44) may present a higher deterministic safety factor than cylindrical or spherical surfaces but they are generally associated to a higher probability of failure and lower reliability. This is because along horizontal planar surfaces, the autocorrelation coefficient function remains close to unity and the variance reduction effect implicit in Eq. (30) is much less pronounced than in the case of a rotational mechanism (Eq. (29)) (Auvinet and González, 2000 [117]).

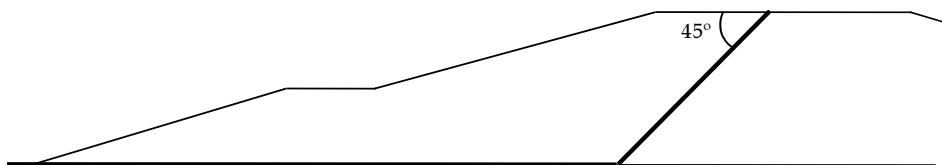


Figure 44. Semi planar failure mechanism.

Figures 45 and 46 present the case of a slope failure in a trial excavation in the former Texcoco Lake area in Mexico City soft clays.

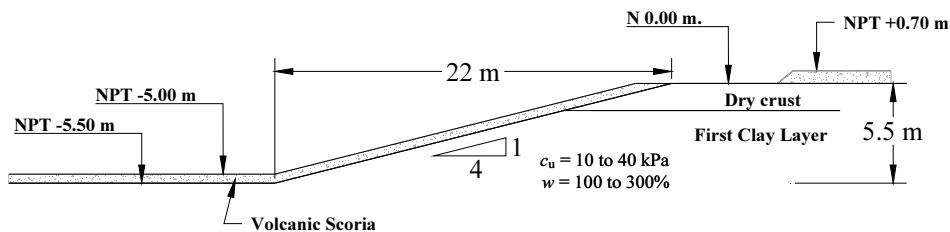


Figure 45. Slope of a trial excavation in Mexico City clay.

The failure occurred along a practically horizontal planar surface similar to the one presented in Figure 44, when the excavation with a 4:1 slope reached a depth of 5.5m (Figure 46) (Mendoza *et al.*, 2018 [119]; Schmitter *et al.*, 2018 [120]).



Figure 46. Semi planar failure mechanism of a trial excavation slope (Courtesy, W.I. Paniagua).

As far as stability of geotechnical structures is concerned, the anisotropy of the correlation structure of the soil mass is thus probably more relevant than the mechanical anisotropy observed in the laboratory at the sample level.

7. Geotechnical solutions for mitigating the effects of spatial variations of soft soils

7.1. Available techniques

When constructing on spatially variable soft soils, geotechnical engineers may consider two options. The first one consists of adapting the geotechnical solution to the varying characteristics of the soil. This will lead to complex designs with varying dimensions of footings, number of piles, etc. When possible, he may however consider a second option aiming at erasing to some degree the mechanical differences between distinct zones of the soil mass. This will make it necessary to use some sort of soil improvement technique (Mitchell, 1981 [121]; Pilot *et al.*, 1985 [122]).

Improvement techniques have been developing considerably in the last decades (Schaefer, 2012 [123]). They may consist of grouting, soil stabilization using admixtures, thermal stabilization, or soil reinforcement. The most common method is probably consolidation by gravitational or vacuum preloading, generally with the help of vertical drains (Mesri and Khan, 2012 [124]).

7.2. Mitigating the effects of soil spatial variations in Mexico City clays by preloading.

The gravitational preloading method has been implemented for different geotechnical structures built on Mexico City clay, including industrial embankments (Auvinet, 1979 [125]) and runways (Mendoza *et al.*, 2018 [51]). This well-known technique consists of placing on the ground a preload (embankment) equal to the final load that will be

transmitted to the soil by the geotechnical structure. This preload is applied during a time sufficient for the total settlement to occur before the end of construction.

To accelerate the settlements and reduce the preloading period, a surcharge may be added and vertical drains be installed (Figure 47).

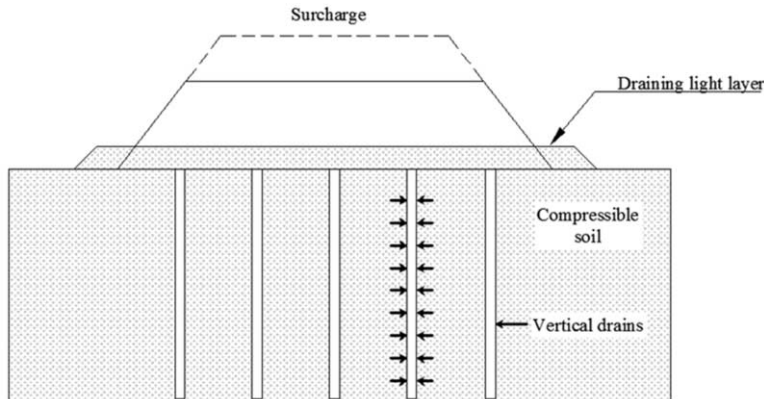


Figure 47. Preloading system.

The surcharge and the temporal part of the preload are removed when the induced vertical displacement reaches a target settlement that guarantees an acceptable behavior of the geotechnical structure during operation and future maintenance works.

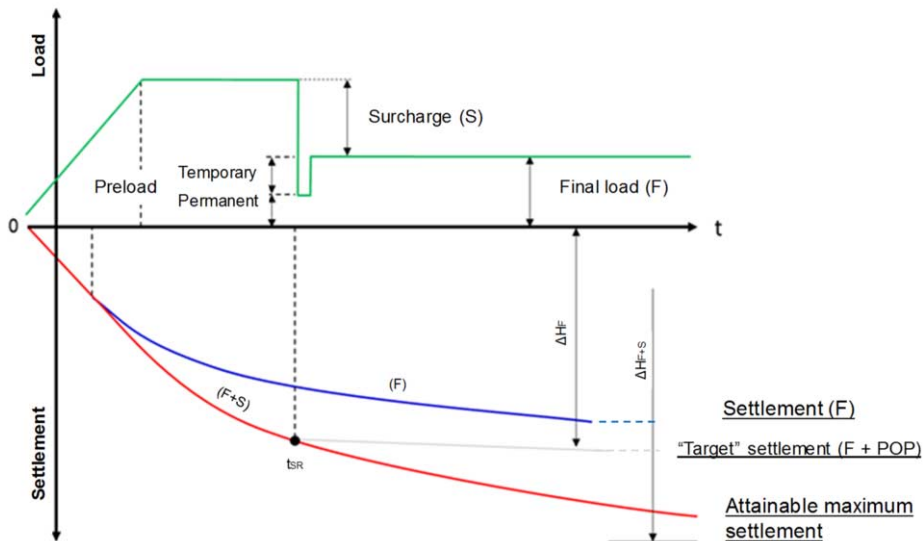


Figure 48. Principle of preloading with surcharge.

As shown on Figure 48, the objective of this technique is to induce with the permanent and temporary preload and the surcharge (red curve) a settlement equal to at least 100% the total settlement ΔH_f (primary plus secondary consolidation) that would

be expected for the final structure without preloading (asymptotic value reached by blue curve). In fact, a settlement clearly larger than ΔH_f should be reached for the soil to attain an overconsolidated state, allowing safe future maintenance works during the lifetime of the geotechnical structure, including those that could require some additional loading of the soil, without inducing significant settlements. Reaching a clearly overconsolidated state also contributes to mitigating the effects of the secondary consolidation of the soil on the final structure (Ladd and De Groot, 2003 [1]).

When applying this technique, it is necessary to take into account that the soil parameters commonly present strong spatial variations due to different factors, including the loading history of the site.

Special attention must be lent to the initial Over Consolidation Ratio (*OCR*):

$$OCR = \frac{\sigma'_p}{\sigma'_0} \quad (32)$$

where σ'_p = yield stress at the considered elevation, and σ'_0 = current effective vertical stress at the considered elevation.

Disposing of an accurate value of *OCR* is essential since consolidation settlement of a soil layer submitted to a stress increment $\Delta\sigma$ is commonly calculated from odometer tests results as:

$$\Delta H = H \left[\frac{C_d}{1+e_0} \log OCR + \frac{C_c}{1+e_0} \log \frac{\sigma'_0 + \Delta\sigma}{\sigma'_p} \right] \quad (33)$$

$$\text{when } \sigma'_{0_z} \leq \sigma'_p \text{ and } \sigma'_{0_z} + \Delta\sigma \geq \sigma'_p$$

where C_c = compression index, C_d = swelling index, e_0 = initial void ratio, and H = layer thickness.

OCR is a parameter difficult to define with accuracy. The actual value of yield stress σ'_p is not easily derived from laboratory tests due to disturbance of samples and differences between competing methods that have been proposed for estimating this stress from the compressibility curve (Note that, as suggested in Appendix 1 for Mexico City clays, the yield stress may be easier to obtain from $n - \log \sigma'$ curve rather than from the classical compressibility curve $e - \log \sigma'$).

On the other hand, for soil close to the surface, the effective stress in the denominator of Eq. (32) is small and very sensitive to the seasonally changing elevation of the water table.

These uncertainties further increase the natural randomness of *OCR* due to spatial variations within the soil mass.

A more stable parameter defining the position of the current effective vertical stress with respect to the yield stress is the pre-consolidation overburden pressure or *POP*:

$$POP = \sigma'_p - \sigma'_0 \quad (34)$$

To avoid future differential settlements associated to spatial variability of the soil and initial conditions, the objective of preloading should then be inducing in the subsoil

along the future geotechnical structure a final pre-consolidation overburden pressure (POP), such that:

$$\text{Min}(POP) > \Delta p \quad (35)$$

where Δp is a stress margin allowing safe future maintenance works during the lifetime of the geotechnical structure, without inducing significant settlements. Stress margin Δp must be taken into account when assessing the target settlement (Figure 48).

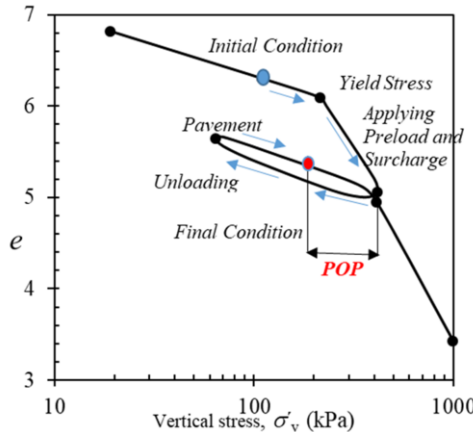


Figure 49. Target final condition.

Following the above rule will guarantee that all future volume changes of the soil will take place along the recompression branch of the compressibility curve, minimizing differential settlements (Figure 49),

This requires a thorough assessment of the spatial variations of current and final effective vertical stress σ'_0 , yield stress σ'_p and/or OCR within the soil.

Figure 50 shows the variation of the estimated initial yield stress σ'_p in the subsoil along an embankment longitudinal axis (runway in former Texcoco Lake) obtained by the estimation techniques of Appendix II.

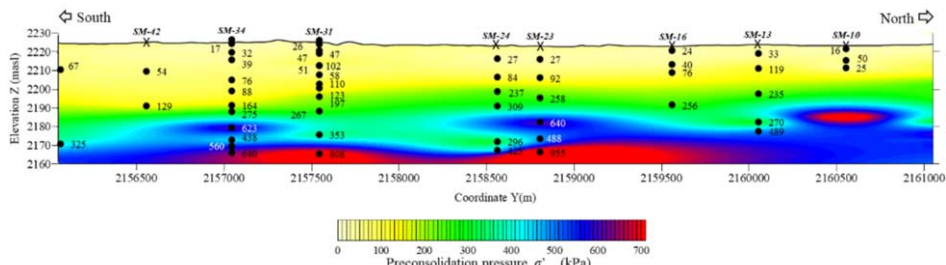


Figure 50. Variations of yield stress σ'_p along embankment longitudinal axis. (Runway 2, NAICM).

A strict evaluation of compliance of condition (35) should in fact be based on simulations of the above field (Figure 51), in order to take into account possible local soft points.

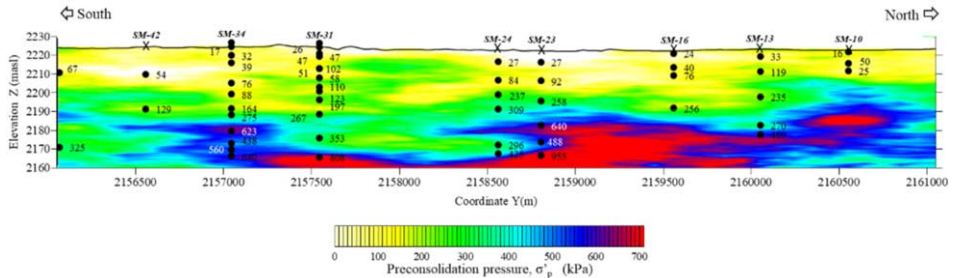


Figure 51. Conditional simulation of the σ'_p field along embankment longitudinal axis (Runway 2, NAICM).

Note that condition (35) can be difficult to attain uniformly in the soil when vacuum preloading is applied on contiguous panels due to the peculiar conditions prevailing in the joints between the panels.

Furthermore, when implementing the preloading technique, the following issues must also be addressed:

- Final load

To reduce the load transmitted to the soil by the final geotechnical structure (and the target settlement), it can be convenient to install in the basis of the preloading embankment a layer of light material whose function will be mainly to absorb settlements and will only contribute marginally to the final weight of the structure. A light granular material (for example volcanic scoria, known locally in Mexico as *Tezonite*) divided by sieving into several uniform size fractions can be installed in successive thin layers separated by geotextile sheets. Uniform size fractions present a higher porosity than the original granular material (Auvinet, 1986 [87]). The wall effect between the granular material and the geotextile sheets also increases porosity. Dry unit weight as low as 9 kN/m^3 can be attained.

- Water table

When the water table is close to the surface, during preloading, the superficial natural soil and the preloading materials become partially submerged. This new condition reduces the efficiency of preloading since the original unit weight γ_m of these materials becomes:

$$\gamma_{sub} = \gamma_{sat} - \gamma_w \quad (36)$$

where γ_{sub} = buoyant unit weight of soil, γ_{sat} = unit weight of saturated soil, and γ_w = water unit weight.

For such situations, a pumping installation aimed at maintaining the materials above the water table can be implemented. This system increases the efficiency of preloading and can, in some cases, make the surcharge unnecessary (Auvinet, 2016 [126]; 2016 [127]).

- Vertical drains

Vertical drains are useful for reducing the time required for the consolidation of a soft soil layer submitted to preloading, especially when the thickness of the layer exceeds about 5m. The designer must then choose between vertical sand drains and Prefabricated Vertical Drains (PVD). Installation time of PVD is generally much shorter. However, it must be taken into account that sand drains can contribute to reduce significantly the target settlement when designed to act as a reinforcement of the soil. They can also contribute to a better homogenization of the soil, eliminating at least part of the effects of spatial variations of soil compressibility and reducing differential settlements.

It must also be taken into account that any kind of vertical drain can modify the hydraulic conditions prevailing in the subsoil. In the case of Mexico City, a drawdown condition generally exists due to deep pumping (Figure 52).

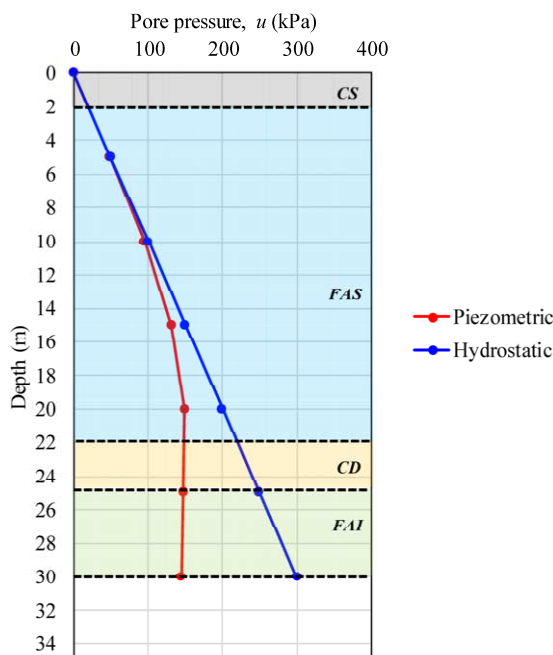


Figure 52. Typical pore pressure depletion within Mexico City subsoil.

When vertical drains are installed, the hydrostatic condition is reestablished down to the tip of the drains. A strong hydraulic gradient then develops between this level and the first hard permeable layer where pore pressure is depleted. This induces a vertical strain concentration in the soil by consolidation at this elevation as shown by extensometers measurements (Figure 53).

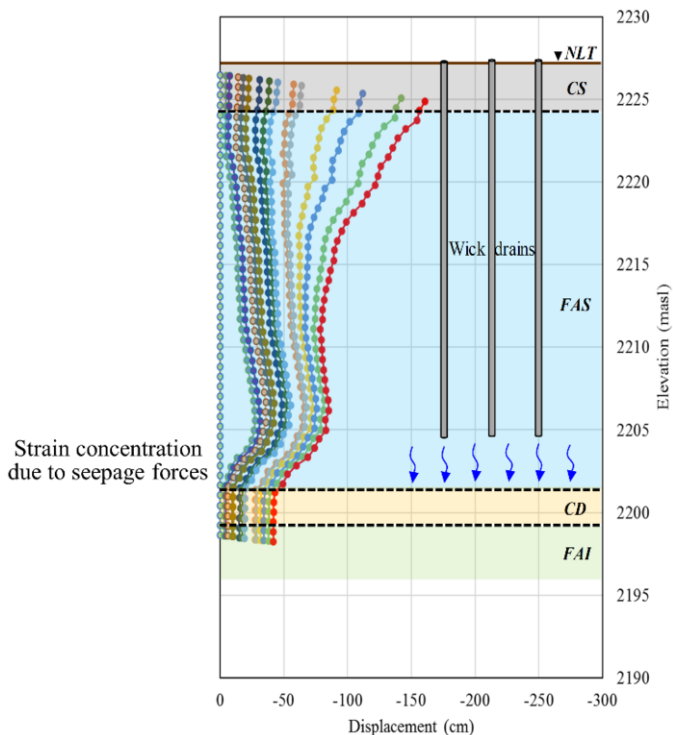


Figure 53. Settlement induced by seepage forces between the tip of PVD drains and first hard permeable layer (CD).

This phenomenon must be taken into account when assessing the target settlement.

8. Conclusions

Among the sources of uncertainty prevailing in the geotechnical characterization of soft soils, spatial variability was singled out as one of the most difficult to deal with. For an accurate evaluation of the subsoil conditions, spatial variations of the soil profile and mechanical properties as well as the groundwater conditions must be assessed by performing a sufficient number of soil explorations and field tests, processing a generally large amount of data and developing either deterministic or probabilistic models representing these variations.

The techniques available to develop such models and some difficulties encountered to implement them in practice were examined in this lecture. Emphasis was placed on geostatistical methods for estimation and simulation of spatial variations of soft soils represented by single or multiple random fields. A discussion showing the limitations of the concepts of void ratio and gravimetric water content commonly used in Geotechnical engineering, in the context of statistical analyses of spatial variations of soft soils was presented.

Geotechnical analysis and design methods that take into account soft soils spatial variations were also reviewed together with some construction techniques aimed at

mitigating consequences of soil variability. The above considerations were illustrated by applications to the Mexico City highly compressible volcanic lacustrine clays. Models of the spatial variability of Mexico City subsoil developed over the years for different projects using traditional and geostatistical techniques were presented. Simple examples of the geotechnical analysis and construction methods that can be used by geotechnical engineers to deal with soil spatial variability were discussed.

During the preparation of this lecture, the author kept constantly in mind the great influence of Professor Arthur Casagrande in the formation of what in time became a buoyant Mexican School of Geotechnical Engineering that, year after year, has faced competently the extremely difficult conditions of Mexico City subsoil as well as other challenging geotechnical problems in the rest of the country.

Acknowledgments

This lecture is a tribute to researchers and practitioners, many of them directly or indirectly former students of Professor Arthur Casagrande, who contributed during the last century to a better knowledge of the subsoil of Mexico City.

The author also wants to acknowledge the most valuable comments and contributions of Moisés Juárez Camarena, Edgar Méndez Sánchez, Marco Pérez Ángeles, Marcos Delgado Muñiz, Felipe Vázquez Guillen, Alma Rosa Pineda and Francisco Hernández Vizcarra and the help of Eduardo Martínez Hernández during the preparation of this lecture.

List of Symbols

Symbol	Nomenclature
a	area
a_v	coefficient of compressibility
c	salt concentration in %
$C(u_1, \dots, u_n)$	n-dimensional copula
$c(u_1, \dots, u_n)$	copula density
C_c	compression index
C_{cn}	compression index in terms of porosity
CD	first hard layer in Mexico City Lake Zone.
CL	low compressibility clay
CH	high compressibility clay
$\text{Cov}[\quad]$	covariance
CPT	Cone Penetration Test
CPTu	Cone Penetration Test with pore pressure measurement
CU	consolidated undrained triaxial test
C_s	swelling index
C_{sn}	swelling index, in terms of porosity
C_s	spatial copula
$C_V(X_1, X_2) = \text{Cov}[V(X_1), V(X_2)]$	random field autocovariance function
$C_V(X_1, X_2) = C_V(X_2 - X_1) = C_V(h)$	stationary random field autocovariance function
$CV[\quad]$	coefficient of variation
d	moment arm

DMT	Marchetti dilatometer test
e	void ratio
$F_V(v; X)$	probability distribution function of field $V(X)$
$E\{ \}$	mathematical expectation operator
$\exp \{ \}$	exponential operator
E	resultant of all horizontal components of forces
E'	drained modulus
FAI	lower clay formation in Mexico City Lake zone
FAS	upper clay formation in Mexico City Lake zone
G_0	small strain shear modulus
G_s	specific density of solids
H	layer thickness
$I_V(v, X)$	indicator function
K	covariance matrix
m	exponent
m_v	coefficient of volume compressibility
ML	low compressibility silt
MH	high compressibility silt.
$\text{Min} ()$	minimum
MM	moment of driving forces
MR	moment of resisting forces
n	porosity
n	number
N_i	total normal force acting on the column base
N_k	cone factor
OCR	Over Consolidation Ratio
OH	high compressibility organic soil
OL	low compressibility organic soil
p	pressure
PCA	test pit
P_f	probability of failure
PI	plasticity index
PND	dynamic cone penetrometer
POP	preconsolidation overburden pressure
q_c	tip resistance in CPT test
q_u	unconfined compressive strength
Q	friction bearing capacity of pile
R_i	moment arm of resisting force i
$R_V(X_1, X_2) = E\{V(X_1)V(X_2)\}$	autocorrelation function
s_u	undrained shear strength
s_{ui}	shear strength at base of column i
s_{uL}	average undrained shear strength along a segment with length L
$s_u(Z)$	1D undrained shear strength random field
S	normally consolidated ratio $(s_u / \sigma'_{v0})_{nc}$
SC	continuous sampling
SDMT	seismic dilatometer test
Sds	suspended logging

SF	safety factor
SM	mixed boring (SPT + undisturbed sampling)
SM	safety margin
SPT	Standard Penetration Test
SS	selective sampling
$s_u $	undrained shear strength
USCS	Unified Soil Classification System
UU	undrained triaxial test
V	random variable
$V(X)$	random field
$V(X,t)$	spatio-temporal random field
Var[]	variance
V_s	shear wave velocity
V_s	volume of solids in sample
VST	vane shear test
V_T	total volume of sample.
V_Ω	average value of field $V(X)$ on subdomain Ω
\mathbf{V}	vector of random variables
$w,$	gravimetric water content (Eq. (1))
w'	gravimetric water content (Eq. (2))
w''	volumetric water content (Eq. (3))
w_{ap}	apparent water content (including salt in solids, Eq. (1)).
W_i	weight of column i
w_L	liquidity limit
w_P	plasticity limit
W_W	weight of water in sample
W_S	weight of solids in sample
W_T	total weight of sample ($=W_W+W_S$)
α_y	angle
β	reliability index
δ	correlation distance
δ_A	settlement of point A
δ_B	settlement of point B
λ	coefficient
ϕ'	internal friction angle
Φ	normalized Gaussian probability distribution function
γ_z	angle
γ_{sub}	buoyant unit weight of soil
γ_{sat}	unit weight of saturated soil
γ_w	unit weight of water
$2\gamma_v(h) = E\left\{ [V(X+h) - V(X)]^2 \right\}$	variogram
$\mu_v(X) = E\{V(X)\}$	expected value of random field $V(X)$
ν	Lagrange multiplier
ν'	Poisson's ratio
$\sigma_v^2(X) = \text{Var}[V(X)]$	variance of random field $V(X)$

$\rho_v(X_1, X_2) = \rho_v(h)$ autocorrelation coefficient (normalized autocovariance) of stationary random field.

σ'_{vo} *in situ* effective vertical stress

σ_0 total vertical stress at the level of the measurement

σ'_p yield stress

Other symbols:

1D uni-dimensional

2D bi-dimensional

3D three-dimensional

References

- [1] Ladd, C.C., and De Groot, Don J., (2003). "Recommended Practice for Soft Ground Site Characterization", Arthur Casagrande Lecture, 12th Pan-American Conference on Soil Mechanics and Geotechnical Engineering, Massachusetts Institute of Technology, Cambridge, MA, USA
- [2] Casagrande, A., (1948). "Classification and identification of soils". Transactions, American Society of Civil Engineers, Vol. 113, 901-930.
- [3] Spangler M.G. and Handy, R., (1982). "Soil Engineering", p. 177, 4th edition, Harper & Row.
- [4] Gutiérrez García, A., (2006). "Determination of Atterberg limits: uncertainty and implications", Journal of the Geotechnical and Geoenvironmental Engineering, March.
- [5] Moreno-Maroto J.M. and Alonso-Azcárate (2018). "What is a clay? A new definition of "clay" based on plasticity and its impact on the most widespread soil classification systems", Applied Clay Science, 161, 57-63.
- [6] ASTM (1989) D2487-85, D2488-84.
- [7] Perrin, J., (1974). "Classifications des sols organiques", Bulletin de Liaison des LPC, France, No 69, 39-47.
- [8] Magnan, J.P.; (1980). "Classification géotechnique des sols", Bulletin de Liaison des LPC, France, No 105, 49-52.
- [9] Akagi, H., (2004). "3D F.E. Analysis of the deformation of underground structure constructed in a soft subsiding reclaimed area", Proceedings, ISSMGE TC36 workshop on "Foundation engineering in difficult soft soil conditions", SMIG-I de I, UNAM, Mexico, 211-216.
- [10] Phien-wei, N., Thepparak, S. and Giao, P.H., (2009). "Prediction of differential settlement of structures in sinking Bangkok ground", Proceedings, ISSMGE TC36 workshop, "Geotechnical Engineering in urban areas affected by land subsidence", SMIG, Mexico City.
- [11] Kempfert, H.G. and Raithel, M., (2005). "Experiences on Dike Foundations and landfills on very soft soils", Proceedings, ISSMGE TC36 workshop on "Foundation engineering in difficult soft soil conditions", SMIG-I de I, UNAM, Mexico, 211-216.
- [12] Kempfert, H.G., (2006). "Excavations and Foundations in Soft Soils", Springer Verlag, Berlin-Heidelberg-NY, 576 Seiten.
- [13] Mitchell, J.K. and Coutinho, R.Q., (1991). "Occurrence, geotechnical properties and special problems of some soils in America", Proceedings, IX Pan-American Conference on Soil Mechanics and Foundation Engineering, Viña del Mar, Chile, Vol. IV, 1651-1735.
- [14] Coutinho, R.Q. and Oliveira, J.T.R., (2005). "Behavior of Recife soft clays", Proceedings, ISSMGE TC36 workshop on "Foundation engineering in difficult soft soil conditions", SMIG-I de I, UNAM, Mexico, 57-86
- [15] Almeida, M.S.S., Futai, M.M. and Marques, M.E.S., (2004). "Theoretical and practical concepts to assess the behaviour of Rio de Janeiro clays", Proceedings, ISSMGE TC36 workshop on "Foundation engineering in difficult soft soil conditions", SMIG-I de I, UNAM, Mexico, 43-56.
- [16] Martínez, J.M., (1991). "Propiedades geotécnicas del subsuelo de Bogotá", Proceedings, IX Pan-American Conference on Soil Mechanics and Foundation Engineering, Viña del Mar, Chile, Vol. 1, 143-154.
- [17] Caicedo, B., Mendoza, C., López, F. and Lizcano, A., (2018). "Behavior of diatomaceous soil in lacustrine deposits of Bogotá, Colombia", Journal of Rock Mechanics and Geotechnical Engineering, 10, 367-379.

- [18] Whitman, R., (1996). "Organization and Evaluating Uncertainty in Geotechnical Engineering". Proceedings "Uncertainty 96", ASCE, New York, 1-28.
- [19] Lacasse, S., and Nadim, F., (1996). "Uncertainty in characterizing soil properties", *Uncertainty in the Geologic Environment*, GSP No 58, ASCE, 49-75.
- [20] Fenton, G., (1997). "Probabilistic methods in Geotechnical Engineering", ASCE GeoLogan'97 Conference Logan, Utah, 1-95.
- [21] Phoon, K., and Kulhawy, F., (1999). "Characterization of Geotechnical Variability", Canadian Geotechnical Journal, 612-624.
- [22] Auvinet, G., (2001), "La gestion de l'incertitude en géomécanique", key-note lecture, Proceedings, First Albert Caquot Conference, Paris, France.
- [23] Auvinet, G., (2002). "Uncertainty in Geotechnical Engineering/Incercidumbre en Geotecnia", Sixteenth Nabor Carrillo Lecture/Decimosexta Conferencia Nabor Carrillo. (English/Español), Sociedad Mexicana de Mecánica de Suelos, Mexico, 131p., ISBN: 968-5350 10-8.
- [24] Baecher, G.B. and Christian, J.T., (2003). "Reliability and Statistics in Geotechnical Engineering", John Wiley & Sons, Ltd ISBN: 0-471-49833-5
- [25] Huber, M., (2013). "Soil variability and its consequences in geotechnical engineering", Doctoral Thesis, Institut für Geotechnik der Universität Stuttgart, Germany
- [26] Del Castillo and Ordoñez, (1893). "Plano geológico y petrográfico de la ciudad de México", Comisión Geológica Mexicana, México.
- [27] Mooser, F., (1978). "Geología del relleno cuaternario de la cuenca de México", Memoria, Simposio "El subsuelo y la ingeniería de cimentaciones en el área urbana del valle de México", SMMS, Ciudad de México, México.
- [28] Mooser, F., Montiel, A. y Zuñiga, A. (1996). "Nuevo mapa geológico de las Cuencas de México, Toluca y Puebla: estratigrafía, tectónica regional y aspectos geotérmicos", Comisión Federal de Electricidad, Ciudad de México, México.
- [29] Mooser, F., (2018). "Geología del Valle de México y otras regiones del país", Colegio de Ingenieros Civiles de México, Volumen 1, Ciudad de México, México.
- [30] Auvinet, G., Méndez, E. and Juárez, M., (2017). "El subsuelo de la Ciudad de México/The Subsoil of Mexico City, Vol. 3", Third edition of 1959 book by Marsal and Mazari, UNAM, Mexico, ISBN 978-607-02-8198-3.
- [31] Robertson, P.K., (2009). "Interpretation of cone penetration tests - a unified approach". Canadian Geotechnical Journal 46 (11): 1337-1345, 2009.
- [32] Robertson, P.K., (2012). "The James K. Mitchell Lecture: Interpretation of in-situ tests-some insights", Geotechnical and geophysical Site Characterization, Porto de Galinhas, Brazil.
- [33] Marsal R.J., and Mazari, M., (2017). "El subsuelo de la Ciudad de México/The subsoil of Mexico City, Vol. 1 and 2", Third edition (first edition: 1959), UNAM, Mexico, ISBN 978-607-02-8198-3.
- [34] Zeevaert, L., (1972). Foundation Engineering for Difficult Subsoil Conditions. Van Nostrand Reinhold Company, New York.
- [35] Santoyo, E. Ovando, E., Mooser, F. y León, E., (2005). "Síntesis geotécnica de la Cuenca del Valle de México", TGC Geotecnia, México. ISBN: 968-5571-06-6.
- [36] Ovando Shelley, E., (2011). "Some geotechnical properties to characterize Mexico City clay", Proceedings, XIVth Pan-American Conference on Soil Mechanics and Geotechnical Engineering, paper 889, Canadian Geotechnical Society, Toronto, Canada.
- [37] Zeevaert, L., (1952). "Estratigrafía y problemas de ingeniería en los depósitos de arcillas lacustre de la Ciudad de México", Congreso Científico del IV Centenario de la Universidad Nacional Autónoma de México, México, pp. 155-176, Mexico.
- [38] Leonards, G. and Girault, P. (1961). "A study on the one dimensional consolidation test", Proceedings, Fifth International Conference on Soil Mechanics and Foundation Engineering, Vol. 1, 213-218.
- [39] Girault, P. (1964). "Mineralogía de las arcillas del Valle de México". Revista Ingeniería, Facultad de Ingeniería, UNAM, México.
- [40] Lo, K.Y., (1962). "Shear strength properties of a sample of volcanic material of the Valley of Mexico, Geotechnique, Vol. XII, 4, U.K., 303-310.
- [41] Mesri, G., Rokhsar, A. and Bohor, B.F., (1975). "Composition and compressibility of typical samples of Mexico City clay", Geotechnique 25 (3): 527-554.
- [42] Peralta y Fabi, R., (1973). Aspectos Micro estructurales del Subsuelo de la Ciudad de México; Informe a la Fundación "Ricardo J. Zevalda", Instituto de Ingeniería, UNAM.
- [43] Diaz-Rodriguez, J.A., (2003). "Characterization and engineering properties of Mexico City lacustrine soils". Characterization and Engineering Properties of Natural Soils, Vol. 1, Balkema, Rotterdam: 725-755.
- [44] Cruz, I.R. and Mayne, P. (2006). "Interpretation of CPTU tests carried out in lacustrine Mexico City clay", Site & Geomaterial Characterization (GSP 149, Proc. GeoShanghai), ASCE, Reston/VA: 24-31.

- [45] Mayne, P., (2017), "Yield stress profile in soft clays by piezocone", TC214 Session, 19th ICSMGE, Seoul, South Korea.
- [46] Rangel-Nuñez, J.L., Almanza-Hernández, F. e Ibarra-Razo, E., (2019). "Caracterización de las series arcillosas del Valle de México con el microscopio electrónico y pruebas convencionales de mecánica de suelos. Pan-American Conference on Soil Mechanics and Geotechnical Engineering, Cancún, Mexico.
- [47] Walkley, A. and Black, A., (1934). "An examination of the Degtjareff method for determining of soil organic matter, and proposed modification of the chromic acid titration method", Soil Science. 37:29-38.
- [48] Díaz-Rodríguez, J.A., Leroueil, S., and Aleman, J.D., (1992). "Yielding of Mexico City clay and other natural clays", Journal of the Geotechnical Engineering Division, ASCE, 118 (7), pp. 981-995.
- [49] Wheeler, S.J., (2003). "An anisotropic elastoplastic model for soft clays", Canadian Geotechnical Journal, 40, Canada, 403-418.
- [50] Santoyo, E., (2010). "Exploración de suelos/Soil exploration", XXa Conferencia Nabor Carrillo/XXth Nabor Carrillo Lecture, Sociedad Mexicana de Ingeniería Geotécnica, México.
- [51] Mendoza, M., Ovando E., Auvinet, G., López-Acosta N., Botero, E., Ossa, A., Flores, O. y Juárez, M. (2018). "Investigaciones y Estudios Especiales Relacionados con Aspectos Geotécnicos del Diseño y la Construcción del Nuevo Aeropuerto Internacional de la Ciudad de México (NAICM)", Convenio GACM-IIUNAM, Informe final, México.
- [52] Santoyo E., Lin R. y Ovando E. (1989). "El cono en la exploración geotécnica", TGC Geotecnia, México.
- [53] Alanis, R., (2003), "Caracterización geotécnica del ex lago de Texcoco", Tesis de maestría, Programa de Maestría y Doctorado en Ingeniería, Ingeniería Civil, Geotecnia, UNAM, Mexico.
- [54] Montañez, L., (1983). "Exploración con cono eléctrico en la Ciudad de México", Tesis de maestría, División de Posgrado de la Facultad de Ingeniería, UNAM, México.
- [55] Rodríguez, J.F., (2011), "Modelado del comportamiento de pilotes e inclusiones sometidos a consolidación regional en la zona lacustre de la Ciudad de México", Tesis doctoral, Programa de Maestría y Doctorado en Ingeniería, Ingeniería Civil, UNAM, Mexico.
- [56] Ossa, A., (2004). "Modelo elasto-visco-plástico (EVP) para el estudio de la consolidación unidimensional de los suelos", Tesis de maestría, Programa de Maestría y Doctorado en Ingeniería, UNAM, Ciudad de México, México.
- [57] Romo, M.P. and Auvinet, G. (1992). "Seismic behavior of foundations on cohesive soft soils" in *Recent advances in Earthquake Engineering and Structural Dynamics*, edited by V. Davidovici, Ouest-Editions, pp. 311-328, Paris, France.
- [58] Marsal, R.J. (1975). "The lacustrine clays of the valley of Mexico", Contribution of Instituto de Ingeniería, UNAM to the 1975 International clay conference, Publication E16, Instituto de Ingeniería, Universidad Nacional Autónoma de México, Mexico.
- [59] GDCDMX, Gobierno de la Ciudad de México (2017a). "Normas Técnicas Complementarias para diseño y construcción de cimentaciones", Gaceta de la Ciudad de México, diciembre, Mexico.
- [60] Murillo, R. y Morales, R., (1991). "El subsuelo del ex Lago de Texcoco", Proceedings, IXth Pan-American Conference on Soil Mechanics and Foundation Engineering, 213-225, Viña del mar, Chile.
- [61] Marsal, R. J. y Graue, R, (1969). "El subsuelo del Lago de Texcoco", Volumen Nabor Carrillo; Ciudad de México, México, 167-202.
- [62] Méndez, E., Auvinet, G., Matus, U. and Juárez, M., (2010). "Caracterización de anomalías geotécnicas en las zonas lacustre y de transición de la ciudad de México", XXVa Reunión Nacional de Mecánica de Suelos e Ingeniería Geotécnica, SMIG, Acapulco, México, Vol. 1, 311-321.
- [63] Carrillo, N., (1948). "Influence of Artesian wells on the sinking of Mexico City", Proceedings, Second international Conference on Soil Mechanics and Foundation Engineering, Vol.7, 156-159, Rotterdam, Netherlands.
- [64] Ovando-Shelley E., Romo, M. P. and Ossa, A. (2007). "The sinking of Mexico city: Its effects on soil properties and seismic response". Soil Dynamics and Earthquake Engineering, 27, No. 4, 333-343.
- [65] Jaime, A. and Méndez, S., (2010), "Evolution of Mexico clay properties affected by land subsidence", International Association of Hydrological Sciences, Publication 339, 232-234, Mexico.
- [66] González Rodriguez, R., (2012), "Estado actual y perspectivas a futuro de las condiciones del Centro Nacional de la SCT desde el punto de vistas geotécnico", Tesis de maestría, Programa de estudios de maestría y doctorado en Ingeniería, UNAM.
- [67] Ovando-Shelley, E., Romo, M.P., Contreras, N. and Giralt, A., (2003), "Effects of regional subsidence on the seismic response of Mexico City clay deposits", Elsevier Science Ltd, 12th European Conference on Earthquake Engineering, paper reference 248, 8p.
- [68] Auvinet, G., (2011). "Soil fracturing induced by land subsidence" in "Land subsidence, Associated Hazards and the Role of Natural Resources Development", 339, 0-26
- [69] Auvinet, G., Sánchez-Guzmán, J. y Pineda, A.R, (2019). "Mitigación de daños ocasionados por grietas en el suelo", Revista Ingeniería Investigación y Tecnología, Facultad de Ingeniería, UNAM, Mexico. (publication pending)

- [70] Steinbrenner, (1934). *Tafeln zur setzungsberechnung*, Die Strasse.
- [71] Button, S.J., (1953). "The bearing capacity of footings on a two layer cohesive subsoil", Third International Conference on Soil Mechanics and Foundation Engineering, Zurich, Switzerland.
- [72] Richardt, F.E., Hall, J.R. and Woods, R.D., (1970). "Vibrations of soils foundations", Prentice Hall.
- [73] Ladd, C.C. and Foote, R., (1974), "A new design procedure for stability of soft clays", Journal of the Geotechnical Engineering Division. ASCE, Vol. 100, No GT7, pp. 763-786.
- [74] Bay, J.A., Anderson, R., Colocino, T.M. and Budge, A.S., (2005). "Evaluation of Shansep parameters for soft Bonneville clays", Report No UT-03.13, Utah State University, Dept. of Civil and Environmental Engineering.
- [75] Vanmarcke, E.H., (1983). "Random fields: Analysis and Synthesis", MIT Press, Cambridge, Ma.
- [76] Vanmarcke, E.H., (2010). "Random fields: Analysis and Synthesis", World Scientific, Princeton University.
- [77] Krige, D. G., (1962). "Statistical application in mine valuation", J. Institute Mine Survey, South Africa
- [78] Matheron, G., (1965). "Les variables généralisées et leur estimation", Masson et Cie, France.
- [79] Juárez, M., (2015). "Análisis geoestadístico del subsuelo de la zona lacustre de la Cuenca de México", Tesis doctoral, Programa de Maestría y Doctorado en Ingeniería, Ingeniería Civil, Geotecnia, UNAM, Ciudad de México, México
- [80] Azzouz, M. et Bacconnet, C., (1988). "Optimisation d'une campagne de reconnaissance par géostatistique", Symposium on Reliability-based design in Civil Engineering, Lausanne, Switzerland, 269-276.
- [81] Wackernagel, H., (2003). Multivariate Geostatistics. An Introduction with Applications. Springer, 3rd Edition, Berlin, Germany, 387p.
- [82] Nelsen, R.B. (2006). "An introduction to copulas", Springer-Verlag, New York, 2nd Edition, pp. 269.
- [83] Phoon, K., and Ching, J., (2015) "Risk and reliability in geotechnical engineering", CRC Press, New York.
- [84] Vázquez, F. y Auvinet, G., (2014). "Simulación de campos aleatorios con dependencia no multigaussiana empleando cópulas", Ingeniería, Investigación y Tecnología, FI-UNAM, Vol. XV, Núm 4, Mexico.
- [85] Vásquez-Guillén, F. y Auvinet, G., (2015). "Simulación de campos aleatorios espacio-temporales utilizando un filtro de Kalman modificado", Ingeniería, Investigación y Tecnología, FI-UNAM, Vol. XVI, Núm 1, 1-12, Mexico.
- [86] Auvinet, G. and Bouvard, D., (1984). "Effet d'échelle géométrique dans les milieux granulaires", Revue Française de Géotechnique, N° 25, 63-69, avril, Paris, France.
- [87] Auvinet, G., (1986) "Estructura de medios granulares", Tesis doctoral, División de Estudios de Posgrado de la Facultad de Ingeniería, UNAM, (2 vol.), México.
- [88] Auvinet, G., (1969), "Desplazamientos horizontales producidos en un subsuelo arcilloso por cargas superficiales y por hincada de pilotes", Tesis para obtener el grado de Maestro en Ingeniería, División de Estudios de Posgrado, Facultad de Ingeniería, UNAM, México.
- [89] GDCDMX, Gobierno de la Ciudad de México (2017b). "Normas Técnicas Complementarias para diseño por sismo", Gaceta de la Ciudad de México, diciembre, México.
- [90] Mazari, M., (1996). "La isla de los perros". El Colegio Nacional, CDMX, México.
- [91] Reséndiz, D. and Herrera, I., (1969). "A probabilistic formulation of settlement-controlled Design", Proceedings, 7th International Conference on Soil Mechanics and Foundation Engineering, Mexico, Vol 2, pp 217-225.
- [92] Auvinet, G., Juárez, M. and Medina, Z., (2001), "Geostatistical interpretation of soil exploration" Proceedings, International Conference on Soil Mechanics and Geotechnical Engineering, Istanbul, Turkey, Vol.1, pp. 373-376.
- [93] Auvinet, G., and Juárez, M., (2002). "Geostatistical characterization and simulation of Mexico Valley subsoil", Proceedings, IASTED International Conference, Modelling and Simulation 2002, Marina del Rey, California, USA. pp. 208-212
- [94] Auvinet, G., Juárez, M. and Valdez P., (2005), "Caractérisation géostatistique du sol de la ville de Mexico", Revue Française de Géotechnique, No 110, Paris, France.
- [95] Delgado Muñiz, M., (2017). "Análisis geoestadístico multivariante de las propiedades geotécnicas del subsuelo lacustre del valle de México", Tesis de maestría, Programa de Maestría y Doctorado en Ingeniería, Ingeniería Civil, Geotecnia, UNAM, Ciudad de México, Mexico.
- [96] Juárez, M., Auvinet, G. and Méndez, E., (2016) "Geotechnical zoning of Mexico valley subsoil", Ingeniería Investigación y Tecnología, Volume XVII (issue 3), July-September, Art. 1036, ISSN 1405-7743 FI-UNAM, Ciudad de México, México.
- [97] Flores Tapia, L.I., (2000). "Contribución a la zonificación geotécnica de la zona sur de la cuenca de México", Tesis profesional, Facultad de Ingeniería, UNAM, Ciudad de México. México.

- [98] Aguilar, R., (2001). "Zonificación geotécnica del Cerro de la Estrella y sus alrededores", Tesis Profesional, Escuela Superior de Ingeniería y Arquitectura, Unidad Zacatenco, Instituto Politécnico nacional, México.
- [99] Pantoja, A., (2002). "Análisis Geoestadístico del subsuelo en el norte de la zona lacustre del Valle de México". Tesis de Maestría, Universidad Nacional Autónoma de México, Ciudad de México, México.
- [100] Morales, A., (2004). "Aplicación de la geoestadística a la descripción estratigráfica del subsuelo de la zona de los ex-lagos de Xochimilco y Chalco", Tesis de Maestría ESIA-UZ, IPN, Ciudad de México, México.
- [101] Valencia, D., (2007). "Contribución a la zonificación geotécnica de la zona norte del Valle de México", Tesis de Maestría, ESIA-UZ, IPN, Ciudad de México, México.
- [102] Jiménez, O., (2007). "Caracterización geoestadística del subsuelo de la zona poniente del Valle de México", Tesis de Maestría, ESIA-UZ-IPN, Ciudad de México, México.
- [103] Tenorio, A., (2013). "Aplicación de la Geoestadística a la Caracterización Geotécnica del Subsuelo de la Zona Central de la Ciudad de México", Tesis de Maestría, Universidad Nacional Autónoma de México, Ciudad de México, México.
- [104] Pérez, D., (2009). "Modelado del hundimiento de la zona lacustre del valle de México. Aspectos estratigráficos y piezométricos", Tesis de maestría, SEPI, ESIA-IPN, México.
- [105] Rodríguez, M.E., (2010). "Caracterización geoestadística del subsuelo del ex lago de Texcoco", Tesis de Maestría, ESIA, Unidad Zacatenco, Instituto Politécnico Nacional, Ciudad de México, México
- [106] Hinojosa, J., (2010). "Comportamiento del suelo en la zona próxima al cerro del marqués y sus efectos en obras de infraestructura", Tesis de Maestría SEPI, ESIA-IPN, Ciudad de México, Mexico.
- [107] Hernández Vizcarra, F., (2013). "Caracterización geotécnica del subsuelo de la zona norte de la Cuenca de México", Tesis de maestría SEPI, ESIA-IPN, Ciudad de México, México.
- [108] Barranco-Eyssautier, A., (2016). "Caracterización geotécnica del subsuelo de la zona sur del valle de México con aplicación a una obra de infraestructura", Tesis de licenciatura, UNAM, México.
- [109] Magnan, J.P., et Bourehaoua, A., (2001). "Analyse probabiliste de la consolidation unidimensionnelle des sols", Revue Française de Géotechnique, 2ème trimestre, pp 10-25, France.
- [110] Auvinet, G., Bouayed, A., Orlandi, S. and López A., (1996). "Stochastic Finite Element Method in Geomechanics", Proceedings, Geotechnical Engineering Congress, "Uncertainty 96", University of Wisconsin, Geotechnical Engineering Division, ASCE Geotechnical Special Publication N° 58, Vol. 2, 1239-1253, ISBN: 0-7844-0188-8, USA.
- [111] Auvinet, G., Mellah R., Masroui F. and Rodríguez, J.F., (2000). "La méthode des éléments finis stochastiques en Géotechnique", Revue Française de Géotechnique N° 93, Paris, France, 67-79.
- [112] Mathews, J. and Walker, R.L., (1964). Mathematical methods of Physics, 2nd edition, Benjamin Publishers, 286-298.
- [113] Rosenblueth, E., (1975). "Point estimates for probability moments", Proceedings of National Academy of Science of the U.S.A., 72(10), 3812-3814.
- [114] Ghanem, R.G. and Spanos, P.D., (1991). "Stochastic finite elements, A spectral approach", Springer-Verlag, New York.
- [115] Pineda A.R., (2015). "Análisis estocástico de estructuras terreas: enfoque espectral", Tesis doctoral, Programa de Maestría y Doctorado en Ingeniería, Ingeniería Civil, Geotecnia, UNAM, Ciudad de México, México.
- [116] Freudenthal, A.M., Garrelts, J.M. and Shinozuka, M. (1964). "The analysis of structural safety", Belvoir Defense Technical Information Center.
- [117] Auvinet, G. and González, J.L., (2000). "Three dimensional reliability analysis of earth slopes", Computers and Geotechnics 26, 247-261, Elsevier.
- [118] Hungr, O., (1987). "An extension of Bishop's simplified method of slope stability to three dimensions", Géotechnique 38, No 1, 155-156, London.
- [119] Mendoza, M.J., Mendoza, S., Rufiar, M. and González, D., (2018). "Slope stability of a slope excavation in the soft clayey soil of the ancient Texcoco lake", Proceedings, XXIX Reunion de Nacional de Ingeniería Geotécnica, León, Guanajuato, Mexico.
- [120] Schmitter, J.J., Pérez, A. and Romero, W. (2018). "Thought about the behavior of the Texcoco former Lake subsoil, while being excavated", Proceedings, XXIX Reunion de Nacional de Ingeniería Geotécnica, León, Guanajuato, Mexico.
- [121] Mitchell, J.K., (1981). "Soil Improvement: State-of-the-Art Report", Proceedings of the 10th International Conference on Soil Mechanics and Foundation Engineering, Stockholm, Sweden, 509-565.
- [122] Pilot, G., Queyroi, D. et Chaput, D., (1985), "Amélioration des sols de fondation. Choix des méthodes d'exécution", LCPC, Ministère de l'urbanisme, du logement et des transports, Paris, France.
- [123] Schaefer, V. (2012). "Ground improvement in the 21st Century. A comprehensive Web-based Information System", ASCE GSP, May, Conference GeoCongress 2012.

- [124] Mesri, G. and Khan, A.Q., (2012) "Ground improvement using vacuum loading together with vertical drains", Journal of Geotechnical and Geoenvironmental Engineering, ASCE, June.
- [125] Auvinet, G., (1979). "Precarga en arcillas del Valle de México", Memoria, Simposio sobre "Mejoramiento masivo de suelos", Sociedad Mexicana de Mecánica de Suelos, 100-102, CDMX, México.
- [126] Auvinet, G., (2016), "Técnica de precarga alternativa para las pistas del NAICM", Nota Técnica del II-UNAM No. GEO-35. Elaborada para: Grupo Aeroportuario de la Ciudad de México (GACM), Mexico.
- [127] Auvinet, G. y Pérez Ángeles M., (2016), "Terraplenes y bordos sobre suelos blandos", Memoria de la XXVIII Reunión Nacional de Ingeniería Geotécnica, SMIG, Conferencia magistral, 23-26 de noviembre, Mérida, Yucatán, México.

Appendix I. Considerations about some physical properties of soft soils

a) Void ratio

In geotechnical engineering, the widely used physical property known as *void ratio* e is defined as:

$$e = \frac{V_v}{V_s} \quad (1)$$

where V_v = volume of voids (including water) in sample, and V_s = volume of solids in sample.

This parameter is extremely unstable for small samples (Auvinet, 1986 [1]) and for soft soils with high water content. When applied to the microstructure of soils, according to Eq. (1) e tends towards extreme values:

$$e = \infty \text{ for } V_s = 0$$

$$e = 0 \text{ for } V_v = 0$$

It is also easy to verify that if a heterogeneous sample is divided into k parts of the same size, the void ratio of the sample as a whole is not the average of the k void ratios of the different subsamples. This is of course a consequence of the high non-linearity of Eq. (1) with respect to V_s . Averaging local void ratios introduces a bias and overestimates the actual void ratio of the whole sample. Void ratio is thus an ill-fitted parameter for statistical analyses of soft soils spatial variations. Note that Compression index C_c and Swelling index C_s are incremental void ratios.

These inconveniences can of course be avoided by sticking to another common physical property, porosity, n , defined as:

$$n = \frac{V_v}{V_T} \quad (2)$$

where V_v = volume of voids in sample, and V_T = total volume of sample.

Porosity is a stable parameter ranging between 0 and unity (100%) that can be averaged over a volume.

Note that, as it is well known:

$$n = \frac{e}{(1+e)} \quad \text{and} \quad e = \frac{n}{(1-n)} \quad (3)$$

However, if porosity n is considered as a random variable with expected value $E\{n\}$ and standard deviation σ_n within an heterogeneous random medium, the corresponding expected value of void ratio $E\{e\}$ will present a biased value that can be estimated using a second order approximation (Papoulis, 1985 [2]) :

$$E\{e\} \cong \frac{E\{n\}}{1 - E\{n\}} + \frac{1}{2} \left[\frac{d^2 e}{dn^2} \right]_m \sigma_n^2 = \frac{E\{n\}}{1 - E\{n\}} + \frac{\sigma_n^2}{(1 - E\{n\})^3} \quad (4)$$

and reciprocally:

$$E\{n\} \cong \frac{E\{e\}}{1 + E\{e\}} + \frac{1}{2} \left[\frac{d^2 n}{de^2} \right]_m \sigma_e^2 = \frac{E\{e\}}{1 + E\{e\}} - \frac{\sigma_e^2}{(1 + E\{e\})^3} \quad (5)$$

Most expressions in terms of void ratio can also be readily expressed in terms of porosity.

As an example, Figure 1 shows a typical $e - \log \sigma'$ compressibility curve for Mexico City clays and the corresponding $n - \log \sigma'$ curve. Comparing these graphs it can be observed that, at least in this case, the second representation looks, as a matter of fact, better-suited than the first one for determining the preconsolidation pressure σ'_p and the slope of the virgin and recompression branches.

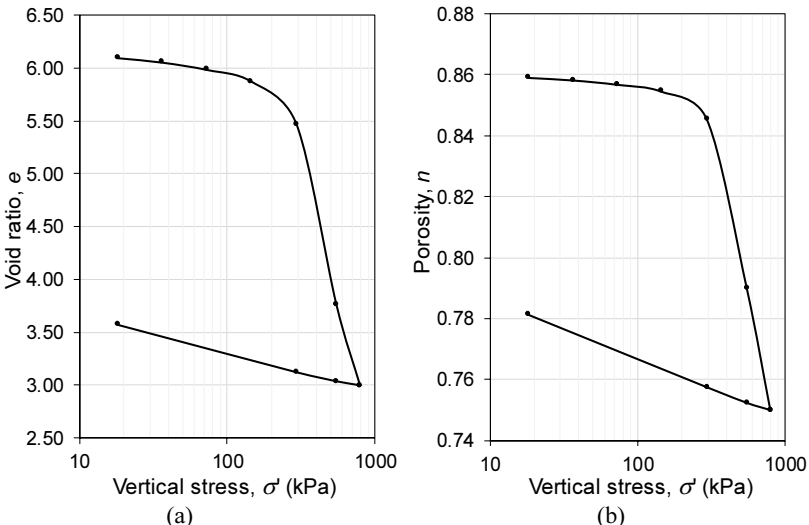


Figure 1. Compressibility curves expressed in term of (a) void ratio e and (b) porosity n .

The settlement ΔH of a layer with thickness H , usually calculated as:

$$\Delta H = \frac{e_0 - e}{1 + e_0} H \quad (6)$$

where e_0 is the initial void ratio and e is the void ratio after the settlement has occurred.

Can also be calculated as:

$$\Delta H = \frac{n_0 - n}{1 - n} H \quad (7)$$

Where n_0 is the initial porosity and n is the porosity after the settlement has occurred.

In a more general form, the settlement of a soil layer submitted to a stress increment $\Delta\sigma$ can be calculated from compressibility curve in terms of porosity as:

$$\Delta H = H \left[\frac{C_{dn}}{1 - n} \log \frac{\sigma_p'}{\sigma_0'} + \frac{C_{cn}}{1 - n} \log \frac{\sigma_0' + \Delta\sigma}{\sigma_p'} \right] \quad (8)$$

when $\sigma_0' \leq \sigma_p'$ and $\sigma_0' + \Delta\sigma \geq \sigma_p'$

where C_{cn} = compression index (from n -log σ' curve), C_{dn} = swelling index (from n -log σ' curve), n = final porosity, and H = layer thickness.

Void ratio thus appears as an unnecessary parameter, redundant with porosity, and with the inconveniences mentioned above in the context of statistical analyses of soft soils spatial variations.

b) Water content

In the same way, in geotechnical engineering, the physical property known as *gravimetric water content* w is defined as:

$$w = \frac{W_w}{W_s} \quad (9)$$

where W_w = weight of water in sample, and W_s = weight of solids in sample.

This is also a very unstable parameter for small samples and for soft soils with high water content. When applied to the microstructure of soils, according to Eq. (9), w tends towards extreme values:

$$w = \infty \text{ for } W_s = 0$$

$$w = 0 \text{ for } W_w = 0$$

It is also easy to verify that if a sample is divided into k parts of the same size, the water content w of the sample as a whole is not the average of the water contents of the k different subsamples. This is again a consequence of the non-linearity of Eq. (9) with

respect to W_s . Averaging local water contents introduces a bias and overestimates the actual water content of the whole sample. Note that Atterberg's limits are also gravimetric water contents.

Taylor (1948 [3]) underlined that definition of Eq. (9) is not standard in all branches of science, the water content being defined in geology, for example, as a percentage of total weight:

$$w' = \frac{W_w}{W_T} \quad (10)$$

where W_T = total weight of sample ($=W_s + W_w$)

This parameter is much more stable than the previous one since it can only vary between 0 and 100%. However, it is also easy to verify that if a sample is divided in k parts of the same size, water content w' of the sample as a whole is not the average of the water content of the k different subsamples. Averaging local water contents introduces a small bias and overestimates the actual water content of the whole sample. Strictly speaking, parameter w' cannot be averaged either over a volume but the error incurred in using this parameter in statistical analyses is generally small.

Note that:

$$w' = \frac{w}{w+1} \text{ and } w = \frac{w'}{1-w'} \quad (11)$$

A volumetric definition of water content is also commonly used:

$$w'' = \frac{V_w}{V_T} \quad (12)$$

where V_w = volume of water in sample, and V_T = total volume of sample ($=V_w + V_s$ for saturated materials).

This stable parameter varies between 0 and 100 % and can be averaged on a volume. In the case of saturated materials, it is equal to porosity. Note that, also for saturated materials:

$$\begin{aligned} w'' &= \frac{G_s w}{1 + G_s w} \text{ and } w = \frac{w''}{G_s(1 - w'')} , \text{ while:} \\ w'' &= \frac{G_s w'}{1 + w'(G_s - 1)} \text{ and } w' = \frac{w''}{w'' + G_s(1 - w'')} \end{aligned} \quad (13)$$

where G_s = specific density of solids.

Figure 2 shows how, for saturated materials with high water content, small increases in volumetric water content w'' (Eq. (12)) correspond to very large increases in gravimetric water content w (Eq. (9)) that do not correspond to really significant changes

in the composition of the soil sample. Water content w' (Eq. (10)) presents a much more stable behavior.

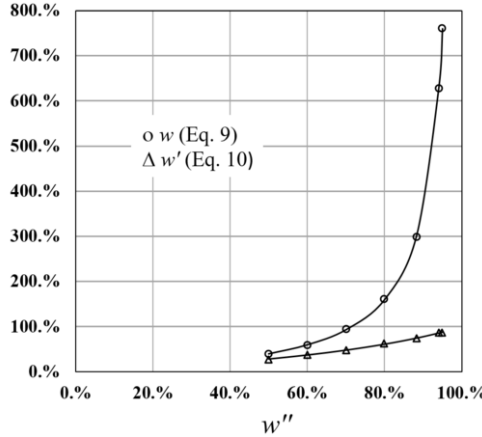


Figure 2. Variations of water contents w (Eq. (9)) and w' (Eq. (10)) as a function of w'' (Eq. (12)).

If the volumetric water content w'' is considered as a random variable with expected value $E\{w''\}$ and standard deviation $\sigma_{w''}$ within an heterogeneous random medium, the corresponding expected value of water content w , $E\{w\}$, can be estimated using a second order approximation as :

$$E\{w\} \approx \frac{E\{w''\}}{G_s(1 - E\{w''\})} + \frac{1}{2} \left[\frac{d^2 w}{dw''^2} \right]_m \sigma_{w''}^2 = \frac{E\{w''\}}{G_s(1 - E\{w''\})} + \frac{\sigma_{w''}^2}{G_s(1 - E\{w''\})^3} \quad (14)$$

and reciprocally:

$$E\{w''\} \approx \frac{G_s E\{w\}}{1 + G_s E\{w\}} + \frac{1}{2} \left[\frac{d^2 w''}{dw^2} \right]_m \sigma_w^2 = \frac{G_s E\{w\}}{1 + G_s E\{w\}} - \frac{G_s^2 \sigma_w^2}{(1 + G_s E\{w\})^3} \quad (15)$$

Similarly,

$$\begin{aligned} E\{w'\} &\approx \frac{E\{w''\}}{E\{w''\} + G_s(1 - E\{w''\})} + \frac{1}{2} \left[\frac{d^2 w'}{dw''^2} \right]_m \sigma_{w''}^2 \\ &= \frac{E\{w''\}}{E\{w''\} + G_s(1 - E\{w''\})} + \frac{G_s(G_s - 1)\sigma_{w''}^2}{[E\{w''\} + G_s(1 - E\{w''\})]^3} \end{aligned} \quad (16)$$

and reciprocally:

$$\begin{aligned} E\{w''\} &\approx \frac{G_s E\{w'\}}{1 + E\{w'\}(G_s - 1)} + \frac{1}{2} \left[\frac{d^2 w'}{dw'^2} \right]_m \sigma_{w'}^2 \\ &= \frac{G_s E\{w'\}}{1 + E\{w'\}(G_s - 1)} - \frac{G_s(G_s - 1)\sigma_{w'}^2}{[1 + E\{w'\}(G_s - 1)]^3} \end{aligned} \quad (17)$$

Most existing geotechnical engineering analytical developments have been expressed in terms of parameters defined by Eqs. (1) and (9). These parameters should however be considered as inadequate in a context of statistical analyses of soft soils spatial variability. To illustrate the above, in Table 1, a hypothetical heterogeneous saturated sample was divided into five equal parts with assumed unitary volumes. The specific density of solid was considered to be $G_s = 2.5$.

Table 1. Comparison of average and true values of void ratio and water content.

Subsample	W_w	W_s	W_t	V_w	V_s	V_t	Gravimetric	Gravimetric	Volumetric	Void	Porosity
							1	2	$w'' = V_w/V_t$	$e = V_w/V_s$	$n = V_w/V_t$
							$w = W_w/W_s$	$w' = W_w/W_t$	$w'',\%$	e	n
1	0.88	0.29	1.18	0.88	0.12	1.00	300	75	88	7.50	0.88
2	0.80	0.50	1.30	0.80	0.20	1.00	160	62	80	4.00	0.80
3	0.70	0.75	1.45	0.70	0.30	1.00	93	48	70	2.33	0.70
4	0.60	1.00	1.60	0.60	0.40	1.00	60	38	60	1.50	0.60
5	0.50	1.25	1.75	0.50	0.50	1.00	40	29	50	1.00	0.50
Average							131	50	70	3.27	0.70
True value							92	48	70	2.29	0.70
Bias							39	2	0	0.98	0

A strong bias is observed between the average of the local values of void ratio e and the true value of this same parameter for the whole sample.

Similarly, a bias exists between the average of local values and the true values of the gravimetric water contents (Eqs. (9) and (10)) for the whole sample. The bias of the average value of w' is however much smaller than the bias of the average value of w . Volumetric water content w'' is clearly the best behaved parameter from a physical and mathematical point of view.

Note that the true value of void ratio e for the whole sample can be calculated directly applying the second relation of Eq. (3) to the unbiased average value of porosity. This true value corresponds to the first term of the development of Eq. (7) while the bias is approximately equal to the second term of this development.

Similarly, the true values of gravimetric water contents w and w' for the whole sample can be calculated directly applying the second and fourth relations of Eq. (13) to the unbiased average value of volumetric water content w'' . These true values correspond to the first terms of the developments of Eqs. (14) and (16) while the biases are approximately equal to the second terms of these developments.

References for Appendix I

- [1] Auvinet, G., (1986). "Estructura de medios granulares", Tesis doctoral, División de Estudios de Posgrado de la Facultad de Ingeniería, UNAM, (2 vol.), México.
- [2] Papoulis, A., (1985). Probability, Random variables and Stochastic Processes, McGraw-Hill, USA.
- [3] Taylor, D.W., (1948). Fundamentals of Soil Mechanics, John Wiley & Sons, New York, USA.

Appendix II. Random fields and Geotechnical engineering

II.1. Definitions

Let $V(X)$ be a geotechnical variable of either physical (e.g. water content), mechanical (e.g. undrained shear strength), or geometric type (e.g. thickness of a certain stratum), defined at points X of a certain domain R^P ($p = 1, 2$, or 3). If at each point of the domain this variable is regarded as random, the set of these random variables constitutes a random field (Auvinet, 2002 [1])

To describe such a field, the following parameters and functions are introduced:

- Expected value:

$$\mu_V(X) = E\{V(X)\} \quad (1)$$

- Variance:

$$\sigma_V^2(X) = Var[V(X)] \quad (2)$$

The square root $\sigma_V(X)$ of the variance is known as *standard deviation* whereas the ratio $CV(X) = \sigma_V(X) / E\{V(X)\}$ is defined as the *coefficient of variation*.

- Autocorrelation function:

$$R_V(X_1, X_2) = E\{V(X_1)V(X_2)\} \quad (3)$$

This function, defined in the $R^P \times R^P$ space is a mixed second order moment that can be centered introducing the concept of autocovariance function:

- Autocovariance function:

$$C_V(X_1, X_2) = \text{Cov}[V(X_1), V(X_2)] = \\ E\{[V(X_1) - \mu_V(X_1)][V(X_2) - \mu_V(X_2)]\} \quad (4)$$

The autocovariance function represents the degree of linear dependence existing between the values of the property of interest in two different points of the medium. It can be written in terms of a dimensionless autocorrelation coefficient (normalized autocovariance function), the value of which always ranges between -1 and +1:

- Autocorrelation coefficient function (normalized autocovariance):

$$\rho_V(X_1, X_2) = \frac{C_V(X_1, X_2)}{\sigma_V(X_1)\sigma_V(X_2)} \quad (5)$$

It should be emphasized that functions (3) to (5) are not intrinsic properties of points X_1 and X_2 since they also depend on the dominion in which the field has been defined. Actually, if a soil deposit is considered as a whole, it may be possible to find a high correlation between the properties corresponding to two points that belongs to the same

substratum; however, this correlation is likely to vanish if the study is limited to analyzing the spatial variations within this particular substratum. Tables providing "typical autocorrelation coefficient functions" found in the literature are thus generally meaningless.

- Probability distribution functions:

$$F_{V_1, \dots, V_n}(v_1, \dots, v_n; X_1, \dots, X_n) = P[V(X_1) \leq v_1, \dots, V(X_n) \leq v_n] \quad (6)$$

among which special mention should be made of the first-order probability distribution function:

$$F_V(v; X) = P[V(X) \leq v] \quad (7)$$

as well as of its derivatives, namely the joint probability densities:

$$f_{V_1, \dots, V_n}(v_1, \dots, v_n; X_1, \dots, X_n) \text{ and } f_V(v; X) \quad (8)$$

If these functions (and the associated moments) are invariant by translation in space for any value of n and for any set of points: X_1, \dots, X_n , the random field is said to be *strictly stationary*.

If, in the domain considered, the expected value and other parameters are constant, the medium is called *statistically homogeneous*. If parameters such as the expected value and variance of the field are not constant, it is said that they present a certain *trend* or *drift*.

When it is possible to accept the hypothesis that the expected value of the variable of interest is constant throughout the whole dominion and that the spatial autocovariance only depends on the distance between points X_1 and X_2 , it is said that the field is *wide-sense stationary*; then:

$$C_V(X_1, X_2) = C_V(X_2 - X_1) = C_V(h) \quad (9)$$

where h = scalar equal to the distance between points X_1 and X_2 .

Eq. (9) implies that variance of $V(X)$ is also a constant in the whole dominion.

Similarly, in this case, the autocorrelation coefficient can be expressed as:

$$\rho_V(X_1, X_2) = \rho_V(h) \quad (10)$$

In many applications, however, it will be more realistic to admit that the previous relationship is only valid along a specified direction, i.e. that the structure of correlation of the medium is anisotropic. In this case, the notations $C_V(h\mathbf{u})$ and $\rho_V(h\mathbf{u})$ can be used, where \mathbf{u} is a unit vector in the direction being considered.

In media with linear drift, the field is not stationary but increments $V(X + h) - V(X)$ can still be stationary. Accordingly, some authors, especially in mining applications,

have opted for using the concept of variogram instead of autocovariance. The variogram $2\gamma(h)$ is the second order moment of increment $V(X+h) - V(X)$:

$$2\gamma(h) = E\left\{[V(X+h) - V(X)]^2\right\} \quad (11)$$

For a wide-sense stationary field:

$$2\gamma(h) = \text{Var}[V(X+h) - V(X)] \quad (12)$$

$$\gamma(h) = C_v(0) - C_v(h) \quad (13)$$

In most engineering applications, using the concept of variogram fails to present any advantage and therefore autocovariance function is commonly employed instead. As a matter of fact, some of the most common geostatistical softwares systematically convert variograms into autocovariance functions to provide better stability to numerical algorithms (Deutsch and Journel, 1992 [2]).

Note that, alternatively, spatial variability of geotechnical variables can be modeled by means of copulas (Vázquez-Guillén, 2014 [3]). Copulas are of interest as random functions because they express dependence without the influence of the first-order distribution functions. Thus, more realistic spatial variability descriptions can be attained. For a random field constituted by continuous random variables, the n -dimensional copula is written as (Nelsen, 2006 [4]):

$$C(u_1 = F_{V_1}(v_1), \dots, u_n = F_{V_n}(v_n)) = F_{V_1, \dots, V_n}\left(F_{V_1}^{-1}(u_1), \dots, F_{V_n}^{-1}(u_n)\right) \quad (14)$$

and the corresponding copula density by:

$$c(u_1, \dots, u_n) = f_{V_1, \dots, V_n}(F_{V_1}^{-1}(u_1), \dots, F_{V_n}^{-1}(u_n)) / \prod_{i=1}^n f_{V_i}\left(F_{V_i}^{-1}(u_i)\right) \quad (14a)$$

For example, the multivariate Gaussian copula can be formulated as:

$$C_\Gamma^G(u_1, \dots, u_n) = \Phi_\Gamma\left(\Phi^{-1}(u_1), \dots, \Phi^{-1}(u_n)\right) \quad (15)$$

where $\Phi_\Gamma(\cdot)$ is the multivariate Gaussian distribution (see 4.4) with zero mean and correlation matrix Γ and $\Phi^{-1}(\cdot)$ is the inverse of the first-order standard Gaussian distribution.

The corresponding Gaussian copula density is written as:

$$c(u_1, \dots, u_n) = f_{V_1, \dots, V_n}(\Phi^{-1}(u_1), \dots, \Phi^{-1}(u_n)) / \prod_{i=1}^n f_{V_i}\left(\Phi^{-1}(u_i)\right) \quad (15a)$$

where $f_{V_1, \dots, V_n}()$ is the multivariate Gaussian density function and $f_{V_i}()$ is the first-order Gaussian density function.

As an example, Figure 1 displays copula density plots of the bivariate Gaussian copula for different correlation coefficients ($\rho=0.95, 0.85$ and 0.45).

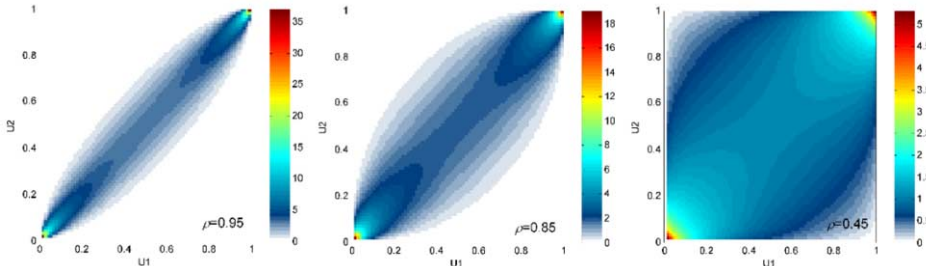


Figure 1. Bivariate Gaussian copula density plots for different correlation coefficients.

Similar to a description with autocovariance functions, bivariate spatial copulas are used to describe spatial variability. For any two locations separated by the vector $h\mathbf{u}$, a spatial copula is defined via Sklar's theorem as (Bárdossy, 2006 [5]):

$$C_S(h\mathbf{u}; u_1, u_2) = C(F_V(V(X), F_V(V(X+h\mathbf{u})) \quad (16)$$

Hence, the copula becomes a function of the separating vector $h\mathbf{u}$. Note that u_1 and u_2 are the quantiles of $V(X)$ and $V(X+h\mathbf{u})$, respectively. For a given $h\mathbf{u}$, the spatial copula $C_S()$ describes thus the spatial dependence between the quantiles u_1, u_2 of pairs of random variables.

Note also that in soils suffering consolidation, the evolution of static and dynamic parameters of the deforming deposit occurs within a context of pronounced uncertainty. Therefore, the use of a spatio-temporal random field may be helpful to increase the degree of realism of long-term predictions made with geomechanical models. Vázquez and Auvinet (2015 [6]) described this type of random fields and proposed a stochastic simulation technique of such random fields. In the work by Vázquez and Auvinet (2017 [7]), such technique is applied to identify hydraulic conductivities from temporal observations of the hydraulic head field.

II.2. Statistical estimation of random field parameters

The descriptive parameters of a random field can be estimated from “discrete” (isolated samples) or “continuous” (boring logs) obtained in an exploratory program. In the latter case, and assuming that the field is statistically homogeneous and ergodic (i.e. its parameters can be estimated from a single sample function or realization), the expected value can be assessed (Auvinet, 2002 [1]) using the following approximation:

$$\mu_V \cong \bar{\mu}^* = \frac{1}{L} \int_0^L V(x) dx \quad (17)$$

where L = depth of the boring.

Similarly, it is possible to estimate the autocovariance function along the \mathbf{u} direction as:

$$C_V(h\mathbf{u}) \approx \frac{1}{L} \int_0^L V(x)V(x+h\mathbf{u})dx - \mu^2 \quad (18)$$

where \mathbf{u} is the unit vector in the direction along which the covariance is evaluated and h is a scalar.

Estimating the autocovariance by means of Eq. (18) introduces a small bias, as can be verified by evaluating the expected value of the second member.

On the other hand, if the following indicator function is introduced:

$$I_V(v, X) = \begin{cases} 1 & \text{if } V(X) \leq v \\ 0 & \text{if } V(X) > v \end{cases} \quad (19)$$

The field's first-order probability distribution function can be estimated from continuous records based on the relationship:

$$F_V(v, X) = P[V(X) \leq v] \approx \frac{1}{L} \int_0^L I_V(v, x) dx \quad (20)$$

Estimation of field parameters in terms of the available data is generally known as *structural analysis*.

In the case of isolated samples, estimations can be performed using discrete expressions equivalent to the previous equations (Deutsch and Journel, 1992 [2]). This situation is the most common whenever the variable of interest is of the geometric type (thickness of a given stratum, as an example).

II.3. Scale effect

Knowing the major parameters of a random field representing the variations of the properties makes it possible to evaluate the expected value and dispersion of the average values of such properties in subdomains (lines, areas or volumes) contained within the medium. In a stationary field, the mathematical expectation of the average value of the property of interest in a subdomain ω is (Papoulis, 1985 [8]):

$$E\{V_\omega\} = E\left\{\frac{1}{\Omega_\omega} \int V(X) dX\right\} = E\{V(X)\} \quad (21)$$

and its variance is:

$$\text{Var}[V_\omega] = E\{V_\omega^2\} - E^2\{V_\omega\} \quad (22)$$

that is to say:

$$\text{Var}[V_\Omega] = \frac{1}{\Omega^2} \left[E \left\{ \int_{\Omega} V(X) dX \int_{\Omega} V(X) dX \right\} - E \left\{ \int_{\Omega} V(X) dX \right\}^2 \right] \quad (23)$$

that can be expressed as:

$$\begin{aligned} \text{Var}[V_\Omega] &= \frac{1}{\Omega^2} \left[\int_{\Omega} \int_{\Omega} E\{V(X_1)V(X_2)\} dX_1 dX_2 \right. \\ &\quad \left. - \int_{\Omega} \int_{\Omega} E\{V(X_1)\} E\{V(X_2)\} dX_1 dX_2 \right] \end{aligned} \quad (24)$$

or:

$$\text{Var}[V_\Omega] = \frac{1}{\Omega^2} \int_{\Omega} \int_{\Omega} C_V(X_1, X_2) dX_1 dX_2 \quad (25)$$

Similarly, it can be shown that the covariance between the average values of a given property in two subdomains Ω_1 and Ω_2 , with or without overlapping, is:

$$\text{Cov}[V_{\Omega_1}, V_{\Omega_2}] = \frac{1}{\Omega_1 \Omega_2} \int_{\Omega_1} \int_{\Omega_2} C_V(X_1, X_2) dX_1 dX_2 \quad (26)$$

Eq. (25) can be also written as:

$$\text{Var}[V_\Omega] = \frac{\text{Var}[V(X)]}{\Omega^2} \int_{\Omega} \int_{\Omega} \rho_V(X_1, X_2) dX_1 dX_2 \quad (27)$$

Since the correlation coefficient is smaller than or equal in absolute value to unity, the variance of the average value of a stationary random property in a given subdomain Ω tends to decrease when the dimensions of such domain increase (except in the trivial case of perfect correlation).

The above consideration applies to any property that can be averaged on a volume. As seen in Appendix I, strictly speaking, this is not the case of soil gravimetric water content.

II.4. Conditional estimation

A problem of utmost interest in geotechnical engineering is the estimation of the value of a property of interest at a point of the medium where no measurement exists (point estimation). A solution to this problem allows interpolating between available data and even defining virtual boring logs and cross-sections of the medium. The problem can be generalized to that of estimating the average value of the same property in any subdomain studied, for instance in a given volume or along a certain potentially critical surface (global estimation).

A technique available to reach this objective is the *unbiased linear conditional estimation with minimal variance*, also known as Wiener's filter. A similar technique used in mining engineering, is known as *kriging* (Krige, 1962 [9]; Matheron, 1965 [10]).

II.4.1. Bivariate linear conditional estimation

Modeling by means of a random field a property defined in a domain, Ω , makes it possible to evaluate the conditional expected value and variance of V_Ω , punctual or average value of this property in a subdomain, Ω_1 , in terms of the value V_{Ω_2} , also punctual or average, obtained through direct measurement in another subdomain Ω_2 .

A linear estimator $V_{\Omega_1}^*$ is used such that:

$$V_{\Omega_1}^* = aV_{\Omega_2} + b \quad (28)$$

that should be unbiased:

$$E\left\{ V_{\Omega_1}^* - V_{\Omega_1} \right\} = 0 \quad (29)$$

It is possible to obtain an expression for the values of a and b , so that Eqs. (28) and (29) are simultaneously satisfied, and the expectation of the square of the error or *estimation variance* is minimized:

$$E\left\{ (V_{\Omega_1}^* - V_{\Omega_1})^2 \right\} = \text{Var}\left[aV_{\Omega_2} + b - V_{\Omega_1} \right] \quad (30)$$

From (29) it can be inferred that the value of b is:

$$b = E\left\{ V_{\Omega_1} \right\} - aE\left\{ V_{\Omega_2} \right\} \quad (31)$$

On the other hand, it is easy to verify that by making equal to zero the derivative of Eq. (27) with respect to variable a , in order to minimize the estimation error, the following result is obtained:

$$a = \frac{\text{Cov}\left[V_{\Omega_1}, V_{\Omega_2} \right]}{\sigma_{V_{\Omega_2}}^2} \quad (32)$$

Eq. (28) providing the estimation becomes:

$$V_{\Omega_1}^* = E\left\{ V_{\Omega_1} \right\} + \rho_V \left(V_{\Omega_1}, V_{\Omega_2} \right) \frac{\sigma_{V_{\Omega_1}}}{\sigma_{V_{\Omega_2}}} \left[V_{\Omega_2} - E\left\{ V_{\Omega_2} \right\} \right] \quad (33)$$

where $\rho_V(V_{\Omega_1}, V_{\Omega_2})$ is the correlation coefficient between V_{Ω_1} and V_{Ω_2} :

$$\rho_V(V_{\Omega_1}, V_{\Omega_2}) = \frac{\text{Cov}[V_{\Omega_1}, V_{\Omega_2}]}{\sigma_{V_{\Omega_1}} \sigma_{V_{\Omega_2}}} \quad (34)$$

The corresponding minimized estimation variance is equal to:

$$E\left\{(V_{\Omega_1}^* - V_{\Omega_1})^2\right\} = \text{Var}[V_{\Omega_1}] (1 - \rho_V^2) \quad (35)$$

If the two variables have the same expected value and variance, two extreme situations can prevail regarding the correlation coefficient:

- If V_{Ω_1} and V_{Ω_2} are perfectly correlated, then: $\rho_V(V_{\Omega_1}, V_{\Omega_2})=1$ and $V_{\Omega_1}^* = V_{\Omega_2}$.
- If V_{Ω_1} and V_{Ω_2} are not correlated, the information regarding Ω_2 is useless for reducing uncertainty on Ω_1 .

It can be observed that, in the general case, the knowledge of the field in a given subdomain leads to a correction of the expected value and to a reduction of variance of the field or of its average value in other subdomains.

II.4.2. Multivariate linear estimation

The previous method can be extended to the estimation of conditional expectations, variances and covariances of punctual or average values taken respectively by a random field in different points or subdomains of the medium studied, based on a certain number of results of measurements also carried out in different points or subdomains.

Let \mathbf{V} be a vector of dimension p containing the k variables to be estimated and the $p-k$ known variables, defined as:

$$\mathbf{V} = \begin{pmatrix} \mathbf{V}_1 \\ \mathbf{V}_2 \end{pmatrix} \text{ with } \mathbf{V}_1 = \begin{pmatrix} V_1 \\ \cdot \\ \cdot \\ \cdot \\ V_k \end{pmatrix} \text{ and } \mathbf{V}_2 = \begin{pmatrix} V_{k+1} \\ \cdot \\ \cdot \\ \cdot \\ V_p \end{pmatrix} \quad (36)$$

\mathbf{V}_1 is the vector of the variables to be estimated and \mathbf{V}_2 is the vector of the known variables.

Let \mathbf{U} be the vector, also with a dimension p , of the expected values of the variables to be estimated and of the known variables, defined as:

$$\mathbf{U} = \begin{pmatrix} \mathbf{U}_1 \\ \mathbf{U}_2 \end{pmatrix} \text{ with } \mathbf{U}_1 = \begin{pmatrix} \mu_1 \\ \cdot \\ \cdot \\ \cdot \\ \mu_k \end{pmatrix} \text{ and } \mathbf{U}_2 = \begin{pmatrix} \mu_{k+1} \\ \cdot \\ \cdot \\ \cdot \\ \mu_p \end{pmatrix} \quad (37)$$

On the other hand, let \mathbf{K} be the covariance matrix for the set of variables known and to be estimated:

$$\mathbf{K} = \begin{pmatrix} \mathbf{K}_{11} & \mathbf{K}_{12} \\ \mathbf{K}_{21} & \mathbf{K}_{22} \end{pmatrix} \quad (38)$$

where:

\mathbf{K}_{11} submatrix of covariances between the variables associated to the different estimation points or domains, of order k .

\mathbf{K}_{22} submatrix of covariances between the variables associated to the different known points or subdomains, of order $p-k$.

\mathbf{K}_{12} and \mathbf{K}_{21} submatrices of covariances between the different data and the variables associated to the various estimation points or subdomains, respectively of order k and $p-k$. It should be observed that $\mathbf{K}_{21} = \mathbf{K}_{12}^T$.

It is possible to obtain a vector \mathbf{V}_1^* , an estimate of vector \mathbf{V}_1 given that \mathbf{V}_2 is known, the elements of which are linear, unbiased and leading to a minimum estimation variance.

The elements of this vector will be linear combinations of the elements of \mathbf{V}_2 :

$$\mathbf{V}_1^* = \mathbf{A}\mathbf{V}_2 + \mathbf{b} \quad (39)$$

The estimation will be unbiased if:

$$E\left\{\mathbf{V}_1^* - \mathbf{V}_1\right\} = \mathbf{A}\mathbf{U}_2 + \mathbf{b} - \mathbf{U}_1 = 0 \quad (40)$$

The submatrix of the estimation variances will be written as:

$$\mathbf{K}_{11,2} = E\left\{(\mathbf{V}_1^* - \mathbf{V}_1)(\mathbf{V}_1^* - \mathbf{V}_1)^T\right\} \quad (41)$$

that is to say:

$$\mathbf{K}_{11,2} = \mathbf{A}\mathbf{K}_{22}\mathbf{A}^T + \mathbf{K}_{11} - \mathbf{A}\mathbf{K}_{12}^T - \mathbf{K}_{12}\mathbf{A}^T \quad (42)$$

Proceeding again by derivation in order to minimize the elements of this matrix, it can be shown that the optimum coefficients matrix is:

$$\mathbf{A} = \mathbf{K}_{12}\mathbf{K}_{22}^{-1} \quad (43)$$

Combining the previous equations, the vector of the estimated values is obtained as:

$$\mathbf{V}_1^* = \mathbf{U}_1 + \mathbf{K}_{12} \mathbf{K}_{22}^{-1} (\mathbf{V}_2 - \mathbf{U}_2) \quad (44)$$

and the submatrix of minimized estimation variances is equal to:

$$\mathbf{K}_{11,2} = \mathbf{K}_{11} - \mathbf{K}_{12} \mathbf{K}_{22}^{-1} \mathbf{K}_{21} \quad (45)$$

This method is useful to estimate punctual or average values of the random field in subdomains of the medium (for instance, finite elements or sets of these elements) taking into account results obtained through sampling.

II.4.3. Multifield linear estimation

The same technique can be used when data from different random fields corresponding to different properties of interest are available. This is of foremost importance in Geomechanics since it allows estimating critical (primary) properties such as mechanical parameters from (secondary) variables more easily determined such as index properties. In this case, two fields $V(X)$ (primary) and $S(X)$ (secondary) will be defined. Their respective expected value, variance and autocovariance will be estimated from the data together with their *cross-covariance* function understood as:

$$\begin{aligned} C_{VS}(X_1, X_2) &= \text{Cov}[V(X_1), S(X_2)] \\ &= E\{[V(X_1) - \mu_V(X_1)][S(X_2) - \mu_S(X_2)]\} \end{aligned} \quad (46)$$

This function represents the linear correlation that may exist between the primary and secondary fields. It can be obtained from the data but also from correlations established in similar geotechnical conditions.

As in 4.2, \mathbf{V}_1 will be the vector of the (primary) variables to be estimated but \mathbf{V}_2 the vector of the known variables will include some values corresponding to secondary field $S(X)$. Where necessary, the expected values of field $S(X)$ will be introduced and autocovariance will be substituted by cross-covariance in covariance submatrices.

This approach improves considerably the results of the one-field approach whenever the different fields present a good spatial cross-correlation. To avoid numerical problems, cross-covariance coefficient must satisfy the Cauchy-Schwartz inequality; $|\rho_{VS}(h)| \leq \sqrt{\rho_{VV}(h)\rho_{SS}(h)}$ for all h ; (Chiles and Delfiner, 1999 [11]).

II.4.4. Gaussian fields

A particular case of utmost importance is that of the *Gaussian* fields. It should be remembered that a random field is *Gaussian* when each random variable of the field, $V(X)$, has a probability density of the type:

$$f_V(v) = \frac{1}{\sqrt{2\pi}\sigma_V} \exp\left[-\frac{1}{2}\left(\frac{v-\mu_V}{\sigma_V}\right)^2\right] \quad (47)$$

and when the joint probability density of any set of n field variables is defined by the following equation (Mood and Graybill, 1963 [12]):

$$f_{V_1, \dots, V_n}(v_1, \dots, v_n; X_1, \dots, X_n) = \frac{1}{\left| \mathbf{K} \right|^{\frac{1}{2}} (2\pi)^n} e^{-\frac{1}{2}(\mathbf{V}-\boldsymbol{\mu})^T \mathbf{K}^{-1} (\mathbf{V}-\boldsymbol{\mu})} \quad (48)$$

for $-\infty < v_i < +\infty$ and $i = 1, \dots, n$

where \mathbf{V} is the vector of the random variables $V(X_1), V(X_2), \dots, V(X_n)$; $\boldsymbol{\mu}$ is a vector of real values such that $\mu_i = E\{V(X_i)\}$ and \mathbf{K} is the positive definite symmetric covariance matrix of the random variables that contains, in the principal diagonal, the respective variances of the different variables and, outside of the diagonal, the paired covariances.

An interesting property of Gaussian fields is that the linear estimators of minimal variance discussed in the previous paragraphs are exact. In other words, for a vector \mathbf{V} of dimension p presenting a p -Gaussian distribution of expectation vector \mathbf{U} and covariance matrix \mathbf{K} , the conditional distribution of vector \mathbf{V}_1 , of order k , knowing \mathbf{V}_2 is a k -Gaussian distribution of the expectation vector \mathbf{V}_1^* , defined by Eq. (41) and with a covariance matrix given by Eq. (42) (Mood and Graybill, 1963 [12]).

The central limit theorem allows for this type of field to develop naturally when the analyzed phenomenon results from adding the effects of multiple fields. In many cases, there is no particular reason to assume that this happens in the case of the geotechnical variables; however, this type of field can be used as a first approximation of more complex fields.

It should also be remembered that any field can be transformed into a Gaussian field. This transformation is known as *anamorphosis*. It can be performed by the classical *Jacobian* method. Transformation to a Gaussian field through anamorphosis may be necessary to ensure that the covariance matrices involved in the procedure described in 4.2 be positive definite and can be inverted, especially in the case of multiple fields.

II.4.5. Kriging

The technique known as *kriging*, widely used in mining engineering (Matheron, 1965, [10]) consists, as in 4.2, of obtaining linear estimators of minimum variance (*Best Linear Unbiased Estimation* or "BLUE"). However, the technique has some variants that can be of interest and that are briefly discussed in what follows for the case of the point estimation.

II.4.5.1. Simple kriging.

The *simple* kriging is a technique that can be applied when the field expected value $E\{V(X)\}$ is a known function of X (eventually a constant). It consists of obtaining the punctual estimators in the field having null mean, $V(X) - E\{V(X)\}$, rather than in $V(X)$. The elements of the vector \mathbf{V}_1^* of Eq. (36), are then substituted by:

$$V^*(X) - E\{V(X)\} = \sum_{i=1}^n \lambda_i (V_i - E\{V_i\}) \quad (49)$$

where V_i represents the known elements of vector \mathbf{V}_2 and $E\{V_i\}$ the elements corresponding to the expectation vector \mathbf{U}_2 .

Coefficients λ_i and the estimators sought for can be obtained by using equations of section 4.2. The *simple* kriging is in fact rigorously equivalent to the conditional estimation technique brought forward in sections 4.3 and 4.4.

II.4.5.2. Ordinary kriging

When dealing with a stationary field, Eq. (43) of the *simple* kriging method can be expressed as follows:

$$V^*(X) = \sum_{i=1}^n \lambda_i V_i + \left[1 - \sum_{i=1}^n \lambda_i \right] \mu_V \quad (50)$$

where μ_V is the field's constant expected value.

It is possible to find an unbiased linear estimator with minimal variance that requires no knowledge of the mean μ_V , by imposing the condition:

$$\sum_{i=1}^n \lambda_i = 1 \quad (51)$$

The estimation variance:

$$\sigma_E^2(X) = \text{Var}[V(X) - V^*(X)] = E\{(V(X) - V^*(X))^2\} \quad (52)$$

can be written as:

$$\sigma_E^2(X) = \text{Var}[V^*(X)] + \text{Var}[V(X)] - 2 \text{Cov}[V^*(X), V(X)] \quad (53)$$

but:

$$\text{Var}[V^*(X)] = \text{Var}\left[\sum_{i=1}^n \lambda_i V_i\right] = \sum_{i,j=1}^n \lambda_i \lambda_j C_V(X_i, X_j) \quad (54)$$

and:

$$\text{Cov}[V^*(X), V(X)] = \text{Cov}\left[\sum_{i=1}^n \lambda_i V_i, V(X)\right] = \sum_{i=1}^n \lambda_i C_V(X, X_i) \quad (55)$$

Therefore:

$$\sigma_E^2(X) = \text{Var}[V(X)] + \sum_{i=1}^n \sum_{j=1}^n \lambda_i \lambda_j C_V(X_i, X_j) - 2 \sum_{i=1}^n \lambda_i C_V(X, X_i) \quad (56)$$

It is possible to minimize $\sigma_E^2(X)$ respecting the unbiasedness condition by resorting to the technique of Lagrange's multipliers. The following system of linear equations is obtained:

$$\sum_{j=1}^n \lambda_j C_V(X_i, X_j) - v = C_V(X, X_i) \quad i = 1 \text{ to } n \quad (57)$$

Including Eq. (49), there is a total of $n+1$ equations that allow the determination of the n coefficients, λ_j , and of Lagrange's multiplier, v .

The corresponding minimized estimation variance is:

$$\sigma_E^2(X) = \text{Var}[V(X)] + v - \sum_{i=1}^n \lambda_i C_V(X, X_i) \quad (58)$$

The estimator provided by *ordinary* kriging has been said to be more *robust* than that obtained by *simple* kriging. Since it does not require the knowledge of the field's expected value, it can adapt itself better to local variations. However, the fact that the method implies no knowledge of the expected value only constitutes a marginal advantage because this parameter is generally better known than the autocovariance function.

II.4.5.3. Cokriging

A solution to the multifield problem identified in 4.3 can also be obtained resorting to the *simple* and the *ordinary* kriging approaches (Wackernagel, 2003 [13]; Delgado Muñiz, 2017 [14]).

The general expression of the multivariate estimator is defined as follow:

$$V^*(X) = \sum_{i=1}^n \lambda_i V(X_i) + \sum_{j=1}^m \beta_j S(X_j) \quad (59)$$

where the left side of the equation represents the primary property $V(X)$ and the right side the secondary property $S(X)$, λ and β are the influence weights of the primary and secondary properties.

In cokriging, the variance of the estimate is reduced because it implicitly considers the spatial correlation between the two properties (Chiles and Delfiner, 2012). The variance of the estimate is:

$$\sigma_{ECK}^2(X) = \text{Var}[V(X)] + \mu_1 - \sum_{i=1}^n \lambda_i C_V(X_n - X_i) - \sum_{j=1}^m \beta_j C_{VS}(X_m - X_j) \quad (60)$$

where $\text{Var}[V(X)]$ is the variance of the primary variable, C_V y C_{VS} are the primary and cross covariances, μ_1 is a Lagrange multiplier.

II.4.6. Nonparametric estimation of the conditional distribution function

When applying the techniques of linear estimation to the indicator function (Auvinet, 2002 [1]) of a field, it is possible to obtain a non-parametric estimation (i.e. not requiring estimating the expected value, variance or other parameters) of the probability distribution function of the field values at any point. In fact, the linear estimation applied to the indicator function provides the conditional expectation of this function, which, being a binary function in 0 and 1, is equal to the probability:

$$P[V(X) \leq v | \text{data}] = F_{V|data}(v; X) \quad (61)$$

The distribution function can be obtained one point at a time for different values of v . This possibility is quite valuable, particularly when characterizing the field through an expected value and variance is insufficient.

II.5. Simulation of random fields

The *simulation* is the process by which a possible configuration of a random field is generated in a way compatible with its descriptive parameters (*unconditional simulation*) or with these parameters and, furthermore, with the available data (*conditional simulation*). Several realizations or images of the field can thus be generated to allow the appreciation, in particular, of potentially critical extreme values.

The easiest way to simulate a random field consists of considering that such a field is represented by n points X_1, X_2, \dots, X_n where realizations of the set of random variables $V(X_1), V(X_2), \dots, V(X_n)$ should be obtained, with the appropriate field structure in what refers to the expected value and covariance matrix. The simulation is generally carried out on a mesh of points in the domain of interest and it therefore suffices to generate a certain number of jointly distributed random variables. An introduction to this topic is presented below.

II.5.1. General technique

The most common technique to sample at random a representative value of a random variable $V(X)$ with a certain probability distribution function, $F_V(v, X)$ consists of adopting a value v such that:

$$F_V^{-1}(v, X) = u \quad (62)$$

where u is a random number with uniform probability density ranging between 0 and 1 (Mood and Graybill, 1963 [12]). The main algorithms that allow generating random numbers with these characteristics have been presented by Fogli (1980 [15]).

If $V(X_1), V(X_2), \dots, V(X_n)$ is the set of n random variables representative of the field intended to be simulated, and these variables are statistically independent, then their joint density and probability distribution functions can be expressed as:

$$f_{V_1, \dots, V_n}(v_1, \dots, v_n; X_1, \dots, X_n) = \prod_{i=1}^n f_{V_i}(v_i; X_i) \quad (63)$$

$$F_{V_1, \dots, V_n}(v_1, \dots, v_n; X_1, \dots, X_n) = \prod_{i=1}^n F_{V_i}(v_i; X_i) \quad (64)$$

where $f_{V_i}(v_i; X_i)$ and $F_{V_i}(v_i; X_i)$ are, respectively, the marginal (individual) functions of density and probability distribution of $V(X_i)$.

In this case, the random values of each variable can be generated separately and independently by means of the technique described before (Eq. (62)).

For a set of dependent random variables $V(X_1), V(X_2), \dots, V(X_n)$, the joint density and probability distribution functions can be expressed as:

$$f_{V_1, \dots, V_n}(v_1, \dots, v_n; X_1, \dots, X_n) = f_{V_1}(v_1; X_1)f_{V_2}(v_2 | v_1; X_2) \dots f_{V_n}(v_n | v_1, \dots, v_{n-1}; X_n) \quad (65)$$

$$F_{V_1, \dots, V_n}(v_1, \dots, v_n; X_1, \dots, X_n) = F_{V_1}(v_1; X_1)F_{V_2}(v_2 | v_1; X_2) \dots F_{V_n}(v_n | v_1, \dots, v_{n-1}; X_n) \quad (66)$$

where functions $f_{V_i}(v_i | v_1, \dots, v_{i-1}; X_i)$ and $F_{V_i}(v_i | v_1, \dots, v_{i-1}; X_i)$ represent, respectively, the conditional probability density and distribution function of $V(X_i)$ given that $V(X_1) = v_1, V(X_2) = v_2, \dots, V(X_{i-1}) = v_{i-1}$.

Because the random variables are dependent, it is no longer valid to use directly a set of uniformly distributed and independent random numbers to generate the desired values. When the field is of the Gaussian type or it has been transformed by anamorphosis into a Gaussian field, it is possible to use the procedure indicated below.

II.5.2. Unconditional simulation

This type of simulation requires initially the generation of a sequence of *normally distributed independent standard random variables* (with zero mean and unit variance), obtained from two random variables, U_i and U_{i+1} , uniformly distributed between 0 and 1 (Fogli, 1980 [15]):

$$\begin{aligned} Z_i &= \sqrt{-2 \ln(1 - U_i)} \cos(2\pi U_{i+1}) \\ Z_{i+1} &= \sqrt{-2 \ln(1 - U_i)} \sin(2\pi U_{i+1}) \end{aligned} \quad (67)$$

Alternatively, uniformly distributed random numbers can be generated using integrated tools accompanying the computational environment in which the simulation process is implemented.

On the other hand, the correlation matrix, ρ , constituted by elements:

$$\rho_V(X_i, X_j) = \frac{C_V(X_i, X_j)}{\sigma_V(X_i)\sigma_V(X_j)} \quad (68)$$

can be broken down in the product of a lower triangular matrix and its transpose:

$$\mathbf{L}\mathbf{L}^T = \rho \quad (69)$$

This operation, known as *Cholesky's decomposition* (Alabert, 1987 [16]), evidences certain shortcomings: it cannot be carried out when some of the variables $V(X_i)$ are perfectly correlated among themselves; it is difficult to calculate when the number of points in the field is too large; and it tends to generate numerical rounding errors. However, efficient standard algorithms are available for its calculation.

From matrix \mathbf{L} of Eq. (69), it is possible to obtain a *correlated normal standard random field*, as a linear combination of the normal independent standard variables, Z_j :

$$G(X_i) = \sum_{j=1}^i L_{ij} Z_j ; \quad i=1,2,\dots, n \quad (70)$$

Finally, the known values of the mean and the variance are introduced to generate realizations of $V(X_i)$, in order to obtain the field simulation:

$$V(X_i) = \mu_V(X_i) + \sigma_V(X_i) G(X_i) \quad (71)$$

When the random field $V(X)$ has already been simulated, the realization obtained can be used as a starting point for a deterministic analysis. The simulation process can then be repeated as many times as desired to evaluate the variability of the results as part of a *Monte Carlo* analysis.

II.5.3. Conditional simulation

It is now assumed that the random field $V(X)$ has been observed at points X_1, X_2, \dots, X_p and that it will be simulated at points $X_{p+1}, X_{p+2}, \dots, X_{p+n}$. It is intended to generate realizations of $V(X)$ that precisely equal the data at p points and that are random in the remaining $n - p$ points.

The *conditional* simulation of a random field can be directly performed by the method discussed in the previous section, but using conditional expected values, variances and covariances of the available data. Points can be generated one at a time or simultaneously in groups of convenient size. The former approach seems to be the most efficient (Shinozuka, 1996 [17]). The simulated values are then incorporated into the data and new points can be generated.

II.5.4. Conditional simulation by copulas

In copula-based random field descriptions, the multivariate copula model accounts for the multivariate dependence of the random field explicitly and is parametrized through bivariate spatial copulas.

Consider the conditioning of the random field $V(X)$ at N locations by the set α consisting of n observations. This task can be completed using the sequential simulation approach. In terms of copulas, the simulation process is formulated as follows (Vázquez-Guillén and Auvinet, 2014 [3]):

$$F_v(X_i; v_i) = C_{x|\alpha}(u_i = F_v(V(X_i) \leq v(X_i)) | u_\alpha = F_v(v(X_\alpha))), \alpha = 1, \dots, n \quad (72)$$

$$F_v(X_2; v_2) = C_{X|a}(u_2 = F_v(V(X_2) \leq v(X_2)) | u_\alpha = F_v(v(X_\alpha))), \alpha = 1, \dots, n+1 \quad (73)$$

$$F_v(X_3; v_3) = C_{X|a}(u_3 = F_v(V(X_3) \leq v(X_3)) | u_\alpha = F_v(v(X_\alpha))), \alpha = 1, \dots, n+2 \quad (74)$$

$$F_v(X_N; v_N) = C_{X|a}(u_N = F_v(V(X_N) \leq v(X_1)) | u_\alpha = F_v(v(X_\alpha))), \alpha = 1, \dots, n+N-1 \quad (75)$$

where $F_V(\cdot)$ is the first-order distribution function and $C_{X|a}(\cdot)$ is the conditional copula.

The simulation process is restricted to local neighborhoods X_i , for $i=1, \dots, n$ closest to the node to be simulated. This decision is supported by the fact that further away conditioning data is “screened” by the information content of nearest data. The values u_α , include both original data (prior distribution) and previously simulated nodes. The simulation process can be performed by visiting unsampled locations at random over a mesh. After visiting all nodes of the mesh, the process is completed (Vázquez-Guillén and Auvinet, 2015 [6]).

References for Appendix II

- [1] Auvinet, G., (2002). “Uncertainty in Geotechnical Engineering/Icertidumbre en Geotecnia”, Sixteenth Nabor Carrillo Lecture/Decimosexto Conferencia Nabor Carrillo. (English/Español), Sociedad Mexicana de Mecánica de Suelos, Mexico, 131p., ISBN: 968-5350 10-8.
- [2] Deutsch, C. and Journel, A., (1992). GSLIB Geostatistical software library and user's guide: Oxford University Press, New York, 340p.
- [3] Vázquez, F. y Auvinet, G., (2014). “Simulación de campos aleatorios con dependencia no multigaussiana empleando cópulas”, Ingeniería, Investigación y Tecnología, FI-UNAM, Vol. XV, Núm 4, Mexico.
- [4] Nelsen, R.B. (2006). “An introduction to copulas”, Springer-Verlag, New York, 2nd Edition, pp. 269.
- [5] Bárdossy, A. (2006). “Copula-based geostatistical models for groundwater quality parameters”, Water Resour. Res., 42, W11416 (1 of 12).
- [6] Vásquez-Guillén, F. y Auvinet, G., (2015). “Simulación de campos aleatorios espacio-temporales utilizando un filtro de Kalman modificado”, Ingeniería, Investigación y Tecnología, FI-UNAM, Vol. XVI, Núm 1, 1-12, Mexico.
- [7] Vázquez-Guillén, F. and Auvinet, G. (2017). “Identification of hydraulic conductivities via ensemble Kalman filtering with transformed data considering the risk of systematic bias”, Geofísica Internacional, 56(4), pp. 317-333.
- [8] Papoulis, A., (1985). Probability, Random variables and Stochastic Processes, McGrawHill, USA.
- [9] Krige, D. G., (1962). “Statistical application in mine valuation”, J. Institute Mine Survey, South Africa
- [10] Matheron, G., (1965). “Les variables généralisées et leur estimation”, Masson et Cie, France.
- [11] Chiles, J.P. and Delfiner, P., (1999). “Geostatistics, Modeling spatial uncertainty”, John Wiley and Sons, INC.
- [12] Mood, A. M. and Graybill, F.A., (1963). “Introduction to the Theory of Statistics”, Mc Graw-Hill Book Company, Inc., New York, USA.
- [13] Wackernagel, H., (2003). Multivariate Geostatistics. An Introduction with Applications. Springer, 3rd Edition, Berlin, Germany, 387p.
- [14] Delgado Muñiz, M., (2017). “Análisis geoestadístico multivariante de las propiedades geotécnicas del subsuelo lacustre del valle de México”, Tesis de maestría, Programa de Maestría y Doctorado en Ingeniería, Ingeniería Civil, Geotecnia, UNAM, Ciudad de México, Mexico.
- [15] Fogli, M., (1980). “L’approche de Monte Carlo dans les problèmes de sécurité: Application à l’estimation du risque de ruine des poutres hyperstatiques en béton armé soumises à des actions aléatoires statiques», Thèse de Docteur Ingénieur, INSA, Lyon, France, 217 p.
- [16] Alabert, F., (1987). “The practice of fast conditional simulations through the LU decomposition of the covariance matrix”. Mathematical Geology, Vol. 19, N° 5, pp. 369-386.
- [17] Shinozuka, M., (1996). “Equivalence between Kriging and CPDF Methods for conditional simulation”. Journal of Engineering Mechanics, ASCE, pp 530-538.

Appendix III. Reduction of variance in a 1D random field with exponential autocorrelation coefficient

III.1. Exponential autocorrelation coefficient

A one-dimensional stationary random field $V(X)$, where X is an abscissa in a one-dimensional domain is said to present an exponential autocorrelation coefficient function (normalized autocovariance), ρ , when for any interval such as $X_1-X_2=\tau$, this function can be expressed as:

$$\rho = e^{\frac{-\tau}{a}}; \tau > 0 \quad (1)$$

where a is the area below the graph of the autocorrelation function:

$$\int_0^\infty e^{\frac{-\tau}{a}} d\tau = \left[\frac{e^{\frac{-\tau}{a}}}{\frac{-1}{a}} \right]_0^\infty = a \quad (2)$$

Distance $\delta=2a$ is known as the *correlation distance*.

III.2. Variance of the average value of a random field in an interval with length L

Taking into account Eq. (25) of Appendix II:

$$\text{Var}[V_L] = \text{Var}[V] \frac{1}{L^2} \int_0^L \int_0^L e^{\frac{|y-x|}{a}} dx dy = 2\text{Var}[V] \frac{1}{L^2} \int_0^L \int_0^y e^{\frac{(y-x)}{a}} dx dy \quad (3)$$

$$\text{Var}[V_L] = 2\text{Var}[V] \frac{1}{L^2} \int_0^L e^{\frac{y}{a}} dy \int_0^y e^{\frac{x}{a}} dx \quad (4)$$

$$\text{Var}[V_L] = 2\text{Var}[V] \frac{1}{L^2} \int_0^L e^{\frac{-y}{a}} \left(\frac{e^{\frac{x}{a}}}{\frac{1}{a}} - a \right)_0^y dy \quad (5)$$

$$\text{Var}[V_L] = 2a\text{Var}[V] \frac{1}{L^2} \int_0^L \left(1 - e^{\frac{-y}{a}} \right) dy = 2a\text{Var}[V] \frac{1}{L^2} \left[L - \left(\frac{e^{\frac{-y}{a}}}{\frac{1}{a}} \right)_0^L \right] \quad (6)$$

$$\text{Var}[V_L] = 2a\text{Var}[V] \frac{1}{L^2} \left[L + \frac{e^{-\frac{L}{a}}}{\frac{1}{a}} - a \right] = \frac{2a^2}{L^2} \text{Var}[V] \left[\frac{L}{a} + e^{-\frac{L}{a}} - 1 \right] \quad (7)$$

III.3. Covariance between average values defined on two non-overlapping segments

The average values of the field are defined in two non-overlapping intervals $(x_1, x_2), (y_1, y_2)$, with length L_1 and L_2 respectively and with $(y_1 > x_2)$. The autocorrelation coefficient (normalized autocovariance) is:

$$\rho = e^{-\frac{\tau}{a}}; \tau > 0 \quad (8)$$

Calling V_{L1} the average value of the field in interval (x_1, x_2) and V_{L2} the average value in interval (y_1, y_2) :

$$\text{Cov}[V_{L1}, V_{L2}] = \text{Var}[V] \frac{1}{L_1 L_2} \int_{y_1}^{y_2} \int_{x_1}^{x_2} e^{-\frac{|y-x|}{a}} dx dy \quad (9)$$

$$\text{Cov}[V_{L1}, V_{L2}] = \text{Var}[V] \frac{1}{L_1 L_2} \int_{y_1}^{y_2} e^{\frac{y}{a}} dy \int_{x_1}^{x_2} e^{\frac{x}{a}} dx \quad (10)$$

$$\text{Cov}[V_{L1}, V_{L2}] = \text{Var}[V] \frac{1}{L_1 L_2} \left[\frac{e^{\frac{-y}{a}}}{\frac{-1}{a}} \right]_{y_1}^{y_2} \left[\frac{e^{\frac{-x}{a}}}{\frac{1}{a}} \right]_{x_1}^{x_2} \quad (11)$$

$$\text{Cov}[V_{L1}, V_{L2}] = \text{Var}[V] \frac{a^2}{L_1 L_2} \left[e^{\frac{-y_1}{a}} - e^{\frac{-y_2}{a}} \right] \left[e^{\frac{x_2}{a}} - e^{\frac{x_1}{a}} \right] \quad (12)$$

This page intentionally left blank

Plenary Lecture ISSMGE President

This page intentionally left blank

Plenary Lecture ISSMGE President



C. W. W. NG

Dr Charles W.W. Ng is currently the CLP Holdings Professor of Sustainability, Chair Professor in the Department of Civil and Environmental Engineering and Associate Vice-President for Research and Development at the Hong Kong University of Science and Technology (HKUST). He is the President of International Society for Soil Mechanics and Geotechnical Engineering (2017-2021).

Professor Ng earned his PhD degree from the University of Bristol, UK in 1993. After carrying out a period of post-doctoral research at the University of Cambridge between 1993 and 1995, he returned to Hong Kong and joined HKUST as Assistant Professor in 1995 and rose through the ranks to become Chair Professor in 2011.

Professor Ng was elected an Overseas Fellow from Churchill College, Cambridge University, in 2005 and was also elected as a Changjiang Scholar (Chair Professor in Geotechnical Engineering) by the Ministry of Education in China in 2010. He is Fellow of the Institution of Civil Engineers, the American Society of Civil Engineers, the Hong Kong Institution of Engineers and the Hong Kong Academy of Engineering Sciences. Currently, he is an Associate Editor of the Canadian Geotechnical Journal.

Professor Ng has published some 320 SCI journal articles and 250 conference papers and delivered more than 50 keynotes and state-of-the-art reports in 6 continents. He is the main author of two reference books: (i) *Soil-structure Engineering of Deep Foundations, Excavations and Tunnels* by Thomas Telford, (ii) *Advanced Unsaturated Soil Mechanics and Engineering*, and (iii) *Plant-Soil slope Interaction* by Taylor & Francis. He has received many awards including the 2017 Telford Premium Prize from the Institution of Civil Engineers, UK, the Henry Adams Award from the Institution of Structural Engineers, UK, the first Tan Swan Beng Award from the Southeast Asian Geotechnical Society, and the R. M. Quigley Award from the Canadian Geotechnical Society three times for his three best papers published in 2007, 2012 & 2016.

Interplay Between Ecology and Unsaturated Soil Mechanics for Bioengineered Landfill Covers and Slopes

C. W. W. NG^a, J. J. NI^{a,1} and C. ZHOU^b

^a*Department of Civil and Environmental Engineering, Hong Kong University of Science and Technology (HKUST), Hong Kong SAR*

^b*Department of Civil and Environmental Engineering, Hong Kong Polytechnic University, Hong Kong SAR*

Abstract. The negative impact of climate change calls for additional sustainable and environmentally friendly techniques to be developed for the improvement of the engineering performance of civil infrastructure, such as landfill covers and slopes. Bioengineering using vegetation can be considered and promoted as a low-cost, aesthetically pleasant solution for greening landfill covers and improving shallow slope stabilisation. The mechanical effects of vegetation as soil reinforcement have been extensively studied, but the hydrological effects of vegetation on soil shear strength and water permeability are unclear. This study therefore presents an interdisciplinary research programme consisting of laboratory and field tests and centrifuge modelling. The programme explores the hydrological effects of plants on the performance of final landfill covers and slope stabilisation. Results show that suction induced by plants under a novel vegetated three-layer landfill cover is preserved better than that under a bare cover even after an extreme rainfall event with a return period of greater than 1000 years in Hong Kong. The laboratory tests and field trials demonstrate that the vegetated three-layer landfill cover system using recycled concrete can effectively minimise percolation at humid climate even without a geomembrane. Novel artificial root systems are developed for the centrifuge model tests. Heart-shaped roots have stronger pull-out resistance and higher preserved suction (hence higher soil shear strength) compared with tap- or plate-shaped roots. The heart-shaped root architecture is thus the most effective type in producing stabilisation effects on slopes.

Keywords. Soil bioengineering, vegetation, matric suction, landfill cover, slope stability

1. Introduction

Bioengineering using vegetation can potentially offer an environmentally friendly, cost-effective and aesthetically pleasant solution for greening landfill covers and improving shallow slope stabilisation. Although vegetation has been used in slope protection for decades, its purpose has mainly been aesthetic [1] probably because the mechanisms of soil–plant–atmosphere interaction have not been fully understood. Thus, the current

¹ J. J. NI, Corresponding author, Department of Civil and Environmental Engineering, Hong Kong University of Science and Technology; E-mail: cenijj@ust.hk.

design practice does not scientifically integrate the engineering function of plant roots into the analysis and design of landfill covers and slope stability.

Plant roots can provide mechanical reinforcement to slope stabilisation [2, 3]. The mechanical effects of root reinforcement have been extensively quantified experimentally and theoretically in the past decades [2, 4, 5]. By contrast, the hydrological effects of plants have received insufficient attention, as stated by Ng [6]. These hydrological effects refer to the increase in soil shear strength and the reduction in water permeability caused by enhanced soil suction [7]. The key to using plants for these purposes is to understand the fundamentals of unsaturated soil mechanics and soil–plant–atmosphere interactions, which are interdisciplinary subjects involving atmosphere science, soil science, botany, ecological and geotechnical engineering.

In this study, an integrated and complementary research approach is reported to investigate plant hydrological effects on the performance of final landfill covers and the stabilisation of shallow soil slopes. Firstly, a series of laboratory column tests was conducted to quantify transpiration-induced soil matric suction in a novel vegetated three-layer landfill cover using recycled crushed concrete without the use of a geomembrane. Two plant species commonly found in Hong Kong were studied. Secondly, a full-scale field trial was performed to investigate the influence of vegetation on the performance of the novel vegetated three-layer landfill cover for two years. Finally, novel artificial model root systems were developed for geotechnical centrifuge tests to study the combined mechanical and hydrological effects of different root architectures on hydrology, slope stability and failure mechanisms. The influence of root architectures on slope deformation and failure mechanism was identified. Additional details of the laboratory, field and centrifuge model tests and findings were given by Ng et al. [7].

2. Fundamentals of unsaturated soil mechanics

Relevant theories of unsaturated soil mechanics are introduced to improve our understanding of soil–plant–atmosphere interaction. For simplicity, the shear strength of unsaturated soil, τ_f , may be expressed in terms of water content and soil matric suction as follows [8]:

$$\tau_f = c' + (\sigma_n - u_a) \tan \phi' + (u_a - u_w) \left[(\tan \phi') \left(\frac{\theta - \theta_r}{\theta_s - \theta_r} \right) \right] \quad (1)$$

where c' is the effective cohesion; σ_n is the normal stress; u_a and u_w are the pore–air pressure and pore–water pressure, respectively; ϕ' is the effective friction angle; θ is the volumetric water content; θ_s is the saturated volumetric water content; θ_r is the residual water content. The difference between u_a and u_w (i.e., $u_a - u_w$) is called matric suction. Advanced theories, such as effects of state-dependent dilatancy on the shear strength of unsaturated soil, were provided by Chiu and Ng [9], Ng and Menzies [10] and many others. According to Eq. (1), plant-induced matric suction would increase soil shear strength due to a reduction in water content (and an increase in soil matric suction). The laboratory findings of Ng and Zhou [11] showed that matric suction can increase the tendency of soil dilation, thereby improving soil shear strength.

Unlike water permeability in saturated soils, that in unsaturated soils not only depends on the void ratio (e) but is also governed by the degree of saturation or the water

content, which in turn affects matric suction in the soils. The relationship between water permeability and matric suction can be expressed as follows [12]:

$$k(\psi) = k_s \left[\frac{\int_{\ln(\psi)}^b \frac{\theta(e^y) - \theta(\psi)}{e^y} \theta'(e^y) dy}{\int_{\ln(\psi_{ave})}^b \frac{\theta(e^y) - \theta_s}{e^y} \theta'(e^y) dy} \right] \quad (2)$$

where ψ is the matric suction; $b = \ln(10^6)$; k_s is the saturated water permeability; y is a dummy variable for the integration of ψ ; θ' is the first derivative of function θ . Water permeability generally reduces with increasing matric suction. Given that pore air is not conducive to liquid water movement in unsaturated soils, an increase in suction (i.e., a reduction in water content) leads to a decrease in water permeability. Eqs. (1) and (2) show that plant-induced suction not only increases soil shear strength but also reduces water permeability, thereby decreasing rainfall infiltration and hence potentially helping preserve a large amount of soil suction in unsaturated landfill covers and soil slopes. The hydrological effects of plant root–water uptake was not fully recognised until comprehensive research was conducted in the recent few years (e.g., Ng et al. [13, 14, 10]; Ni et al. [15, 16, 17]; Ng [8]).

3. Hydrological effects of vegetation on matric suction in landfill covers

To improve the effectiveness of a traditional landfill cover with capillary barrier effects (CCBE) in humid regions, Ng et al. [18] proposed an all-weather three-layer landfill cover system comprising a fine-grained layer underlying the traditional two-layer CCBE. Recycled construction waste was also proposed as cover materials for landfills to reduce cost and achieve environmental sustainability [19, 20]. The new three-layer landfill cover was vegetated with plants. In this study, the effects of plant roots on the hydrological performance of the three-layer landfill cover system during drying and wetting were studied.

One-dimensional soil column tests were conducted in a plant room at Hong Kong University of Science and Technology (HKUST) to quantify the effects of evapotranspiration (ET, which is the sum of soil evaporation and plant transpiration) on suction in the novel landfill covers in this study. Three columns were used, each with an inner diameter of 300 mm and a height of 1500 mm (Figure 1). Each column was compacted with completely decomposed granite (CDG), fine recycled concrete aggregate (FRC) and coarse recycled concrete aggregate (CRC) overlying completely decomposed volcanic rocks (CDV). The selected grass species (*Cynodon dactylon*, G) and shrub species (*Schefflera arboricola*, S) are native to southern China, including Hong Kong [20]. Bare soil (B) was used as reference. All the three columns were subjected to daily irrigation with a constant amount of water of 200 mL per day for 4 months. After drying, 48 h ponding with a constant water head of 100 mm (equivalent to a rainfall of more than a 1000-year return period in Hong Kong; [21]) was applied. Soil matric suction was measured continuously during the drying and wetting periods.

A three-dimensional full-scale test was conducted in the Xiaping landfill site in Shenzhen, China to evaluate the field performance of the novel three-layer cover system that uses recycled crushed concrete without the use of a geomembrane (Figure 2; [19]). The field test plot was located in a humid subtropical climate region with approximately

80% of rainfall occurring between May and September. Unsieved CDG and CRC were used for the top and intermediate layers, respectively, and sieved CDG was used as the lowest layer. One section was transplanted with *C. dactylon*, whereas the other section was left bare (Figure 2). Water percolation was measured for two years (June 2016 to June 2018) by using a lysimeter installed at the bottom of the landfill cover.

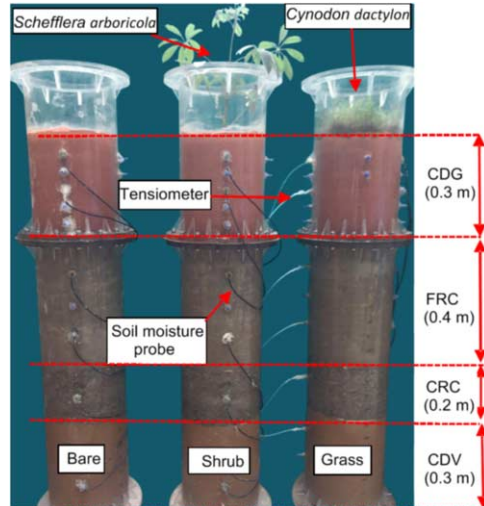


Figure 1. Overview of the three columns.



Figure 2. Front view of the Xiapeng landfill site in Shenzhen, China.

3.1. ET-induced soil matric suction

Figure 3 shows the laboratory test results and compares the suction response under the bare and vegetated three-layer landfill covers. Suction under the vegetated covers was up to 95% higher than that under the bare cover due to ET before ponding. Compared with grass, shrub induced an additional 25%–30% suction in the FRC and CRC layers. After 48 h of ponding, suction in the top CDG and FRC layers was reduced to nearly zero. For the bare cover, suction in the bottom layer of CDV decreased from 52 kPa to 3 kPa during ponding. Percolation was observed under the bare cover, with a total of 35 g

of water, which was equivalent to 0.5 mm water depth in the column. By contrast, for the vegetated covers, large amounts of suction (52 kPa for the grass and 57 kPa for the shrub cover) were maintained in the bottom layer of CDV. According to a comparison of the two vegetated cover systems, suction maintained under the cover with shrub in the FRC, CRC and bottom CDV layers was higher than that under the cover with grass by 2–6, 6 and 5 kPa, respectively. No percolation was observed under the covers with shrub and grass. Therefore, the vegetated three-layer cover system using recycled concrete aggregate can effectively minimise water infiltration under extreme rainfall events (more than 1000-year return period).

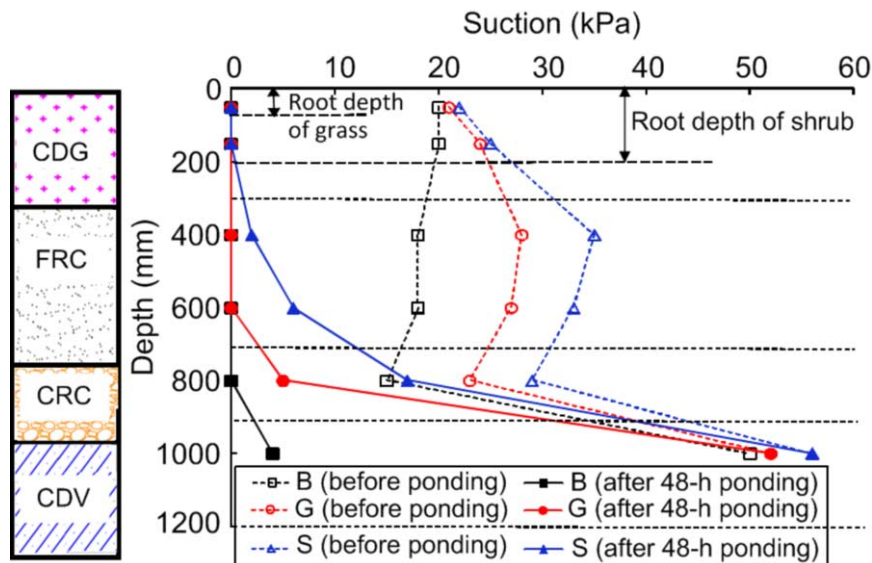


Figure 3. Suction distributions before and after ponding.

3.2. Root effects on water percolation in vegetated landfill covers

Figure 4 shows the cumulative percolation in the bare and grass-covered three-layer landfill covers in Shenzhen, China, from June 2016 to June 2018. The lines correspond to cumulative percolation at three different locations in the slope (i.e., crest, middle, toe). The cumulative rainfall depth of about 4900 mm for two years is also provided in the figure for reference. At the end of the monitoring period, percolation results were approximately 47 and 37 mm for the bare and grass-covered landfill covers, respectively. The difference was likely because of the presence of grass roots, which induced higher soil suction and hence reduced water permeability [7], thereby leading to decreased percolation. The cumulative percolation amount in the bare (47 mm) and grass-covered (37 mm) three-layer landfill covers met the recommended design criterion of 60 mm for two years [22]. These results demonstrated the effectiveness of grass in reducing excessive water percolation in the novel three-layer landfill cover system, which uses recycled crushed concrete and does not have a geomembrane in humid climates.

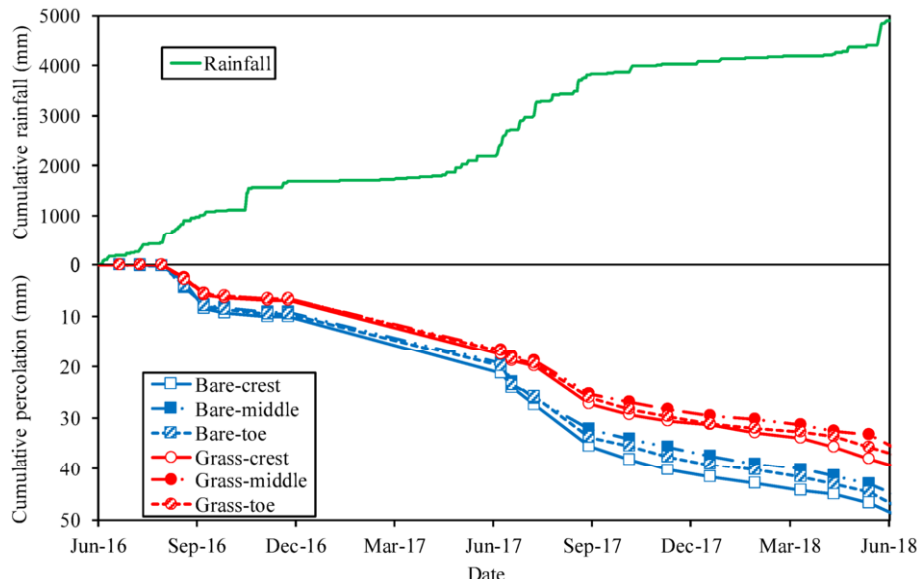


Figure 4. Cumulative percolation in the bare and grass covered three-layer landfill cover system.

4. Hydromechanical effects of plant roots on slope stability and failure mechanisms

Although the mechanical effects of plant roots on slope stability have been reported [4, 23], the combined hydromechanical effects remain unclear. Therefore, novel artificial root systems were developed for geotechnical centrifuge model tests to study the combined mechanical and hydrological effects of different root architectures on hydrology, slope stability and failure mechanisms [24, 25, 7, 26]. All dimensions reported in this section are in prototype scale unless stated otherwise.

4.1. Principle and properties of the novel root model

Figure 5 shows the artificial root models of the three different architectures (tap, heart and plate) created by Ng et al. [24]. They were developed on the basis of the idealisation and simplification of real roots retrieved from three species that are commonly used for slope rehabilitation and ecological restoration in tropical and subtropical regions, namely, *Schefflera heptaphylla*, *Rhodomyrtus tomentosa* and *Melastoma sanguineum* [27]. These artificial root models are made of a porous material called cellulose acetate (CA), whose tensile strength and elastic modulus are fairly close to those typically identified in real roots [28]. In the design of Ng et al. [24], these root models connect with a vacuum system, which includes a vacuum chamber that is partially filled with de-aired water. Through the vacuum source connected to the chamber, different vacuum pressures can be applied to the CA; hence, different vacuum pressures up to -100 kPa can be induced in the water reservoir. Given that the CA is in contact with soil, any applied vacuum (and hence reduction in total head inside the root model) would enable

water to flow from the soil to the chamber through the filter. The decrease in soil moisture would then induce soil suction. Leung et al. [26] showed that the distribution of root area ratio with root depth is reasonably captured by the three root models, given the natural variability of plants in fields. Additional details of the test results and interpretation can be found in Ng et al. [7].

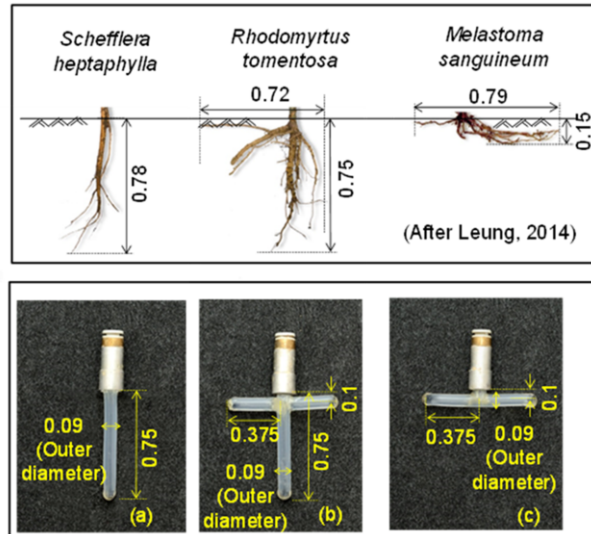


Figure 5. Idealisation and simplification of plant roots with different root architectures (unit: m; converted to prototype scale).

4.2. Root architecture effects on pore water pressure after rainfall

Figure 6 shows a typical centrifuge model setup. Three centrifuge tests were conducted to compare the contributions of three different root architectures, namely, tap, heart and plate, to the hydrology and stability of 45° model slopes made of CDG. Each model slope was supported by 15 artificial roots and subjected to a five-day simulated transpiration by the root system, followed by an intense 8 h rainfall event with a constant intensity of 70 mm/h (equivalent to a rainfall of 1000-year return period in Hong Kong; [21]). Six pore pressure transducers were installed to monitor the suction (negative pore water pressure, PWP) in each slope. All tests were performed at 15 g in the geotechnical centrifuge facility at HKUST. The soil properties, model setup, instrumentation and test procedures are detailed in Leung et al. [26] and Ng et al. [7].

Figure 7 compares the measured PWP profiles of the three model slopes with different root architectures during rainfall. Before rainfall, suction within the depths of the tap- and heart-shaped roots increased substantially during the transpiration process. The heart-shaped root could induce higher suction because it had two branches. For the plate-shaped roots, which did not have any taproot component, suction was noticeable only at a depth of 0.3 m. After a 2 h rain with a constant intensity of 70 mm/h (equivalent to a return period of 10 years), suction at all depths in all types of roots was reduced as expected. In the case of the heart-shaped roots, slightly higher suctions of 2–3 kPa were

retained within the root depth. As the rainfall continued for another 6 h with the same intensity (equivalent to a return period of 1,000 years), a positive PWP of approximately 2 kPa resulted within the root depth. However, the plate-shaped roots showed the highest positive PWP amongst the three root types. This finding suggests that any transpiration performed by this type of root does not quite effectively help reduce the PWP below the root depth under extreme rainfall.

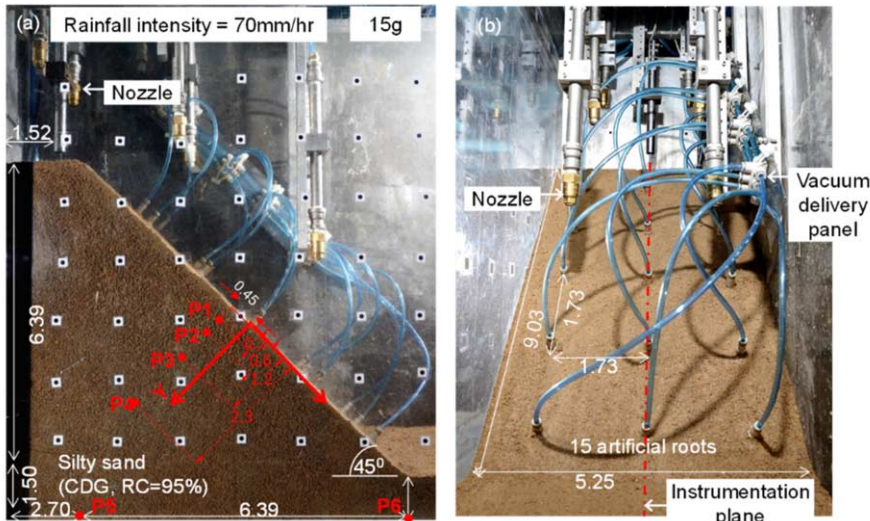


Figure 6. (a) Elevation and (b) side views of the centrifuge model package and instrumentation (all dimensions are in metres and in prototype scale).

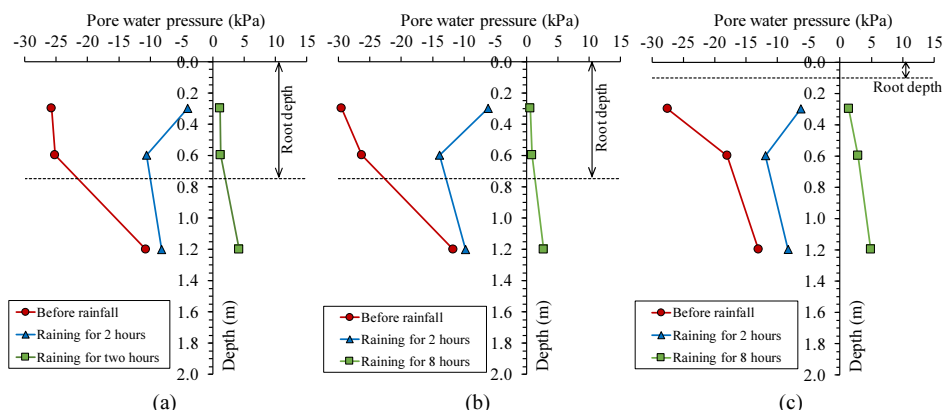


Figure 7. Distribution of measured and computed pore water pressure along various depths before and after rainfall in the slope models supported by (a) tap-, (b) heart- and (c) plate-shaped roots.

4.3. Effects of root architecture on pull-out resistance

Apart from hydrological reinforcement via plant transpiration, the pull-out resistance of plant root systems contributes substantially to the mechanical reinforcement of slopes

[29, 30]. Figure 8 compares the relationships between pull-out force and displacement of the tap-, heart- and plate-shaped architectures. All pull-out tests were conducted after 8 h of rainfall, when the soil was saturated (Figure 7). After peaking, the pull-out force in all three cases decreased as the soil–root contact area reduced continuously during the pull-out process. The peak resistance of the heart-shaped root (3.9 kN) was slightly higher than that of the tap-shaped root (3.5 kN). Moreover, the postpeak behaviour of the former architecture was more brittle, given that less pull-out displacement was required to mobilise the same amount of resistance in the former than in the latter. Given the similar positive PWP induced after 8 h of rainfall (Figs. 7(a) and (b)), the difference in pull-out behaviour between these two architectures was primarily attributed to the mechanical reinforcement given by the two branches of the heart-shaped root model. By contrast, the plate-shaped root architecture was not effective against pull-out force. This is because (i) the peak pull-out resistance (1.2 kPa) was three to four times lower and (ii) the postpeak load displacement response was much more brittle than those of the two former architectures. The major reason was that for this root architecture, the two horizontal branches located at much shallower depths failed to provide considerable pull-out resistance. The heart-shaped root architecture therefore had the highest pull-out resistance due to its multiple branching.

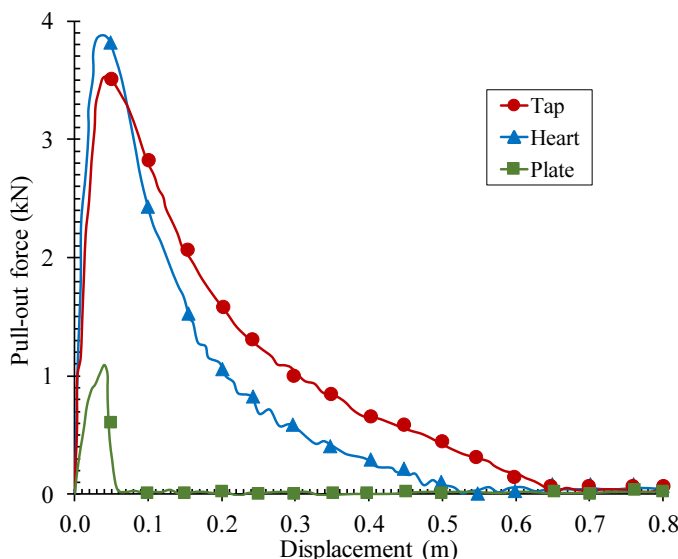


Figure 8. Comparison of the pull-out behaviour of tap-, heart- and plate-shaped root models [31].

4.4. Effects of root architecture on slope stability and failure mechanisms

On the basis of the measured PWP response (Figure 7) and pull-out resistance (Figure 8), the combined hydromechanical effects of the plant roots on slope stability and failure mechanisms were studied. In accordance with the back-analysed PWP responses, slope stability analysis was conducted using SLOPE/W [32] to determine the factor of safety (FOS) in each case. The artificial roots were modelled as a beam element to capture the elastic axial and bending responses [25, 7]. The computed FOS results are shown in

Figure 9. Before transpiration, the FOS was similar for the three slopes and exceeded 1.0 (i.e., the slopes were stable.). When suction was created by simulating transpiration, the FOS of each slope increased but not substantially (less than 4%) because transpiration affected mainly the PWP in the top 1.2 m of each slope. After the 8 h rain, the FOS of the three slopes dropped significantly, following a reduction in PWP upon infiltration. Despite the reduction in FOS, all slopes remained stable, as observed in the model tests. The FOS values of the slope supported by the heart-shaped roots were 16% and 28% higher than those of slopes supported by the tap- and plate-shaped roots, respectively. The greater stability provided by the heart-shaped roots came from the substantial suction preserved after rainfall and their higher mechanical pull-out resistance compared with that of the two other root architectures (Figs. 7 and 8). If the transpiration effects before the rainfall event were ignored, then the values of FOS after rainfall in all the cases would decrease below 1.0. Regardless of the root architecture, neglecting the effects of transpiration on slope stability resulted in a significant underestimation of FOS of up to 50%.

Two more centrifuge tests were conducted for steeper model slopes (i.e., 60°) vegetated with tap- and heart-shaped root models to study the role of root architecture in the slope failure mechanism. The two slopes were continuously subjected to an 8 h extreme rainfall event with a constant intensity of 70 mm/h (equivalent to a rainfall with a return period of 1000 years in Hong Kong) until failure. A comparison of the postfailure geometries between the two slopes in Figure 10 suggested that a shallower slip was formed and a smaller volume of soil failed when the slope was reinforced with heart-shaped roots in comparison with the tap-rooted slope. The runout distance from the heart-shaped slope toe was approximately 9% (4.3 m versus 4.7 m) shorter than that from the tap-shaped one, suggesting that the heart-shaped roots were more effective for stabilising slopes and reducing runout distance in comparison with the tap- and plate-shaped roots.

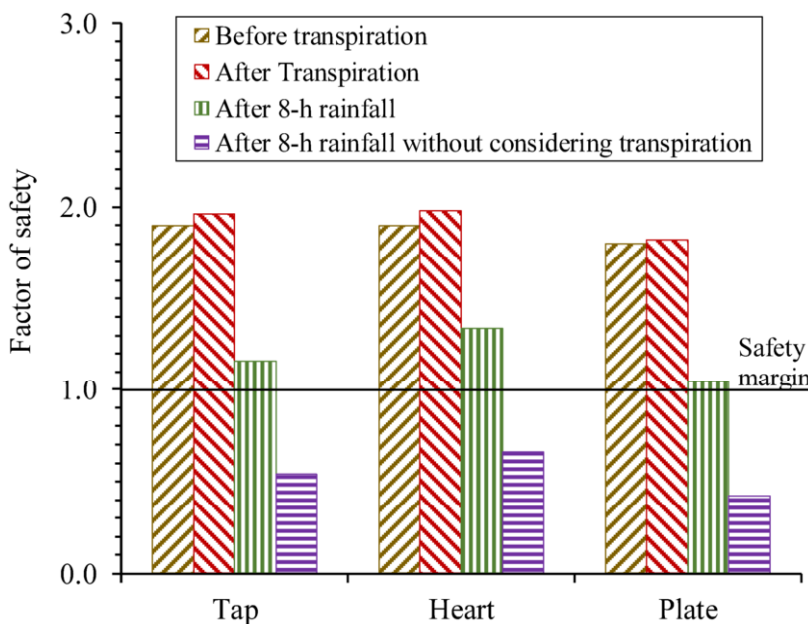


Figure 9. FOS of slopes supported by different root architectures.

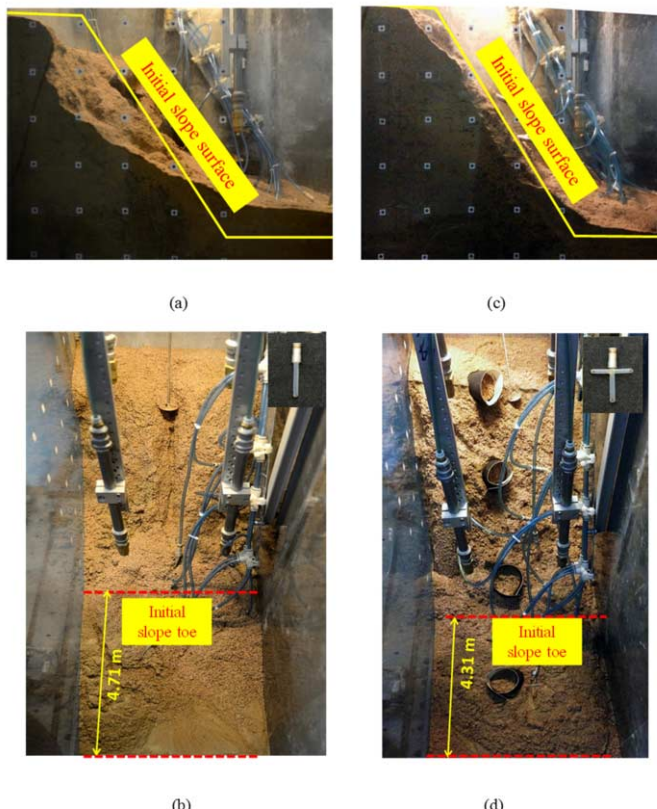


Figure 10. (a) Side view and (b) plan view of a 60° steep slope reinforced by tap-shaped roots; (c) side view and (d) plan view of a 60° steep slope reinforced by heart-shaped roots.

5. Conclusions

Sustainable and ecologically bioengineered landfill covers and slopes that use plants were studied through an interdisciplinary research programme. Three different plant species were studied. The species included tree (*S. heptaphylla*), shrub (*S. arboricola*) and grass species (*C. dactylon*) native to southern China. After 48 h of ponding (equivalent to a rainfall with a return period greater than 1000 years in Hong Kong), suction maintained under the novel vegetated three-layer landfill covers was higher than that under the bare cover. The shrub was more effective than the grass in preserving soil matric suction after intense rainfall. With the presence of plant roots, percolation in vegetated landfill covers was decreased significantly. Therefore, the vegetated three-layer landfill cover system, which uses recycled concrete and does not have a geomembrane, can effectively minimise infiltration and percolation in humid climates.

Novel artificial root systems with different idealised root architectures were developed to study the combined hydrological and mechanical effects of plant roots on slope stability in centrifuge model tests. The centrifuge experiments were conducted in the geotechnical centrifuge facility of HKUST. Findings showed that the heart-shaped roots were more effective in providing stabilisation effects in that they preserved higher

suction (hence higher soil shear strength and lower water permeability) and exhibited stronger pull-out resistance compared with the two other root types during rainfall due to multiple branching. The FOS was greatly improved (up to 50%) when plant hydrological effects were considered. Therefore, vegetation should be an excellent alternative for developing sustainable and ecologically engineered landfill covers and slopes around the world.

Acknowledgements

The authors acknowledge Research Grant No. T22-603/15N funded by the Theme-based Research Scheme and Research Grant No. AoE/E-603/18 awarded by the Areas of Excellence (AoE) Scheme of the Hong Kong Research Grants Council of the Government of Hong Kong SAR.

References

- [1] N.J. Coppin, I.G. Richards, Use of Vegetation in Civil Engineering. Construction Industry Research and Information Association/Butterworths, London, UK, 1990.
- [2] T.H. Wu, W.P. McKinnell, D.N. Swanston, Strength of tree roots and landslides on Prince of Wales Island, Alaska, *Canadian Geotechnical Journal* **16** (1979), 19–33.
- [3] A. Stokes, C. Atger, A.G. Bengough, T. Fourcaud, R.C. Sidle, Desirable plant root traits for protecting natural and engineered slopes against landslides, *Plant and Soil* **324** (2009), 1–30.
- [4] N. Pollen, A. Simon, Estimating the mechanical effects of riparian vegetation on stream bank stability using a fiber bundle model, *Water Resources Research* **41** (2005), W07025.
- [5] D. Boldrin, A.K. Leung, A.G. Bengough, Root biomechanical properties during establishment of woody perennials, *Ecological Engineering* **109** (2017), 192–206.
- [6] C.W.W. Ng, Atmosphere-plant-soil interaction: Theories and mechanisms, *Chinese Journal of Geotechnical Engineering* **39** (2017), 1–47.
- [7] C.W.W. Ng, A.K. Leung, J.J. Ni, *Plant-Soil Slope Interaction*. Taylor & Francis, USA, 2019a. ISBN 978-1-13819755-8
- [8] S.K. Vanapalli, D.G. Fredlund, D.E. Pufahl, A.W. Clifton, Model for the prediction of shear strength with respect to soil suction, *Canadian Geotechnical Journal* **33** (1996), 379–392.
- [9] C.F. Chiu, C.W.W. Ng, A state-dependent elastoplastic model for saturated and unsaturated soils, *Géotechnique* **53** (2003), 809–829.
- [10] C.W.W. Ng, B. Menzies, *Advanced Unsaturated Soil Mechanics and Engineering*, Taylor & Francis Group, London, UK, 2007.
- [11] C.W.W. Ng, R.Z.B. Zhou, Effects of soil suction on dilatancy of an unsaturated soil. In Proceedings of the 16th International Conference on Soil Mechanics and Geotechnical Engineering. Osaka, Japan, 2005, 559–562.
- [12] D.G. Fredlund, A. Xing, S. Huang, Predicting the permeability functions for unsaturated soils using the soil-water characteristic curve, *Canadian Geotechnical Journal* **31** (1994), 533–546.
- [13] C.W.W. Ng, K.X. Woon, A.K. Leung, L.M. Chu, Experimental investigation of induced suction distributions in a grass-covered soil, *Ecological Engineering* **52** (2013), 219–223.
- [14] C.W.W. Ng, A.K. Leung, K.X. Woon, Effects of soil density on grass-induced suction distributions in compacted soil subjected to rainfall, *Canadian Geotechnical Journal* **51** (2014a), 311–321.
- [15] J.J. Ni, A.K. Leung, C.W.W. Ng, Investigation of plant growth and transpiration induced suction under mixed grass-tree conditions, *Canadian Geotechnical Journal* **54** (2017), 561–573.
- [16] J.J. Ni, A.K. Leung, C.W.W. Ng, Modelling soil suction changes due to mixed species planting, *Ecological Engineering* **117** (2018), 1–17.
- [17] J.J. Ni, A.K. Leung, C.W.W. Ng, Unsaturated hydraulic properties of vegetated soil under single and mixed planting conditions. *Géotechnique* (2019), <https://doi.org/10.1680/jgeot.17.T.044>.
- [18] C.W.W. Ng, J.L. Coo, Z.K. Chen, R. Chen, Water infiltration into a new three-layer landfill cover system, *Journal of Environmental Engineering ASCE* **142** (2016a), 04016007.
- [19] C.W.W. Ng, R. Chen, J.L. Coo, J. Liu, J.J. Ni, Y.M. Chen, L.T. Zhan, H.W. Guo, B.W. Lu, A novel vegetated three-layer landfill cover system using recycled construction wastes without geomembrane, *Canadian Geotechnical Journal* (2019b), <https://doi.org/10.1139/cgj-2017-0728>.

- [20] C.W.W. Ng, B.W. Lu, J.J. Ni, Y.M. Chen, R. Chen, H.W. Guo, Effects of vegetation types on infiltration rate in three-layer landfill cover with recycled concrete, *The Journal of Zhejiang University-Science-A* **20** (2019c), 1–9.
- [21] C.C. Lam, Y.K. Leung, Extreme rainfall statistics and design rainstorm profiles at selected locations in Hong Kong, Royal Observatory, Hong Kong, 1995.
- [22] USEPA (U.S. EPA), Solid waste disposal facility criteria, Technical manual EPA530-R-93-017, Washington DC, 1993.
- [23] R. Sonnenberg, M.F. Bransby, P.D. Hallett, A.G. Bengough, S.B. Mickovski, M.C.R. Davies, Centrifuge modelling of soil slopes reinforced with vegetation, *Canadian Geotechnical Journal* **47** (2010), 1415–1430.
- [24] C.W.W. Ng, A.K. Leung, V. Kamchoom, A. Garg, A novel root system for simulating transpiration-induced soil suction in centrifuge, *Geotechnical Testing Journal* **37** (2014b), 1–15.
- [25] C.W.W. Ng, V. Kamchoom, A.K. Leung, Centrifuge modelling of the effects of root geometry on the transpiration-induced suction and stability of vegetated slopes, *Landslides* **13** (2016b), 1–14.
- [26] A.K. Leung, V. Kamchoom, C.W.W. Ng, Influences of root-induced soil suction and root geometry on slope stability: a centrifuge study, *Canadian Geotechnical Journal* **54** (2017), 291–303.
- [27] B.C. Hau, R.T. Corlett, Factors affecting the early survival and growth of native tree seedlings planted on a degraded hillside grassland in Hong Kong, China, *Restoration Ecology* **4** (2003), 483–488.
- [28] A. Stokes, C. Mattheck, Variation of wood strength in tree roots, *Journal of Experimental Botany* **47** (1996), 693–699.
- [29] L.J. Waldron, S. Dakessian, Soil reinforcement by roots: Calculation of increased soil shear resistance from root properties, *Soil Science* **132** (1981), 427–435.
- [30] A.R. Ennos, The anchorage of leek seedlings: The effect of root length and soil strength, *Annals of Botany* **65** (1990), 409–416.
- [31] V. Kamchoom, A.K. Leung, C.W.W. Ng, Effects of root geometry and transpiration on pullout resistance, *Géotechnique Letters* **4**(2014), 330–336.
- [32] Geo-Slope International Ltd., Stress-Deformation Modeling with SIGMA/W, An Engineering Methodology, 4th edn., 2009.
- [33] F.T.Y. Leung, The use of native woody plants in slope upgrading in Hong Kong. PhD thesis, The University of Hong Kong, Hong Kong, China, 2014.

Keynote Lectures

This page intentionally left blank

Technical Session #2

“Analytical and Physical Modelling in Geotechnics”



Jorge ZORNBERG

Dr. Jorge G. Zornberg is Professor in Geotechnical Engineering at the University of Texas at Austin. He earned his B.S. from the National University of Cordoba (Argentina), his M.S. from the PUC of Rio de Janeiro (Brazil), and his Ph.D. from the University of California at Berkeley (USA).

As a researcher, his focus has been on soil reinforcement interaction, geosynthetics, earth retaining structures, roadways, urban and mining waste containment, unsaturated soils, and numerical and physical (centrifuge) modeling of geotechnical systems. As consultant, he has often served as expert witness in forensic investigations. Prof. Zornberg served as President of the International Geosynthetics Society (IGS) from 2010 to 2014. He was elected “fellow” of ASCE, society in which he currently serves as chair of its G-I Technical Committee on Geosynthetics.

He has authored over 400 technical publications, edited a number of proceedings and book chapters, and been awarded three patents. Prof. Zornberg has been invited to deliver keynote lectures in numerous events around the world. He has also received many prestigious awards, including the Mercer Lecture, ASCE’s Croes Medal, IGS’ Award, ASCE’s Collingwood Prize, and IGS’ Young Member Award, as well as the Presidential Early Career Award for Scientists and Engineers (PECASE) awarded by the President of the United States.

Centrifuge Technology for Characterization of Expansive Clays

Jorge ZORNBERG^{a,1}

^a *The University of Texas at Austin*

Abstract. In addition to the already common use of geotechnical centrifuges to represent, in a reduced-scale model, the state of stresses corresponding to a full-scale geotechnical structure, centrifuge techniques have increasingly been used for an additional purpose: accelerating flow process through geotechnical systems. This is particularly relevant in geotechnical problems involving low hydraulic conductivity scenarios, including flow through low-hydraulic conductivity shales, through unsaturated soils in general, and through unsaturated soils subjected to volumetric changes during infiltration (i.e. expansive clays). This paper provides an overview of recent analytical and experimental advances involving the use of centrifuge technology for the hydraulic and volumetric evaluation of expansive clays. In particular, a new centrifuge approach is presented for practical characterization of expansive clays aimed at implementation in conventional laboratories rather than research centers. The results indicate that, in spite of the significantly highly practical and expeditious characteristics of the new approach, the predicted swell-stress curve is the same as that obtained using time-consuming conventional experimental techniques.

Keywords. Centrifuge testing, Expansive clays, Unsaturated flow, Soil Water Retention Curve, Swell-stress curve

1. Introduction

The typical philosophy for centrifuge modelling in geotechnical is based upon the requirement of similitude between model and prototype. If a model of a prototype structure is built with dimensions reduced by a factor $1/N$, then an acceleration field of N times the acceleration of gravity, g , will generate stresses by self-weight in the model that are the same as those in the prototype structure. In addition to this approach, centrifuge techniques can also be used for an additional purpose: to accelerate flow processes through geotechnical systems. This may be particularly beneficial in geotechnical problems involving flow through: (1) low hydraulic conductivity materials (e.g. flow through low-hydraulic conductivity shales), (2) unsaturated soils that do not undergo significant volume changes (e.g. sandstones), and (3) unsaturated soils subjected to possibly significant volumetric changes during infiltration (e.g. high plasticity clays).

A practical problem, which is the focus of this paper, is the use of centrifuge principles for hydraulic and volumetric characterization of expansive clays, a particularly costly geotechnical problem. As early as 1973, the annual cost of expansive soil damage in the US was estimated at \$2.2 billion [1]. The US Department of Housing and Urban

¹ Corresponding Author, 301 E. Dean Keeton, Austin, Texas 78712, USA; E-mail: zornberg@mail.utexas.edu

Development subsequently estimated that foundation damage caused by swelling clays reached \$9 billion per year in 1981 [2]. Estimates by Whitterspoon [3], based on data collected from foundation repair contractors, places this damage at an approximate \$13 billion per year. Finally, and allowing for annual inflation and population growth, Wray & Meyer [4] estimate that total annual damage from swelling clays in the US well exceeds \$15 billion. Although not life-threatening as compared to other natural disasters, expansive soils constitute a natural hazard with an average annual damage that exceeds that caused by floods, hurricanes, earthquakes and tornados combined [4, 5, 6, 7].

Important advances have been made towards a better understanding of the swelling of clays and their treatment. These include new moisture diffusion and volume change models (e.g. El-Garhy & Wray [8]), verification of numerical simulations (e.g. Houston et al. [9]), the effect of clay structure on its mechanical response [10, 11], evaluation of new stabilizers (e.g. Miller & Zaman [12]), assessment of properties governing the unsaturated characteristics of expansive soils (e.g. Likos & Lu [13, 14], Puppala et al. [15], Lin & Cerato [16]), coupled interactions between clay microstructure and macrostructure (e.g. Likos & Wayllace [17]), and characterization of the mechanical behavior of swelling clays (e.g. Zhan & Ng [18]).

Yet, our ability to measure the one variable that is ultimately responsible for damages exceeding \$15 billion per year (i.e. the vertical rise itself) remains, at best, limited. This is because conventional "free-swell" tests often require excessive testing time for their completion in practical applications. Also, since water infiltration into the specimen is solely driven by suction gradients, the termination of swelling tests is ill-defined and constitutes a source of error that compromises the repeatability of test results. Finally, proper design would require a comprehensive battery of swelling tests, as design typically requires the determination of the entire relationship between swelling and confining stresses. Probably because of these shortcomings, the current state of practice relies heavily on (often crude) empirical correlations between vertical rise and clay index properties. In Texas, for example, widespread practice has been to rely solely on the PI of soils to predict vertical heave using correlations developed in the 1950's.

The study discussed in this paper focuses on the characterization of expansive clays using centrifuge technology as an alternative to alleviate the shortcomings associated with using soil index properties. Specifically, centrifuge technology was used for the continuous and expeditious, direct measurement of the swelling of clays. Also, the centrifuge approach is well-suited for characterization of swelling clays because it is expected to be practical to define the entire relationship between swelling and vertical stresses. This is a significant advantage over conventional free swell tests, which are often prohibitively long and provide swelling for a single stress value.

This investigation capitalized on the availability of a centrifuge facility at The University of Texas at Austin, which was specially tailored to investigate flow-related problems in geotechnical applications. This is a high-g centrifuge capable of continuously, non-destructively, and non-intrusively measuring suction, moisture content, and fluid flow rate in a soil specimen during centrifugation. It allowed expedited determination of both the Soil Water Retention Curve (SWRC) and the hydraulic conductivity function (K-function) from a single specimen in a single test [19, 20, 21]. In this new application, the centrifuge capabilities were expanded to determine both the unsaturated hydraulic properties and the swelling response of soils showing significant volume changes.

In addition, a comparatively simple and inexpensive centrifuge environment was developed for direct quantification of swelling. Accordingly, a comparatively small

centrifuge, used commercially for multiple industrial purposes, was adapted and also used for expansive soil characterization. Ultimately, this study highlights that the use of centrifuge testing is no longer restricted to research activities, but it has the potential of becoming a conventional equipment in geotechnical laboratories.

2. Background

2.1. *Expansive Clays*

Expansive clays are soils that increase in volume, often substantially, when given free access to water. One of the most commonly accepted theories to explain the expansion of soils is based on the diffuse double layer (DDL) that develops between clay platelets [22, 23]. Negatively charged soil particles attract cations in order to remain electrically neutral, forming areas of high cation concentration in between particles. When wetted, the higher concentration of cations creates a hydraulic gradient due to differences in osmotic pressure, which in turn induces the flow of water in between the particles, ultimately causing an increase in volume [24].

Studies have been performed to compare the theoretical swell potential (pressure) of pure clays, predicted using the DDL theory, against that measured in the laboratory [25, 26, 27, 28]. These studies have generally found a good relation between theoretical and experimental results, with the exception of soils in which the structure of soil particles affects the compression or expansion (e.g. soils with relatively large particles or with flocculated soil structure). Even in soils for which the experimental observations do not match the theoretical predictions, the trend of experimental results has been found to compare well with theoretical predictions.

As previously mentioned, problems caused by swelling clays throughout the US result in billions of dollars a year in damages [4]. Damages can occur to nearly any structure built on or in expansive soils, including deep and shallow foundations, retaining walls, and roadways. The most problematic areas are those with abundance of swelling clays and a climate that promotes seasonal changes in the water content of clays. In these cases, the key to the design is to predict the magnitude of swelling and/or the magnitude of pressures that are expected from expansive soils. Only with this information can a geotechnical design be conducted to accommodate the expected pressures or movements.

Conventional free swell tests [29] are performed in consolidation frames. Clay samples are compacted in consolidations cells and subjected to overburden pressure. Water is then poured to submerge the sample and vertical deflections are subsequently measured. There is no clear termination point and tests often run for months until the sample height appears to reach equilibrium. Because of their long duration, conventional free swell tests are rarely used in geotechnical practice. This is probably what led to the proliferation of correlations based on soil index properties to predict swelling. This includes correlations with the Plasticity Index (PI) developed by McDowell [30]. Vijayavergiya & Ghazzaly [31] and Nayak & Christensen [32] suggested relations using the dry unit weight and either the PI or Liquid Limit. Rao et al. [33] showed good predictions using a correlation based on dry unit weight, compaction water content, overburden pressure, and free swell index results.

A good example of the imperative need to develop approaches for expeditious, direct measurement of the swelling of clays is the state of the practice throughout Texas (and probably in several other states). Specifically, government agencies and geotechnical

designers in Texas rely heavily on the correlations developed by McDowell [30] for their geotechnical designs. The method correlates the PI of a soil with the predicted volume change. Unfortunately, this correlation is based on laboratory swell testing of only three test soils that were subjected to wetting through capillary adsorption. This capillary approach involved placing a specimen atop a water reservoir and allowing swelling by water drawn by capillary rise for a period of time (in days) equal to the PI of the soil. The percent volume change was then corrected for the overburden pressure to yield a predicted vertical rise. While the study by McDowell [30] was valuable at its time, the lack of reliable procedures for direct measurement of the swelling of clays has led to its continued use until today, in spite of the deficiencies of these correlations. First, the method is based on a small number of tests in which all of the samples were remolded. Also, no tests were conducted on soils at comparatively low initial water content. Finally, the correlations have been extrapolated (e.g. Tex-124-E [34]) to PI values as high as 140, which is well beyond the range of testing. Despite these limitations, the method has been used for over fifty years throughout the state of Texas.

2.2. Water Flow through Unsaturated Porous Media

Flow of water in unsaturated soils can be described using three non-linearly related variables, namely the volumetric water content θ (or degree of saturation), the matric suction ψ (or capillary pressure if the air pressure is non-zero), and the hydraulic conductivity K . These variables are quantified experimentally by determining the soil-water retention curve (SWRC) and the hydraulic conductivity-function (K-function), a set of relationships that govern the soil's moisture storage and impedance to water flow, respectively. An important challenge, however, is that measurement of the hydraulic characteristics of unsaturated soils involves lengthy testing periods. Consequently, most projects requiring the use of hydraulic characteristics of unsaturated soils rely heavily on empirical correlations or theoretical models rather than on experimental measurements. Centrifuge testing has been recently used to alleviate the shortcomings, allowing a comparatively expeditious determination of the unsaturated hydraulic characteristics [19, 20, 21].

The SWRC is the relationship between θ and ψ , and represents the energy needed (i.e. ψ) to de-saturate the soil to a given θ . The K-function is the relationship between K and ψ (or θ), and reflects the decrease in available pathways for water flow as a soil de-saturates. The typical SWRC and K-function of a low plasticity clay are shown in Figure 1. The experimental SWRC data shown in this figure were obtained using three of the four approaches described by ASTM D6836 [35] (i.e. hanging column, pressure plate, and thermodynamic tests). It should be noted that each point on the SWRC in Figure 1 was defined using a different water flow mechanism. The hanging column and pressure plate tests involve monitoring the transient outflow of water from the soil specimen during application of ψ (i.e. the difference between the pore air and pore water pressures), while the thermodynamic test involves monitoring the total suction (i.e. the sum of matric and osmotic suction values) during evaporation of water from the soil. Instead of using experimentally-derived data as in the SWRC, the K-function shown in Figure 1 was defined using a theoretical model. Specifically, the van Genuchten-Mualem [36] model was used to define the K-function. This model assumes that the soil behaves as a bundle of capillary tubes having properties described by the parameters of a function fitted to the experimental SWRC of the soil. The predicted K-function is only shown up

to 10^{-14} m/s as this value nears the low end of K values that have been measured in the laboratory [37]. The K-function represents the proportionality between the hydraulic gradient and water flow rate, and is thus only relevant for conditions in which the water phase in the soil is continuous. When the water phase in the soil becomes discontinuous, hydraulic gradients applied to the water phase will not result in water flow. Instead, vapor transport by diffusion will dominate the migration of water. Because the theoretical prediction of the K-function provides no lower bound on the K of a soil, the boundary between liquid and vapor phase transport is difficult to assess. This boundary is likely to occur in the vicinity of the ψ value where the slope of the SWRC starts to decrease, or at about 200 kPa for the data in Figure 1.

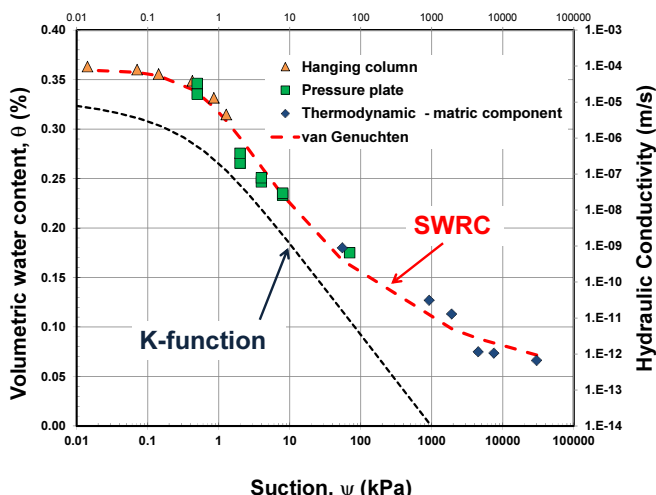


Figure 1. Hydraulic characteristics of an unsaturated clay of low plasticity.

The common practice of predicting the shape of the SWRC and K-function using empirical observations or theoretical models is well documented (e.g. Zapata et al. [38], van Genuchten [36], Brooks-Corey [39]). A SWRC is typically quantified by fitting experimental data to power law, hyperbolic, or polynomial functions [39, 36, 40]. Although the Brooks & Corey [39] model is able to represent a sharp air entry suction, the van Genuchten [36] model is most commonly used in numerical analyses because it is differentiable for the full range of suction values. Preliminary estimates of the SWRC could be obtained using databases that rely on the granulometric distribution of soils [40].

Experimental evaluations to validate the K-functions predicted using theoretical models are rarely conducted in practice. This is especially problematic as the SWRC and K-function are sensitive to soil structure variables such as pore size distribution [41, 42, 43, 44], soil fabric [45], mineralogy [46], compaction conditions [47, 48], use of admixtures [15], volumetric changes [49, 50, 51, 52], and stress state [53]. Khaleel et al. [54] observed that predicted K-functions could be in error by several orders of magnitude due to some of these effects. The broad range of potential impacts and the high magnitude of errors point to the need for direct measurement of the hydraulic characteristics of unsaturated soils.

One of the few tests available to directly measure the hydraulic characteristics using controlled infiltration is the column flow test, performed in either a rigid-wall permeameter, with flow controlled by surface infiltration and gravity drainage or in a flexible-wall triaxial permeameter with flow controlled by a pump [55, 47, 56]. Specifically, a column flow test can be used to measure the SWRC and K-function by imposing a known flow rate through the specimen and monitoring the corresponding gradient in hydraulic head, or by imposing a gradient in hydraulic head on the specimen and monitoring the ensuing flow rate. In either approach, there will be a transient period during which θ and ψ will change, followed by steady-state water flow conditions. Although the transient changes in θ and ψ can be used to measure the soil hydraulic characteristics [37], the calculated flow rates and gradients are prone to significant error. Steady-state flow data can be used to measure the hydraulic characteristics with more confidence, but a significantly long time is needed to establish steady flow conditions [57].

2.3. Centrifuge Techniques for Characterization of Unsaturated Hydraulic Properties

Much of the basis used in this study for characterization of the swelling of clays upon water infiltration relies on recent studies on the characterization of unsaturated flow using centrifuge techniques. This is because centrifugation was recently used to alleviate shortcomings of conventional characterization of the SWRC and K-function of soils. The key benefit stems from the fact that time in flow processes through soil has been shown to decrease quadratically with increasing g-level. The conditions of similarity for geotechnical structures tested in a centrifuge have often been inferred from general scaling relationships. Although modeling limitations are often difficult to overcome when the purpose of the investigation is to compare the performance of model and prototype structures, many of these limitations can be taken into account when the purpose is to identify mechanisms or to determine properties of the tested soils.

Centrifuge modeling has been used in investigations involving contaminant transport phenomena [58, 59, 60, 61, 62, 63], movement of immiscible fluids [64, 65, 66, 67, 68], unstable infiltration [69, 70], and soft soil desiccation [71]. Centrifuge modeling has the distinct advantage of being able to reproduce similitude of the suction-moisture content regime in unsaturated soils. Centrifuges were first used in the early 1930's to define the SWRC by soil scientists and petroleum engineers [72, 73]. The specific scaling relations for unsaturated soils have been investigated both analytically using dimensional analysis and experimentally using "modeling of models" [74, 58, 59, 75, 76]. These investigations showed that unsaturated flow problems should be analyzed using the same scaling relations as (saturated) laminar flow problems. However, only a limited number of studies has focused on centrifuge modeling of expansive clays [77, 78], with focus on the performance of earth structures rather than on clay characterization.

Centrifuge technology has been used in previous studies to decrease testing time when using steady-state infiltration for characterization of unsaturated soils. This was the motivation behind the development of the Steady-State Centrifuge (SSC) by Nimmo et al. [79] and of the Unsaturated Flow Apparatus (UFA) by Conca & Wright [80]. The UFA approach has been employed in geotechnical design to measure the hydraulic characteristics of the soil used in an alternative landfill cover [81]. However, the SSC and UFA use relatively small medical ultracentrifuges, which do not include a data acquisition system that is operational under high accelerations. Consequently, these systems did not permit concurrent measurement of the SWRC and K-function of soils.

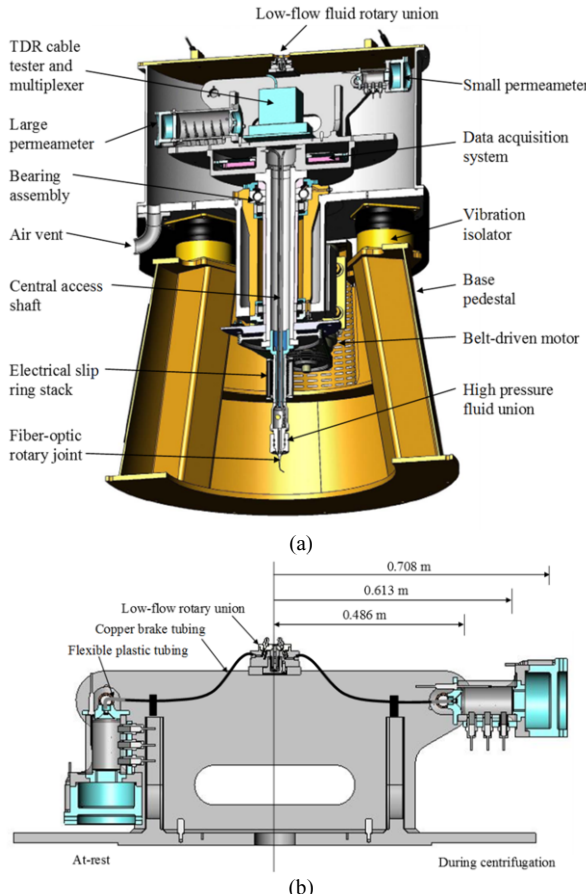


Figure 2. Centrifuge permeameter at the University of Texas at Austin for characterization of unsaturated flow: (a) Centrifuge detail; (b) Testing environment.

The recent studies at the University of Texas at Austin have focused on the concurrent experimental measurement of both the SWRC and K-function using a new centrifuge permeameter [19, 20, 21]. Figure 2 shows the centrifuge permeameter, which allows expeditious measurement of the three key variables that govern water flow under unsaturated conditions (i.e. θ , ψ and K) in soils that are not subject to significant volume changes during infiltration (e.g. silts, clays with low plasticity). A key aspect of the testing approach developed in that study is that steady-state flow conditions could be achieved in a comparatively short testing time. Reaching steady-state conditions significantly facilitates the experimental measurement of the unsaturated hydraulic properties of soils.

A cross section of the centrifuge permeameter available at The University of Texas at Austin is shown in Figure 2(a). The centrifuge includes a testing environment and data acquisition hub resting atop a spindle and bearing assembly, which is supported by three vibration isolators mounted on a conical base pedestal. A central access shaft in the spindle permits wires and plumbing lines to pass through rotary joints from the data acquisition system and testing environment to the stationary environment. The testing

environment is shown with added details in Figure 2(b). Two identical, instrumented permeameters are mounted on a swinging bucket assembly. The swinging buckets permit the longitudinal axis of the permeameter to be aligned with the resultant of the acceleration field. Characterization permeameters at rest (left) and spinning (right) are shown in Figure 2(b). A low-flow rotary union was designed to transmit low flow rates while preventing water loss and minimizing heat generation. The centrifuge is equipped with a solid-state data acquisition board (no moving disc drives).

The centrifuge permeameter at UT Austin has a maximum angular velocity of 875 RPM, which translates to a g-level of 600 at the base of the permeameter. The swinging buckets of the permeameter have a maximum payload of 50 kg for a g-ton rating of 30. This investigation capitalizes on the recent advances in unsaturated soil characterization using the centrifuge permeameter, but incorporates the additional ability to characterize the swelling of clays. This required that the testing environment be capable of measuring volume changes (ε_v) induced during infiltration. Ultimately, the overall goal is to concurrently and expeditiously measure the four variables that continuously change during infiltration of water into swelling clays (i.e. θ , ψ , K , and ε_v).

3. Analytical Framework

The analytical framework for water infiltration under unsaturated conditions in a centrifuge environment provides insight into the experimental approach developed in this study. Water flow occurs in response to a gradient in hydraulic potential, the dominant components of which are gravity and matric suction. These components are independent, as gravity is a body force, while suction is an air-water interface phenomenon. Unlike suction gradient, which varies over orders of magnitude, the gradient of elevation head is constant and equal to 1. Centrifugation is an alternative approach to increase the body force component of the hydraulic potential, the gradient of which may be greater in magnitude than the suction gradient. Centrifugation increases the body forces on a specimen by imposing a centripetal acceleration, a :

$$a = \omega^2 r = N_r g \quad (1)$$

where ω is the angular velocity of the centrifuge, r is the radius at a certain point in a soil specimen, g is the acceleration of gravity, and N_r is the ratio between the centripetal acceleration and g . The r subscript in N_r signifies that N varies with radius. When a single N_r is considered, it corresponds to the value at mid-height of the soil specimen $N_{r,mid}$ (also referred to as “g-level”). A control volume for water flow in the centrifuge is shown in Figure 3. A coordinate z_m is used, with datum at the base of a soil specimen, defined as:

$$z_m = r_0 - r \quad (2)$$

where z_m is the distance from the datum at the base of the specimen, r is the radius from the center of rotation, and r_0 is the radius of the base of the specimen. The cylindrical specimen with length L_m has an inlet face at a radius of r_T , and an outlet face at a radius of r_O . As z_m is defined as positive toward the axis of rotation, the water discharge velocity v_m is positive in the direction of positive z_m , toward the axis of rotation.

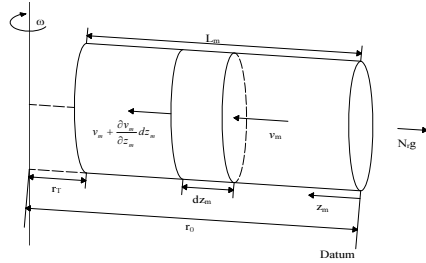


Figure 3. Centrifuge control volume [76].

The self-weight of water in the centrifuge acceleration field increases the driving force for water flow. The hydraulic potential in the centrifuge model Φ_m is quantified as:

$$\Phi_m = -\frac{1}{2} \left(\frac{I\omega^2}{m} \right) + \frac{1}{2} \left(\frac{v_m}{n} \right)^2 + \frac{P_w + P_o}{\rho_w} \quad (3)$$

where I is the rotational inertia of a point mass m in a centrifuge field. The components on the right hand side correspond to the rotational potential energy per unit mass induced by centrifugation, the kinetic energy per unit mass due to the relative linear velocity of the fluid with respect to the solids, the energy per unit mass due to the water pressure, and energy per unit mass due to the osmotic pressure. The sign of the first term is negative because the rotational kinetic energy increases in the opposite direction of the coordinate z_m . For a point mass m in a centrifuge field, the moment of inertia is given by:

$$I = m(r_0 - z_m)^2 \quad (4)$$

Assuming that centrifugation does not cause turbulent water flow, the kinetic energy term may be neglected. Also, the air pressure is assumed to be negligible, so the suction can be substituted for the water pressure as $P_w = -\psi$. Finally, the osmotic pressure can be assumed not to vary with moisture content for unsaturated soils, so the last term is not considered. Considering these assumptions, the hydraulic potential in the centrifuge is:

$$\Phi_m = -\frac{1}{2}\omega^2(r_0 - z_m)^2 + \frac{(-\psi)}{\rho_w} \quad (5)$$

Alternatively, the hydraulic potential can be written in terms of hydraulic head:

$$h = \frac{\Phi_m}{g} = -\frac{\omega^2}{2g}(r_0 - z_m)^2 - \frac{\psi}{\rho_w g} \quad (6)$$

where h is the total hydraulic head having units of length, the suction head equals the suction divided by $\rho_w g$. Similar to water flow under 1-gravity, the discharge velocity through a soil specimen in the centrifuge is proportional to the gradient in the total hydraulic potential. Darcy's law in the centrifuge is given by:

$$v_m = -\frac{K(\psi)}{g} \frac{d\Phi_m}{dz_m} \quad (7)$$

The gradient of the hydraulic potential with respect to z_m in Eq. (7) is:

$$\frac{d\Phi_m}{dz_m} = \omega^2 (r_0 - z_m) - \frac{1}{\rho_w} \frac{\partial \psi}{\partial z_m} \quad (8)$$

This equation can be incorporated into Eq. (7) to determine the discharge velocity:

$$v_m = -\frac{K(\psi)}{g} \left[\omega^2 (r_0 - z_m) - \frac{1}{\rho_w} \frac{d\psi}{dz_m} \right] \quad (9)$$

The first term within the brackets is the centrifuge acceleration, while the second term represents the suction gradient. This equation indicates that the discharge velocity varies with the radius of the centrifuge. Flow continuity requires that:

$$\frac{d\theta}{dt} = -\frac{dv_m}{dz_m} \quad (10)$$

Combining the continuity equation with Eq. (9), Richards' equation for one-dimensional flow of water through an unsaturated soil in a centrifuge results in:

$$\frac{d\theta}{d\psi} \frac{d\psi}{dt} = \frac{d}{dz_m} \left[K(\psi) \left[\frac{\omega^2}{g} (r_0 - z_m) - \frac{1}{\rho_w g} \frac{d\psi}{dz_m} \right] \right] \quad (11)$$

This equation has been solved numerically by Bear *et al.* [82] and Simunek and Nimmo [83]. Alternatively, analytical solutions can be derived for the case in which the K-function is represented using Gardner's [84] model. Dell'Avanzi *et al.* [76] derived an analytical solution for suction profiles during steady state water flow in the centrifuge, as follows:

$$\begin{aligned} \psi(z_m) &= -\frac{1}{\alpha} \ln \left[e^{\left(\ln \left(\frac{v_m}{N_r K_s} \right) + e^{-\alpha \psi_0} \right) - \alpha \omega^2 \rho_w z_m \left(r_0 - \frac{z_m}{2} \right)} \right] - \frac{v_m}{N_r K_s} & \text{if } \left(\frac{v_m}{N_r K_s} \right) + e^{-\alpha \psi_0} > 0 \\ \psi(z_m) &= -\frac{1}{\alpha} \ln \left[-e^{\left(\ln \left(\frac{v_m}{N_r K_s} \right) + e^{-\alpha \psi_0} \right) - \alpha \omega^2 \rho_w z_m \left(r_0 - \frac{z_m}{2} \right)} \right] - \frac{v_m}{N_r K_s} & \text{if } \left(\frac{v_m}{N_r K_s} \right) + e^{-\alpha \psi_0} < 0 \end{aligned} \quad (12)$$

where ψ_0 is the suction at the outflow face of the centrifuge specimen. Suction profiles for a soil layer with an imposed surface discharge velocity and a saturated bottom boundary are shown in Figure 4 for values $\alpha = 1 \text{ kPa}^{-1}$ and $K_s = 10^{-6} \text{ m/s}$, and a normalized specimen geometry representative of the centrifuge permeameter used in this study.

The average g-level tends to influence both the distribution of suction with height as well as the suction in the upper portion of the specimen. v_m tends to influence the suction

in the upper portion of the specimen. The magnitudes of suction in this figure are not important as they depend on the assumed values of α and K_s . However, a more important feature of these graphs is the distribution of suction with height in the specimen. Independent of the suction (or saturation) condition at the bottom, the suction does not vary significantly in the upper portion of the specimen length, even for low $N_{r,mid}$. Because N_r varies with radius, the suction distribution in the upper portion of the specimen shows a minor gradient. However, for this particular set of hydraulic characteristics and specimen geometry, it may be assumed that the suction is constant in this zone. Accordingly, the suction magnitude at the outflow boundary does not have a significant effect on the shape of the suction profile in the upper zone of the specimen, as indicated by the suction profiles in Figure 4.

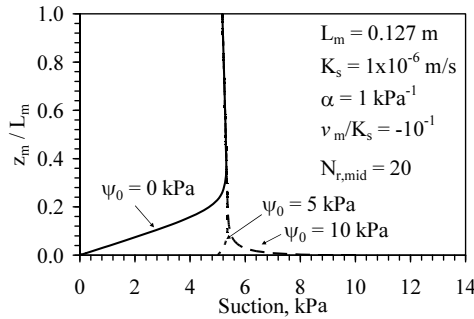


Figure 4. Steady state suction profiles for different: (a) $N_{r,mid}$; (b) v_m ; (c) ψ_0 .

Given the value of α in the Gardner [84] model, the limiting suction in the upper zone of the soil layer may be predicted as [76]:

$$\psi_\infty = -\frac{1}{\alpha} \ln \left(-\frac{v_m}{N_{r,mid} K_s} \right) \quad (13)$$

Unlike the 1-g case, the limiting suction is valid when $N_r = N_{r,mid}$ throughout the profile. Using the calculated components of the total head gradient, the distribution in K under steady state water flow can be determined using Darcy's law, as:

$$K(\psi, z_m) = \frac{-v_m}{\left[\frac{\omega^2}{g} (r_0 - z_m) - \frac{1}{\rho_w g} \frac{d\psi}{dz_m} \right]} \quad (14)$$

where v_m is an imposed, discharge velocity (equal to Q/A) and ω is an imposed centrifuge angular velocity.

4. A New Centrifuge for Characterization of Expansive Clays

The recent experimental and analytical developments that led to the expeditious determination of the properties governing water flow in soils under unsaturated conditions (i.e. SWRC and K-function) were adopted for the expeditious determination

of the swelling of soils. This is because the time involved in the swelling process, which is often significantly long and has compromised its direct determination in practical applications, is directly governed by the time involved in the water infiltration process. Accordingly, adding monitoring of volumetric changes to the previously described equipment would result in the ultimate goal of concurrently and expeditiously measuring the four variables that continuously change during infiltration of water into swelling clays (i.e. θ , ψ , K , and ε_v). While this ambitious goal was pursued at the University of Texas at Austin (see Quaglia [85]), the focus of this paper is on a new experimental technique that simplifies the experimental approach for cases in which the focus is strictly the characterization of volumetric changes.

4.1. Centrifuge components

The centrifuge used in this research study is a floor-mounted centrifuge used for a variety of industrial purposes. This is a considerably simpler equipment than the one described in Section 2.3, which involves a hydraulic rotary joint and a comprehensive in-flight data acquisition system. The floor-mounted centrifuge contains six hangers that hold freely swinging aluminum centrifuge cups. The setup of the centrifuge is fairly customizable, as the contents of the centrifuge cups were altered to fit requirements of different tests. Plastic permeameter cups that fit inside the centrifuge cups were designed and manufactured specifically for this equipment. A view of the centrifuge cups and the floor-mounted new centrifuge is shown in Figure 5 [86].



Figure 5. Centrifuge equipment for characterization of expansive clays: (a) Centrifuge permeameters, (b) centrifuge system [86].

The original testing approach involved ponding water on top of a compacted soil sample and spinning the sample at comparatively high g levels (ranging from 25 to 400 g). As previously discussed, the increased g level leads to an increased hydraulic gradient that forces the water through the samples at an increased rate, promoting expeditious swelling of the clay. The centrifuge cups (Figure 6a) hang from the spinning centrifuge arms. The holders have an inner diameter of 63.5 mm and a usable inside depth of 114.3 mm. The base of the specimen holder includes a small vent hole to allow air and water outflow. While in-flight, the distance from the base of a sample to the center of rotation in the small centrifuge is 165 mm.

The permeameter cups (Figure 6b) fit inside the centrifuge cups with an outside diameter of 63.3 mm and a depth of 114.3 mm. The cups have an inside diameter of 57.2 mm at the top, which is reduced to 47.1 mm approximately 25 mm from the base of the cups. This reduction was adopted to form a ledge that allows a porous plate to support soil samples. The base of the cup is removable and is used as a liquid collection system. Outflow can be measured by measuring the increase in weight of the collection cup. A small air vent (visible in Figure 6b) connects the collection cup to the area above the sample to allow equalization of air pressure between the chambers located above the ponded water and at the bottom of the sample [87].

The porous supporting plate (Figure 6c) sits on top of the ledge in the permeameter cup and creates a firm yet pervious surface to place specimens. The plate contains 0.8 mm-diameter holes that allow water to flow freely from the base of the specimen. To avoid migration of soil particles, a filter paper is placed between the porous plate and the soil specimen. A rubber permeameter cap fits inside the top of the permeameter cup in order to minimize evaporation during testing. The rubber cap provides an airtight seal once the centrifuge is in flight.

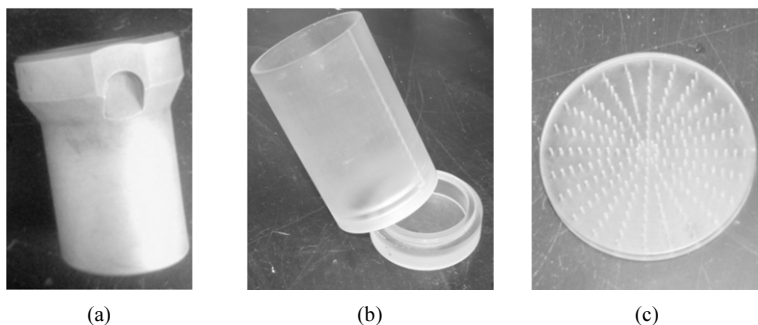


Figure 6. Centrifuge components: a) Centrifuge cup b) Permeameter cup c) Porous disc.

An alternative centrifuge cup was developed, which allows for testing undisturbed soil specimens collected in the field using Shelby tube samplers. In order to accommodate testing of field specimens from push samplers, the boundary conditions and permeameter cup design were changed to incorporate cutting rings. A comparison between the original centrifuge cup design and the double infiltration cup design is shown in Figure 7.

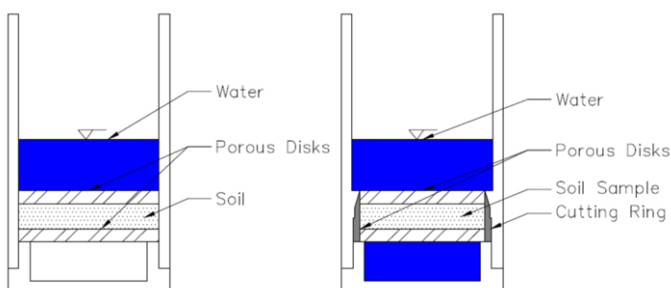


Figure 7. Single infiltration and double infiltration permeameter cups.

In order to allow centrifuge testing of undisturbed soil specimens, a method was developed to moisture condition (dry) the field-collected specimens. The procedure was developed after verifying that a rapid rate of drying results in shrinkage cracks that compromise the subsequent centrifuge testing [88]. To retard the rate of drying, an environmental chamber with a relatively constant, high relative humidity was developed, which involves a glove box and the use of saturated salt solutions. The time to reach the targeted moisture content (e.g. 3 moisture percentage points dry of optimum) may be as long as 36 to 72 hours, but the approach allowed reaching the target initial moisture content without developing shrinkage cracks in the soil specimens.

4.2. Instrumentation and in-flight data acquisition

A data acquisition system (DAS) was developed for the new centrifuge. The system includes a battery housing unit, a linear position sensor (LPS) for each permeameter cup that records changes in height of the clay specimen, a JeeNode (Version 6) Arduino along with the analog-to-digital converter (ADC), and an accelerometer to measure the g-level experienced by the specimen. These components are displayed in Figure 8.

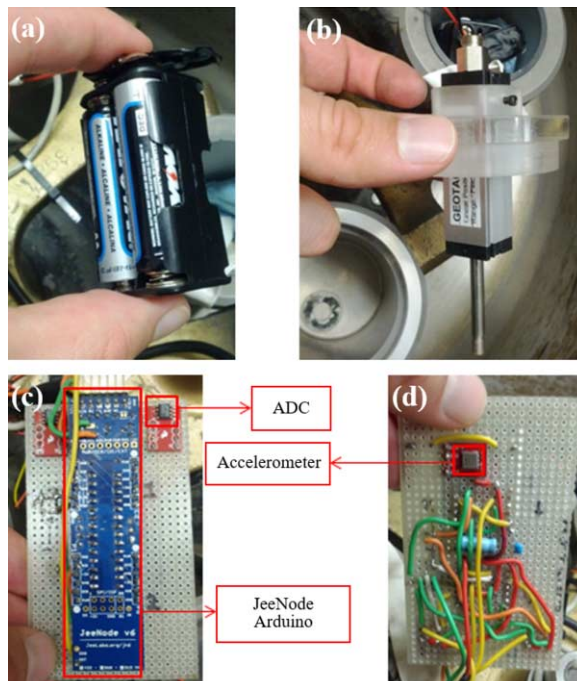


Figure 8. Components of the Data Acquisition System in the Swell Centrifuge: (a) Battery Housing Unit; (b) Linear Position Sensor; (c) JeeNode Arduino and Analog-to-Digital Converter; (d) Accelerometer [89].

The JeeNode Arduino involves a programmable microchip that controls and interfaces with the other DAS components through serial communication (RS232). The microchip sends a signal, notifying the ADC to take displacement and acceleration readings. The ADC converts the voltage to digital readings and sends them to the Arduino along with the digital accelerometer reading. The internal JeeNode Arduino,

communicates the readings to an external JeeNode Arduino via wireless radio. The external Arduino transfers the readings to a Labview program, which translate the readings into specimen heights.

5. Testing Procedure

Reconstituted soil specimens are prepared to a target density using kneading or static compaction. The soil specimen is initially subjected to a seating load by raising the g-level to 2 to 3 g's and allowing the compression of the soil at a low seating pressure. This cycle is consistent with the seating load applied in conventional swell tests.

The compression cycle involves raising the g-level on the soil specimen (without access to water) for several minutes and then stopping the centrifuge. This allows measuring the compression due to the increased load during centrifugation. In tests involving undisturbed in-situ soil specimens, the g-level should be selected to replicate in-situ field stresses. In tests involving reconstituted soil specimens, they have been generally tested at the g-levels of 5, 25, and 200. These g-levels result in effective stresses ranging from approximately 0.47 kPa up to 95.76 kPa, which are representative of the stress range typical to the active zone for expansive clays.

After the initial compression cycle, the specimen is removed from the centrifuge, decreasing the applied overburden. Water is then added to the cups, which are subsequently placed in the centrifuge. The centrifuge is then run again, and allowed to spin for 24 to 48 hours. Primary swelling of the sample is typically reached within one day, and the sample is often tested for some additional time to ensure that secondary swelling has begun. After the test is completed, cups are removed from the centrifuge, and the cup and cup base with water are then weighed. Final sample heights are measured to determine the final swell in comparison to that recorded by the sensors while spinning. The soil is then extruded and placed on a metal tray for oven-drying to measure the gravimetric water content of the soil.

6. Typical Centrifuge Swell Test Results

6.1. Swell vs. Time Test Results

Test results from three soils are presented herein: Eagle Ford shale, Houston Black clay, and Black Taylor clay. The initial specimen conditions considered as baseline are an initial moisture corresponding to the soil optimum moisture content and an initial unit weight corresponding to the soil compacted to a relative compaction of 97% in relation to the Standard Proctor test. For example, the Eagle Ford baseline condition consisted of a soil with a moisture content of 24% ($\pm 0.5\%$) and a dry unit weight of 14.34 kN/m^3 . A parametric evaluation was conducted, which involved specimens prepared at a moisture content ranging from the soil optimum moisture content -3% to the optimum moisture content + 3%. The specimens were prepared to relative compaction values of 94%, 97%, and 100% in relation to the dry unit weight as determined by the standard proctor test. The specimens were tested under g-levels of 5, 25, and 200 g's in order to generate the stress-swell curves. These g-levels correspond to confining stresses of approximately 1.44, 4.79, and 47.88 kPa.

For each test, the data recorded is the change in height of a soil at a specified time interval. From this data, the swelling of a specimen can be continuously defined throughout the test, generating a swell versus time curve. A typical swell-over-time curve is shown in Figure 9. The conditions for this Eagle Ford clay specimen are those corresponding to its baseline conditions.

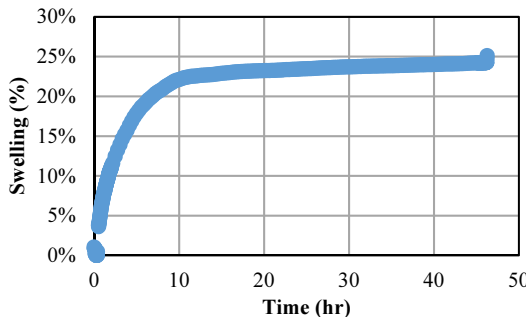


Figure 9. Time-history of swelling in a centrifuge test using a specimen of Eagle Ford clay.

As the figure illustrates, the first portion of the swelling curve is where the primary swell occurs, involving significant swell changes as the water enters the voids. This stage may take some 10 hours, until the swelling reaches an inflection point, and then continues to increase at a slower rate corresponding to the secondary swelling. The inflection point is often used to report the soil swelling.

Table 1 contains the average swelling data at the baseline conditions for the three most tested soils (Eagle Ford, Houston Black, and Black Taylor) for each of the tested g-levels.

Table 1. Baseline conditions for the clays evaluated in this study.

Soil	w_{opt} (%)	Target Dry Unit Weight, (kN/m ³)	Swelling (%) @ 5g	Swelling (%) @ 25g	Swelling (%) @ 200g
Eagle Ford	24	14.79	24.68	15.65	7.26
Houston Black	25.5	14.28	6.13	5.34	1.46
Black Taylor	23.3	14.28	3.92	2.65	2.26

The most highly plastic soil, the Eagle Ford shale, shows the highest average swelling per test. However, the Houston Black clay does show a higher average swelling for the 5-g and 25-g tests than the Black Taylor, even though the Houston Black clay has a higher PI than the Black Taylor clay.

6.2. Swell-Stress Curves

The swell-stress curves were defined for three soils for which a large suite of tests were conducted. They include the Eagle Ford, Black Taylor, and Houston Black clays. The resulting curves are shown in Figure 10. The Eagle Ford clay shows significantly higher swelling potential than the Black Taylor and Houston Black. The Black Taylor and

Houston Black clays show similar swelling, with the Black Taylor having a slightly higher swell-stress curve.

Curves based on samples with varied compaction moisture and density were also obtained. The results in Figure 10b show the effect of compaction moisture content on swelling for the case of the Houston Black Clay.

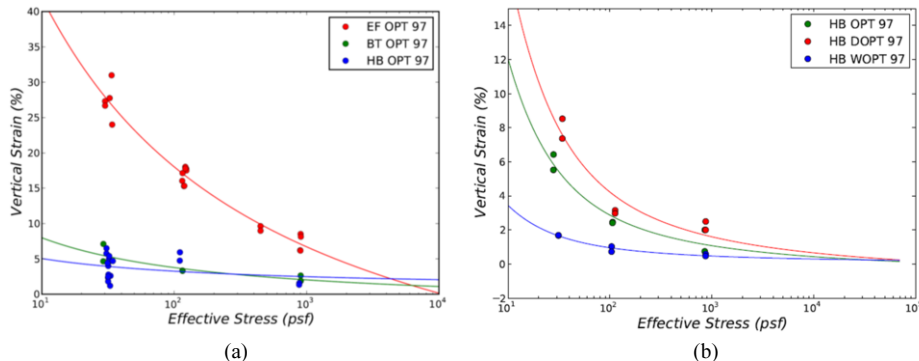


Figure 10. Swell stress Curves: (a) for three different soils; (b) for Houston black at three different initial moisture content values. Notes: EF = Eagle Ford; BT = Black Taylor; HB = Houston Black

6.3. Comparison between Centrifuge with Standard Swell Test Results

The swell results obtained from the centrifuge testing were compared against those from standard swell test results, using specimens with the same initial unit weight and water content. The results are shown in Figure 11. The centrifuge results showed excellent consistency with the standard swell test results, as shown in Figure 11 for the case of Eagle Ford clay. Equally consistent results were obtained for the other clays.

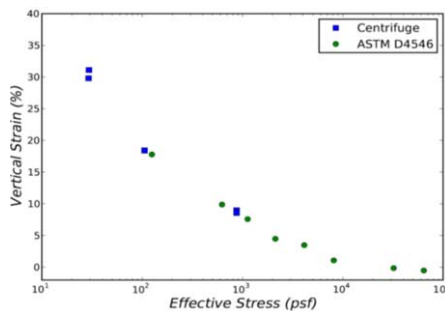


Figure 11. Comparison between centrifuge and standard swell test results (Eagle Ford clay)

7. Conclusions

Characterization of soil volumetric strains as an additional variable within the framework of unsaturated hydraulic characteristics adds complexity to the already intricate, non-linear relationships representing the response of the volumetric water content and hydraulic conductivity as a function of matric suction. From the experimental point of view, proper characterization of the unsaturated hydraulic characteristics of expansive

clays is not only complicated by the need to control an additional variable (volume changes), but also because these soils have particularly low hydraulic conductivity values, which adds significant challenges in terms of testing time and accuracy of measurements.

This investigation used centrifuge technology as an alternative to alleviate the shortcomings in the characterization of the unsaturated hydraulic characteristics, and associated volumetric changes, of expansive clays. Specifically, centrifuge technology was adopted for continuous and expeditious measurement of the changing soil moisture content, suction, hydraulic conductivity and void ratio that occur during unsaturated flow processes. The use of centrifuge technology allowed accurate and expeditious determination of the swelling of clays, including the determination of the swell-stress relationship. Determination of this relationship is particularly relevant because the financial losses caused by problems associated with expansive clays correspond to the highest costs associated with natural hazards in the US.

The new centrifuge approach developed in this study for characterization of swelling of clays involves subjecting soil specimens to water infiltration during comparatively small testing periods. The results indicate that, in spite of the significantly more practical and expeditious characteristics of the new approach, the predicted swell-stress curve is the same as that obtained using time-consuming conventional experimental techniques. The centrifuge approach was found to be particularly appropriate for determination of the Potential Vertical Raise, a magnitude that has often been used for the design of roads founded on expansive clays.

References

- [1] Jones, D.E., and Holtz, W.G. (1973). "Expansive Soils – The Hidden Disaster." Civil Engineering, New York, pp. 87-89.
- [2] Jones, D. E. (1981). "Perspectives on needs for an availability of scientific and technical information. Department of Housing and Urban Development, presented at the 1st meeting of Committee on Emergency Management, Commission on Sociotechnical Systems, National Research Council, April 30-May 1, 1981.
- [3] Whitterspoon, W.T. and Litke, S. (2000). "Residential Foundation Performance: A Study of Repaired Foundations." ADSC, pp. 156.
- [4] Wray, W.K. and Meyer, K.T. (2004). "Expansive Clay Soil... A Widespread and Costly Geohazard." Geo-Strata, Vol. 5, no. 4, pp. 24-28.
- [5] Adams, A.G., Dukes, O.M., Tabet, W., Cerato, A.B. and Miller, G.A. (2008). "Sulfate Induced Heave in Oklahoma Soils due to Lime Stabilization." GeoCongress 2008: GSP 179, Characterization, Monitoring, and Modeling of GeoSystems, New Orleans, LA, March 9-12, 2008, pp. 444-451.
- [6] Puppala, A. J., and Cerato, A. (2009). "Heave distress problems in chemically-treated sulfate-laden materials." Geo-Strata, 10(2), 28-32.
- [7] Rendon-Herrero, O. 2011. "Special Issue on Construction on Expansive Soils," Guest Editor Introduction, ASCE Journal of Performance of Constructed Facilities, pp. 2-4.
- [8] El-Garhy, B.M. and Wray, W.K. (2004). "Method for Calculating the Edge Moisture Variation Distance." Journal of Geotechnical and Geoenvironmental Engineering, ASCE, Vol. 130, pp. 945-955.
- [9] Houston, S.L., Dye, H.B., Zapata, C.E., Waslh, K.D., and Houston, W.N. (2011). "Study of Expansive Soils and Residential Foundations on Expansive Soils in Arizona." J. Performance of Constructed Facilities, ASCE, Vol. 25, No. 1, pp. 31-44.
- [10] Miao, L., Houston, S.L., Cui, Y., and Yuan, J. (2007). "Relationship between Soil Structure and Mechanical Behavior of an Expansive Unsaturated Clay." Canadian Geotechnical Journal, Vol. 44, No. 2, pp. 126-137.
- [11] Cerato, A., Miller, G., and Hajjat, J. (2009). "Influence of Clod-Size and Structure on Wetting-Induced Volume Change of Compacted Soil." *J. Geotech. Geoenviron. Eng.*, 135(11), 1620-1628.
- [12] Miller, G.A., and Zaman, M. (2007). "Field and Laboratory Evaluation of Cement Kiln Dust as a Soil Stabilizer." Transportation Research Record 1714, pp. 25-31.

- [13] Likos, W.J., and Lu, N. (2003). "Automated Humidity System for Measuring Total Suction Characteristics of Clay." *Geotechnical Testing Journal*, Vol. 26, No. 2, pp. 1-12.
- [14] Likos, W.J., and Lu, N. (2003b). "Filter paper column for measuring transient suction profiles in expansive clay," *Journal of the Transportation Research Board*. No. 1821, 83-89.
- [15] Puppala, A.J., Punthataechea, K., Vanapalli, S.K. (2006) "Soil water characteristic curves of stabilized expansive soils." *Journal of Geotechnical and Geoenvironmental Engineering*, ASCE, 132(6):736-750.
- [16] Lin, B., and Cerato, A.B. (2012). "Investigation on Soil-Water Characteristic Curves of Untreated and Stabilized Highly Clayey Expansive Soils." *Journal of Geotechnical and Geological Engineering*, Vol. 30, No. 4, pp. 803-812.
- [17] Likos, W.J. and Wayllace, A. (2010). "Porosity Evolution of Free and Confined Bentonites during Interlayer Hydration." *Clays and Clay Minerals*, Vol. 58, No. 3, pp. 399-414.
- [18] Zhan, T.L.T., Ng, C.W.W. (2006). "Shear strength characteristics of an unsaturated expansive clay." *Can Geotech J* 43:751-763.
- [19] Zornberg, J.G., and McCartney, J.S. (2010). "Centrifuge Permeameter for Unsaturated Soils I: Theoretical Basis and Experimental Developments." *Journal of Geotechnical and Geotechnical Engineering*, ASCE, Vol. 136, No. 8, August, pp. 1051-1063.
- [20] McCartney, J.S., and Zornberg, J.G. (2010). "Centrifuge Permeameter for Unsaturated Soils II: Determination of the Hydraulic Characteristics of an Unsaturated Clay." *Journal of Geotechnical and Geotechnical Engineering*, ASCE, Vol. 136, No. 8, August, pp. 1064-1076.
- [21] McCartney, J.S., and Zornberg, J.G. (2010). "Effects of Infiltration and Evaporation on Geosynthetic Capillary Barrier Performance." *Canadian Geotechnical Journal*, Vol. 47, No. 11, November, pp. 1201-1213.
- [22] Gouy, G. 1910. Sur la constitution de la charge electrique a la surface d'un electrolyte, *Annales Physique* (Paris), Serie 4, Vol. 9, pp. 457-468.
- [23] Chapman, D. L. 1913. A contribution to the theory of electrocapillarity, *Philosophical Magazine*, Vol. 25, No 6, pp. 475-481.
- [24] Mitchell, J. K. and Soga, K. 2005. Fundamentals of soil behavior (3rd edn). Hoboken, NJ: John Wiley & Sons. ISBN 13: 978-0-471-46302-7.
- [25] Bolt, G. H. 1956. Physico-chemical analysis of the compressibility of pure clays, *Géotechnique*, Vol. 6, No. 2, pp. 917-928.
- [26] Warkentin, B. P., Bolt, G. h., and Miller, R. D. 1957. Swelling pressure of montmorillonite, *Soil Science Society of America Proceedings*, Vol. 21, No. 5, pp. 495-497.
- [27] Madsen, F. T., and Müller-Vonmoos, M. 1989. The swelling behaviour of clays, *Applied Clay Science*, Vol. 4, No. 2, pp. 143-156.
- [28] Di Maio, C. 1996. Exposure of bentonite to salt solution: Osmotic and chemical effects, *Géotechnique*, Vol. 46, No. 4, pp. 695-707.
- [29] ASTM (2008). D-4546-08. Standard test methods for one-dimensional swell or collapse of cohesive soils. American Society for Testing and Materials.
- [30] McDowell, C., 1956, "Interrelationships of loads, volume change, and layer thickness of soils to the behavior of engineering structures." Highway Research Board, Proc. 35th Annual Meetings, Pub. No. 426, Washington, DC, pp. 754-772.
- [31] Vijayavergiya, V and Ghazzaly, O. 1973. Prediction of swelling potential for natural clays. In Proceedings of the 3rd International Conference on Expansive Soils, Haifa.
- [32] Nayak, N. V and Christensen, R. W. 1974. Swelling characteristics of compacted expansive soils. *Clays and Clay Minerals*, 19 (4):251-261.
- [33] Rao, A., Phanikumar, B., and S. R.S. 2004. Prediction of swelling characteristics of remoulded and compacted expansive soils using free swell index. *Quarterly Journal of Engineering Geology and Hydrogeology*, 37:217-226.
- [34] TEX-124-E. Determining potential vertical rise. Texas Department of Transportation.
- [35] ASTM (2008) D6836-02 e2. Standard Test Methods for Determination of the Soil Water Characteristic Curve for Desorption Using a Hanging Column, Pressure Extractor, Chilled Mirror Hygrometer, and/or Centrifuge.
- [36] van Genuchten, M. (1980). "A closed-form equation for predicting the hydraulic conductivity of unsaturated soils." *Soil Sci. Soc. Am. J.* 44, 892-898.
- [37] Olson, R., and Daniel, D. (1981). "Measurement of the hydraulic conductivity of fine grained soils." *Permeability and Groundwater Contaminant Transport*, ASTM STP 746. T.F. Zimmie and C.O. Riggs, Eds., ASTM. 18-64.
- [38] Zapata, C., Houston, W., Houston, S., and Walsh, K. (1999). "Soil-water characteristic curve variability." GSP No. 99, Advances in Unsaturated Geotechnics, Proc. of sessions of Geo-Denver 2000. ASCE. Denver, CO.

- [39] Brooks, R.H., and Corey, A.T. (1964). "Hydraulic properties of porous medium." Colorado State University (Fort Collins). Hydrology Paper No. 3. March.
- [40] Fredlund, D.G. and Xing, A. (1994). "Equations for the soil-water characteristic curve." *Canadian Geotechnical Journal*, 31, 521-532.
- [41] Arya, L.M., Leij, F.J., Shouse, P.J., and van Genuchten, M. (1999). "Relationship between the hydraulic conductivity function and the particle-size distribution." *Soil Sci. Soc. Am. J.* 63:1063-1070.
- [42] Burger, C. and Shackelford, C. (2000). "Soil-water characteristic curves and dual porosity of sand-diatomaceous earth mixtures." *ASCE J. Geotech. Geoenviron. Eng.* 127(9), 790-800.
- [43] Simms, P. and Yanful, E. (2002). "Predicting soil-water characteristics curves of compacted plastic soils from measured pore-size distributions." *Geotechnique*, 52(4) 269-278.
- [44] Chiu, T.F., and Shackelford, C.D. (1998). "Unsaturated hydraulic conductivity of compacted sand-kaolin mixtures." *Journal of Geotechnical and Geoenvironmental Engineering*, ASCE, Vol. 124, No. 2, February 1998, pp. 160-170.
- [45] Vanapalli, S., Pufahl, D., and Fredlund, D. (1999). "The influence of soil structure and stress history on the soil-water characteristic of a compacted till." *Geotechnique*, 49(2):143-159.
- [46] Miller, C., Yesiller, N., Yaldo, K., and Merayyan, S. (2002). "Impact of Soil Type and Compaction Conditions on Soil Water Characteristic." *J. Geotech. Geoenviron. Eng.* 128(9), 733-742.
- [47] Meerding, J. S., Benson, C. H., and Khire, M. V. (1996). "Unsaturated hydraulic conductivity of two compacted barrier soils." *Journal of Geotechnical and Geoenvironmental Engineering*, ASCE, 122(7), 565-576.
- [48] Tinjum, J., Benson, C., and Blotz, L. (1997). "Soil-Water Characteristic Curves for Compacted Clays." *J. Geotech. Geoenviron. Eng.* 123(11), 1060-1069.
- [49] Huang, S., Fredlund, D. and Barbour, S. (1998). "Measurement of the coefficient of permeability for a deformable unsaturated soil using a triaxial permeameter." *Can. Geotech. J.* 35: 426-432.
- [50] Parent, S.E., Cabral, A.R., Dell'Avanzi, E., and Zornberg, J.G. (2004). "Determination of the Hydraulic Conductivity Function of a Highly Compressible Material Based on Tests with Saturated Samples." *ASTM Geotechnical Testing Journal*, November 2004, Vol. 27, No. 6, pp. 1-5.
- [51] Parent, S.E., Cabral, A.R., Dell' Avanzi, E., and Zornberg, J.G. (2007). "Determination of the Hydraulic Conductivity Function of a Highly Compressible Material Based on Tests with Saturated Samples - Closure." *ASTM Geotechnical Testing Journal*, Vol. 30, No.3, May, pp. 242-243.
- [52] Parent, S.E., Cabral, A.R., and Zornberg, J.G. (2007). "Water Retention Curve and Hydraulic Conductivity Function of Highly Compressible Materials." *Canadian Geotechnical Journal*, Vol. 44, No. 10, October, pp. 1200-1214.
- [53] Ng, C. and Pang, Y. (2000). "Influence of stress state on soil-water characteristics and slope stability." *J. Geotech. Geoenviron. Eng.* 126(2):157-166.
- [54] Khaleel, R. Relyea, J., Conca, J. (1995). "Evaluation of van Genuchten-Mualem relationships to estimate unsaturated hydraulic conductivity at low water contents." *Water Resour. Res.* 31(11), 2659-2668.
- [55] Benson, C. and Gribb, M. (1997). "Measuring unsaturated hydraulic conductivity in the laboratory and field." *Unsaturated Soil Engineering Practice*. Houston, S. and Wray, W. (eds.). ASCE. Reston, VA. p. 113-168.
- [56] Lu, N. and Likos, W.J. (2005). *Unsaturated Soil Mechanics*. Wiley. New York. 584 p.
- [57] Moore, R. (1939). "Water conduction from shallow water tables." *Hilgardia*, 12, 383-426.
- [58] Arulanandan, K., Thompson, P.Y., Kutter, B.L., Meegoda, N.J., Muraleetharan, K.K., and Yogachandran, C. (1988). "Centrifuge modeling of transport processes for pollutants in soils." *Journal of Geotechnical Engineering*, Vol. 114, No. 2, February 1988, pp. 185-205.
- [59] Cooke, A.B., and Mitchell, R.J. (1991). "Physical modelling of a dissolved contaminant in an unsaturated sand." *Canadian Geotechnical Journal*, Vol. 28, pp. 829-833.
- [60] Hensley, P.J., and Schofield, A.N. (1991). "Accelerated physical modelling of hazardous-waste transport." *Géotechnique*, Vol. 41, No. 3, pp. 447-465.
- [61] Li, L., Barry, D.A., and Stone, K.J.L. (1994). "Centrifugal modelling of non-sorbing, nonequilibrium solute transport in a locally inhomogeneous soil." *Canadian Geotechnical Journal*, Vol. 31, pp. 471-477.
- [62] Mitchell, R.J. (1994a). "Matrix suction and diffusive transport in centrifuge models." *Canadian Geotechnical Journal*, Vol. 31, pp. 357-363.
- [63] Mitchell, R.J. (1994b). "Centrifuge techniques for testing clay liner samples." *Canadian Geotechnical Journal*, Vol. 31, pp. 577-583.
- [64] Illangasekare, T.H., Znidarcic, D., Al-Sheridda, M., and Reible, D.D. (1991). "Multi-phase flow in porous media." *Centrifuge '91*, H.-Y. Ko and F. G. McLean, eds., Balkema, Rotterdam, The Netherlands, pp. 517-523.
- [65] Knight, M.A. and Mitchell, R.J. (1996). "Modelling of light nonaqueous phase liquid (LNAPL) release into unsaturated sand." *Canadian Geotechnical Journal*, Vol. 33, No. 4, pp. 913-925.

- [66] Culligan, P.J., Savvidou, C., and Barry, D.A. (1996). "Centrifuge modelling of contaminant transport processes." *Electr. J. of Geot. Eng.*, <<http://geotech.civen.okstate.edu/ejge/Ppr9606/index.htm>>.
- [67] Abu-Hassanein, Z., Riemer, M. F., and Pantazidou, M. (1998). "Infiltration of High Viscosity Low Density DNAPLs in Saturated Porous Media." *Centrifuge '98*, Tokyo, pp. 23-25.
- [68] Pantazidou, M., Abu-Hassanein, Z.S., and Riemer, M.F. (2000). "Centrifuge study of DNAPL transport in granular media." *Journal of Geotechnical and Geoenvironmental Engineering*, Vol. 126, No. 2, February, pp. 105-115.
- [69] Culligan, P.J., Barry, D.A., and Parlange, J.-Y. (1997). "Scaling unstable infiltration in the vadose zone." *Canadian Geotechnical Journal*, Ottawa, No. 34, pp. 466-470.
- [70] Griffioen, J.W., and Barry, D.A. (1999). "Centrifuge modeling of unstable infiltration and solute transport." *Journal of Geotechnical and Geoenvironmental Engineering*, ASCE, Vol. 125, No. 7, July 1999, pp. 556-565.
- [71] Oliveira, W.L. and Znidarcic, D. (1998). "Instrumentation for soft soil desiccation testing." *Centrifuge '98*, T. Kimura, O. Kusakabe, and J. Takemura, eds., Balkema, Rotterdam, The Netherlands, pp. 47-54.
- [72] Gardner, R. (1937). "The method of measuring the capillary pressures in small core samples." *Soil Science*, 43, 277-283.
- [73] Hassler, G. L. and Brunner, E. (1945). "Measurements of capillary pressure in small core samples." *Trans. AIME*. 160, 114-123.
- [74] Goodings, D.J. (1984). "Relationships for modelling water effects in geotechnical centrifuge models." *Application of Centrifuge Modelling to Geotechnical Design*, W.H. Craig, ed., pp. 1-24.
- [75] Garnier, J., Lynch, R., Bolton, M., Kecharvarzi, C., Treadaway, A., Coumoulos, H., Soga, K., Konig, D., Rezzoug, A., Heibrock, G., Weststrate, F.A., Van der Poel, J.T., Ouung, O., Schrijver, R.R., Allersma, H.G.B., Esposito, G.M., Davis, M., Burkhardt, S., Merrifield, C.M., and Craig, W.H. (1998). "NECER: network of European centrifuges for environmental geotechnical research: Special Report." *Centrifuge '98*, Balkema, Rotterdam, pp. 33-55.
- [76] Dell'Avanzi, E., Zornberg, J.G., and Cabral, A.R. (2004). "Suction Profiles and Scale Factors for Unsaturated Flow under Increased Gravitational Field." *Soils and Foundations*, June, Vol. 44, No. 3, pp. 79-89.
- [77] Frydman, S. and Weisberg, E (1991). "Study of centrifuge modeling of swelling clay." *Proceedings of the International Conference Centrifuge*, p. 113.
- [78] Gadre, A. and Chandrasekaran, V. (1994). "Swelling of black cotton soil using centrifuge modeling." *Journal of Geotechnical Engineering*, Vol. 5, p. 914-919.
- [79] Nimmo, J.R., Rubin, J., and Hammermeister, D. P. (1987). "Unsaturated flow in a centrifugal field: Measurement of hydraulic conductivity and testing of Darcy's law." *Water Resources Research*, Vol. 23, pp. 124-134.
- [80] Conca, J., and Wright, J. (1992). "Diffusion and flow in gravel, soil, and whole rock." *Applied Hydrogeology*. 1, 5-24.
- [81] Zornberg, J.G., LaFountain, L., and Caldwell, J.C. (2003). "Analysis and design of evapotranspirative cover for hazardous waste landfill." *J. Geotech. Geoenv. Eng.* 129(5), 427-438.
- [82] Bear, J., Corapcioglu, Y. and J. Bulkarnishna. 1984. "Modeling of centrifugal filtration in unsaturated deformable porous medium." *Adv. in Water Resour.* 7(4), 150-167.
- [83] Simunek, J., and Nimmo, J.R. 2005. "Estimating soil hydraulic parameters from transient flow experiments in a centrifuge using parameter optimization technique." *Water Resour. Res.* 41(4)
- [84] Gardner, W. R. (1958) "Some steady -state solutions of the unsaturated moisture flow equation with application to evaporation from a water table. *Soil Sci.* 85: 228-232
- [85] Quaglia, G. (2017). Ph.D. dissertation: "Hydro-mechanical Characterization of Unsaturated Clays using Centrifuge Technology." Department of Civil, Architectural, and Environmental Engineering. The University of Texas at Austin.
- [86] Blake, C., Summerlin, K., and Zornberg, J.G. (2019). Characterization of Swelling for Natural and Stabilized Clays using Centrifuge Technology. Center for Transportation Research (CTR), Product Report No. FHWA/TX-19/5-6048-05, Austin, Texas, August, 184 p.
- [87] Zornberg, J.G., Plaisted, M.D., Armstrong, C.P., and Walker, T.M. (2013). Implementation of Centrifuge Testing for Swelling Properties of Highly Plastic Clays. Center for Transportation Research (CTR), Product Report No. 5-6048-01-1, Austin, Texas, August, 90 p.
- [88] Armstrong, Christian, P. (Spring 2018). Ph.D. dissertation; "Characterization of Expansive Clay Behavior using Centrifuge and Field Evaluations." Department of Civil, Architectural, and Environmental Engineering. The University of Texas at Austin.
- [89] Zornberg, J.G., Armstrong, C.P., and Potkay, A. (2017). Implementation of Centrifuge Testing of Expansive Soils for Pavement Design. Center for Transportation Research (CTR), Product Report No. 5-6048-03-1, Austin, Texas, March, 222 p.

Technical Session #4

“Unsaturated Soils”



Eduardo ROJAS

Dr. Eduardo Rojas is a Civil Engineer from CeNETI (Mexico) and got his master and PhD degrees at the Institut de Méchanic de Grenoble (France). He is presently a research-professor at the University of Querétaro, Mexico. He is chairman of the Geotechnical Section of the Postgraduate program and president of the Technical Committee on Unsaturated Soils of the Mexican Society of Geotechnical Engineering. He has been entitled as National Researcher from the National Research Agency and has obtained the González Flores Award in the area of Research from the Mexican Society of Geotechnical Engineering. He has been granted three times the Alejandrina Award in Research and Technology by the University of Querétaro. He has written 3 books and published 72 peer reviewed papers. He is consultant engineer for retaining walls, shallow and deep foundations and foundations for expansive soils. He also has been involved in projects for the levelling of inclined buildings.

A General Fully Coupled Model for Unsaturated Soils

Eduardo ROJAS^{a,1}

^aUniversidad Autónoma de Querétaro, México

Abstract. Different phenomena influence the strength and volumetric behavior of unsaturated soils. Among the most important are suction hardening, hydraulic hysteresis and the influence of volumetric strains on the soil-water retention curves. Fully coupled hydro-mechanical models require including all three phenomena in their constitutive relationships. Among these phenomena, suction hardening is the most influencing as it determines the apparent preconsolidation stress, the position of the loading-collapse yield surface and the shift of both the isotropic consolidation and the critical state lines. In this paper, a simple fully coupled hydro-mechanical model is presented. Numerical simulations on both suction controlled and undrained triaxial tests show comparable results to more complex models.

Keywords. Unsaturated soils, coupled model, effective stresses, suction hardening

1. Introduction

In the last fifteen years many hydro-mechanical coupled models for unsaturated soils have been developed using the effective stress concept. Some models use non-normal flow rules requiring a plastic potential function in addition to a yield surface. Others use elaborated hardening coefficients to reproduce the volumetric behavior of unsaturated soils. Some others include fitting parameters for hydro-mechanical coupling. Models based on the modified Cam-Clay model (MCCM) have been largely used with fair results. Some of the most representative models are those proposed by Russell and Khalil [1], Zhou and Sheng [2] and Ma et al. [3].

The aim of this paper is demonstrate that constitutive models based on the Critical State theory for saturated soils can be easily adapted as fully coupled models for unsaturated soils when the phenomena of suction hardening, hydraulic hysteresis and dependency of the soil water retention curves (SWRCs) on plastic volumetric strains are properly considered. Specifically, this paper shows that the MCCM can properly simulate the behavior of unsaturated soils with minor changes. In this way, very simple fully coupled constitutive models for soils can be generated with similar precision to other models.

In this paper, the mean effective stress (p') is represented by Bishop's equation, in the form:

¹ Corresponding Author: Eduardo Rojas, UAQ, Facultad de Ingeniería, Cerro de las Campanas, Querétaro, Qro., México. E-mail: erg@uaq.mx.

$$p' = p_n + \chi s \quad (1)$$

where $p_n = p - u_a$ is the mean net stress defined as the total stress (p) in excess of air pressure (u_a). The term χs represents the suction stress where χ is Bishop's parameter and $s = u_a - u_w$ represents suction with u_w as the water pressure. Bishop's parameter can be obtained through a porous-solid model described in the next section.

When loading is preceded by drying in soil samples, the phenomenon of suction hardening occurs. It is one of the most influencing phenomena when modeling the behavior of unsaturated soils. This phenomenon arises because the components of the effective stress: suction and net stresses, act independently one from the other. When a soil dries, the apparent preconsolidation stress increases in a quantity dependent on the increment of suction stress. Consider Figure 1(a) representing the volumetric behavior of the soil in the axes logarithm of the effective mean stresses (p') versus void ratio (e). Suppose that a saturated normally consolidated soil is initially subjected to a mean net stress p_{n0} indicated by point 0 in Figure 1(a). If this sample is subjected to drying, the mean effective stress increases in the quantity $\chi_0 s_0$, where s_0 represents the maximum suction reached at drying and χ_0 represents the value of Bishop's parameter at this suction. This behavior is sketched in Figure 1(b) in the axes of mean effective stress against suction. During drying, the mean effective stress moves from 0 to A in Figure 1(a). If at this stage, the sample is loaded by an increment of the mean net stress, an initial elastic behavior occurs (path AB) until the apparent preconsolidation stress (p'_0) is reached. This apparent preconsolidation stress (point B) is represented by the mean effective stress at the end of drying (point A) added by the suction stress ($\chi_0 s_0$) as indicated in Figure 1(b). If the net mean stress increases further, elastoplastic strains occur (dotted path beyond B in Figure 1(a)). This means that the increment in the apparent preconsolidation stress after drying (point B) with respect to the initial preconsolidation stress (p_{n0}) is twice the suction stress $\chi_0 s_0$, as indicated in Figure 1(b). Therefore, the loading collapse yield surface (LCYS) runs parallel to the drying path at a horizontal stress equal to the suction stress $\chi_0 s_0$ (see Figure 1(b)). In other words, when the effective stress increases in the quantity $\Delta(\chi s)$, the apparent preconsolidation stress increases in the quantity $2\Delta(\chi s)$. This explains why unsaturated soils rapidly show highly preconsolidated behavior when suction increases. This increase of twice the suction stress increment for the preconsolidation stress is not considered by most constitutive models. The Barcelona Basic Model considers this phenomenon by coupling the displacements of the LCYS with those of the suction increase yield surface (SIYS).

In contrast, when the effective stress increases by a net stress increment Δp_n beyond the LCYS, the apparent preconsolidation stress (p'_0) only increases in this same quantity. Suction hardening not only affects the position of the isotropic consolidation line (ICL) but it pulls along the critical state line (CSL) as reported by different researchers (see for example Wheeler and Sivakumar [4]). The shift of both lines is indicated in Figure 1(a) where $CSL_{s=0}$ and CSL_{s_0} represent the position of the CSL for suction equal 0 and s_0 , respectively.

Related to this phenomenon comes another issue. When suction hardening is taken into consideration to include the shift of the ICL and CSL in the constitutive model, an anisotropic hardening of the yield surface in the effective mean stress (p') against the deviator stress (q) plane occurs. Consider the elliptic yield surface of the MCCC depicted in Figure 1(b). When suction hardening occurs, the ICL and the CSL displace in the quantity $\chi_0 s_0$. However, the critical state point (center) of an ellipse showing

isotropic hardening only displaces in the quantity $\chi_0 s_0/2$. Therefore, in order to displace the CSL in the quantity $\chi_0 s_0$, anisotropic hardening of the elliptic yield surface has to be considered as shown in Figure 1(b). In spite of this, most constitutive models do not include anisotropic hardening in their developments.

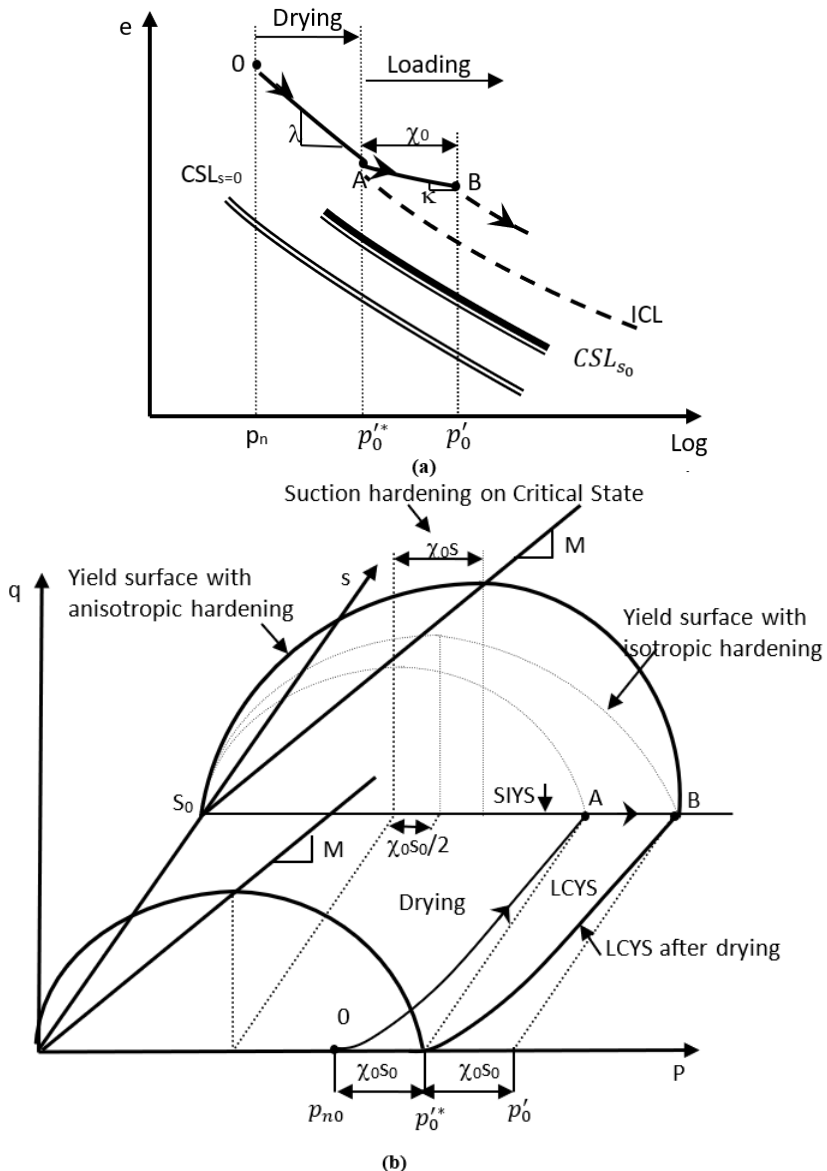


Figure 1. (a) Suction hardening displaces the ICL and the CSL in the quantity $\chi_0 s_0$, (b) the yield surface shows anisotropic hardening.

Moreover, suction stress (and therefore suction hardening) does not keep increasing with suction but it shows a maximum value and then decreases for sandy and silty soils

subjected to drying (Rojas [5], Lu et al. [6]). Consider a saturated soil sample subjected to drying up to suction s_0 . As suction increases, elastoplastic strain occurs (path 0A in Figure 2(a)) and the LCYS runs aside the drying path as indicated by line LCYS_B in Figure 2(b). Observe that in this last figure, the effective mean stress (horizontal axis) is plotted in logarithmic scale, and therefore, the drying path and the LCYS_B do not run parallel to each other as previously shown in Figure 1(b). If at some point, suction stress reaches its maximum value (point A, in Figure 2), the drying path curves to the left hand side and shows the shape sketched in Figure 2(b). When the maximum suction stress is reached, the apparent preconsolidation stress reaches its maximum value (p'_0)_C and the SIYS is locked at this position indicated by line SIYS_{max} in Figure 2(b). Because further drying produces the effective stress to reduce, soil sample shows a volumetric elastic rebound (path AB in Figure 2(a)). Therefore, from the maximum suction stress and for increasing values of suction, the LCYS_B shows a vertical slope (line CC' in Figure 2(b)). This means that at this stage, no further yielding occurs with increasing values of suction. This behavior has been experimentally reported by Cunningham et al. [7] and Fleureau et al. [8]. If at the end of drying (point B), the soil is loaded by a net stress increase, it shows an initial elastic recompression (path BC) until the apparent preconsolidation stress is reached (point C) with a maximum suction hardening value of (χs)_{max}. With further loading, the sample shows elastoplastic behavior (path CD). By the end of loading the LCYS has displaced to the position indicated by line LCYS_D.

2. Hydraulic model

The hydraulic model employed here has been presented elsewhere (Rojas [5] and [9]) and will be only briefly described here. According to an equilibrium analysis, Bishop's parameter can be expressed as:

$$\chi = f^s + S_w^u f^u \quad (2)$$

where f^s and f^u represent the saturated and unsaturated fractions of the soil, respectively, and S_w^u is the degree of saturation of the unsaturated fraction. The saturated fraction represents the volume of all solids exclusively surrounded by saturated pores added by the volume of these pores and divided by the total volume of the soil. The unsaturated fraction represents the volume of solids surrounded by a combination of saturated and dry pores added by the volume of these pores and divided by the total volume of the soil. Finally, the degree of saturation of the unsaturated fraction is the volume of saturated pores divided by the total volume of pores both within the unsaturated fraction of the sample. For fully coupled models, these three parameters depend on the current value of suction and the whole wetting-drying and loading-unloading paths applied to the soil sample. Their value can be obtained using a porous-solid model based on the pore size distribution (PSD) and grain size distribution of the material (Rojas [5]). The PSD of a soil can be obtained indirectly from the porous-solid model when the experimental SWRCs at wetting and drying are provided. This can be accomplished, by successively proposing different values for the mean size and standard deviation for bonds and sites until the best fit between numerical and experimental curves is reached. This procedure is eased by the fact that bonds control the drying curve while the wetting curve is controlled by sites (Dullien [10]).

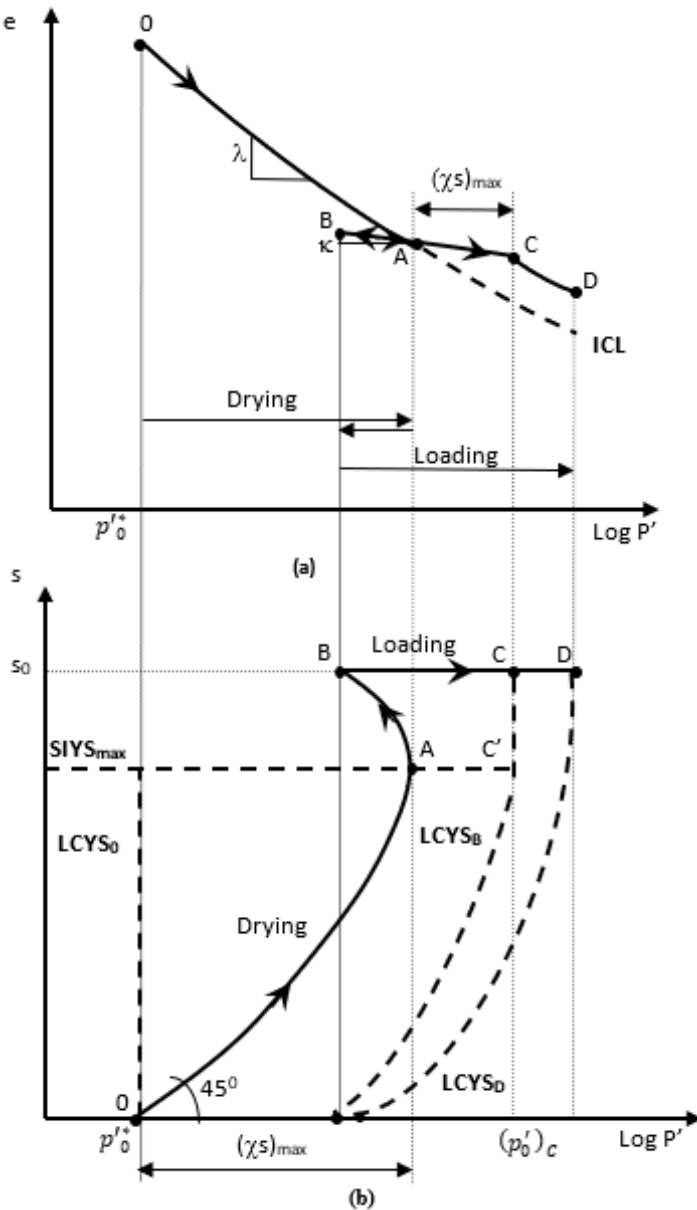


Figure 2. Loading after elastic rebound during drying. (a) Volumetric behavior and (b) stress path and yield surfaces at different stages.

3. Mechanical model

Anisotropic hardening was included in the model by Loret and Khalil [11]. This model considers a yield surface that can modify the position of the critical state with respect to the apparent preconsolidation stress. This feature was implemented by splitting the yield

surface in two ellipses that meet horizontally at the critical state in the axes of effective mean stress versus deviator stress. Here a similar approach is considered except that the two curves forming the yield surface can have different shapes (not only ellipses) and therefore a large number of combinations can be considered for the geometry of the yield surface in addition to the position of the critical state. The proposed equations for the left (dilating behavior) and the right side (compressive behavior) of the yield surface are:

$$\begin{aligned} q^{a_1} - M^{a_1} \{(b p'_0)^{a_1} - |p' - b p'_0|^{a_1}\} &= 0 \\ q^{a_2} - \left(\frac{M b}{1-b}\right)^{a_2} \{(p'_0(1-b))^{a_2} - |p' - b p'_0|^{a_2}\} &= 0 \end{aligned} \quad (3)$$

where a_1 and a_2 represent the exponent of the left and right side of the yield surface, respectively, while b is the ratio between the preconsolidation effective stress and the effective mean stress at the critical state. The left and right side of the yield surface are established according to the position of the critical mean stress $b\bar{p}'_0$.

Equations (3) ensures that for any combination of values where $a_1, a_2 > 1$, and $0 < b < 1$, both segments of the yield surface meet horizontally at the critical state and reach vertically the effective mean stress axis. Different combinations for parameters a_1, a_2 and b are represented in Figure 3. The three numbers for each surface, represent the values of parameters a_1, a_2 and b , in this order.

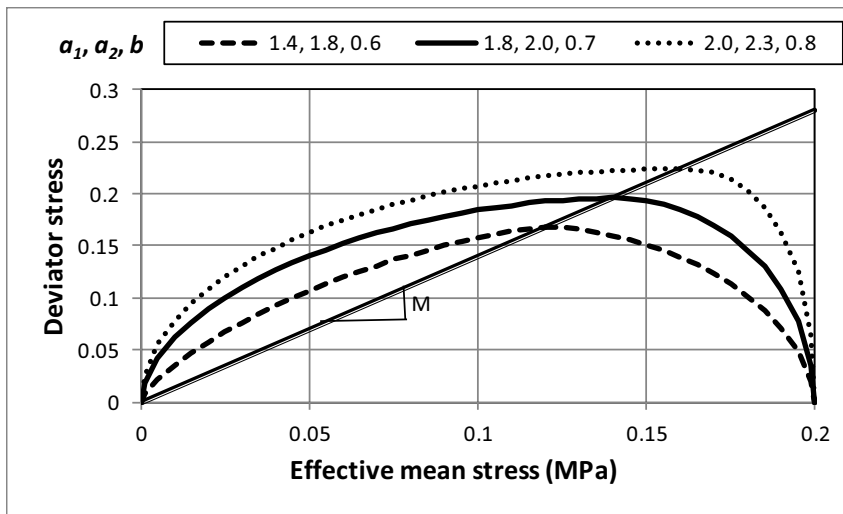


Figure 3. Different shapes and positions of the critical state for the yield surface in the (p', q) plane.

When few experimental results are available, the yield surface can take the usual ellipsoidal shape of the MCCM ($a_1 = a_2 = 2$) while the position of the critical state with respect to the preconsolidation stress (parameter b) can take values in the range between 0.4 - 0.6.

Accordingly, the stiffness matrix for the mechanical model used herein is similar to the Modified Cam Clay Model and results in:

$$\begin{bmatrix} d\epsilon_v^p \\ d\epsilon_q^p \end{bmatrix} = \frac{1}{H} \begin{bmatrix} a_x(M\beta_1)^{a_x}(p' - p'_0 b)^{(a_x-1)} & a_x q^{(a_x-1)} \\ a_x q^{(a_x-1)} & \frac{[a_x q^{(a_x-1)}]}{a_x(M\beta_1)^{a_x}(p' - p'_0 b)^{(a_x-1)}} \end{bmatrix} \begin{bmatrix} dp' \\ dq \end{bmatrix} \quad (4)$$

with

$$H = \left\{ \frac{\lambda - \kappa}{vp'_0 a_x [M\beta_1]^{a_x}} \right\} \left\{ \frac{1}{\beta_2 [p'_0 \beta_3]^{(a_x-1)} + \beta_4 (p' - p'_0 f)^{(a_x-1)}} \right\} \quad (5)$$

$$\beta_1 = \left(\langle h_1 \rangle + \langle h_2 \rangle \left(\frac{b}{1-b} \right) \right), \quad \beta_2 = (\langle h_1 \rangle + \langle h_2 \rangle (1-b)), \quad \beta_3 = (\langle h_1 \rangle b + \langle h_2 \rangle (1-b)), \quad \beta_4 = (\langle h_1 \rangle + \langle h_2 \rangle b).$$

a_x can take the value a_1 or a_2 depending which side of the yield surface hits the stress path: a_1 for the left side and a_2 for the right side. Similarly, $\langle h_1 \rangle$ and $\langle h_2 \rangle$ represent the step function for the left and right side of the yield surface, respectively, and can take the value 1 or 0, depending on the side reached by the stress path. It can be observed that the stiffness matrix remains symmetric which makes this model suitable for finite elements algorithms.

The elastic behavior is considered dependent on the effective mean stress and current void ratio. In this way, the bulk (K) and shear modulus (G) are given by the equations:

$$K = \frac{1+e}{e} \frac{p'}{\kappa} \quad G = \frac{3(1-2\nu)}{2(1+\nu)} \frac{(1+e)p'}{e \kappa} \quad (6)$$

where ν represents the Poisson ratio and κ the slope for the URL. Finally, the common hardening law for the yield surface is adopted here

$$dp'_0 = \frac{vp'_0}{\lambda - k} d\epsilon_v^p \quad (7)$$

Then, in order to simulate the behavior of unsaturated soil samples during triaxial tests, the proposed model requires the following parameters: M , λ , κ , v , a_1 , a_2 and b in addition to the grain size distribution, the main wetting and drying retention curves for a certain confining stress and the initial state of the sample (e_0 , p_0^{*} , \bar{p}_0 , q_0 , s_0).

4. Numerical and experimental comparisons

Two sets of controlled suction drained triaxial tests performed by different authors were compared with the numerical results to verify the precision of the proposed model. The first set of tests was carried out by Futai and Almeida [12]. These authors performed suction controlled triaxial tests on undisturbed tropical soil samples obtained at the depths of 1 and 5 m. The PSD of samples obtained at 1m in depth show a bi-modal structure and were chosen for the simulations presented here. The degree of saturation during sampling was of the order of 80 to 96%. Suction in the triaxial cells was controlled

using the axis translation technique. Volume change of soil samples in the triaxial cell were obtained using an automated rolling diaphragm device. Some isotropic tests at different values of suction were also performed and are shown in Figure 4. These results were used to obtain the values of parameters λ and κ . A set of saturated triaxial tests were performed on this material and reported elsewhere (Futai and Almeida [13]). These tests were used to obtain parameters M , a_1 , a_2 and f of the soil. Figure 5 shows the experimental points with the numerical fitting for these tests. The adopted values of the parameters of the model are listed in Table 1.

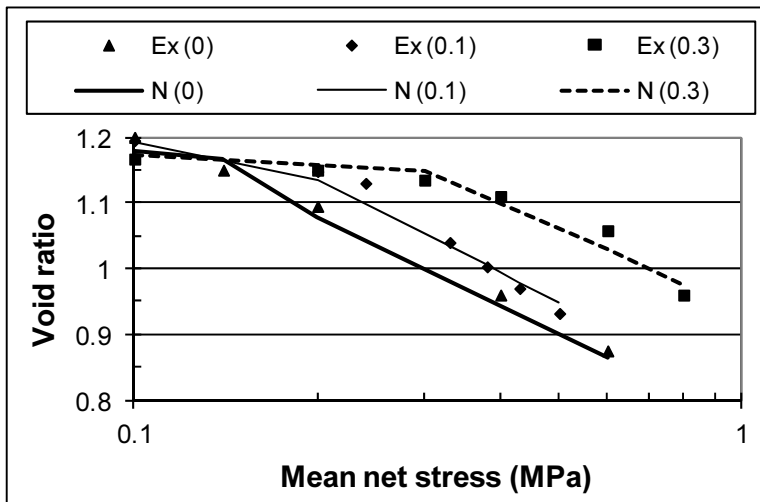
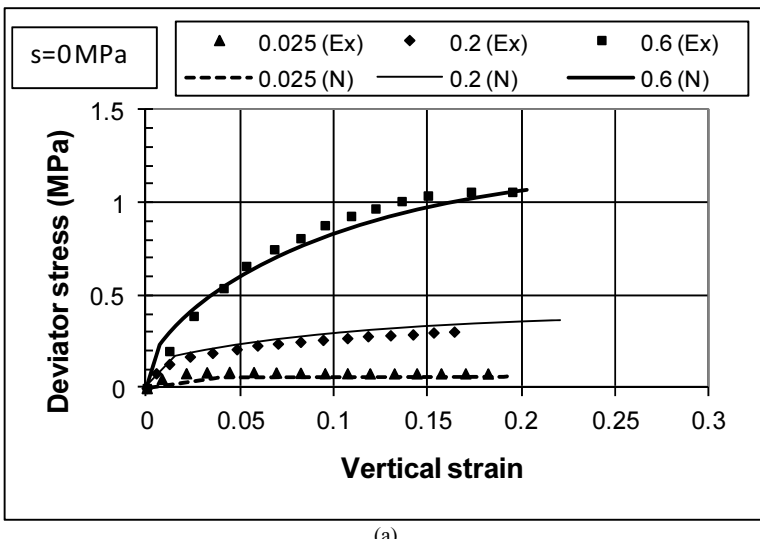


Figure 4. Experimental isotropic compression tests performed at different suctions (in MPa) and numerical fitting to set model parameters. Experimental data after Futai and Almeida [12].



(a)

Figure 5. Experimental results from saturated samples at different confining stresses (in MPa) and numerical fitting to set model parameters. Experimental data after Futai and Almeida [13].

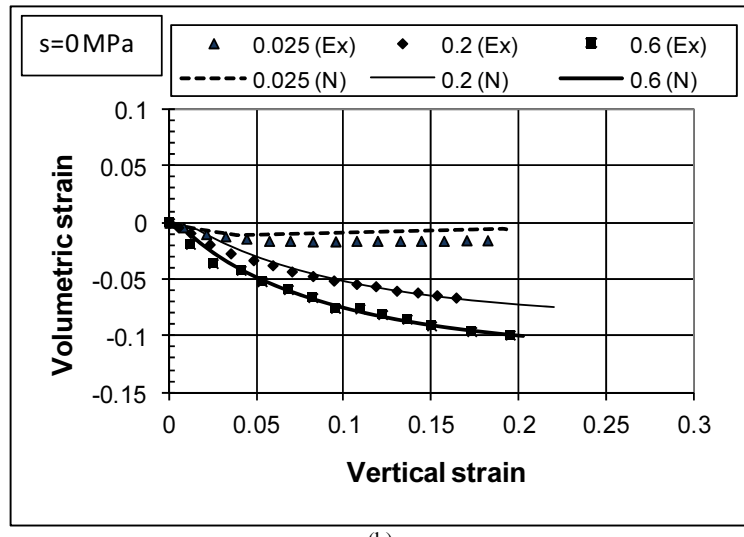


Figure 5. (continued) Experimental results from saturated samples at different confining stresses (in MPa) and numerical fitting to set model parameters. Experimental data after Futai and Almeida [13].

Table 1. Parameters of the model for test reported by Futai and Almeida [13].

Parameter	M	λ	κ	ν	a_1	a_2	f
Value	1.3	-0.25	-0.04	0.25	1.8	2.0	0.6

The experimental and numerical results of tests performed at two constant values of suction (0.1 and 0.3 MPa) and different confining stresses are shown in Figure 6.

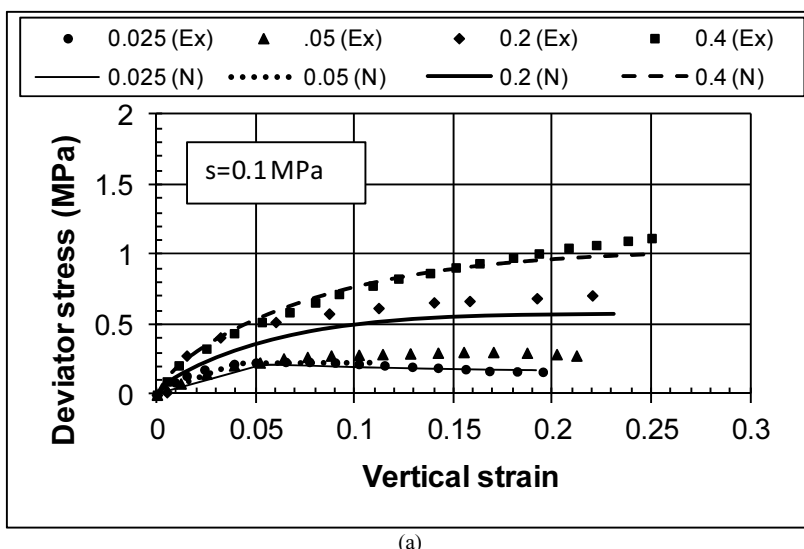


Figure 6. Experimental and numerical results comparison for triaxial tests at suction of 0.1 and 0.3 MPa and different confining stresses (in MPa). Experimental data after Futai and Almeida [12].

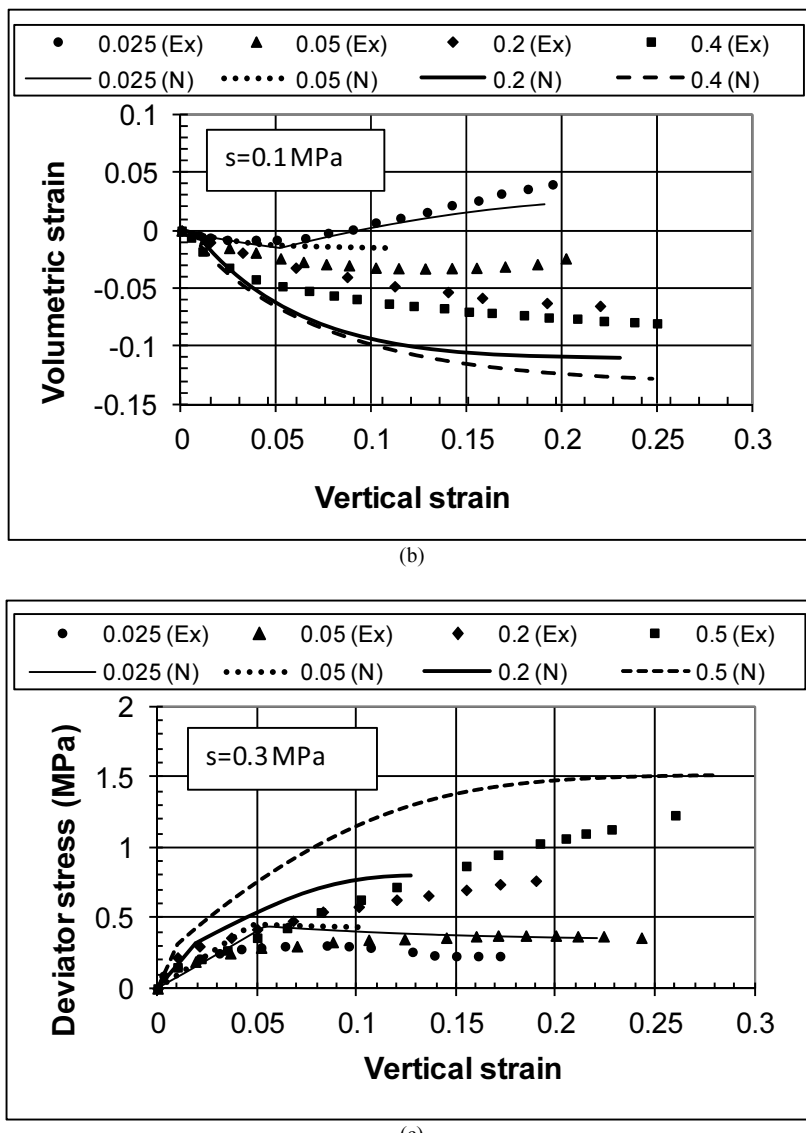
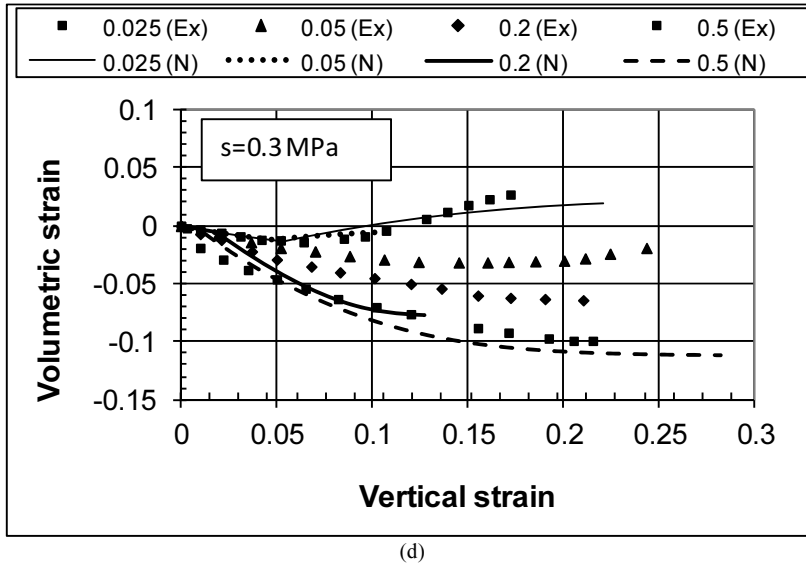


Figure 6. (continued) Experimental and numerical results comparison for triaxial tests at suctions of 0.1 and 0.3 MPa and different confining stresses (in MPa). Experimental data after Futai and Almeida [12].



(d)

Figure 6. (continued) Experimental and numerical results comparison for triaxial tests at suctions of 0.1 and 0.3 MPa and different confining stresses (in MPa). Experimental data after Futai and Almeida [12].

Although numerical results fit well with saturated experimental data, some differences are observed when modeling unsaturated samples. In general, for samples tested at a suction of 0.1 MPa, the numerical deviator stress at failure results smaller with respect to experimental results (see Figure 6(a)) except for the test performed at a confining stress of 0.05 MPa. In contrast the predicted volumetric strain during shearing show larger values during compression (see Figure 6(b)). For samples tested at a suction of 0.3 MPa, the numerical results agree better with experimental data except for the sample tested at a confining stress of 0.5 MPa. In that sense, the experimental results in the stress-strain plot (Figure 6(c)) show some inconsistencies related to the low stiffness and strength of this sample with respect to the other tests performed at the same suction (see Figure 6(c)).

The second set of experiments was performed by Garakani, et al [14]. They conducted suction controlled triaxial tests in a modified triaxial cell. Suction was controlled using the axis translation technique. Volume changes in the triaxial cell and soil sample were measured using automated volume change devices. These volume changes were corrected after a careful calibration of the equipment. Before shearing, samples were subjected to suction equilibrium followed by isotropic compression. Suctions varied from 0.1 to 0.4 MPa while isotropic stresses varied from 0.05 to 0.4 MPa. Figure 7 shows some numerical and experimental comparisons for triaxial tests performed at a constant suction of 0.4 MPa and different confining stresses. Table 2 shows the parameters used to simulate these tests.

Table 2. Parameters of the model for test reported by Garakani et al. [14].

Parameter	<i>M</i>	λ	κ	ν	a_1	a_2	b
Value	1.15	-0.25	-0.015	0.25	2.0	1.8	0.5

Experimental and numerical simulations show fair agreement except for the initial stiffness of samples tested at 0.05 and 0.15 MPa where experimental results show a much lower value. However, this behavior is inconsistent with results of sample tested at a confining stress of 0.3 MPa where the initial stiffness of experimental results agree well with the numerical simulation.

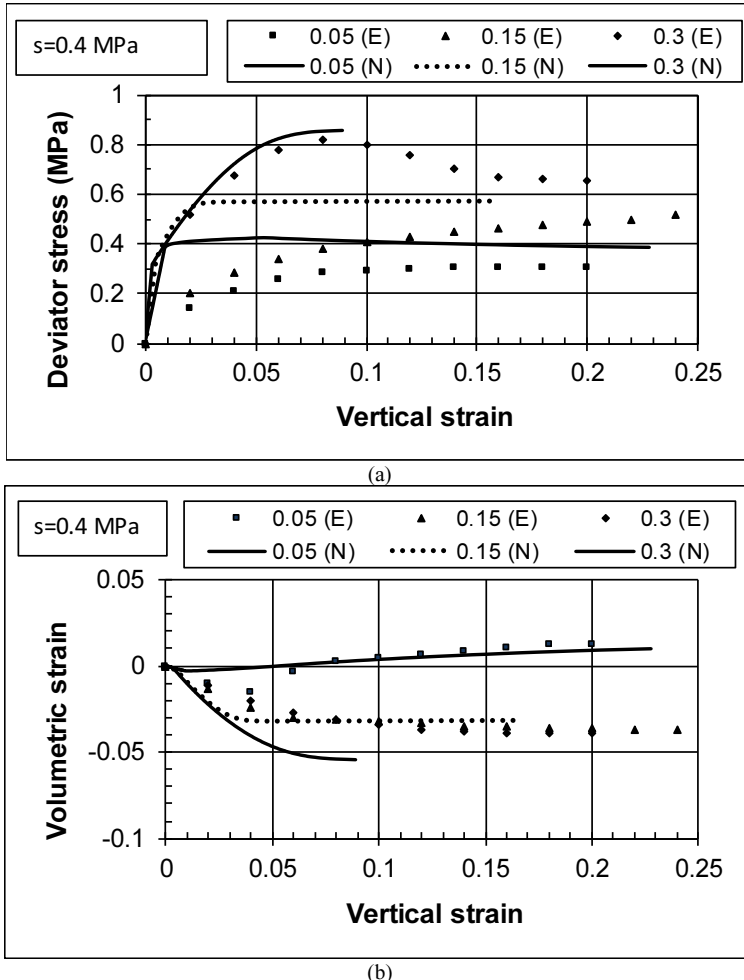


Figure 7. Numerical and experimental comparison for triaxial tests performed at constant suction and different confining stresses. Experimental data after Garakani et al. [14].

Additionally, Jotisankasa et al. [15] performed undrained triaxial tests on a mixture of 70% silt, 20% kaolin and 10% London clay. These materials were mixed at a water content 1.5 times de liquid limit. Then the slurry was dried at 70°C , grounded and passes into sieve N° 40. This material shows a liquid limit of 28% and plasticity index of 18%. This mixture was hydrated to reach a water content of 10.1% and statically compacted in nine layers at a maximum vertical pressure of 0.8 MPa to reach an initial void ratio of 0.706 with degree of saturation of 0.38. These samples were dryer and looser than the optimum of standard compaction.

The results of a series of undrained triaxial tests performed at the confining stresses of 0.2 MPa are shown along with the numerical simulations in Figure 8. The initial suction for each sample is indicated in top of this figure in MPa. Suction during shearing was measured in the triaxial cell using two suction probes located at two different heights of the sample. The volume change of the soil was estimated from the readings of both radial and local axial strain measurements. The axial strain was measured using a pair of inclinometer-type local strain devices. Radial displacements were measured at the mid-height of the sample using a single linear variable displacement transducer. The global volume change of the sample was estimated with a similar approach to that proposed by Klotz and Coop [16] using the recorded local strain measurements. Table 3 shows the values of the parameters of the model employed to simulate these tests.

Table 3. Parameters of the model for tests reported by Jotisankasa et al. [15].

Parameter	M	λ	κ	ν	a_1	a_2	b
Value	1.3	-0.21	-0.01	0.25	1.3	3.0	0.7

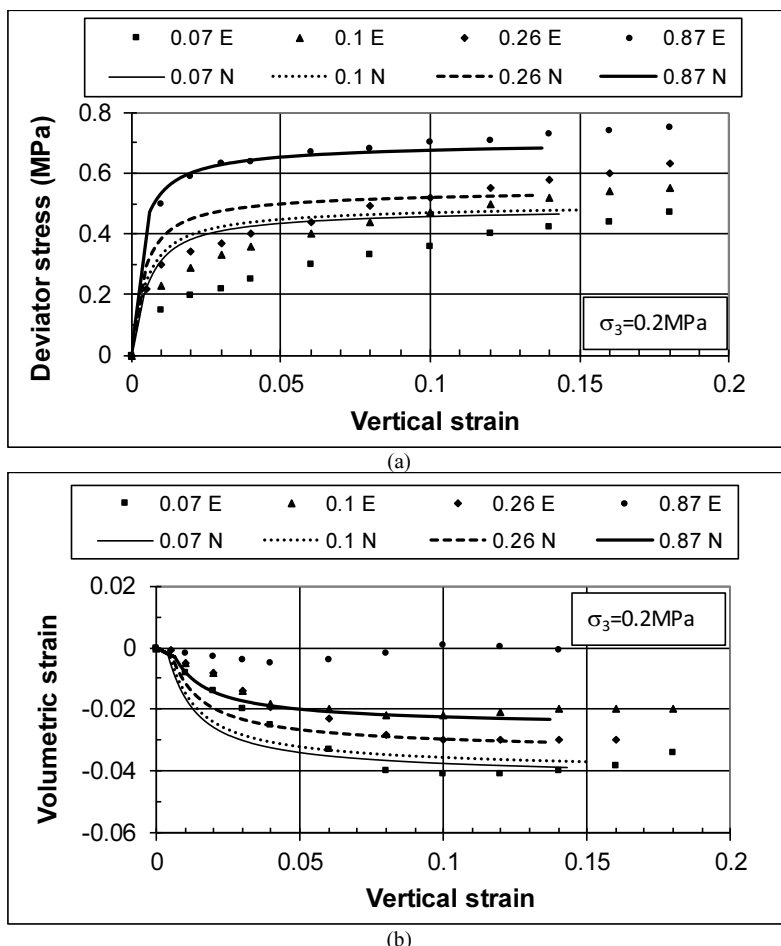


Figure 8. Undrained triaxial tests performed at a confining stress of 0.2 MPa and different water contents. Experimental data from Jotisankasa et al. [15].

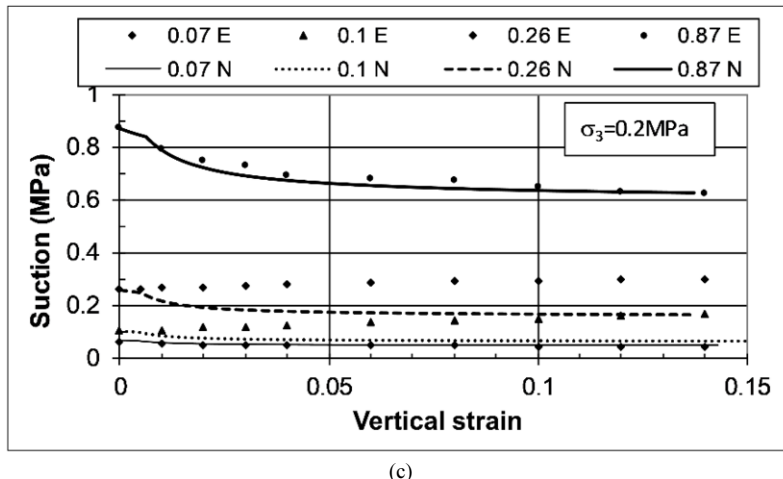


Figure 8. (continued) Undrained triaxial tests performed at a confining stress of 0.2 MPa and different water contents. Experimental data from Jotisankasa et al. [15].

Related to the strength, the numerical simulations show fair agreement. Related to the volumetric strain, discrepancies occur mainly for the sample tested at the initial suction of 0.87 MPa in Figure 8(b) where the model predicts compression while the experimental results show a small dilation. In spite of these discrepancies, the variation in suction during shearing is well predicted by the model as shown in Figure 8(c).

5. Conclusions

By including the phenomena of suction hardening, the shift of retention curves with volumetric strains and the hysteresis of the SWRCs, the modified Cam-Clay model can fairly simulate the behavior of unsaturated soils. The inclusion of these phenomena does not affect the symmetry of the stiffness matrix which results advantageous for analysis based on the finite element method. In this way, this model keeps the simplicity of the modified Cam-Clay model.

The yield surface proposed herein can adopt different shapes and includes the phenomenon of anisotropic hardening meaning that the location of the critical state point on the yield surface displaces according to the suction hardening phenomenon.

References

- [1] Russell A and Khalil N. (2006). "A unified bounding surface model for unsaturated soils". *International Journal for Numerical and Analytical Methods Geomechanics*, 30: 181-212.
- [2] Zhou A and Sheng D. (2015). "An advanced hydro-mechanical constitutive model for unsaturated soils with different initial densities". *Computers & Geotechnics*, 63: 46-66.
- [3] Ma T, Wei C, Wei H and Li W. (2015). "Hydraulic and mechanical behavior of unsaturated silt: experimental and theoretical characterization". *International Journal Geomechanics*, 16(6): D4015007:1-13.
- [4] Wheeler SJ and Sivakumar V. (1995). "An elastoplastic critical state framework for unsaturated soil". *Géotechnique*; 45: 35-53.
- [5] Rojas E. (2008). "Equivalent stress equation for unsaturated soils. Part II: The porous-solid model".

- International Journal of Geomechanics, 8, 291-300.
- [6] Lu N, Kim YK, Lee SJ and Lee SR. (2012). "Relationship between the soil-water characteristic curve and suction stress characteristic curve: experimental evidence from residual soils". *Journal of the Geotechnical Geoenvironmental Engineering*, 138: 47-57.
- [7] Cunningham MR, Ridley AM, Dineen K and Burland JB. (2003). "The mechanical behavior of reconstituted unsaturated silty clay", *Géotechnique*, 53: 183-194.
- [8] Fleureau J-M, Kheirbek-Saoud S, Soemiro R. and Taibi S. (1993). "Behavior of clayey soils on drying-wetting paths". *Canadian Geotechnical Journal*, 30: 287-296.
- [9] Rojas E. (2013). Towards a unified soil mechanics theory, Bentham Science Publishers, Open access ebook, UAE, 190 p.
- [10] Dullien FAL. Porous media, fluid transport and pore structure, Academic Press, USA; 1992.
- [11] Loret B and Khalil N. (2002). "Effective stress elastic-plastic model for unsaturated porous media". *Mechanics of Materials*, 34: 97-116.
- [12] Futai MM and Almeida SS. An experimental investigation of the mechanical behavior of an unsaturated gneiss residual soil. *Géotechnique* 2005; 55: 201-213.
- [13] Futai MM and Almeida SS. Yield, strength, and critical state behavior of a tropical saturated soil. *J Geotech Geoenviron Engng*, 2004; 130: 1169-1179.
- [14] Garakani AA, Haeri SM, Khosravi A and Habibagahi G. (2015). "Hydro-mechanical behavior of undisturbed collapsible loessial soils under different stress state conditions". *Engineering Geology*, 195: 28-41.
- [15] Jotisankasa A., Coop M. and Ridley A. (2009). "The mechanical behavior of an unsaturated compacted silty clay". *Géotechnique*, 59, 415-428.
- [16] Klotz E. U. and Coop M. R. (2002). "On the identification of critical state lines for sand". *ASTM Geotech. Test. J.*, 25(3), 289-302.

Technical Session #5 “Soft Soils”



Marcio S. S. ALMEIDA

Professor Marcio Almeida graduated in 1974 with a degree in Civil Engineering from the Federal University of Rio de Janeiro (UFRJ), where he also received his MSc. In 1984 he was awarded a PhD by the University of Cambridge, England. Marcio has lectured at the Federal University of Rio de Janeiro since 1977 where he was granted a full professorship in 1997. The French Geotechnical Society honored him the Coulomb Lecturer prize in 2015. Throughout his career, he has published over 300 journal and conference articles and has been awarded prizes by the Geosynthetics International and Ground Improvement Journals for his work. He is also a recipient of the Terzaghi & José Machado Awards from the Brazilian Geotechnical Society, ABMS. The primary focus of his research includes: soft clay engineering, ground improvement, offshore geotechnics and physical modelling. Marcio authored a book on soft clay construction in 2013 and another on geosynthetic-encased columns in 2018.

Field Studies of Stone Columns and Geosynthetic-Encased Columns

Marcio S.S. ALMEIDA^{a,1}, Iman HOSSEINPOUR^b and Bruno LIMA^c

^aGraduate School of Engineering (COPPE), Federal University of Rio de Janeiro (UFRJ), RJ, Brazil

^bDepartment of Civil Engineering, Faculty of Engineering, University of Guilan, Rasht, Iran

^cDepartment of Foundations and Structures, Rio de Janeiro State University (UERJ), RJ, Brazil and at Fluminense Federal University (UFF), Niterói, Brazil

Abstract. Ground improvement techniques are commonly required for construction on soft clays. In general, the most traditional construction techniques use a combination of prefabricated vertical drains, temporary surcharge, reinforcement, stabilising berms or staged construction. In order to achieve shorter construction times, alternative techniques may be adopted. Examples of these include: lightweight fills, vacuum preloading, temporary surcharge, geosynthetic-reinforced pile-supported embankments, stone columns, geosynthetic-encased columns and cement injection techniques such as deep mixing. This keynote lecture will present the results of two recent case studies in which vibro stone columns and encased columns were used to strengthen a soft clayey foundation supporting embankment loading.

Keywords. Stone columns, embankment, soft clay, geosynthetics, field test

1. Introduction

Stone columns and encased columns are increasingly used as ground reinforcement to support a wide variety of structures such as buildings and embankments. They accelerate the consolidation of soft soil resulting from a shortened drainage path, and can increase load-bearing capacity and reduce settlement [1].

Stone columns were probably first used by French military engineers in 1830, to provide heavy foundation support for cast iron resting on soft soil deposits in an estuary [2]. FHWA [3] published a report presenting their basic principles, the column types and equipment used, and other details of their construction and quality. More information about the vibro-replacement method of constructing stone columns can be found in [3-5].

In very soft soil ($s_u < 15$ kPa), encasing granular columns with suitable geosynthetics improves the lateral column confinement, thus increasing the load-bearing capacity and reducing the total deformation of the supporting subsoil [6-9]. Additionally, encasement prevents the lateral squeezing of stones and aggregates into the surrounding soft soil, and vice versa.

¹ Corresponding author, COPPE/UFRJ, RJ 21941-972, Brazil, e-mail: mssal@gmail.com.

With regard to the practical application of encased columns, many successful case histories with geotextile-encased gravel and sand columns for the stabilisation of embankments on soft soils have been reported [9-10].

To understand the behaviour of soft soil foundation under embankment loading, two instrumented field load tests were performed in a steel power plant located in the State of Rio de Janeiro, Brazil. In Case Study A, vibro stone columns (VSCs) were installed and in Case Study B geotextile-encased columns (GECs) were installed [11]. The monitored area was a small part of a large stockyard where stone columns and encased columns were installed in 2008 [12]. An aerial view of the complex, which occupies an area of 9.0 km², is shown in Figure 1. In Case A finite element (FE) analysis was also performed using Plaxis software to assess the field measurements and to provide further insight into the technique.



Figure 1. Aerial view of the project site.

The main purposes of the ground treatment at the stockyard were to control the stability, reduce the settlement and speed up the construction process. Accordingly, instrumentation was used to investigate the behaviour of the composite ground in terms of settlement, soil horizontal deformation, vertical and horizontal stresses, excess pore water pressure, and hoop strain in the geotextile encasement.

2. Case Study A

A field load test was performed inside the stockyard of ThyssenKrupp CSA with the purpose to investigate the performance of the installed columns under vertical loading (Figure 2).

The detail of the soil profile is shown in Figure 3. The upper soft soil layer extends up to 6.5 m to 7.5 m deep. A sand layer (1.0 m to 3.0 m thick) is found underneath, followed by another soft clay layer whose thickness varies between 3.0 m and 5.0 m. The remaining soil profile consists mainly of sand layers, often without continuity. A large working platform of 2.0 m to 3.0 m thick was constructed by means of a hydraulic fill on the ground surface to start the construction process.

The geotechnical site investigation involved 14 standard penetration tests (SPTs), 20 cone penetration test (CPTu) with pore pressure measurement, three vane shear test (VST) and six dilatometer test (DMT). Total 16 undisturbed samples were extracted using stationary Shelby piston tubes for laboratory testing.

The details of Case Study A are shown in Figures 2, 3 and 4. The surcharge was composed of rails laid over a concrete slab with four concrete beams ($6.50\text{ m} \times 0.40\text{ m} \times 0.40\text{ m}$) to create a span between the rails and the ground surface. The field test was performed on a mesh of 4×4 VSCs, with plan dimensions of $6.5\text{ m} \times 6.5\text{ m}$. The columns were 1.0 m in diameter and spaced 1.85 m with a total length of 11.25 m , as shown in Figure 3.



Figure 2. Field test with rails surcharge [12].

As shown in Figure 5, the surcharge was applied in steps, and the maximum load of 180 kPa was achieved after 27 days. The loading was reduced to about 100 kPa after 70 days. The instrumentation included 28 sensors as described below:

- Eleven settlement plates (S) were installed at a depth of 0.50 m (settlement plate S6 was damaged);
- Two inclinometers (I) with lengths of 23.0 m , positioned on the west side of the test area 0.75 m and 6.05 m from the edge of the concrete slab;
- The installation depths of the nine vibrating wire piezometers (P) were 4.0 m , 4.5 m , 6.0 m (two sensors), 7.0 m , 7.5 m , 8.3 m (damaged sensor), 11.7 m , and 12.0 m ;
- Magnetic extensometers (EX) were installed at depths of 6.0 m , 11.0 m , 14.0 m , 23.5 m , and 27.0 m .
- Four total stress cells (EP) inserted vertically, with the objective of measuring the variation in horizontal effective stress. These were installed at depths of 4.5 m , 6.0 m , 7.5 m , and 8.3 m (damaged sensor).

The soil profile was determined via CPTu tests performed after the installation of VSCs and working platform (three months before the beginning of field loading). In the test area the water table was at 0.80 m below ground level [12].

The field test was also useful in calibrating the numerical model for predicting the behaviour of the permanent stockyard. Two-dimensional (2D) and three-dimensional (3D) FE analyses were carried out and the results of field measurements and numerical calculations were compared for better understanding.

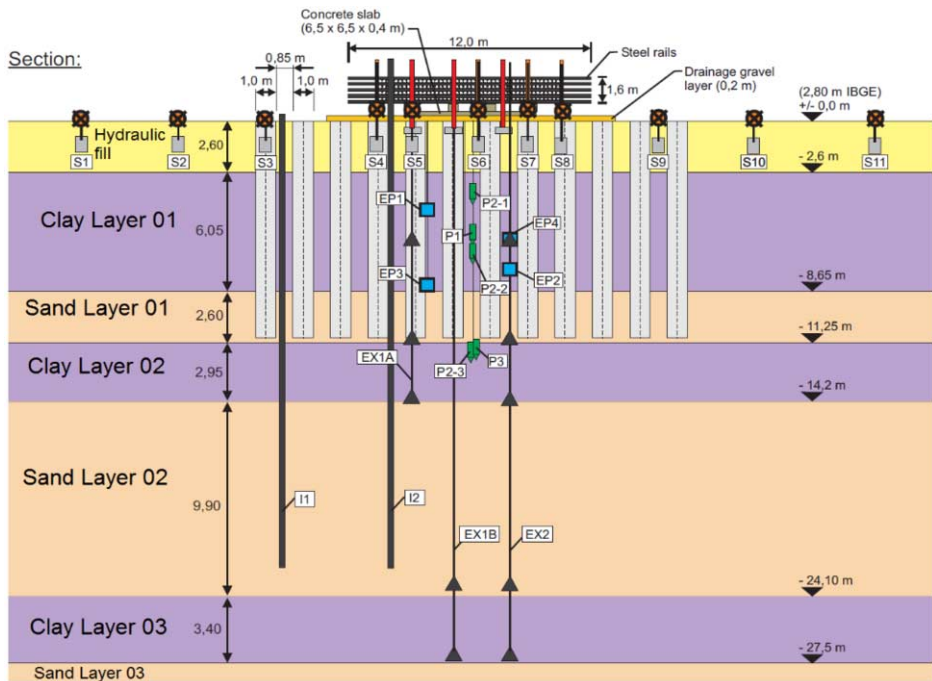


Figure 3. Cross sectional view of the test area with instrumentation [12].

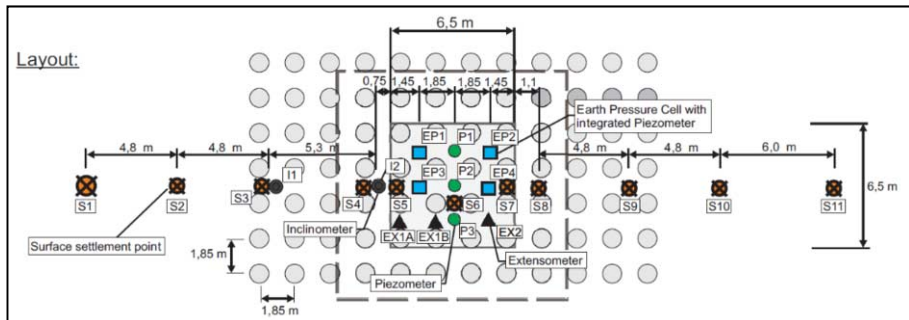


Figure 4. Plan view of the test area [12].

2.1. Numerical Modelling

Numerical analyses under plane strain (2D) and three-dimensional conditions were performed using PLAXIS software with the purposes of better understanding the field behaviour and to assess the capability of the numerical models. Clay layers were modelled with the soft soil constitutive model [13]. All column granular materials, sand layer and hydraulic fill were modelled using Mohr-Coulomb constitutive model [14]. To simulate the smear damage due to the installation of VSCs coefficient of permeability of the clay were reduced [15].

The geometric relationship between the smear zone and the stone column was equal to 2.0 [14]. Due to the effect of the installation of columns, the pressure coefficient was increased (K^*), and parametric analyses provided the best fit with a value of 1.25.

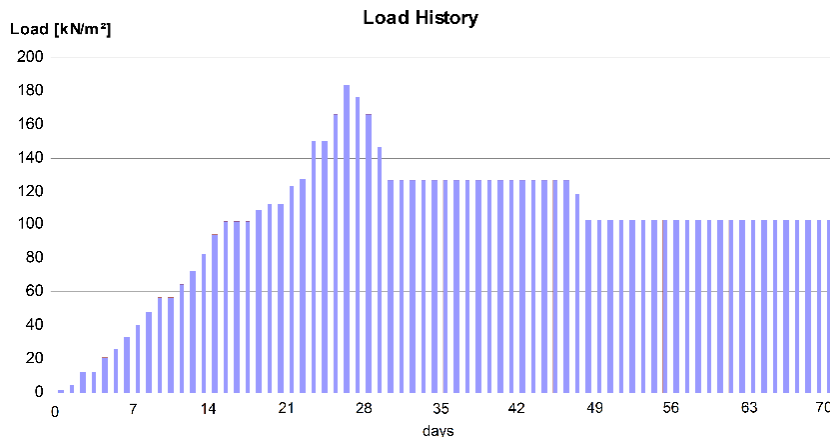
**Figure 5.** Loading sequence during the test [12].

Table 1 summarises the parameters used for the clay layers, while Table 2 presents the parameters used for granular materials. .

Table 1. Parameters of the clay layers [14].

Material	Clay layer 1	Clay layer 2	Clay layer 3
γ [kN/m³]	13.4	16.0	15.6
ϕ' [°]	25.0	25.0	25.0
c' [kPa]	0.0	0.0	0.0
K^* or K_0 [-]	1.25	0.60	0.60
C_c [-]	1.92	1.07	1.00
C_s [-]	0.29	0.13	0.12
C_a [-]	0.04	0.04	0.04
e_0 [-]	3.05	1.68	1.85
OCR [-]	1.08	1.08	1.08
k_h [m/day]	7.9×10^{-5}	7.8×10^{-5}	14.0×10^{-5}
k_v [m/day]	3.9×10^{-5}	3.9×10^{-5}	7.0×10^{-5}
C_k [-]	1.27	0.60	0.60

γ = soil bulk weight; ϕ' = friction angle obtained from CIU tests; c' = cohesion; C_c = compression index; C_s = swelling index; C_a = secondary compression index; e_0 = initial void ratio; OCR = overconsolidation ratio; k_h and k_v = coefficient of horizontal and vertical permeability, respectively; C_k = slope of the e versus $\log k_v$ data

Table 2. Parameters of the granular materials.

Material	γ [kN/m³]	K^* or K_0 [-]	ϕ' [°]	E' [kPa]	ν' [-]
Stone column	20.0	0.35	40.0	80.000	0.3
Hydraulic fill	18.0	1.25	30.0	2.000	0.3
Sand 01	18.0	1.25	30.0	30.000	0.3
Sand 02 and 03	18.0	0.50	30.0	30.000	0.3

E' = Young's modulus; ν' = Poisson ratio

In case of 2D plane strain analysis, the cylindrical columns were transformed into trenches [16] of 0.4 m wide. The drainage capacity of the VSCs in the plane strain model is same as the axi-symmetric unit cell model.

The 2D FE mesh was made of 5,213 triangular elements with 15 displacement nodes and 12 stress calculation integration points. The 3D FE mesh used 28,930 tetrahedral elements (10 displacement nodes and four Gauss points). More information about these FE analyses can be found in [14]. The results of the FE analysis are presented below along with the field measurement data.

2.2. Results and Discussion

The results of the 2D and 3D FE analyses are presented for comparison with field measurements, including the displacements, pore pressure, and horizontal stresses.

2.2.1. Displacements

The settlement versus time results (settlement plates S5, S6, S7, and S8) are compared with the 2D and 3D numerical analyses (named MFE 2D and MFE 3D, respectively) in Figure 6, and a good agreement can be seen between the numerical results (2D and 3D) and the measured data. After the 22nd day, the vertical displacements increased rapidly, indicating that the limit state condition was achieved. The agreement between the 2D and 3D results suggests that the procedure for geometric transformation was satisfactory.

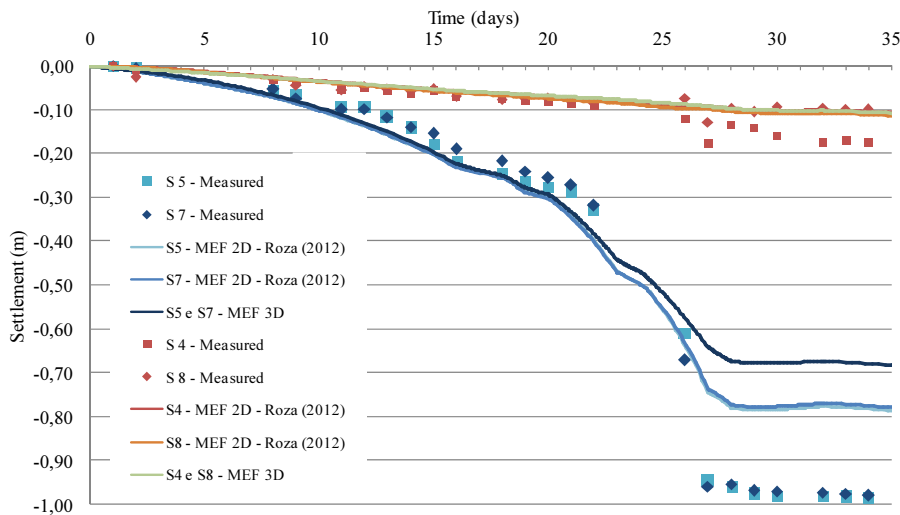


Figure 6. Vertical displacements versus time.

The numerical results for the horizontal displacements and the field measurements given by inclinometers I1 and I2 at depths of 3.5 and 8.0 m are compared in Figure 7. It can be seen that the results of the 3D and 2D analyses are quite close and both match well with the data obtained from the Inclinometer 1 [14]. Similarly, for the vertical displacements, good agreement is obtained between the predicted and measured values

of the horizontal displacements, and the displacements at 3.5 m increase after the 22nd day. Limit state conditions appeared to be reached on the 22nd day of loading, when the displacement values found to increase rapidly (observed both in the field and in the FE analyses). The numerical analysis was assumed to be qualitative, since it was not possible to simulate the discontinuous soil mass caused by failure in continuum FE analysis.

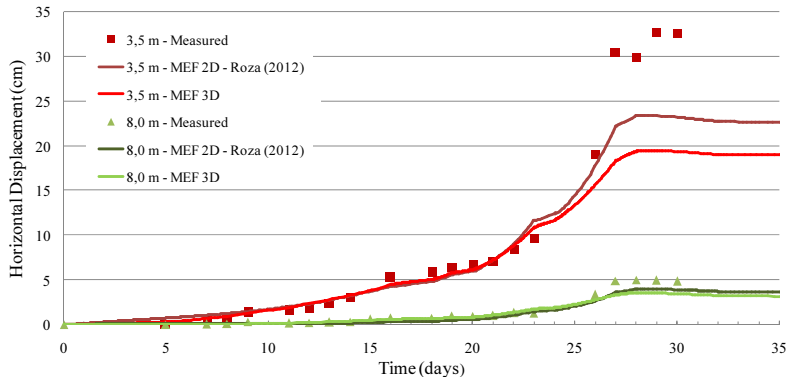


Figure 7. Variation of horizontal displacement with time.

2.2.2. Pore Pressures and Total Stresses

The excess pore pressures measured by the piezometers located at depths of 4.0 m, 6.0 m, and 7.0 m are compared in Figure 8. Although the values obtained from numerical calculation are greater than the measured values, the curve patterns are similar.

The differences may arise both from the positioning of piezometers in relation to the VSCs and the differences in the values of the coefficients of permeability used in the numerical analyses, compared to the actual field values. The effect of piezometer position was verified by, comparing the FE results with points adjacent to the column and at the centre of two columns (location used on results presented here). The above comparison showed that the field data lay between the two results.

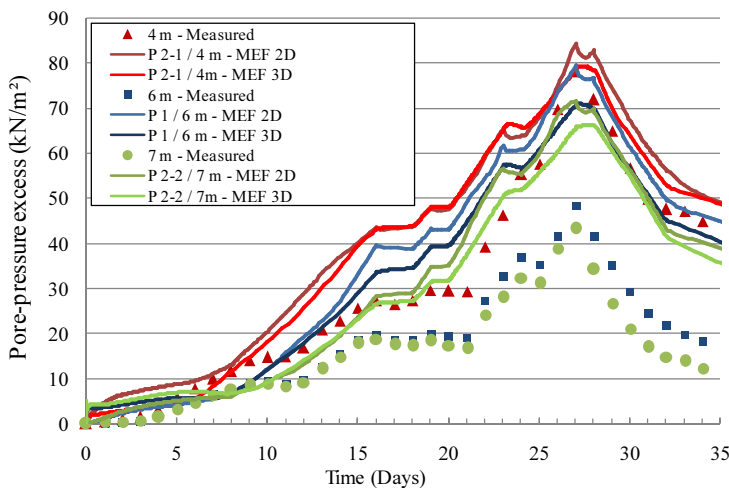


Figure 8. Variation of excess pore pressure with time.

Figure 9 shows the values for the excess pore pressure obtained from the 3D FE analysis at a depth of 6.0 m on the 20th day. As expected, the obtained values are higher in the centre of the loading application area (left-hand columns, Figure 9), and decreases towards the central loading area, with a pronounced gradient (differences of up to 50 kPa surrounding the stone columns). A small difference in the position of the piezometer may therefore cause a significant difference in the value of the measured pore pressure.

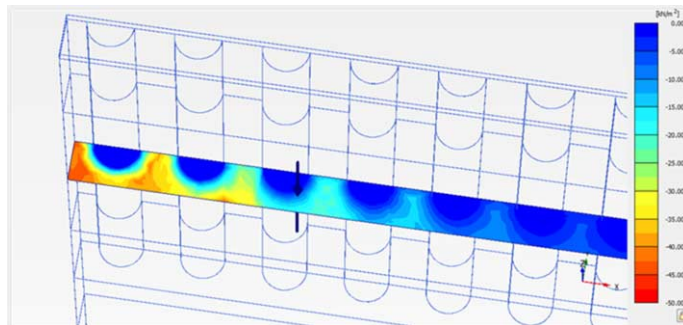


Figure 9. Excess pore pressure at a depth of 6.0 m, 20th loading day.

Total stress cells were installed in the vertical position in the first clay layer to measure the increase in the total horizontal stress ($\Delta\sigma_h$) during loading. Figure 10 compares the measurements of the numerical values of $\Delta\sigma_h$ at depths of 4.5 m, 6.0 m, and 7.5 m. It can be seen that the numerical analyses reproduce the measured values fairly well, and in particular the trends showing increasing and decreasing values with time. From the 11th day onwards, particularly at a depth of 7.5 m, the predicted 2D and 3D results are fairly close to the field data. The differences in the results can be due to the deviation of the cell from its designated position during the installation.

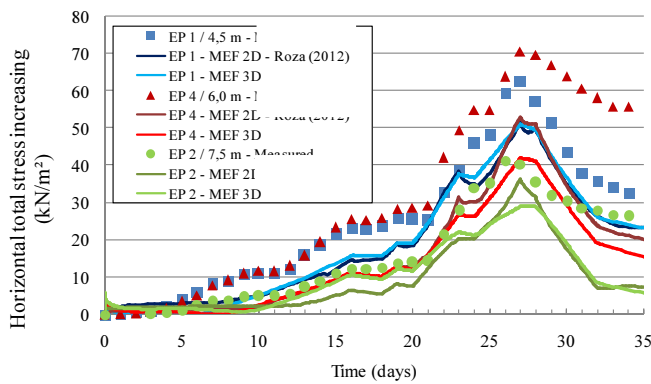


Figure 10. Variation of total horizontal stresses with time.

3. Case Study B

The second field load test was also performed in the test area located inside the stockyard of ThyssenKrupp CSA Company [17, 18] on GECs.

The soil profile in the test area was mainly characterised by a 10 m-thick soft clay deposit stabilised by 36 GECs installed in a square pattern. The granular columns were 11 m in length, 0.8 m in diameter, and had an average centre-to-centre spacing of 2.0 m. The geosynthetic used for the encasement was a seamless woven geotextile with a ring tensile stiffness of 1750 kN/m.

Prior to construction of the embankment, a detailed site investigation was carried out and the geotechnical parameters of the soft clay were obtained by means of in-situ and laboratory tests. The site investigation consisted of SPTs, VST, and CPTu performed in three boreholes. Due to the high water table, a blanket of sand 1.5 to 2.0 m thick was placed over the ground surface to allow access for construction equipment. The variation in the compressibility ratio ($CR = C_s / (1 + e_0)$) indicated an average ratio of 0.3 along the soil profile, which is a common value for Brazilian soft clay [19]. The undrained strength (s_u) determined from the VST data also showed an average value of around 15 kPa.

Figure 11 shows cross sectional view of the embankment and the positions of the instruments, as described below:

- Three surface settlement plates, two of which are placed on top of the soft soil (S1; S2) and one on top of an encased column (S3) to measure the total and differential settlement;
- Three piezometers installed in the soft soil at the depth of 3 m (PZ1), 6 m (PZ2) and 8 m (PZ3), respectively, positioned midway between two columns near the embankment centreline;
- Four total stress cells to assess soil arching and to measure the embankment stresses transmitted to the surrounding soil (CP1, CP3) and to the GECs (CP2, CP4);
- Three radial extensometers (EX) attached to the geotextile encasement at a depth of about 1.0 m below the top of the column to measure the geotextile hoop strain
- Two inclinometers (IN) installed at the embankment toes to measure the distribution and magnitude of the maximum lateral deformation of the soil beneath the embankment.

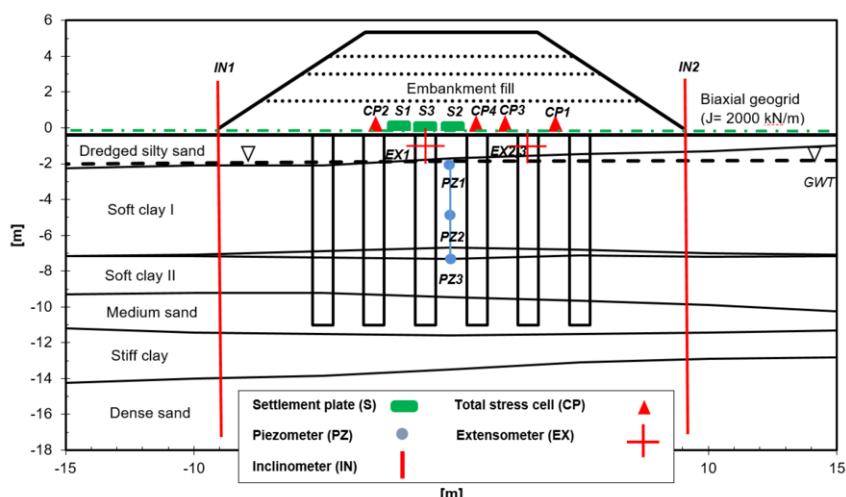


Figure 11. Test embankment: sectional view and positions of instruments [16].

The embankment load test was performed in four stages, as defined by the consolidation interval between the stages. The final height of the embankment was 5.35 m which corresponds to 150 kPa of vertical stress. The embankment was left in place for 180 days after the final layer was placed to allow the dissipation of excess pore water pressure.

3.1. Measured Results

In this section, the results from the field test are briefly described. It should be noted that due to the page limitation, the results of the numerical analyses for this case study are not reported here. The details about the numerical analysis can be found in [8, 18].

3.1.1. Settlements

Figure 12(a) shows the settlements on top of the GECs (measured by S3) and the surrounding soft soil (measured by S1 and S2). It can be seen that these settlements increased sharply during the construction of embankment and show a gradual increase after the construction. It can be observed that 65% of the total settlement was found to be achieved at end of the embankment construction. Both the settlement sensors placed on top of the surrounding soil (i.e. S1 and S2) showed quite similar behaviour during construction stages. The settlement measured by S2 was about 2% greater than that measured by S1 at the end of the monitoring period.

The reason for this may be the location of these sensors; S2 was placed in a diagonal half span between the columns, where greater settlement was expected to occur, while S1 was located in the halfway between the columns. The differential settlement (DS) measured between the top of the column and the soft soil was normalised by the half of the diagonal span between the GECs, as shown in Figure 12(b). Similar to the trend observed in case of total settlement, the normalised differential settlement increased with the embankment height and continued to increase gradually during post-construction period, resulting in 6% of the normalised differential settlement at end of the monitoring period.

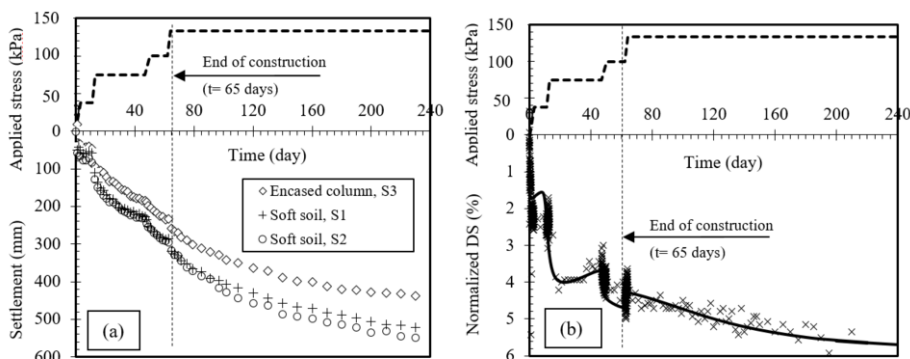


Figure 12. Measured settlements and normalised differential settlement at the embankment base versus time.

Figure 13(a) shows the profile of the horizontal deformation during embankment construction. As expected, the maximum horizontal deformation increases with the height of the embankment. For instance, the results of measurement by inclinometers indicate that the horizontal displacement increased from 10 mm just after first loading stage to about 80 mm just after the embankment was completed. It is also seen that the maximum soil horizontal deformation occurred in the middle of the soft clay, as confirmed by both the inclinometers.

The profile of the horizontal deformation post-construction is also plotted in Figure 13(b). It can be seen that the maximum horizontal deformation increases as excess pore pressure dissipates, although at a slower rate than during the construction period. The maximum value was about 150 mm, which is twice the value measured at end of the construction period.

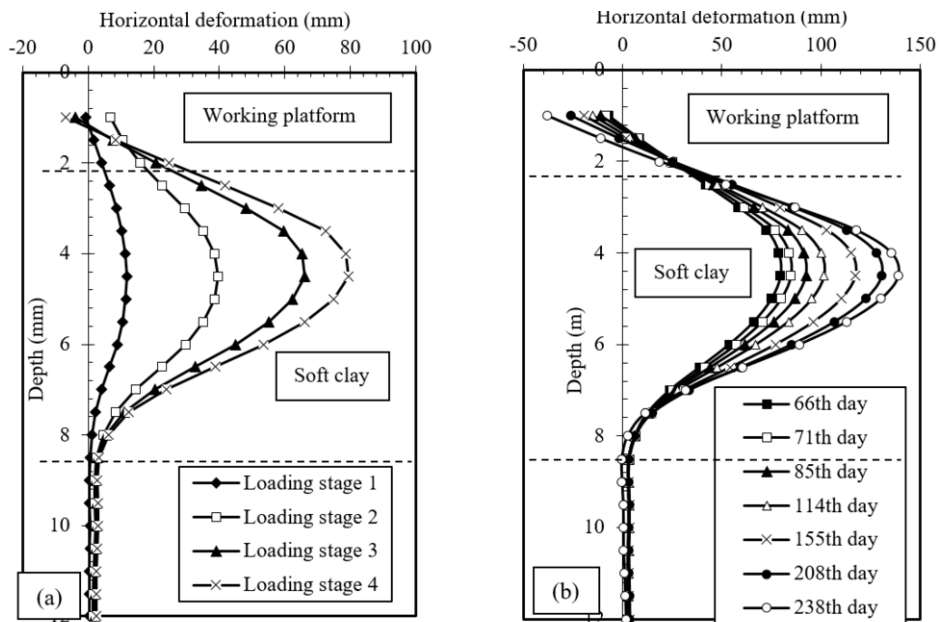


Figure 13. Measured soil horizontal deformation under the embankment toes.

The maximum horizontal deformation measured in the middle of the soft clay layer was correlated with the maximum settlements measured at the centreline of the embankment, as shown in Figure 14. It can be observed that the horizontal deformation increased linearly, with settlement resulting in a slope (DR) varying from 0.16 to 0.2. From the analyses of 15 embankments on soft soil deposits without ground improvement, the authors of [20] reported an average DR ratio of 0.91 at yield conditions during construction and 0.16 during consolidation. It can be concluded that unlike embankments on non-improved foundations, GECs improved foundation resulted in a uniform DR during the construction and consolidation stages.

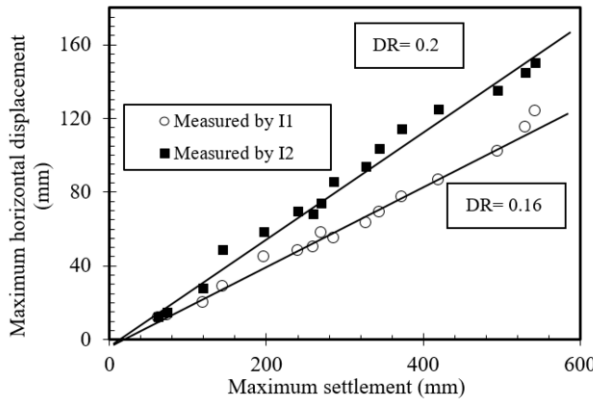


Figure 14. Measured relationship between vertical and horizontal displacements.

Figure 15(a) shows the hoop strains developed in the geotextile encasement measured by three extensometers installed 1.0 m distance below the top of the GECs. The geotextile hoop strain was determined by the ratio of increase in diameter measured by the extensometers to the original column diameter (i.e. 0.8 m). It can be seen that the hoop strains increased rapidly during the loading stages and then continued to increase gradually during consolidation. A sharper increase is seen in the first two loading stages, due to the greater total vertical stress applied in these stages.

The variation in the column diameter (Δd_c) was used to compute the ring force (T_{mob}) mobilised in the geotextile encasement using $T_{mob} = \Delta d_c \cdot J/d_c$, where d_c (diameter of granular column) and J (ring tensile modulus) were 0.8 m and 1750 kN/m, respectively. The mobilised ring tensile force in the geotextile encasement vs time is plotted in Figure 15(b). An average value for the geotextile expansions measured by the three extensometers was used to calculate the mobilised ring force. Figure 15(b) shows that the mobilised ring tensile force increased upon the placement of each layer, and then continuously increase during post-construction period. It can be seen that the mobilised ring force at the end of the monitoring period is 33.6 kN/m, i.e. around 35% of the allowable tensile force.

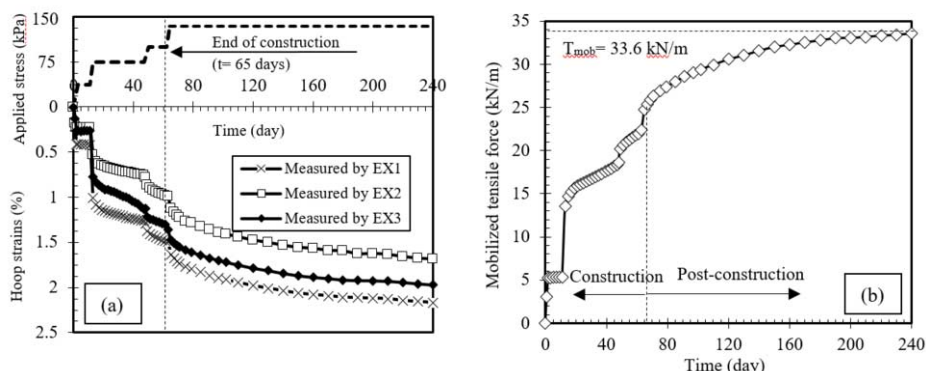


Figure 15. Measured tensile force in geotextile encasement.

The excess pore water pressures measured by the piezometers located at depths of 3 m, 6 m and 8 m are shown in Figure 16(a). As expected, the excess pore pressure rises sharply due to increase in embankment height resulting a quick loading conditions induced in the soft clay. It is observed that the excess pore pressure dissipates during the construction intervals and during the post-construction consolidation (i.e. after the 65th day) phase. The maximum excess pore pressure was measured by PZ2, located in the middle of the soft clay I, which had the longest drainage path. In contrast, PZ3 showed the lowest excess pore pressure as it was located close to the sand zone between the two clay layers. Figure 16 (b) shows the incremental excess pore pressure (Δu), normalised by the increases in vertical stress in the surrounding soil ($\Delta \sigma_{vs}$) measured during the construction stages. The average value of the vertical stresses measured by the cell pressures CP1 and CP3, located on top of the surrounding soil, was used to normalise the excess pore pressure measured by PZ2, located in the middle of the soft clay.

Figure 16(b) indicates that the ratio of $\Delta u / \Delta \sigma_{vs}$ ranges from 0.65 to 0.9, and thus is not equal to unity, as expected for strictly undrained loading conditions. It is frequently reported in case histories that this ratio starts at a relatively low value for the initial loading stage, and increases to a maximum value close to unity during subsequent loading stages. Thus, the initial ratio of 0.78 for stage 1 loading and an increase to 0.91 for stage 2 loading does not appear unreasonable. However, the decrease in the ratio of applied stress to pore pressure in stages 3 and 4 may be due to soil arching effect.

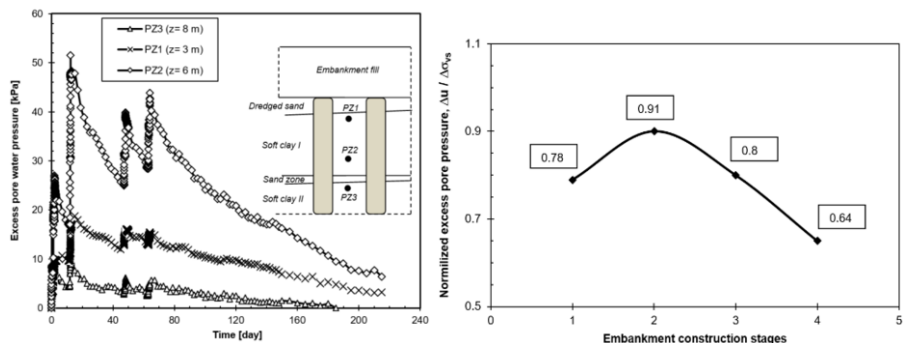


Figure 16. Measured excess pore pressure in soft soil.

4. Conclusions

This paper describes the behaviour of a soft clayey foundation reinforced with VSCs and GECs using field load test. A numerical analysis of the VSCs was also performed to assess the field measurements. The main conclusions derived from the above studies are as follows:

Case Study A: Vibro stone columns (VSCs)

In general, the vertical and horizontal displacements obtained from the numerical prediction showed good agreement with the field measurements up to the 22nd day of loading; at this point, the limit state condition was observed close to failure, which was not adequately modelled in the numerical analyses.

The magnitudes of the excess pore pressures predicted by the numerical analysis were generally greater than the measured ones. This difference could be due to inadequacies in modelling the consolidation or due to uncertainties in the exact in situ position of the piezometers.

The values of the horizontal stress measured in the field lie within the range of values provided by the numerical calculations. The differences may be related to the positions of the total stress cells, which could not be installed exactly perpendicular to the horizontal ground surface.

Case Study B: Geotextile-encased columns (GECs)

A differential basal settlement was observed at the embankment base, due to soil arching induced by the fill. This differential settlement was found to increase with the height of the embankment.

The ratio between the maximum horizontal and the maximum vertical displacements was in the range 0.16 to 0.2, and remained relatively constant throughout the loading and consolidation stages.

The radial expansion of the geotextile increased when each layer was placed. This increase became slower as consolidation progressed, tending to a final asymptote achieved at about three months after end of the construction.

The test embankment with a total applied vertical stress of around 150 kPa showed satisfactory overall performance, with maximum horizontal and vertical displacements of 0.15 m and 0.5 m, respectively. The pore pressure and the settlement value found to stabilise 6 months after the placement of final loading stage.

Acknowledgements

The results presented here were parts of two PhD studies supported financially by Brazilian National Funding Institutes CAPES and CNPq whom are greatly appreciated. ThyssenKrupp CSA and Huseker Brasil are also thanked for their assistance through the field load tests and providing geosynthetics. The authors also would like to thank to Dr. Sunil Mohapatra for his comments on the final version of the paper.

References

- [1] J.K. Mitchell & T.R. Huber, Performance of a stone column foundation, *Journal of Geotechnical Engineering* **3** (1985), 205–223.
- [2] W. Hu, Physical modelling of group behaviour of stone column foundations, *PhD Thesis*, Glasgow University, Scotland p. 312, 1995.
- [3] FHWA, *Design and Construction of Stone Columns*, vol 1. Report FHWA/RD-83/027, R.D. Barksdale & R.C. Bachus (eds.), Federal Highway Administration, 1983.
- [4] V.R. Raju, R. Hari Krishna & R. Wegner, Ground improvement using vibro-replacement in Asia 1994 to 2004 – A 10 years review, *5th International Conference on Ground Improvement Techniques*, Kuala Lumpur, 2004.
- [5] Y.W. Yee & V.R Raju, Ground improvement using vibro-replacement (vibro stone columns) – historical development, advancements and case histories in Malaysia, *16th Southeast Asian Geotechnical Conference*, Kuala Lumpur, Malaysia, 2007.
- [6] I. Hosseinpour, M. Riccio & M.S.S. Almeida, Field measured Poisson's ratio of geotextile encased granular column, *Proceedings of the Institution of Civil Engineers-Ground Improvement*, 2019. DOI: <https://doi.org/10.1680/jgrim.18.00097>.

- [7] I. Hosseinpour, M.S.S. Almeida & M. Riccio, Ground improvement of soft soil by geotextile-encased columns, *Proceedings of the Institution of Civil Engineers-Ground Improvement*, **169**(4) (2016), 297–305.
- [8] I. Hosseinpour, C. Soriano & M.S.S. Almeida, A comparative study for the performance of encased granular columns, *Journal of Rock Mechanics and Geotechnical Engineering* (2019). DOI: <https://doi.org/10.1016/j.jrmge.2018.12.002>.
- [9] M.S.S. Almeida, M. Riccio, I. Hosseinpour & D. Alexiew, *Geosynthetic Encased Column for Soft Soil Improvement*, CRC Press, London, UK, 2018.
- [10] M. Raithel, H.G. Kempfert & A. Kirchner, Geotextile encased columns (GEC) for foundation of a dike on very soft soils, *Proceedings of the 7th International Conference on Geosynthetics*, Balkema, Netherland, 1025–1028, 2002.
- [11] D. Alexiew, C. Moermann & H. Jud, Foundation of a coal/coke stockyard on soft soil with geotextile encased columns and horizontal reinforcement, *Proceedings of the 17th International Conference on Soil Mechanics and Geotechnical Engineering*, Alexandria, Egypt, 2236–2239, 2009.
- [12] TKCSA, *TKCSA Design And Quality Documents for Soil Improvements*, Report, 2007.
- [13] R.B.J. Brinkgreve, *Finite Element Code for Soil and Rock Analyses - PLAXIS - 2D User's Manual*. Rotterdam, Netherlands, Balkema, 2010.
- [14] M.S.S. Almeida, B.T. Lima, M. Riccio, H. Jud, M.C.F. Almeida & F. Roza, Stone columns field test: monitoring data and numerical analyses, *Geotechnical Engineering Journal of the SEAGS & AGSSEA*, **45** (2014), 103–112.
- [15] Indraratna, B., Sathananthan, I., Bamunawita, C. & Balasubramaniam, A.S. Theoretical a numerical perspectives and field observations for the design and performance evaluation of embankments constructed on soft marine clay. *Ground Improvement, Case Histories*. (eds Indraratna & Chu) Elsevier, London: (2005), 51-89.
- [16] S.A. Tan, S. Tjahyono & K.K. Oo, Simplified plane-strain modeling of stone-column reinforced ground *Journal of Geotechnical and Geoenvironmental Engineering ASCE*, **134**(2) (2008), 185–194.
- [17] M.S.S. Almeida, I. Hosseinpour, M. Riccio & D. Alexiew, Behavior of geotextile-encased granular columns supporting test embankment on soft deposit, *Journal of Geotechnical and Geoenvironmental Engineering ASCE*, **141** (2014), 0401416.
- [18] I. Hosseinpour, M.S.S. Almeida & M. Riccio, Full-scale load test and finite-element analysis of soft ground improved by geotextile-encased granular columns, *Geosynthetics International*, **22**(6) (2015), 428–438.
- [19] I. Hosseinpour, M.S.S. Almeida, M. Riccio & M. Baroni, Strength and compressibility characteristics of a soft clay subjected to ground treatment, *Geotechnical and Geological Engineering*, **35**(3) (2017), 1051–1066.
- [20] F. Tavenas, C. Mieussens & F. Bourges, Lateral displacement in clay foundations under embankments, *Canadian Geotechnical Journal*, **16** (1975), 532–550.

Technical Session #6

“Foundations and Retaining Structures”



Anne LEMNITZER

Anne Lemnitzer is an Associate Professor at the University of California, Irvine (USA). She received her Engineering Diploma Degree (Dipl.-Ing.) at the University of Applied Science in Leipzig, Germany, Master's degrees from the California State University Long Beach and the University of CA, Los Angeles (UCLA), and a PhD degree from UCLA. Her research interests include experimental soil-structure-interaction, underground structures, deep foundations, and sensor instrumentation. She serves in many capacities and is currently Co-editor in chief for the Deep Foundations Journal, Associate Editor for the ASCE's Journal of Geotechnical & Geoenvironmental Engineering (JGGE), and Chair of the Geo-Institute's Earth Retaining Structures Technical Committee. She recently won DFI's President's Award, NSF's Career Award and ADSC's President's Award. At UC Irvine she teaches the undergraduate and graduate coursework in geotechnical engineering. If not in the lab or at the construction site, Anne loves spending time pursuing her passion for photography and challenging herself on ski slopes around the world

Laterally Loaded Pile Behavior at Soil-Rock-Impedance Contrast

Anne LEMNITZER^{a,1}, Carter COX^b, Rabie FARRAG^a and Benjamin TURNER^c

^a*University of California, Irvine, Department of Civil & Environmental Engineering*

^b*Independent Consultant*

^c*Dan Brown and Associates*

Abstract. At zones of strong impedance contrast in which there is a significant change in stiffness between adjacent geomaterial layers, Winkler-based analysis methods predict abrupt changes in the internal pile reaction force effects for laterally-loaded foundation elements. In particular, the sudden de-amplification of moment when transitioning from a soft to stiff layer is accompanied by amplification of pile shear. From a design perspective, this is problematic when considering large lateral loads and moments acting on drilled shafts, because it can result in bulky transverse reinforcement designs that pose constructability challenges. This paper will review the challenges associated with the lateral performance of piles in zones with strong stiffness contrasts and present a large-scale experimental research program that investigates the lateral load transfer of rock-socketed deep foundation elements. The study seeks to better understand the ability of numerical and analytical methodologies in capturing the behavior at impedance interfaces, compare such with experimental observations, and derive lessons for the construction industry in how to optimize the design requirement using performance-based predictions for deep foundations embedded in stiff materials.

Keywords. Pile foundations, lateral loading, impedance contrast, rock sockets

1. Introduction

Pile foundations are extensively used in the construction of various types of superstructures, including tall buildings, bridges, freeways and offshore structures. Hereby, a fully constrained tip embedment such as a rock-socket offers an attractive solution for achieving maximal tip resistance and improving the load transfer capabilities of the foundation element. In soil profiles with very soft surface soils, rock-socketing often provides the only reliable source of axial and lateral resistance.

Previous research predominantly focused on geotechnical response aspects of rock-socketed piles without considering complex interaction effects inherent to the pile curvature integration and differentiation procedures and their effect on the pile's structural response behavior. Impedance contrasts between strong rock layers and softer surface soils yield abrupt changes in the pile's moment profiles which translate into amplified shear forces at the rock-socket interface, originating from differentiation of the fourth order differential beam equation. The validation of potential shear amplification (or the lack thereof) with field load tests and verified advanced numerical analysis is very

¹ Corresponding Author, Anne Lemnitzer, PhD, Department of Civil & Environmental Engineering, University of California, Irvine, United States; E-mail: alemnitz@uci.edu.

limited in existing literature. However, the correct evaluation of shear demands at soil-rock socket interfaces is vital since the shear demand may govern the drilled shaft's structural design and the overall constructability of the foundation system. This amplification behavior is not unique to rock-soil interfaces but accompanies most deep foundation elements when interfaces separating soil layers have substantially different stiffnesses, or when head or tip restraints control the lateral pile bending behavior. It is particularly pronounced when predicting a pile's lateral load behavior with the $p-y$ method of analysis and inherent to the mathematical process by which internal pile reactions, such as shear forces are derived.

2. Experimental Studies

To better understand the lateral load behavior of deep foundations embedded in stratigraphies with strong impedance boundaries, an experimental research program consisting of three reinforced concrete pile foundations was developed. Testing was executed at the Structural Engineering Testing Hall at the University of California, Irvine. The test specimens were embedded in a two-layer soil system and subjected to reverse cyclic lateral loading until complete structural failure was reached. This paper will present the iteration of the specimen geometry, the test setup, specimen configuration, material properties, test results, failure observations, and an abbreviated comparison between analytically predicted and experimentally observed specimen behavior for two of the pile foundations.

2.1. Specimen Selection and Analytical Pre-test Predictions

The $p-y$ method of analysis, as implemented in the software platform LPile [1], was used to predict the general foundation response of two pile specimens due to cyclic lateral loading at the pile head. The analytical results enabled the iteration of suitable specimen geometries and reinforcement configurations that would serve two objectives: (1) to gain general insight into the piles' nonlinear performance behavior and failure development under small and large lateral deformations, and (2) to learn whether the potential amplification of shear forces at the impedance boundary is experimentally verifiable. The soil layers were analytically replicated using $p-y$ springs for weak rock [1] as well as sand [4] which are readily embedded in the LPile software. The soil properties were initially estimated based on supplier data sheets for typical sand-type fill materials. Concrete strengths were taken as design strengths with an overstrength factor. One pile specimen, hereafter referred to as Specimen 1, was designed to satisfy all predicted internal pile reactions (moment, shear) and reinforced extensively to provide sufficient capacity to accommodate all amplified internal pile reactions, while another specimen (Specimen 2) was designed to only satisfy the code requirements associated with the applied lateral load. If the amplification of shear demands at the interface between soft and stiff soil layers is real, this specimen would be expected to fail due to insufficient shear capacity at the respective boundary. Table 1 presents the structural design summary of Specimens 1 and 2. In accordance with typical reinforcement ratios used in U.S. foundation deep foundation design, the longitudinal reinforcement ratio was chosen as $\rho = 1.41\%$.

Figure 1 shows the predicted load-deflection relationship of both pile specimens (Figure 1a) and suggests a lateral load of 13.34 kN [3kips] at the point of concrete

cracking, a load of 40.92 kN [9.2kips] at specimen yield and a load of 62.27 kN [14kips] when reaching the ultimate pile capacity. Moment and shear profiles are predicted in Figures 1(b) and (c), respectively. Figure 1(c) illustrates the shear amplification prediction explained above. For an applied lateral pile head load of 62.27 kN [14 kips], the Winkler-type analysis predicts an internal pile shear magnification of 591.61 kN [133 kips], which corresponds to 9.5 times of the applied head load. This strong analytical amplification ratio was chosen to exaggerate the pile reaction effects and obtain maximum pile reactions experimentally. The soil was selected in a manner to support this amplification effect (i.e., a relatively loose sand material across a limited specimen height overlaying a stiffer rock layer, as described hereafter).

Table 1. Predictions of pile capacities using LPile [1] and selected reinforcement.

	Specimen 1	Specimen 2
Longitudinal reinforcement	8#6	8#6
Transverse reinforcement (Inside rock socket)	#4@11.43 cm [4.5 in]	#4@15.24 cm [6.0 in]
Transverse reinforcement (Outside rock socket)	#4@15.24 cm [6.0 in]	#4@15.24 cm [6.0 in]
Nominal shear strength, V_n , kN [kips]	618.30 [139]	395.89 [89]
Nominal flexural strength, M_n , kN-m [kip-ft]	157.27 [116]	157.27 [116]
Predicted failure mechanism / limit state	Flexure	Amplified shear
Predicted lateral head load @ failure	62.3 kN [14 kips]	44.5 kN [10 kips]

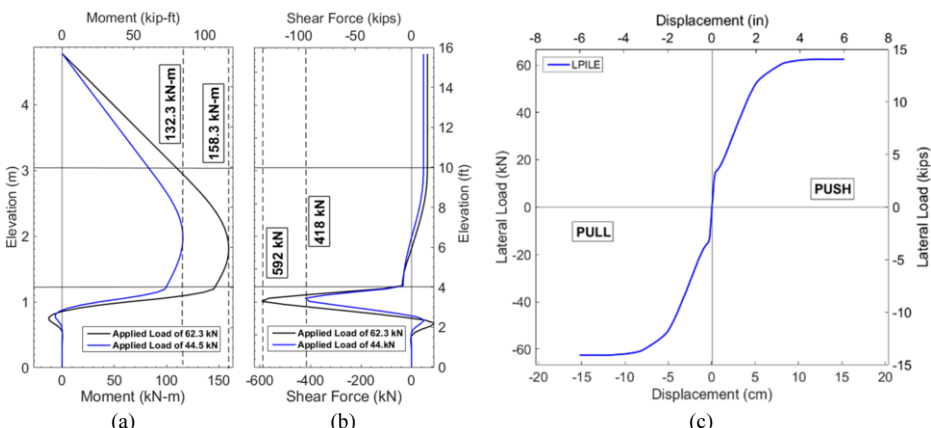


Figure 1. Prediction of pile head load-displacement relationships (a), pile moment (b) and pile shear forces (c) due to lateral loads of 44.5 kN (10kips) and 62.3 kN (14 kips) at the pile head.

2.2. Specimen Geometry and Reinforcement

The two reinforced concrete piles were 4.57 m [15.0 ft] in length and 0.46 m [18.0 in] in diameter. As shown schematically in Figure 2a, the piles were embedded in 1.20 m [4.0 ft] of “rock”, simulated experimentally through high strength concrete ($f'_c = 48.3$ MPa [7 ksi]). The concrete blocks (i.e., the “rock sockets”) had dimensions of 1.83 m [6.0 ft] in length, 1.22 m [4.0 ft] in width, and 1.22 m [4.0 ft] in height. The blocks were secured to the reinforced concrete floor of the testing facility using pre-drilled, epoxy grouted, high strength steel anchors. The piles extended a total of 3.35 m [11.0 ft] outside the rock. A pile cap with cross-sectional dimensions of 0.61 m by 0.61 m [24 x 24 in] and a height of 0.41m [16 in] was constructed at the pile head and used for lateral load application. The two pile specimens had different reinforcement configurations as explained in

section 2.1 above and shown in Figure 2(b) and (c) below. The longitudinal reinforcement of both specimens consisted of eight number 6 bars ($A_{s,\text{total}} = 22.71 \text{ cm}^2$ [3.52 in^2]), Grade 60 A 706 steel, aligned in equal spacings around the circumference of the pile. The longitudinal reinforcement ratio was 1.41 %. The clear concrete cover was 5.08 cm [2.0 in]. The transverse reinforcement consisted of Number 4 spirals. Specimen 1's transverse reinforcement was spaced at a pitch of 11.43 cm [4.5 in] in the zone of the rock socket, i.e., approximately up to 1.2 m [4.0 ft], and at a pitch of 15.24 cm [6.0 in] along the remaining pile height. The closer spiral pitch at the bottom of the pile was satisfies the amplified shear demand within the rock socket as predicted by the $p-y$ analysis in Figure 1. Specimen 2 was reinforced with transverse spirals at a pitch of 15.24 cm [6.0 in] along the entire specimen height. The reinforcement scenario of Specimen 2 ignores the amplified shear demand in the impedance zone and satisfies the code requirements for shear and confinement based on the applied lateral load per ACI 318-14 [4] only.

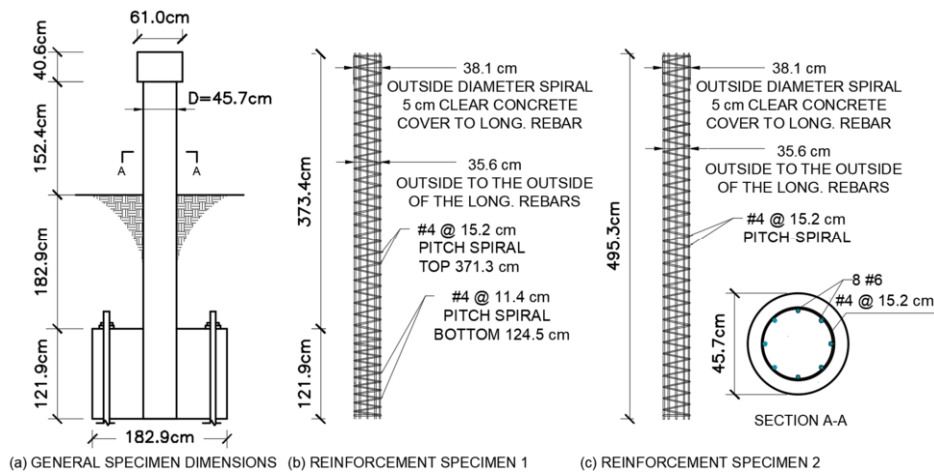


Figure 2. Schematic specimen configuration.

2.3. Specimen Instrumentation

Specimen instrumentation consisted of internal and external sensors, such as inclinometers, linear voltage differential transducers (LVDTs), strain gauges in longitudinal, rosette, and tetrahedral configurations, and string potentiometers. An example schematic instrumentation plan for Specimen 1 is shown in Figure 3.

2.4. Specimen Construction

Figure 4 shows photographs during specimen construction. Upon instrumenting all rebar cages outside the soil pit, the cages were placed inside Sonotubes and aligned along the walls of the soil pit. Concrete was poured and manually vibrated to avoid sensor damage. The pile caps were constructed after the piles had cured for approximately one week. Piles were then placed and secured inside the formwork of the rock sockets prior to casting the rock socket concrete as shown in Figure 4.

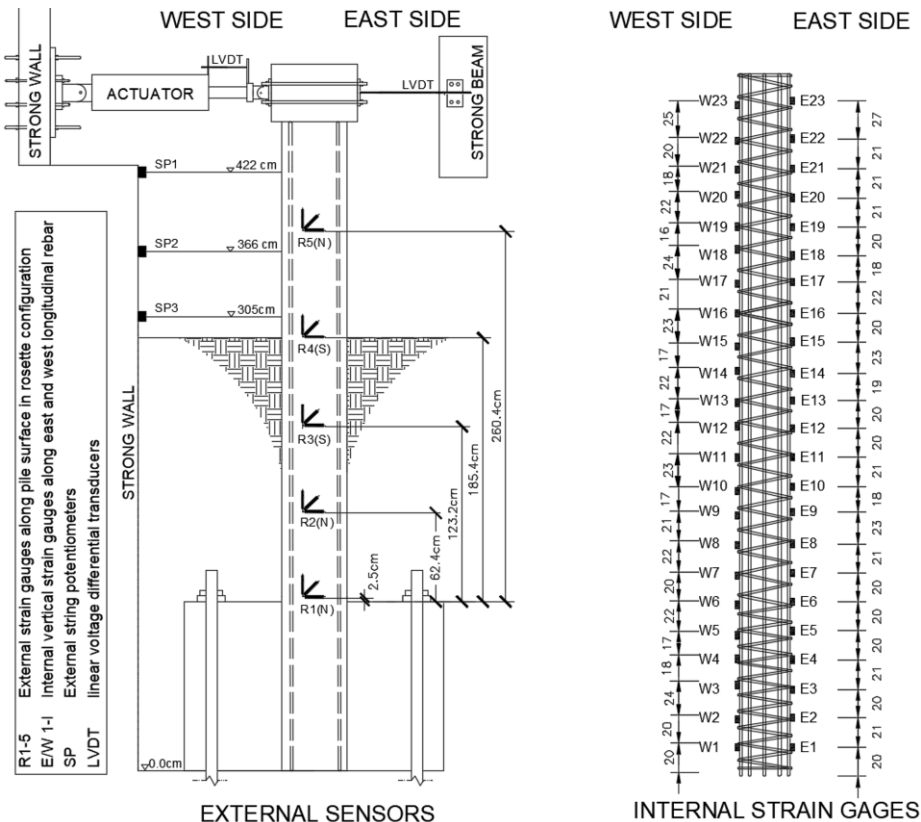


Figure 3. Instrumentation layout for Specimen 1 (tetrahedral sensors not shown, all dimensions in cm).

Along the height of the rock socket (i.e., along the bottom 1.22 m [4ft] of the pile) the concrete surface was roughened with a pneumatic needle scaler to ensure a good concrete to concrete adherence. The rock-socket concrete had a design strength of 34.5 MPa [5ksi], and an average in-situ strength of 48.3 MPa [7ksi] at the day of testing. Pile Specimens 1 and 2 had a design strength of 27.58 N/mm² [4ksi], and an in-situ compressive strength of 40.7 MPa [5.9ksi] and 39.3 MPa [5.7ksi] at the day of testing respectively.

The space between the rock-sockets, which is unaffected by the load application at the pile cap was filled with geofoam. The remaining soil pit was then filled with sand pluviated from a minimum height of 3.66 m [12ft] to yield a relative average in-situ density of 20% (Figure 4(e)). Pluviation was accomplished by designing a sieve system to be attached at the bottom of a concrete hopper and calibrating the fall heights as well as the sieve openings until the desired relative density was reached. The relatively low in-situ density of 20% provided a strong impedance contrast between the soil and rock materials. Additional laboratory testing of the soil material revealed a friction angle of 34.6 degrees (direct shear testing), a cohesion of 4.96 kN/m² [0.72 psi], and a max dry density of 21 kN/m³ [134pcf] (Modified Proctor test). Cone penetration (CPT) and Dilatometer testing (DMT) were used to estimate the soils E-modulus and shear wave velocity; test results are omitted for brevity. The in-situ moisture content of the soil was 6%.



Figure 4. (a) Pile rebar cages, (b) Instrumented specimens prior to concrete pouring, (c) Concrete piles placed in rock-socket formwork, (d) Specimens with rock-sockets anchored into the floor after formwork removal (e) Sand pluviation, (f) Completed test setup for SP 2.

2.5. Load Application

The loading protocol was developed based on the predictive analyses shown in Figure 1 and followed the general guidelines of ASCE 41-06, in which applied displacement levels are selected as fractions or multipliers of the anticipated yield displacement. Quasi-static, reverse-cyclic loading was applied at the pile head by three cycles per displacement level up to ultimate capacity. Hereafter two cycles per displacement level were performed until substantial degradation of the load-displacement relationship was noticeable.

Loading was applied under displacement control at the center of the pile cap using a 76.2 cm [30 in] stroke, 667 kN [150 kips] capacity hydraulic actuator (see Figure 2a). The strong wall of the UCI laboratory served as reaction wall. The actuator was controlled by an MTS 407 dual channel controller and data were recorded using a National Instrument data acquisition system. A total of 115 channels were utilized for each test. An externally installed LVDT, mounted between an independent reference frame and the backside of the pile cap was used to control the experiment and record the pile head displacement.

3. Test Results

3.1. Post-test Failure Observations

To better track the crack patterns around the pile specimen a spray-paint grid was printed on the sand surface as shown in Figure 5. The grid spacing was 15.24 x 15.24 cm [6 x 6 in]. An example of the circumferential crack expansion and the formation of a “crater-type” hole around the pile for displacements beyond 4 in displacement is the depicted in the photographs. Each pile was manually excavated (in push direction) to identify substantial cracking and the location of the plastic hinge (Figure 5 d, e). The most substantial cracking concentrated within 61 cm [24 inch] above the rock socket but extended to higher elevations with larger spacings. Almost all cracks formed perpendicular to the pile axis, i.e. very few diagonal cracks were recorded. There was no sign of cracking or damage along the socket surface or within the rock socket itself.

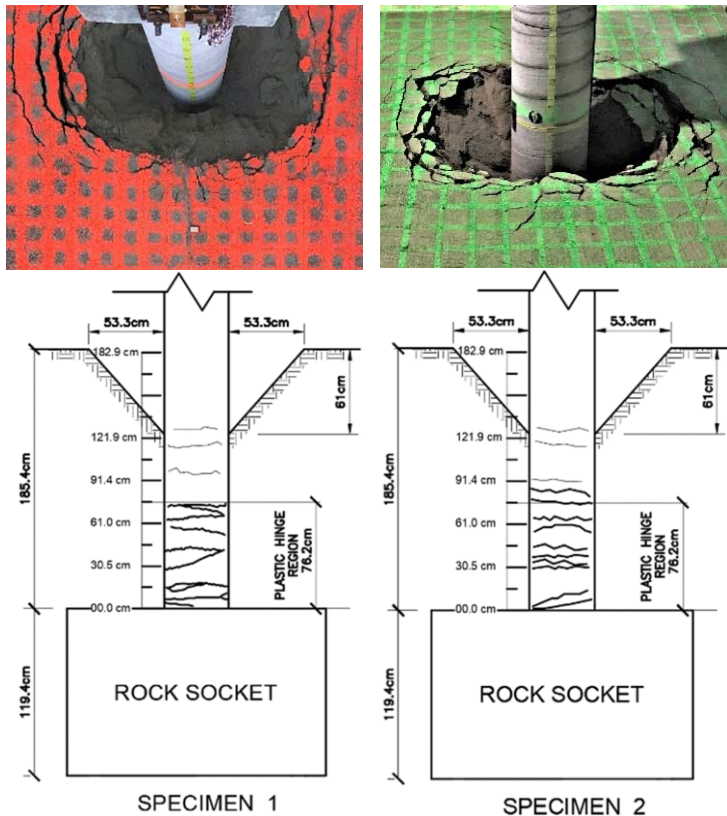


Figure 5. Major cracks along the pile depth and around the surface soil at test completion.

3.2. Selected Experimental Data

Figure 6 shows the experimental load displacement behavior of Specimens 1 and 2 with their respective backbone curves. Specimen 1 reached an ultimate load of approximately 68.5 kN [15.4 kips] at a corresponding pile head displacement of 11.4 cm [4.5 in] in push

direction, and approximately 65 kN [14.7 kips] at a corresponding pile head displacement of 11.4 cm [4.5 in] in the pull direction. Similarly, Specimen 2 reached ultimate resistance at 64.5 kN [14.5 kips] and 11.4 cm [4.5 in] in push direction, and approximately 71.2 kN [16 kips] at a corresponding pile head displacement of 11.4 cm [4.5 in] in pull direction.

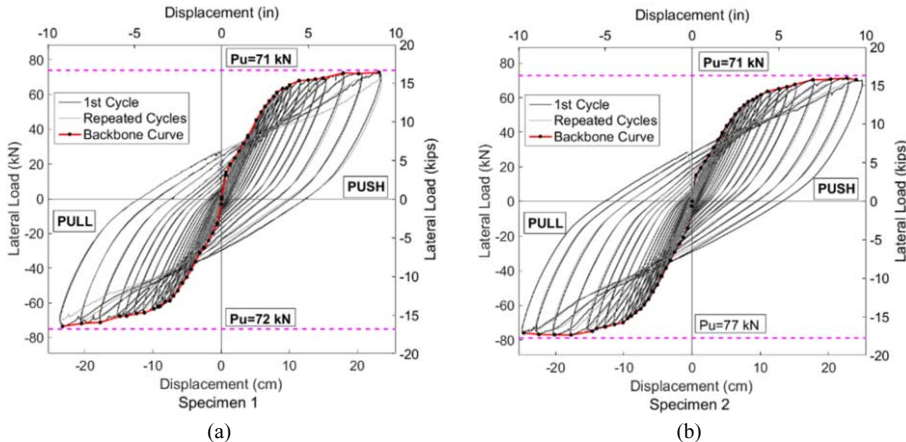


Figure 6. Experimental load-displacement relationships with backbone curve: (a) specimen 1, (b) specimen 2.

Both specimens behaved identically up to “concrete cracking”, i.e., up to a displacement level of 0.64 cm [0.25 in] and a corresponding load of 13.34 kN [3 kips] (about 20% of the ultimate load). The yield displacement was approximately 6.35 cm [2.5 in] at a corresponding load of 8 kips (about 50% of the ultimate load) after which the piles accumulated substantial permanent deformations for repeated loading cycles.

Figure 7 shows the lateral deformation profile recorded through the inclinometer instrumentation. Measurements indicate that no deformation occurred within the rock socket. Small lateral pile deformations are noticeable beyond 15 cm [0.5 ft] above the rock socket. Deformed shapes were similar in both “pull and push” directions, as well as for SP1 and SP 2. Curvature profiles, as shown in Figure 8 suggest the formation of a plastic hinge within 60 cm [2 ft] above the rock-socket which corresponds to 1.2 m [4 ft] below the ground surface (i.e., about 3 pile diameters (3D)) which agrees well with crack patterns observed upon excavation.

3.3. Comparison with Analytical Predictions

Figure 9 compares the experimental backbone curves for Specimens 1 and 2 with the predicted load-displacement curve. Relatively good agreement can be observed up to specimen yield. The predictions slightly underestimate the specimens’ ultimate capacity by about 10%. This deviation could be attributed to the yield strength assumption of the longitudinal reinforcement. Figure 9 also illustrates the predicted failure limits in flexure and shear. The identical specimen behavior suggests flexural failure modes for both, SP1 and SP2. Specifically, the predicted shear failure due to potential shear amplification near the rock-socket interface would have caused an early failure of Specimen 2 at approximately 44.5 kN [10 kips], which was not observed experimentally. Instead the pile specimen SP2, which was insufficiently reinforced for the potential shear

amplification, performed identically to the pile (SP1) which was sufficiently reinforced for the shear amplification and resisted a lateral load of 1.6 times the predicted failure limit state.

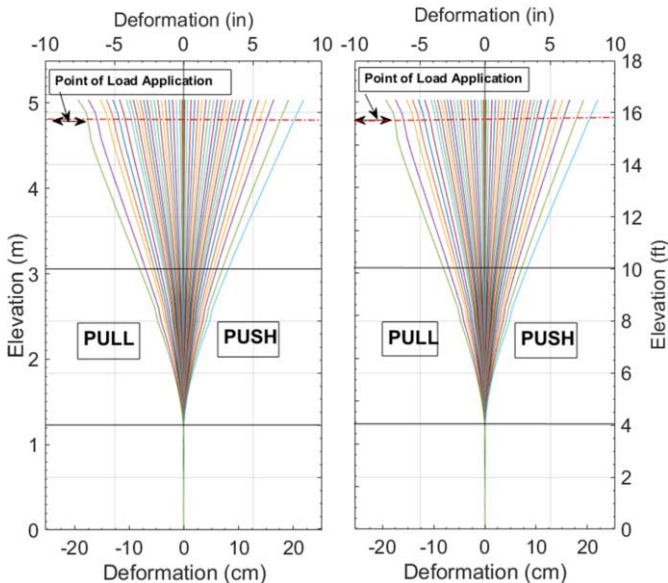


Figure 7. Deformed shape of Specimen 1(left) and Specimen 2 (right) at each applied displacement level (inclinometer readings).

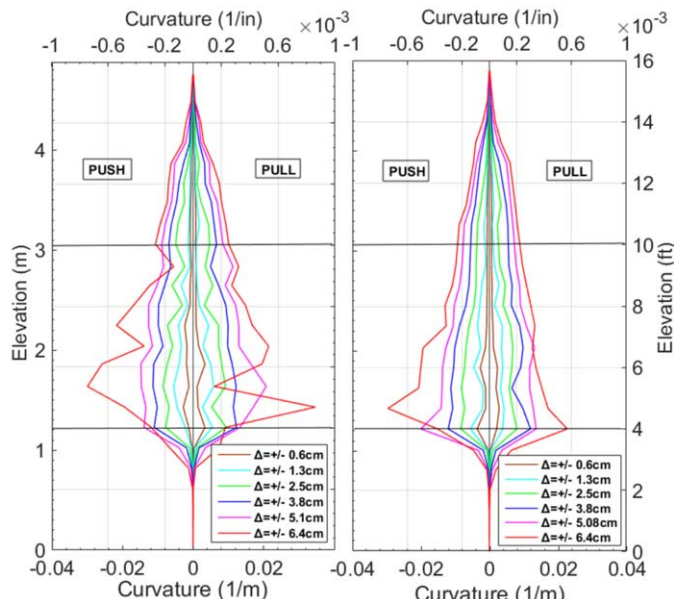


Figure 8. Curvature profiles derived from longitudinal strain gauge instrumentation for Specimen 1 (left) and Specimen 2 (right).

4. Summary

Two pile specimens with different transverse shear reinforcement were examined under identical test conditions and subjected to reverse cyclic lateral loading. The specimens were installed in a two-layer soil system with a strong stiffness contrast, namely a loose, silty sand underlain by rock, experimentally simulated through high-strength concrete. Specimens were tested to complete structural failure and excavated after test completion. No damage (i.e., cracking) and no lateral pile deformations were observed in the rock socket. Predominantly flexural cracking occurred along the pile within 60 cm [2 ft] above the rock socket. This elevation corresponds to a depth of three pile diameters below ground surface, which is a typical location of plastic hinges of flexible piles. The differently reinforced pile specimens were expected to fail in different failure modes according to their transverse reinforcement ratio and the predicted shear amplification by the Winkler-based analysis. The experimental specimen behavior suggests that the analytically predicted shear dominated failure did not occur. These preliminary observations could be of future benefit to the construction industry as heavy transversely instrumented section could be minimized and potential issues such as restrictions of concrete flow or air-pocket formation due to too closely spaced hoops could be reduced.

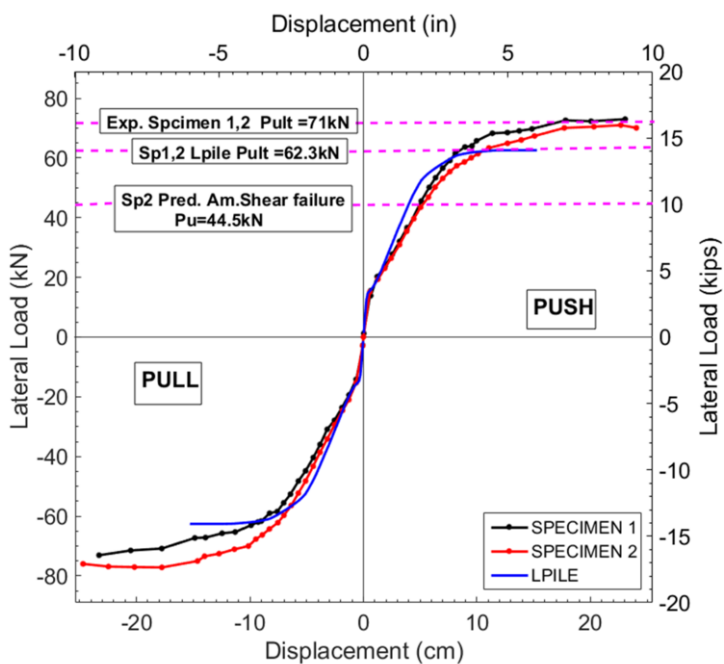


Figure 9. Comparison of experimental and predicted load-displacement responses.

Acknowledgements

This research idea was partially developed through the DFI Drilled Shaft Committee and executed under the leadership of Prof. Anne Lemnitzer and Dr. Ben Turner. The experimental work was partially enabled through DFI's Committee project fund, as well

as the first author's NSF funding (1752303), as well as generous industry support. We would like to gratefully acknowledge material and equipment donations by: PJ Rebar, Atlas Geofoam, Williams Form Engineering, and Gregg Drilling and Testing.

References

- [1] Lymon C Reese et al. "Computer program Lpile plus version 10.0, A Program for the Analysis of Piles and Shafts Under Lateral Loads technical manual". In: Ensoft, Inc., Austin, Texas (2018).
- [2] Reese, L. C., Analysis of Piles in Weak Rock, Journal of the Geotechnical and Geoenvironmental Engineering Division, ASCE, pp.1010-1017, 1997.
- [3] M. W. O'Neill and J. M. Murchinson "An Evaluation of p-y Relationships in Sands,". A report to the American Petroleum Institute, May 1983.
- [4] Building Code Requirements for Structural Concrete (ACI 318-14) and Commentary (ACI 318R-14), American Concrete Institute, 2014.

Technical Session #7

“Excavations and Tunnels”



Werner BILFINGER

Dr. Werner Bilfinger is a civil engineer graduated from the University of São Paulo, where he also got his Master and PhD degrees. He works with design and consultancy since graduation mainly in infrastructure projects, including tunnels, dams, hydro projects, roads and railroads, maritime structures, airports, slopes and foundations in Brazil, the Americas, Europe and Africa. His activities also include the analyses of losses for insurers and insured, as well as participation in arbitrations as technical advisor. He is active member of technical societies, being Brazilian representative in Working Group 19 (Conventional Tunnelling) of the International Tunnelling Association, and Technical Committee 207 (Soil Structure Interaction) of the ISSMGE. He published more than 40 papers in journals and conferences. He participated in the organization of several conferences, being co-editor of the World Tunnel Congress 2014 proceedings and chairman of 9th International Symposium on Geotechnical Aspects of Underground Excavations in Soft Ground. He was chairman of the Brazilian Tunnelling Committee for the term 2017-2018.

Tunneling Through the Rock-Soil Interface

Werner BILFINGER^{a,1}

^aVector Projetos Ltda

Abstract. Constructive methods, tunnel lining, and soil treatment and conditioning depend fundamentally on ground and hydro-geological conditions. Regardless of specific difficulties, construction in homogeneous ground becomes, after adequate definition of the parameters above and the initial learning curve, a repetitive and uniformly controlled process, either through conventional or mechanical tunneling methods. Difficulties often arise when varying ground conditions are encountered along the tunnel alignment, especially if ground behavior presents significant contrasts in deformability, shear strength and permeability. In geological environments where soft ground overlays rock and tunnels have to be built crossing this interface, the above-mentioned contrasts normally occur at the same location. The most significant recent tunnel failures in Brazil occurred close to rock soil interface, showing the necessity of a review of current design and construction practice. This paper intends to discuss main challenges associated to the rock-soil interface in the light of recent tunnel failures and present suggestions for robust design and construction methods.

Keywords. Soil Treatment, Rock-Soil Interface, Constructive Methods, Design

1. Introduction

In tunnel construction, geological-geotechnical contrasts along tunnel alignment are among the main challenges. Changes in material behavior, shear strength, deformability and permeability have often led to problems, including reduction of production rates, need for additional and unexpected treatments, and failures.

This paper presents the main topics associated to design and construction, focusing on the soil-rock interface. Although most of the discussed topics are known and available in the literature, it is important to revisit these topics in the light of recent tunnel failures.

The paper is focused on tunnels built using the so-called NATM or SEM (Sequential Excavation Method); however, the discussed concepts may also be used for mechanically excavated tunnels.

2. Background

Unfortunately, few publications discuss failures and their causes in tunneling. Some compilations with case histories are presented in [1], [2], [3], [4] and [5]. When analyzing these databases, it becomes clear that a significant part of the published failures is associated to singularities and unexpected ground conditions. The soil-rock interface is

¹ Corresponding Author, Vector Projetos Ltda, Rua Cardeal Arcoverde 1749 cj. 103, São Paulo, Brazil;
E-mail: werner@vector.com.br

one of these singularities, where often some critical conditions are encountered at the same place:

- great variability of materials (deformability, shear strength and permeability), with non-regular geometry;
- concentration of high permeability layers, leading to high water inflow and its associated problems;
- Necessity to change the constructive method: at the interface the constructive method has to be changed often from conventional excavation of soil (using excavators or road headers), to the necessity to excavate rock (or vice-versa), using drill and blast.

The shape and position of the soil-rock interface is often difficult to determine precisely prior to tunnel excavation. Figure 1 below present data from [2], showing the soil-rock interface as presented in the final design documents, as well as a re-interpretation based on additional site investigations performed after a failure at the Lausanne Metro in 2005. The failure, according to [2], is related to the difference in ground conditions between the design profile and the real site conditions, including a “pocket filled with water.”

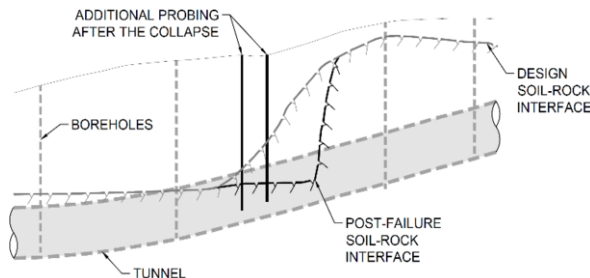


Figure 1. Longitudinal geological profile with soil-rock interface as presented in final design and after post-failure site investigations [2].

An analogous problem occurred during the construction of Salvador Metro: during the design phase, the soil-rock interface was analyzed using a number of boreholes. However, between two boreholes, an undetected depression reduced significantly the rock cover above tunnel crown, which led to a failure that, fortunately, did not progress to the surface.

Figure 2 presents an example of a soil-rock interface, reproduced from [6], as interpreted after the forensic evaluations of the failure of the Pinheiros Station, in São Paulo. It becomes clear that the often idealized straight line used to identify the soil-rock interface can be misleading and has to be adequately interpreted.

The difficulties of mapping the soil-rock interface is not limited to tunneling projects: in [7], a case history is presented where, due to an undetected paleo-channel, the design of a dam had to be changed from an earth-rock fill dam, to a concrete structure.

The different characteristics of the geo-materials normally lead to the need of using additional measures, when compared to the routine, to ensure tunnel stability, like installation of (additional?) soil treatments, reduction of excavation sections and groundwater lowering. The efficiency of different stabilizing measures has to be carefully evaluated. For example, a jet-grouted pre-lining, including a “plug”, closing the pre-lining, could be considered a safe solution at first glance. However, minor defects

in the pre-lining can lead to almost catastrophic situations, with significant water ingress into the tunnel, piping of loose material and surface settlement velocity of more than 120mm/day, as described in [8].

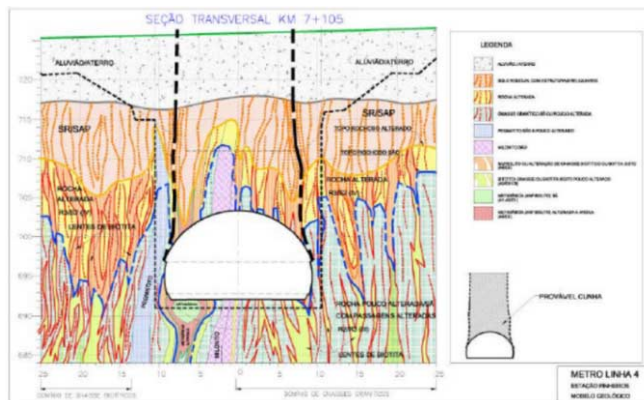


Figure 2. Geological cross section of the Pinheiros Station, reproduced from [6].

Therefore, the difficulties associated to the soil-rock interface can be divided into at least three different aspects:

- Mapping its position and shape;
- Identifying its characteristics;
- Identifying possible treatments and their limitations.

3. Site Investigations – State of Practice and Limitations

Site investigations are the tool to predict the geotechnical profile and geomechanical properties of its materials. Without the proper site investigations, the risk of not identifying important geological-geotechnical features increases and, therefore, of facing non-predicted behavior during and after tunnel excavation. Following general rules regarding site investigations are proposed in [9] and discussed by Parker [10]:

- Between 1.5 and 2.25 % of the construction cost should be spent with site investigations, and a contingency of up to 3% should be foreseen;
- For every meter of tunnel, between 0.75 and 1.2 m of boreholes should be foreseen. It is interesting to mention that, historically, in the Metro of São Paulo, the meter of borehole / meter of tunnel ratio is 1, in line with this recommendation.

These quantities have to be seen as broad guidelines, bearing in mind that every project has its particularities. Fookes, in [11], states very properly that “if you do not know what you are looking for in a site investigation you are not likely to find much of value.”

3.1. Site investigation sequence

Site investigations influence tunneling projects in all its phases, starting at the feasibility studies, until actual tunnel construction. Site investigations are influenced by several

factors, including, geology, hydrogeology and geomorphology, project characteristics and use, construction method and environmental considerations [12].

Usual site investigation types consist of:

- desk studies;
- field mapping;
- field investigations, including direct (trial pits, borings, in situ tests) and indirect investigations (geophysical methods), surveys and monitoring;
- laboratory tests, and
- exploratory investigations.

A suggestion of strategy to develop site investigations is presented in [12]. This strategy divides the tunnel design in three phases and associates 3 respective phases of site investigations:

- feasibility studies – first campaign, to assess the main ground conditions and identify major risks. Table 1 presents a summary of expected results and investigation means.
- preliminary design – second campaign, to quantitatively assess soil and rock behavior, and validate methods and sequence. Table 2 presents a summary of expected results and investigation means.
- detailed design – identify properties of ground units and reduce uncertainties. Table 3 presents a summary of expected results and investigation means.

The names of the phases may not be the same in different parts of the world, but the 3 phases approach can be considered conventional.

Table 1. Site Investigations for feasibility studies, based on ITA recommendations [12].

Expected results	Investigation means
Geological and hydrogeological maps	Regional topographic, geological, hydrogeological / groundwater, seismic hazard map
Natural risk maps, when appropriate	Information from field surveys and/or adjacent similar projects
Longitudinal geological profile	Geophysics may provide useful information.
Longitudinal geotechnical and geomechanical profile and identification of major hazards	Limited site investigations to confirm extremely critical geological or groundwater conditions
Preparation of risk register	

Table 2. Site Investigations for preliminary design, based on ITA recommendations [12].

Expected results	Investigation means
Longitudinal geological profile (1:5000 to 1:2000)	Geophysics and boreholes at portals and shafts
Longitudinal geotechnical-geomechanical profile (1:5000 to 1:2000) with ground behavior classes	Boreholes along the alignment
Geological and geotechnical cross sections at the portals (1:500 to 1:200)	Water sources and groundwater monitoring
Geological and geotechnical cross sections at access and ventilation shafts	Laboratory tests
Preliminary characterization of the hydrogeological regime	Outcrop and surface mapping
Update of risk register	In situ measurements and permeability tests, when appropriate
	Exploratory galleries / shafts, if needed

Table 3. Site Investigations for detailed design, based on ITA recommendations [12].

Expected results	Investigation means
Longitudinal geological profile (1:2000 to 1:1000)	Additional boreholes at portals and along alignment
Longitudinal geotechnical-geomechanical profile (1:2000 to 1:1000) with ground behavior classes	Laboratory and field tests
Geological and geotechnical cross sections at the portals and shafts (1:200 to 1:100)	In specific cases / locations, geophysics may provide useful information
Definition of detailed set of design parameters and their variability	Excavation of experimental sections along tunnel alignment, if needed
Detailed characterization of the hydrogeological regime	Continue the monitoring of water sources and groundwater
Update of risk register	

3.2. Desktop studies and field mapping

Desktop studies and field mapping are activities performed normally in the initial site investigation phases. The main objective is identifying materials that will be excavated, geomechanical classes and possible hazards that will be encountered along tunnel alignment. This information is obtained by the analyses of regional and local geology data, mapping of faults, shear zones and other possible discontinuities. Data about structural geology are also obtained. All this information is obtained from literature and/or in field mapping activities.

During these initial phases the soil-rock interface is interpreted normally with the main objective of defining the tunnel length to be excavated in different materials and to estimate quantities.

3.3. Direct investigations

Direct investigations evaluate type of material and measure soil and rock properties by the insertion of some type of tool into the ground. Material may be extracted or not. The most common direct investigations in soil are ([13], [14], [15]):

- Trial pits;
- Standard penetration test (SPT);
- Cone and Piezocone Test (CPT / CPTU);
- Vane test;
- Pressuremeter tests;
- Flat Dilatometer test (DMT).

Interpretation of the results of these tests can provide geomechanical parameters using different theoretical or empirical approaches [13]. Permeability may also be measured using constant head (Le Franc) or variable head tests in boreholes.

In rock, tests are usually associated to core drilling, complemented by other tests:

- Discontinuity measurements, with borehole video or acoustic televiewing. In the past the impression packer was used for this purpose, but the televiewing technique replaced it almost completely;
- Permeability measurements, using Lugeon tests with packers;
- Uniaxial compressive strength performed on recovered specimens.

Special tests, like hydraulic fracturing, may also be performed on boreholes, but are less common. A complete list of ISRM standardized – SM Suggested Methods – can be found in the “Blue Book” [16] and in the more recent “Orange Book” [17].

It can be seen that the direct investigations in soil and in rock are different and, exactly at the boundary between these materials, difficulties may arise in identifying and characterizing materials: SPT and CPT/CPTU tests may reach refusal to penetration before rock is actually reached. On the other hand, core drilling, when drilling close to the soil-rock interface, may not recover material and, therefore, no information may be obtained in this region.

3.4. Indirect investigations - geophysics

Indirect investigations aim to identify different materials and its properties of the subsoil profile without the necessity of drilling boreholes or driving probes. Most of the geophysical methods have the advantage of generation sections, in contrast to direct investigations, where only a vertical "line" is investigated.

Main geophysical investigation methods are ([18], [19]):

- Seismic – reflection, refraction, borehole seismic, surface waves;
- Gravity;
- Magnetics;
- Geoelectrics;
- Electromagnetics;
- Radar.

Geophysical methods focus mainly on profiling – preparation of geological profiles and geomechanical parameters are generally not obtained. Seismic tests measure seismic velocity of the different layers, which then can be correlated to stiffness and other geomechanical parameters.

In the experience of the author, for usual tunnel projects, seismic refraction and electrical resistivity tests are commonly used. To obtain more accurate dynamic soil parameters, cross hole or down the hole tests are performed. The use of the seismic refraction technique may be limited by external sound sources, typical in urban environment.

In [20] case histories are discussed, where different geophysical methods are combined to map the geology along tunnel alignment.

3.5. Discussion

The recommendations regarding site investigations presented in 3.1, as well as the available techniques, direct and indirect, show that there are several tools to investigate soils and rocks. However, the interface, which is normally not the idealized straight line, is often very difficult to investigate. Figures 2 and 5 present examples of more realistic shapes of the soil-rock interface. To investigate the interface, in the opinion of the author, a combination of methods is necessary:

- Initial geological assessment, to evaluate possible shapes, thicknesses, existence of boulders, geohydrological conditions, orientation of discontinuities, etc.
- Borings, focusing on maximum core recovery (large diameter, careful boring – limiting the use of water circulation). Orientation of boreholes should take into consideration the orientation of the discontinuities of the rock;
- Televiwing of boreholes, where boreholes are sufficiently stable;

- Geophysical investigation, calibrated using the borings, if possible, using more than 1 method.
- Recovered core samples should be inspected and tested in the laboratory.

After the site investigation campaign, which could be performed in phases, like the recommendation presented in 3.1, its interpretation should be equally careful. The interpretation should focus specially on:

- Identification of different materials;
- Identification of geohydrological conditions;
- Characterization of shear strength, deformability and permeability of the identified materials;
- Mineralogical characterization of the materials, evaluating the possibility of swelling or other deleterious properties.

It is, however, important to state that with current practices and technologies, it is not possible to preview with precision the location, dimension and particularities of the so-called soil-rock interface. In reality, the interface is not a line or plane, but a transition zone.

The use of probe-drilling during construction has been an important tool to improve the knowledge about the ground. More recent techniques, including seismic ([21],[22]) investigations from inside the tunnel are an evolution that may add information to the pre-tunneling geological-geomechanical model.

4. Lining and Support - concepts

There is no universal nomenclature that defines the system of elements that support the soil or rock mass, stabilizing the tunnel opening. In [23], primary support, also called lining, and secondary linings are associated to construction phases. The primary support is defined as having the purpose of "...to stabilize the underground opening until the final lining is installed". The usual elements of a primary support / lining are shotcrete (reinforced or not), rock bolts, steel ribs and lattice girders.

The definitions above encompass both tunnels in soil and in rock. There is, however, an important difference between tunnels in these materials: to stabilize the soil around a tunnel opening in soil, a shell-like structure is necessary, normally consisting of shotcrete and/or concrete. This shell stabilizes ground pressures as a structure – resisting to axial forces, bending moments and shear forces.

For tunnels in rock other ways to stabilize the rock mass are normally used, mainly rock-bolts, that make a part of the rock mass work as a supporting rock arch. This mechanism is only possible if the rock has a) sufficient strength to support the acting stresses and b) the rock bolts are adequately anchored to resist the tensile stresses.

Figure 3 below presents the conceptual differences of both linings / supports.

To differentiate linings / support of tunnels in soil and rock, the following definitions are used in this paper:

- "lining" is associated to the shell-like structure that stabilizes ground pressure resisting mainly to axial forces, typical for a tunnel in soil. This type of lining is sometimes called structural lining;
- "support" is associated to the combination of rock-bolts and shotcrete, typical for tunnels in rock.

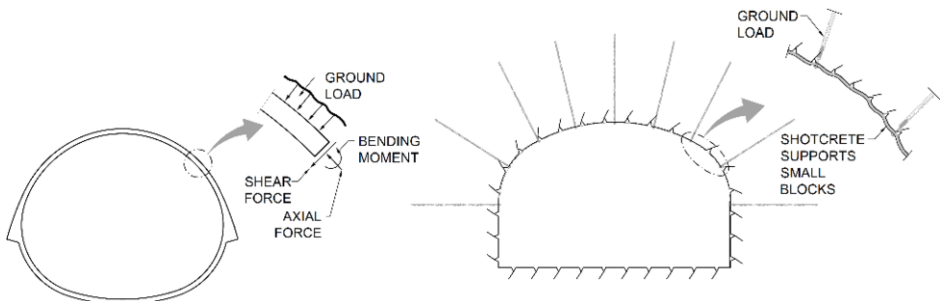


Figure 3. Concept of tunnel support in rock and in soil.

It is important to mention that the differences between linings and the concepts discussed above are far more complex, but for the purpose of this paper, the simplifications above are sufficient.

Considering the mechanisms above and the discussion in item 2, it becomes clear that in the region of soil-rock interface it is not possible to consider that a rock arch can be formed. Therefore, a structural lining is necessary to safely equilibrate ground loads.

The definition of the loads, to be considered acting on the lining and which will be used to define it (shape, thickness, strength, reinforcement, etc.) is a topic which extrapolates the scope of this paper. Comprehensive literature, like [24], may be used, as well as design standards.

Some particularities regarding lining loads are important to emphasize, specifically when designing close or at the soil-rock interface:

- Normally, the ground is not homogenous, but has anisotropic behavior, and includes discontinuities, planes of weakness, etc.
- If the lining is founded on rock, with relatively low deformability, and the surrounding ground settles due to, for example, groundwater lowering, lining loads may be higher than the total soil overburden, i.e., no soil arching will occur;
- Along the tunnel axis, foundation conditions may vary significantly, and usual 2D analyses and their simplifications may not be representative.

5. Typical Failure Mechanisms

The HSE – Health and Safety Executive [5] presented a summary of typical failure mechanisms associated to tunnels excavated using the SEM (sequential excavation method), dividing them into three main categories:

- Ground collapse in heading;
- Failure of lining before ring closure;
- Failure of lining before or after ring closure.

The location of the failures is divided into regions A and B, as presented in Figure 4. It is important to mention that the HSE, when developing his studies, focused on failures in soil, like London Clay.

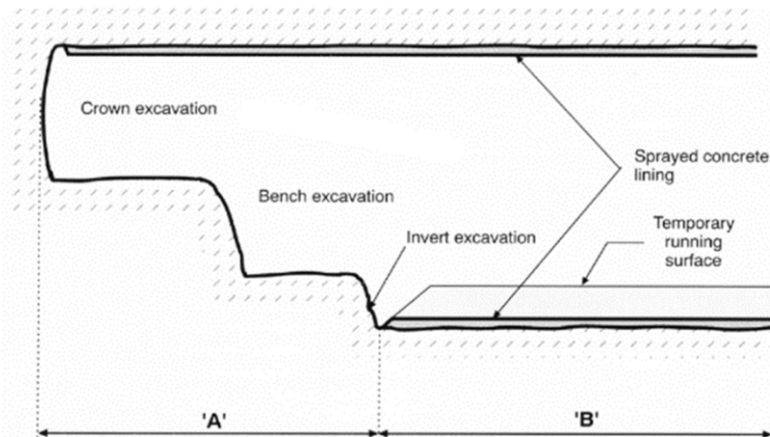


Figure 4. Possible locations of failures – regions A and B, reproduced from [5].

Typical failure mechanisms described in [5] for region A are:

- Bench, crown or full-face failures;
- Weakness in crown due to vertical fissures, pipes and manmade features;
- Insufficient cover to overlaying permeable water bearing strata;
- Insufficient cover to surface;
- Lining bearing failures and failures due to horizontal movement of arch footing.

Typical failure mechanism for region B (and in region A) are:

- Shear and compression failure;
- Combined bending and thrust;
- Punching.

The most common failures, whether published in the literature or not, occur in region A, where no or limited stabilizing effect of the tunnel lining is available. In the experience of the author in several cases, smaller failures are not even made public, if they do not progress to the surface.

Failures in region B, where the lining is already installed, are fewer, but often have a much more severe impact, because a longer tunnel stretch may be affected. If one analyzes, for example, the failure of the Pinheiros Station ([6], [25], [26]), the tunnel length affected by the accident was significant because the failure mechanism occurred not in region A, close to the tunnel face, but region B, affecting a relatively long already lined tunnel stretch. Two other recent tunnel failures in Brazil affected also a significant stretch of the tunnel and can be associated to failures in region B. This type of failure is associated to a condition where the tunnel lining, or its foundation, is not capable of supporting the load of the soil / rock mass and the failure is only interrupted where a change of either the lining or the lining loads occurs.

In addition to the failure mechanisms described in [5], at the soil rock interface other mechanisms may develop due to the presence of non-homogeneous materials, with discontinuities of the original rock mass. An interesting representation of the soil-rock interface can be visualized in Figure 5, reproduced from [27]. It can be seen, that the soil rock interface is not a clearly defined line – interface, as often idealized, but a region where the transition from soil to rock occurs. Discontinuities inherited from the original rock mass, blocks, immersed in the soil mass, soil filling rock discontinuities are some

of the potential problems that are faced when tunneling through the soil-rock interface. In the majority of the cases, this region lies below the groundwater level and local high permeability stretches can lead to localized high flow rates. Water inflow with soil erosion [28] is described as an important destabilizing mechanism that occurs at the soil-rock interface.

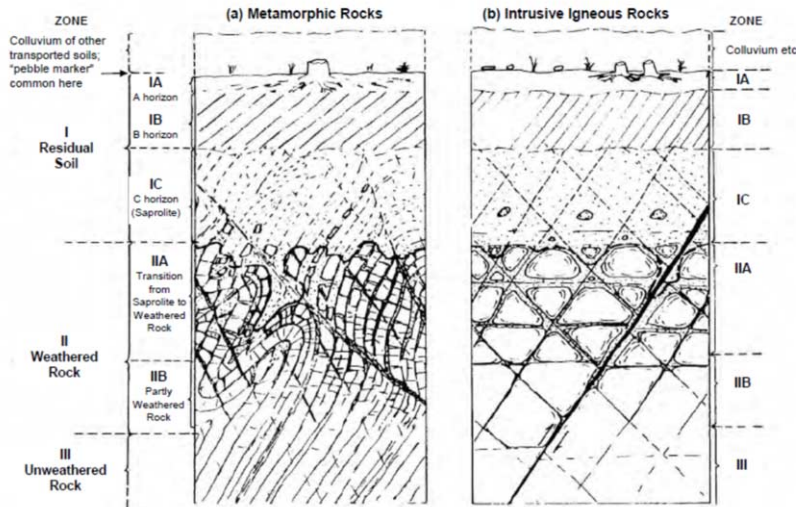


Figure 5. Typical weathering profile for metamorphic and igneous rocks, reproduced from [28].

6. Ground Treatments

The need for ground treatment arises in material that cannot be excavated due to stability problems. Possible solutions are normally:

- Reduction of excavated cross section, generating a more stable condition;
- Ground Treatments (soil and/or rock), including reduction of pore pressures.

Typically, ground treatments can be divided into following types [23]:

- Ground improvement;
- Ground reinforcement;
- Dewatering.

These types of treatments may be installed from inside the tunnel or from the surface, depending on local conditions.

An important issue that often is overseen is the fact that in the region of the soil-rock interface it will be necessary to drill through different materials: soft ground and rock. Drilling through both materials in a same hole may generate the necessity to use special tools or to "telescope", using casings with different diameters. Drilling through rock blocks may be particularly complicated, depending on their size, because of possible movements of the blocks with relation to the surrounding ground, "trapping" drill rods. Therefore, when designing and prior to starting actual ground treatment, a careful evaluation of possible scenarios should be done.

6.1. Ground Improvement

This type of treatment improves mechanical and/or hydraulic properties of the ground. Typical ground improvement techniques are grouting, jet grouting and ground freezing.

6.1.1. Grouting

Grouting is a traditional soil and rock treatment used not only in tunneling, but in several other civil engineering applications, like foundation treatments of dams. Grouting *per se* is a very extensive theme and extrapolates the scope of this paper. [29], [30], [31] and [32] are examples of interesting literature about grouting.

Grouting can be divided according to the way the grout interacts with the soil or rock mass:

- Permeation grouting – filling soil voids, by permeation, i.e., substituting normally water by the grout and not “disturbing” the soil structure;
- Fracture grouting – the grout fills discontinuities or creates (“hydro fracture grouting”) and fills discontinuities;
- Compaction grouting – the grout generates compaction of the soil mass by displacement.

Grouting can also be divided according to the material that is injected:

- Conventional Portland cement;
- Other types of cements, like micro-cements, with much smaller granulometry, allowing penetration in significantly smaller voids;
- Different types of chemical grouts – polymers – like acrylic, polyurethane, silicates or epoxy.

The first step of assessing a grouting solution is evaluating its main purpose: reinforcing the soil / rock, reducing its permeability or both. The “groutability” of the massif should also be evaluated: depending of the massifs condition, grouting can even be deleterious due to a possible destruction of an existing structure. Another important issue is existence of water flow: depending on flow velocity, cementitious grouts may be inefficient, because of the cement being carried away by the water. Therefore, a grouting solution should be evaluated considering its purpose, type, material, injection pressure, injected volumes and existence of water flow.

6.1.2. Jet Grouting

The jet grouting technique “transforms” the local ground, using a high pressure grout jet (sometimes with additional air and water jets), into a soil-cement mix. Comprehensive information about it can be found, for example, in [33].

The jet grouting technique forms soil-cement cylindrically shaped columns and can be built from the surface, for shallow tunnels, or horizontally from inside the tunnel. Jet grouting is a very versatile technique, in which the ground can be improved in several ways and shapes:

- installation of a sequence of secant columns can form a “pre-tunnel,” including or not a “plug,” to configure an impervious pre-lining [34],[35];
- Foundation for tunnel lining in weak ground;
- Tunnel face reinforcement.

One key issue when using jet-grouting is the definition of different operational parameters to achieve the desired column diameter. In relatively homogeneous material, theoretical approaches are possible ([33], [36]). However, in very heterogeneous material, this type of prediction is almost impossible. If rock blocks are part of the ground mass, due to a “shadow” effect, no column will be formed behind this block and the jet grouting solution may be inefficient. Therefore, in the region of the soil-rock interface, jet grouting solutions have to be carefully evaluated, especially if waterproofing action is expected (i.e. one single defect can compromise the whole solution).

6.1.3. Ground Freezing

The ground freezing technique is based on the principle of transforming temporarily the water in the ground into ice, which has the advantage of a relatively high shear strength, as well as being impermeable. The ground is frozen circulating a coolant through previously installed tubes.

Although being a relatively costly and slow process, in some cases this is the only technique of stabilizing the ground, to allow excavation and lining installation.

In addition of being costly and slow, a disadvantage of the process is the expansion of the water when turning into ice, which can lead to ground heave, and, during thawing, volume reduction and settlements.

6.2. Ground Reinforcement

Ground reinforcement are methods where elements are inserted into the ground, to improve its properties by mechanical action. The most common types are pipe umbrellas, spiles and face nails / bolts. Pipe umbrellas and spiles are also known as forepolings.

6.2.1. Pipe Umbrellas

The so called “pipe umbrellas” are usually 10 to 15 m long and the pipes have a 75 to 100 mm diameter, with a 30 to 50 cm spacing between tubes. They introduce a stabilizing effect, acting like a beam, with one end fixed in the soil mass ahead of tunnel excavation face and the other end, on the existing lining (Figure. 6 below).

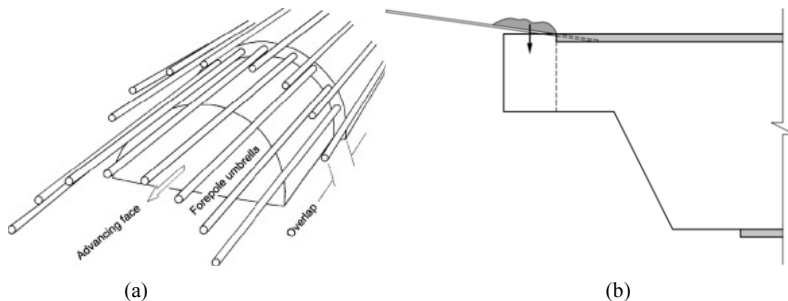


Figure 6. (a) Schematic view of pipe umbrella, reproduced from [35], (b) “beam” effect of individual pipe.

Pipe umbrellas are often associated to grouting: using rubber sleeves and injection packers, the tube can be used to inject grout. This injection can be used solely to make sure that the tube is adequately fixed to the surrounding ground, or to tentatively improve it.

Topics that should be considered with this type of solution are:

- Installation of tubes can be done:
 - In unlined borings, if the soil is sufficiently stable;
 - In unstable ground, cased borings or selfboring tubes have to be used;
- The installation of the individual tubes may generate, by itself, settlements;
- The space between tubes will remain “open” and the local soil exposed, which can be a problem in the case of cohesionless soils;
- Pipe umbrellas, in principle, do not reduce settlements. Settlement reducing effects can only be expected when large diameter tubes are used [37].
- Considering the necessity of installation from inside the tunnel, pipe umbrellas (as all other similar treatments) have to be installed following a conical shape. Therefore, the initial stretch of each tube will be located inside the tunnel (and will have to be destroyed during excavation), and the longer the tubes, the greater is the distance from the tunnel to them, reducing their efficiency.

6.2.2. Spiles

Spiles are relatively short bars (usually made of steel, 20 to 25 mm diameter) installed locally to protect excavation roof or sidewalls, allowing safe excavation and installation of the lining or support. Spiles are 2 to 3 m long, being manually driven or installed in pre-drilled holes.

6.2.3. Face nailing

Face nailing are installed to stabilize the excavation face and also improve global stability. Usually face nails are made of glass fiber, to facilitate its removal, as they are located in a region that will be excavated in the future. Face nails are installed in pre-drilled, grouted holes. Different length and spacings are possible; usual spacing between nails vary from 1 to 2 m and nail length between 8 to 12 m.

Some nailing systems have not only the reinforcement purpose, but also work as drains.

6.3. Groundwater lowering

The control of groundwater is one of the most important issues in tunneling. When the groundwater level is located above the tunnel, the difference in porepressures will generate water flow in the direction of the tunnel face and unsupported areas. This flow, even in low permeability ground, is highly destabilizing and, in the case of ground with low cohesion, can lead to piping and generalized destabilization. Controlling porepressures is often one of the keys to successfully building a tunnel.

The groundwater can be lowered from the surface, by deep wells, or from inside the tunnel, with horizontal drains, with or without the help of vacuum.

Important topics that have to be considered with relation to the groundwater:

- Existence of more than one groundwater level (perched groundwater levels);
- Ground stratification, with different materials and permeabilities;
- Concentrated flow in discontinuities, in rock, weathered rock or saprolitic soils;
- Constructive difficulties, considering that for the installation of deep wells it may become necessary to perforate rock, or rock blocks. Under these conditions,

the use of special tools or equipment may become necessary, increasing costs and reducing productivity.

7. Other particularities

7.1. Over-excavation

In the region of the interface, during a certain tunnel length, part or even the full cross section, has to be excavated in rock, but a structural lining needs to be installed. Depending on the rock type, drill and blast has to be used to excavate the rock. When using drill and blast, the so-called perimeter holes have to be drilled slightly outwards, which automatically leads to an over-excavation. It is very complicated to obtain a regular shape when installing a structural lining; therefore, the outer face of the excavation usually has a "sawtooth" shape, while the internal face has the designed regular shape. Figure 7 shows an example of the excavation and lining shape.

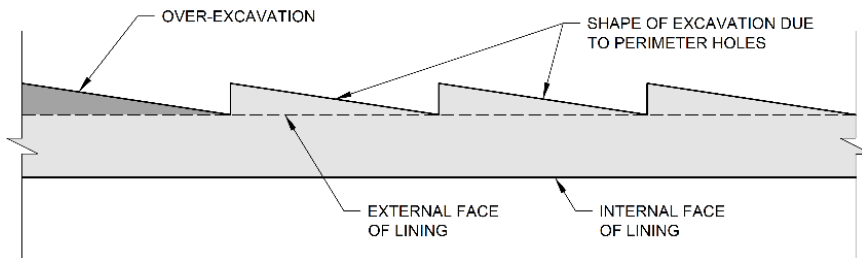


Figure 7. Excavation in rock using drill and blast and structural lining – plan view.

The condition above is theoretical and in reality, considering that the round length has to be small due to potential stability problems, over-excavations are significantly higher: to drill the perimeter holes for the next stretch to be excavated, the drill rod can only drill at an angle compatible with the installed lining, Figure 8.

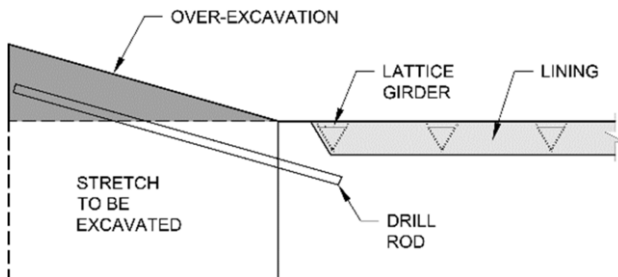


Figure 8. Excavation in rock using drill and blast and structural lining – plan view – including geometry conditioned by installed lining and drill rod.

These over-excavations, depending on the shape of the tunnel, lining thickness, available equipment and round length can easily generate average lining thickness increases of more than 100 %.

7.2. Variable cross sections

When tunneling through the soil-rock interface, its position varies along the tunnel alignment from the invert to tunnel crown, generating cross sections with very different geomechanical conditions, as presented in Figure 9:

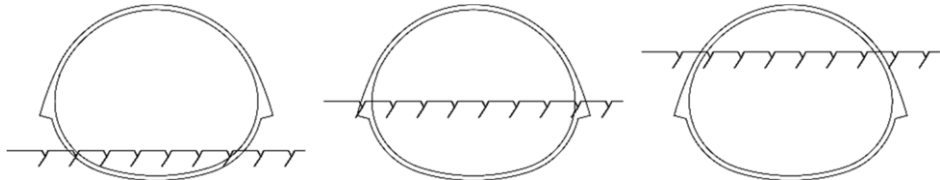


Figure 9. Variable cross sections along a soil-rock interface.

The horizontalized interface is hypothetical; normally it is sloping, generating asymmetric conditions. Its variable position generates different particular conditions:

- Interface close to the invert – possible elimination of the invert, if bearing capacity of the rock below the interface is adequate. This decision has to be investigated and evaluated carefully, due to possible high variabilities, as presented in Figure 2.
- Interface close to the center of the tunnel – possible excavation in two phases;
- Interface close to tunnel crown – difficulties to excavate in two phases.

A relatively common practice in tunneling is to install a structural lining only in the part of the cross section excavated in soil and use the rock support in the part of the section excavated in rock. This type of hybrid solution has to be evaluated carefully. The structural lining may generate high localized loads on the interface, which may not be supported by the rock. Additionally, the part of the section with rock support did not configure a continuous rock arch – Figure 10.

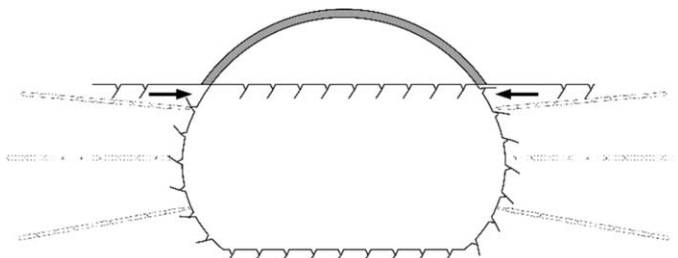


Figure 10. Cross section with crown in soil and side walls in rock.

7.3. Different Constructive Method at the same Cross Section

Figure 10 of item 7.2 above shows a common practice with relation to the lining / support. However, the geomechanical conditions at the same cross section lead to the necessity to excavate part of it by conventional means and the rest of the cross section, using drill and blast. This condition generates the following potential problems:

- Blasting will be used very close to the relatively fresh shotcrete of the conventionally excavated part of the cross section;

- The foundation of the lining will be removed, generating an unfavorable condition;
- Often more time is necessary to install the lining of the stretch excavated by drill and blast, because of the construction phases of drill and blast: drilling, loading, blasting, ventilation, muck removal, scaling, installation of shotcrete and rockbolts.

8. Case Histories

In this item, 4 unsuccessful cases are briefly presented and discussed, including some lessons learned to avoid similar problems in the future.

8.1. Case 1 – Face and Crown Stability Problems – Region A

Figure 11 presents a geological longitudinal section of a 15 m wide tunnel built recently in Brazil. The tunnel lining consisted of a 25 cm thick shotcrete shell in soil and, in rock, 4 m long rock bolts with variable spacing and shotcrete support, defined according to the rock mass classification.

Approximately 20 m from the tunnel portal, a depression of the soil-rock interface was foreseen (using boreholes and geophysical site investigations) and, due to its proximity to the tunnel, a pipe umbrella was designed to protect the excavation.

The real interface was encountered closer to the tunnel portal and extended a few meters deeper, inside the tunnel cross section. During excavation severe stability problems occurred, with soil and water ingress into the tunnel. Excavation was paralyzed and the tunnel heading protected with backfill and shotcrete.

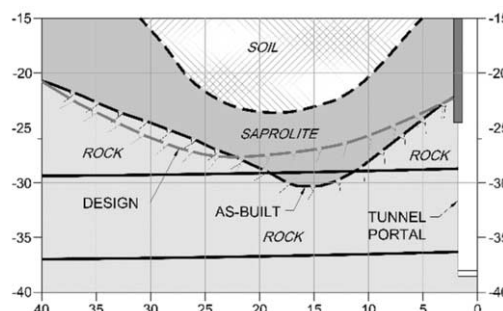


Figure 11. Longitudinal geological cross section with the idealized design soil-rock interface and the “as built” interface.

Different attempts were done to restart excavation, using:

- Conventional pipe umbrella, with pipes being installed in uncased holes. However, the holes proved not to be stable and water (pressure of almost 300 KPa) and soil was washed into to tunnel.
- Conventional pipe umbrella, and face nailing, installed using cased holes. However, water and soil were washed through the casings into the tunnel.
- Jet grouting pre-tunnel and face stabilization. However, no continuous columns were formed in the heterogeneous saprolite, and additionally, part of the soil-

grout mix was washed into the tunnel, even with the use of a so called "preventer".

Finally, a solution that included groundwater lowering with deep wells, horizontal drains and a grouted pipe umbrella, using self-boring pipes, was successfully used, allowing the excavation to proceed.

Tunnel excavation was paralyzed for several months and significant settlements occurred.

8.2. Full Collapse in Region B

Three recent tunnel failures that occurred in Brazil involved significant tunnel stretches and could be typically classified as collapses in Region B, i.e., failures associated to a regular tunnel stretch and not limited to the region close to the tunnel face.

Constructive method to build the three tunnels was the so called NATM (SEM), with excavation done partially through conventional means and partially with the use of drill and blast.

Causes and responsibilities about the failures are still being discussed and it is not the aim of this paper to evaluate or interpret them. However, some important lessons should be learned from them.

8.2.1. Case 2 - Pinheiros Station

The failure of the Pinheiros Station, in 2007, has been presented by different authors ([6], [25], [26]), with different views about its causes and failure mechanisms. A convergent view, however, is that the overstressing of the tunnel walls by the loads of the structural tunnel lining and the immediately adjacent rock mass are an important factor (figure 12).

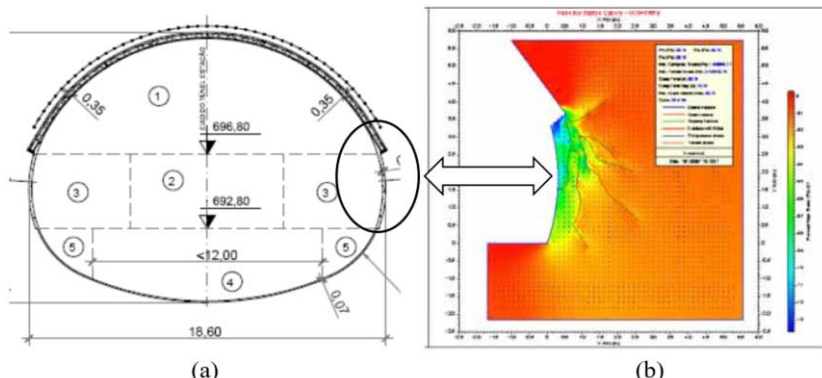


Figure 12. (a) Cross section of the Pinheiros Station, reproduced from [6]. (b) Failure mechanism presented for the Pinheiros Tunnel Station failure by [24]

8.2.2. Case 3

To present date, no technical information was published about Case 3, a failure of a four-lane road tunnel. Failure occurred when excavation reached the transition zone from soil to rock, with relatively high cover. The upper half of the tunnel was being excavated without side-drifts or other subdivision. Figure 13 presents a schematic cross section of the tunnel and simplified geological model.

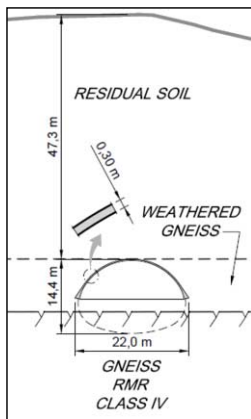


Figure 13. Cross section and simplified geological profile of Case 3.

Failure of the tunnel initiated with signs of overstress in the lining, close to tunnel face and progressed for several meters, probably due to the combination of high lining loads, overstressing of the shotcrete, and difficulties of the ground mass to properly arch and transfer loads. Fortunately, the failure did not cause casualties.

8.2.3. Case 4

To present date, no technical data was published about Case 4. This case is a failure of one of two parallel four-lane road tunnels. Failure occurred during the excavation of the central part of the cross section, connecting the two previously excavated side-drifts. Figure 14 presents a typical cross section of the tunnels. The tunnel that failed was the tunnel on the right side of figure 14 below.

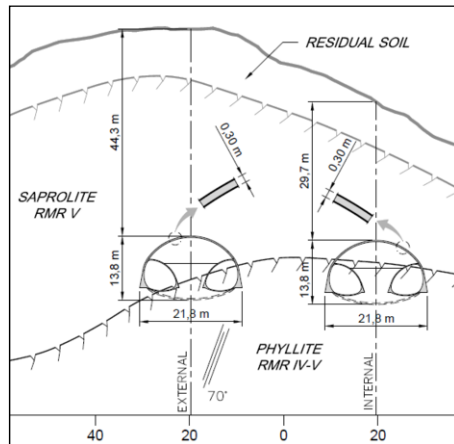


Figure 14. Cross section and simplified geological profile of Case 4. The tunnel on the right side failed.

Failure initiated, also, with signs of overstress in the lining, close to the excavation face and progressed until the tunnel portal for around 130 m. After the failure of the right tunnel, the left tunnel lining showed significant distress.

8.3. Lessons Learned

Problems in tunneling associated to the rock-soil interface generate often as consequence delays and cost increases. Therefore, a generalized conservative approach during design and construction are advisable.

The soil-rock interface is very difficult to map and is not the often idealized "line" drawn between boreholes. In Case 1 the interface was locally encountered approximately 3 m deeper than foreseen and this difference led to significant problems, including a delay in construction and settlements on the surface. If tunnel stability depends on a precise location of the interface, a conservative design approach i.e., evaluation of different scenarios, is advisable. Local vertical variations of the interface for at least 3 m can be considered normal.

In Cases 2 to 4, discussions associated to the failure mechanisms always included the relevance of geological features, that make the ground behave in a non-homogeneous way. In all cases, the foliation / main discontinuities were steeply dipping and oriented approximately parallel to the tunnel axis, and in all cases, tunnel lining failed due to overstresses. Therefore, a conservative approach regarding lining design (shape, thickness, strength, adequate foundation) is strongly recommended, based on a comprehensive evaluation of geological and geomechanical design models.

With relation to ground treatments, an equally conservative approach is recommended, including the evaluation of possible constructive problems:

- Stability of holes bored to install soil treatments (pipe umbrellas, face nails), influencing the decision of using unlined, cased or selfboring elements;
- Water pressures and associated flow rates, leading to soil-piping and "washing" grout out of the ground, reducing / eliminating its effect;
- Difficulties in obtaining jet-grouting column diameters in variable strength ground.

Planning and installing ground treatment as preventive and mitigating action is always more efficient than using ground treatment as remedial measures.

9. Concluding Remarks

This paper presented a brief summary of the main issues associated to the soil-rock interface:

- The knowledge of a representative geological-geomechanical model is crucial. This model should be continuously revised and improved with information obtained from face mappings, probe drillings and other means, updating and adjusting design if necessary;
- Site Investigations:
 - o with the current state of practice, a precise location and definition of the soil-rock interface is almost impossible. Variations of a few meters should be considered as being normal. This reality should be considered when designing and building tunnels;
 - o A comprehensive site investigation campaign, including quality boreholes (with high recovery rates) and geophysical testing should be foreseen for every important tunnel. The rule of thumb of one m of boring for one m of

tunnel is generally valid, but should be complemented by at least another type of investigation.

- Lining concepts: the use of a structural lining is important, considering that a typical rock tunnel lining will only be efficient if the rock mass, together with rock bolts and shotcrete, form a “rock arch” that supports the overlaying ground. Extreme care should be taken considering the fact that the idealized geometry that supports design studies never occurs during excavation. For this reason, the shotcrete / concrete used to fill the irregular shape of the so called “overbreaks” should not be considered part of the structural lining thickness;
- Ground treatments: different types are available, applicable for different conditions. There is no ground treatment, applicable and efficient for all conditions. A robust solution, in the opinion of the author, includes more than one type of ground treatment, from which, in most cases, groundwater lowering is a very effective part. It is also important to bear in mind that mitigation is normally much better than remediation, i.e., preventive ground treatments are much more effective than tentative remedial ground treatments, often under difficult conditions.
- The presented case histories showed that a conservative approach regarding lining design (shape, thickness, strength, adequate foundation) is important, based on a comprehensive evaluation of geological and geomechanical models. This conservative approach should include a continuous update of geological and monitoring information, verifying if the idealized design conditions are met and, if necessary, adjusting the design to real on-site conditions.
- The concepts of robust and resilient design are important tools to mitigate construction and operational risks during the design phase. It is however fundamental that a risk mitigation philosophy continues during construction and the entire operational life of the tunnel.

Acknowledgements

The author wishes to thank Prof. Luiz Guilherme de Mello and Prof. Georg R. Sadowski for valuable discussions and Engineer Cristiano Yai for his valuable help with the illustrations.

References

- [1] GEO Geotechnical Engineering Office. *Catalogue of Notable Tunnel Failures – Case Histories (up to April 2015)*. Available at: https://www.cedd.gov.hk/eng/publications/geo/notable_tunnel.html, 2015.
- [2] Seidenfuss, T. *Collapses in Tunnelling – MSc Thesis*. EPFL Lausanne. 2006.
- [3] Souza, R.L. *Risk Analysis for Tunnelling Projects - PhD Thesis*, Massachusetts Institute of Technology, 2010.
- [4] Spackova, O. *Risk Management of tunnel construction projects*. PhD Thesis, Czech Technical University in Prague, 2012.
- [5] Health & Safety Executive. *Safety of New Austrian Tunnelling Method (NATM) Tunnels*. HSE Books, Sudbury. 1996
- [6] Hight, D.W. *Comments on the Foreseeability of some Geotechnical Failures*. XV Brazilian Soil Mechanics and Geotechnical Engineering Conference, Gramado. 2010.
- [7] Hachich, W., de Mello, L.G., Bilfinger, W., Bucalem. *Análise Tridimensional das Tensões em uma barragem e suas fundações: implicações na avaliação da segurança*. Geotecnia, **100**, p. 1-20. 2004.

- [8] Bilfinger, W. *Recalques nas Obras do Porto Maravilha*. Presentation at Geosul. 2017.
- [9] U.S. National Committee on Tunnelling Technology. *Geotechnical Site Investigations for Underground Projects*. National Academy Press, Washington D. C. 1984
- [10] Parker, H. W. *Planning and Site Investigation in Tunnelling*. I Brazilian Tunnelling and Underground Structures Congress / International Seminar South American Tunnelling. 2004.
- [11] Fookes, P.G. *Judging the Lie of the Land – Meeting Report of the First Glossop Lecture*. Ground Engineering (10(8):36. 1998.
- [12] ITA WG 2. *Strategy for Site Investigation of Tunnelling Projects*. ITA-AITES. 2015
- [13] Schnaid, F. *In Situ Testing in Geomechanics*. Taylor and Francis. Oxon. 2009
- [14] Clayton, C.R.I., Mathews, M.C., Simons, N.E. *Site Investigation. 2nd ed.* Blackwell Science. Oxford. Available at <http://www.geotechnique.info/>. 1995
- [15] FHWA. *Technical Manual for Design and Construction of Road Tunnels – Civil Elements*. National Highway Institute. New York. Available at: <https://www.fhwa.dot.gov>. 2009.
- [16] Ulusay, R. Hudson, J.A. *The complete ISRM suggested methods for rock characterization, testing and monitoring: 1974 – 2006*. ISRM Turkish National Book. 2007.
- [17] Ulusay, R. *The ISRM Suggested Methods for Rock Characterization, Testing and Monitoring: 2007 – 2014*. Springer, Cham. 2015.
- [18] Lehmann, B., Orlowsky, D., Misiek, R. *Exploration of Tunnel Alignment using Geophysical Methods to Increase Safety for Planning and Minimizing Risk*. Rock Mechanics and Rock Engineering. **43**. 2010.
- [19] Andersen, N., Croxton, N., Hoover, R., Sirles, P. *Geophysical Methods Commonly Employed for Geotechnical Site Characterization*. Transportation Research Board. Washington. Available at <http://onlinepubs.trb.org>. 2008.
- [20] Satum, M., McClement, B., Arsenault, J-L. *Imaging soil and rock along tunnel alignments with combined geophysical seismic techniques, case histories*. 14th PCSMGE, Toronto. 2011.
- [21] Dickmann, T., Sander, B.K. *Drivage-Concurrent Tunnel Seismic Prediction (TSP)*. Felsbau. **14**. 1996.
- [22] Dickmann, T. *3D Tunnel Seismic Prediction: A Next Generation Tool to Characterize Rock Mass Conditions Ahead of the Tunnel Face*. Journal of Rock Mechanics & Tunneling Technology. **20**. 2014.
- [23] ITA WG 19. *General Report on Conventional Tunnelling Method*. ITA-AITES. 2009.
- [24] British Tunneling Society; Institution of Civil Engineers. *Tunnel Lining Design Guide*. Thomas Telford Ltd., London. 2004
- [25] Assis, A. P., Barros, J. M., Iyomasa, W., Azevedo, A. A. *Accidents and Failures of Underground Structures in Large Cities: An Independent and Outsider View of the Pinheiros Station Accident*. XIV Brazilian Soil Mechanics and Geotechnical Engineering Conference, Búzios,. 2008
- [26] Barton, N. *The main causes of the Pinheiros Cavern Collapse*. XIV Brazilian Soil Mechanics and Geotechnical Engineering Conference, Búzios. 2008
- [27] Deere, D. U., Patton, F.D. *Slope Stability in Residual Soils*. Proc. 4th. Pan. Am. Conf. Soil Mech. Found. Engng., Puerto Rico. 1971
- [28] Eriksson, L. O. *Soil Rock Interfaces: Problem Identification and Conceptualisation for Sealing Strategies*. MSc. Thesis, Chalmers University of Technology, Gothenburg. 2014.
- [29] Warner, J. *Practical Handbook of Grouting*. Wiley. 2013.
- [30] Bowen, R. *Grouting in Engineering Practice*. Applied Science Publishers. 1975
- [31] Stille, H. *Rock Grouting – Theories and Applications*. BeFo Rock Engineering Research Foundation. 2015
- [32] Norwegian Tunneling Society. *Rock Mass Grouting – publication no. 20*. NFF. Available at <http://nff.no>. 2011
- [33] Croce, P., Flora, A., Modoni, G. *Jet Grouting – Technology, Design and Control*. Taylor and Francis, London. 2014.
- [34] Bilfinger, W.; Mello, L. G. F. S.; Primo, C. P.; Carvalho, F. C.; Cortes, M. J. *Rio de Janeiro Subway System: Settlements due to Horizontal Jet Grouting and Their Control*. In: Progress in Tunnelling After 2000? World Tunnel Congress, Miloano. 2000.
- [35] Mello, L. G. F. S., Bilfinger, W., Primo, C. P.; Carvalho, F. C.; Cortes, M. J. *Rio de Janeiro Subway System: Jet-Grouting Treatment Design and Control*. In: Progress in Tunnelling After 2000? World Tunnel Congress, Milano. 2000.
- [36] Shen, S-L., Wang, Z-F, Yang, J., Ho, C-E. *Generalized Approach for prediction of Jet Grout Column Diameter*. Journal of Geotechnical and Geoenvironmental Engineering, ASCE, v. **139**. 2013
- [37] Schumacher, F. P., Kim, E. *Modeling the pipe umbrella roof support system in a Western US underground coal mine*. International Journal of Rock Mechanics and Mining Sciences. v **60**. 2013,
- [38] Fillibeck, J. *Herstellung und Tragwirkung von Schirmgewölbesicherungen*. In Tunnelbau 2015. DGGT – Ernst & Sohn. 2015.

Technical Session #8

“Offshore Geotechnics”



Per SPARREVIK

Per Sparrevik, Technical Adviser at NGI (MSc. 1985), with more than 29 years' experience from various offshore and subsea projects. His expert skills are especially related to instrumentation systems for real-time installation control and structural health monitoring of offshore structures and foundations. In addition he has a solid track record developing monitoring solutions for large scale field testing, geohazard assessment, and geophysical applications. He has a broad professional background that combined with extensive field experience covers both geotechnical and monitoring applications as well as practical aspects related to marine and subsea operations. His trademark is "Development of customized monitoring solutions in a practical setting". Mr Sparrevik has been a pioneer within the development of bucket foundations and suction pile technology. Since 2009 Mr. Sparrevik has supervised development and installation of offshore wind turbine foundations.

Offshore Wind Turbine Foundations

State of the Art

Per SPARREVIK^{a,1}

^aNorwegian Geotechnical Institute

Abstract. The huge growth and intense development in the European offshore wind power sector over the last decade have created significant achievements within the wind turbine foundation technology. The state of the art focusing on geotechnical design aspects for Offshore Wind Turbine (OWT) foundations and important aspects for installation are presented in this paper. In place operational experience based on structural health monitoring campaigns and future trends are also discussed.

Keywords. Offshore wind turbines, foundations, loads, soil conditions, holding capacity, dynamic response, offshore installation, in place behavior, future trends.

1. Introduction

The Offshore wind energy industry has greatly matured during the last decade, presently the annually installed energy capacity exceeds 3.5 GW in Europe, with UK and Germany as the largest offshore wind energy producers, see Figure 1. Europe has a total installed offshore wind capacity of 18 499 MW generated by 4 543 grid-connected wind turbines across 11 countries [1].

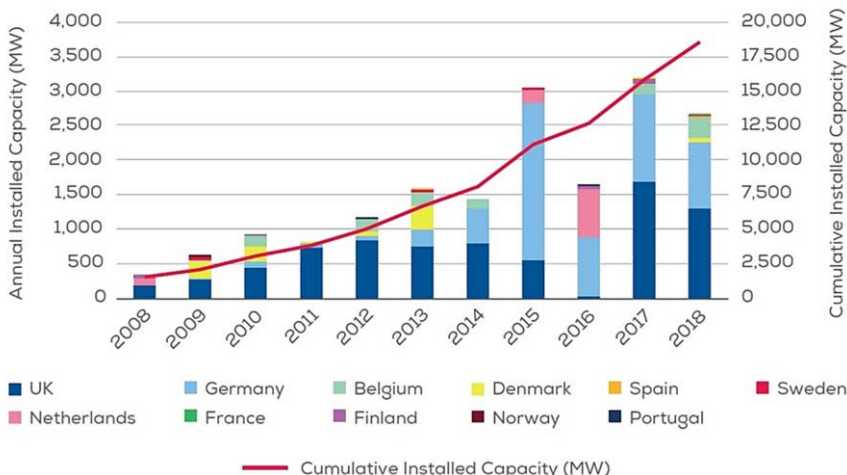


Figure 1. Installed offshore wind energy capacity in Europe and distribution among countries [1]. China is now in the third place globally in terms of offshore wind power (2790 MW in 2017 and rapidly growing).

¹ Per Sparrevik, Norwegian Geotechnical Institute, Norway; E-mail: Per.Sparrevik@ngi.no.

The large-scale development of offshore wind farms requires considerable investments. However, as the costs for construction and production of offshore wind power are falling and the energy prices are rising, tenders for new wind farm developments in Europe are now being submitted without subsidiaries. Both the embedded part and the substructure up to the base of the turbine tower are often referred as the "foundation" to the offshore wind turbine (OWT). The wind turbine is the most expensive part, fabrication and installation of the foundation represent the second largest partial cost (25-30%) of the total wind farm development [1]. Therefore, and especially for deeper waters, developers have high focus on optimizing the design and fabrication cost for the foundations and reduce the installation time such that the overall development costs can be cut down.



Figure 2. The Walney Wind Farm operated by Ørsted in the Irish Sea is presently (2018) the world's largest operating offshore wind farm with 189 OWT's producing 659 MW of power (photo: Ørsted).

2. Environmental conditions

The OWT foundations involve significant technical challenges, including design requirements to withstand the harsh marine environment, storm periods with intense wave loading, wind turbulence, fatigue and at least 25 years operational life.

The ideal condition for an offshore wind farm is a location with high and persistent wind speed to ensure sufficient energy harvesting and economic operation considering the required investments. Wind turbines start to operate at wind speeds of 4 to 5 m/s and reach maximum power output at around 15 m/s. At very high wind speeds, gale force winds of >25 m/s, the wind turbines automatically shut down. On site mapping of the wind conditions is therefore performed before the decision of full development is made.

Normally a Met mast is installed at the field 1-2 years in advance, lately Lidar buoys are becoming more popular as these can record the wind profiles on site at much lower total costs and can easily be moved and reused, see Figure 3.

Secondary conditions affecting the total wind farm costs are distance from shore (grid connection and offshore access), water depth, seabed topography and geotechnical conditions. The seabed outside the European coastline many times comprise complex geology and diversified layering.

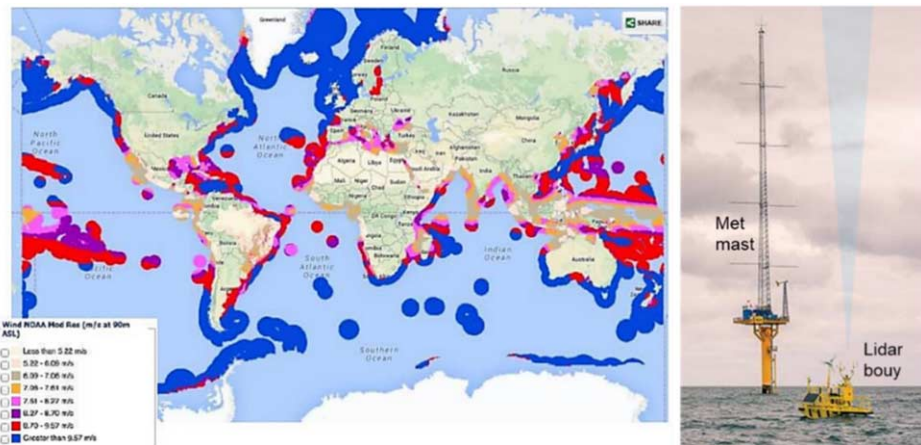


Figure 3. Average wind speed 90m above sea level outside the global coastlines (source: NOAA). Right: Met mast and AXYS Lidar buoy installed at Blyth wind farm for validation tests (photo: AXYS Tech.).

2.1. Foundation loads

An OWT foundation is subjected to a combination of axial loads, low-amplitude cyclic loads, bending and torsional moments generated by waves acting on the upper part of the foundation and the wind loads acting on the turbine and tower, see Figures 4 and 5.

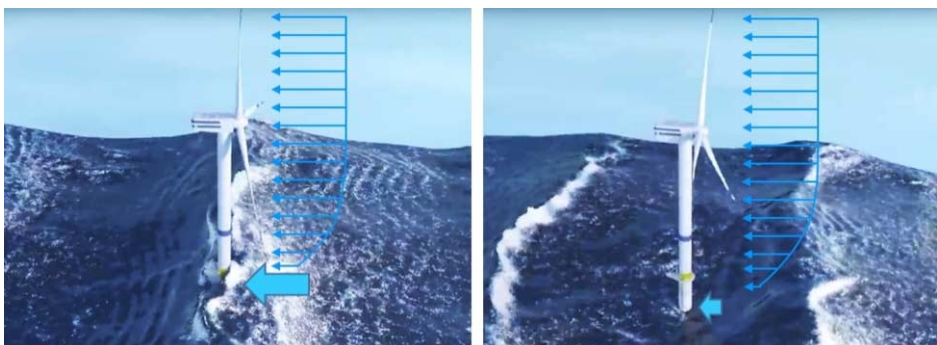


Figure 4. Breaking waves that may occur at shallow banks far out in the sea can be a severe loading condition.

The main design driver is often the dynamic performance (stiffness) of the foundation. To prevent resonance amplification effects, the rotor blades are automatically pitched to change the rotor speed and the turbine eventually shuts down at a certain amplitude of vibrations. With towers, stretching more than 150m above sea level and rotors spanning 160m, the tolerances for differential settlements or tilt are obviously small.

The loads acting on the wind turbine tower are ultimately transferred to the foundation and can be classified into two types: static or dead load because of the self-weight of the components and the environmental loads generated by waves and wind with different peak periods, mean levels and cyclic amplitudes see Figure 5.

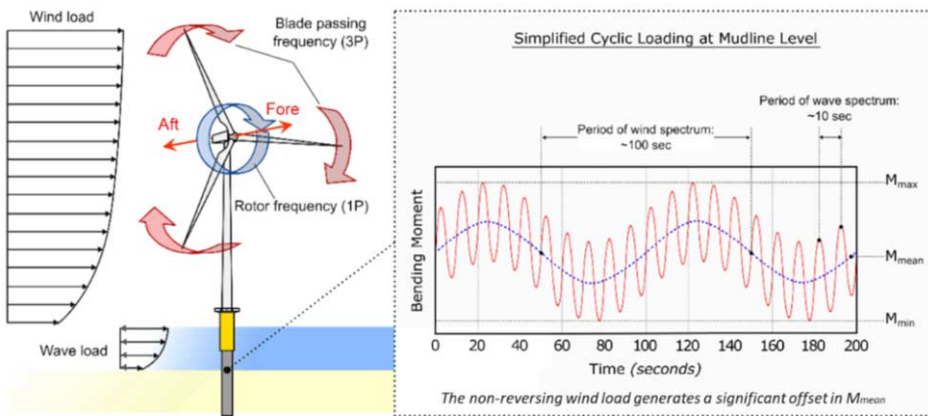


Figure 5. Characteristic of the combined wave and wind loads acting on an OWT foundation [2].

The following categories of dynamic loads are the most significant for design:

1. The lateral load acting at the top of the tower produced by the turbulence in the wind and the drag of the rotating blades
2. The load caused by waves crashing against the foundation substructure. The magnitude of this load depends on the wave height and wave period.
3. The load caused by the vibration at the hub level because of the mass and aerodynamic imbalances of the rotor. This load has a frequency equal to the rotational frequency of the rotor and referred to as the 1P load
4. Loads in the tower because of the vibrations caused by blade shadowing effects and loss of wind load on the tower (referred to as 3P for rotors with three blades), see Figure 6.

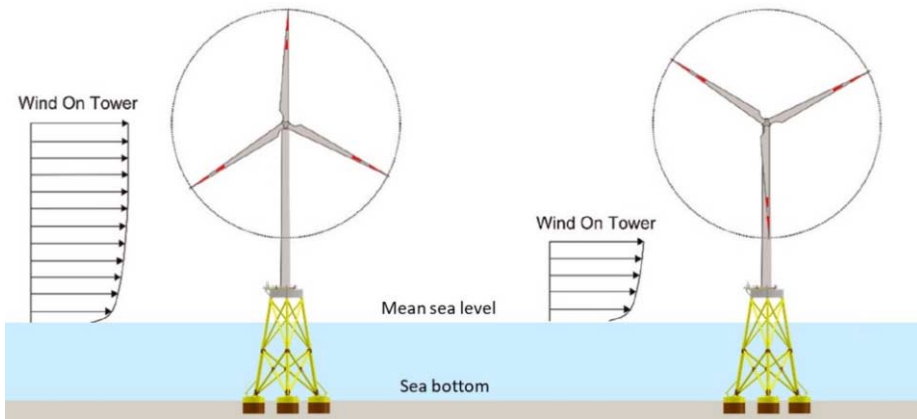


Figure 6. Variation in wind load acting on the tower due to rotor blade shadowing.

Representative power spectra are constructed by means of analyzing site-specific data in the time and frequency domains. The design of the wind turbine and foundation must make sure that the system Eigen frequency do not coincide with any of the dynamic load peak frequencies. Presently the system frequencies for commercial viable

OWT foundations lies between the 1P and 3P peaks, which is a quite narrow frequency band, see Figure 7.

For deeper waters and larger turbines, the Eigen frequency will decrease and approach the 1P frequency that also will move closer to the wave frequency. Due to limitations in the lateral stiffness this will ultimately limit the feasible turbine size and maximum water depth for a traditional monopile foundation.

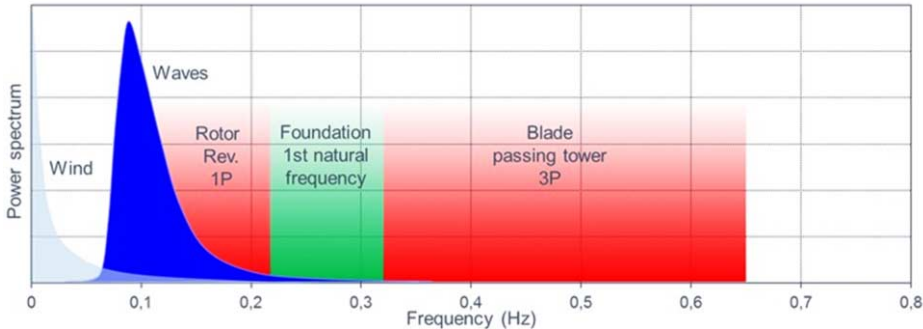


Figure 7. Example of power spectra for forces acting on a monopile foundation.

2.2. Soil conditions and design parameters

An offshore wind farm involves many turbine foundations (tens to hundreds of units) and covers a large area (tens to hundreds of km²). The ground stratigraphy, the mechanical properties of materials and their lateral and vertical variability should be accurately determined at each OWT location. Furthermore, a solid knowledge of the mechanical properties of the shallow sediments is required along the cable routes, between wind turbines and to the coast.

The development of a wind farm requires significant investment decisions at early stages when in many cases the geotechnical information for many of the proposed turbine locations not is available or only performed to a limited depth. Initially an integrated desk study is performed making use of existing data and knowledge (geology, seabed mobility, depositional environment, formation variability, seismic risk, etc.). Geophysical and preliminary borehole data are key input for the evaluation of future survey strategies, foundation concepts, construction risks and cost estimates of the foundation scope to be used for final investment decisions.

Typical steps to define the soil conditions for a Wind farm development are [3]:

1. Desk study, initial conceptual ground model and risk register
2. Specification and Implementation of geophysical surveys, geotechnical soil investigation and lab testing
3. Geophysical and Geotechnical Data interpretation, including identification of formations, ground boundaries and unitization of relevant layers and derivation of characteristic properties.
4. Compilation of the integrated ground model
5. Derivation of final geotechnical design profiles

At shallow water depths, rather complex soil conditions can be expected at many potential offshore wind farm sites in Europe. For example, the coastal waters in the North Sea around UK consist of diverse materials, such as loose mobile sand banks, glacial till, stiff and soft clay. Along the west coast of Denmark, Germany and Benelux, dense sand

with silt layers is dominating. Further south, offshore France, the soil conditions are even more diversified, spanning from soft clay to shallow limestone and chalk-based formations. The Baltic seabed consist mainly of clay but sometimes contains significant chalk layers and boulders, ice conditions must be considered in the Baltic Sea. The diversity of expected soil conditions may call for different foundation solutions also within the same wind farm.

2.2.1. Ground model

The initial and preliminary ground model of the wind farm site is mainly based on geophysical data including seafloor surveys from multi-beam bathymetry and side-scan sonar, see Figure 8. The stratigraphy of different sediment layers is mapped by means of seismic multichannel reflection survey. The data is used to establish the seafloor bathymetry and morphology, to define lithological units and tectonic structures, and to establish the stratigraphic profiles.

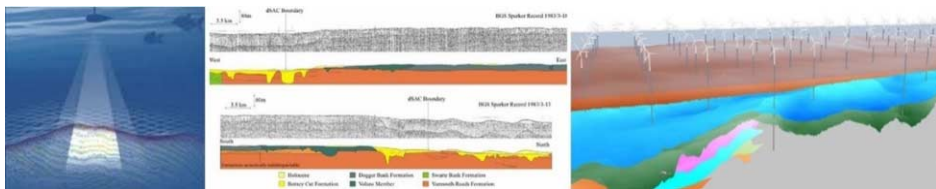


Figure 8. Establishment of ground model based on geophysical data.

In many cases, high quality seismic data can be used for preliminary assessment of suitable types of foundations and required pile embedment length or effect of changed wind farm layout, see Figure 9.

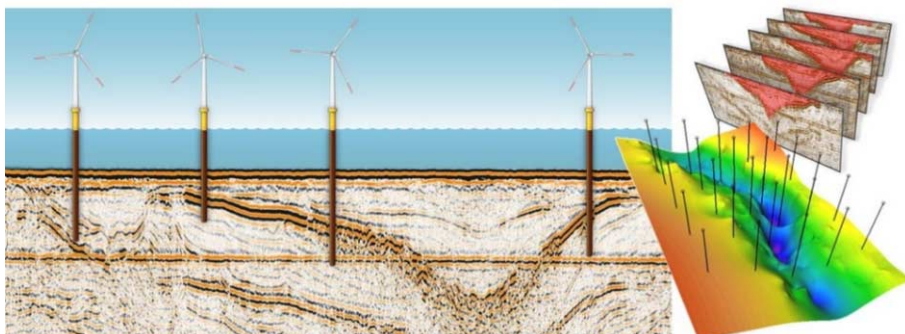


Figure 9. Preliminary pile design based on multichannel high resolution seismic profiles (Illustrations Fraunhofer Institute for Wind Energy Systems).

2.2.2. Determination of soil parameters

The specifications for the soil investigation program are based on the ground model and preliminary wind farm layout. CPT's are normally required at each location of an OWT foundation, see Figure 10. Bore holes and samples for laboratory testing are required to determine the geotechnical design parameters for the different sediment layers.



Figure 10. Left to right: Borehole and wind turbine location plan [5], geotechnical drilling vessel and seabed CPT rig.

Once the geotechnical parameters have been determined for the different layers, the ground model with the stratigraphy of different sediment layers can be used to establish new site-specific soil parameter profiles if the positions of the wind turbines should be rearranged, see Figure 11.

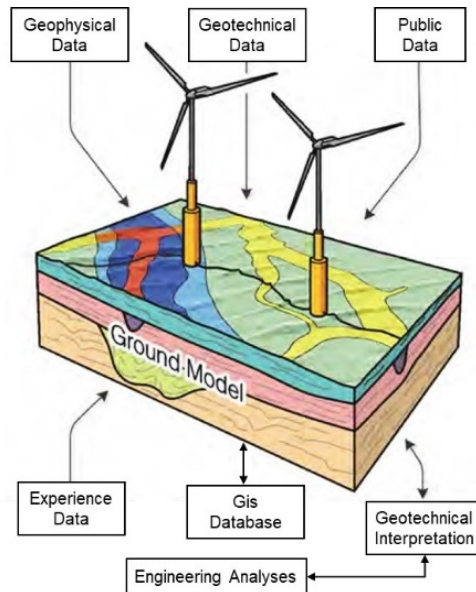


Figure 11. The evolutionary ground model [4].

2.2.3. Other seabed conditions

For seabeds with sand at the surface and strong currents (usually tidal) the risk for scour development and hence the need for scour protection must be assessed. Significant scour can develop rapidly around seabed foundation and have critical impact on the dynamic behavior and stability of the foundations, see Figure 12. Other conditions that must be investigated is the seabed topography (sand dunes etc.) and the presence of embedded boulders.



Figure 12. Scour development around a monopile foundation (illustrations: EIWA).

In some areas the presence of UXO's (unexploded ordnance), mainly old mines or shells from the 2nd World War buried in the seabed must be checked, see Figure 13. An UXO survey is conducted by means of sonars, sub-bottom profilers and magnetometer survey methods.



Figure 13. Marine mine (UXO) from 2nd World War.

3. Different types of OWT foundations

Presently, the main alternatives for offshore wind turbine foundations can be divided into four different categories, see Figure 14:

1. Monopiles (or monopods if suction bucket is used), normally relevant for water depths down to 30-50m. Represent 89% of the OWT foundations presently installed in European waters [1].
2. Gravity base structures with skirts, normally relevant at 25 to 60m water depth. Represent 6.6% of the OWT foundations presently installed in European waters [1].
3. Jackets or tripods, pre-piled or with suction buckets, normally relevant at 25 to 60m water depth. Represent 9.8% of the OWT foundations presently installed in European waters [1].
4. Floating foundations, normally relevant from 50m and deeper waters. Represent 0.2% of the foundations presently installed in European waters [1].

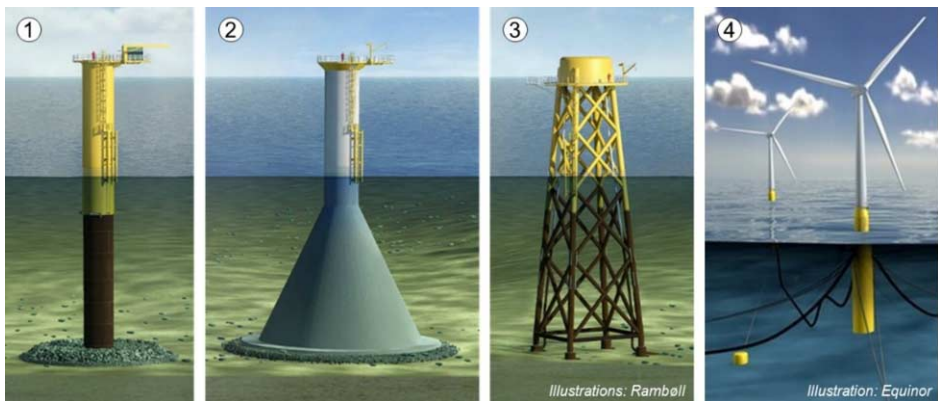


Figure 14. Main foundation alternatives for offshore wind turbines (Illustrations: Rambøll and Equinor).

The monopile is presently the most cost-efficient foundation solution (including fabrication and installation) and has therefore been the dominating type of foundation in Europe, see Figure 15. However, as the trend is larger turbines in deeper waters it is expected that other types of foundation will become more common in the future when the limit for feasible monopile design is met. 12 MW turbines are expected to enter the market in 2020 and more expensive foundation alternatives become attractive if the energy output from each installation can be increased.

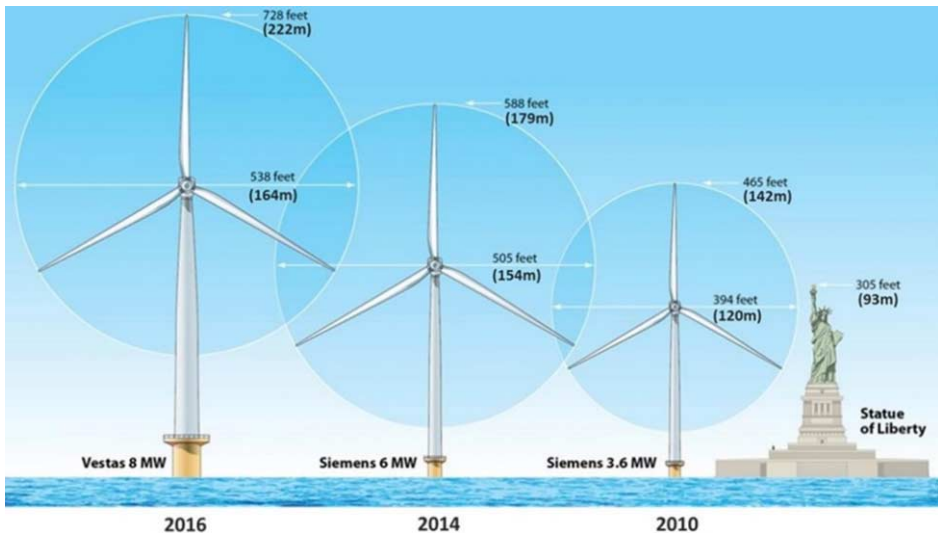


Figure 15. Size trend for wind turbines on monopiles (Illustration: Sierra magazine).

An important aspect concerning offshore wind turbines is the sensitivity to verticality, even for a small inclination a wind turbine loses its ability of effective energy production. Therefore, requirements for Serviceability Limit State, SLS, set the limits on the permanent accumulated inclination (typical 0.25° to 0.5°). As discussed earlier the dynamic motions (vibrations) or stiffness of the foundation are also important for the

serviceability and fatigue limit state. ULS (Ultimate Limit State) conditions, requiring the maximum load-carrying capacity, is usually not the main foundation design driver.

3.1. Monopiles

The sizing of a monopile is an iterative process, typically starting with selecting an initial diameter (usually identical for all monopiles in the wind farm). In the second step, the required pile length is determined, primarily governed by the foundation capacity. Due to the sediment stratigraphy varied pile embedment depth may be required at different wind turbine locations within the wind farm, see Figure 16.

Note that the capacity of a monopile is in general defined by a maximum deformation criterion, which is essentially a performance-based design. The wall thickness is typically in the range of 1/80-1/120 of the diameter and is governed by the structural fatigue design. With decreasing length to diameter ratio, the foundation serviceability becomes gradually more important than mainly affects the required monopile diameter. In the early days, the monopile dimensions were determined to meet a certain soil-foundation stiffness values such that the first eigen-frequency of the OWT is in the range between 1P and 3P (see Figure 7). Although this criterion still is relevant, the foundation design should not only be based to meet a certain target stiffness, since other structural components of an OWT support structure may be adjusted more easily.

The actual sizing is often done using distributed Winkler springs, describing the soil response of a loaded monopile. Several different types of Winkler springs have been proposed in the literature. These can be linear elastic or non-linear (elastic). Most commonly used in the past were the non-linear API [5] p-y springs.

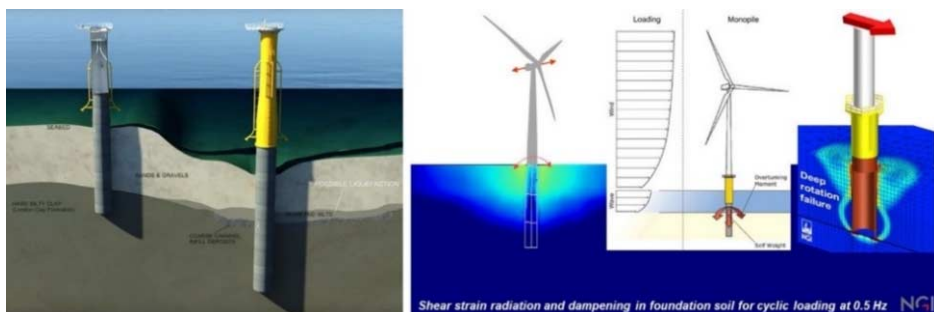


Figure 16. Monopile embedment depth adapted to sediment stratigraphy (illustration COWI/IMS). Soil dampening, transfer of loads and ULS deep rotation failure for monopoles (illustration NGI).

Non-linear springs are crucial for an optimized monopile design but it is demonstrated through numerous studies that the traditional approach using API springs is not appropriate for the sizing of an OWT monopile foundation with relatively small L/D ratios (where L is embedded length and D is pile diameter). Therefore, offshore monitoring campaigns with strain gauges on full scale monopiles have been conducted as well as large scale onshore lateral pile load tests, see Figure 17.

The performed tests and recorded data from offshore piles suggest that the piles often show a considerable stiffer lateral response than predicted using API p-y curves.



Figure 17. Large scale lateral pile load tests performed for investigation of P-Y response for monopiles: (1) Rødbyhavn (Denmark) - hard clay and driving shoes, performed by NGI/Bilfinger for Equinor (2014); (2) Cuxhaven (Germany) - dense sand and vibrated piles, performed by Bilfinger for RWEInnogy (2014); (3) PISA project, Cowden (UK) - stiff clay and Dunkirk (France) - dense sand, performed by ESG for Carbon trust consortium (2014-15); (4) Gouvieux (North France) - Sandstone, performed by Fugro for EMF (2016).

In the PISA project (3) the monopile design model has been updated with sets of distributed lateral and rotational Winkler-springs [6] for monotonic loading. In the REDWIN Joint research project headed by NGI, the soil-pile system is replaced by a macro element at the mudline [7]. The REDWIN model can reproduce different foundation stiffness during monotonic and cyclic unloading/reloading and foundation damping dependent on the loading history, which is observed in real pile behavior.

By increasing the size of the monopiles, support of 10-12 MW turbines at water depths down to 50-70m is feasible. The so called XXL monopiles have a tapered shape with an outer diameter up to 10m or more at the mudline that is gradually decreased to 5-6m at the top, see Figure 18. The substantial weight will require lifting vessels with upgraded crane capacity and bigger hammers are needed to install the very large diameter piles.



Figure 18. The world's largest monopiles produced by EEW 2016 for the German "Veja Mate" wind farm, total weight 1 300 tons, 7.8m diameter at mudline and 82m long.

A mono bucket foundation appears as a monopile topside, however the complete foundation is integrated and installed in one operation, see Figure 19. Instead of pile driving, the caisson foundation (bucket) is penetrated into the seabed by self-weight and the generated under pressure when water is pumped out from the confined void inside the caisson.

As for monopiles, the rocking stiffness may be design driving and the main limitation for this type of foundation. The moment capacity is mainly provided by skin friction along the skirt walls and contact pressure across the lid of the bucket.

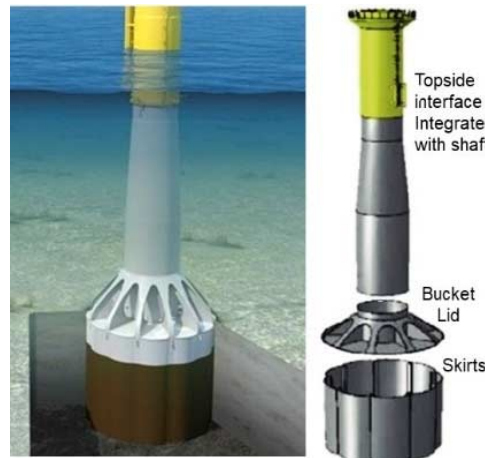


Figure 19. Mono bucket foundation (illustration: Universal foundations).

3.2. Gravity base foundations

The significant weight of the gravity base foundations is distributed across the large base area and provides the rocking stiffness and over turning stability. The hollow base is in general built of concrete with a steel shaft. The structure is floated to site and ballasted by filling the hollow concrete base with sand; see Figure 20. The foundation is suitable for a large variety of soil conditions, best viable at locations with stiff sediments near the seabed or shallow bedrock. The gravity base foundation is normally equipped with shallows skirts for increased bearing and sliding capacity and to prevent undermining by scour.

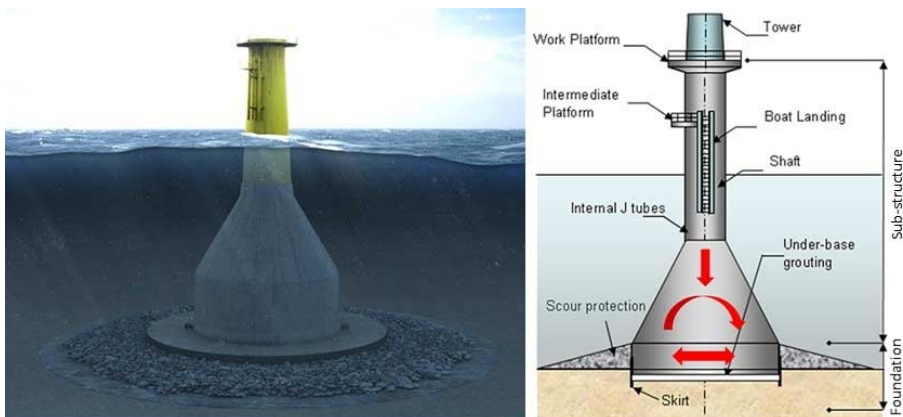


Figure 20. Gravity Base foundation (Seatower) for Offshore Wind turbines.

3.3. Jackets and tripods

Jackets and tripods usually consist of braced steel structures with three or four legs fixed to the seabed by piles or suction buckets. A three-legged foundation constitutes a static determined system and is the most cost-efficient solution for OWT's. The environmental overturning moment loads are mainly transferred to vertical loads on the embedded foundations and the rocking stiffness is high, see Figure 21.

The friction piles are usually pre-installed using a piling template, the jacket with stabs is inserted and grouted to the piles during a subsequent lifting operation. A suction bucket jacket comprises a complete foundation that is installed in one operation.

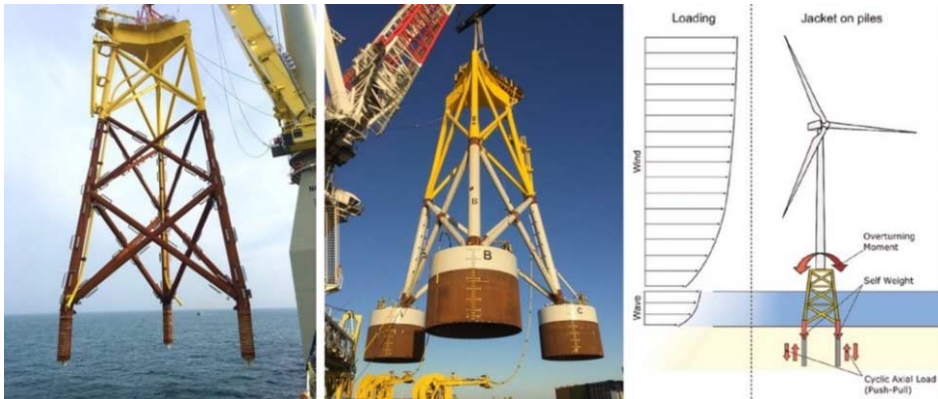


Figure 21. Pre-piled (left) and suction bucket jackets (middle). Loads acting on the jacket foundation (right).

In the design of shallow foundations such as suction buckets, more effort is required to achieve optimized dimensions considering both installation feasibility and in-place performance [8]. The behavior of the suction bucket is especially sensitive to the drainage conditions in the soil during installation, tensile and cyclic loading; see Figure 22.

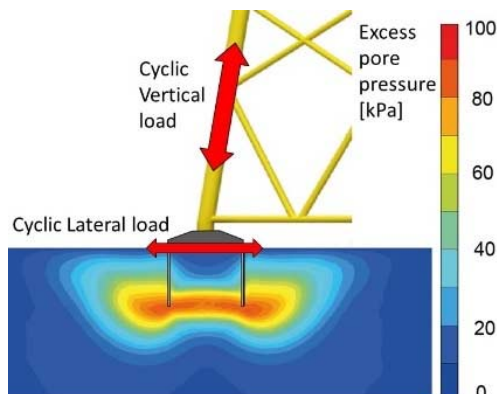


Figure 22 Finite element analysis of pore pressure build up when a suction bucket is subjected to combined vertical and horizontal cyclic loading. The contour plot shows the excess pore pressure at the end of the peak phase during a 35-hrs design storm (source: NGI).

3.4. Floater

Floating OWT foundations become relevant at water depths >50m and can be placed far out in deeper seas where the wind conditions are favorable. The floater can be of a Spar or Semisubmersible type, see Figure 23. The floater is anchored by catenary or taut leg moorings. The optimal seabed anchors depend on the type of mooring and seabed conditions. Presently suction piles have been used for catenary moored floaters. The amount of seabed anchors can be reduced by combined mooring systems, i.e. several OWT's share common anchor points in the floating wind farm.



Figure 23. From left to right: SPAR, Semisub and TLP type of OWT floaters (Illustration: DNV-GL).

Design of anchors for floating structures follow the standard practice applied in the offshore Oil and Gas industry. The main design challenge is to ensure that the loading response in the mooring system not is affecting the overall dynamics of the floating OWT.

3.5. Offshore substations

An internal grid connects the wind turbines to offshore substations, where the AC voltage is increased to reduce the transmitted current and transmission losses. For clusters of remote wind farms, the High Voltage Alternating Current (HVAC) is converted to High Voltage Direct Current (HVDC) to minimize transmission losses over long distance in the subsea export cable to shore, see Figure 24.

The foundations for offshore substations carry heavy equipment and usually have facilities for accommodation and maintenance acting as a hub for offshore operations. Thus, the foundation loads are dominated by waves and comparable with offshore oil and gas installations. The smaller HVAC stations can be fitted on monopiles, the larger

HVDC stations may require foundations with increased bearing capacity such as multi column gravity base structures or jackets with piles or suction buckets.

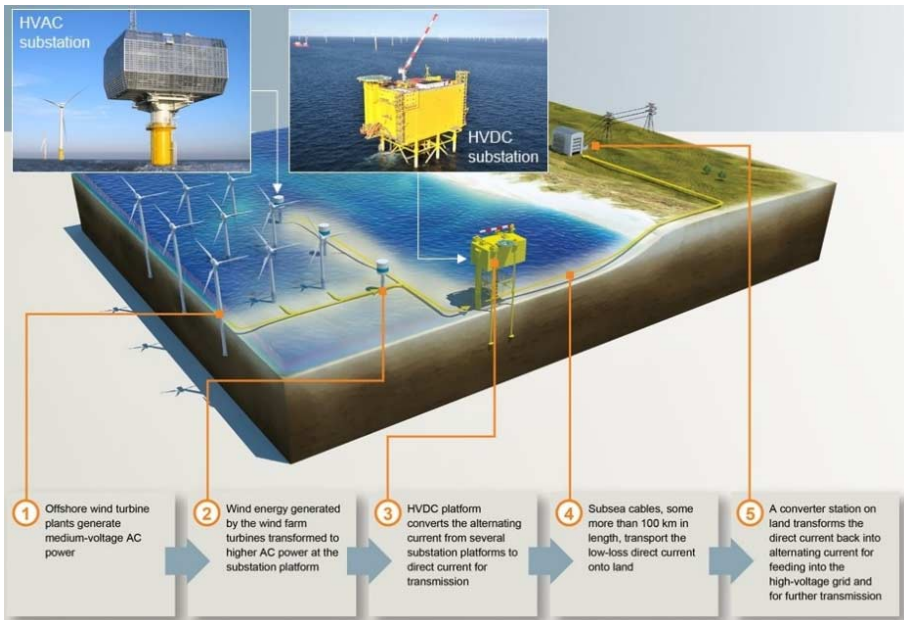


Figure 24. Transmission of energy captured by offshore wind farms (Illustration Siemens AG). The photos show a HVAC substation on a monopile at Gunfleet Sands wind farm (UK) and Dolwin Alpha HVDC substation, (six-legged jacket) 75 km outside the German coast.

4. Offshore installation

The offshore installation work represents a major cost in the development of a wind farm and includes foundations, turbines, grid and shore connections. Optimized operations are a priority for the developers and serial production is required for the large numbers of structures involved. Due to the size and weights of the complete OWT, the standard approach is to first install the foundations and sub-structures and subsequently install the tower and turbines, using vessels dedicated for each task and overlapping operations.

4.1. Monopile installation

The monopiles are normally driven by hydraulic hammers, during initial stabbing and driving the pile is guided by pile grippers controlling the verticality, see Figure 25.

After the piles have been driven to target depth, the transition pieces (TP's) are mounted on top of the piles. The TP's act as an adaptor on the pile top and are equipped with secondary steel components including J-tubes for grid hook-up, boat landing, access ladders with platform, and flange for mounting of the turbine tower at required elevation above the sea surface. Presently the size of the monopiles that can be installed is limited by the vessels lifting capacity and hammer size available in the market.



Figure 25. Monopile driving from a floating vessel with motion compensated pile grippers for control of the pile verticality. The transition pieces are installed after completed pile driving and stored upright on deck to the left in the picture (Illustration: Quest Offshore).



Figure 26. Pile driving with double bubble curtains (left) and with pile driving muffler (right). Images: Geosea and IHC.

In Europe, the noise and disturbance to the marine life during pile driving is a big environmental issue. Arrangement for noise mitigation such as bubble curtains and/or pile driving mufflers is therefore required at many locations; see Figure 26.

To reduce the pile driving noise and fatigue effects on the pile, vibratory hammers can be used for driving the piles. Vibrations are especially efficient for pile installation in sand and faster than conventional pile driving. The main question is if and how much vibro-piling may affect the lateral stiffness of the installed pile and the efficiency for driving through clay layers. A large vibro-pile test was conducted in 2014 by a consortium headed by RWE comparing the installation and lateral capacity of large piles in sand installed by impact and vibratory hammers; see Figure 27. Installation of very large diameter monopiles to moderate depth may also be possible by silent suction driving.



Figure 27. Vibro test in Cuxhaven (Germany), Photo: RWE.

4.2. Pre-piled jacket installation

To optimize the installation process for piled jackets or tripods, the piles can be driven in advance using a seabed template with pile sleeves. The larger (and more expensive) lifting vessels are then only required to deploy the jacket or tripods directly on the pre-piled foundation; see Figure 28. The jacket legs have flanged stabs in the bottom that are inserted into the top of the piles and secured by grouting.



Figure 28. Pile driving using seabed template and subsequent jacket installation (Illustration: Jumbo shipping).

The pre-piling method requires that the pile stick up is monitored during pile driving and the pile top elevation differences must be measured with high precision after all piles in a group are installed. These measurements are directly used for shimming beneath the flange of the pile stab and crucial for final leveling of the structure supporting the wind turbine. By means of instrumented piling templates, the measurements are performed during pile installation; see Figure 29. So far, more than 1000 pre-installed piles are in use for OWT foundations and pre-piling is considered as a proven solution although

special skills are required for the metrology. The only uncertainty may be the long-term performance of the grouted pile connections.

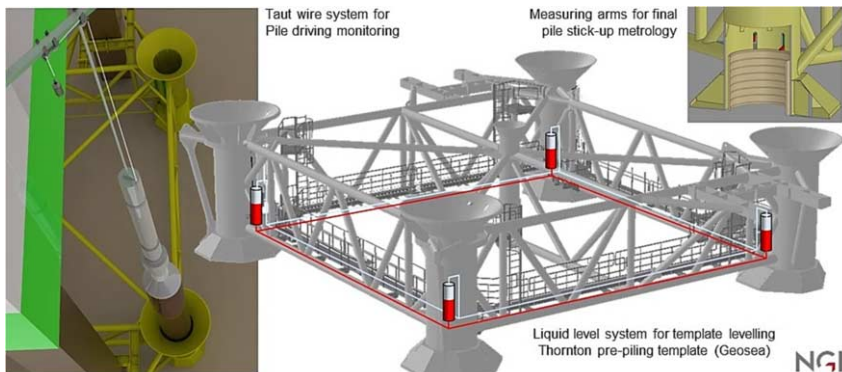


Figure 29. Example of instrumentation provided by NGI for pre-piling metrology.

4.3. Suction bucket jacket installation

The seabed foundations are integrated in the Suction Bucket Jacket (SBJ) and the offshore installation can be completed in one operation. Suction pumps with integrated instrumentation is used to for driving the buckets to the required penetration depth and controlling the installation process, see Figure 30. After the buckets have been landed on the seabed and penetrated by self-weight, the entrapped water inside the buckets is pumped out. Dependent on the penetration resistance a suction pressure is created inside the buckets, driving them further into the seabed. The added driving force by suction can be more than 20 times larger than the complete weight of the SBJ and is a very efficient and silent installation method.

The verticality of the SBJ can be precisely controlled during the suction operations and no further levelling arrangement is required. The ultimate limit of the suction force that can be generated when entrapped water is evacuated is determined by cavitation (vacuum) and may limit the feasible suction penetration in shallow waters (<20m). Normally the gap that may remain inside the buckets after completed suction penetration is backfilled with mortar to improve the effective stress contact between the seabed and the lid of the bucket foundations.



Figure 30. Suction pump arrangement used for Ørsted's Borkum Riffgrund 02 SBJ installation (Photos: NGI-FRAMO).

4.4. Installation of Gravity base foundations

The gravity base foundations are large and floated out to location; see Figure 31. The hollow interior of the foundation is de-ballasted to obtain buoyancy for float-out. During installation the structure is ballasted by water and sand such that the structure sinks down to the seabed. The foundation base is often outfitted with shallow skirts that are penetrated by the increased weight during ballasting. If required, longer skirts can also be penetrated to target depth by the added force from suction driving.



Figure 31. Tow-out of Gravity base foundations constructed by BAM for Blyth offshore windfarm.

4.5. Drilled and grouted piles

For seabeds consisting of weak rock or carbonite soils, the only reliable foundation alternative may be drilled and grouted piles. Special seabed templates and drilling rigs are then required, see Figure 32. The installation operations are usually more time consuming and expensive compared to traditional pile driving.

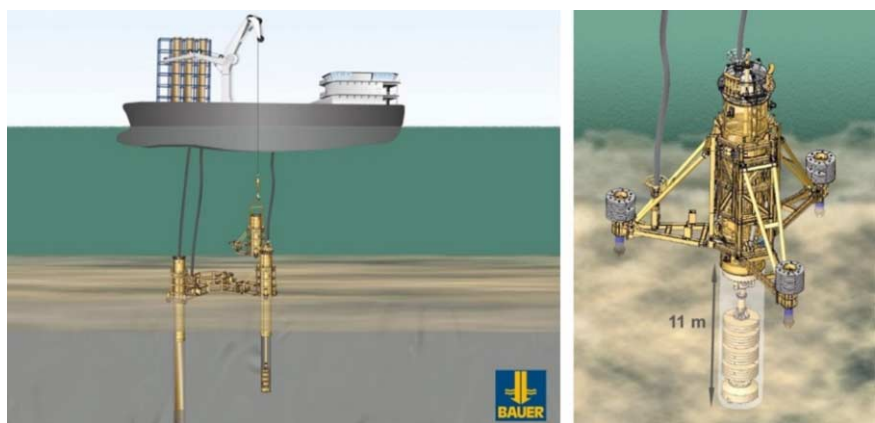


Figure 32. Seabed templates and drilling rigs for drilled and grouted piles operated by Bauer Renewables.

5. Operational experience

Long term Structural Health Monitoring (SHM) is an important tool for reducing risks and costs in development and management of offshore wind farms. Due to the amount of installations in a wind farm, systematic flaws or problems can be very expensive. Consequently, potential savings are big if the design can be improved and optimized based on observed response to environmental loads in the field; see Figure 33.



Figure 33. In-situ observations of structural Health and Response.

An example of a systematic fault with large consequences was the problems with the grouted connections between the transition piece and the monopile detected in 2010. Cracks and severe deterioration of the grout was discovered on a large amount (hundreds) of monopile foundations in Europe. The problem was solved by a re-designed conical joint, however the offshore repair of the old joints has costed enormous sums.

The in-situ dynamic response, for example lateral stiffness and dampening of the monopiles, is important to monitor for design optimization. With respect to the long-term behavior and operational life of the foundations, the degradation due to corrosion is probably the most critical parameter to observe in the field [9]. The amount of SHM data recorded in-situ is sparse, presently the most comprehensive field monitoring campaigns have been conducted by Ørsted in conjunction with their prototype SBJ foundations installed at BKR01 and 02 windfarms; see Figure 34.

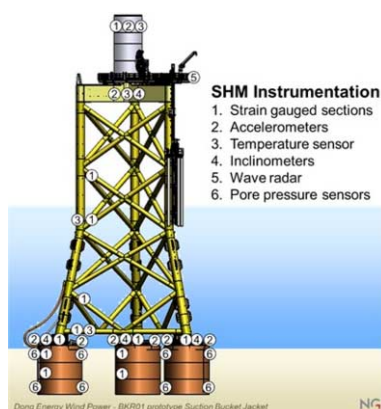


Figure 34. Example of integrated SHM system with 141 sensors implemented on Ørsted's prototype Suction Bucket Jacket BKR01 installed in 2014. (SHM system provider: NGI).

Initial interpretation of data from BKR 01 Suction bucket jacket [10] revealed that undrained conditions are present for cyclic load periods less than 2.5 minutes and drained conditions appears for periods longer than 46 minutes. The nonlinear stiffness anticipated in the design was confirmed and the eigen-frequency is higher (foundation is stiffer) than conservatively assessed in design.

6. Future trends

Due to the cost efficiency, the limiting depth and maximum turbine size for monopile foundations will be pushed as far as possible. Major operators such as Ørsted consider monopiles with up 12 MW turbines at water depths down to 70m as feasible in the near future. 12 MW offshore wind turbines are already being developed such as General Electrics Haliade-X turbine; see Figure 35.

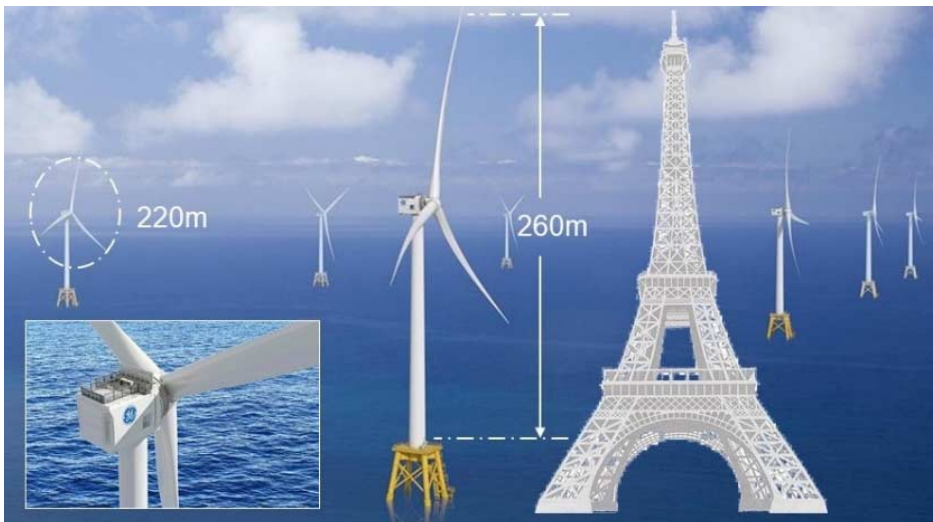


Figure 35. The 12 MW Haliade-X turbine presently being developed by General Electrics.

Due to the dominating place in the market, fabrication and installation costs for monopiles have been optimized over the years, the cost gap may be reduced when alternative solutions mature. Due to increasing turbine size and/or water depth, tripod jackets with buckets or piles (if required due to the soil conditions) may be the preferred bottom fixed foundation in the future, however the fabrication costs must be decreased. Development of new installation methods and vessels (for example with regard to lifting capacity and pile driving noise) are also important factors affecting the optimal foundation concept in the future. Local soil conditions, infrastructure, resources and regulations are also important. Crane free gravity base solutions may be attractive at some locations but not in other places.



Figure 36. Floating deep-water foundations with Vertical Axis Wind Turbines (VAWT's), Image: InFLOW.

Although the opinion among the operators is diversified, the general approach is that the water depth must exceed ~70m before floating wind farms are considered as competitive with bottom fixed structures. New technology may however change this opinion. Significant development work is ongoing for Vertical Axis Wind Turbines (VAWT's). These types of turbines imply a low Centre of gravity and significant less moment loads on the foundation. VAWT solutions are especially attractive for floating foundations see Figure 36, but mechanical problems with bearings etc. remain to be solved.

Power generating kites can harvest the strong winds at very high altitude, up to 3 km; see Figure 37. The technology is being developed by several actors in the market. Due to air traffic and other hazards they are difficult to operate on land, but may be suitable for floaters far out in the sea.

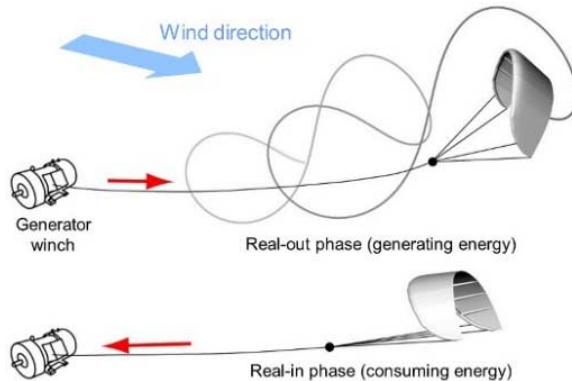


Figure 37. Example showing the operation principles of a power generating wind kite (illustration: Xsens).

Acknowledgement

Hendrik Sturm, NGI for review and useful comments to this paper.

References

- [1] Annual report by Offshore Wind in Europe, Key trends and statistics 2018 Published by Windeurope.org, February 2019
- [2] G. Nikitasa, Nathan J Vimalanb and S.Bhattacharyaa, "An innovative cyclic loading device to study long term performance of offshore wind turbines", Soil Dynamics and Earthquake Engineering, Volume 82, March 2016, Pages 154–160
- [3] Guidance Notes for the Planning and Execution of Geophysical and Geotechnical Ground Investigations for Offshore Renewable Energy Developments, The Society for Underwater Technology, May 2014
- [4] Rattley M., Salisbury R., Carrington T., Erbrich C., and Li G. (Fugro) "Marine site characterization and its role in wind turbine geotechnical engineering", Proceedings of TC 209 workshop 19th ICSMGE - Seoul, 20 September 2017
- [5] American Petroleum Institute, Recommended Practice for Planning, Designing and Constructing Fixed Offshore Platforms, 2011.
- [6] Burd H. J., Byrne B. W., McAdan R.A., Houlsby G. T., Marten C. M., Beuckelaers W. J.A.P. (Oxford University), Zdravković L., Taborda D.M.G., Potts D. M., Jardine R. J. (Imperial College), Gavin K., Doherty P., Igoe D., Gretlund J. S., Andrade M. P., and Wood A. M. "Design aspects for monopile foundations" Proceedings of TC 209 workshop 19th ICSMGE - Seoul, 20 September 2017
- [7] Page, A. M., Grimstad, G., Eiksund, G. R. and Jostad, H. P. "A macro-element pile foundation model for integrated analyses of monopile-based offshore wind turbines." Ocean Engineering Vol. 167 (2018): pp. 23–35. DOI 10.1016/j.oceaneng.2018.08.019.
- [8] Sturm H. (NGI), "Design Aspects of Suction Caissons for Offshore Wind Turbine Foundations" Proceedings of TC 209 workshop 19th ICSMGE - Seoul, 20 September 2017
- [9] Sparrevik P., Rahim A. (NGI) " Guidelines for Structural Health Monitoring for Offshore Wind Turbine Towers & Foundations", BSSE Offshore Wind Recommendations, 9. June 2017
- [10] Shonberg A., Harte M., Aghakouchak A., Brown C. S. D., Andrade M. P., and Liingaard M. A. (DONG Energy) "Suction bucket jackets for offshore wind turbines: applications from in situ observations" Proceedings of TC 209 workshop 19th ICSMGE - Seoul, 20 September 2017

Technical Session #8 “Offshore Geotechnics”



Phil WATSON

Phil is the Shell Professor of Offshore Engineering and Director of the ARC Industrial Transformation Research Hub on Offshore Floating Facilities at University of Western Australia. He is a highly experienced offshore geotechnical engineer, with over 25 years oil and gas experience and previously held the position of Global Director of GeoConsulting for Fugro. At Fugro he was a champion of innovation and technology development, working to integrate specialist consulting teams around the world, and with a commitment to sharing expertise and streamlining access to leading edge design approaches. Prior to joining Fugro, Phil was a Director of specialist geotechnical consulting firm Advanced Gemicnics, based in Perth.

Phil is a Fellow of The Australian Academy of Technology and Engineering, a Fellow of the Institution of Engineers Australia, the current Chair of ISSMGE Technical Committee 209 ‘Offshore Geotechnics’, and a committee member of ISO Working Group 10 / API Resource Group 7

Foundation Design in Offshore Carbonate Sediments – Building on Knowledge to Address Future Challenges

Phil WATSON^{a,1}, Fraser BRANSBY^a, Zine Labidine DELIMI^b, Carl ERBRICH^b, Ian FINNIE^b, Henry KRISDANI^b, Chris MEECHAM^b, Michael O'NEILL^b, Mark RANDOLPH^a, Mike RATTLEY^b, Marcelo SILVA^b, Bob STEVENS^b, Stephen THOMAS^b, and Zack WESTGATE^b

^a*The University of Western Australia*

^b*Fugro*

Abstract. Carbonate sediments are prevalent in many major offshore oil and gas basins, as well as a growing number of regions assigned to offshore wind development. Identified as difficult from an engineering perspective, the failure to properly characterize and design for these sediments has adversely influenced several projects. This paper provides a brief geological perspective, and identifies broad trends and characteristics to be considered when defining the engineering properties of such materials. An overview of the challenges faced when founding offshore structures in such sediments is provided, drawing on experience gained over the last 30 years, and with an emphasis on current and emerging issues.

Keywords. Carbonate, site investigation, sensitivity, foundation

1. Introduction

Carbonate sediments are found across the world, influencing offshore development from the oil and gas sector to the offshore renewable industry. When thinking about carbonate sediments, what features might a geotechnical engineer identify – grain structure, cementation, high variability, crushability, extreme sensitivity? These are all valid attributes, and highlight the complex behavior of such sediments – and the care needed in dealing with them.

The nature of carbonate sediments can influence the design process from concept stage through to operation, and ultimately to decommissioning. Challenges associated with the recovery of intact (high quality) sample, and difficulty developing design lines for a site lead to uncertainty; while high sensitivity and variability, as well as other engineering features, drive a need for bespoke design methods.

This paper briefly reviews the geology underlying the formation of carbonate sediments and where they are encountered, identifies and discusses aspects of their interpretation, and provides an overview of select foundation solutions that overcome the design challenges posed by these sediments.

¹ Corresponding Author, Oceans Graduate School, The University of Western Australia, 35 Stirling Hwy, Nedlands, Australia, 6009; E-mail: phillip.watson@uwa.edu.au.

1.1. Context

The challenges associated with foundation design in carbonate sediments have been appreciated for many years, and there have been two international conferences on this topic. The first conference [1] was held in Perth in 1988 and focused both on the broader topic, but also included papers dedicated to the lessons learned from design and installation of the North Rankin A Platform. The second conference [2] was held in Bahrain in 1999 and introduced more recent engineering experiences. The period between the two events saw the release of a book dedicated to foundation design in carbonate sediments [3]. Since the late 1990s there have been numerous research studies and industry projects aimed at better understanding specific issues.

The current paper has been prepared by practicing engineers who work routinely on offshore projects encountering carbonate sediments – and the focus is on identifying practical aspects relevant for design.

2. A brief overview of carbonate sediments

2.1. What are carbonate sediments?

The term ‘carbonate sediment’ holistically defines both the origin and transportation/deposition processes that control individual grains, and the sedimentary package as a whole. In this context, ‘carbonate’ generally relates to the mineral polymorphs of calcium carbonate (CaCO_3). For sediments encountered offshore these are principally calcite and aragonite. Other polymorphs, such as dolomite, are typically less abundant offshore, as are non-calcium carbonates (magnesite, ankerite, siderite). In this paper, the term ‘sediment’ generally correspond to the very broad range of whole and detrital fragments of the skeletons and conglomerations generated by biogenic and authigenic carbonate production. Importantly in an offshore context, the term sediment also implies that individual grains have been subject to reworking, transportation and/or deposition, densifying and consolidation.

In classification terms, ‘pure’ carbonate sediments are defined as comprising greater than 90% CaCO_3 [4]. However, the term carbonate is also applied when the sediments include greater than 50% CaCO_3 (i.e. siliceous or clayey carbonate [4]). In contrast, calcareous sediments (or soils) are generally considered to contain between 10 and 50% CaCO_3 and can be considered ‘transitional’. Such sediments generally do not exhibit the unique engineering properties attributed to carbonate sediments. This paper focuses on sediments with high CaCO_3 – but with a cautionary note that there is no fixed percentage at which such sediments should be treated as carbonate for engineering purposes.

Carbonate sediments are distinctive from other sediments in several ways. Perhaps most pertinent from an engineering perspective is the intragranular porosity inherent in some ‘fresh’ carbonate sediments, where the fragile grains have not collapsed. Combined with an open structure, this attribute explains the extreme sensitivity of some fine-grained carbonate soils and, for example, explains the very low pile shaft friction that can be mobilized in such soils during installation. To put this in perspective, carbonate sediments are frequently composed of more void space than solids.

Carbonate sediments can also extend into the rock realm – reflecting the fact that diagenesis of these sediments can occur independent of deep burial. Near-surface diagenetic processes are covered in more detail in the section below but it is important

to note that the end product is that carbonate geology can be considered to present a sediment-rock continuum rather than a discrete divide.

The appropriate description of carbonate sediments can be problematic, and existing engineering logging standards often note the need for supplementary references. For example, the definition of grain shape, angularity and sorting/grading may give rise to misleading inferences about sedimentary processes, and subsequent engineering behavior. Reference to supplementary published geological standards can allow for greater flexibility, but this is hampered by key conflicts such as the definition of grain-size boundaries and the possibility that the added complexity detracts from the key message(s) relating to parameters for engineering consideration. To this end, there remains a need for a globally accepted classification system that acts as a bridge from geological observation to engineering parameterization.

2.2. How are they formed?

Carbonate sediments mainly originate either through biogenic primary production or authigenic precipitation. Both forms of production are intrinsically linked to the marine environment – biogenic through fauna habitats, and authigenic by the migration of hydrocarbons and bicarbonate ions of hydrothermal fluids [5]. Deposition in the marine environment means sediments are typically subject to multiple phases of degradation from wave, tidal, and current action, bioturbation and biodegradation (eg. borers, digestion), and/or mass transport processes. At any given time much, if not most, of the world's carbonate sediments are reworked – often to a state that has become unrecognizable from their original form.

Calcareous skeletons (see Figure 1) are produced by a wide variety of organisms, ranging from bacteria to a wide variety of marine plants and animals. Diversity in organisms is reflected in diversity of habitat, and carbonate sediments are accordingly produced in most marine environments – although the greatest abundance is noted in warm, clear, shallow water environments with sufficient nutrients and exposure to sunlight. Biogenic production takes place on the sea floor (benthic organisms) as well as in the water column (planktonic organisms). Unsurprisingly, the resulting sediments exhibit highly variable morphology – ranging from delicate balloon-like planktonic foraminifera to solid ooids. Biogenic production can also form carbonate rocks through coral reefs and cyanobacteria communities, such as stromatolites.

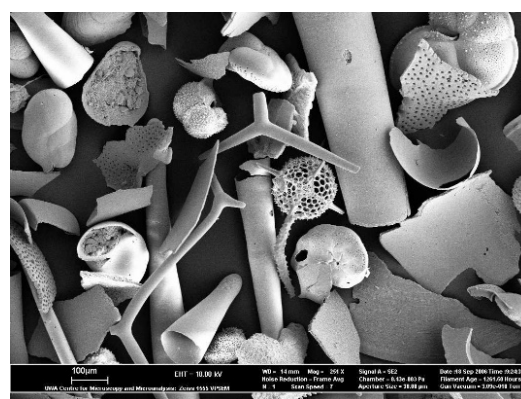


Figure 1. Example microscopic image of a carbonate sediment.

Authigenic carbonate sediments are less common or, perhaps more accurately, are more restricted in their distribution. Such sediments occur where a sulfate-methane interface intersects the seabed. At and above this interface, venting gases can react with the interstitial, near-surface pore water in shallow sediments to produce carbon dioxide and bicarbonates [6]. This anaerobic oxidation of methane catalyzes the production of calcium and magnesium carbonates. The result is the generation of cemented, boulder-scale hard-rock outcrops, which can also act as large caps or seals over vented areas. Biogenic carbonate production in the form of hard-shell chemosynthetic communities may be found proximal to authigenic carbonate mounds, illustrated in Figure 2.

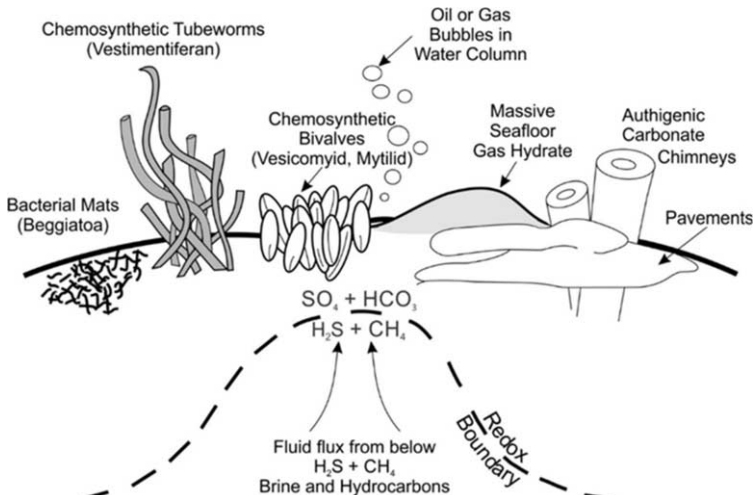


Figure 2. Illustration of authigenic carbonate production and associated biogenic communities (after [7]).

Lithification of carbonate sediments does not depend on deep burial and the associated increases in temperature and pressure – although limestone, chalk and marble can be derived from such processes. At shallow burial depths, diagenesis of carbonate sediments, and the inverse dissolution of carbonate rocks, is primarily influenced by the chemical composition of the surrounding water. This reflects the fact that calcite and aragonite may be either soluble or insoluble depending on water chemistry. The precipitation/dissolution balance is controlled by factors including water temperature, acidity and the prevalence of ions. These factors themselves vary through time in response to climate driven eustatic sea-level change. Sea-level fluctuations therefore exhibit significant control on the geology of the carbonate platforms noted on modern day continental shelves – both in terms of biogenic production and subsequent diagenesis and/or weathering of the sediment package.

2.3. The importance of geology

Carbonate geology – the nature of the sediments and any diagenetic alteration – results from the complex interplay of a range of factors: water depth, temperature, salinity and clarity, metocean conditions, climate, distance from land, and pore water chemistry. Importantly, these factors themselves change over geological time, particularly in response to climate-driven eustatic sea level change. Assessment of any carbonate

dominated region requires the development of a geological ground model to establish a framework for the relevant geological processes and to predict how those processes have impacted the region. Ideally, the model will evolve with the project and will be a useful tool to aid planning related to field layout, site surveys, geohazard avoidance and/or mitigation, and engineering design and installation.

The focus of this paper is on carbonate sediments formed in (open) continental shelves, and a simplified schematic is shown in Figure 3. This schematic is essentially a generic ground model and facilitates assessment of how factors such as biogenic production, chemical alteration, physical and biogenic reworking may change both spatially and temporally. In general, carbonate dominated seabeds in less than 120 m water depth exhibit the highest degree of variability as this isopach roughly delineates the maximum extent of subaerial exposure during the last glacial maxima [8]. Variability is typically inversely proportional to water depths with notable exceptions relating to mass transport processes and authigenic carbonate production.

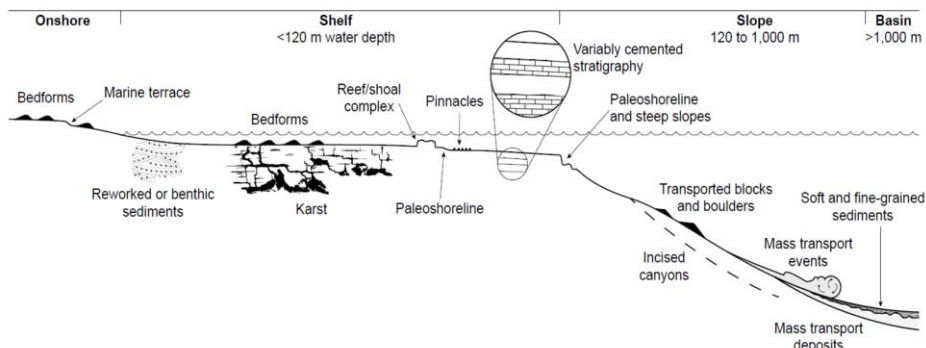


Figure 3. Illustrative shelf cross section, highlighting key geological processes.

Although not the principal focus of this paper, it is valuable to provide a brief discussion on chalk, as this group of carbonate sediment plays an important role in design of offshore structures in the North Sea and other regions. Chalk forms an extensive deposit, generally between about 200 m and 800 m in thickness, and is present over large areas (offshore) Northern Europe. Chalk was formed by the sedimentation of microscopic coccolithophores through the water column and consists of a very weak to moderately weak fine-grained limestone with coccolith bioclasts, in a matrix of coarser calcite components with localized concentrations of gravel to boulder-sized flint nodules. The CaCO_3 content of chalk is high, while its porosity is highly variable due to bioturbation, large-scale slumping and recrystallisation soon after deposition. In addition, zones of hard grounds consisting of gravel, nodules, horizons of hardened chalk and increased fossil content are present locally within the strata.

2.4. A comment on geohazards

Typical offshore geohazards, such as slope instability and debris flows, also occur in carbonate sediment profiles. The discussion below identifies geohazards that are more closely associated with carbonate sediments, with a more complete discussion (relative to carbonate sediments on the North West Shelf of Australia) provided in [9].

Carbonate sediments are different from silica sediments, and not all carbonate grains are the same. Arguably the most significant engineering geohazard relating to carbonate sediments is also the most widely acknowledged – that being the contrast in engineering behavior of carbonate sediments when compared to silica equivalents. For example, the impacts of this contrast are well documented in literature pertaining to foundation installation of the earliest offshore infrastructure on the North West Shelf of Australia [10]. While it is now well understood that carbonate sediments are not the same as silica sediments, it should also be noted that not all carbonate sediments are the same. For example, the engineering behavior of well sorted, solid ooid carbonate grains will significantly differ to that of planktonic foraminifera assemblages. Detailed geological inspection coupled with specialized geotechnical laboratory testing can mitigate against the potential risks posed by this geohazard.

Carbonate geology is highly variable, both laterally and vertically. Discussed previously, carbonate geology on continental shelves is inherently variable, particularly in water depths less than 120 m. Reliable site characterization can be problematic, and experience is needed in selecting both the types and quantities of data collected to support engineering analysis. A famous example of this variability is the (limestone) pinnacle formations in Cervantes, Western Australia (Figure 4). Related to geological variability but worth specific mention are karst features. Dissolution of calcium carbonate has the potential to result in the formation of voids – in the marine environment such features appear generally (but not always) filled with uncemented sediment, presenting a stark contrast to the surrounding rock.



Figure 4. Local variability observed at the Pinnacles, Western Australia (photo from [11]).

Sample recovery requires bespoke equipment and methods. Engineering analysis of cemented carbonate sediments is often hampered by uncertainty stemming from data acquisition – or more specifically a lack thereof. Weakly cemented and dense sediments can exhibit similar in situ testing properties, while being fundamentally different with respect to certain key engineering parameters. Both types of sediment may result in refusal using standard push sampling techniques. Further, standard rotary coring can lead to little or no recovery when the degree of cementation is low. Specialized coring equipment and drilling parameters are needed to maximize the chance of successful recovery. The absence of high quality samples can lead to additional uncertainty being

carried through to engineering design and installation, potentially leading to unconservative or excessively conservative outcomes.

Steep slopes may reflect sediment interlocking and may be aided by biogenic silicas. Steep slopes are noted at the shelf break of many carbonate dominated continental shelves. These slopes are often over-steepened relative to the apparent strength of the sediments – and in some case, overhanging sections have been observed despite the lack of any apparent cementation in the sediment. In such cases oversteepening may be explained by granular interlocking of the varied and irregular grain shapes often associated with carbonate sediments. Particulate interlocking may also contribute to the often very high peak friction angles typically noted in carbonate sediments. However, such interlocking is not unique to the carbonate component of these sediments – biogenic silicas such as spicules, diatoms and radiolaria almost certainly contribute as well.

3. Interaction with offshore development

In this section we identify regions where carbonate sediments are either known or expected to influence offshore development. Commentary is divided by region and is based on the experience of the authors – and is not intended to be exhaustive. While focus is on the oil and gas sector, the behavior of carbonate sediments can influence all offshore development. Examples of this are the recent expansion of offshore wind in the North Sea and the Baltic Sea, where chalk (and in some cases limestone) may be encountered, and potential wind farm projects offshore southeast US and southeast Australia where carbonates sediments are prevalent.

Figure 5 identifies many areas with carbonate sediment, taken initially after [12] which specifically identified areas of carbonate sand. In the current paper other known regions with carbonate sediment are also considered, particularly including locations where such materials might be found to impact offshore developments. These are also highlighted on Figure 5.

3.1. Known regions where carbonate sediments are encountered

Regions where carbonate sediments are encountered include:

- Central and North America – carbonates are found on the Yucatan Shelf in the Gulf of Mexico, the Belize Shelf in the Caribbean Sea, extending further south to Nicaragua and Columbia; and on the South Florida Shelf between the Gulf of Mexico and the Atlantic Ocean (extending out to the Bahamas). Carbonates are (often) encountered as silty sand in layers of variable thickness, typically interbedded with sediments of (significantly) lower carbonate content.
- South America – the Campos Basin in Brazil is an area where carbonates are found in relatively shallow water, occurring in layers of silty sand to sand, and often with sand at the seabed [13]. As exploration pushes further into deep water, it is possible that regions of finer grained carbonate sediment will also be encountered – although this is not currently documented in the literature.
- Europe – extensive regions of variably weathered chalk are found throughout the southern North Sea, English Channel and the southern Baltic Sea, typically of significant thickness for engineering purposes and sometimes overlain by

- younger (non-carbonate) sediments. Limestone and calcarenite are also prevalent in some areas, particularly off the west and northwest coasts of France.
- Middle East – the Arabian Sea is a well-known region where high carbonate content sediment is encountered, in particular offshore Qatar and the UAE. In shallow waters the stratigraphy is dominated by variable strength calcarenite, whereas carbonate sands (sometimes lightly cemented) are encountered as water depth increases (and may be interbedded with calcareous silts and clays).
 - Africa – activities off the east coast have identified cemented carbonate reefs and uncemented carbonate sediments in shallow waters associated with shelf breaks and lagoonal areas, particularly offshore Mozambique. Mass transport processes have carried some of these sediments, including extremely large boulders (> 1 km in diameter, or olistoliths, [14], [15]) through the numerous canyons which line the Mozambique coast and onto the continental slope near locations associated with well sites. Authigenic carbonate mounds have also been observed on the continental slope, related to fluid seeps and/or bioherm communities. Carbonate sediments have also been encountered to the north of Africa, in Mediterranean waters offshore Libya.
 - Asia – oil and gas activities offshore India have encountered carbonate sediments, although these are more common off the west coast (with the east coast heavily impacted by terrestrial outflow). Carbonates are also encountered offshore the Philippines, where carbonate sediment is found as sand in modest water depth, becoming finer grained with increasing depth.
 - Australia – north west Australia is another well-known region for carbonate sediments, extending from the North West Shelf to Browse Basin, and into the Timor Sea. Carbonates occur over the full depth profile, with shallow waters dominated by coarser grained particles, transitioning to mixed material (silty sand / sand silt) with depth, and to silt and mud in deeper waters. Carbonates are also prevalent in the Bass Strait off the southeast coast, comprising predominantly sandy sediment in shallow waters, becoming silty sand (to silt) with increasing water depth. Varying degrees of cementation are prevalent throughout these areas, particularly in shallow water and at shallow depths (i.e. within the depth range of subaerial exposure during the last glacial maximum) – although significant cementation is also often encountered at greater depths in shallow water sediment profiles and, more rarely, in deep water.

3.2. Potential areas where carbonate sediments may be influential

This section highlights areas of current and future development, which may encounter carbonate sediments and require particular attention:

- North America – it is understood that the southeast coast is proposed for future wind farms. Carbonates are anticipated in this region, as indicated in [16].
- Central America – deep water areas of the Caribbean Sea, including offshore Venezuela and Guyana have potential to encounter soft carbonate sediments, as indicated in [17].
- Middle East – new areas of the Red Sea are currently being explored. Shallower depths are expected to comprise calcarenite with some uncemented layers, while deeper waters may contain finer grained carbonate sediments.

- Africa – additional areas along the east coast of Africa, are being developed by the oil and gas industry. Experience to date suggests that carbonate silts and sands, possibly with variable cementation, may be found offshore Tanzania – potentially similar to the northern parts of Western Australia. Off the west coast of Africa, carbonates have been encountered offshore Mauritania and Senegal, although generally in deeper water and with $\text{CaCO}_3 < 50\%$ and so may not be ‘true’ carbonates.
- Asia – oil and gas exploration offshore Vietnam has potential to encounter carbonate sediments, which (depending on water depth) may also be the case for proposed offshore renewables projects.
- Australia – ongoing development along the northwest and northern coasts will largely occur in seabeds that mostly comprise carbonate sediments. The southern Australian coast is also anticipated to see an increase in offshore exploration with carbonate sediments similar to those found in the Bass Strait region likely to be encountered, although generally reflecting a higher energy environment.



Figure 5. Map showing where carbonate sediments are important for offshore development.

4. Select aspects of carbonate sediment behavior

This section highlights a selected range of key engineering properties of carbonate sediments, based on the experience of the authors. General trends describing the range of observed behavior are provided to avoid focusing on individual data and to facilitate a broader discussion. Noted above, a key characteristic of carbonate sediments is their high spatial variability and accordingly, care should always be used (and experience valued) when evaluating engineering parameters.

In Section 4.1 to Section 4.6 below, the presented parameters originate (primarily) from testing of normally to moderately overconsolidated samples, with and without cementation. In contrast, Section 4.7 provides commentary on the heavily overconsolidated chalks found in the southern North Sea.

4.1. CPT based interpretation

The cone penetrometer test (CPT) is widely used to characterize offshore sediments, and Figure 6 presents example CPT data from testing in water depths between 100 m and 130 m on the North West Shelf of Australia. All four profiles come from an area roughly 10 x 15 km. The profile comprises a sequence of interbedded carbonate silt and carbonate sand, with (relatively thin) layers of variably cemented material.

A comparison with traditional CPT correlations (after [18]) is provided in Figure 7, using the same CPT profiles (and color scheme), where it is seen that the data plots at the low end of the normally consolidated range. While the silts overlap with zones characterized by high sensitivity, the high sensitivity of the sands (in particular) is not immediately apparent.

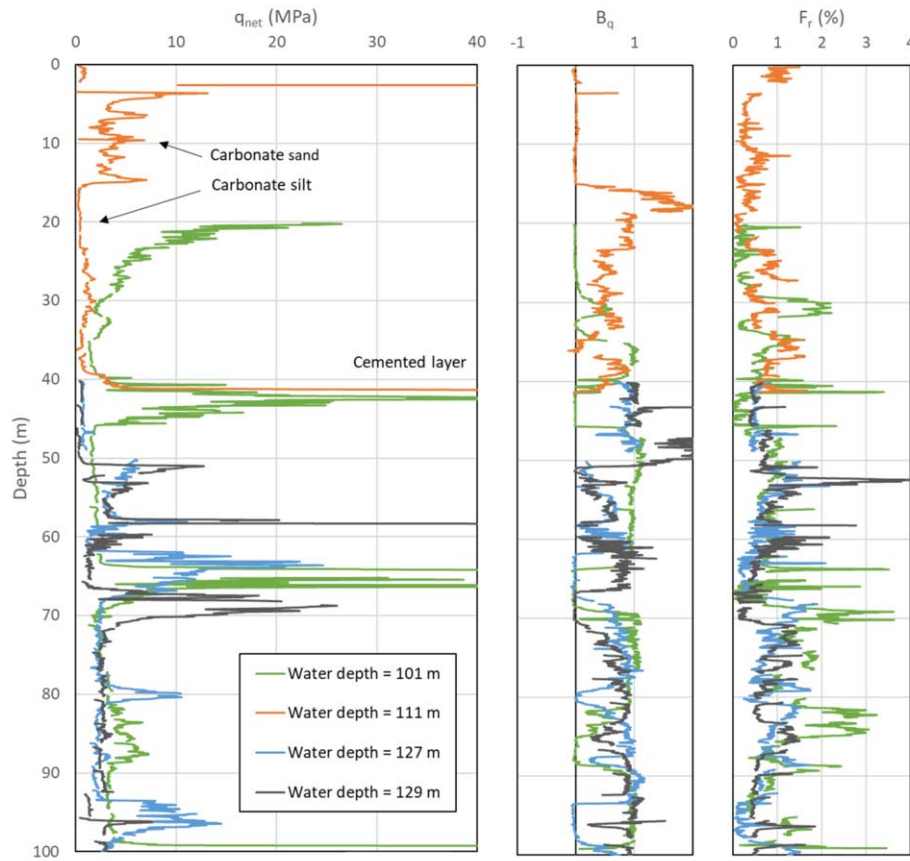


Figure 6. Example CPT data from the North West Shelf, Australia.

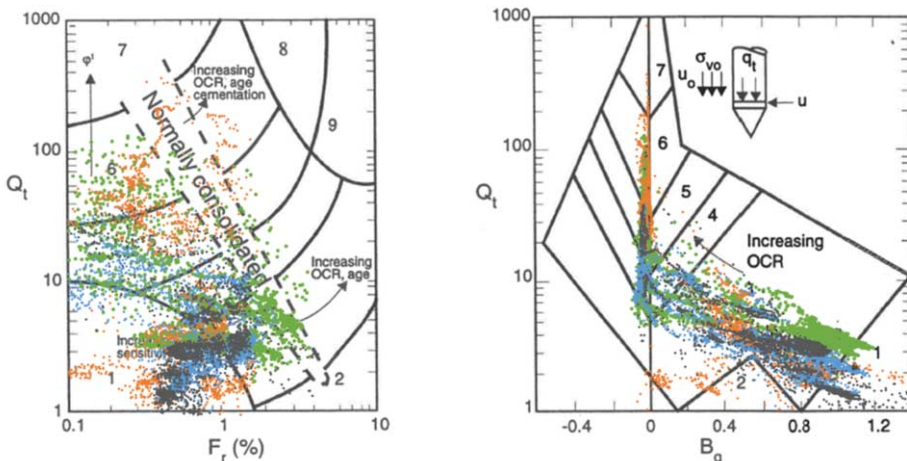


Figure 7. Comparison with CPT correlations after [18].

4.2. Shear strength (uncemented sediments)

The monotonic undrained shear strength ($s_{u\text{ mono}}$) of uncemented carbonate sediments is a critical parameter for many aspects of engineering design. However, the high degree of variability in fines content often associated with many carbonate sediment profiles makes correlation of the undrained strength with CPT data a challenging task.

However, in general terms, $s_{u\text{ mono}}$ can be determined from q_{net} using N_{kt} values that vary with fines content, ranging from around 10 to 15 where the profile is strongly influenced by clay/silt sized particles, to over 40 (and sometimes much higher) where the profile comprises predominantly carbonate sand. In the latter case, the high N_{kt} values reflect the effect of partial drainage and also generally vary with density. Typical strength ratios ($s_{u\text{ mono}}/\sigma'_v o$), which serve as a type of state parameter, range from around 0.3 for normally consolidated fine grained strata (such as on the outer shelf and in deep water) to well over 2 where dense carbonate sand is encountered – although these should be considered broad guidelines only.

Sensitivity (S_t) is a measure of the reduction in undrained shear strength due to remoulding. High S_t is generally associated with carbonate sediments, and can be investigated through both field and laboratory testing. Figure 8 shows a typical result from insitu cyclic T-bar testing (as discussed in [19]), for a sediment with S_t in the range 25, which is reached after 10-15 cycles. Alternatively, either the fall cone test or minivane may be used in the laboratory; with the former more common outside the United States. The high sensitivity of many carbonate sediments is associated with the fragile nature of the particles, which can break during shearing; and may also result from hollow particles being filled with water, which is released on breaking leading to an apparent increase in free water content.

A useful ‘rule of thumb’ to determine whether a carbonate sediment will exhibit high sensitivity is where the Liquidity Index (LI) exceeds 1. When $LI > 1$, the remolded strength of carbonate sediments (over the depth ranges of interest to most design) often tends towards an absolute value of 1-2 kPa, regardless of the initial stress ratio – which leads to higher sensitivity being observed for samples with high undrained shear strength ratio or from significant depth. Sensitivities well over 100 have been observed in some

cases. Relatively high ‘apparent’ sensitivities can also be observed due to water entrainment effects, which are relevant to subsea pipelines due to the seabed disturbance during the installation process.

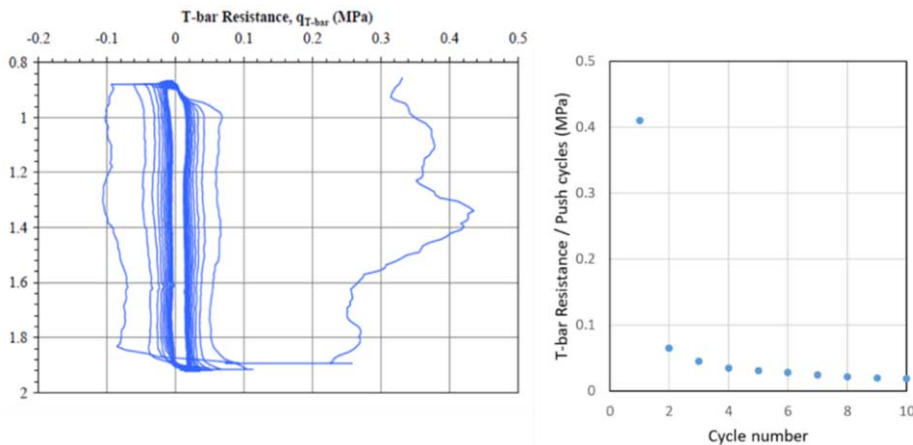


Figure 8. Typical cyclic T-bar test.

While high sensitivity is a manifestation of highly destructive processes at very large shear strains, uncemented carbonate sediments also typically exhibit significant strength degradation during cyclic loading at relatively small strains. This is due to classical softening as a result of compaction induced excess pore pressure generation, as the samples attempt to densify under cyclic loading. Most carbonate sediments are prone to reaching a state of cyclic mobility (initial liquefaction) under sufficiently intense cyclic loading, although this tendency reduces with an increasing component of clay minerals. Cyclic degradation can be explored through cyclic simple shear tests, allowing the impact of number of cycles (N) and load bias (1-way or 2-way) to be investigated. Figure 9a presents typical results from testing of carbonate silt / sandy silt / silty sand across a range of locations offshore Australia, and shows the ratio of cyclic to monotonic soil strength plotted against normalized monotonic soil strength. In this case a reference of $N = 10$ was adopted, and all results are shown for a maximum strain $\gamma = 10\%$. Consistent with the nature of carbonate sediments, considerable spread is observed in the data. However, the potential for cyclic loading to lead to significant strength reduction is clear – and is greatest for 2-way testing and generally increases for higher initial soil strength.

Two further characteristics related to undrained shear strength merit further comment:

- Carbonate sediments typically display only modest response to strain rate changes. Typically explored through simple shear testing at different rates, experience suggests that (while local variations may occur) strength increases of less than 5% per log cycle of shear strain rate may be expected in most cases (albeit once again, an increasing clay mineral fraction may enhance the rate effect).
- When designing foundations in carbonate sediments, especially shallow foundations, the potential for strength increase with application of additional

vertical stress can be useful for optimizing design. Again, simple shear tests can be used to explore this – typically using samples from the same depth, and performing tests at varying vertical stress. Figure 9b shows (illustrative) relationships typically observed from testing of carbonate sediments ranging from silt to sand. The stress ratio decreases with increasing levels of applied stress – with larger decreases observed for samples with higher initial stress ratio. For design purposes, undrained strength increases in the range 25-50% of the applied increase in vertical stress are common.

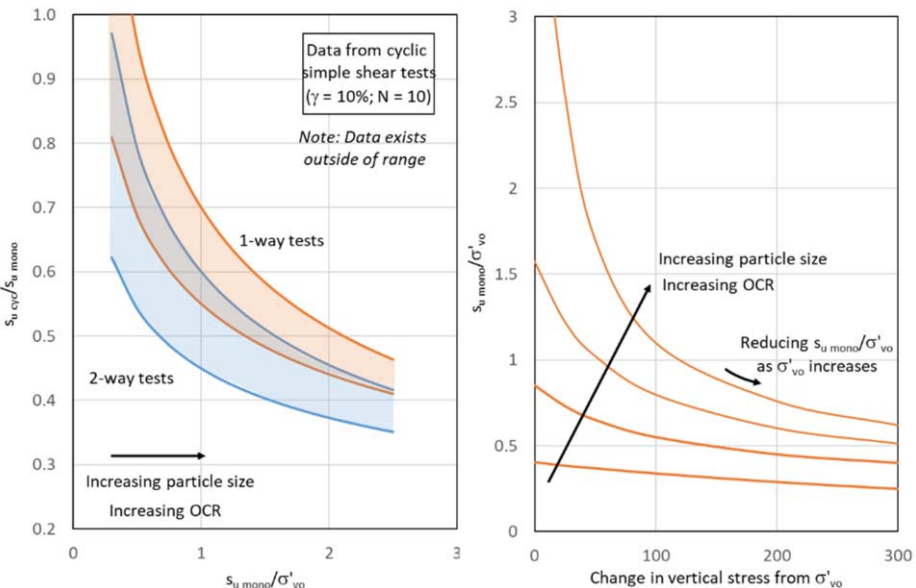


Figure 9. Undrained shear strength (a) degradation of soil strength due to cyclic loading; (b) changes in stress ratio for (applied) increases in vertical stress.

Aside from undrained shear strength, cohesion (c') and friction angle (ϕ') are other important engineering properties, used to explain (for instance) the steep slope angles often observed in uncemented carbonate sediments (Section 2.4). Methodology has been developed to combine results from UCS testing with stress path testing (triaxial and simple shear) to evaluate both of these parameters. In the case of simple shear, an important consideration in the interpretation of stress path is device type, with studies showing that the ‘Berkeley’ type apparatus leads to a diagonal failure plane, and shear stress mobilized on this plane considered more representative of the true stress path (noting that the shear stress on the diagonal plane tends to be slightly higher than on the applied horizontal plane). Tests performed on a range of uncemented carbonate sediment supports the presence of cohesion caused (presumably) by particle interlocking, which also explains the (high) peak friction angles often observed. Peak friction angles greater than 50° are often observed, which reduce (post-peak) to closer to 40° as the interlocking is broken.

4.3. Shear strength (cemented sediments)

Many cemented carbonate sediments demonstrate a brittle response, with significant post-peak softening, which requires careful consideration in design. The discussion below focuses on defining the shaft friction response for design of drilled and grouted piles, although this can be extended to other foundation types.

A critical challenge in dealing with cemented material relates to variability over the zone of interest. As noted previously, high geological variability may be experienced in such materials. Further, interpreters often face incomplete data sets – with complete CPT profiles often difficult to achieve (even with small diameter cones), and high quality sample recovery often challenging. Correlations are needed, with one example illustrated in Figure 10a, comparing q_{net} to unconfined compressive strength (UCS) – showing that in this case $\text{UCS} \sim q_{\text{net}}/20$ (but note that this is not a general rule).

The peak interface strength (τ_{peak}) can be explored via constant normal stiffness (CNS) testing in a direct shear device, with the adopted normal stiffness (K) determined as a function of small strain shear stiffness (G_{\max}) and pile diameter. Testing is usually performed for a soil-soil interface, as it is anticipated this will generally govern design; although testing can also be performed to examine soil-grout and grout-steel interfaces in a similar manner. Figure 10b shows a typical monotonic (soil-soil) response, highlighting the brittle nature of these materials. Historical correlations exist to link τ_{peak} to q_{net} , including those in [20] and [21], and noting that other factors (grout pressure, borehole roughness and pile diameter) are also important and can influence τ_{peak} [22]. These suggest τ_{peak} typically in the range 2-2.5% of q_{net} , thereby implying $N_k \sim 40-50$ (which, coincidentally, is consistent with the above example UCS relationship). While the authors have experience indicating that higher ratios of $\tau_{\text{peak}}/q_{\text{net}}$ may be observed in some cases, the stated range is generally considered reasonable for design – especially where highly brittle behavior is observed.

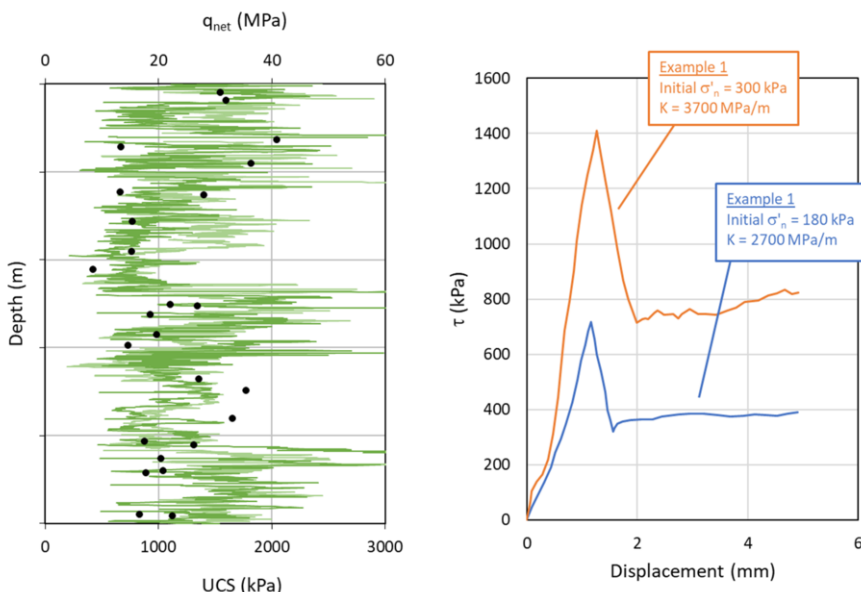


Figure 10. Strength of cemented sediments (a) q_{net} versus UCS; and (b) brittle response from CNS testing.

The cyclic response of cemented materials is also of interest, especially in cases where the design loading could lead to progressive failure. Given the brittle behavior of such materials, two types of CNS test may be used to explore the cyclic behavior:

- Displacement controlled cyclic CNS testing – where the displacement of each cycle is fixed, and the (changing) shear stress is measured. This type of test can be used to explore the ‘post peak’ behavior on the interface.
- Stress controlled cyclic CNS testing – where the sample is sheared between preset stress limits, typically a fraction of the peak shear strength. This type of test can be used to evaluate the ‘pre-peak’ behavior of the interface, in a similar manner to cyclic simple shear testing in uncemented sediment.

Figure 11 presents examples of the different test types. As the results are heavily influenced by site specific conditions, it is difficult to draw broad conclusions. However, experience suggests that when cycling ‘pre-peak’ (generally stress controlled) it is normally possible to apply stress levels > 50% of τ_{peak} without rapid failure; whereas cycling ‘post peak’ (generally strain controlled) leads to residual cyclic strengths as low as 10% of τ_{peak} after a moderate number of cycles.

As a final comment, given the conditions under which cemented layers form, high variability should be anticipated in these materials. A range of stress-controlled conditions is needed during testing to bound the likely range in response, and appropriate engineering judgement employed in design.

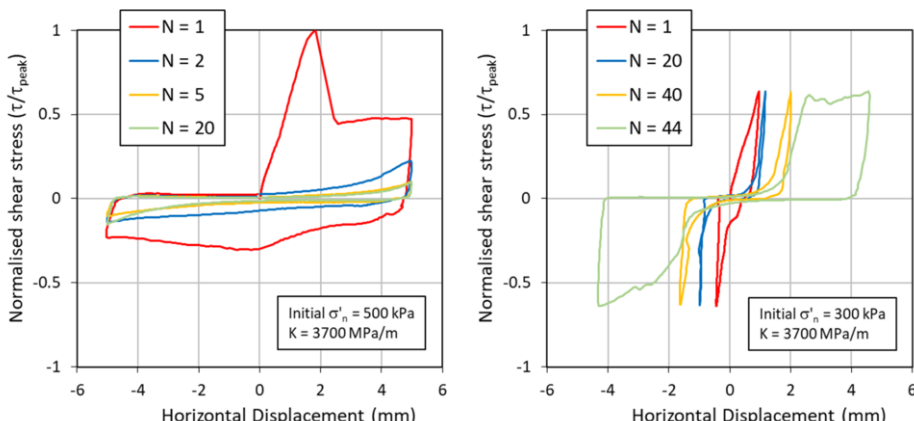


Figure 11. Response from (a) strain controlled; and (b) stress controlled cyclic CNS tests.

4.3.1. Chalk

Presenting design challenges broadly similar to cemented materials found on open carbonate shelves, chalk is a highly variable engineering material that is generally characterized in terms of intact dry density and fracture state. The latter is based on the classification system proposed in [23] and designates chalk from structureless through various grades of structured chalk. Figure 12 illustrates typical variations of cone resistance and UCS values with dry density and grade, as measured in the southern North Sea. CPT refusals are common in high density chalk especially where flint bands are present – and the latter can be problematic for driven pile installation.

A specific challenge when defining the mechanical response of chalk for foundation design is understanding the transition from strongly dilatant to highly contractive response, which can result from the large strains induced during foundation installation (remolding during pile driving) or under severe environmental loading – and this aspect typically governs the design capacity of deep foundations in chalk.

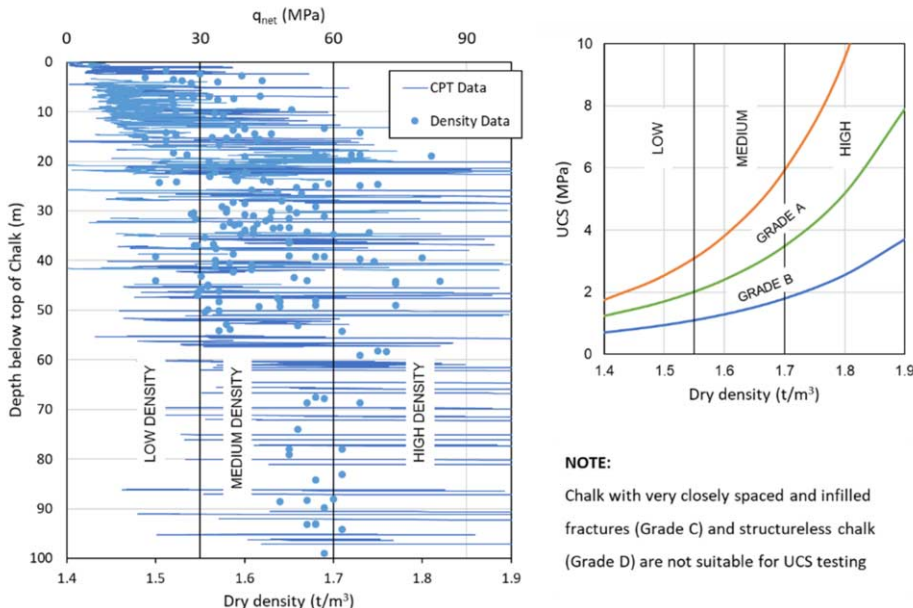


Figure 12. Typical CPT and UCS variations by chalk dry density and grade.

4.4. Interface strength

A brief comment is warranted on the importance of direct shear testing to evaluate, for example, the friction characteristics of pipeline-soil interfaces. Testing is generally performed using representative interfaces manufactured from the appropriate material (e.g. polypropylene or concrete) and with the appropriate roughness, selected in collaboration with the client based on the expected pipeline coating and surface finish. At the stage when this testing is conducted (e.g. as part of a geotechnical interpretative report) these pipeline details are often unknown and so it may be necessary to test a range of interface roughness, or supplement the testing later in a project when these interface properties are known. Tests may be conducted on either intact or reconstituted soil samples (depending on the expected amount of soil disturbance during pipe lay), normally with multiple tests required per soil zone/type to estimate the range of interface properties for that zone.

Shearing is performed under conditions of constant (total) normal stress and can be performed at rates (or for durations) to measure undrained, drained, or partially drained shearing conditions. Slow monotonic tests are generally performed to measure drained interface shear resistance with tests performed at different normal stress levels to quantify how the interface shear resistance changes with normal stress. Faster tests are performed to measured undrained shearing behavior and these may include cyclic events

to explore the transition of shear resistance with increasing number of cycles (or drainage time).

There is general understanding on how qualitatively the interface shear resistance varies with interface roughness, soil stress history, normal stress and drainage conditions. However, pipeline and zone specific testing is required to quantify the range of interface properties for a particular pipeline and soil zone combination.

4.5. Shear stiffness

Small strain stiffness (G_{\max}) is typically measured via resonant column testing, or from bender element tests performed on (for example) triaxial samples. As tests are typically performed on a modest number of samples, correlations are used to develop profiles of G_{\max} with depth. One such approach is outlined in [18], based on q_{net} and σ'_{vo} giving:

$$\frac{G_{\max}}{q_{\text{net}}} = A \left(\frac{\frac{q_{\text{net}}}{p_a}}{\sqrt{\frac{\sigma'_{\text{vo}}}{p_a}}} \right)^n \quad (1)$$

where p_a is atmospheric pressure (100 kPa). From experience with a wide range of uncemented silt to sand samples, indicative values for A in the range 200 – 800 are observed, with $n = -0.75$, although site-specific values should be determined. In contrast, for cemented carbonate materials the stiffness ratio (G_{\max}/q_{net}) may be 2-3 times higher.

For dynamic analysis in soft soil sites, resonant column tests may be used to examine both the degradation of shear stiffness (G) with strain, and the associated damping ratio. A recent study reported in [24] developed relationships for G/G_{\max} and damping ratio for a range of soils types encountered in the Bay of Campeche, including carbonate sediments. The relationships proposed in this study are compared on Figure 13 with select data obtained from testing uncemented carbonate sediments (varying from sandy silt to sand) from the North West Shelf of Australia. It is seen that the Australian data compares reasonably well with that reported in [24], although tends towards the upper bound for low strain levels, but with more rapid degradation as strain level increases.

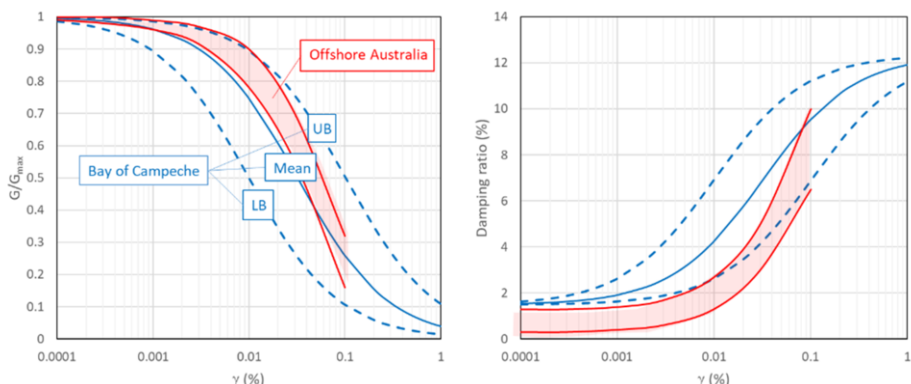


Figure 13. Stiffness degradation and damping ratio, Bay of Campeche vs offshore Australia.

In contrast, cemented carbonate sediments tend to show limited degradation in shear stiffness until approaching the peak response.

4.6. Compression behavior

By the nature of their deposition, uncemented carbonate sediments are highly compressible. Typical ranges of compression index (C_c) are shown on Figure 14(a), plotted against in situ voids ratio (e_o) – where low voids ratio typically reflects coarser grained materials or higher OCR, and high void ratios are typical of (very) soft soil profiles. As is evident, both voids ratio and compressibility are significantly higher than typical ranges for siliceous sands and silts at practical stress levels. An alternative perspective is that the yield stress ratio (YSR) for carbonate sediments is generally low, so that high compressibility is encountered at stress levels relevant for foundation design. The coefficient of consolidation (c_v) controls the rate of settlement. It is a function of stress level, stress history (loading vs unloading) and soil type – and for carbonate sediments may vary from less than $1 \text{ m}^2/\text{yr}$ for mud/silt to over $10^6 \text{ m}^2/\text{yr}$ for carbonate sands, with a wide range in data often observed.

Under cyclic loading, carbonate sediments will exhibit an increase in pore pressure, consistent with their compressible nature. Subsequent dissipation of the excess pore pressure results in further settlement, which can be explored by measuring the compression in simple shear tests after cyclic loading. This is discussed in [25] for a selected carbonate silt / sand, where the response in that case was shown to be comparable to recompression behavior under 1D conditions – as highlighted on Figure 14(b).

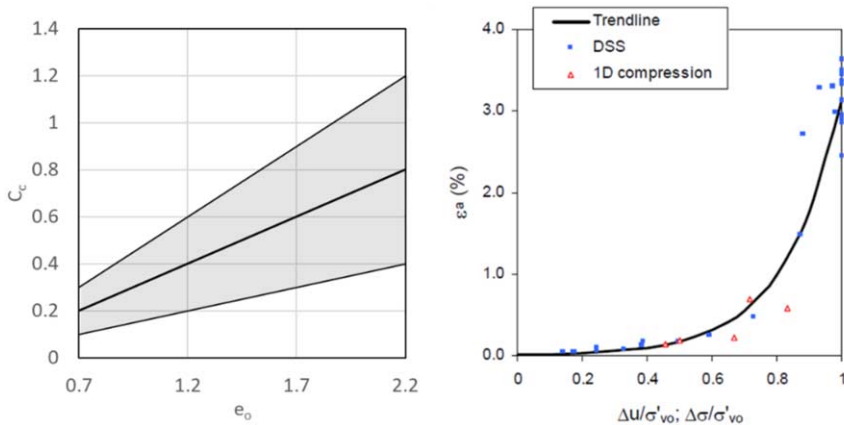


Figure 14. Compression behavior (a) typical C_c vs e_o and (b) post cyclic recompression, after [25].

4.7. Resistance to scour

The resistance to scour governs both the magnitude and rate at which erosion will occur around subsea structures, as highlighted in Section 6.2. Recent testing reported in [26], [27] have shown some differences in the erosion response of carbonate sediments relative to silica sand and silt. In general, similar threshold velocity to initiative erosion is observed for sand sized particles, while considerably higher resistance to scour is

observed for silts. This is illustrated in Figure 15, where the critical shear stress of undisturbed carbonate sediments is compared to siliceous soils as reported in [28].

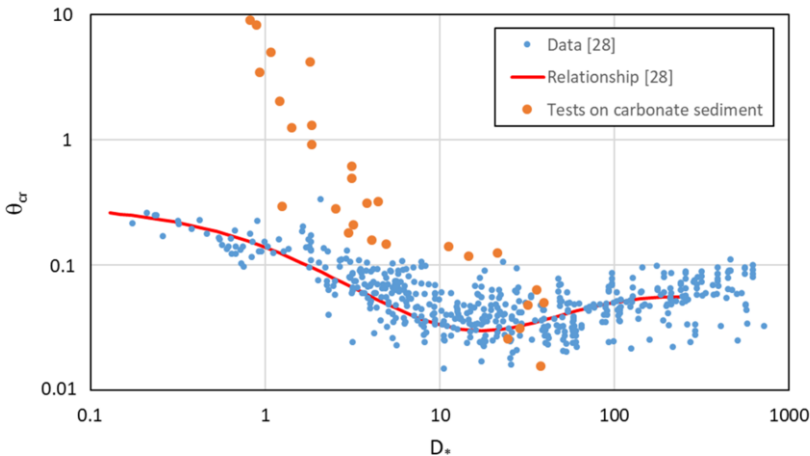


Figure 15. Erosion resistance of carbonate sediments.

5. On the importance of sample quality and interpretation

Section 4 highlighted the high sensitivity of many carbonate sediments, while Section 2 noted that the difficulty in sampling these materials – both uncemented and cemented – represents a geohazard, owing to the potential impact on engineering studies. Careful ‘management’ of sample quality is therefore of paramount importance.

Such management starts with the development of specialist drilling/sample techniques to minimize disturbance during recovery, continuing to sample storage and transportation to the laboratory. The effect of the latter can be tracked via accelerometers, and the data used as a semi quantitative tool to understand quality issues and potential variability between samples. Close inspection of each sample, including any observed settlement in sample tubes before and after transport, can also provide insights into sample disturbance – and is undertaken routinely in our practice prior to laboratory testing.

Once in the laboratory, non-destructive approaches are available to enhance our understanding of the material, as well as to aid selection of sub-samples for testing. The use of x-ray or CT scanning are common means to inspect samples prior to extrusion, while more advanced techniques (such as the use of a Multi-Sensor Core Logger) can provide valuable early information to characterize an offshore site.

Selection of an appropriately experienced soil laboratory and specification of test standards is critical. As highlighted in [29], results from different laboratories can vary significantly – especially in regards to characterization testing, although this is also true for advanced testing.

Owing to the wide variability of carbonate sediments, it is important to take advantage of existing data from past projects wherever possible. As well as being a valuable in assessing sample quality, such databases can be used to increase confidence in the relatively modest amount of testing often performed to characterize individual

offshore sites, while also allowing trends to be developed. With sufficient data, it also becomes possible to adopt data science based approaches, allowing uncertainty from characterization to be captured explicitly in the design process.

6. Foundation design in carbonate deposits

The previous sections have focused on the physical and engineering properties of carbonate sediments. In this section, we outline aspects of foundation design that have been adapted to address the challenges posed by these sediments.

6.1. Deep foundations

As for all soil types, the vast majority of offshore pile foundations comprise steel tubular piles, with the two most common pile types being (i) driven and (ii) drilled and grouted. The latter is relatively rare in non-carbonate sediments but common in many sediments with high carbonate content because of the potential for low shaft capacity, although driven piles are often used in chalk. Excluded from this list are the so-called suction piles (or buckets) which, for most applications, do not rely on axial shaft friction as the principal support mechanism, instead mobilizing direct bearing on the baseplate and/or skirts to resist vertical and lateral loads respectively. In any case, applications for deep pile foundations are numerous, ranging from supporting jacket platforms and wind turbines to tethering tension-leg platforms or anchoring floating production vessels. Over the last two decades, typical offshore pile diameters have increased substantially – from less than 2.5 m historically, to extremes of over 8 m for monopiles supporting offshore wind turbines, and 3 to 6 m diameter for jackets and anchoring systems.

6.1.1. Driven piles

While driven piles are generally installed open-ended, a limitation of in carbonate materials is the potentially low shaft resistance that is mobilized during installation, especially in carbonate silt and sand. This is attributed to the tendency for carbonate materials to either be crushed (coarse-grained) or remolded (fine-grained) during the large strain shearing induced during penetration at the soil/pile interface. In addition, cyclic loads applied during dynamic pile driving will also tend to cause liquefaction in the surrounding soils, further reducing available shaft friction.

This behavior can result in uncontrolled pile penetration, i.e. ‘pile runs’ or free-falls, if appropriate mitigation measures are not taken, for example as per ([30] and [31]). In many carbonate soils, particularly the more compressible varieties that also exhibit high friction angles or may have a modest degree of cementation, the shaft resistance is expected to remain at very low levels when the piles are later subject to operational loads, with only modest set-up (i.e. increase in shaft friction) expected over time. Even where driving can be controlled by an arrestor device, for example using a hydraulic brake to limit free-fall velocities ([31] and [32]), use of driven piles as bearing piles in such sediments is generally limited to cases where loads are predominantly compressive and a hard layer exists that can provide significant end-bearing support.

Driven open-ended piles are used widely in carbonate sediments where there is either somewhat lower carbonate content or where carbonates are interbedded between

significant non-carbonate layers. However, even in these conditions piles often exhibit relatively high embedment ratios in order to achieve the required capacity.

Pile monitoring data has been widely used worldwide to justify and improve axial pile design in carbonate soils, and this has resulted in site specific methods where sufficient geotechnical and pile monitoring data are available. Site specific methods combine both geotechnical and pile monitoring data and have significantly improved the pile design methods, especially where partially drained carbonate silts (which are difficult to characterize) are encountered.

While chalk is also a carbonate sediment that often exhibits low shaft friction during driving, significant set-up is commonly observed shortly after installation. This allows driven piles to be used more successfully in chalk than in more common carbonate materials, as discussed further in Section 6.1.3.

Driving through cemented carbonate layers can lead to installation difficulties. This may include early refusal on such hard layers, pile damage and/or uncontrolled pile runs. While the pile may pass through a hard layer, it may undergo what is referred to as 'extrusion buckling' whereby the pile tip is distorted from its original circular shape. As the pile is driven further, the magnitude and extent of the distortion increases, leading to increased driving resistance and enhanced risk of premature refusal. Such failure modes have been known to occur when open ended piles are driven into variably cemented materials [33]. In general, extrusion buckling refers to the potential for initial imperfections in the structural geometry of the primary pile, either pre-existing or initiated by heterogeneities in the sediments (such as boulders, [34]), to propagate upwards as the pile is driven into the seabed. This phenomenon occurs in sediments that have a much higher stiffness than the elastic hoop stiffness of the pile itself, causing pile deformations to propagate at an accelerating rate [35]. Where such risks are identified, analyses should be conducted to eliminate the risk of extrusion buckling.

6.1.2. Drilled and grouted piles

In contrast to driving, drilled and grouted piles generally provide superior axial support by mobilizing shaft resistance along the grout-soil interface. This is because the drilling out process does not generally impart significant damage to sediment at the grout-soil interface, hence eliminating the main problem with driven piles in these soil types.

Drilling and grouting is essential where driving is not possible, for example through strata of medium to strong cementation (including calcarenites and limestones) – where the design objective is to take advantage of these hard (cemented) strata to provide the required axial capacity.

The depth at which a suitably thick hard stratum is found, and the competence of the shallower sediments, determines whether a drilled and grouted pile can be installed as a single-stage pile, or whether a multi-stage construction process is required. For example, multi-stage piles are only occasionally used in the Middle East, but are common in Australia where considerable depths of overlying unstable silts and sands preclude drilling of an unsupported hole. In these cases, an open-ended primary pile is driven first to the top of the hard stratum in order to restrain the overlying sediments. This section of pile also provides the lateral resistance, which can be assessed using appropriate methods [36].

Following installation of the primary pile, a rotary drill is lowered through the primary pile to remove the internal soil plug, then advanced to sufficient depth to accommodate an insert pile. The insert pile is then grouted in the drilled hole and to the

primary pile. The drilled and grouted section of the pile generally provides most of the required axial capacity. The process is illustrated in Figure 16.

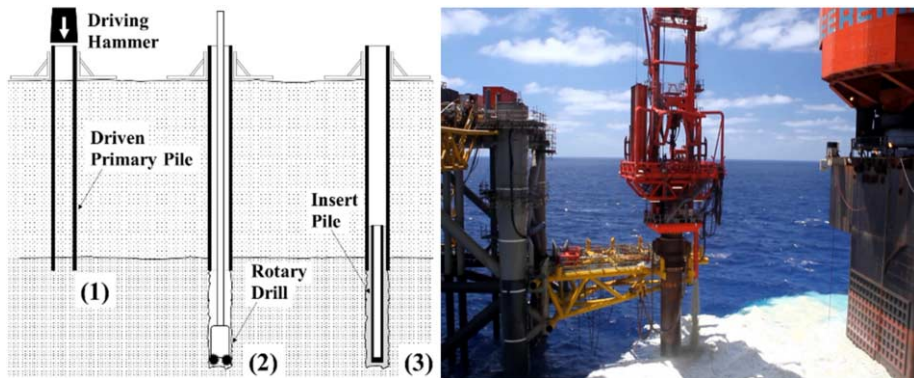


Figure 16. Installation of a drilled and grouted pile in carbonate soil.

For drilled and grouted piles, the following installation aspects should be considered as appropriate:

- Where a primary pile is used to provide support in the upper soil, it is essential to consider any risks of extrusion buckling, which may lead to excessive pile deformation. The resulting enhanced driving resistance may cause premature refusal and the distorted shape may preclude subsequent passage of a drill bit to allow further construction (as was the case for the Goodwyn A Platform on the North West Shelf).
- To maximize shaft friction capacity, insert pile holes are generally drilled offshore without any active stabilization such as drilling muds. This can lead to a risk of hole collapse if there is insufficient cementation. While open holes may be stable where there is sufficiently high cementation, or where undrained conditions prevail in the soil for a sufficient duration, holes drilled in insufficiently cemented carbonate sediments that exhibit drained or partly drained responses are at high risk of collapse. To mitigate this risk, a technique that has been used with high success for projects in Australia's Bass Strait involves using an elevated drill riser and the application of a positive water head (i.e. above hydrostatic) to enhance the effective stresses acting at the hole wall, through seepage induced drag. With an appropriate head and ensuring a sealed riser (particular care being required to avoid breaching at the tip of the primary pile) this has proven to provide sufficient hole stabilization to allow the drilling, pile lowering and grouting operations to be completed successfully.
- In most weakly cemented carbonate sediments a 'rough' interface is expected to arise naturally as a result of drilling operations. However, in some cases where there is potential to realize particularly high shaft friction, reliance on natural roughening may be insufficient. This was the case for the Pluto Platform on the North West Shelf offshore Australia where the grouted piles were installed within high quality limestone. In this case a reaming tool was used to 'roughen' the hole wall by gouging circumferential 'grooves' in the hole wall at regular intervals [37].

With regard to pile performance, geotechnical models with a strong theoretical basis have been developed and utilised over the last 15 years for modelling pile interaction with carbonate materials. Models such as CYCLOPS and pCyCOS, both described in [36], define complex t-z and p-y load transfer algorithms that simulate both the non-linear and cyclic (softening) aspects observed in specialized laboratory element strength tests on carbonate materials. CYCLOPS can be applied in both cemented and uncemented soil, with parameters calibrated from CNS direct shear or simple shear tests, respectively. Conversely, pCyCOS only applies for uncemented soil, with static and cyclic simple shear tests defining the required input information. Where cemented materials are found near the surface, p-y models that can address potential brittle failure should be adopted instead. The 'CHIPPER' model [38] was developed for this purpose and accounts explicitly for wedges of 'chipped' material forming in the upper meters of the seabed below which 'full-flow' failure occurs. The p-y curves in this model incorporate both the brittle nature and the high compressibility that is typically found in many cemented carbonate sediments. Such models have been applied with great success to the design of piles offshore Australia and can be readily applied in other regions where carbonate sediments are prevalent or more generally for laterally loaded piles in weak rock.

6.1.3. Specific considerations related to axial capacity of piles in chalk

During driving of small-displacement piles in structured chalk, crushing occurs leading to the formation of an annulus of chalk 'putty' around the pile, which has significantly lower strength than the structured chalk. This is somewhat analogous to, but less extreme, than the processes that result in high sensitivity seen in many other types of carbonate soil, as discussed earlier. A similar local de-structured zone of width comparable to the pile wall thickness also occurs when driving piles into weak limestone. Allowing for this, common offshore design practice for axial capacity in chalk is to apply the recommendations of CIRIA [23]. These are based on a cautious interpretation of a small number of short-term static pile load tests, which lead to the adoption of unit shaft resistance values of 20 kPa in low to medium density chalk and 120 kPa in high density chalk, the lower value being particularly challenging for piles in the southern North Sea – and does not take account of the potentially highly significant magnitude of set-up that occurs in the chalk putty following pile installation.

Site-specific variations to the CIRIA limits have been proposed previously in [39], but still do not account for set-up. An approach outlined in [40] provides a framework for evaluating long-term pile shaft capacities in chalk, including set-up for the chalk putty annulus, and were calibrated to full-scale field testing from [41]. The procedures provide a more fundamental (and less cautious) approach to design than the CIRIA limits.

While the above relates to driven piles, drilled and grouted piles may also be used in chalk. Design requires the use of analysis calibrated to the (local) shear response of chalk as measured under CNS conditions – similar to that proposed in [22].

6.1.4. Other technologies

An approach to overcome the risk of premature refusal during driving is the 'drive-drill-drive' method, which has been successfully used for many years ([42], [43]). This technique was recently employed in carbonate sediments for a project on the North West Shelf of Australia [44], in this case utilizing a newly developed riserless drilling system. In this project, anchor piles were initially driven towards target penetration but with a

pre-determined limiting acceptable blow count. Where the limiting acceptable blow count was reached prior to target penetration, relief drilling was performed through the pile centre, after which driving was recommenced. The main risk with this approach is that if the piles are driven excessively hard before commencing drill-out, extrusion buckling of the pile may occur, which could then preclude a successful drilling operation. For this project extensive analysis was conducted to ensure that this risk was minimal for the prescribed acceptable blow count.

A less conventional approach, which may be viable where shallow strata contain only thin or weakly cemented layers, is the use of tubular piles that are driven closed-ended. This concept was proven and adopted successfully in calcareous sediments in the Campos Basin offshore Brazil [45], using a strengthened conical tip to close the tubular piles. Field data demonstrated improved axial shaft friction and also a significant increase in the end-bearing resistance that could be relied upon. Where such piles are driven through highly sensitive surficial sediments, consideration needs to be given to the more extensive zone of remolded soil that would form around the pile compared with an open-ended pile, which might compromise any required lateral resistance.

As an alternative to both driven and drilled and grouted piles, offshore versions based on onshore continuous flight auger piles are starting to be developed per [46], avoiding creation of an open hole and allowing a grouted pile to be constructed from seabed level.

6.2. Shallow foundations

Shallow foundations support a wide range in offshore structures – from large gravity structures to small subsea structures, and also including mudmats of piled jacket structures. Designs in carbonate soil tend to be bespoke, and are tailored to the specific challenges for each structure. This section build (in part) on previous discussion in [47].

6.2.1. Evolving use of shallow foundations

The late 1990s saw the adoption of large gravity structures in carbonate sediments for the first time. Two key structures include the West Tuna Platform for ExxonMobil [48] and the Wandoo B Platform for the Wandoo Alliance [49]. Foundation challenges are well documented for the Wandoo B platform, which is founded on a thin layer of carbonate sand overlying cemented strata. Dominated by large (environment) lateral loads, and varying on-bottom weight in response to GBS storage needs, the sensitivity of the sand to cyclic loading was a critical consideration. To maximize the sliding resistance, the underside of the base was roughened (maximizing the interface friction), and a drainage blanket was used to minimize the build up of excess pore pressure (thereby reducing the equivalent number of cycles, and hence the degradation of strength). Scour protection, comprising placed rock, was used to mitigate the risk of undermining of the foundation.

A more recent large gravity structure is the Wheatstone Platform, which moved away from concrete to adopt a steel substructure design. In this case, the foundation design took advantage of a region of weakly cemented seabed to allow the platform to be supported on (individual) shallow foundations. The seabed required placement of a rock blanket and, similar to Wandoo B, scour protection was used to protect both the blanket and the surficial sand. In optimizing the foundation design, the effect of

consolidation under the weight of the structure, cyclic loading and post-peak behavior of the cemented sediment were all addressed explicitly.

Other steel gravity platforms include the Yolla A Platform [25] and more recently the Ichthys Riser Support Structure [50]. Both of these structures are on much softer sediments than the foregoing cases and therefore utilize deep skirts penetrating into seabeds comprising uncemented carbonate muds, silts and sand through a combination of self-weight and suction. In each case, the design was undertaken through a combination of analytical and numerical approaches, with both capacity and settlement addressed. For the Ichthys RSS in particular, seismic design proved particularly challenging [51]. Although Australia is not in general a highly seismic area, there is sufficient seismic activity in northern areas under the rare ductility level events to cause a significant problem in the very soft, uncemented carbonate sediments that are generally highly susceptible to liquefaction [52].

As the offshore sector pushes into deeper water, shallow foundation design has shifted to that needed to support subsea structures. A typical development requires a large number of seabed structures, with foundations ranging from small seabed structures to support individual valves to large structures supporting complex manifold systems. Foundation design needs to address installation (including the penetration of skirts where used) and capacity issues, the latter allowing for cyclic degradation. Of particular importance is the assessment of settlement, including that resulting from self-weight consolidation as well as from design events such as earthquakes, and reliable estimates of lifetime settlement is needed in order to ensure the integrity of connectors between individual structures.

Figure 17 illustrates the evolving use of shallow foundations in carbonate sediments.

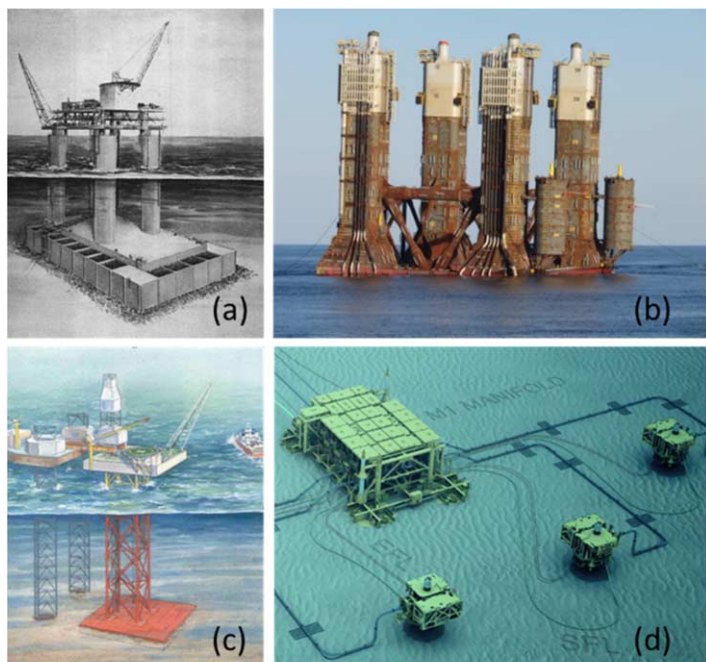


Figure 17. Shallow foundations in carbonate sediments, (a) Wandoo B CGS [49]; (b) Wheatstone Platform [53]; (c) Yolla A Platform [25]; (d) Gorgon subsea manifold [54].

6.2.2. Select aspects of design

While many of the design issues associated with shallow foundations are not unique to carbonate sediments, the properties of such materials can lead to a need for bespoke design methods. Consideration is now routinely given to the incorporation of strength increase due to consolidation, and design tools exist to capture the effects of cyclic loading in an efficient way, both of which lead to smaller foundations being acceptable. However, there are aspects that require specific attention, and are worth capturing here:

- Installation considerations are important for shallow foundations. For instance, local variability may impact the penetration of skirts, while low strength at mudline or insufficient drainage can lead to aquaplaning or higher than anticipated initial embedment.
- Noted previously, settlement is a key consideration – and is especially important when considering its impact on tie-in spools (or other stiff connections). While calculation approaches are relatively standard, it can be challenging to determine appropriate input parameters for carbonate sediments. A particular challenge is the case of settlement after seismic events – whereby excess pore pressures are generated in the seabed that, while perhaps not leading to liquefaction or flow failure, still result in large post-event settlement. This may vary significantly between structures, leading to stress on connectors.
- Subsea systems are required to accommodate large axial expansion of pipelines, associated with thermal effects. While it may be possible to accommodate this through design of the structure, another option is to allow the foundation to slide directly on the seabed. The key consideration in this case is ensuring that over the life of the development, and for the full range of thermal expansions (which may be several meters), the foundation does not penetrate excessively into the seabed. The critical design considerations for such foundations are discussed in [55] and, in accordance with these, several structures of this type have now been installed in carbonate sediments.
- While sliding foundations are required to accommodate large movements, opportunities also exist in regards the development of ‘compliant foundations’. This is particularly important in the design of manifolds, or other subsea structures that include a number of tie-in spools. Loads associated with tie-in and operation can be a high proportion of the design loads – but reduce significantly in response to (small) foundation movement. Accordingly, allowing for the ‘compliance’ of the foundation can significantly reduce the requirements for foundation design and in turn, lead to more cost-effective outcomes.
- The potential for scour to influence the performance of shallow foundations is well understood. Traditional design approaches are based on assessing the susceptibility of the soil at seabed to scour and, where deemed necessary, the installation of scour protection – such as rock blankets or concrete mats. It was noted in Section 4.7 (Figure 15) that for specific particle size ranges, carbonate sediments demonstrate greater resistance to scour than silica materials of comparable (silt to sand) particle size. This can be assessed for individual sites, with testing extended to assess not just the threshold but also the rate at which scour will occur. In some cases, this can lead to opportunities (via adoption of probabilistic approaches) to avoid early placement of scour protection, and adopt a ‘wait and see’ (i.e. observational design) approach [56].

6.3. Spudcan foundations

The installation of jack up rigs on uncemented silty carbonate sediments has proven to be challenging, with key considerations being the assessment of spudcan penetration during installation and preloading, and spudcan capacity under storm loading.

6.3.1. Penetration

In regards to spudcan penetration, the key risks relate to the potential for deeper than expected penetration and unexpected punch-through events, driven by the high sensitivity and transitional drainage conditions often associated with carbonate sediments. Case histories where this has proven significant are presented in [57], from jack up rigs installed off south east Australia. For one of these cases, where the jackup was installed adjacent to the Yolla A Platform, unexpectedly large penetrations occurred as the maximum preload was approached - with punch-through involving a ‘free-fall’ of about 4 m for each spudcan. Significant tilt of the jack up rig occurred, with the rig itself coming to within a few meters of the Yolla A Platform topside. Following the punch through, each spudcan was successfully loaded to the maximum preload with minimal additional penetration.

In this case, it is important to note that punch-through was not predicted, despite assessments being made by multiple parties, and the presence of high quality in situ (and laboratory) test data. Based on the lessons learned, [57] proposed an approach to assess spudcan resistance to penetration based directly on in situ T-bar penetrometer data, and take account of (i) consolidation properties and drainage behavior, (ii) rate effects, and (iii) geometry effects.

A second phase of jackup operations occurred at the Yolla A Platform location, with spudcans installed through the existing crater, as described in [58]. Given the complexity of this operation, and inherent risks to the adjacent platform from further punch-through, a rigorous design approach involving both analytical and large deformation finite element analysis was adopted. These studies confirmed and highlighted the significant impact that the high sensitivity and transitional drainage conditions have on the spudcan penetration response in such soils.

The other significant case study presented in [57] was from a nearby site (Trefoil). At that location, initial static preloading led to legs at very different depths, which was deemed unacceptable. A program of cyclic preloading was therefore undertaken at the site, where the ‘high’ legs were cycled as rapidly as possible (albeit only about 1 or 2 cycles per hour). Eventually, all legs were lowered to an acceptable level using this approach, as a result of soil softening induced by the cyclic loads. This was considered a great success, but also an alarming surprise to the jackup owner, who had never encountered such ‘unusual’ soil behavior before. It should be appreciated that cyclic preloading of this type can cause significant structural distress to a jackup rig and it is recommended that appropriate geotechnical and structural studies should be conducted to confirm the safe operating limits prior to any such operation.

6.3.2. Capacity under storm loading

Similar to the design of shallow foundations, the offsetting effects of strength gain due to consolidation (under self-weight) and cyclic degradation need to be addressed when assessing the response of spudcans under the imposed loads from storms.

Assessment of spudcan capacity is typically undertaken using the approaches in [59], where the applied preload is used to anchor the size of a foundation yield envelope, from which the applicable material factor under storm loads is determined. However, this approach does not account for either consolidation or cyclic loading effects. Accordingly, a 'Modified SNAME' approach was proposed in [57], where the measured preload is replaced with a calculated vertical capacity that accounts for both consolidation and cyclic degradation. Since a calculated (rather than measured) capacity is used to anchor the yield envelope in this case, a higher material factor is appropriate and is specified to be consistent with 'conventional' design practice for most offshore shallow foundations.

This approach has been adopted successfully for multiple jack up rig installations conducted offshore Australia, as reported for example in [60] and [61].

6.4. Anchoring solutions

Anchoring of floating facilities, whether for temporary (such as exploration drilling) or permanent (such as for production facilities) purposes, requires design approaches that address both the characteristics of the seabed and the applied loading conditions. This section outlines considerations for common anchor types.

6.4.1. Drag anchors

The design of drag embedment anchors requires a thorough understanding of anchor behavior in various soil conditions, in order to ensure an adequate margin of safety in the anchor holding capacity and to ensure that no anchor movement ('dragging') occurs during a design storm event. This is particularly important for carbonate sediments, where the complex interacting effects of sensitivity, consolidation and cyclic loading will dictate the minimum level of preload at installation that is required to ensure no in-place anchor movement. Importantly, for carbonate sediments, the combination of these effects often results in drag anchor preload levels exceeding the in-place design loads, as outlined in [62] and [63], a situation that is rarely found in other soil types.

Drag anchors are also susceptible to premature refusal (i.e. insufficient embedment during installation) in layered soil profiles, which is a common feature of carbonate sediments – where such layering often takes the form of shallow cemented horizons. In this scenario, the resistance offered by the cemented materials may be sufficient to prevent the anchor fluke tips from embedding through the horizon, resulting in the fluke tips 'scraping' along the 'weak-strong' interface, and the anchor being unable to attain the required preload.

A similar but more subtle scenario can occur in carbonate soils with transitional drainage conditions, where drained (i.e. 'strong') soil resistance is mobilized on the shank but undrained (i.e. 'weak') soil resistance is mobilized on the fluke. In fact, this appears to be the critical mechanism in many drag anchor installations and seems to explain the often very low anchor efficiencies (i.e. ratio of static capacity to weight) that has been reported during field installations in carbonate soil.

6.4.2. Anchor piles

Despite a well-documented history of problems associated with driving piles into carbonate sediments, large diameter driven piles have recently been used successfully in seabeds comprising highly variable weak carbonate sediments [31]. Design issues for

such anchors include pile free-fall during installation, driving through localized hard (cemented) layers, the assessment of the pile in-place lateral and axial response, and assessment of the post-seismic response of the pile.

Special consideration must be given to the influence of the embedded portion of the anchor chain – where locating the anchor pad eye below mudline level may lead to excessive uplift loads due to low shaft resistance. While the simplest solution for this is to move the pad eye close to mudline, this is inefficient in terms of lateral capacity. Drilled and grouted piles may be considered in this case in order to enhance the axial capacity, although this introduces other installation challenges in uncemented soils. For cemented seabeds, drilled and grouted piles are generally a preferred anchoring option and can now be installed using riserless heave-compensated reverse circulation drilling equipment (as in [44]).

6.4.3. Suction anchors

Suction caisson anchors have also been installed successfully in carbonate sediments, where seabeds have comprised predominately softer materials, per [64], [65] and [66]. Due to the low shaft friction offered by carbonate sediments, suction anchors can have reduced application in deeper waters where semi-taut or taut mooring configurations are generally adopted, as applied vertical loads (at the pad eye) are long term and rely on frictional resistance to provide stability. However, should the vertical loads be of a transient nature (as for catenary moorings) then suction may provide adequate resistance.

6.5. Pipelines

The design of an untrenched (or surface laid) pipeline must account for how it interacts with the seabed as it is loaded by waves and currents, experiences cycles of heating and cooling, and is required spans over an uneven seabed (affecting pipeline fatigue). Geotechnical design input is normally provided in terms of ‘friction factors’, which quantify the limiting soil resistance (relative to its own self-weight) when the pipeline moves laterally or axially on the seabed, and in terms of soil springs describing how the lateral, axial, and vertical soil resistance changes as a function of pipeline displacement and through cycles of loading.

Despite increased documentation of approaches to assess pipe-soil interaction (as in [67], [68]) many of the methodologies are disputed. Importantly, guidelines provided in key codes are rarely appropriate for carbonate sediment conditions [69]. This was stated explicitly in the now superseded [70] where it was stated that “*Special considerations should be made if the sand contains a high fraction of calcium carbonate*”. While this text was not included in the more recent code [71], the same carbonate sediment section from the earlier document is included.

With specific regard to the properties of carbonate sediments vs non-carbonate soil, the following is noted in regard to surface-laid pipelines:

- Higher sensitivity results in deeper as-laid embedment for surface-laid pipelines in carbonate sediment [72], in particular carbonate silts that can be subject to greater water entrainment effects than non-carbonate fine-grained soils. Calculations must include consideration of ‘apparent’ S_t values, which may be greater than measured values in a laboratory fall cone or miniature vane device. Calibration of as-laid embedment methods may be informed by back-analysis

- of lay records for nearby pipelines, but needs to account for differences in seastate conditions and/or lay vessel characteristics.
- Higher angles of internal friction (due to grain angularity) and higher pipe-soil interface shear resistances often leads to higher axial and lateral seabed resistances – although specialized laboratory interface testing [73] is required to measure this directly.
 - Drainage conditions may vary for different pipeline loading events in carbonate sediment, depending on the load duration, the drainage path length and the soil c_v . For instance, carbonate silty sands are likely to behave in an undrained to partly drained manner during a wave loading event, though may be fully drained during a slow (multi-hour) axial pipeline expansion – and design methods must encompass this transitional behavior rather than assuming (for example) that any ‘sand’ is drained. Drainage conditions in shallow sediments are best assessed using specialist in situ tools [74].
 - As highlighted earlier, high spatial variability may be expected along the pipeline length, while variability may also occur within individual zones. Soil parameter ranges are often wide compared to uniform soil deposits, and the ranges of associated pipeline design parameters must take account of this. Since both low and high seabed resistance may govern design as outlined in [75], statistical approaches to assess the pipe-soil resistance parameters are often used to narrow ranges for input to structural reliability analysis.
 - Outcropping (and shallow subcropping) cemented layers are common in shallow and intermediate water depths. Rock-pipeline interface friction coefficients will depend on the level of rock cementation, the pipeline surface coating roughness and the anticipated normal contact force between the pipeline and rock surface and may vary from other rock types. Site-specific rock-pipeline interface testing is required. Consideration should also be given to the influence of macroscale features - extremely outcropping (extending above seabed) can act to constrain the pipeline from lateral movement.
 - Seabed mobility may lead to changes in pipeline burial state after lay, which can vary both spatially and temporally through the life of operation ([26]). These changes may have to be accounted for to provide inputs to ensure effective thermal management (lateral buckling, end-expansion, pipeline walking), as outlined in [76], or can potentially be ‘banked’ to improve long-term hydrodynamic stability per [77].

Reliable, fit-for-purpose, inputs to pipeline design can be generated for carbonate sediment conditions, by considering the above differences and performing the following activities:

- Zoning the site by integration of geophysical and geotechnical information along the pipeline length (as illustrated in Figure 18 after [78]) and ensuring appropriate geophysical and geotechnical investigation is conducted.
- Conducting appropriate advanced element testing (such as interface testing, strength testing, c_v measurement) combined with in situ testing to provide site-specific (and pipeline-relevant) ranges of seabed parameters.
- Using calculation methods that explicitly account for the relevant mechanical properties of the seabed. Ideally such approaches will have a sound theoretical basis (such as the failure approach for lateral breakout resistance calculation

proposed by [79]), although where semi-empirical methods are used they should be based on evidence on similar carbonate sediments. This can include project-specific centrifuge testing, as outlined in [80].

- Accounting for the drainage conditions experienced by the pipeline in different design conditions.
- Considering of sediment mobility effects.
- Employing statistical methods (such as Monte Carlo analysis) to quantify the output design ranges for the specific probability levels required by the project. This will typically narrow the adopted design ranges, by reducing the influence of unrealistic (extreme) parameter combinations.

As a final comment, when approaches have been used that do not take account of the key difference in dealing with carbonate sediments, regular inspection of operational pipelines is recommended to ensure that the embedment conditions are as anticipated and that the pipeline is responding as expected.

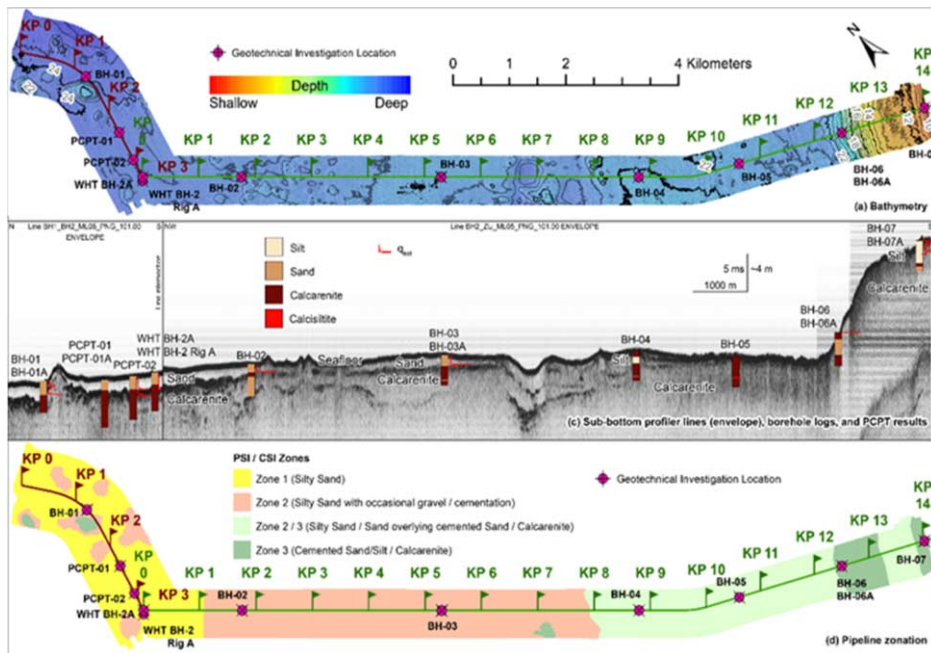


Figure 18. An example of seabed zonation along a pipeline in carbonate sediment conditions after [78] showing (a) bathymetry; (b) sub-bottom profile; and (c) zonation.

7. Concluding remarks

Soils with moderate to high carbonate content are prevalent in many regions of the world offshore, especially in mid latitudes. In this paper we have focused on sediments with high carbonate content and have summarized selective important characteristics – such as the high spatial variability, varying levels of cementation, high compressibility, high shear resistance, high sensitivity, often transitional drainage conditions and propensity for cyclic degradation. We have then explained how these characteristics have important

influences on the selection and behavior of appropriate foundation and pipeline systems for a variety of conditions.

The presence of such materials has had an important influence on many oil and gas projects and is likely to become important for the renewable industry as it moves into new territory – although the challenges are not unique to these sectors.

The last 30 (or so) years has seen substantially increased exposure and experience in dealing with carbonate sediments, from characterization to foundation performance, and many lessons have been learned. However, there continue to be challenges – and it is important to remain vigilant when dealing with carbonate sediments.

Acknowledgements

We acknowledge the support of Fugro colleagues including Neil Winman, Bryan Bergkamp, Steve Varnell, KC Gan, Yosmel Sanchez, Shailesh Singh and Romain Clavaud. Additionally, we recognize the contribution of Shambhu Sharma (formerly Fugro). Phil Watson acknowledges the support of Shell Australia, provided via the Shell Chair of Offshore Engineering at UWA. Fraser Bransby acknowledges the support of Fugro, provided via the Fugro Chair in Geotechnics at UWA.

References

- [1] Jewell, R.J and Andrews, D.C. 1988. Engineering for calcareous sediments: Proceedings of the International Conference on Calcareous Sediments, Perth.
- [2] Al-Shafei, K.A. 1999. Engineering for Calcareous Sediments: Proceedings of the Second International Conference on Engineering for Calcareous Sediments, Bahrain.
- [3] Le Tirant, P. and Nauroy, J-F. 1994. Foundations in carbonate soils, Editions Technip, Paris.
- [4] Clarke, A.R. and Walker, B.F. 1977. A proposed scheme for the classification and nomenclature for use in the engineering description on Middle Eastern sedimentary rocks, *Geotechnique*, 27(1), 93-99.
- [5] Lein A. Y., 2004. Authigenic Carbonate Formation in the Ocean. *Lithology and Mineral Resources* Vol 39, pp. 3-35.
- [6] Roberts, H.H., P. Ahern, J. Carney, J. Larkin, and R. Sassen, 1990. Seafloor responses to hydrocarbon seeps, *Texas Continental Slope: Geo Marine Letters*, Vol 10, pp. 232-243.
- [7] McConnell, D., Gharib, J., Henderson, J., Danque, H.W., Digby, A., and Orange, D., 2008. Seep-hunting in deepwater for frontier basin prospectivity assessment. *World oil*, 229(4).
- [8] Clarke, P. U., Dyke, A. S., Shakun, J. D., Carlson, A. E., Clark, J., Wohlfarth, B., Mitrovica, J. X., Hostetler, S. W., McCabe, A. M., 2009. The Last Glacial Maximum. *Science* Vol 325, pp. 710-714.
- [9] Hogan, P. Finnie, I., Tyler, S. and Hengesh, J. 2017. Geohazards of the North West Shelf Australia, Offshore Site Investigation and Geotechnics, Proceedings of the 8th International Conference, London.
- [10] Jewell, R.J and Khorshid, M.S. 1988. Engineering for calcareous sediments, Volume 2 – North Rankin ‘A’ Foundation Project, State of the Art Reports, Perth.
- [11] <http://www.geologypage.com/2016/05/the-pinnacles-western-australia.html>
- [12] Murff, J.D. 1987. Pile capacity in calcareous sands: State of the art, *J. Geotech. Engrg.* 113(5), 490-507.
- [13] Morrison, M.J. and Machado, C.F. 1986. Generalised soil conditions encountered in the Campos and Sergipe Basins, Offshore Brazil, Offshore Technology Conference, Houston, Texas.
- [14] Heubeck, C. 1992. Sedimentology of large olistoliths, South Cordillera Central, Hispaniola, *J. Sedimentary Petrology*, 63(3), 474-482.
- [15] Playton, T. 2008. Characterisation, variations and controls on reef rimmed carbonate foreslopes, PhD. UTexas, Austin.
- [16] Milliman, J.D. 1972. Atlantic Continental Shelf and Slope of the United States - Petrology of the Sand Fraction of Sediments, Northern New Jersey to Southern Florida, Geological Survey Professional Paper 529-J.

- [17] Valent, P.J., Altschaeffl, A.G. and Lee, H.J. 1982. Geotechnical properties of two calcareous oozes, Geotechnical properties, behaviours and performance of calcareous soils, ASTM STP 777, K.R. Demar and R.C. Chaney, Eds., ASTM, 1982, 79-95.
- [18] Lunne, T., Robertson, P.K. and Powell, J.J.M. 1997. Cone Penetration Testing in Geotechnical Practice, Blackie Academic and Professional, London
- [19] Randolph, M.F., Hefer, P.A., Geise, J.M. and Watson, P.G. 1998. Improved seabed strength profiling using T-bar penetrometer, Proc Int. Conf. Offshore Site Investigation and Foundation Behaviour - "New Frontiers", Society for Underwater Technology, London, 221-235.
- [20] Abbs, A.F. 1992. Design of grouted offshore piles in calcareous soils, 6th ANZ Conference on Geomechanics, Christchurch.
- [21] Joer, H.A. and Randolph, M.F. 1994. Modelling of the shaft capacity of grouted driven piles in calcareous soil, Int Conf on Design and Construction of Deep Foundations, Orlando.
- [22] Randolph M.F., Joer H.A. and Airey D.W. 1998. Foundation design in cemented sands, 2nd Int. Seminar on Hard Soils, Soft Rocks, Naples, Vol. 3, pp 1373-1387.
- [23] Lord, J.A., Clayton, C.R.I. and Mortimore, R.N. 2002. Engineering in Chalk, CIRIA
- [24] Flores Lopex, F.A., Taboada, V.M., Gonzalez Ramirez, Z.X., Cruz Roque, D and Barrera Nabor, P. 2018. Normalised modulus reduction and damping ratio curves for Bay of Campeche carbonate sand, Offshore Technology Conference, Houston.
- [25] Watson, P.G. and Humpheson, C. 2007. Foundation design and installation of the Yolla A Platform, 6th Int. Conf. on Offshore Site Investigation and Geotechnics, London, UK.
- [26] Leckie, S.H.F., Draper, S., White, D.J., Cheng, L. and Fogliani, A. 2015. Lifelong embedment and spanning of a pipeline on a mobile seabed, Coastal Engineering, Vol. 95, pp. 130-146.
- [27] Mohr, H. Draper, S. Cheng, L and White, D.J. 2016. Predicting the rate of scour beneath subsea pipelines in marine sediments under steady flow conditions, Coastal Engineering, Vol 110, pp 111-126.
- [28] Soulsby, R.L. and Whitehouse, R.J.S. 1997. Threshold of sediment motion in coastal environments, Pacific Coasts and Ports' 97: Proc. of the 13th Australasian Coastal and Ocean Engineering Conference and the 6th Australasian Port and Harbour Conference; Volume 1, Centre for Advanced Engineering, University of Canterbury.
- [29] Joer, H., Sharma, S. and Le, F. 2013. Problems in testing of carbonate sediments, Australian Geomechanics, Vol. 48 No. 4.
- [30] Banimahd, M., Chow, F.C., Tyler, S. Senders, M and Stewart-Wynne, R. 2017. Hold-back anchor piles with free-fall potential on the Australian North-West Shelf, Proc. 8th Int. Conf. on Offshore Site Investigation and Geotechnics, Vol. 2, pp. 1198-1205.
- [31] Erbrich, C., Lam, S.Y., Zhu, H., Derache, A., Sato, A. and Al-Shawaiter, A. 2017. Geotechnical Design of Anchor Piles for Ichthys CPF and FPSO, Proc. 8th Int. Conf. on Offshore Site Investigation and Geotechnics, Vol. 2, pp. 1186-1197.
- [32] Boylan, N., Roux, A., Colliat-Dangus, J-L and Sato, A. 2017. Installation response of 5.5 m diameter anchor piles in carbonate soils – the Ichthys development, Proc. 8th Int. Conf. on Offshore Site Investigation and Geotechnics, Vol. 2, pp. 674-681.
- [33] Barbour, R.J. and Erbrich, C., 1994. Analysis of In-situ Reformation of Flattened Large Diameter Foundation Piles Using ABAQUS, UK ABAQUS Users Conference, September 1994, Oxford, UK.
- [34] Stevens, R.F., Westgate, Z. and Kocjan, J. 2019. Assessing the Pile Driving Risk due to the Presence of Boulders, Offshore Technology Conference, Houston.
- [35] Erbrich, C.T., Barbosa-Cruz E and Barbour R. 2010. Soil Pile Interaction during Extrusion of an Initially Deformed Pile, Proc. 2nd International Symposium on Frontiers in Offshore Geotechnics, Perth, Australia.
- [36] Erbrich, C.T., O'Neill, M.P., Clancy, P. and Randolph, M.F. 2010. Axial and Lateral Pile Design in Carbonate Soils, Proc. 2nd International Symposium on Frontiers in Offshore Geotechnics, Perth, Australia.
- [37] Senders, M., Banimahd, M., Zhang, T. and Lane, A. 2013. Piled foundations on the North West Shelf, Australian Geomechanics Vol. 48, No. 4, 149-160 pp.
- [38] Erbrich, C.T. 2004. A new method for the design of laterally loaded anchor piles in soft rock. Offshore Technology Conference, Houston.
- [39] Carrington, T.M., Li, G. and Rattley, M.J. 2011. A new assessment of ultimate unit friction for driven piles in low to medium density chalk. Proc. European Conference on Soil Mechanics and Geotechnical Engineering, Athens.
- [40] Jardine, R.J., Buckley, R.M., Kontoe, S., Barbosa, P. and Schroeder, F.C. Behaviour of driven piles in chalk, Proc. of the Engineering in Chalk 2018 conference, London.
- [41] Barbosa, P., Geduhn, M., Jardine, R.J. and Schroeder, F.C. 2017. Large Scale Offshore Static Pile Tests – Practicality and Benefits, Proc. 8th Int. Conf. on Offshore Site Investigation and Geotechnics, London

- [42] Sullivan, R.A. and Ehlers, C.J. 1972. Practical Planning for Driving Offshore Pipe Piles, Offshore Technology Conference, Houston.
- [43] Stevens, R.F., Wiltsie, E.A., and Middlebrooks, J.R. 1984. Controlled Hard Driving, Proc 2nd International Conference on the Application of Stress Wave Theory on Piles, Stockholm.
- [44] Finnie, I., Gillinder, R., Richardson, M., Erbrich, C., Wilson, M., Chow, F., Banimahd, M. and Tyler, S. 2019. Design and Installation of Mobile Offshore Drilling Unit Mooring Piles using Innovative Drive-Drill-Drive Techniques, 13th Australia New Zealand Conference on Geomechanics, Perth.
- [45] Mello, J.R.C., Amaral, C.D.S., Costa, A.M., Rosas, M.M., Coelho, P.S.D. and Porto, E.C. 1989. Closed-ended pipe piles: testing and piling in calcareous sand, Proc Offshore Technology Conference, Houston.
- [46] Spagnoli, G. and Doherty, P. 2016. Comparison of two calcareous sands in relation to a novel offshore mixed-in-place pile, Oil Gas European Manazine 2/2016, pp 91-94.
- [47] Randolph, M., & Erbrich, C. 1999. Design of shallow foundations for calcareous sediments. Proc. Second International Conference on Engineering for Calcareous Sediments, Bahrain.
- [48] Titus, P.G. 1997. West Tuna, Bream B: Application of concrete technology offshore Australia. The APPEA Journal, 37(1) 546-559.
- [49] Humpheson, C. 1998. Foundation design of Wandoor B Concrete Gravity Structure, Proc. Offshore Site Investigation and Foundation Behavior, London, 353-382.
- [50] Lee, K.K., Erbrich, C.T., Aravind, M. and Ravappa, J.W. 2016. Foundation design and installation of the Ichthys Riser Support Structure. Offshore Technology Conference, Houston.
- [51] Erbrich, C. Wallbridge, P., Yamamoto, N. 2016. Numerical Modelling of Seismically Induced Settlement for Ichthys Riser Support Structure. Offshore Technology Conference Asia, Kuala Lumpur.
- [52] O'Driscoll, D., Yamamoto, N., Amadio, A., Bransby, M. F., Erbrich, C. T., & Westgate, Z. J. 2016. Seismic assessments for offshore shallow foundations in carbonate sediments. Offshore Technology Conference, Houston.
- [53] <https://hmc.heerema.com/projects/wheatstone/>
- [54] <https://www.chevron.com/stories/underneath-the-great-gorgon>
- [55] Deeks, A., Zhou, H., Krisdani, H., Bransby, F., and Watson, P. 2014. Design of direct on-seabed sliding foundations. ASME 2014, 33rd International Conference on Ocean, Offshore and Arctic Engineering.
- [56] Tom, J. Draper, S. White, D and O'Neill, M. 2016. Risk-based assessment of scour around subsea infrastructure, Offshore Technology Conference, Houston.
- [57] Erbrich CT. 2005. Australian Frontiers – Spudcans on the Edge, Int. Symposium on Frontiers in Offshore Geotechnics (ISFOG) 2005. Australia.
- [58] Erbrich CT, Amadio A, Lam, S, Krisdani H., Lam S., Xu X. and Tho K.K. 2015. Revisiting Yolla – New Insights on Spudcan Penetration. International Conference: The Jack-up Platform, London, UK
- [59] SNAME. 2008. Guidelines for Site Specific Assessments of Mobile Jack-up Units, The Society of Naval Architects and Marine Engineers. New Jersey.
- [60] Amadio A., Chang T.M., Kong V. and Erbrich C.T. 2015. The Effects of Jack-up Installation Procedures on Spudcan Capacity in Offshore Carbonate Sediments, The International Symposium on Frontiers in Offshore Geotechnics (ISFOG). Australia.
- [61] Amadio A., Erbrich CT., Murugavel V. and Moyle I. 2015. Re-visiting Yolla – Managing Storm Stability; Geotechnical Assessment. International Conference: The Jack-up Platform, London, UK.
- [62] Neubecker, S.R., O'Neill, M.P. and Erbrich, C.T. 2005. Preloading of Drag Anchors in Carbonate Sediments, Proc. Int. Symp. on Frontiers in Offshore Geotechnics: ISFOG 2005.
- [63] O'Neill, M.P., Neubecker, S.R. and Erbrich, C.T. 2010. Installation and In-Place Assessment of Drag Anchors in Carbonate Sediments, Proc. Int. Symp. on Frontiers in Offshore Geotechnics II: ISFOG 2010.
- [64] Randolph, M.F., O'Neill, M.P., Stewart, D.P. and Erbrich, C. 1998. Performance of Suction Anchors in Fine Grained Calcareous Soils, Offshore Technology Conference, Houston.
- [65] Erbrich, C. and Hefer, P. 2002. Installation of the Laminaria Suction Piles – a Case History, Offshore Technology Conference, Houston.
- [66] Frankenmolen, S.F., Erbrich, C.T. and Fearon, R.E. 2017. Successful Installation of Large Suction Caissons and Driven Piles in Carbonate Soils, Proc. 8th Int. Conf. on Offshore Site Investigation and Geotechnics, Vol. 1, pp. 539-548.
- [67] White, D.J., Clukey, E.C., Randolph, M.F., Boylan, N.P., Bransby, M.F., Zakeri, A., Hill, A.J. and Jaek, C. 2017. The State of Knowledge of Pipe-Soil Interaction for On-Bottom Pipeline Design. Offshore Technology Conference, Houston.
- [68] White, D., and Bransby, F. 2017. Pipe–Seabed Interaction, Encyclopedia of Maritime and Offshore Engineering, 1-25.
- [69] Zhang, J., Stewart, D.P. and Randolph, M.F. 2002. Modeling of shallowly embedded offshore pipelines in calcareous sand, J. Geotechnical and Geoenvironmental Engineering, ASCE, 128(5): 363–371
- [70] DNV-RP-F109. 2010. DNV-RP-F109. On-bottom Stability Design of Submarine Pipelines, DNV Recommended Practice.

- [71] DNVGL-RP-114. 2017. Pipe-soil interaction for submarine pipelines. Recommended practice, DNVGL.
- [72] Westgate, Z.J., White, D.J. and Randolph, M.F. 2012. Field observations of as-laid pipeline embedment in carbonate sediments. *Géotechnique* 62 (9), 787-798.
- [73] White, D.J., Campbell, M., Boylan, N., and Bransby, M.F. 2012. A new framework for axial pipe-soil resistance: illustrated by shearbox tests on carbonate soils, Proc. 8th Int. Conf. Offshore Site Investigation and Geotechnics, London: Society for Underwater Technology.
- [74] White, D.J., Stanier, S., O'Loughlin, C., Chow, S.H., Randolph, M., Draper, S., Mohr, H., John, M., Peuchen, J., Fearon, R., Roux, A., and Chow, F. 2017. Remote intelligent geotechnical seabed surveys – technology emerging from the RIGSS JIP, Offshore Site Investigation and Geotechnics: Smarter solutions for future offshore developments, London.
- [75] White, D.J., Westgate, Z.J., Ballard, J-C., de Brier, C., Bransby, M.F. 2015. Best practice geotechnical characterization and pipe-soil interaction analysis for HTHP design, Offshore Technology Conference, Houston.
- [76] Bransby, M. F., Borges Rodriguez, A., Zhou, H., Tom, J. and Low, H.E. 2014. Sediment Mobility Effects on Seabed Resistance for Unburied Pipelines, Offshore Technology Conference, Houston.
- [77] Griffiths, T., Draper, S., White, D., Cheng, L., An, H., and Fogliani, A. 2018. Improved Stability Design of Subsea Pipelines on Mobile Seabeds: Learnings From the STABLEpipe JIP, ASME 2018, 37th International Conference on Ocean, Offshore and Arctic Engineering.
- [78] Abdel-Hakim, M., Abdel Azeem, M., Bransby, F., Low, H. E., Clavaud, R., Bergkamp, B., and Kizhikkilod, J. 2018. Cost Savings for Subsea Pipelines Using Enhanced Pipe-Soil Interaction Assessment, Abu Dhabi International Petroleum Exhibition and Conference, SPE.
- [79] Randolph, M. F., and White, D. J. 2008. Upper-bound yield envelopes for pipelines at shallow embedment in clay, *Géotechnique*, 58(4), 297-301.
- [80] Bransby, M.F., White, D.J., Low, H.E. and Borges Rodriguez, A. 2013. The use of centrifuge model testing to provide geotechnical input parameters for pipeline engineering, OMAE2013-11484.

Technical Session #9 “Transportation in Geotechnics”



Erol TUTUMLUER

Dr. Erol Tutumluer is a Professor specializing in Transportation Geotechnics in the Department of Civil and Environmental Engineering (CEE) at the University of Illinois at Urbana-Champaign (UIUC). Professor Tutumluer holds Paul F. Kent Endowed Faculty Scholar and serves as the Director of International Programs. Dr. Tutumluer has research interests and expertise in characterization of pavement and railroad track geomaterials, i.e., subgrade soils and base/ballast unbound aggregates, soil/aggregate stabilization, geosynthetics, modeling granular foundation systems using innovative techniques, sustainable use of foundation geomaterials and construction practices for transportation infrastructure, discrete element analysis of ballast, dynamic response measurement and analyses of track systems, and mechanistic analysis and design. Dr. Tutumluer has served as an investigator on over 100 research projects and graduated 17 PhD and 39 MS students, and authored/co-authored over 300 peer reviewed publications from his research projects. Dr. Tutumluer is the Editor-in-Chief of the new Transportation Geotechnics Elsevier journal and he is the Chair of the ISSMGE Technical Committee 202 on Transportation Geotechnics. Dr. Tutumluer is a member of the ASCE T&DI and Geo-Institute and served as the Chair of the ASCE Geo-Institute's Pavements Committee in 2006-2012. He is a member of the AREMA Committee 1 on Ballast. Dr. Tutumluer is an active affiliate of the Transportation Research Board (TRB) and serves as the Chair of TRB's AFP00 Geological and Geoenvironmental Engineering Section. He served as the Chair of TRB's AFP70 Aggregates Committee in 2011-2016 and he is a member of the AFS70 Geosynthetics Committee. Dr. Tutumluer was the 2000 recipient of the TRB's Fred Burgraff award for Excellence in Transportation Research; he also received TRB's Geology and Earth Materials Section Best Paper Awards in 2009 and 2012 and TRB's Soil Mechanics Section Best Paper Award in 2016. He was selected and honored with Yangtze River Scholar Award by China Ministry of Education in 2016.

Sustainable Pavement Foundations with Chemically Stabilized Quarry By-Products

Erol TUTUMLUER^{a,1}, Issam QAMHIA^b, and Hasan OZER^c

^a Professor, Paul F. Kent Endowed Faculty Scholar

^b Postdoctoral Research Associate

^c Research Assistant Professor

Department of Civil and Environmental Engineering, University of Illinois at Urbana
Champaign. Urbana, Illinois – USA

Abstract. Quarry by-products (QB) are an industrial by-product of aggregate quarry processes. They are typically less than ¼ in. (6 mm) in size and consist of coarse, medium, and fine sand particles, and a small clay/silt fraction. Quarry by-products are found abundantly all over the crushed rock extraction facilities in Illinois where they are produced during blasting, crushing, washing, and screening operations. Recent research conducted at the Illinois Center for Transportation (ICT) has evaluated the characteristics of QB materials collected from different quarries across the State of Illinois, and studied potential uses of QB in pavement applications. Because the Unconfined Compressive Strength (UCS) for QB materials was quite low, Portland cement and Class C fly ash chemical admixture stabilizers were used to improve the strength properties of QB materials which resulted in 10 to 30 times increases in laboratory determined UCS compared to virgin unstabilized QB samples. Such significant increases observed in the strength of stabilized QB materials have indicated suitability of QB for sustainable pavement applications. Full-scale test sections were constructed next with chemically stabilized QB base/subbase applications over a subgrade having a California Bearing Ratio (CBR) of 6% to represent medium volume flexible pavement applications. The test sections were evaluated for performance using Accelerated Pavement Testing (APT), which spanned over two years to include effects of harsh winter freeze. Field testing and forensic analysis techniques included Falling Weight Deflectometer (FWD) tests before and after trafficking, hot mix asphalt coring, Dynamic Cone Penetrometer (DCP) profiling of subsurface layers, and trenching to determine actual thicknesses and contribution of each pavement layer to the measured surface rutting. In general, results from APT and forensic analyses indicated satisfactory results and improved rutting performance.

Keywords. Quarry By-products, Pavements, Accelerated Pavement Testing, Field Performance, Sustainability, Chemical Stabilization, Nondestructive Testing, DCP

1. Introduction

Quarry by-products, usually less than 6 mm in size, are produced during quarry operations such as blasting, crushing, screening, and washing. QB are mostly coarse-, medium-, and fine-grained sand particles, with a small fraction of silts and clays. QB can

¹ Corresponding Author, Department of Civil and Environmental Engineering, University of Illinois at Urbana-Champaign, 205 N. Mathews, Urbana, Illinois – USA, 61801; E-mail: tutumlu@illinois.edu.

exist in aggregate production sites in three distinct types: screenings, pond fines, and baghouse fines [1]. During the crushing stages, QBs are generally carried out in three stages, i.e. primary, secondary, and tertiary crushing [2].

The importance of utilizing aggregate quarry by-products in pavement applications stem from the vast quantities that are produced and remain excessive with many quarries each year. QB stockpiling and disposal is a serious issue facing the aggregate industry as they accumulate in stockpiles and interfere with quarry operations [3]. A report by the Federal Highway Administration estimated the quantity of quarry by-products generated in the United States each year to exceed 159 million metric tons, little of which is being put into use for pavement applications [1]. The same report also estimated that aggregate QB accumulation in the US alone exceeded 3.6 billion metric tons from the 3,000 operating quarries. In the state of Illinois, where this study was conducted, the annual production of crushed stone QB was estimated through a survey conducted among aggregate producers in the state and was found to be as high as 855,000 tons (950,000 US tons) [4]. Research conducted by Kumar and Hudson (1992) showed that stockpiled fines comprised an average of approximately 12% of the total annual aggregate production [5]. More recently, NCHRP Synthesis 435 (volume 4) reported that, depending on the type of rock quarried, QB could make up to 25% of the total aggregates produced [6].

Given these massive quantities, the investigation of successful applications of QB as a sustainable and inexpensive construction alternative for pavements has become imperative. However, only a few number of research studies have been conducted to date to evaluate the use of QB as a geotechnical pavement material in subbase or base applications, and especially the use of QB as an unbound material, which was found to be scarce in literature. NCHRP synthesis 435 (volume 4) being a main source of information on the QB use, summarizes the different QB applications in pavements by the different states in the US [6].

1.1. Laboratory characterization of stabilized QB materials

Based on laboratory testing results, some researchers have utilized chemical stabilization and accordingly recommended specific field applications for QB. According to Kalcheff and Machemehl (1980), the stabilization of QB with cement developed relatively high rigidity with a small amount of Portland cement compared with granular soil-cement stabilization [7]. The use of low-cement content has the advantage of decreasing the shrinkage cracking. Kumar and Hudson (1992) examined the unconfined compressive strength, tensile modulus of elasticity, and Poisson's ratio of cement-treated QB materials [5]. They concluded that stabilizing QB with cement could produce the adequate compressive strength, modulus of elasticity, and tensile strength required for subbase materials. They proposed a base course material additive, flowable fill, under slab granular fill, and cement-stabilized subbase/base layers as possible pavement applications of QB.

Stabilized QB mixes were also evaluated for applications such as flowable fills, soil modification and Self-Consolidating Concrete (SCC). According to the results presented in the study by Wood and Marek (1995), using 3% cement, 8% fly ash, and 89% QB resulted in a flowable fill with adequate performance [8]. Naik et al. (2005) examined the use of QB in SCC and reported that the addition of QB minimized the needed quantity of admixtures without reducing the strength of the SCC [9]. Koganti and Chappidi (2012)

reported that using up to 40% QB by weight proved to be beneficial in improving the strength of black cotton expansive soil [10].

Recent laboratory studies investigated the use of QB (or quarry fines) for pavement applications. Abdullah et al. (2018) conducted workability tests, flexural strength tests, and compressive strength tests on concrete samples with 100% quarry dust used for sand replacement in concrete [11]. The study concluded that concrete samples with 100% QB as fine aggregates produced more sustainable concrete samples with better durability, compressive strength and furnishing properties. The same study reported that concrete samples with QB had higher water absorption and workability at lower water cement ratios. Schankoski et al. (2017) evaluated the rheological properties of fresh cement paste with QB (diabase or gneiss quarry rock powders). They concluded that cement pastes containing QB had lower yield stress and lower viscosity than samples with cement pastes only [12].

Puppala et al. (2008) reported that the addition of 2.3% cement increased the unconfined compressive strength of QB materials to 174 psi (1,200 kPa). They concluded that the strength and resilient modulus of the cement-treated QB were similar to those of sandy materials with very few fines [13]. Mwumvaneza et al. (2015) conducted Unconfined Compressive Strength (UCS) tests on 10% Class 'C' fly ash and 2% Portland cement-stabilized QB samples, and they examined that the chemically stabilized QB specimens exhibited up to 30 times strength improvement when compared with untreated QB materials [14].

Finally, in a laboratory study conducted by LaHucik et al. (2016; 2016a), various proportions of cement-treated mixes of QB and Fractionated Reclaimed Asphalt Pavement (FRAP) or virgin coarse aggregates were evaluated [15, 16]. Based on aggregate packing tests conducted with different proportions of QB and FRAP by weight, an optimal blending ratio of 70% QB with 30% FRAP was found to maximize density/minimize void content. LaHucik et al. (2016) also evaluated mix design performances through strength tests (compression/split tension) and modulus tests. Higher cement content increased both the strength and elastic modulus properties of all the tested mixes. Mixtures containing virgin aggregates with QB yielded statistically greater elastic moduli than mixtures with FRAP and QB. Fibers were used as additives in some of the mixtures. From statistical analysis, the fibers did not have a considerable influence on strength or elastic modulus but did provide residual shear capacity across cracks. The QB and FRAP or QB and virgin aggregate mixtures with 3% to 4% cement content exceeded the strength of typical cement-stabilized base materials reported in the literature [15, 16].

1.2. Pavement applications of stabilized QB materials

Only few researchers in the United States have investigated the use of QB as a chemically stabilized base/subbase layer in pavement applications. In a study in Lynn County, Iowa, the use of emulsion-stabilized limestone screening was investigated as a base material [17]. Several test sections with base thicknesses of 4 to 6 in. (100 to 150 mm) and asphalt-cement contents of 2.5%, 3.5%, and 4.5% were inspected. The 4-in. (100-mm) thick base did not produce a satisfactory low cost maintenance roadway, based on periodic crack survey data and structural adequacy assessment using a Road Rater equipment. Thus, the researchers recommended a 6-in. (150-mm) thick emulsion-stabilized QB base with

more than 3.5% asphalt cement, topped with 2 in. (50 mm) HMA surface, which could provide a low maintenance roadway [17].

In a study in Arlington, Texas, the use of limestone QB was evaluated as a base material for sections of State Highway 360 [18]. A 36-in. (914-mm) thick layer of quarry fines stabilized with 2.3% cement was used as the base overlain by a 4-in. (102-mm) thick HMA and 8-in. (203-mm) thick Continuously Reinforced Concrete Pavement (CRCP) surface. Field monitoring using horizontal inclinometers showed that the sections experienced low permanent deformation during service. Additionally, the International Roughness Index (IRI) values were measured to be within 32-158 in./mile (0.5-2.5 m/km) after 30 months of service, which is lower than the threshold value of 200 in./mile (3.15 m/km), thus indicating good performance [18].

2. Studied aggregate quarry by-product applications

In total, seven pavement test sections investigating bound applications of aggregate quarry by-products were selected for performance evaluation. These applications were selected based on successful previous studies that provided initial evaluations of these applications through laboratory testing [4, 14, 15-16]. In light of the outcomes of these previous research projects, the following set of applications were selected for studying QB usage as chemically-stabilized materials:

- For base course applications, blending QB with coarse aggregate fractions of recycled materials [Fractionated Reclaimed Asphalt Pavements (FRAP) or Fractionated Recycled Concrete Aggregates (FRCA)] and stabilizing the blends with 3% cement or 10% class C fly ash by weight; and
- Using QB as a cement-treated base material; and
- Using QB as a cement or fly ash-treated subbase (i.e. in inverted pavements).

2.1. Materials selection

In total, five aggregate materials were collected to construct the test sections: one virgin aggregate material, two QB materials, and two recycled coarse aggregates. The two QB materials, i.e. QB2 and QB3, were obtained from quarries in Illinois near Thornton and Falling Springs, respectively. The FRAP originated from milling operations for an existing flexible pavement in Illinois, while the FRCA was obtained from a concrete recycling yard in Urbana, Illinois. The CA06_R material was a well-graded dolomite aggregate obtained from a quarry in Fairmont, Illinois and has a grain size distribution conforming to the Illinois Department of Transportation (IDOT) CA06 gradations for base course materials.

The grain size distributions of all aggregate materials and material blends used to construct the test sections are shown in Figure 1(a). Note that for test sections utilizing QB blended with coarse recycled aggregates, a central plant mix of 70% QB2 with 30% FRAP or FRCA by weight was brought to the construction site. The grain size distributions for these blends are shown in Figure 1(a). The Maximum Dry Densities (MDD) and Optimum Moisture Contents (OMC) for all material combinations used to construct the test sections were determined from laboratory testing using the standard

compaction effort as per ASTM D698. Figure 1(b) shows the moisture-density relationships for all material combinations used to construct full-scale pavement test sections.

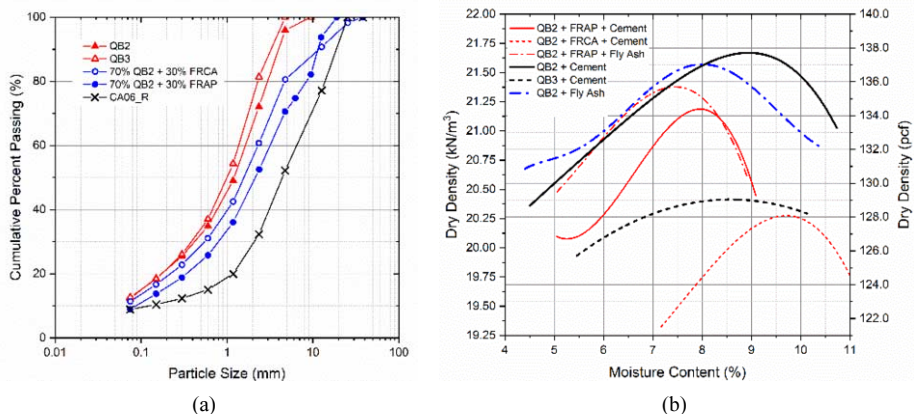


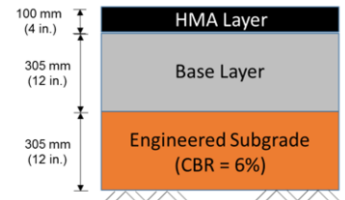
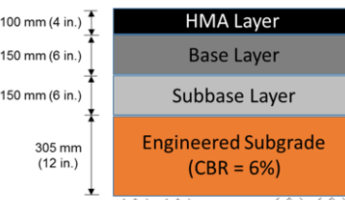
Figure 1. (a) Grain size distribution curves, and (b) moisture-density relationships for the various aggregate material combinations used in construct pavement test sections.

2.2. Details of constructed test sections

The construction of the pavement test sections took place at the accelerated pavement testing facility of Illinois Center for Transportation (ICT). In total, seven test sections were constructed to evaluate chemically stabilized applications of QB in base and subbase layers. All sections were constructed on top of a subgrade soil having an engineered CBR of 6%. The details of these sections are presented in Table 1. All base layers had a nominal design thickness of 12 in. (305 mm). For inverted pavement test sections (i.e. C3S2 and C3S3), the thicknesses of the base and subbase layers were 6 in. (152 mm) each. All test sections were overlain with 4 in. (102 mm) of Hot Mix Asphalt (HMA).

Note that the test sections presented in this paper are part of a larger study aimed to evaluate bound and unbound applications for quarry by-products by constructing 12 flexible pavement test sections and four unsurfaced construction platform sections. Four ‘test Cells’ (Cell 1S, 1N, 2 and 3), each having four test sections, were constructed for field evaluation. The sections presented in this paper are part of ‘Cell 2’ and ‘Cell 3’, which evaluated the performance of seven bound applications of QB and a conventional flexible pavement section. The details for the unbound QB applications evaluated were presented elsewhere [19, 20]. The beginning and end parts of each cell were designed to have 22.5 ft. (6.8 m) long crawler zones where the crawlers of the Accelerated Testing and Loading ASsembly (ATLAS) were placed. The innermost 7.5 ft. (2.3 m) in each crawler area was the speed stabilization zone for the acceleration/deceleration of the wheel to ensure that all test sections were tested at a constant speed of 5 mph (8 km/h). A 10 ft. (3 m) long transition zone was also added at the middle of each cell to minimize any possible influence of changing materials on the APT results.

Table 1. Base and subbase materials constructed in the test sections to study stabilized QB applications.

Section ID	Description	Pavement cross sections
C2S1	A blend of 70% QB2 and 30% Fractionated Reclaimed Asphalt Pavements (FRAP) by weight, mixed with 3% Type I cement by weight.	
C2S2	A blend of 70% QB2 and 30% Fractionated Recycled Concrete Aggregates (FRCA) by weight, mixed with 3% Type I cement by weight.	
C2S3	A blend of 70% QB2 and 30% FRAP by weight, mixed with 10% Class 'C' fly ash by weight.	All test sections (except C3S2 and C3S3)
C2S4	A Blend of QB2 and 3% Type I cement by weight.	
C3S1	A Blend of QB3 and 3% Type I cement by weight.	
C3S2	Subbase layer: A Blend of QB2 and 3% Type I cement by weight. Base layer: CA06_R (A dense-graded unbound dolomite aggregate layer conforming to the CA06 aggregate gradation band of the Illinois Department of Transportation)	C3S2 and C3S3
C3S3	Subbase layer: A Blend of QB2 and 10% Class 'C' fly ash by weight. Base layer: CA06_R	

2.3. Construction of test sections

The top 12 in. (305 mm) portion of the in situ subgrade at the full-scale testing site was prepared and engineered to a CBR of 6% by an iterative procedure. The desired CBR was achieved through the adjustment of the soil's moisture content and compaction levels. A moisture content of 12% and a dry density of 19.1 kN/m³ (121.6pcf) resulted in the targeted CBR of 6%. The details for the iterative procedure utilized for engineering the subgrade was presented elsewhere [19, 20]. Qamhia et al. (2019) presented the achieved subgrade CBR at the various measuring points [21].

QB2 blends with FRAP and FRCA for test sections C2S1, C2S2, and C2S3 were plant-mixed in a local asphalt plant and then delivered to the construction site. To ensure proper setting and curing of the test sections, a maximum of two hours was allowed between mixing with the stabilizing agent and compaction. For the purpose of this project, where relatively small road sections were constructed with each material, the construction procedure involved the following steps: (1) stockpiles of known volumes of the QB materials or QB blends with FRAP/FRCA were dry-mixed using the bucket of a backhoe to ensure the consistencies of targeted moisture contents and particle size distributions, (2) moisture samples were collected to measure the in situ moisture

contents, and calculate the dry weights of the stockpiles accordingly, (3) the stabilizing agent (3% cement or 10% fly ash, by weight) was added and mixed several times, for uniformity, using a backhoe bucket, (4) additional moisture was added, as needed, to adjust the moisture content to the optimum moisture content, and the blends were further mixed to uniformly distribute the moisture and the stabilizing agent, (5) the mixes were placed and tilled several times for mixing uniformity using a soil tiller, then compacted using a smooth-drum vibratory roller. The test sections were typically constructed and compacted in 152-mm (6-in.) lifts. Construction steps involved in constructing the chemically stabilized layers are presented in Figure 2. Note that the use of a pugmill mixer or a single shaft travelling mixer is recommended to achieve better blending for a larger scale construction.



Figure 2. Construction steps of chemically stabilized test sections studying QB applications.

Finally, the HMA structural layer was paved in two equal 50-mm (2-in.) thick layers. The same mix design was used for both layers. The mix design had an asphalt binder with a Performance Grade of PG 64-22 and a 9.5-mm (0.375-in.) nominal aggregate size.

3. Performance monitoring and evaluation

3.1. Accelerated pavement testing conditions

The constructed test sections were monitored for performance through accelerated pavement testing (APT). Heavy vehicle loads were applied using the Accelerated

Transportation Loading ASsembly (ATLAS). A super-single tire (455/55R22.5) was used to traffic the test sections. The first number (455) refers to the tire width from wall to wall in mm, the second number (55) corresponds to the side wall height expressed as a percentage of tire width, and the third number (22.5) is the rim diameter in inches.

A constant unidirectional wheel load of 10 kip (44.5 kN), a tire pressure of 110 psi (760 kPa), and a constant speed of 5 mph (8 km/h) were assigned to load the constructed sections, and to evaluate their rutting potential. Channelized wheel loading was applied with no wander considered. Once the test sections were done receiving 100,000 wheel passes at the above listed standard load/pressure, the wheel load was increased to 14 kips (62.3 kN) and the tire pressure was increased to 125 psi (862 kPa), and additional 35,000 passes were applied at these increased load/pressure levels.

3.2. Surface rutting accumulation and subgrade pressures

Performance monitoring was accomplished by periodic surface profile measurements after a certain number of passes. The transverse surface rut profile measurements for the HMA-surfaced test sections were measured using an automated laser profiler. Transverse rut measurements at the two measuring points in each test section were taken up to a distance of 16 in. (405 mm) on each side of the centerline of the wheel path. At each measuring point, a total of six 31.9 in. (810 mm) lateral scans were performed at 0.2 in. (5 mm) spacing, and the rut depth was reported as the average rutting of the centermost 11.8 in (300 mm) of the wheel path from the six measurements.

Comparisons of maximum wheel path rutting progressions of the test sections intended to study chemically stabilized layer applications of QB, are made in Figure 3. Overall, for the stabilized sections, the two sections chemically stabilized with 10% class 'C' fly ash (C2S3 and C3S3) consistently accumulated higher rut amounts and showed higher rates of rutting progression at the increased load level when compared to the other test sections chemically stabilized with 3% Portland cement. For the two sections, intended to study the effect of QB source, i.e. C2S4 with cement-stabilized QB2 base and C3S1 with cement-stabilized QB3 base, the trends of rutting progression were similar, indicating little effect of the source of QB on performance. Further, satisfactory rut performance was achieved for C3S2 inverted test section with a cement-stabilized QB subbase. The best performances with the lowest rut amounts were obtained for C2S1 and C2S2 having stabilized base courses of the QB blends with FRAP/FRCA, and the highest rutting accumulation was observed for C3S3 with a fly ash-stabilized QB subbase.

Three of the test sections with stabilized QB applications, namely C2S1, C2S4, and C3S2, had soil pressure cells installed on top of the subgrade to measure the vertical stress on top of the subgrade. A comparison of the measured wheel load deviator stresses on top of the subgrade for these test sections is presented in Figure 4. These test sections with stiff chemically stabilized QB base/subbase layers consistently recorded low pressures on top of the subgrade, indicating negligible subgrade rutting; which was also validated from the trenches which showed no signs of subgrade rutting. Note that a conventional test section with the same layer thicknesses and subgrade properties had significantly higher measured vertical pressures on top of subgrade of around 9 psi (61 kPa). Clearly, the stiffer stabilized base materials are changing the mechanism of stress distribution in the pavement structure, allocating a higher share of the load to the stiffer base/subbase layers, and thus reducing subgrade pressures and subgrade rutting potential.

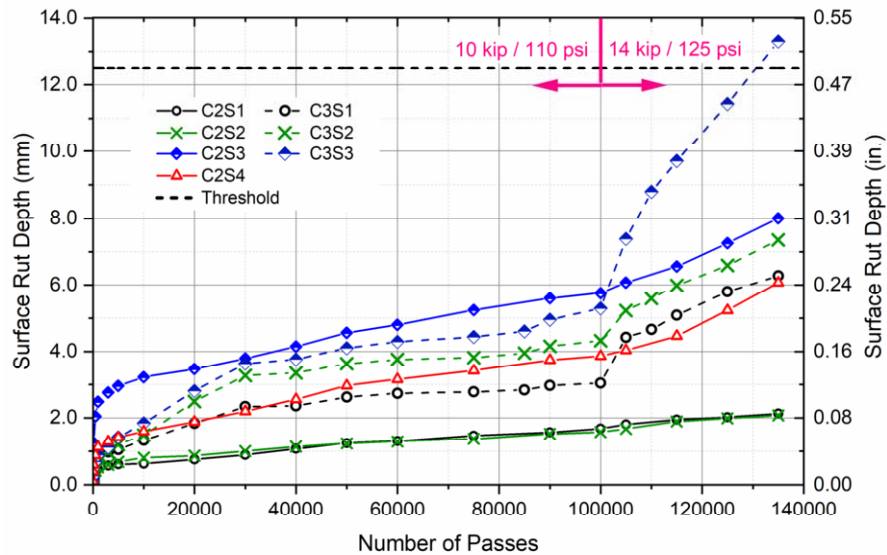


Figure 3. Wheel path maximum rut progression in test sections utilizing QB applications.

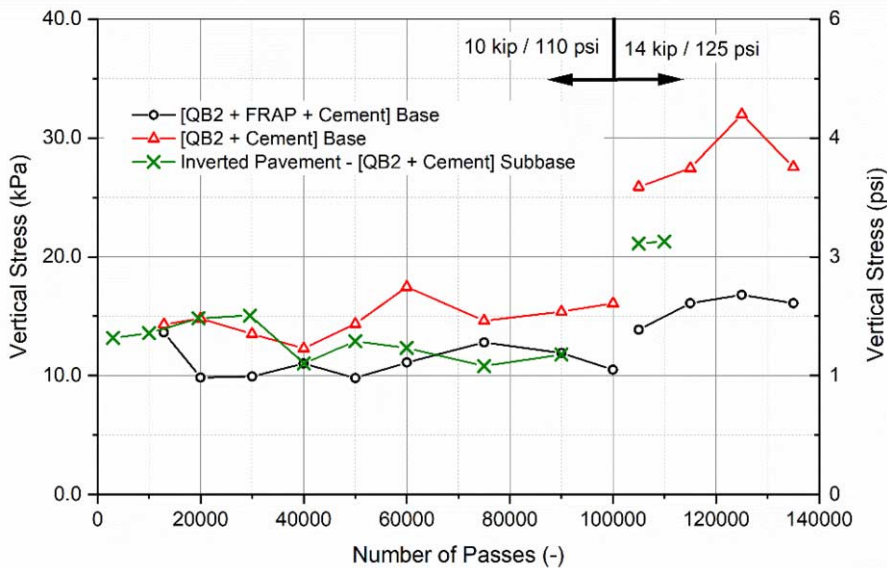


Figure 4. Vertical stress measured on top of subgrade using the installed pressure cell sensors.

3.3. Falling Weight Deflectometer Test Results and Interpretations

FWD tests were conducted by dropping three different load levels at each measuring point to induce variable stress states in pavement layers, and detect the surface deflections from seven geophones that are set 12 in. (305 mm) apart; including a center

geophone directly under the load drop location. The complete data covering all deflection basins from the conducted tests are presented elsewhere [19, 20].

Figure 5 shows the FWD deflections from the load dropped geophones (D_0 - D_3), spaced 12 in. (305 mm) apart. For each individual test section, the trends for the progression of rutting and FWD deflections are matching (i.e. typically greater maximum ruts were accumulated in the wheel path at the sections where higher FWD deflections were recorded). For sections with a cement-stabilized QB base material (i.e. C2S1, C2S2, C2S4, and C3S1), the measured FWD deflections were lower than those in section C2S3 with a fly ash-stabilized QB/FRAP base and inverted pavement section C3S2 with a cement-stabilized subbase, largely due to a higher stiffness of the pavement structure due to the chemically stabilized QB base. For section C3S3 with a fly ash-stabilized subbase, significantly higher deflections were measured, indicating a weaker pavement structure. The engineered subgrade stiffness was also likely similar in sections C2S1 - C3S2 according to the similar shapes of the deflection basins. The higher sensor deflections measured for sensors D_2 and D_3 in C3S3 were an indication of a weaker engineered subgrade for this section.

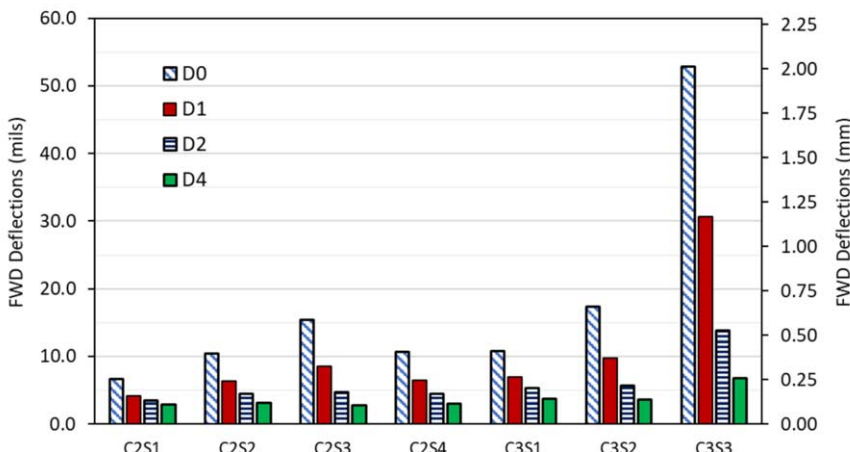


Figure 5. Recorded FWD deflections for sensors D_0 – D_3 .

Based on the FWD sensor deflections, the AREA parameter and the Area Under Pavement Profile (AUPP) were calculated. AREA parameter, measured in units of inches (mm), calculates the area of deflection basin over a radial distance of 36 in. (914 mm) from the center of the load plate, normalized with respect to D_0 sensor deflection. AUPP, measured in units of mils (μm), calculates the area beneath the deflection basin over a radial distance of 36 in. (914 mm) from the center of the load plate. These parameters are calculated using the following equations:

$$AREA = \frac{6[D_0 + 2D_1 + 2D_2 + D_3]}{D_0} \quad (1)$$

$$AUPP = \frac{5D_0 - 2D_1 - 2D_2 - D_3}{2} \quad (2)$$

The AREA parameter combines multiple measured deflections into one value and thus minimizes the contribution of malfunctioning sensors, if any [22]. The AUPP deflection basin parameter is complementary in definition to the AREA profile, and a lower AUPP is typically indicative of a higher pavement stiffness and better integrity. Higher AREA values generally indicate better structural integrity. From the results shown in Figure 6, the constructed pavement test sections with bound bases/subbases, the calculated AREA values and the measured surface ruts from field evaluation all follow the same trends; sections with higher AREA values accumulated the least rut depths. Note that FWD deflections are resilient, and they relate to pavement responses directly, but do not directly relate to performance trends. In most cases, however, FWD deflections and rut accumulations followed similar trends. Similarly, the AUPP values follow the trends of surface rut accumulations.

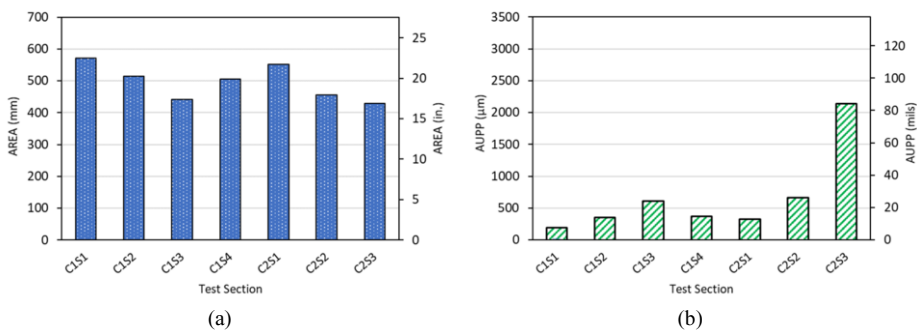


Figure 6. FWD deflection basin parameters: (a) AREA parameter, and (b) AUPP.

3.4. Subsurface layer DCP profiling

Following HMA coring, DCP testing was conducted into the underlying base and subbase layers of all test sections. The DCP tests were conducted directly in the center of the wheel path through the holes of the cored HMA. All DCP tests were conducted in dry weather conditions after several days/few weeks of no rain. The results for all test sections are summarized in Figure 7, which shows the number of DCP drops normalized for 1 in. (25 mm) of penetration. Higher numbers correlate with higher shear strength characteristics of the stiffer subsurface layers since DCP results produce shear strength profiles. For example, it took 852 DCP hammer drops for penetrating 12.25 in. (311 mm) into the C2S1 cement-stabilized QB/FRAP blend, i.e. 70 DCP drops per 1 in. (25 mm) of penetration.

The strength profiles of the subsurface pavement base/subbase layers were found to correlate well with performance trends, where sections accumulating the least rutting had the highest number of DCP drops per 1 in. (25 mm). In particular, C2S1 and C2S2 with blends of QB with FRAP/FRCA accumulated the least rutting, and had the strongest DCP profiles.

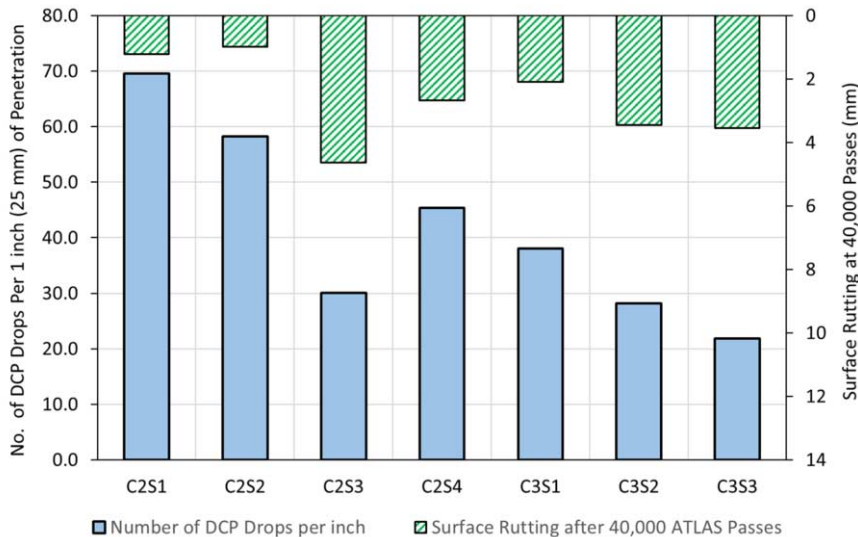


Figure 7. DCP penetration rates in base and subbase closely match with rutting progression trends.

3.5. Unconfined compressive strength tests for stabilized test sections

Following trenching of the test sections, some of the stabilized materials were recovered in intact pieces that were large enough to extract laboratory samples for Unconfined Compressive Strength (UCS) testing. Earlier on, attempts to extract and test cores of the stabilized base/subbase layers from the wheel path were not successful as the materials eroded with the presence of water from the coring process. In another attempt, a dry coring technique was employed to extract cylinders from the stabilized base and subbase layers for UCS testing. However, the lightly cemented layers eroded under the drilling action, producing fine fragments that clogged the coring bit; creating high friction and preventing the recovery of fully intact cores.

Test cubes, 3 in. (76 mm) in size, were saw-cut in the laboratory from the recovered intact blocks cut using a dry-sawing process. The size of the test cubes were 4 times the nominal maximum aggregate size (NMAS) for the FRAP course aggregate particles used in C2S1 and C2S3 test sections (NMAS of FRAP was 0.75 in. or 19 mm), thus conforming with ASTM recommendations for sample size. For C2S2 with QB/FRCA blends, 95% of the material blend was smaller than $\frac{3}{4}$ in. (19 mm) in accordance with the combined QB/FRCA gradation.

Three test cubes were prepared and tested for each stabilized test section in Cell 2, as well as for stabilized QB3 base in C3S1 and the stabilized subbase layers in C3S2 and C3S3. Prior to testing, the cubes were capped using a sulfuric compound to ensure more uniform loading distribution, and then tested for unconfined compressive strength at a rate of 0.04 in./minute (1 mm/minute). Figure 8 summarizes the UCS results for the different mechanically stabilized QB combinations and compares the achieved field UCS of the tested cubes. Since only three cubes were tested for each test section, which is insufficient for conducting statistical analyses, the minimum, average, and maximum cube strengths are shown. Also shown in Figure 8 are the UCS for the laboratory tested

cylinders. Note that for concrete specimens, it is generally agreed that cube strengths are 18-30% higher than cylinders with a 2:1 aspect ratio of height: diameter [23, 24].

On average, the highest UCS was achieved for the QB2 with 3% cement combination (C2S4 and C3S2), which was significantly higher than the USCS for laboratory cylinders, followed by cement-stabilized QB/FRCA and QB/FRAP (C2S2 and C2S1), respectively. The lowest strength was achieved for the fly ash-stabilized QB2/FRAP combination, which was the only combination that achieved a lower average UCS than the laboratory cylinders. Note that the reported strength values for the field cubes can be considered to represent the UCS for the recovered intact blocks. The presence of internal cracks resulting from trenching and handling might have contributed to lower strength. Generally, the strength values of these cubes are expected to be on the higher end since they were extracted from the intact blocks recovered after trenching, while the weaker parts of the stabilized pavement layers would not be found intact. A discussion of the UCS of laboratory prepared cylinders with the different material combinations was presented elsewhere [19-21].

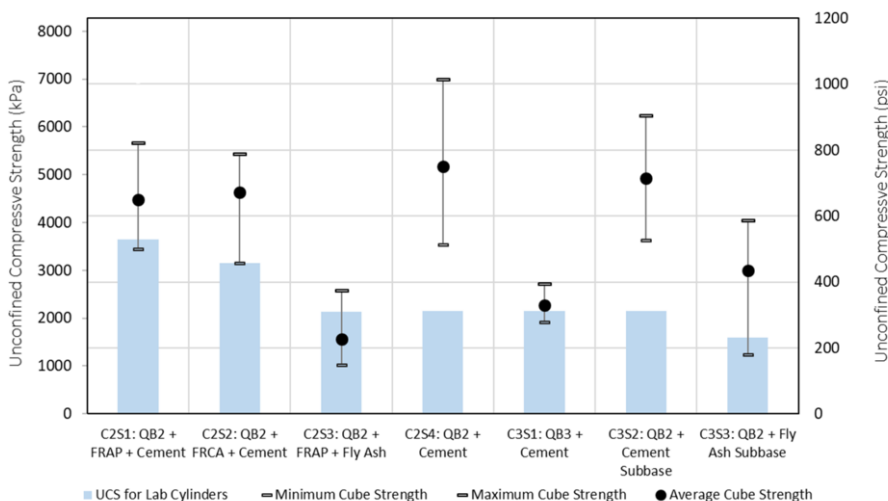


Figure 8. Unconfined compressive strength (UCS) values of stabilized QB material combinations retrieved from field test sections.

4. Summary and conclusions

This paper presented research findings from a study conducted at the Illinois Center for Transportation (ICT) to investigate sustainable bound applications for Quarry By-products (QB) in base and subbase layers. Three categories of chemically stabilized QB applications were selected and tested for field performance: (1) Blending QB with coarse aggregate fractions of reclaimed asphalt pavement (FRAP) and recycled concrete aggregates (FRCA); (2) using QB as a cement-treated base material; and (3) using QB as a cement or fly ash-treated subbase material in inverted pavements.

Satisfactory rutting performance trends were achieved for all chemically stabilized QB layer applications. No fatigue cracking was observed in any of the test sections with chemically stabilized QB applications. QB blends with FRCA or FRAP and cement had

higher and statistically different unconfined compressive strengths from laboratory tests. They also showed the most satisfactory rutting performance trends, with the lowest Falling Weight Deflectometer (FWD) deflections, and the highest number of drops per inch (25.4 mm) of penetration by Dynamic Cone Penetrometer (DCP) from field testing. Sections stabilized with fly ash had somewhat inferior and more variable performance trends when compared to the cement-stabilized sections. Test sections that utilized two different sources of QB for the cement-stabilized base application (i.e. QB2 and QB3) did not show any significant difference in performance, which is in agreement with the laboratory unconfined compressive strength test results.

The performance monitoring of the stabilized test sections before and after trafficking with accelerated pavement testing in general indicated relatively low FWD deflections for the stabilized test sections utilizing QB applications. Additionally, measured wheel load stresses from pressure cells installed on top of the subgrade indicated relatively low subgrade pressures of around 2 psi (14 kPa) recorded for the three cement-stabilized base/subbase test sections, and thus low subgrade rutting potential. Further, inverted pavement sections (C3S2 and C3S3) showed satisfactory performance. In particular, C3S2 with a cement-stabilized QB subbase resulted in better performance demonstrating the suitability of using cement-stabilized QB in inverted pavement applications.

Acknowledgements

The support for this study was provided by the Illinois Department of Transportation (IDOT) as part of the Illinois Center for Transportation (ICT) R27-168 research project. Special thanks go to IDOT Technical Review Panel, Dr. Imad Al-Qadi, Greg Renshaw, Michel Johnson, James Meister, and all the ICT students for their help during construction and testing at the Advanced Transportation Research and Engineering Laboratory (ATREL). The contents of this paper reflect the views of the authors who are responsible for the facts and the accuracy of the data presented. This paper does not constitute a standard, specification, or regulation.

References

- [1] Chesner, Warren H., Robert J. Collins, Michael H. MacKay, and John Emery. *User guidelines for waste and by-product materials in pavement construction*. No. FHWA-RD-97-148, Guideline Manual, Report No. 480017. Recycled Materials Resource Center, 2002.
- [2] Petavratzi, E. and S. Wilson. Incinerated Sewage Sludge Ash in Facing Bricks. *Characterization of mineral wastes, resources and processing technologies-integrated waste management for the production of construction material*. Publication WRT177/WR0115, 2007
- [3] Hudson, W. Ronald, Dallas N. Little, Arslan M. Razmi, V. Anderson, and Angela Jannini Weissmann. *An investigation of the status of by-product fines in the United States*. University of Texas at Austin. International Center for Aggregates Research, 1997.
- [4] Tutumluer, Erol, Hasan Ozer, Wenting Hou, and Vincent Mwumvaneza. *Sustainable Aggregates Production: Green Applications for Aggregate By-Products*. Illinois Center for Transportation/Illinois Department of Transportation, 2015.
- [5] Kumar, Doraiswamy Senthil, and W. R. Hudson. *Use of quarry fines for engineering and environmental applications*. Special Report, National Stone Association, Centre for Transportation Research, University of Texas, Austin, 1992.

- [6] Stroup-Gardiner, Marry and Tanya Wattenberg-Komas. *Recycled materials and by-products in highway applications. Volume 4: Mineral and quarry by-products*. NCHRP Synthesis of Highway Practice (Project 20-05, Topic 40-01), Transportation Research Board, 2013
- [7] Kalcheff, I. V., and C. A. Machemehl Jr. *Utilization of crushed stone screenings in highway construction*. In 59th Annual Meeting of the Transportation Research Board, Washington, DC, vol. 135. 1980.
- [8] Wood, Sandra A., and Charles R. Marek. *Recovery and utilization of quarry by-products for use in highway construction*. In ICAR 3rd annual symposium, volume 10. 1995.
- [9] Naik, Tarun R., N. Rudolph, Yoon-moon Chun, C. Fethullah, and W. Bruce. *Use of fly ash and limestone quarry byproducts for developing economical self-compacting concrete*. In International Congress on Fly Ash Utilization, 4th–7th December, 2005.
- [10] Koganti, Shyam Prakash, and Hanumantha Rao Chappidi. Effective utilization of quarry dust in flexible pavements as per IRC-37: 2012. *ARP Journal of Engineering and Applied Sciences* **13**, no. 5, (2012), 1545-1552.
- [11] Abdullaah, Jahaarul Dini Karen Lee, Nazri Ali, Roslli Noor Mohamed, and Mohammed Mu'azu Abdullaah. The effect of quarry dust with cement by-products on properties of concrete. *Malaysian Journal of Civil Engineering* **30**, no. 3 (2018), 415 - 428.
- [12] Schankoski, Rudiele Aparecida, Ronaldo Pilar, Luiz Roberto Prudêncio Jr, and Raissa Douglas Ferron. Evaluation of fresh cement pastes containing quarry by-product powders. *Construction and Building Materials* **133** (2017), 234-242.
- [13] Puppala, Anand J., Sireesh Saride, and Richard Williammee. Sustainable reuse of limestone quarry fines and RAP in pavement base/subbase layers. *Journal of Materials in Civil Engineering* **24**, no. 4 (2011), 418-429.
- [14] Mwumvaneza, Vincent, Wenting Hou, Hasan Ozer, Erol Tutumluer, Imad L. Al-Qadi, and Sheila Beshears. Characterization and Stabilization of Quarry Byproducts for Sustainable Pavement Applications. *Transportation Research Record* **2509**, no. 1 (2015), 1-9.
- [15] LaHucik, Jeffery, Scott Schmidt, Erol Tutumluer, and Jeffery Roesler. *Characterization of Cement Treated Base Course Using Reclaimed Asphalt Pavement, Aggregate By-Products, and Macro-Synthetic Fibers*. In Proceedings of Geo-Chicago Conference, pp. 523-533. 2016.
- [16] LaHucik, Jeffrey, Scott Schmidt, Erol Tutumluer, and Jeffery Roesler. Cement-treated bases containing reclaimed asphalt pavement, quarry by-products, and fibers. *Transportation Research Record* **2580**, no. 1 (2016): 10-17.
- [17] Nelson, Jerry D., Shane Tymkowicz, and Mark Callahan. *An Investigation of Emulsion Stabilized Limestone Screenings*. Office of Materials, Highway Division, Iowa Department of Transportation, 1994.
- [18] Puppala, Anand J., Sireesh Saride, Sunil K. Sirigiripet, R. Williammee, and V. Dronamraju. Evaluation of cemented quarry fines as a pavement base material. *ASCE Geotechnical Special Publication* **177** (2008), 312-319.
- [19] Qamhia, Issam, Erol Tutumluer, and Hasan Ozer. *Field Performance Evaluation of Sustainable Aggregate By-product Applications*. Illinois Center for Transportation/Illinois Department of Transportation, 2018.
- [20] Qamhia, Issam. *Sustainable pavement applications utilizing quarry by-products and recycled / nontraditional aggregate materials*. Doctoral Dissertation. University of Illinois at Urbana Champaign, 2019.
- [21] Qamhia, Issam, Erol Tutumluer, Hasan Ozer, Heather Shoup, Sheila Beshears, and James Trepanier. Evaluation of Chemically Stabilized Quarry Byproduct Applications in Base and Subbase Layers through Accelerated Pavement Testing. *Transportation Research Record* (2019): 0361198118821099.
- [22] Hoffman, Mario S. *Mechanistic interpretation of nondestructive pavement testing deflections*. Doctoral Dissertation, University of Illinois at Urbana Champaign, 1980.
- [23] Townsend, James M., W. Craig Jennings, Christopher Haycocks, George M. Neall III, and Lawrence P. Johnson III. *A relationship between the ultimate compressive strength of cubes and cylinders for coal specimens*. In The 18th US Symposium on Rock Mechanics (USRMS). American Rock Mechanics Association, 1977.
- [24] Kumavat, Hemraj R., and Vikram J. Patel. Factors influencing the strength relationship of concrete cube and standard cylinder. *International Journal of Innovative Technology and Exploring Engineering (IJITEE)* **3**, no. 8 (2014), 76-79.

Technical Session #10

“Natural Hazards”



Murray D. FREDLUND

Dr. Fredlund received his training from the University of Saskatchewan and Texas A&M University and has published over 50 research papers on topics related to database design, finite element modeling, and unsaturated soil knowledge-based systems. In 1997 he started SoilVision Systems Ltd. with a database software product called SoilVision which could be used to estimate unsaturated soil behavior. He has since directed the development of eight finite element software packages covering areas of groundwater flow, contaminant transport, geothermal analysis, air-flow analysis, stress / deformation, and slope stability.

More recent work has involved supervising the development of the state-of-the-art 2D/3D SVSLOPE slope stability software and the SVDESIGNER 3D conceptual modeling software. This work has continued with the expansion of 3D slope stability analysis into the areas of mining such as the analysis of open pits, tailings dams, power dams and performing landslide risk analysis.

Developments in Landslide Analysis Methodologies

Murray D. FREDLUND^{a,1}, Delwyn G. FREDLUND^b and
Gilson de F. N. GITIRANA Jr.^c

^aBentley Canada Inc.

^bUniversity of Saskatchewan, Saskatoon, SK, Canada

^cFederal University of Goias, Goiania, GO, Brazil

Abstract. Some of the first analytical tools developed in soil mechanics aimed at evaluating the stability of slopes. In recent years there has been numerous changes proposed on how best to model the behavior of slopes and the mechanisms of instability. “Limit Equilibrium” methods of slices have gone through a series of changes as the computer has provided increased ability to solve complex and nonlinear formulations. In recent years numerous new methods have been proposed for the analysis of slopes. These methods have provided new methodologies for the calculation of the normal forces along any proposed slip surface as well as new search routines that attempt to directly determine the shape and location of the most critical slip surface. Each new method of analysis required testing against a history of experience and previous methods of analysis. Recent developments in the analysis tools used for slope stability have augmented the ability of the practicing engineer to analyze slopes. Three-dimensional (3D) analysis is today easily possible and, therefore, its use in the regulatory environment dominated by 1.3 and 1.5 factors of safety must be understood. The influences of slip shape, new searching methods in 3D, geostrata, loading conditions, anchors, water tables as well as advanced methods of representing surface topology must be considered. How do we now consider the influence of 3D anisotropic bedding planes in rock environments? How do we account for probability? What are new searching methods to determine the slip surface in 3D? How do we determine spatial factors of safety over large land areas? The objective of this paper is to provide the practicing geotechnical engineer with information that allows the assessment of newly proposed methods for determining the factor of safety of soil and rock masses.

Keywords. 3D slope stability, stability, limit equilibrium, factor of safety, rock stability, 3D stability analysis

1. Introduction

Slope stability studies have constituted an important part of geotechnical engineering practice. The ability to analyze a soil or rock mass and calculate a factor of safety has lent considerable credibility to the engineering profession. This analytical ability has also been profitable for geotechnical engineers.

Changes in methodologies for the analysis of slopes have been considerable over a matter of a few decades and this has given rise to concerns over what is the best

¹ Corresponding Author, Murray Fredlund, Bentley Canada Inc., Saskatoon, SK, Canada E-mail: murray.fredlund@bentley.com

methodology to use in practice. Some slope stability methods emerged in the early years of soil mechanics. More recently new analytical forms of analysis have emerged. This often leaves the practicing geotechnical engineer with questions regarding the significance of the new methodologies. The advent of the computer has proven to be a valuable tool for analysis purposes. At the same time the computer has birthed other more complex computational tools.

The main objective of this paper is to provide a summary of the history of slope stability analysis while at the same time clarifying some strengths and weaknesses associated with the analyses. Another objective is to summarize some of the new methods associated with 3D analysis which have the potential to improve the current state of practice. This paper emphasizes the gradual change that has taken place with the use of limit equilibrium methods. However, changes in slope stability analyses have spread beyond the restrictions of limit equilibrium analyses. This has been largely due to the growth and availability of computing ability.

The geotechnical engineer is left with the task of sorting out the strengths and weaknesses of various slope stability techniques. This paper attempts to not only show the progressive changes that have taken place in slope stability analyses but also illustrate how one methodology has built upon the findings of another technology. This has lead to the place where today it is possible to extend two-dimensional analyses involving one central section through a soil mass into complex three-dimensional analyses. The potential differences with 3D analysis are clarified as well as the new issues that 3D analysis introduces. The methodologies developed to date for improving 3D analysis are presented and clarified. A particular focus of the paper is related to handling probability and the spatial variation of the computed factor of safety in real-world settings. The scope of this paper is limited to sliding earth & rock masses that are quite readily amenable to analysis.

2. History of Limit Equilibrium Analyses

The earliest application of statics to a sliding mass considered a planar sliding surface because of its ease of analysis. The movement of a large earth mass into the Goteborg harbour in Sweden showed the characteristics of a circular shape [1]. The entire sliding mass was considered as a single unit and the tending overturning moment was used to estimate the shear resistance of the soft sediments (Figure 1).

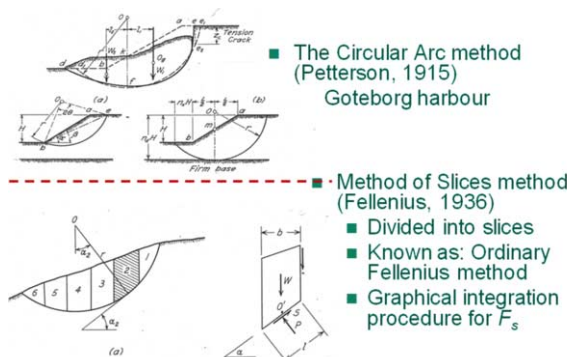


Figure 1. Early history of slope stability analysis by Petterson [1] and Fellenius [2].

Further landslides in the same harbor almost 20 years later resulted in a re-visititation of possible stability analysis that could be performed. Fellenius [2] subdivided the sliding mass into vertical slices, consequently, the name “method of slices”. Assumptions were made regarding the inter-slice shear and inter-slice normal forces existing between each of the slices as shown in Figure 2. The assumption was to simply ignore all inter-slice forces. The analysis was considerably simpler to perform but later would become the focus of concerns related to the accuracy of the analysis.

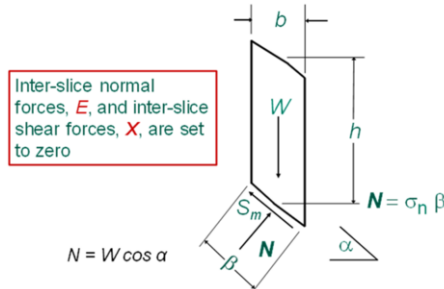


Figure 2. Free-body diagram for Fellenius method.

Little additional research was undertaken to improve the method of slices until the 1950s. In 1955 Bishop (Imperial College, London) published the results of his PhD thesis. Figure 3 shows the free-body diagram of one slice for a sliding mass with a circular shaped slip surface. All inter-slice forces were shown along with a separation of the pore-water force and the force associated with the effective stresses (i.e., an effective stress analysis). Also indicated was the force related to partial submergence of the slope.

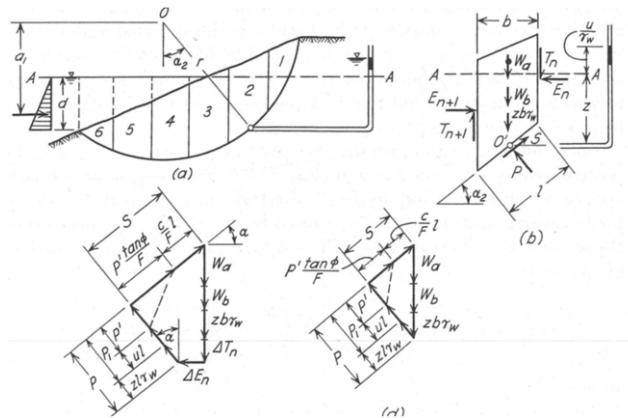


Figure 3. Bishop's Simplified method of slices [3].

Bishop [3] derived three main equations; namely, i.) a moment equilibrium equation for the overall mass with respect to the center of rotation, ii.) a force equilibrium equation for the overall mass in the horizontal direction, and iii.) a vertical force equilibrium equation for each slice comprising the sliding mass. While the equations associated with complete equilibrium of the sliding mass were derived, it was not possible to simultaneously satisfy both the horizontal equilibrium and moment equilibrium

equations using longhand calculations. Consequently, it was suggested that the overall horizontal force equilibrium be ignored along with the inter-slice shear forces, for the calculation of the factor of safety, giving rise to the Bishop Simplified method of slices (Figure 4).

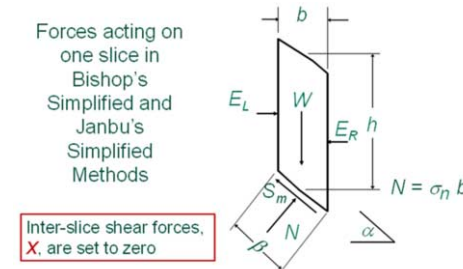
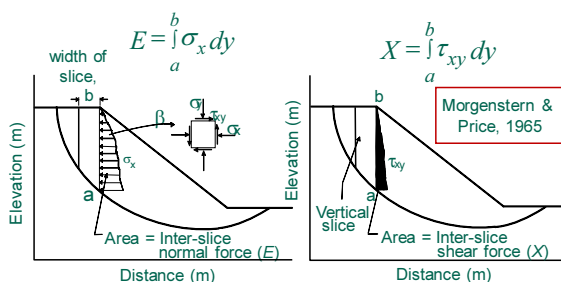


Figure 4. Free-body of a slice for the Bishop's Simplified and Janbu's Simplified methods.

In 1954, Janbu had suggested using the overall force equilibrium equation along with an omission of the inter-slice shear forces and moment equilibrium during the calculation of the factor of safety of a slope. This gave rise to the Janbu Simplified method of slices. Janbu also suggested a more elaborate analysis referred to as the Janbu Generalized method. This method made use of a moment equilibrium for each slice to generate a “line of thrust” to define the point of application of the inter-slice forces [4, 5].

Mainframe digital computers came on the scene in the mid 1960s and with them came additional computing power. Morgenstern and Price [6] were some of the first to take advantage of the increased computational ability. Most importantly it became possible to obtain a factor of safety solution that satisfied both moment and force equilibrium conditions if one additional variable, referred to as Lambda, λ , was introduced into the formulation [6]. It was also suggested that the inter-slice shear and inter-slice normal forces be related through use of an arbitrary but reasonable mathematical function. Morgenstern and Price [6] noted that the slope stability analysis was indeterminate because of a lack of physical understanding of the internal stress state along the sides of each slice. It was also suggested that it might be possible to introduce additional elements of physics into the analysis to render the analysis determinate (Figure 5). While the use of an additional stress analysis might be possible, it was not done until 1983 by Wilson and Fredlund.



It is possible to calculate E forces first and invoke an assumption for the calculation of X forces

Figure 5. Morgenstern-Price [6] method of analysis.

In 1967 Spencer published a method of slices analysis for calculating the factor of safety of a soil mass [7]. The method satisfied both force and moment equilibrium conditions and assumed that the slope of the inter-slice resultant be maintained at a constant slope. Consequently, the formulation was a special case of the Morgenstern-Price [6] method.

In 1977, Fredlund and Krahn published a general set of force and moment equilibrium equations based on the basic assumptions associated with a limit equilibrium analysis. This did not result in a new method of slope stability analysis; however, it showed the inter-relationship and the limitations associated with each of the methods of analysis that had previously been published. The summary of limit equilibrium analytical methods could be visualized through a common set of Newtonian equilibrium equations and a shear strength criterion. Other suggested limit equilibrium methods of slices were also shown to be related to the common set equilibrium equations [8, 9].

3. Fundamentals of Limit Equilibrium Analysis

The evolution of limit equilibrium methods can be presented in terms of a consistent set of Newtonian equations of statics. Within this context, all limit equilibrium methods of slices can be visualized in terms of the i.) elements of statics that have been satisfied in the formulation, and ii.) the assumption(s) invoked to render the analysis determinate.

A limit equilibrium analysis must start with a designated free-body diagram. Herein lies the first problem since the boundaries of the free-body are not known (Figure 6). The ground surface geometry and the stratigraphy associated with the soil layers may be known but the shape and location of a sliding mass are not known at the start of the analysis. All proposed limit equilibrium methods of slices have made the following recommendations to resolve these problems; namely, i.) the shape of the slip surface is assumed, and ii.) the location of the critical slip surface will be found through a trial and error process.

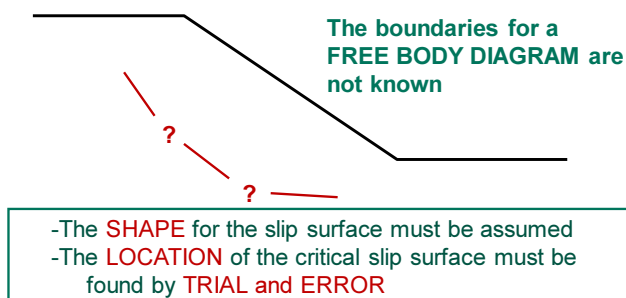


Figure 6. Basic limitations of limit equilibrium methods of analysis.

Figure 7 shows all the forces that need to be applied to an individual slice from the sliding mass. The forces are all shown as total forces without a need to separate the forces between total and effective stress conditions. The selected slip surface was first assumed to be circular but might also deviate from a circular shape.

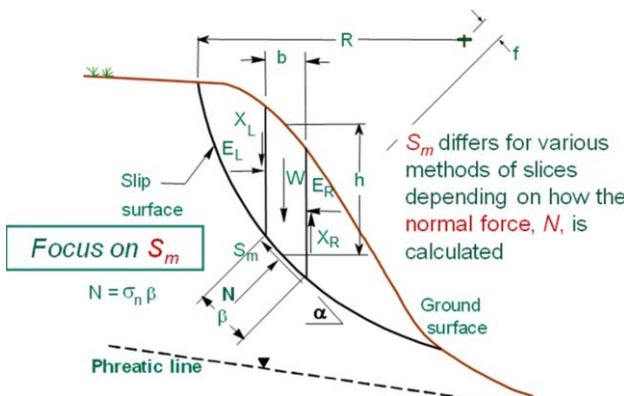


Figure 7. Forces acting on each slice.

The force of greatest interest in Figure 7 is the shear force mobilized, S_m . It is of interest because it is the variable that is calculated by different means in each of the methods of slices. The shear force mobilized changes in the various methods of slices because it is dependent upon the normal force, N , which is calculated differently in the various methods of slices.

All limit equilibrium methods assume that the soils involved behave as Mohr-Coulomb materials. In other words, the soil has a frictional component and a cohesive component. The frictional component is most fundamentally designated as the effective angle of internal friction, ϕ' , and the cohesion intercept is designated as the effective cohesion, c' . Another commonality of all limit equilibrium methods is the assumption that the factor of safety for the cohesive component is equal to that of the frictional component. In addition, the factor of safety is assumed to be the same for all slices of the sliding mass.

It is noteworthy that the pore-water pressure does not appear on the free-body diagram because it is internal to the shear strength equation which is part of the shear force mobilized, S_m . The shear force mobilized can be written as follows in terms of the shear strength criteria.

$$S_m = \frac{c' \beta}{F_s} + \frac{[(\sigma_n - u_w) \tan \phi'] \beta}{F_s} \quad (1)$$

where β = length along the base of a slice; σ_n = normal stress along the base of a slice; u_w = pore-water pressure at the base of a slice; and F_s = factor of safety for the entire sliding mass. The designation of the shear strength mobilized can also be written in a form such that it applies for both saturated and unsaturated materials as shown in Eq. (2).

$$S_m = \frac{c' \beta}{F_s} + \frac{[(\sigma_n - u_a) \tan \phi'] \beta}{F_s} + \frac{[(u_a - u_w) \tan \phi^b] \beta}{F_s} \quad (2)$$

where u_a = pore-air pressure at the base of a slice, and u_w = pore-water pressure at the base of a slice; and ϕ^b = friction angle with respect to matric suction. Other variables have been previously defined.

Before attempting to formulate factor of safety equations within the context of a limit equilibrium framework, a list should be made of the known element of statics and physics available for solving the problem. The following is a list of the known elements of physics that are available for the derivation of factor of safety equation.

Equations that can be listed as “knowns” are:

- n moment equilibrium equations
- n vertical force equilibrium equations
- n horizontal equilibrium equations
- n Mohr-Coulomb failure criterion equations

The above elements of physics can be applied to each slice giving a total of $4n$ “knowns” where n is equal to the number of slices into which the sliding mass has been divided. The “unknowns” variables associated with the analysis can be listed as follows:

- n total normal forces at the base of a slice
- n shears forces at the base of each slice
- $n-1$ inter-slice normal forces, E
- $n-1$ inter-slice shear forces, X
- $n-1$ points of application of the inter-slice E forces
- n points of application of the normal force on each slice
- 1 factor of safety, F_s

The tabulation of “knowns” and “unknowns” show that there are a total of $(6n - 2)$ “unknowns” that need to be computed while there are $4n$ equations to use. Since $(6n-2)$ is greater than $4n$, the analyst must conclude that the problem is indeterminate. The analyst has a choice to make regarding solving for the factor of safety. Either he/she can attempt to invoke further elements of physics to solve the problem or he/she can estimate (or omit) some of the known forces. An examination of the research literature shows that the choice has been made to assume a relationship between some forces or else simply omit some of the forces.

It is possible to derive a general force and moment equilibrium factor of safety equation even prior to a decision being made with regard to rendering the problem determinate. Eq. (3) shows the moment equilibrium that is applicable for both saturated and unsaturated soils. The pore-air pressure has been assumed to be zero in this equation.

$$F_m = \frac{\sum \left\{ c' \beta R + \left(N - u_w \beta \frac{\tan \phi^b}{\tan \phi'} \right) R \tan \phi' \right\}}{\sum Wx - \sum Nf} \quad (3)$$

Eq. (4) shows the horizontal force equilibrium that is applicable for both saturated and unsaturated soils with pore-air pressure equal to zero.

$$F_f = \frac{\sum \left\{ c' \beta \cos \alpha + \left(N - u_w \beta \frac{\tan \phi^b}{\tan \phi'} \right) \tan \phi' \cos \alpha \right\}}{\sum N \sin \alpha} \quad (4)$$

A general form for vertical force equilibrium on each slice can also be derived as shown in Eq. (5).

$$N = \frac{W - (X_R - X_L) - \frac{c' \beta \sin \alpha}{F} + u_w \frac{\beta \sin \alpha \tan \phi'}{F}}{\cos \alpha + \frac{\sin \alpha \tan \phi'}{F}} \quad (5)$$

The normal force equation applies for both saturated and unsaturated soils; however, the pore-air pressure has been set to zero. Various limit equilibrium methods differ with respect to how the inter-slice shear force term, $(X_R - X_L)$ will be computed and which overall statics will be satisfied. All methods of slices, except for the Fellenius method, are nonlinear in the sense that the variables being computed by moment and force equilibrium also appears in the equation to compute the normal force at the base of the slice. Consequently, an iteration procedure is required to obtain convergence to the factor of safety.

At this point a decision must be made regarding how to render the analysis determinate. This must be done before proceeding to solve for the factor of safety. Table 1 contains a summary of the equilibrium conditions that have been satisfied and the assumptions that have been made regarding the inter-slice forces for various methods of analysis. The Fellenius method completely ignores all inter-slice forces while the Bishop Simplified and Janbu Simplified methods ignore the inter-slice shear force but keep the inter-slice normal forces. The Morgenstern-Price (GLE) and Spencer methods attempt to calculate the inter-slice shear forces and then use these values in the calculation of the factor of safety that satisfies both moment and force equilibrium.

Table 1. Equilibrium conditions that are satisfied and assumptions that are made for various limit equilibrium methods of slices.

Method of Analysis	Equilibrium Satisfied	Assumptions
Ordinary or Fellenius	Moment, Perpend. to base	E and X = 0
Bishop's Simplified	Vertical, Moment	E is horizontal, X = 0
Janbu's Simplified	Vertical, Horizontal	E is horizontal, X = 0; empirical factor f_0 applied
Janbu's Generalized	Vertical, Horizontal	E is located by an assumed line of thrust
Spencer	Vertical, Horizontal, Moment	X/E constant
Morgenstern-Price & GLE	Vertical, Horizontal, Moment	X/E = $\lambda f(x)$
Corps of Engineers	Vertical, Horizontal	X/E is equal to the slope of the ground surface
Lowe & Karafiath	Vertical, Horizontal	X/E is equal to the average of the slopes of the ground surface and base of slice

The Morgenstern-Price [6] method introduced an additional unknown, λ , and a functional distribution as shown in Eq. (6):

$$X = E\lambda f(x) \quad (6)$$

where $f(x)$ is a mathematical function that defines the slope of the ratio X/E . Various inter-slice force functions suggested by Morgenstern-Price [6] are shown in Figure 8.

Wilson and Fredlund [10] used a linear elastic analysis in an attempt to compute typical inter-slice force functions.

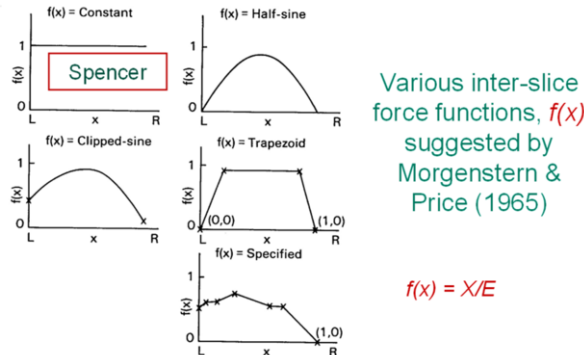


Figure 8. Suggested forms for the inter-slice force function [6].

The results consistently showed that the inter-slice force function took the form of an extended error function as shown in Figure 9 with the peak of the function near the middle of the slope.

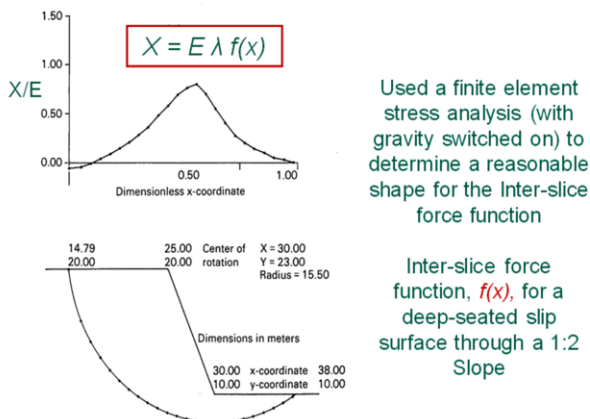


Figure 9. Inter-slice force function based on a linear elastic stress analysis [10].

The interslice force function takes the form of an extended error function [10]. Once the crest and the base of the slope is defined, other variable in the function bear a unique relationship to the steepness of the slope.

$$f(x) = e^{-C^n \omega^n / 2} \quad (7)$$

where: e is the base of the natural log, C is a variable used to define the inflection point along the interslice force function, n is a variable used to describe the steepness of the slope, and ω defines the dimensionless distance along the x -axis.

3.1. Comparison of Moment and Force Equilibrium Factors of Safety

It is possible to compare moment equilibrium and force equilibrium solutions for various geometries (i.e., ground surface profiles) and various shapes of slip surfaces. It is also possible to compare the computed factors of safety from methods that do not satisfy all the elements of statics with methods that satisfy both moment and force equilibrium. Various inter-slice force functions can also be compared through use various percentages of the Lambda, λ , variable.

Figure 10 shows a comparison of the various computed factors of safety when considering a circular slip surface.

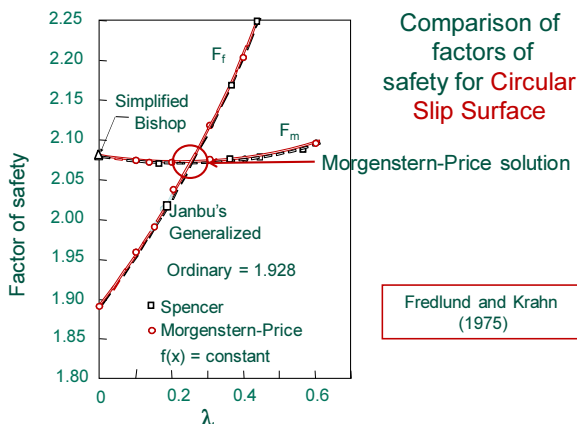


Figure 10. Comparison of moment and force equilibrium factor of safety equations [11].

The following observations can be made from Figure 10 regarding a slope stability analysis where the slip surface is circular.

1. The Morgenstern-Price factor of safety is the cross-over point where moment and force equilibrium are satisfied.
2. The moment equilibrium factors of safety are quite insensitive to the inter-slice force function.
3. Consequently, the Bishop Simplified factor of safety is quite close to the Morgenstern-Price method factor of safety which satisfies both moment and force equilibrium.
4. The Fellenius (or Ordinary) method gives a factor of safety that is lower than the factor of safety satisfying moment and force equilibrium.
5. The force equilibrium factor of safety is quite sensitive to the selected inter-slice force function.
6. The Spencer method is a special case of the Morgenstern-Price method.

Figure 11 shows the results of a comparison of the various computed factors of safety when considering a planar slip surface.

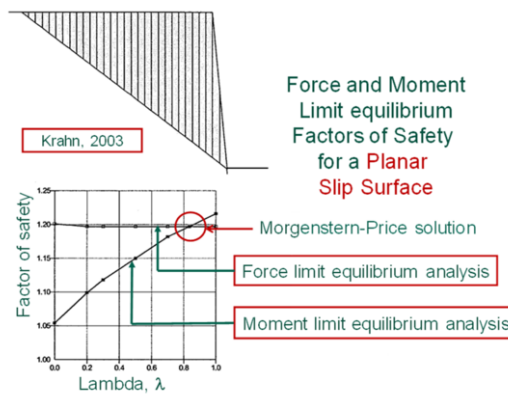


Figure 11. Comparison of moment and force equilibrium factors of safety when the slip surface is planar.

The following observations can be made from Figure 11 regarding a slope stability analysis where the slip surface is planar.

1. The Morgenstern-Price factor of safety is the cross-over point where moment and force equilibrium are satisfied.
2. The moment equilibrium factors of safety are quite sensitive to the inter-slice force function.
3. The Bishop Simplified factor of safety is below the Morgenstern-Price method factor of safety which satisfies both moment and force equilibrium.
4. The moment equilibrium factor of safety is quite sensitive to the selected inter-slice force function.
5. In general, the independent solving of the moment equilibrium and force equilibrium factor of safety equation shows the relationship of the shape of the slip surface to the relationship between moment and force equilibrium.

Figure 12 shows the results of a comparison of the various computed factors of safety when considering a composite slip surface (i.e., part circular and part planar).

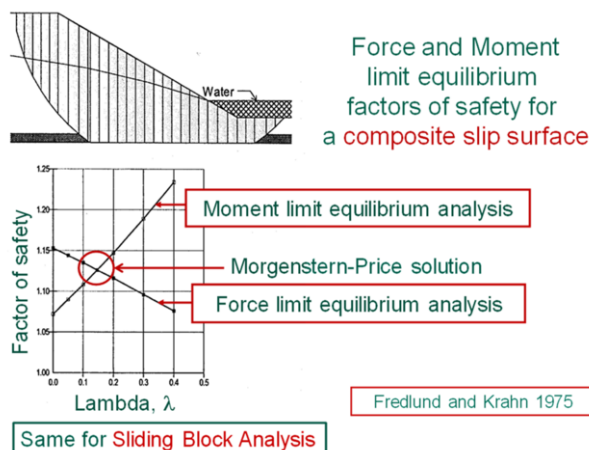


Figure 12. Comparison of moment and force equilibrium factors of safety when the slip surface is composite (i.e., part circular and part planar).

The following observations can be made from Figure 12 regarding a slope stability analysis where the slip surface is composite.

1. The Morgenstern-Price factor of safety is the cross-over point where moment and force equilibrium are satisfied.
2. Both the moment and force equilibrium factors of safety are quite sensitive to the selected inter-slice force function.
3. The Bishop Simplified factor of safety is below the Morgenstern-Price method factor of safety which satisfies both moment and force equilibrium.
4. The independent solving of the moment equilibrium and force equilibrium factor of safety equation shows the relationship of the shape of the slip surface to the relationship between moment and force equilibrium.

The Morgenstern-Price (and GLE) methods of analysis satisfy both moment and force equilibrium conditions and provide considerable flexibility with respect to the selection of an inter-slice force function. The proposed Wilson and Fredlund [10] inter-slice force function is based on a linear elastic analysis of the soil mass. It could be argued that this function is not an accurate reflection of the actual stress state in the soil mass; however, the function has features that are supported by earth pressure theory and appears to always ensure convergence of the factor of safety calculations.

All limit equilibrium methods, (with the exception of the Fellenius method), use Eq. (5) for the calculation of the normal force at the base of the slice. An examination of Eq. (5) shows that under certain conditions it is possible for the denominator to come close to (or exactly) zero and as a result the calculated normal force approaches infinity. This is one of the limitations associated with limit equilibrium methods and in part, has given rise to the consideration of other methodologies.

4. Other Methodologies for Determination of Normal Force on a Slice

One of the first methodologies given consideration for the calculation of the stress state in a soil mass involves the use of a numerical modeling approach such as the finite element method. The search can be put in the form of a question, “Can the stress state within a soil mass be more accurately calculated by switching-on the gravity force (i.e., unit weight of the soil)?” Stated another way, the question can be asked, “Can the complete stress state from a finite element analysis be “imported” into a limit equilibrium framework where the normal stresses and the actuating shear stresses are computed along any selected slip surface?” (See Figure 13).

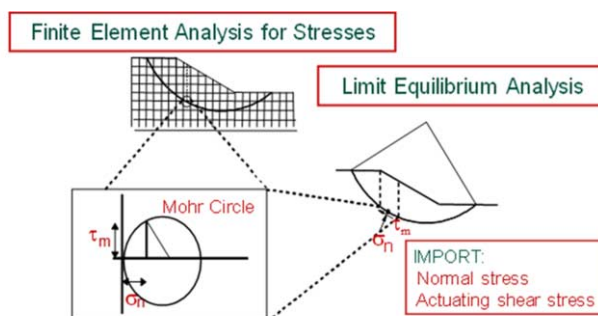


Figure 13. Procedure for “importing stresses” from a finite element analysis into a limit equilibrium analysis.

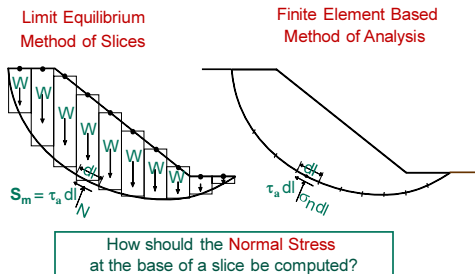


Figure 14. Comparison of the limit equilibrium and stress analysis calculations of the normal stress at the base of a slice.

It can be argued that the stresses computed from “switching-on” gravity are more reasonable than the stresses computed when using a single vertical slice as the free body diagram even though stress-strains conditions might be nonlinear and near failure. Let us compare the free-body diagrams shown in Figure 14. The limit equilibrium free-body diagram shows that the normal force on the base of a slice is largely dependent upon the single slice being analyzed. On the other hand, the finite element simulation also considers overall changes in the ground surface when calculating the stress state at the base of a slice.

The difference in the normal stress at the base of slices can be calculated by comparing the results of a limit equilibrium analysis and a finite element stress analysis. Figure 15 compares the two sets of normal stresses for a slip surface the exits at the toe of the slope. The finite element simulation produces results that reveal that the ground surface geometry goes horizontal after the toe of the slope. However, the limit equilibrium analysis does not show any effect of the geometry past the toe of the slope. In this sense, the finite element analysis would appear to produce a more accurate indication of the normal stresses.

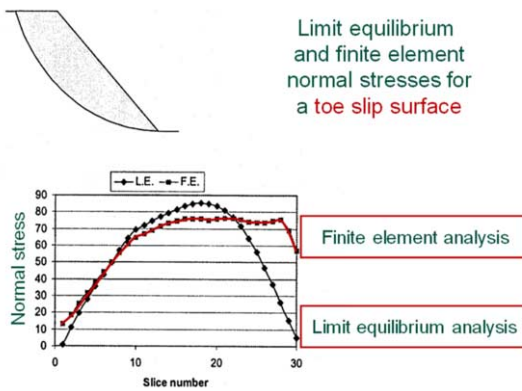


Figure 15. Comparison of limit equilibrium and stress analysis normal forces for slip surface exiting at the toe.

Finite element stress-deformation analyses have been used in different ways for analyzing the stability of a slope. The methodologies can be divided into two broad categories. In the first category there are methods where the stress state information from the stress-deformation analysis are used within the framework of a limit equilibrium

analysis. In this case, the normal stress and the actuating shear stresses are “imported” into a limit equilibrium analysis framework. This class of analysis is referred to an “Enhanced Limit” analysis. There are several “Enhanced Limit” analyses that have been proposed and the methods mainly differ in terms of the equation used to define the factor of safety as shown in Figure 18. It appears that the factor of safety definition proposed by Kulhawy [12] seems to have gained the widest acceptance in geotechnical engineering.

4.1. Enhanced Limit Analyses

There are two categories of slope stability analysis that make use of the results from a finite element analysis. The first category, (i.e., Enhanced Limit analyses) where a linear elastic analysis is used to calculate the stress state throughout the soil mass and the second category (i.e., Strength Reduction analyses) where an elasto-plastic analysis is used. There are also two types of Strength Reduction methodologies that have been proposed; namely, i.) methods where the applied load (or gravity forces) are increased until failure occurs or ii.) methods where the strength of all soils is decreased until failure occurs. The two categories of finite element slope stability are first explained followed by an explanation of the relationship between the two analytical procedures.

Figure 16 is a flowchart that shows the types of finite element stress-deformation analyses that have been proposed for slope stability studies. Consideration is first given to the use of an “Enhanced Limit” type of analysis.

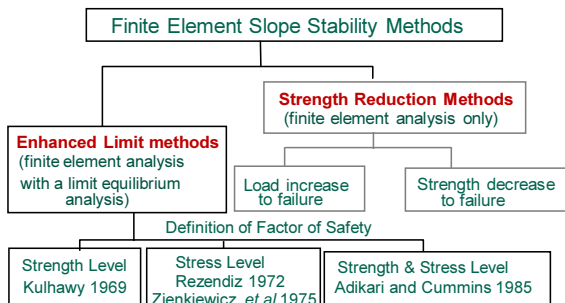


Figure 16. Classification of methodologies that can be used to incorporate stress analysis results.

The factor of safety equation proposed by Kulhawy [12] is shown in Eq. (8) and is most consistent with the equation used in geotechnical engineering.

$$F_K = \frac{\sum (c' + \sigma' \tan \phi') \Delta L}{\sum (\tau) \Delta L} \quad (8)$$

where ΔL represents increments along the slip surface.

5. Use of the “Enhanced Limit” Analysis

There are some distinct differences between a “Limit Equilibrium” analysis and an “Enhanced Limit” analysis. A stress analysis is first performed when undertaking an

Enhanced Limit analysis. The normal stress on any orientation of a slip surface can be calculated because the complete stress state is known. In other words, the Enhanced Limit analysis becomes determinate and the factor of safety equation becomes linear. On the other hand, there are some similarities to a limit equilibrium analysis. It is still necessary to assume a shape for the slip surface and the location of the critical slip surface must be located by trial and error. The Kulhawy [12] definition for the factor of safety is illustrated in Figure 19. For every section along the base of a slip surface, there are two stresses that must be retrieved from the stress-deformation analysis. These are: i.) the normal stress, and ii.) the mobilized shear force. The normal stress is inserted into the shear strength numerator of the factor of safety equation while the shear force mobilized is used in the denominator as shown in Eq. (9).

$$F_{FEM} = \frac{\sum S_r}{\sum S_m} \quad (9)$$

where F_{FEM} is the Kulhawy [12] factor of safety definition, S_m is the shear force mobilized and S_r shear strength resistance.

An example problem illustrates the similarities and the differences between an Enhanced Limit analysis and a limit equilibrium analysis. As part of the Enhanced Limit analysis it is possible to calculate a local factor of safety corresponding to each section along the slip surface, in addition to the global factor of safety. Let us consider a 2:1 slope that is 20 meters high with a piezometric line at 2/3 the height of the slope but exiting at the toe of the slope. Any Young's modulus can be assumed for the analysis. The Poisson's ratio is set to 0.33 since it has some effect of the calculated stresses. Figure 17 shows a plot of the shear strength and the actuating shear stresses at each section across the slope. Note that at all points along the slip surface, the shear strength values are consistently higher than the actuation shear force meaning that all local factors of safety are greater than 1.0.

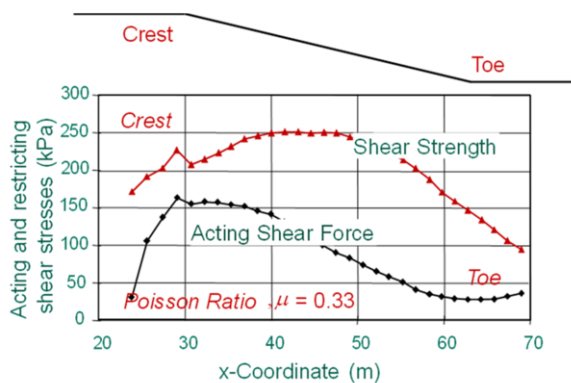


Figure 17. Shear strength and actuating shear force across the slope.

The results from an Enhanced Limit analysis can also be plotted as shown in Figure 18. The results are shown for Poisson's ratios of 0.33 and 0.48. The plots of local factor of safety are different for the two Poisson's ratio values; however, the global factors of safety differ by only 0.1%. Also shown are the global factors of safety obtained when

the example problem is analyzed using the various limit equilibrium methods of analysis. The global factor of safety using the Morgenstern-Price method was 2.356 or a difference of about 1.0% from the Enhanced Limit analysis. It may seem to be a surprise to find such a similarity in the factors of safety when using two dis-similar methods of analysis.

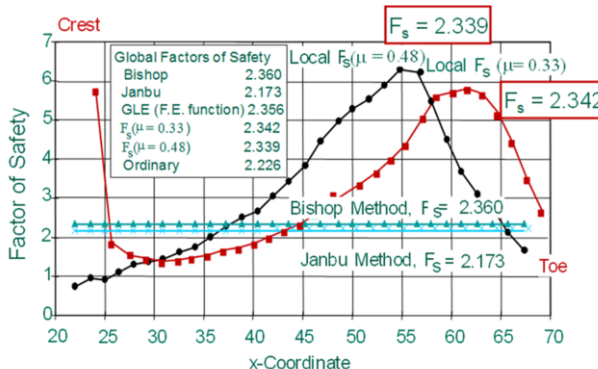


Figure 18. Comparison of Local and Global factors of safety.

The most logical explanation would appear to lie in the fact that both methodologies conserve the potential energy of problem and for this reason are quite similar.

Figure 19 provides a comparison between the results of a parametric study of limit equilibrium analyses and Enhanced Limit analysis. A wide range of cohesion and friction angles were selected and the results are plotted versus the Stability Number. The results are extremely close to each other but it must also be remembered that the problem being analyzed only consists of simple slopes.

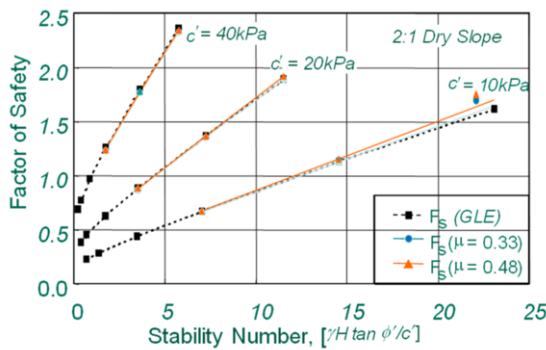


Figure 19. Comparison of factors of safety versus stability number for a range of soil properties.

In general, the global factors of safety appear to be similar between Enhanced Limit and limit equilibrium methods. There is; however, some differences in the location of the critical slip surface locations. This appears to be mainly related to the differences in the calculated normal stresses between the two methodologies. Figure 20 illustrates how the critical slip surface determined by the limit equilibrium method exists at the toe of the slope while the critical slip surface may extend beyond the toe for the Enhanced Limit analysis.

There appears to have been limited interest in geotechnical engineering practice for the use of Enhanced Limit analyses for calculating the factor of safety of a slope.

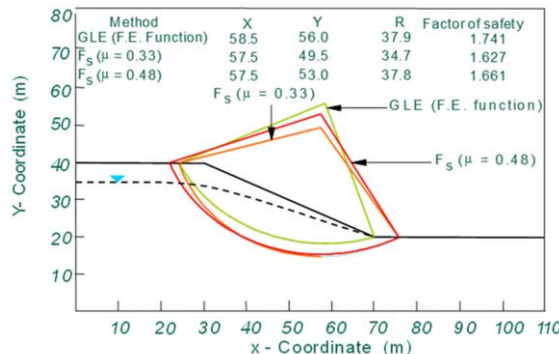


Figure 20. Comparison of the location of the critical slip surfaces.

There may be several reasons for its slow acceptance. First, additional soil properties are required when performing a stress-deformation analysis (e.g., Young's modulus and Poisson's ratio). While the effect of Young's modulus appears to be negligible, there is less confidence in working with deformation soil properties. There is also the perception of inaccuracy in the stresses when performing an analysis corresponding to near failure conditions. There is also the lack of an experience database associated with the Enhanced Limit method. There is the possibility that consideration might be given to use of the Enhanced Limit method when analyzing complex geometries but at present, geotechnical engineering practice is quite committed to using limit equilibrium methods of analysis.

5.1. Comparison Between a Linear Elastic and Elasto-Plastic Stress Analyses

The above comparisons between Enhanced Limit analysis and limit equilibrium analyses were undertaken using a linear elastic stress-deformation analysis. The next question to be addressed is related to whether it might be preferable to use an elasto-plastic analysis rather than using an elastic analysis. This question is examined by comparing the results of a linear elastic and an elasto-plastic analysis when the computed overall factor of safety is; i.) well above 1.0, ii.) near 1.0, and iii.) below 1.0 [13, 14]. The soil properties for the dry slope are shown in Figure 23. The Dynamic Programming technique, described later in this paper, was used to perform the analyses.

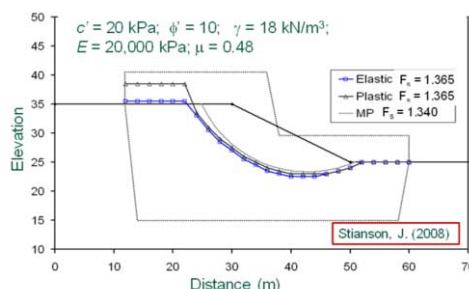


Figure 21. Stress-deformation analysis of a homogeneous dry slope with a factor of safety of approximately 1.3.

Figure 21 shows the computed factors of safety along with the location of the critical slip surfaces for an elastic and elasto-plastic analysis when the factor of safety is approximately 1.3. Also shown are the results of a limit equilibrium analysis (i.e., Morgenstern-Price method). All of the critical slip surfaces have a similar location and the overall factors of safety are the same (i.e., $F_s = 1.365$).

Figure 22 shows a comparison of the calculated local factors of safety across the slip surface. The calculation of the local factors of safety provides an indication of whether there was a re-distribution of stresses along the slip surface (i.e., any plastic zones).

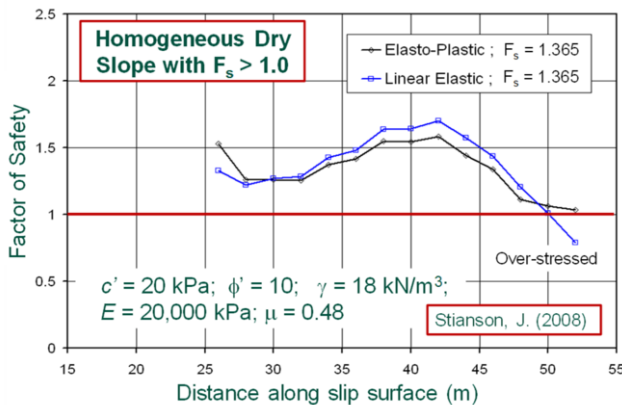


Figure 22. Local factor of safety when the global factor of safety is about 1.3.

The local factors of safety were similar across the slip surface with the exception of some re-distribution of stresses near the toe of the slope, preventing the local factor of safety from going below 1.0.

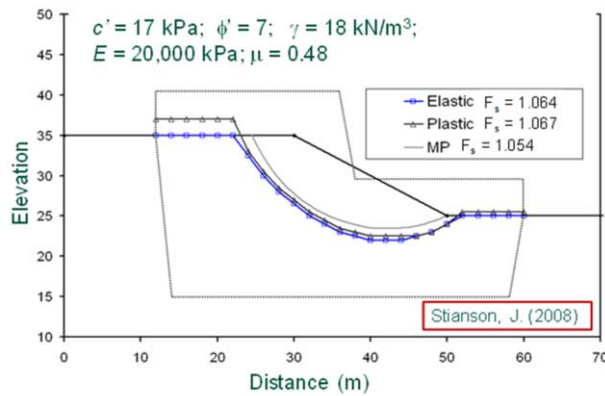


Figure 23. Stress-deformation analysis of a homogeneous dry slope with a factor of safety of approximately 1.0.

Figure 23 shows the computed factors of safety along with the location of the critical slip surfaces for an elastic and elasto-plastic analysis when the overall factor of safety approaches 1.0. The shear strength parameters have been adjusted to bring the overall (global) factors of safety close to 1.0. Also shown are the results of a limit equilibrium

analysis (i.e., Morgenstern-Price method with $F_s = 1.054$). The critical slip surfaces have a similar location and the global factors of safety show very slight differences.

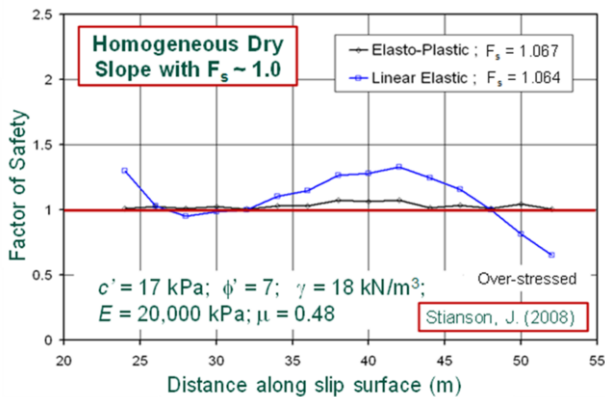


Figure 24. Local factor of safety when the global factor of safety is about 1.0.

Figure 24 shows the computed local factors of safety along the slip surfaces for an elastic analysis and an elasto-plastic analysis. The results correspond to the case where the global factor of safety approaches 1.0. There is clearly a significant redistribution of stresses forcing the shear strength to move into the plastic mode. Consequently, the local factors of safety for the elasto-plastic analysis move towards 1.0. The local factors of safety from the elastic analysis show an over-stressing of the soil near the crest and near the toe of the slope.

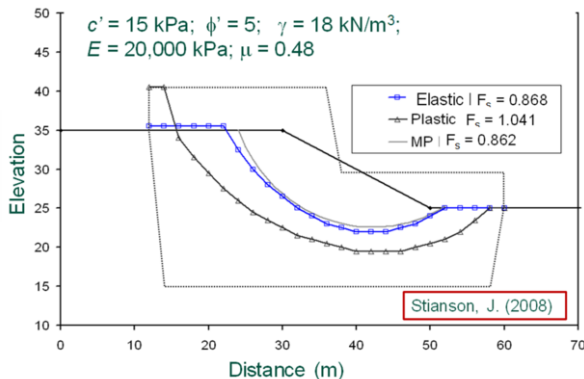


Figure 25. Stress-deformation analysis of a homogeneous dry slope with a factor of safety less than 1.0.

Figure 25 shows the computed factors of safety along with the location of the critical slip surfaces for an elastic and elasto-plastic analysis when the global factor of safety from a limit equilibrium analysis goes less than 1.0. The shear strength parameters have been adjusted to bring the limit equilibrium factor of safety less than 1.0 (i.e., $F_s = 0.862$). The location of the critical slip surface, and the global factors of safety, for the limit equilibrium analysis and the elastic stress analysis remain essentially the same. However, the elasto-plastic stress analysis undergoes a wide re-distribution of stresses causing the

global factor of safety to remain near 1.0. The re-distribution of stresses is clearly shown in Figure 26.

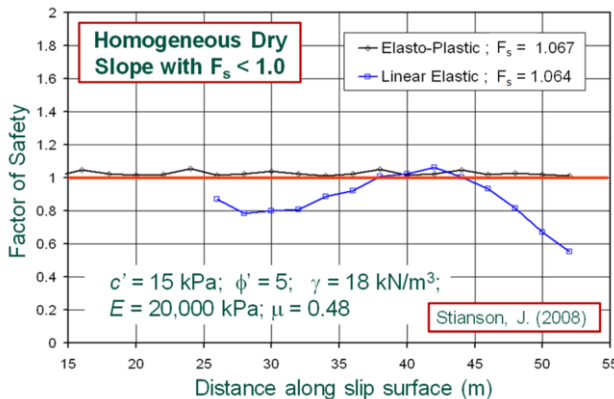


Figure 26. Local factor of safety when the global factor of safety is less than 1.0.

The conclusion from this small comparative study shows that an elastic stress model and an elasto-plastic stress model give similar values in a slope stability analysis as long as the global factor of safety is greater than 1.0. However, an elasto-plastic model should not be used to calculate the *in-situ* stress state when using a finite element stress-based analysis for calculating the factor of safety in a slope stability analysis. Rather, it is an elastic stress-strain model that should be used to estimate the *in-situ* stresses in a soil mass. An elasto-plastic model results in a re-distribution of stresses thereby preventing the factor of safety from ever going below 1.0.

Earlier in this paper (i.e., Figure 16) it was shown that there were two ways in which the results from a finite element stress analysis could be used to assess the factor of safety of a slope; namely, i.) the Enhanced Limit approach and the ii.) Strength Reduction approach. Whereas the Enhanced Limit approach made use of the results from an elastic model, the Strength Reduction approach makes use of an elasto-plastic model of behavior.

5.2. Strength Reduction method

The Strength Reduction method constitutes an approach whereby the results of a finite element analysis can be used as part of a slope stability analysis. There are two ways whereby the strength reduction method can be implemented. For example, the load (e.g., gravity forces) could be increased until the calculated deformation showed that failure was imminent, or the strength of the soil could be decreased until failure was imminent. It is the latter case that has received most attention in geotechnical engineering [15].

The definition for the factor of safety must be changed to be based on a deformation criterion that signifies a “failure state” for the Strength Reduction method. “Failure state” is related to an excessive deformation state such that convergence was not attainable in the finite element stress-deformation model. For this to happen, it is necessary to use a Mohr-Coulomb shear strength type soil model. The factor of safety is equal to the ratio of the actual shear strength parameters (e.g., c' and $\tan \phi'$), to the reduced shear strength parameters corresponding to a non-converged solution. Stated another way, the factor of

safety is equal to the maximum reduction in the original shear strength parameters where convergence could still be obtained. One of the driving forces behind the Strength Reduction method is the fact that fewer “*a priori*” assumptions are required regarding the failure mechanism.

Figure 27 uses a measure the amount of movement on the ordinate versus the factor of safety on the abscissa. Two example analyses are shown. When the full value of the strength parameters is used, the measure of deformation for example 1 was approximately 0.4 (unitless).

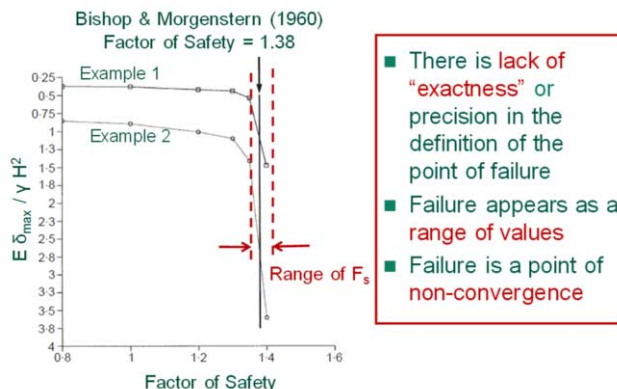


Figure 27. Failure condition specified for the Strength Reduction, method, SRM.

As the shear strength parameters are reduced, the deformation measure slowly decreases to about 0.5 and suddenly the deformation measure rapidly increases to more than 1.5. Further reductions in the shear strength analysis causes the analysis to become unstable (i.e., non-convergence). There is no clear or distinct value for the factor of safety at failure. Rather, failure is defined as a range of values as shown in Figure 29. This behavior is somewhat bothersome to the geotechnical engineer who has been used to working with a precise value for the computed factor of safety when using other methodologies.

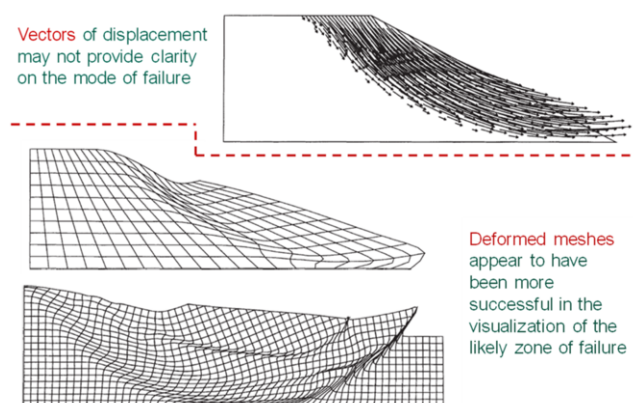


Figure 28. Use of deformed meshes to show zones of excessive deformation.

Figure 28 illustrates how the deformed mesh reveals the zone (or zones) where failure conditions are being approached. In other words, the Strength Reduction method provides the geotechnical engineer with information on the shape and location of failure surfaces.

Additional soils information (e.g., Young's modulus and Poisson's ratio) must be input by the modeler when using an elasto-plastic model. Consequently, the Strength Reduction method require more "know how" than limit equilibrium methods. While this may appear to be a disadvantage for the Strength Reduction methodology, it is noted that the Mohr-Coulomb strength envelope dominates the analysis as failure conditions are approached. The convergence rules (i.e., criterion) may require some user intervention in refining the failure tolerance and this has been viewed as a negative aspect by initial users of the Strength Reduction method. Countering the negative concerns is the fact that the Strength Reduction method provides additional valuable information particularly when analyzing complex geological and geometric conditions.

Figure 29 shows one more example where the results of a Strength Reduction analysis are compares with the results of a limit equilibrium analysis. The values differ slightly but can be considered to be essentially the same from a practicing engineering standpoint.

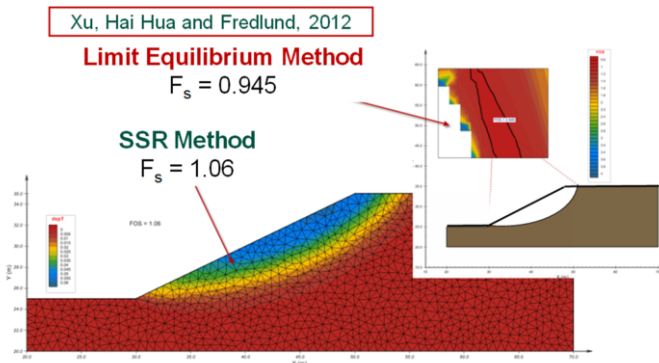


Figure 29. Comparison of the results of a Strength Reduction analysis and a Limit Equilibrium analysis.

The shear strength reduction methodology has also been extended to three-dimensional analyses [16, 17].

6. 3D Analysis and Digital Twins

The traditional application of the limit equilibrium method (LEM) has been in the context of a 2D plane strain analysis. Geotechnical engineers have become complacent with the use of 2D slope stability as it is easy to perform. 2D analysis suffers from fundamental limitations foremost of which are i) the slip shape is assumed to be cylindrical, ii) the slope geometry is assumed to be unchanged in the 3rd dimension, iii) the geo-strata is assumed to not vary in the 3rd dimension, iv) the water table must only vary in the down-slope direction, v) the application of distributed and point surface loads is not considered in the 3rd dimension, and vi) the application of anchors, micropiles, and geomembranes is approximated [18]. Such assumptions have proven 2D analysis to be conservative with

respect to the true 3D factor of safety in the amounts between 10-50% [19]. If unsaturated aspects of slope stability are considered then the difference can be as high as 60% [20]. Therefore, significant opportunity exists to optimize existing designs through the application of 3D slope stability analysis. It should be noted that the difference between a 2D and a calculated 3D factor of safety is different in each situation. Therefore, it is impossible to assume a specific 2D/3D difference for a particular scenario.

The theory for the 3D LEM has been in existence for decades and is therefore not new. Early theoretical development efforts are available in research literature [21, 22, 23, 24, 11]. The primary limitation of all presented theory is that the slip direction is assumed to happen exactly along the x-coordinate axis. Such a limitation introduces a significant problem for the practical application of 3D slope stability analysis. This paper presents an extension to the traditional 3D LEM, which allows for the analysis of slips at any direction. Several benchmark examples are presented such that the implementation of the methodology is proven sound. The technique may be applied to Bishop, Morgenstern-Price, GLE, Spencer and other analysis methods.

The application of 3D slope stability LEM in practical geotechnical analysis requires consideration of the aforementioned 3D influences on the factor of safety. This paper focuses on the effects of slip surface shape and ground surface shape. A recommended approach for the application of 3D slope stability analysis in the practice of geotechnical engineering is also presented.

The application of software tools to analyze slope stability in 3D has traditionally been highly limited. Recent developments allow for the easy application of 3D stability analysis in typical problems [20, 25, 26]. The SVSLOPE software developed by SoilVision Systems Ltd. is utilized for the analysis presented in this paper.

6.1. Continuity between 2D and 3D LEM

It is of importance to understand the difference between the slip shape analyzed in a 2D analysis as opposed to a 3D analysis. In a 2D analysis the slip shape is ultimately extended infinitely in the 3rd dimension and shear on the end surfaces is not considered. An example 2D analysis is presented in Figure 30. The equivalent 3D analysis is shown in Figure 31 where there is no shear strength applied to the vertical end surfaces.

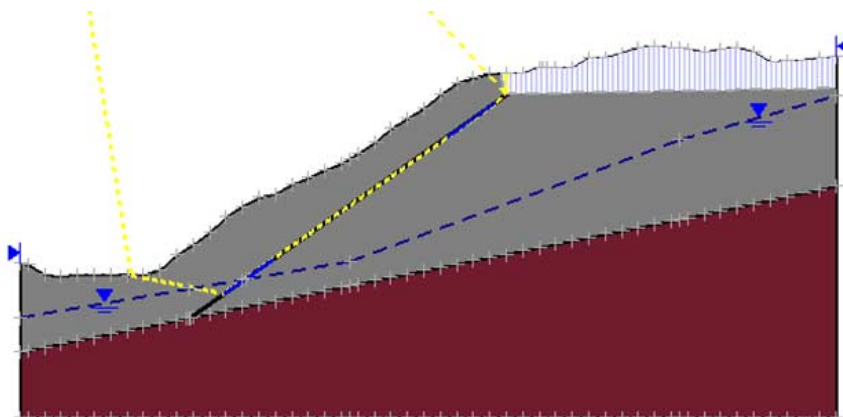


Figure 30. Example 2D stability analysis.

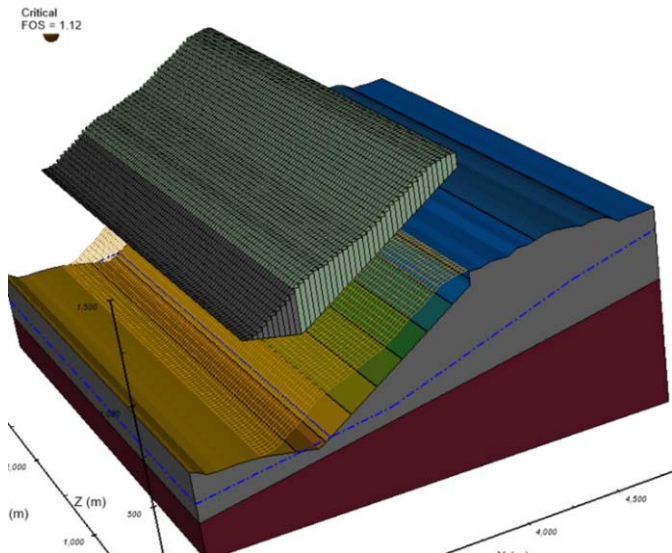


Figure 31. Equivalent 3D analysis (slip surface exploded out of slope).

It should be noted that a simple proof of a 3D analysis can be done by creating a 3D model of a 2D extruded slip surface and applying zero shear strength to the end-walls. This is an easy way to prove the 3D equivalent scenario of any 2D analysis. It also highlights the fundamental limitation of a 2D analysis which i) considers the slip to be of infinite length in the 3rd dimension and ii) does not consider the influence of shear strength on the end surfaces.

7. Directional Three-Dimensional Slope Stability Analysis

Three-dimensional stability analysis of asymmetrical geometries requires the determination of the critical slide direction. Yamagami and Jiang [27, 28] presented a relatively simple solution to this problem by computing the factor of safety using regular one-direction methods and varying the slide direction. The critical slide direction becomes the result of an optimization analysis in search for the minimum factor of safety. Huang and Tsai [29] presented a 3D two-directional moment equilibrium analysis that allow the determination of the critical slide direction. The authors considered semispherical and composite slide surfaces. The developed method is based on the principles of the method of columns and Bishop's assumption regarding the interslice shear forces. The equations for the moment equilibrium factor of safety in two directions is made as a function of the slide direction and the critical slide direction is shown to correspond to equal values of factors of safety. The critical direction is determined in a iterative manner. The method was verified using three different asymmetrical slopes, demonstrating is potential to identify failure mechanisms with lower factors of safety. Later, Cheng and Yip [30] presented a more general approach, based on moment and force equilibrium, the corresponds to extensions of Bishop's simplified, Janbu's simplified, and Morgenstern-Price's methods. The authors explain that past approaches are unstable when the slope is subjected to transverse horizontal forces and that the

proposed methods eliminate such instability. A careful examination is presented of the relevance and implications of assuming that all columns move in the same direction or that divergent movement takes place.

Figure 32 presents an illustration of the use of directional 3D slope stability analyses to asymmetrical slopes. The problem consists of a wedge failure with dimension of 2 and 4 m for which the analytical solution is $FS = 0.280$, a slide direction of 26.5° , and a dip angle of 65.91° . This problem was analyzed by Huang and Tsai [29] and by Cheng and Yip [30] and is analyzed here using SVSLOPE and two implemented approaches: a brute force method similar to what was introduced by Yamagami and Jiang [27, 28] and a one-directional automated method (Gao's method). Both methods produce correct results that match the analytical solution. However, the automated method required approximately 10% of the computation time of the brute force approach.

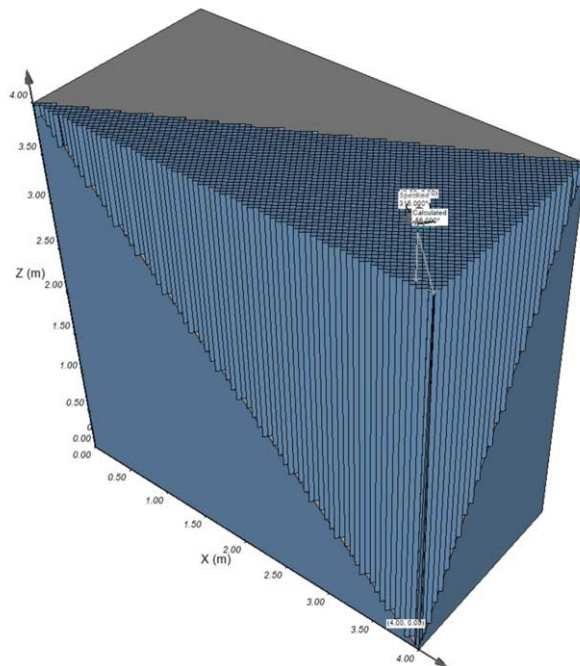


Figure 32. Asymmetrical wedge surface model.

8. Probabilistic approaches for slope stability analysis

From a deterministic standpoint, a slope with an expected factor of safety $E[FS] = 1.5$ is safer than a slope with $E[FS] = 1.2$. The two probability density functions (PDFs) presented in Figure 1 show that a PDF with higher $E[FS]$ may also present a higher probability of failure. Therefore, $E[FS]$ alone may provide incomplete or misleading information about the stability of a slope. Reliability-based approaches provide a way of incorporating parameter uncertainty into the slope modeling process. Reliability-based approaches are based on a method of computation of the probability density function (PDF) of the performance variable (e.g., the factor of safety, FS). Measures of reliability are defined based on the central tendency and variability of FS [31].

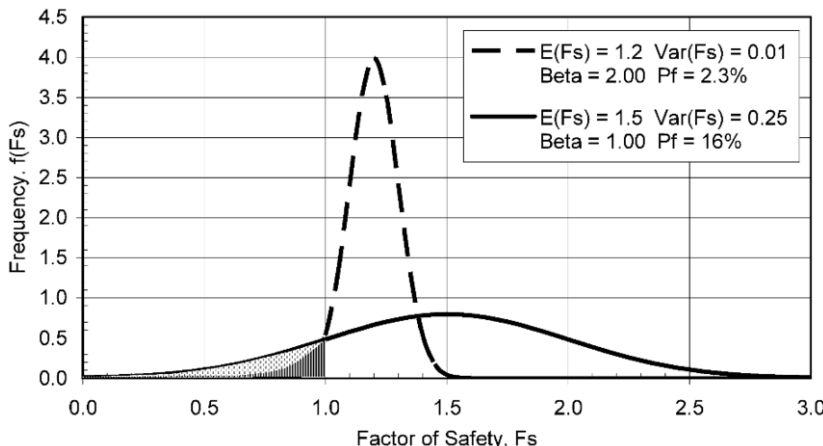


Figure 33. Probability density function of the factor of safety, FS, and probability of failure, Pf.

The design and decision-making process for slope stability requires not only the quantification of geo-hazards, but also the assessment of the vulnerability and risks, the establishment of acceptable risk levels and the selection of managing actions. Several techniques for assessing vulnerability and selecting acceptable risk levels are available and a number of management actions can be taken. Finally, it is important to point out that slope hazard assessment approaches may be implemented at various scales and that most slope hazards occur in the vadose zone and depend on the near ground surface soil characteristics and state. Unsaturated soil mechanics provides the required theoretical background for the quantification of slope hazards because slides are often triggered by the reduction in soil suction and shear strength.

8.1. Overview of reliability analysis methods

A probabilistic method that yields the PDF of the factor of safety is required in order to assess slope stability hazards. The main probabilistic methods available are the Monte Carlo simulation, the Taylor series method, and the Point Estimate methods. The Monte Carlo method was first developed by Hammersley and Handscomb [32]. Sets of input variables are obtained using random number generators. Each randomly generated set must be used to calculate a realization of FS and then used to define the PDF of FS. The Monte Carlo method requires a large number of trials, as shown by Harr [33].

The Taylor series method provides an approximate approach for obtaining the first few moments of the PDF of a function of random variables, such as the factor of safety, FS. Unlike the Monte Carlo method, the Taylor series method does not provide the complete PDF of FS. Therefore, the PDF of FS must be assumed for the computation of the probability of failure, Pf. The use of the first-order, second-moment equation provides a good approximation if FS is a linear function of the input parameters. Unfortunately, the derivatives of FS must be approximated using numerical approaches.

Point Estimate methods (PEM) are probabilistic methods for calculating the moments of the PDF based on the calculation of FS at pre-determined input variable values. The pre-determined values are combined with corresponding discrete probabilities. Evans [34] proposed an early PEM for independent random variables.

However, the first popular PEM approach is generally credited to Rosenblueth (1975)[35]. Several other point estimate methods were proposed (e.g., Li [36]; Panchalingam and Harr [37]). More recently, Gitirana Jr. [38] and Franco et al. [39] introduced a hybrid or alternative PEM based on the combination of the Taylor series approximation and the Rosenblueth two-point estimation for the estimation of the derivatives in Taylor's expansion. The method was shown to be as accurate as previous method, and yet required a reduced number of analyses. Figure 34 presents a comparison of the number of evaluations required by different probabilistic approaches.

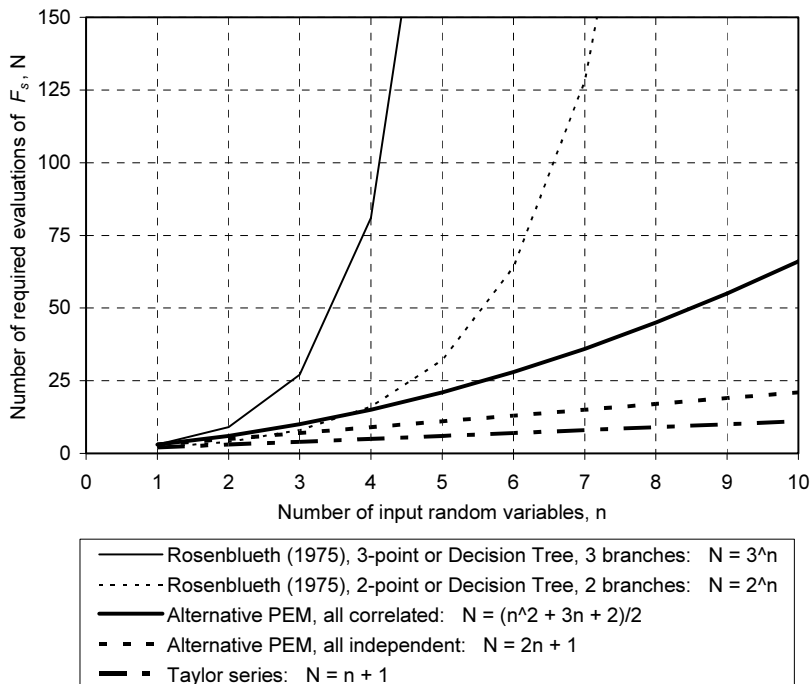


Figure 34. Number of evaluations of FS required by several probabilistic methods.

8.2. Implementation of probabilistic analysis in practice

A variety of issues must be addressed for the use of probabilistic methods in the practice of slope stability analysis and design. Many issues are related to protocols for data collection and the definition of the level of detail required for data collection. Soil properties may be accessed with various levels of detail. Estimates of soil properties may be obtained based on predictive approaches or knowledge-based systems [40]. Site vulnerability and risk levels must be accessed. There are several approaches available for the assessment of vulnerability based on the travel distance of a slide mass and the presence of neighboring structures and facilities. Probability of failure, site vulnerability and consequences must be combined with clearly defined levels of acceptable risks. According to Whitman [31] and Becker [41], the typical range of acceptable probabilities of failure adopted in slope and foundation engineering projects varies from 0.1 to slightly

lower than 1%. Acceptable risk levels can be established by compiling observed frequencies and consequences of natural and man-made events and use these values as a comparative basis. Computationally software is now available for computing probabilities of failure in 2D and 3D analysis.

9. Rock Stability Analysis Considering Anisotropy

The analysis of anisotropy is especially relevant in rock masses. Anisotropy can result from the geologic deformation of rock structures. A shear plane failing across a anisotropic structure is typically a strong failure plane while a shear plane that follow parallel to the bedding plane typically demonstrates weak behavior.

The modeling of such anisotropy in slope stability software has encountered two challenges historically. Firstly, the constitutive strength model to represent anisotropy needed to be developed. Pioneering work was performed by Mercer [42] in the Snowden Mining Industry Consultants in 2005 related to development of the Anisotropic Linear Models (ALM).

When the ALM constitutive model was first developed by Snowden Mining Industry Consultants in 2005, it assumed a linear relationship, both upslope and downslope between shear strength and the orientation in the rock mass. This orientation in the rock mass is known as the Angle of Anisotropy, which is measured as the orientation of an arbitrary slice relative to the orientation of the bedding plane (usually the weakness plane). As the ALM strength model evolved, the fourth generation ALM4 now has differences from its predecessors. Most notably, it now includes defined equations to represent the relationship between the Angle of Anisotropy and the shear strength at any orientation. Simply put, this advancement allows the user to determine shear strength at any orientation in the rock mass.

ALM4 presents other significant information, such as shear strength differentials in the upslope and downslope directions; percentages of shear strength differential; and relationships between the Angle of Anisotropy and the percentage of shear strength differential. ALM4 accommodates simple input parameters to provide valuable modeling information in anisotropic environments.

The second challenge of modeling anisotropy is having a methodology to represent anisotropic weak planes in 2D and 3D numerical models. Historical effort has focused on specifying weak surfaces as lines in 2D or as flat planes in 3D. However, this configuration rarely fits the real-world. Therefore a methodology of representing bedding planes in 3D space was developed (Figure 35; Figure 36).

Bedding Guides are surfaces used to conveniently define a series of beddings for rock layers. They are an ordered series of grids or meshes that define two or more known geometries for beddings. Any number of beddings are linearly interpolated between each adjacent pair of guides during model analysis. The effect of a bedding is to modify the shape of the generated trial slip surfaces such that they may follow the weak bedding. This is particularly useful for Anisotropic Linear Model materials, where the slip surface shape must be able to interact with the rock beddings in order to find an accurate factor of safety.

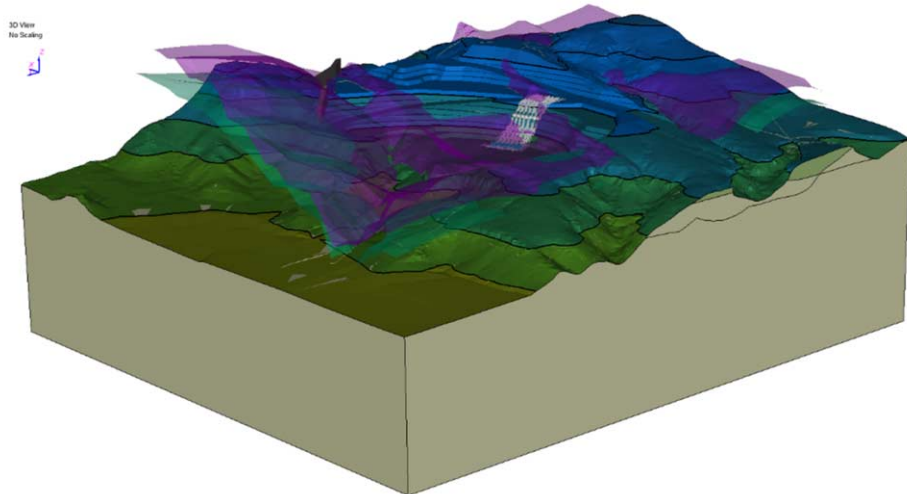


Figure 35. Bedding planes defined in 3D space showing daylighting above the ground.

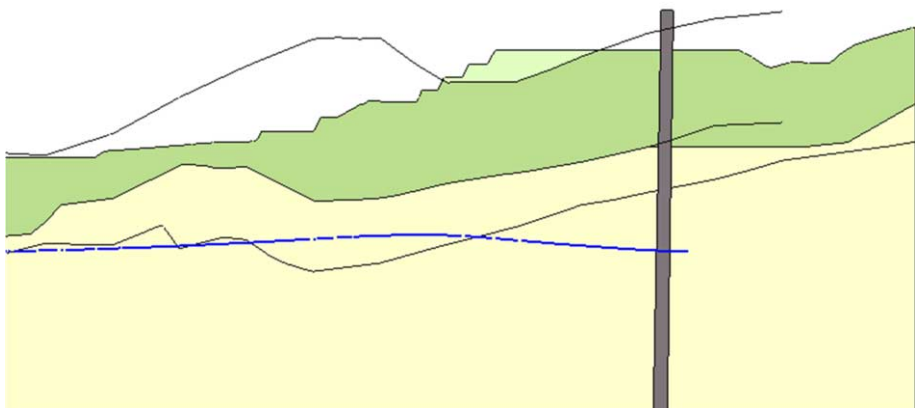


Figure 36. Projection of bedding planes onto 2D space.

Beddings influence a trial slip surface ellipsoid similarly to fully specified wedges or weak surfaces. Where the ellipsoid would cut through and beneath the bedding, instead it follows the bedding (the bedding effectively clips the ellipsoid below the bedding). This allows for parts of the sliding mass to be ellipsoidal shaped while other parts to follow the bedding shape.

Beddings are special in that each ellipsoidal trial will be tested with each individual bedding, one at a time (in addition to only the ellipsoid with no beddings). This means that it's not necessary to know ahead of time which bedding a slip surface should follow. Because only one bedding is active at a time it is not possible for a slip surface to follow one bedding in one area and a different bedding in another area.

10. Spatial Stability Analysis

One of the secondary issues with a standard 2D geotechnical analysis is that the geotechnical engineer may not know the correct location of the 2D plane which produces a critical factor of safety. A classic example of such a problem was presented by Jian [43]. The example presents a simple slope to illustrate two problems with conventional 2D plane-strain stability analysis; namely that the location of the slip as well as the correct factor of safety can be difficult to determine from this relatively straightforward example.

Multi-plane analysis (MPA) allows the engineer to quickly perform hundreds or thousands of analyses around a slope quickly using parallel computations. In the 2D MPA analysis method the slope is sliced into 2D profiles each of which is a full 2D LEM analysis. Each slice is analyzed, and the results are then plotted over top of the original 3D slope therefore giving a spatial perspective to the many 2D slices. Each slice is oriented such that the primary slip direction is the steepest slope. Since the slip may not happen on the steepest slope the MPA analysis method can be specified such that multiple orientations, such as +/- 10 degrees can be analyzed. In this way the most likely slip orientation can also be determined.

The analysis of slope can be seen in Figure 37. From the analysis we can see the critical zone clearly outlined as to the left of the nose of the hill. This is counter-intuitive from the sense that most engineers would feel that the point of the nose of this model would yield the lowest FOS value. Therefore, this illustrates the value of using analytical procedures to determine the correct location of a probable failure zone in an irregular topology. This result must also be noted that it is only the result of 2D slices through differing spatial locations in the 3D model. There is no relation implied or computed between the slices so the 3D lateral effects on the slope are not considered. Therefore, the model must be considered as an indication of a probable failure zone but not a definitive analysis which considers 3D effects.

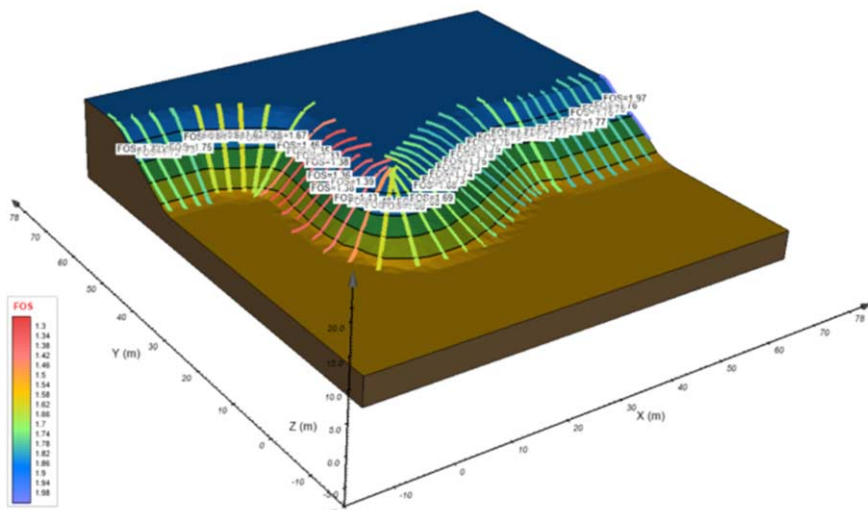


Figure 37. Example of slope difficult to analyze in 2D plane strain [43] – analysis by 2D MPA.

10.1. 3D Spatial Stability Analysis

The benefit of the multi-plane analysis is that it can easily be applied in 3D space using the same slicing planes established for the 2D analysis only with the analysis of a 3D ellipsoid at each slicing plane location. Similar searching techniques such as Entry & Exit, Cuckoo Search, Slope Search, or Auto Refine methods can be applied to the searching technique. The aspect ratio of the ellipsoid as well as faults and fractures can be considered as well in the analysis.

An enormous amount of information is generated with each slice being considered as a full 3D analysis. The 3D results can therefore be presented as a series of individual critical slip surfaces or contoured to produce a contoured map of the relative factor of safety over an area. The results of such an analysis for an open pit are shown in Figure 38. It can be seen that MPA is a useful methodology for i) understanding the relative factor of safety of a large spatial area as well as ii) locating potential zones of instability which may exist. The 3D results also provide a higher and computationally more realistic analysis of the true 3D FOS.

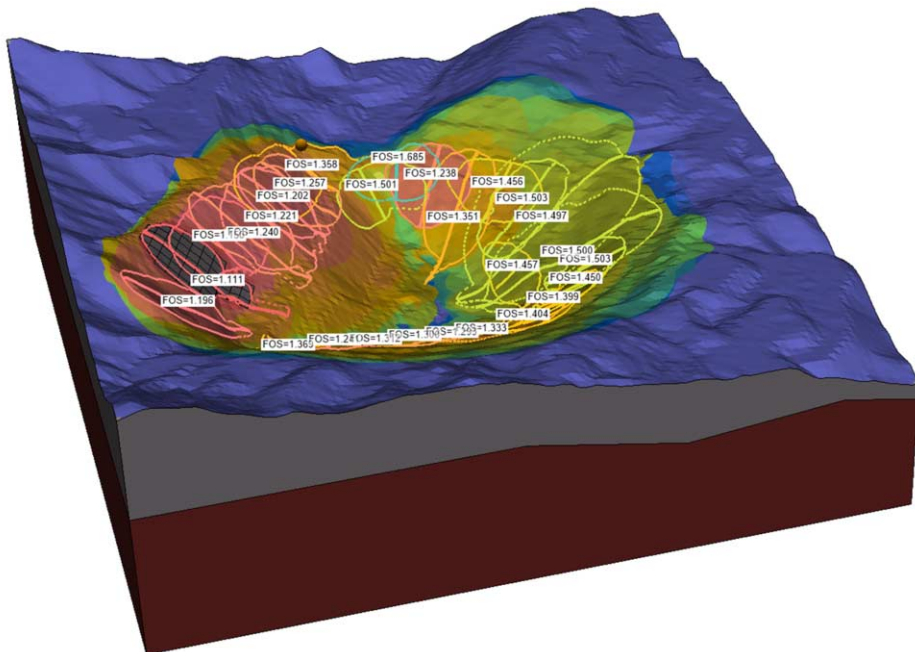


Figure 38. Example of 3D MPA applied to the analysis of an open pit.

11. Summary and Conclusions

Following are a few general conclusions that can be made regarding some of the more recently proposed methods of slope stability analysis and the historically proposed limit equilibrium methods of analysis.

- 1.) The Morgenstern-Price (or GLE) method of analysis is recommended for use when the limit equilibrium methodology is selected for the calculation of the

factor of safety. Other limit equilibrium methods may not give an accurate assessment of the factor of safety depending on the shape of the slip surface (i.e., whether the slip surface is circular or planar). This recommendation holds true for both 2D and 3D analysis.

- 2.) Most of the more recent alternate methods of analysis appear to give factors of safety quite similar to the Morgenstern-Price (or GLE) method when simple slope geometries are analyzed. The reason for the similarities in the calculated factors of safety appears to be mainly due to the common ground surface geometry which controls the overall potential energy imparted to the slope.
- 3.) Some general conclusions can be made with regard to the finite element based methods of analysis:
 - a.) First, it is recommended that the Kulhawy [12] definition for the factor of safety be used when using the Enhanced Limit method of analysis. Also, the finite element stress-deformation analysis should be performed using a linear elastic model.
 - b.) A Mohr-Coulomb model should be used when performing a Strength Reduction finite element stress-deformation analysis. The Strength Reduction method does not provide the engineer with as precise a calculation for the factor of safety; however, the values appear to be essentially the same as those obtained for a limit equilibrium analysis where both moment and force equilibrium are satisfied. The Strength Reduction method can provide the geotechnical engineer with additional concerning the shape and location of the critical slip surface.

There are other aspects associated with the analysis of slopes where consensus would be of value to the geotechnical engineer. Some of these areas are as follows:

- 4.) There has been considerable attention given to the use of three-dimensional slope stability analyses in recent years [44]. It is commonly concluded that in general, the calculated three-dimensional factor of safety is higher than the two-dimensional factor of safety and as a result it has been brushed aside as being of limited value. However, this does not appear to be a wise conclusion since many slope geometries are truly three-dimensional and cannot be modeled using a two-dimensional analysis. In addition, all slope failure in the field are three-dimensional in character. Two-dimensional and three-dimensional analysis should be performed in the majority of cases.

- 5.) Mass movements are often used to back-calculate the shear strength parameters for the soil. While a “forward or design” analysis of a slope involves a search for the minimum factor of safety, the “back-analysis” of a failed slope required a search for the opposite soil parameter conditions.

Stated another way, the factor of safety from a 3-dimensional “forward or design analysis” may typically be 4 to 20% higher than the F_s obtained from a 2-dimensional analysis. On the other hand, the factor of safety is fixed at 1.0 for a “back-analysis” and the shear strength parameters are computed. As a result, the shear strength parameters (i.e., c' and ϕ') may be 4 to 20% lower in a 3-dimensional analysis than in a 2-dimensional analysis. Or it can be said that the search is for the minimum factor of safety in a “forward analysis” whereas the search is for the maximum required shear strength parameters in a “back analysis”. Consequently, the role of the “searches” reverses when considering a “forward analysis” as opposed to a “backward analysis”. Understanding the

reversed roles is complicated when taking into consideration the differences between a 2-D and a 3-D slope stability analysis.

It should also be noted that a “forward or design” analysis involves a search for one variable (i.e., minimum F_s), whereas a “back-analysis” involves a search for two variables (i.e., maximum required c' and ϕ'). Consequently, further information related to the relationship between the two variables is required to make the analysis determinate.

- 6.) Geotechnical engineers need to be aware of the limitations associated with so-called three-dimensional slope stability methods. For example, it can be argued that present three-dimensional formulations are not truly three-dimensional in character since all movement must be limited to a single direction. Recent developments where the direction of movement can be searched for critical conditions are welcomed and useful in the assessment of mining pit and riverbank stability studies.

The calculation and importation of pore-water pressures from either an independent saturated-unsaturated seepage analysis is of considerable value in geotechnical engineering. The imported pore-water pressures may also be induced by applied loads under undrained or partial drainage conditions. These interactions between slope stability and pore-water pressures requires the ability to “combine” more than one software package.

As 3D analysis techniques become more common and easily applied the geotechnical engineer must understand the differences between a 2D and a 3D analysis. A 2D equivalent “cylindrical” shape failure can be simulated with a 3D analysis. Probabilistic analysis can provide a more reliable understanding of the risk related to a certain slope and can be performed in 2D and 3D with reasonable computing times. Anisotropy and complex 3D bedding planes can now be accommodated in a 2D or 3D limit equilibrium analysis. Spatial analysis of slopes is possible with multi-plane technologies over larger areas and opens up new analysis possibilities for determining the location of the most critical failure surface.

References

- [1] Pettersson, K. E. (1916). Kajraset I Goteborg des 5re Mars 1916 (Collapse of a quay wall at Gothenburg, March 5th, 1916). *Teknisk Tidskrift*, 46:289.
- [2] Fellenius, W. (1936). Calculation of the stability of earth dams, *Proceedings of the Second Congress on Large Dams*, Washington, DC, 4.
- [3] Bishop, A. W. (1955). “The use of the slip circle in the stability analysis of slopes”, *Geotechnique*, Vol. 5, pp. 7-17.
- [4] Janbu, N. (1954). Stability analysis of slopes with dimensionless parameters. Doctoral thesis, Harvard University, Cambridge.
- [5] Janbu, N. (1968). Slope stability computations. *Soil Mechanics and Foundation Engineering Report*, Trondheim, Technical University of Norway.
- [6] Morgenstern, N. R. and Price, V.E. (1965). “The analysis of the stability of general slip surfaces”, *Geotechnique*, Vol. 15, pp. 79-93.
- [7] Spencer (1967), “A method of analysis of the stability of embankments assuming parallel interslice forces”, *Geotechnique*, vol. 17, pp. 11-26
- [8] Fredlund, D.G. (1984). Analytical methods for slope stability analysis. State-of-the-art. *Proceedings of the Fourth International Symposium of Landslides*, Toronto, Canada, Vol. 1, pp. 229-250.
- [9] Fredlund, D.G., Krahn, J., and Pufahl, D.E. (1981). The relationship between limit equilibrium slope stability methods, *Proceedings of the 10th International Conference on Soil Mechanics and Foundation Engineering*, Stockholm, Sweden, Balkema-Rotterdam, Vol. 3, pp. 409-416.

- [10] Wilson, G.W., and Fredlund, D.G. (1983). The evaluation of the interslice side forces for slope stability analysis by the finite element method. Proceedings of the 9th Canadian Congress of Applied Mechanics, Saskatoon, Saskatchewan, May 30-June 3.
- [11] Fredlund, D.G. and Krahn, J. (1977). Comparison of slope stability methods of analysis, Canadian Geotechnical Journal, Vol. 14, pp. 429-439.
- [12] Kulhawy, F. (1969). Finite element analysis of the behavior of embankments. Ph.D., thesis, University of California, Berkeley, California, USA.
- [13] Stianson, J. (2008) Three-dimensional Slope Stability Analysis Using the Dynamic Programming Method of Analysis, PhD. Thesis, University of Alberta, Edmonton, AB., Canada.
- [14] Stianson, J.R., Chan, D. and Fredlund, D.G. (2004). Comparing slope stability analysis based on linear-elastic or elasto-plastic stresses using Dynamic Programming technique, Proceedings of the 2004 Canadian Geotechnical Conference, Quebec City, Quebec, ON, Canada.
- [15] Griffiths, D.V. and Lane, P.A. (1999). Slope stability analysis by finite elements, Geotechnique, 49, No. 3, pp. 387-403.
- [16] Lu, Haihua, Xu, L.M., Fredlund, M.D., and Fredlund, D.G. (2014). Comparison between three-dimensional limit equilibrium and shear strength reduction methodologies, Geotechnical Special Publication, Geo-Congress, ASCE, DOI 10.1061/9780784413272.3, February, Atlanta, Georgia.
- [17] Lu, H.H., Xu, L.M., Fredlund, M.D., and Fredlund, D.G. (2014). "Comparison between 3-D limit equilibrium and shear strength reduction methodologies", Proceedings of the Geo-Congress on Geo-Characterization and Modeling for Sustainability, Atlanta, Georgia, February 23-26.
- [18] Lam, L. and Fredlund, D.G. (1993). A General Limit Equilibrium Model for Three-Dimensional Slope Stability Analysis. Canadian Geotechnical Journal, Vol. 30, pp. 905-919.
- [19] Domingos, V.H. (2016). Three-Dimensional Slope Stability Using the Limit Equilibrium Method. M.Sc. dissertation. Federal University of Goias, Goiania, Brazil.
- [20] Zhang, L., Fredlund, M., Fredlund, D.G., Lu, H., and Wilson, G.W. (2015). The Influence of the Unsaturated Soil Zone on 2D and 3D Slope Stability Analyses, Elsevier - Engineering Geology, May 14, 2015.
- [21] Hovland, H.J., (1977).Three-dimensional slope stability analysis method. ASCE J. Geotech. Eng. Div. 103 (GT9), 971–986.
- [22] Hungr, O. (1987). An Extension of Bishop's Simplified Method of Slope Stability Analysis to Three Dimensions. Geotechnique, Vol. 37, No. 1, pp. 113-117.
- [23] Hungr, O. (1997). Slope Stability Analysis. Keynote paper, Proc., 2nd. Panamerican Symposium on Landslides, Rio de Janeiro, Int. Society for Soil Mechanics and Geotechnical Engineering, 3: 123-136.
- [24] Hungr, O., Salgado, E.M., and Byrne, P.M. (1989). Evaluation of a Three-Dimensional Method of Slope Stability Analysis. Canadian Geotechnical Journal, Vol. 26, pp. 679-686.
- [25] Reyes A., Pilar G., Denys P. (2014). 3D Slope Stability Analysis of Heap Leach Pads Using the Limit Equilibrium Method, Heap Leach Solutions, November 10 - 13, Lima, Peru.
- [26] Reyes A., Denys P. (2014). 3D Slope Stability Analysis by the Limit Equilibrium Method of a Mine Waste Dump, Tailings and Mine Waste 2014, October 5 - 8, Keystone, CO, USA.
- [27] Yamagami, T., Jiang, J. C. (1996). Determination of the sliding direction in three-dimensional slope stability analysis. Proc., 2nd Int. Conf. on Soft Soil Engineering, Vol. 1, 567–572, Nanjing, China.
- [28] Yamagami, T., Jiang, J. C. (1997). A search for the critical slip surface in three-dimensional slope stability analysis. Soils and Foundations, 37(3): 1–16.
- [29] Huang, C.C., Tsai, C.C. (2000). New method for 3D and asymmetrical slope stability analysis. ASCE Journal of Geotechnical and Geoenvironmental Engineering, 126(10): 917-927.
- [30] Cheng, Y.M., YIP, C.J. (2007). Three-dimensional asymmetrical slope stability analysis extension of Bishop's, Janbu's, and Morgenstern-Price's techniques. ASCE Journal of Geotechnical and Geoenvironmental Engineering, 133(12): 1544-1555.
- [31] Whitman, R.V. (1984). Evaluating calculated risk in geotechnical engineering. ASCE Geotechnical Engineer Journal. 110(2): 145-189.
- [32] Hammersley, J.M., Handscomb, D.C. (1964). Monte Carlo Method. John Wiley & Sons, New York.
- [33] Harr, M.E. (1987). Reliability-Based Design in Civil Engineering. John Wiley and Sons. New York. 291p.
- [34] Evans, D.H. (1967). An application of numerical techniques to statistical tolerancing. Technometrics, vol. 9.
- [35] Rosenblueth, E. (1975). Point estimates for probability moments. Proc. National Academy of Sciences, 72(10): 3812-3814.
- [36] Li, K. S. (1992). Point-estimate method for calculating statistical moments. Journal of Engineering Mechanics, 118(7), 1506-1511.
- [37] Panchalingam, G., Harr, M.E. (1994). Modelling of many correlated and skewed random variables. Applied Mathematical Modelling, 18: 635-640.

- [38] Gitirana JR., G.F.N. (2005). Weather-related geo-hazards assessment model for railway embankment stability. PhD Thesis. University of Saskatchewan, SK, Canada. 411p.
- [39] Franco, V.H., Gitirana JR., G.F.N., Assis, A.P. (2019). Probabilistic assessment of tunneling-induced building damage. *Computers and Geotechnics*, 113: 97-112.
- [40] Phoon, K.-K., Kulhawy, F.H. (1999). Characterization of geotechnical variability. *Canadian Geotechnical Journal*, 36: 612-624.
- [41] Becker, D.E. (1996). Eighteenth Canadian Geotechnical Colloquium: Limit states design for foundations. Part I. An overview of the foundation design process. *Canadian Geotechnical Journal*, 33: 956-983.
- [42] Mercer, K. (2013). The history and development of the Anisotropic Linear Model: part 2, Australian Center for Geomechanics, Volume No. 40, July 2013
- [43] Jiang, J.-C., Baker, R., and Yamagami, T. (2003). The Effect of Strength Envelope Nonlinearity on Slope Stability Computations, *Canadian Geotechnical Journal*, Vol. 40, No. 2, pp. 308-325.
- [44] Zhang, L., Fredlund, M., Fredlund, D.G., Lu, H. (2014). Comparison of 2D and 3D Slope Stability Analysis for Unsaturated Slopes, 67th Canadian Geotechnical Conference Regina, GeoRegina 210, SK, Canada Sept 28 - Oct 1, 2014.

Technical Session #15 “Preservation of historic sites”



Carlo VIGGIANI

Carlo Viggiani graduated in Civil Engineering in 1960 at the University of Napoli; PhD in Geotechnical Engineering in Napoli in 1969.

He has been teaching in the Universities of Pavia, Cosenza, Potenza; from 1974 to 2011 he has been Professor of Foundation Engineering at the University of Napoli Federico II, where is at present Emeritus Professor.

C.V. has been State of the Art Reporter at the International Conferences on Soil Mechanics and Geotechnical Engineering in New Delhi, 1994 (Mitigation of Natural Hazards: Landslides and Subsidence) and in Osaka, 2005 (Pile foundations).

He is Author or Co-Author of 4 books and more than 200 technical papers.

His research topics include Theory of Consolidation, Soil-Structure Interaction for Shallow and Deep Foundations, Geotechnics for the Conservation of Monuments and Historic Sites. He has been Chairman of TC19 (later TC301) (Preservation of Monuments and Historic Sites) of the ISSMGE and has been involved in the conservation of a number of monuments affected by geotechnical problems.

From 1990 to 2002 he has been member of the International Committee for the Safeguard of the Leaning Tower of Pisa and is presently member of the Monitoring and Surveillance Committee of the Tower. His interest to the Tower dates back to 1963.

C.V. has been involved, as geotechnical consultant, in the design and construction of a number of civil engineering structures; among them earth dams, civil and industrial buildings, bridges, tunnels and underground constructions, stabilisation of landslides. He acted as consultant for Italian Railways and Underground Transportation Systems in Rome, Napoli, Torino, Bologna, Firenze. He has been involved in the design of the suspension bridge over the Messina Straits

The Behaviour of an Ancient Tower Through History and Monitoring

Carlo VIGGIANI^{a,1}

^a*University of Napoli Federico II, Italy*

Abstract. Geotechnical Engineering plays often a significant role in the conservation of historical buildings and monuments; this is particularly true for ancient towers, where soil structure interaction is a very important aspect.

From the viewpoint of an engineer, the peculiarity of any intervention on historical structures is the requirement of respecting their integrity, besides guaranteeing the safety. While the attainment of safety is a relatively straightforward matter for a well trained and experienced engineer, the respect of integrity is a much more difficult matter, since the concept itself of integrity has many facets and is somewhat elusive.

To conceive and implement any intervention intended to safeguard a monument, a clear understanding of its mechanisms of behaviour is essential. Such an understanding may be obtained by a careful reconstruction of its history and a complete observation of its actual behaviour by a proper monitoring program.

These concepts are exemplified referring to a famous medieval Italian tower: the leaning tower of Pisa.

Keywords. Integrity, monitoring, leaning instability.

1. Introduction

To defend, not to attack; to see further afield; to challenge the sky, or simply to observe it; to call to prayer or to sound the alarm; to look inside oneself and lift oneself above and away from the struggle of daily life. A tower can be used for all these things, a creation which sews together East and West and has its roots in the Bible and the Koran, and indeed in the origins of our common civilisation [1].

Consequently, there is an unbelievable number and variety of towers in the ancient and recent history of humankind: from the mythical tower of Babel, erected by Nebuchadnezzar in the 6th century BC, and the lighthouse of Alexandria, one of the seven wonders of the antiquity, to the Eiffel Tower, the Burj Khalifa and other skyscrapers, the modern towers for communication [2, 3]. In Christianity, since the 6th century, many churches and practically all monasteries have a tower, or a campanile. In Islam, the muezzin calls to prayer from a minaret. In the 10th century, Chinese pagodas had already reached a height of 150 m.

Many of these towers, especially the ancient ones, are affected by geotechnical (and structural) problems, due to their slenderness, the high stresses acting in their structure

¹Carlo Viggiani; E-mail: viggiani@unina.it.

and foundations, the lateral actions such as wind and earthquakes. Here engineers, and among them geotechnical engineers, come into play.

2. Integrity

For the ancient towers, any engineering intervention must of course satisfy the requirements of safety (a task relatively easy to fulfil for a well trained and experienced engineer), but also respect the integrity of the monument. The integrity is an elusive concept, with many facets (formal integrity, material integrity, historical integrity) and varies in space and time, as does the prevailing culture of different regions and different ages. It is exactly this elusive value, however, that any intervention on a monument should preserve.

When dealing with this kind of problems, the safety and the integrity are often in conflict. The engineer, in charge of the safety, is influenced by his rational formation and tends to be suspicious about elusive concepts; on the other side the restorer, called to watch over the respect of integrity, is afraid about a possible oversimplifying and invasive approach of the engineer.

The first position may be exemplified by the following episode. Fernando Lizzi (1914-2003) was a very bright Neapolitan engineer, considered the father of micropiles technology. He is author of books on the restauration of ancient constructions [4]; the IMS (International Micropiles Society) has promoted a Lizzi lecture, that has reached the 9th edition. In a paper presented to an international symposium [5] Lizzi recalls that, in 1973, there was an international tender for the stabilisation of the Leaning Tower of Pisa. He participated with a project based on the use of micropiles, signed by himself and Jean Kerisel: names that are a guarantee of quality.

Lizzi writes: "The Competition was not awarded; no decision was taken and, at the date of the present paper (2000), the problem is still in the hands of a special Committee, appointed ten years ago. As for the above project, based on a network of Pali Radice, the present Committee admits its full validity from the engineering point of view; but its members solemnly declare that it cannot be accepted because the execution of piles, although concealed in the low masonry and in the subsoil ... spoils the integrity of the Monument Therefore, the Committee is looking for a solution which can be carried out *without touching* the Monument".

Lizzi makes ironic references to the Committee (italic and dots are in the original paper), and a large majority of the civil engineers would probably agree with his position. The common sense of a familiar, good, reliable underpinning to be obviously preferred to the apparently meaningless pretension of stabilising the Tower without even touching it!

The opposite position, the sacerdotal position of the strict respect of the integrity, may be exemplified by a book by Pierotti [6], a professor at the University of Pisa. In his enjoyable book Pierotti lays out a very documented and complete history of the Tower; in the final part, however, he seriously suggests that the monument could tend to a spontaneous self-equilibrating state, behaving as a biologic organism, and hence it does not need any stabilisation measure.

Trying to find the right way between these irreducible opposites, we will show that the rational, merely mechanistic approach of the engineer may suggest respectful solutions to some difficult restoration problems. As a matter of facts, in the case of Pisa, a solution which can be carried out *without touching* the Monument.

3. Mechanics

As noted above, towers are often affected by geotechnical problems, due to the high stresses acting on their foundations and the lateral actions of wind and earthquakes. Cadignani et al. [7] claim that the historic towers we observe today survived to an initial stage of their life in which they were probably close to a bearing capacity failure, due to insufficient strength of the foundation soils. A long duration of the construction period, and possibly delays or interruptions of the construction, allowed the foundation soil to improve its strength by consolidation and the tower to be successfully finished; this has been actually the case for the Tower of Pisa, whose case history will be dealt with in this paper, and other famous towers as the Ghirlandina in Modena [8]. Due to uneven settlement, many of these towers appear today inclined; this recall the danger of a different form of failure, due to insufficient stiffness of the soil, the so called leaning instability.

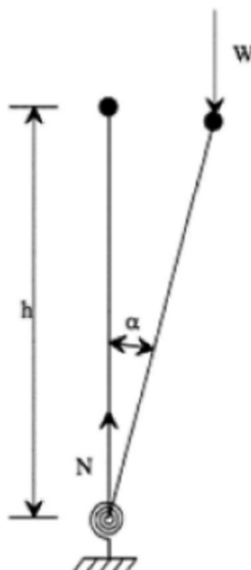


Figure 1. The inverted pendulum.

To introduce leaning instability, the simple conceptual model of an inverted pendulum may be used. It is a rigid weightless vertical pole (Figure 1) with a concentrated mass W at the top and hinged at the base to a constraint that reacts to a vertical displacement w with a vertical force $F = wk_w$ and to a rotation α with a stabilizing moment $M_S = \alpha k_\alpha$. On the other hand, the rotation induces an offset of the mass and hence an overturning moment $M_O = W h \sin \alpha$. If the stabilising moment is larger than the overturning one, the equilibrium is stable; the system returns to its initial configuration. If the contrary occurs, the equilibrium is unstable; the system collapses. If the two moments are equal, the equilibrium is neutral: the system stays in the displaced configuration. The stability of the equilibrium may be characterized by the ratio $FS = M_S/M_O$ between the stabilizing moment and the overturning one.

Modelling the tower as an inverted pendulum, the restraint exerted by the foundation may be evaluated, as a first approximation, by assimilating the foundation to a rigid circular plate of diameter D resting on an elastic half space of constants E, v . The plate is subjected to a vertical force W applied at the height h of the centre of gravity and hence with an eccentricity $e = h \sin\alpha$. Calling $M = We$ the overturning moment and w, α the settlement and the rotation of the foundation, it may be shown that k_α and k_w are given by:

$$k_w = \frac{ED}{i - v^2}; \quad k_\alpha = \frac{ED^3}{6(1 - v^2)} \quad (1)$$

In this simple linear model, there is no coupling between settlement and rotation, and the terms k_α, k_w are intrinsic properties of the ground – monument system. The stability may be characterized by a factor of safety FS given by the ratio between the stabilising moment and the overturning one:

$$FS = \frac{M_s}{M_o} = \frac{k_\alpha \alpha}{Wh \sin \alpha} = \frac{ED^3}{6(1 - v^2)} \frac{1}{Wh} \quad (2)$$

having posed $\sin\alpha \approx \alpha$ for small rotations. In the linear model, hence, the safety factor is also an intrinsic property of the ground – monument system, not depending on the value of the rotation.

In undrained conditions and in terms of total stress, the elastic constants of a linearly elastic, saturated porous medium are given by $E_u = 3E/2(1+v)$ and $v_u = 0.5$ (incompressible medium), where E and v are the constant of the solid skeleton in terms of effective stress. It follows that:

$$2 \geq \frac{FS_u}{FS} = 2(1 - v) \geq 1$$

showing that the safety against leaning instability *decreases* passing from undrained to drained conditions. This underlines the difference between the mechanisms of bearing capacity failure (lack of strength) and of leaning instability (lack of stiffness).

4. A case history: Pisa

4.1. The Monument

The Leaning Tower of Pisa, bell tower of the Pisa Cathedral (Figure 2), is undoubtedly one of the world's most beautiful and famous monuments. Its weight is 14.500 t, its height nearly 60 m, the foundation is 19.6 m in diameter, the centre of gravity is 22.6 m above the foundation plane. It is inclined to south at 5.5° and the seventh cornice overhang the ground by about 4.5 m.

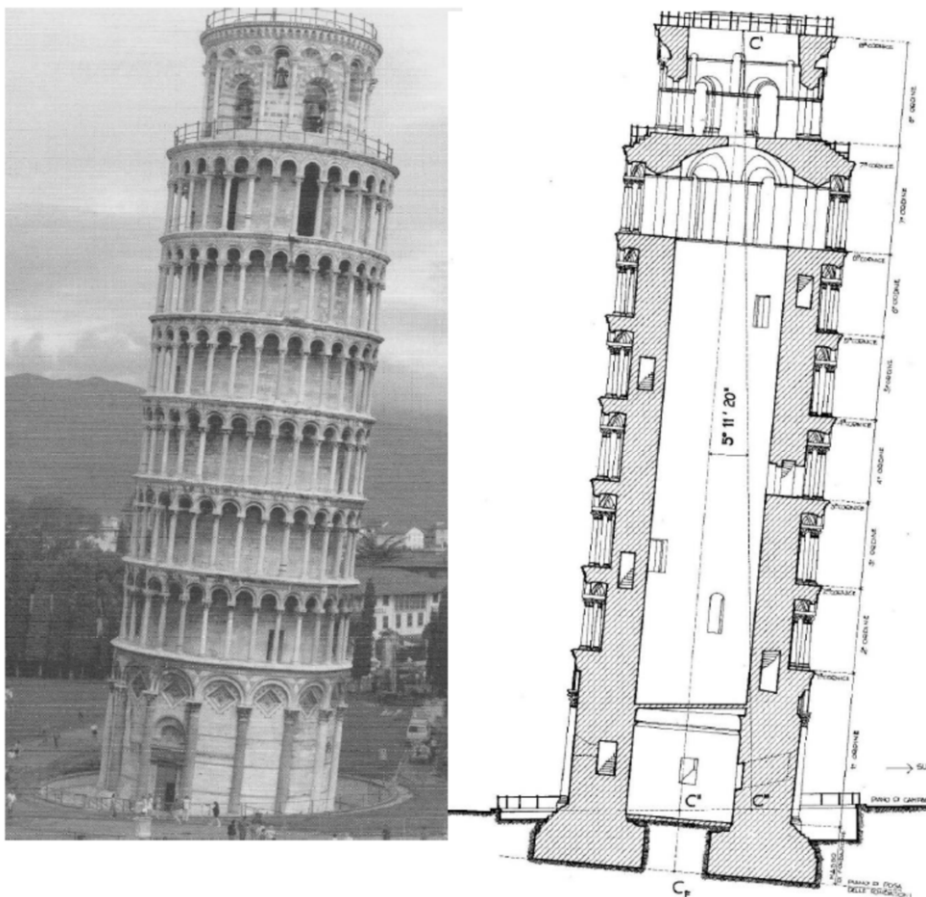


Figure 2. The Leaning Tower of Pisa.

The Tower is founded on weak, highly compressible soils and its inclination had been inexorably increasing over the years to a point at which it was very close to collapse.

As shown in Figure 3, the ground profile below the monument may be schematized in three layers. Layer A is about 10 m thick and consists of soft estuarine deposits of sandy and clayey silts laid down under tidal conditions. Layer B consists of soft, sensitive, normally consolidated or slightly overconsolidated marine clay, which extends to a depth of 40 m. Layer C is a dense sand, which extends to considerable depth. The surface of layer B is dished beneath the Tower, showing that the average settlement is about 3 m.

The construction of the Tower began in 1173, under Bonanno Pisano, architect and sculptor. Work progressed to the fourth order, reached in 1178, and was then suspended for a century; had the construction proceeded without interruption, the Tower would have collapsed due to an undrained bearing capacity failure. Work resumed in 1271 under Giovanni di Simone and reached the seventh cornice in 1278; then a second 80 years interruption followed. Once again, the interruption saved the monument from collapsing. Between 1360 and 1370 Tommaso di Andrea built the belfry, completing the construction two centuries after it had first begun.

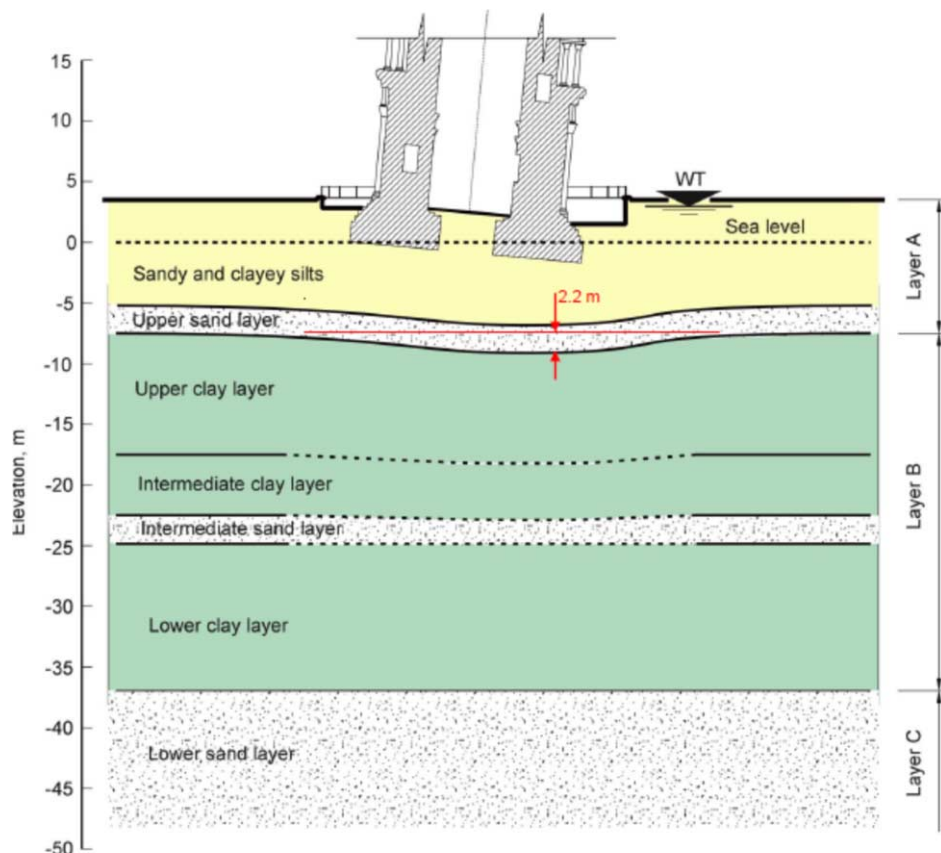


Figure 3. The subsoil of the Tower.

The tower began leaning during construction, as it is apparent from the corrections made by the ancient masons to compensate for the inclination that was progressively occurring. The most evident correction can be seen in the belfry: between the seventh cornice and the floor of the belfry there are six steps on the South side, and only four on the North.

The corrections carried out during the construction may be used to work out the inclination at that time [9]. As we see in Figure 4, at the beginning the Tower leaned to North to an inclination of 0.2° in 1272. In 1278, at the seventh cornice, the inclination was 0.6° to South. During the 80 years of the second interruption, it increased to 1.6° ; at this point the belfry was added.

After the end of construction, indications on the lean may be obtained by pictures (e.g., a fresco by Antonio Veneziano dating back to 1385) or by documents (e.g., a passage of the Arnolfo's life by Giorgio Vasari, 1566). In 1817 two English architects, Cresy and Taylor [10], carried out a detailed survey; another one was performed 40 years later by Rohault de Fleury [11].

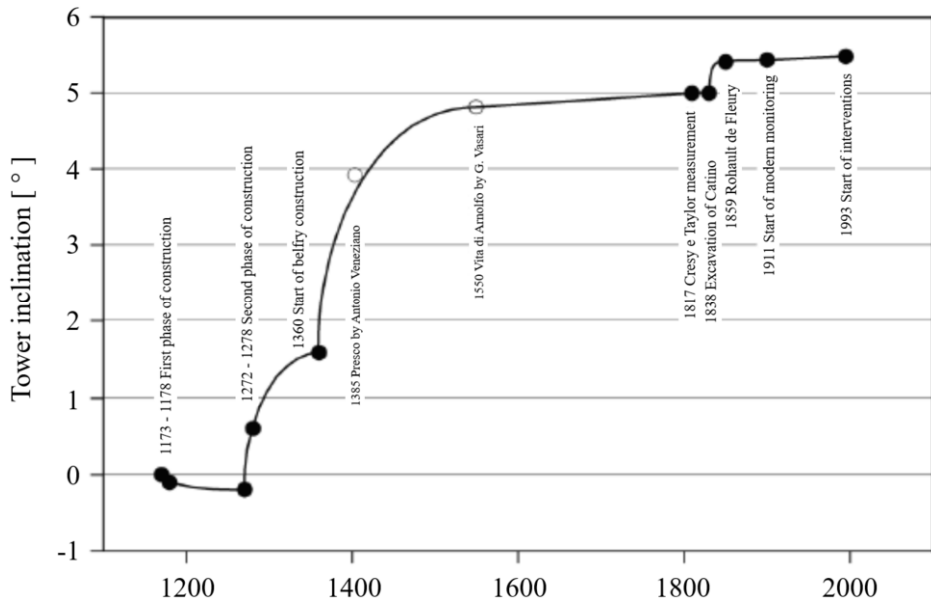


Figure 4. History of the inclination of the Tower.

Between the two measurements, an important event in the history of the Tower had occurred: the excavation of the walkway around the base of the Tower, known as the “catino” (the basin), with the purpose of exposing the column plinths and foundation steps, for all to see as originally intended (as mentioned above, the base of the tower had sunk into the soil due to the 3 m settlement). The excavation of the catino produced a sudden increase of the inclination of the Tower, but also a variation of the characteristics of its motion. Before the excavation, the Tower had come to rest or, in any case, its motion was going on at a very small and progressively decreasing rate. After the excavation, the Tower moves at a progressively increasing rate, ineluctably destined to end in a collapse.

Since 1911 the inclination of the Tower has been observed by a monitoring system, progressively improved and completed [9], [12]; between 1911 and 1990 it has been increasing each year by about six seconds, equivalent to about 1.5 mm horizontal displacement at the top. There has been much debate about the cause of this progressive increase in inclination. It has usually been attributed to a differential settlement due to creep in the underlying soft clay. It has also been suggested that the Tower is affected by impending bearing capacity failure in the underlying soft clay.

4.2. Monitoring

An International Committee, installed in 1990 with the task of conceiving, designing and implementing the stabilisation of the Tower, examined in detail the historical documentation and the available monitoring results. The history of the inclination, as depicted in Figure 4, was one of the outputs of this work.

If one plots the inclination of the Tower against its weight, progressively increasing during construction, the diagram in Figure 5 is obtained. It shows that the Tower kept

essentially vertical till the end of construction, and afterward it inclined significantly. This behaviour suggests the occurrence of a stability problem.

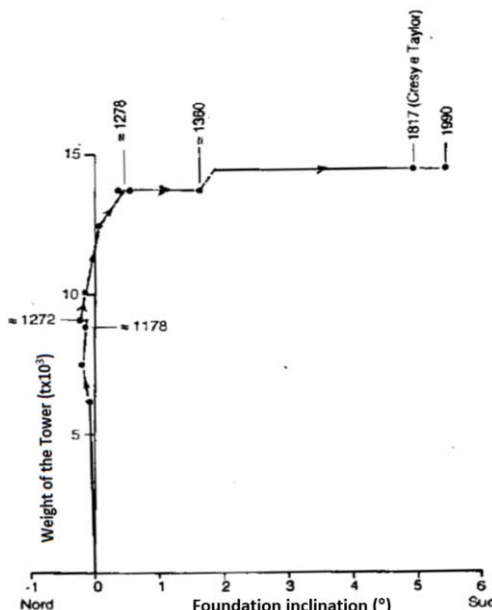


Figure 5. Inclination vs. weight.

A study of the geodetic survey measurements revealed a surprising form of motion, different to previously held ideas. They showed that the first cornice (point V1 in Figure 6) had not moved horizontally, apart from periods when there were external disturbances. Precision levelling, furthermore, showed that the centre of the foundation had not displaced vertically relative to the surrounding ground. Therefore, the rigid body motion of the Tower could only be as shown in Figure 6, with a centre of rotation at the level of the first cornice and vertically above the centre of the foundation. Again, the motion of the Tower shown in Figure 6 is typical of a leaning instability.

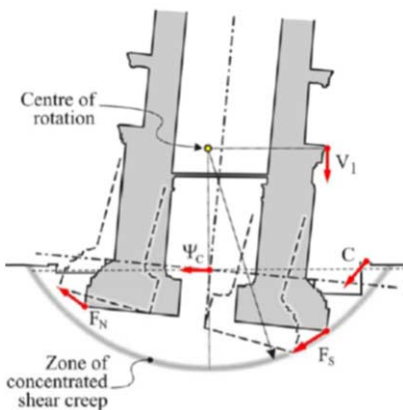


Figure 6. Observed kinematic of the Tower motion.

We can try to describe the phenomenon with the simple linear model outlined in § 4. From the first Eq. (1) one gets:

$$w = \frac{W}{k_w} = \frac{W(1 - v^2)}{ED}$$

With $W = 14,500$ t, $w = 3$ m, $D = 19,6$ m, one obtains:

$$\frac{ED}{1 - v^2} = 4,833 \text{ t/m}$$

With $h = 22.6$ m, Eq. (2) gives:

$$FS = \frac{ED}{1 - v^2} \frac{D^2}{6Wh} = 0.95 \approx 1$$

Even the very rough linearly elastic half space model confirms that the Tower is very nearly in a situation of neutral equilibrium, and that its impending instability is not due to a bearing capacity problem, but to leaning instability due to the very compressible foundation soil.

4.3. The intervention

The discovery of the motion shown in Figure 6 was crucial in many respects; it suggested the application of a lead counterweight to the north side of the foundation as a temporary stabilising measure and the underexcavation beneath the north side as a long term stabilisation measure. A complete description of these interventions and their effect on the Tower may be found in the Proceedings of the International Committee for the Safeguard of the Tower of Pisa [13].

The study of the movements of the Tower, depicted in Figure 6, led to the conclusion that the seat of the continuing long-term rotation of the Tower lies in Horizon A. It was then concluded that, probably in addition to creep, the most likely cause of the progressive rotation was the fluctuating ground water level due to rainstorms.

Piezometric measurements made over years have shown that the average ground water level close to the south side of the Tower in Horizon A is 200 to 300 mm higher than that to the north. This difference generates a small, but not negligible stabilising moment for the monument that is so close to falling over. In the autumn and winter, when the rainfall events are more intense, the water table raises sharply, reducing the difference in piezometric level and thereby producing southward rotations of the Tower, which are not fully recovered. It is believed that the cumulative effects by ratchetting of these repeated impulses has been one of the factors producing the steady increase of inclination in the long term.

To minimise this effect a drainage system controlling the water table was installed; it led to a significant reduction in its seasonal fluctuation and to another northward rotation of the Tower.

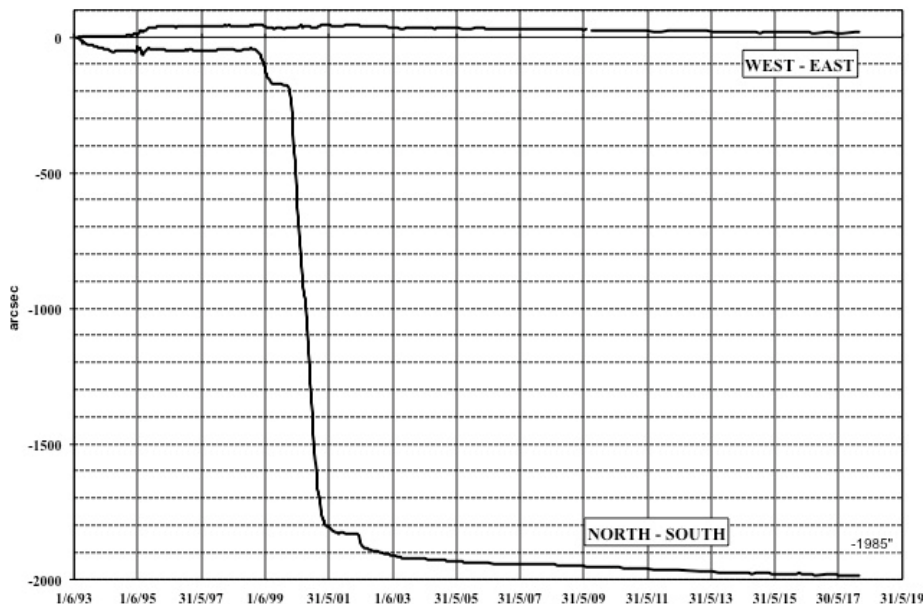


Figure 7. Rotation of the foundation of the Tower since 1993.

The results of these interventions may be seen in Figure 7. Figure 8 shows the effect of underexcavation on the history of the inclination from the beginning of the construction.

The stabilisation work may be seen as a mere reparation to the detrimental effect of the excavation of the catino; there is a kind of poetic justice in the fact that the detrimental effects of an incautious excavation have been repaired by another excavation, this time well conceived and carefully executed.

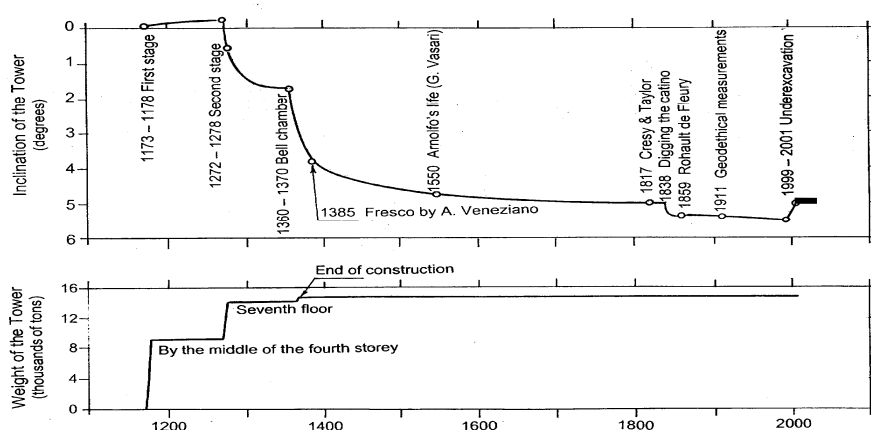


Figure 8. The complete history.

4.4. Has the stabilisation been achieved?

After the intervention of the International Committee and the publication of its results, Fernando Lizzi, already quoted in § 2, believes that the Tower has not been stabilised and expresses his doubts in a letter to a newspaper [14]. The model outlined in § 3 above seems to enhance his opinion: the safety factor is an intrinsic property of the ground-monument system and does not depend on the inclination. So, why a reduction of the inclination should increase the safety?

Albert Einstein used to say that things should be made as simple as possible, but not simpler! And the linear model of subsoil that we have used above is surely oversimplified. Figure 9 reports the results of a series of model tests in the centrifuge, on the rotation of a circular rigid plate resting on a clay bed. It appears evident that the process is non linear and that there is coupling between normal force and rotation. At unloading, only a minor part of the rotation is reversed, and at reloading the behaviour is quasi elastic until the previous load is reached. All these are characters of an elasto-plastic hardening behaviour.

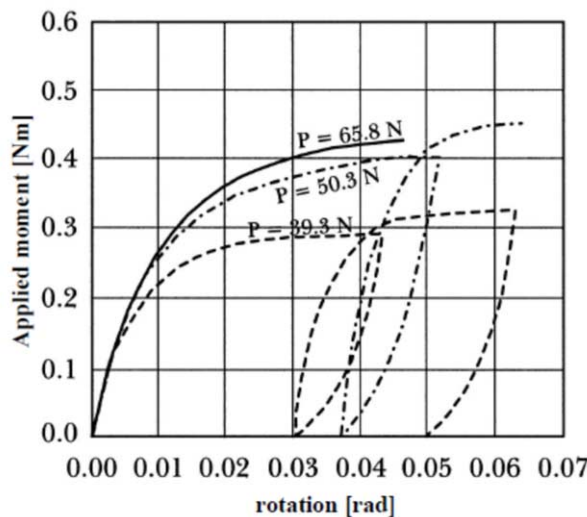


Figure 9. The tests by Cheney et al. [15].

With a non linear, elasto-plastic behaviour the relation between the external actions (W, M) and the displacements (w, α) becomes:

$$\begin{Bmatrix} \partial w \\ \partial \alpha \end{Bmatrix} = \begin{bmatrix} \frac{1}{k_w} & \frac{1}{k_{w\alpha}} \\ \frac{1}{k_{\alpha w}} & \frac{1}{k_\alpha} \end{bmatrix} \begin{Bmatrix} \partial W \\ \partial M \end{Bmatrix}$$

in which the terms of the stiffness matrix are not constant of the soil-monument system but vary as a function of the current stress state and of the previous stress history. Consequently, the safety against overturning is also a function of the current state and of the previous history.

In simple terms, the rotational stiffness of the soil-monument system is but the tangent $\partial M/\partial \alpha$ to the curves depicted in Figure 9. On a first loading curve, such a stiffness decreases with increasing α , and this explain why with increasing inclination the Tower was approaching the collapse: the situation was evolving from neutral equilibrium to instability. On the unloading branch, however, the stiffness is much larger than that at first loading, and this explains why even a small decrease of the inclination produces a substantial increase in the safety.

A question, however, remain to be answered: how will the Tower behave in the future? Attempting an answer is not easy, due to the complexity of the phenomena involved and the number and variety of factors influencing them.

4.5. Future scenarios

The International Committee, upon concluding its work, outlined two possible future scenarios [16].

In the first one, rather conservative, the Tower will remain motionless for some decades (a time span that the Committee called the honeymoon) and then gradually resume a southward rotation, first at a rather slow rate and then progressively accelerating. In this scenario, the Tower would reach the value of the inclination it had in 1999 in a time span of the order of three centuries. Should better options not be available, before reaching this point one could repeat the underexcavation intervention.

In a more optimistic scenario, the rotation will cease, apart the cyclic movements caused by daily sun irradiation, seasonal changes in the water table and the influence of the generalized subsidence of the whole Pisa plain, which affects the Piazza and the Tower [17].

Going back to Figure 7, let us have a look to the observed inclination of the Tower, almost twenty years after the stabilisation works. At present, the situation appears satisfactory; the Tower is still slowly moving northwards and approaching a motionless state with a decreasing rate. There are, however, several more detailed questions that can be asked. Is the honeymoon finishing? Have the stabilisation works modified the daily and seasonal cyclic movements? What about the east-west movements? Is the Tower stable in the east-west direction? The answers to these questions are to be searched in the careful observation of the behaviour of the monument, by going on monitoring it in the next decades.

References

- [1] T. Montanari, On the importance of towers. In: R. Lancellotta *et al.* eds.: *Geotechnics and Heritage: Historic Towers*, 1-4. Taylor & Francis, London, 2018.
- [2] E. Heinle, F. Leonhardt, *Türme aller Zeiten, aller Kulturen*. Deutsche Verlags-Austalt GmbH, Stuttgart, 1997, 336 pp.
- [3] A. Flora, R. Lancellotta, D. Sabia, C. Viggiani, A first insight into towers' behaviour: geotechnical and structural mechanisms. In: R. Lancellotta *et al.* eds.: *Geotechnics and Heritage: Historic Towers*, 15-14. Taylor & Francis, London, 2018.
- [4] F. Lizzi, *The static Restoration of Monuments*. SGEP Publisher, 1981
- [5] F. Lizzi, *Micropiles: past, present and future*.
- [6] P. Pierotti, *Una torre da non salvare*. Pacini, Pisa 1990, 194 pp.
- [7] R. Cadignani, R. Lancellotta, D. Sabia, 2019
- [8] R. Lancellotta, La Torre Ghirlandina: una storia di interazione struttura-terreno. *Rivista Italiana di Geotecnica*, Patron, Bologna 2013, XLVII, 2, 7-37

- [9] J.B. Burland, C. Viggiani, Osservazioni sul comportamento della Torre di Pisa. *Rivista Italiana di Geotecnica*, 1994, 28(3) 179-200
- [10] E. Cresy, G.L. Taylor, *Architecture of the Middle Age in Italy*. London, 1829
- [11] G. Rohault de Fleury, *Le Campanile de Pise*. Encyclopédie de l'Architecture, Bance, Paris, 1859
- [12] J.B. Burland, et al. 2003
- [13] S. Settim, M. D'Elia, M. Jamiolkowski, G. Macchi, F. Veniale, C. Viggiani, *La Torre Restituita*. Bollettino d'Arte, Roma 2005, Numero Speciale, vol. II, 185 pp.
- [14] F. Lizzi, La Torre raddrizzata di 44 cm. Ma dopo undici anni il pericolo permane. *Il Mattino*, Napoli July 1, 2001, 10.
- [15] J.A. Cheney, A. Abghari, B.L. Kutter, Leaning instability of tall structures. *Journ. Geot. Eng., Proc. ASCE*, CXVII (2) 297-318
- [16] M. Jamiolkowski, Introduction. S. Settim, M. D'Elia, M. Jamiolkowski, G. Macchi, F. Veniale, C. Viggiani, *La Torre Restituita*. Bollettino d'Arte, Roma 2005, Numero Speciale, vol. I, 7-10.
- [17] A. Croce, A. Burghignoli, G. Calabresi, A. Evangelista, C. Viggiani, The Tower of Pisa and the surrounding square: recent observations. *Proc. X Int. Conf. Soil Mech. Found. Eng., Stockholm 1981*, vol. III, 61-70

Technical Session #17 “Rock Mechanics”



C. CARRANZA-TORRES

Dr. Carlos Carranza-Torres is a Professor in the Department of Civil Engineering at the University of Minnesota, Duluth Campus (UMD). Dr. Carranza-Torres has 20 years experience working in the industry of geotechnical engineering (full time since 1998 and as part-time consultant since 2008) and 10 years experience working in academia (since 2008 as an Associate Professor and since 2017 as a full-time tenured Professor at UMD). At the university he teaches or have taught undergraduate and graduate courses in rock mechanics, soil mechanics, geotechnical design, engineering geology, numerical analysis, design of excavations and others. His field of research is in the development of analytical and numerical techniques for the practical treatment of geo-mechanics problems. In the geotechnical engineering industry, he has worked first as project engineer and later on, as independent consultant for various geotechnical engineering groups involved in excavation projects for civil and mining engineering applications, in the US and overseas. Dr. Carranza-Torres has served in the editorial board of various geotechnical engineering journals, including the role of co-editor-in-chief of *Engineering Geology* (from 2013-2015).

Analytical and Numerical Study of the Stability of Shallow Circular Cavities in Weak Rocks

C. CARRANZA-TORRES^{a,1}

^a*University of Minnesota, Duluth Campus, Minnesota, USA*

Abstract. This keynote lecture addresses the problem of determining the mechanical stability of shallow circular cavities in cohesive-frictional ground (weak rocks and soils) assumed to obey a Mohr-Coulomb shear failure criterion. Methods traditionally used to analyze stability of shallow excavations are reviewed first. A method based on the application of limit analysis and shear strength reduction technique in full numerical analysis is chosen for evaluating stability conditions of shallow cavities. Application of a scalar factor of safety for shallow tunnels is introduced and dimensionless groups of variables controlling the stability of the openings are identified. The stability of shallow circular cavities in purely cohesive ground and in cohesive-frictional ground are discussed and observations of practical interest are highlighted. Comparison of stability results obtained with the proposed analytical equations, with full numerical analyses, and with approaches used by other authors in the published literature are discussed. The effect of water in the ground and inside the excavation on the obtained factor of safety is reviewed. Similarities of controlling groups of variables for the cases of shallow tunnels and slopes are highlighted.

Keywords. Stability of shallow circular cavities. Factor of Safety. Limit Analysis. Limit Equilibrium. Finite Difference Method. Shear Strength Reduction Technique. CAES system.

Extended Abstract

This keynote lecture presents a study of mechanical stability of shallow circular cavities carried out as part of a multidisciplinary project that looked into the feasibility of using abandoned underground openings (drifts and shafts) from iron ore mining in northern Minnesota (USA), for Compressed Air Energy Storage (CAES) applications (Fosnacht et al. [1]; Carranza-Torres et al. [2]).

The lecture addresses the problem of establishing the stability conditions of shallow cylindrical or spherical openings excavated in cohesive-frictional ground, and subject to either decreasing or increasing internal pressure, associated with the process of ‘contraction’ or ‘expansion’ of the cavities during operation of a CAES system (Succar and Williams [3]). It is worth noting that the problem of *contracting* cavities not only has applications in the design of CAES systems, but has broad applications in civil

¹ Professor of Geotechnical Engineering, Department of Civil Engineering, University of Minnesota, Duluth Campus. 1405 University Drive, Duluth, Minnesota, MN 55812, USA; E-mail: carranza@umn.edu.

engineering, when assessing support requirements for shallow tunnels in soils for subway/metro projects (Carranza-Torres et al. [4]).

There exists several methods to assess the stability conditions of shallow cavities in geotechnical engineering. Potts and Zdravkovic [5] provide a general classification of available methods as follows: *i*) closed-form; *ii*) limit equilibrium; *iii*) stress field; *iv*) lower bound (or statically admissible); *v*) upper bound (or kinematically admissible); *vi*) beam-spring; and *vii*) full numerical analysis methods.

Contracting and expanding cavities in CAES systems have been traditionally analyzed using Terzaghi's type of limit equilibrium methods (Terzaghi [6]; Sofregaz U.S. Inc. [7]).

An alternative approach to assess stability, which is the one discussed in this lecture, is to use a combination of statically admissible solutions derived from the lower bound theorem of plasticity, and full numerical analysis solutions.

The statically admissible solution presented in this lecture is based on a classical model presented by Caquot [8], that allows to compute a conservative estimate of the internal support pressure for a section of shallow cylindrical tunnel, or spherical cavity, when the ground is assumed to obey a Mohr-Coulomb shear failure criterion. The full numerical analysis solution considered in this lecture is based on the application of the shear *Strength Reduction Technique* implemented in the finite difference code FLAC (Itasca, Inc. [9]).

In this study, the model by Caquot is adapted to express the stability of the cavity in terms of a single scalar value, i.e., a factor of safety, as traditionally done to assess stability of slopes in geotechnical engineering. The model is also adapted to consider both, internal pressure values below the stress existing prior to excavation (the *in situ* stress at the crown of the cavities), to represent the case of *contracting* cavities; and internal pressure values above the *in situ* stress, to represent the case of *expanding* cavities (Carranza-Torres et al. [2, 10]). In the extended model, all input variables representing geometry (e.g., radius and depth of the cavity), loading conditions (e.g., internal pressure, surcharge at the ground surface) and material properties (unit weight, cohesive-frictional properties of the Mohr-Coulomb ground) are scaled and expressed in dimensionless form, with the objective of obtaining equations to relate the conservative estimate of the resulting factor of safety with the scaled input variables. For example, the scaled depth of the cavity is defined as the depth of the cavity axis divided by the cavity radius. Introducing a 'converted' unit weight, defined as the unit weight of the ground multiplied by the cavity radius, the scaled internal pressure is defined as the internal pressure divided by the *converted* unit weight; the scaled ground surcharge is defined as the surcharge acting on the ground surface divided by the *converted* unit weight; the scaled cohesion is defined as the cohesion of the ground divided by the *converted* material unit weight, etc.

The stability of shallow cavities for the case of purely cohesive ground is discussed first. A closed form solution to compute factors of safety for both *contracting* and *expanding* cavities is presented. With all other scaled input variables being the same, it is shown that contracting and expanding *spherical* cavities do have always a value of factor of safety that is twice the value of the factor of safety for the corresponding *cylindrical* section of tunnel. For both, contracting and expanding cavities, the factor of safety is shown to increase with increase of the scaled cohesion of the ground, and to decrease with increase of (scaled) depth of the cavity, when the internal pressure is null or the internal pressure is a fixed ratio of the *in situ* stress, respectively (Carranza-Torres et al. [10]). For the case of contracting cavity, it is shown that the factor of safety becomes

a minimum when there is no internal pressure, and becomes infinite when the internal pressure is equal to the in situ stress prior to excavation. A similar but opposite behavior is shown to occur for the case of expanding cavities, with the factor of safety being infinite for internal pressure equal to the in situ stress, and the factor of safety decreasing when the internal pressure increases. In particular, it is found that for a scaled internal pressure equal to two times the scaled in situ stress prior to excavation, the factor of safety for the expanding cavity is the same as for the contracting cavity with null internal pressure. This implies that the range of factors of safety for cavities in a CAES system can be bounded to a minimum prescribed design value, provided the expanding cavity does not have a scaled internal pressure that is larger than two times the scaled value of the in situ stress prior to excavation.

Results obtained with the extended Caquot's model, for both *contracting* and *expanding* cavities, are compared with results obtained with the finite-difference code FLAC (Itasca, Inc. [9]). Numerical (FLAC) models confirm the behavior of the factor of safety with the scaled input variables observed earlier on. Comparison of both methods show that the values of factors of safety obtained with the lower bound solution are within 10% (on the conservative side) of the values of factors of safety obtained with the numerical models.

With the extended Caquot's model and numerical (FLAC) models providing equivalent results of factor of safety, a comparison of results obtained with the extended Caquot's solution and with other approaches published in the literature is presented.

The Terzaghi's type of equilibrium models (Terzaghi [6]; Sofregaz U.S. Inc. [7]) are evaluated first. The comparison shows that for purely cohesive ground, limit equilibrium models can lead to both over conservative (i.e., too safe) and nonconservative (i.e., unsafe) factor of safety values, for both, *contracting* and *expanding* cavities, depending on the scaled depth of the cavity (the ratio of the depth to the axis of the cavity and the cavity radius). In general, the factor of safety is highly conservative for very shallow cavities, and this degree of conservatism decreases with the scaled depth of the cavity. With all scaled input variables being the same, at the scaled depth (axis depth vs cavity radius) equal to ~18:5 for *contracting* cavities, and equal to ~3:5 for *expanding* cavities, both extended Caquot's solution and limit equilibrium solution yield the same factor of safety. For cavities with scaled depths larger than the mentioned values, the factor of safety values obtained with limit equilibrium methods become now nonconservative (i.e., unsafe).

Results obtained with the proposed limit analysis solution are also compared with the results obtained with a semi-analytical stress-field solution presented by Davis et al. [11]. The solution by these authors allows prediction of the required support pressure for a circular cylindrical tunnel in purely cohesive ground. Obtaining a prediction of the required support pressure using the extended Caquot's solution introduced in this lecture, requires considering a factor of safety equal to one, and solving for the internal pressure at the critical state of equilibrium. Comparison of the results reported in Davis et al. [11] and those obtained with the proposed limit analysis solution are shown to be in good agreement—Carranza-Torres and Reich [12].

An extension of the proposed limit analysis model to account for water in the ground is presented next. Cases of cylindrical sections of tunnel in purely cohesive ground with a water surface at or above the ground surface, and limiting conditions of flooded and dry openings are considered. The analytical model shows that for the case of flooded cavity, the factors of safety are typically two times higher than for the same cavity in dry ground, provided the cohesion values of the saturated and dry ground are similar. For the

limiting case of dry cavity and hydrostatic water pressure in the ground surrounding the cavity, the factors of safety are typically 80% to 90% lower than for the same cavity in dry conditions, again for cohesion values of saturated and dry ground being similar, and provided that no tensile failure occurs (i.e., when a mechanical support pressure that is at least equal to the hydrostatic pressure in the ground on the periphery of the cavity is considered).

Finally, the lecture presents the solution of factor of safety for *contracting* and *expanding* cavities in cohesive-frictional ground. The stability formulation for cohesive-frictional ground uses the same compact scaling law introduced by Hoek and Bray [13], when analyzing stability of slopes using limit equilibrium methods—see also, Carranza-Torres and Hormazabal [14]. It is shown that as for the cases of slopes considered by Hoek and Bray, the factor of safety divided by the tangent of the internal friction angle, when the ‘converted’ material unit weight introduced earlier on is used, depends on the scaled depth of the cavity, the scaled internal pressure, the scaled ground surcharge (with the scaling law as introduced earlier on), and the scaled material cohesion (i.e., the cohesion of the ground divided by the *converted* unit weight) divided by the tangent of the internal friction angle.

As for the case of cavities in purely cohesive ground discussed earlier on, several observations of theoretical and practical relevance on the dependence of the resulting factor of safety for *contracting* and *expanding* cavities, with the scaled input values introduced earlier are discussed. Comparison of results obtained with numerical finite difference (FLAC) models and with the proposed extension of Caquot’s limit analysis solution for cohesive-frictional ground are presented. The comparison suggests that the analytical solution can provide a reasonable conservative measure of the stability conditions for the cavities.

References

- [1] D. R. Fosnacht, E. J. Wilson, J. D. Marr, C. Carranza-Torres, S. A. Hauck, and R. L. Teasley. Compressed air energy storage (CAES) in northern Minnesota using underground mine workings and above ground features. Technical Report NRRI/TR-2015/54, Natural Resources Research Institute, University of Minnesota Duluth, 2015. 478 p. (Available for downloading at <http://www.nrri.umn.edu>, see Publications).
- [2] C. Carranza-Torres, D. Fosnacht, and G. J. Hudak. Analytical and numerical study of the stability of shallow underground openings for mining and compressed air energy storage applications. In P. G. Ranjith and J. Zhao, editors, *Keynote Lecture. Proceedings of the IC3G International Conference on Geomechanics, Geoenergy and Georesources. September 28-29, 2016*. Monash University. Melbourne. Australia, 2016. (Available for downloading at www.d.umn.edu/~carranza/IC3G).
- [3] S. Succar and R. H. Williams. Compressed air energy storage: Theory, resources and application for wind power. Technical report, Prepared by the Energy Systems Analysis Group: Princeton Environmental Institute, Princeton University, 81 p., 2008.
- [4] C. Carranza-Torres, T. Reich, and D. Saftner. Stability of shallow circular tunnels in soils using analytical and numerical models. In J. Labuz and J. Bentler, editors, *Proceedings of the 61st Annual Geotechnical Engineering Conference*, Minnesota, 2013.
- [5] D. M. Potts and L. Zdravkovic. *Finite element analysis in geotechnical engineering. Theory*. Thomas Telford, London, 1999.
- [6] K. Terzaghi. *Theoretical soil mechanics*. John Wiley & Sons, Inc., New York, 1943.
- [7] Sofregaz U.S. Inc. Commercial potential of natural gas storage in Lined Rock Caverns (LRC). Technical report, Prepared for the U.S. Department of Energy, Morgantown, WV, 101 p, 1999.
- [8] A. Caquot. *Équilibre des massifs à frottement interne*. Paris: Gaunthier-Villars, 1934.
- [9] Itasca, Inc. *FLAC (Fast Lagrangian Analysis of Continua) Version 8.0*. Itasca Consulting Group, Inc., Minneapolis, Minnesota, 2015.

- [10] C. Carranza-Torres, D. Fosnacht, and G. J. Hudak. Geomechanical analysis of the stability conditions of shallow cavities for compressed air energy storage (CAES) applications. *Geomechanics and Geophysics for Geo-Energy and Geo-Resources*, 3:131–174, 2017. Springer. In press.
- [11] E. H. Davis, M. J. Gunn, R. J. Mair, and H. N. Seneviratne. The stability of shallow tunnels and underground openings in cohesive material. *Geotechnique*, 30(4):397–416, 1980.
- [12] C. Carranza-Torres and T. Reich. Analytical and numerical study of the stability of shallow underground circular openings in cohesive ground. *Engineering Geology*, 226:70–92, 2017. Elsevier.
- [13] E. Hoek and J. Bray. *Rock slope engineering*. Institution of Mining and Metallurgy. London. (First, second and third editions, respectively), 1974, 1977, 1981.
- [14] C. Carranza-Torres and E. Hormazabal. Computational tools for the determination of factor of safety and location of the critical failure surface for slopes in Mohr-Coulomb dry ground. In *Proceedings of the International Symposium Slope Stability 2018. April 11-13, 2018*, Sevilla. Spain, 2013. (Available for download at www.d.umn.edu/~carranza/SLOPE18).

Technical Session #18 “Education”



Jorge E. ALVA HURTADO

Jorge Alva Hurtado obtained the Doctor in Philosophy degree, PhD in Geotechnical Engineering at the University of Massachusetts, Amherst – Massachusetts (1977-1980) and the Master of Science (MSCE) with mention in Material Testing (1974-1976) and Civil Engineer (CE) with mention in Geotechnics (1976-1977) at the Massachusetts Institute of Technology (MIT) – USA. He is Professor in the Faculty of Civil Engineering of the National University of Engineering, in undergraduate and graduate studies in the area of Geotechnics.

He is currently President of the National Engineering University (Period 2016-2020). He was National Dean of the Peruvian Association of Engineers (Period 2016-2018) and President of the Peruvian Association of Geotechnical Engineering (Period 2015-2018) and the National Association of Public Universities of Peru (Period 2016-2019).

He has published approximately 80 articles in national and international specialized magazines in Civil Engineering; as well as books of its authorship. He has been an exhibitor, speaker and / or lecturer in approximately 200 seminars and / or conferences of Civil Engineering of national and international character, representing various institutions and / or national organizations.

He has received distinctions as Doctor Honoris Causa and Honorary Professor in different Universities of Peru, is a member of the Pan-American Academy of Engineering, Medal of the Engineering Order of the Peruvian Association of Engineers and Member of the National Academy of Sciences of Peru.

He is a Consulting Engineer for state companies and private national and foreign organizations, in large-scale engineering works located throughout Peru during the last 40 years; being specialist in seismic hazard studies and geotechnical engineering.

Advances in the Teaching of Geotechnical Engineering in Peru

Jorge E. ALVA HURTADO^{a,1}

^aProfessor, Researcher - National University of Engineering, Lima-Peru

Abstract. In Peru, the university formation in geotechnical engineering has a starting point in the contribution of professor Emilio Le Roux Catter in 1946 in the old School of Engineers, today National University of Engineering. It is then that the Soil Mechanics course was created within the civil engineering teaching curriculum.

In the decade of the 60th, thanks to the visit of renowned experts in Soil Mechanics, the specialty of Soil Mechanics receives dynamism, giving courses on: Soil Mechanics applied to Transport Roads and Soil Mechanics applied to Earth Dams. The Soil Mechanics and Pavement Laboratories were implemented in the National University of Engineering and in the Pontifical Catholic University of Peru.

In 1971, the UNI created the Graduate School and later the Master of Science Civil Engineering with a major in Geotechnics, giving a great boost to the teaching and application of Geotechnics in Peru, which came to fruition during the 1980s and in the mid-1980s, with the work of the Peruvian Committee on Soil Mechanics, Foundations and Rocks Mechanics and with the implementation of the first Peruvian Technical Standard for Soil Mechanics E-050.

Since 2011, techniques for measuring stress, deformation and water flow have been improved both in-situ and in laboratory. On the other hand, the continuous presence of seismic movements has motivated that twenty universities from the country led by the National University of Engineering, consider that the topics of dynamic characterization of soils should be integrated into the training of Civil Engineering students for which have installed a network of accelerographic stations, which favor the research carried out by undergraduate and graduate students and teachers in the area of Geotechnical Seismic Engineering.

Keywords. Courses, teaching, Geotechnical Seismic Engineering.

1. Introduction

Given the importance of this event for geotechnical engineering, I consider that examining the advances in the teaching of geotechnical engineering in Peru, including the contributions that I have been able to collect from other colleagues and from the students themselves in my dual condition as professor of geotechnical engineering, specialty of soil mechanics, at the National University of Engineering (both undergraduate and postgraduate) and as specialty consultant, it is necessary.

Among the contributions mentioned that I consider significant to approach the subject under discussion, we have: "La Mecánica de Suelos en el Perú", by Eng. Genaro Humala [1], the articles "Academia y ejercicio Profesional en Geotecnia, experiencia en

¹ Corresponding Author, Jorge E. Alva Hurtado, Professor, National University of Engineering, Lima-Peru; E-mail: jorgealvah@gmail.com.

Méjico" by Eng. Gabriel Moreno Pecero [2]; "La Formación en Geotécnica del Ingeniero Civil en América Latina, una visión global" by Eng. Mercedes Beltrán [3] and the "Historia de la Geotecnia Peruana" by Eng. Manuel Sánchez[4], "la Ingeniería y la Mecánica de Suelos" by Eng. Alfonso Alcedán [5] among others.

In his professional practice, the civil engineer has many different and important encounters with the soil. He uses the soil as a foundation for structures and embankments; and also as construction material. Likewise, he must design retention structures for excavations and underground openings, and, in general, he finds the soil in a large number of special problems. In the development of these tasks, the engineer is based on Soil Mechanics, a discipline that systematically organizes the principles and knowledge of the engineering properties of the soil.

In the Andean region of South America, before the arrival of the Spaniards, in Inca and pre-Inca times, the experts responsible for the construction of tunnels, cities, dams and canals, achieved a remarkable development solving complex foundation problems. (Wright y Valencia, 2006 [6], Wright, 2008[7], Wright et al., 2017 [8])

This paper presents the historical sequence since the middle of the last century, in the development of the teaching of geotechnical engineering in Peru, a review of the courses taught in the main universities and a proposal to redefine the programs in order to incorporate new topics associated with the latest advances in geotechnical seismic engineering, considering that education should be more than training, as well as incorporating elements of the latest technologies.

2. Process

In Peru, the contemporary university formation in geotechnical has a starting point in the contribution of the Eng. Emilio Le Roux Catter in 1946 in the old School of Engineers, today National University of Engineering. It was when the Soil Mechanics course within the civil engineering teaching curriculum was created.

In the decade of the 60th, thanks to the visit of renowned experts in soil mechanics such as doctors José Antonio Jiménez Salas, Raul Marsal and Eulalio Juárez Badillo, the specialty of Soil Mechanics receives dynamism, giving courses on: Mechanics of Soils I, Mechanics of Soils II, Soil Mechanics III, Soil Mechanics applied to Transport Roads and Soil Mechanics applied to Earth Dams. The Soil and Pavement Mechanics Laboratories are also implemented. In 1970, the "Soil Mechanics II" course is replaced by the course on Soil Mechanics Applied to Foundations".

In 1971 the Graduate School, fist, and the Master of Science with a major in Geotechnics, later, were created, meaning a great boost to the teaching and application of Geotechnics in Peru. There, courses such as Advanced Soil Mechanics, Foundations Design, Soil Dynamics, Rock Mechanics, Applied Geology to Engineering and other elective courses are taught.

On the other hand, at the Pontifical Catholic University of Peru (PUCP) the Soil Mechanics course has been taught since 1957, with Engineer Ricardo Valencia Menegotto as its creator and first Professor. Subsequently, courses such as Soil Mechanics I, Soil Mechanics II, Soil Mechanics III and Pavements were dictated. Later prominent professionals, such as the Msc José María Corzo López de Romaña, who was a disciple of Professor Arthur Casagrande at Harvard, made their appearance. In the 60's, also in the PUCP, the corresponding laboratories were implemented. After the earthquake of 1970, the PUCP dictates the course of Soil Dynamics in the Graduate

section, being the Msc. Pedro Repetto Peirano, disciple of Professor Harry Bolton Seed, one of his teachers [1].

During the decade of the 80s and in the mid-90s, a major advance in geotechnics came with the creation and contribution of the Peruvian Committee on Soil Mechanics, Foundations and Rocks Mechanics, organizing a series of symposia and courses, establishing the Emilio chair Roux Catter course. The implementation of the first Peruvian Technical Standard for Soil Mechanics E-050 was also very significant.

Since 1990, there is a new momentum in the field of Geotechnical Engineering. The techniques of stress measurement, deformation and water flow have been improved both in-situ and laboratory. The seismic effects in the soil are investigated by accelerographs, geophysical equipment and in the laboratory by cyclic triaxial tests, among others. In the static part tests on large samples to minimize scale effects have been developed.

3. Results

In the last International Congresses of the International Society of Soil Mechanics and Geotechnical Engineering (ISSMGE) and in the Pan-American Soil Mechanics Congresses, the concern for the training in Geotechnical Engineering received by future civil engineers has been well known. In our Latin American region, the pioneering work of the Mexican Society of Soil Mechanics stands out, expressed in its Biannual Congress and National Meeting of Teachers, an event in which not only what to teach, but also how to teach has been analyzed, as an example to follow for other countries.

As professor Moreno Pecero G. (2005) [2] suggests, to teach engineering, including of course Geotechnical Engineering, the teacher requires to have certain special qualities:

- Teaching should not be his main task, but rather make students learn to think.
- In addition to his knowledge he must provide the generous and guiding plenitude of his being in balance with his appearance.
- That title is received not by normative mechanisms but by spontaneous consensus.
- He must fully trust and feel genuine respect for the students.
- He must preach with the example that education is not only the work of intelligence but also of the heart.

Starting from such premises, Professor Beltrán M (2005) [3] considers that the experiences lived by the student of Geotechnical Engineering will be indelible if he can observe "first hand" the behavior of the soil, "check the existence of the flow of water in the various types of soil, verify the consequences of the expansion of soils or faults that occur in an embankment built on soft ground. The experience organized by didactic models that ensure the understanding of principles and processes, will transform the opinion on geotechnics of "a subject that must be approved as a requirement to continue his studies, in an interesting subject".

On the other hand the question of what is the minimum level of knowledge that the student of Civil Engineering must acquire in the area of Geotechnics to be able to solve the engineering problems either at the level of design, construction or supervision arises. The answer varies according to the reality of each country, however a minimum group of subjects for basic training in Geotechnics will always exist.

Currently in Peru, it is observed that the curricular plans corresponding to the area of Geotechnics, in the different universities, both public and private, are heterogeneous,

both of the subjects included, and in the time dedicated to them, as can be seen in Tables 1 to 5.

Table 1. Curriculum Plan of the National University of Engineering (UNI).

Category	Course	Credits	Weekly hours
Obligatory	General Geology	4	6
	Soil Mechanics I	4	5
	Soil Mechanics II	4	5
	Applied Geology	4	6
	Total		22
Electives	Soil Dynamics	3	4
	Rocks Mechanics applied to Civil Engineering	4	5
	Finite Elements applied to Geotechnics	3	4
	Soil Mechanics applied to foundations	4	5
	Soil Mechanics applied to transport routes.	3	4

Table 2. Curricular Plan of the Pontifical Catholic University of Peru (PUCP).

Category	Course	Credits	Weekly hours
Obligatory	Geology	3	3
	Geology Laboratory	0.5	1
	Soil mechanics	4.5	5
	Soil Mechanics Laboratory	1	2
	Foundation Engineering	4.5	5
Total			16
Electives	Geotechnical design	3.5	3
	Floors	3.5	3
	Geotechnical Engineering Topics	3.5	3
	Design with Geosynthetics	3.5	3
	Design of Earth Dams and Tailings	3.5	3
	Advanced Soil Mechanics	3.5	3

Table 3. Curricular Plan of the Ricardo Palma University (URP).

Category	Course	Credits	Weekly hours
Obligatory	Geological Engineering	2	3
	Soil Mechanics I	3.5	5
	Soil Mechanics II	3.5	5
	Foundations	3	4
	Floors	4.5	4
Total			21
Electives	Geotechnical design	4	4

Table 4. Curricular Plan of the San Ignacio de Loyola University (USIL)

Category	Course	Credits	Weekly hours Semanales
Obligatory	Geology	2	4
	Soil Mechanics	4	6
	Geotechnical Engineering	4	4
	Foundations	2	4
	total		18

Table 5. Subjects of the area of Geotechnics, taught in other Universities.

Other Universities	Compulsory Subjects
University of Piura	Applied Geology, Soil Mechanics, Geotechnical Design
Peruvian University of Applied Sciences	Geology, Soil Mechanics, Geotechnical Engineering.
National University Federico Villarreal	Geology, Soil Mechanics I, Soil Mechanics II, Floors
Private University Antenor Orrego	Geology, Soil Mechanics I, Soil Mechanics II, Floors

The professional practice in soil mechanics is complex, since knowledge and experience are required. For example, when a hydroelectric project has a dam component, a detailed geotechnical study of the foundation and quarries is required. Normally it will be necessary to apply analytical methods to the design to evaluate infiltration, slope stability, static deformation and seismic action. In addition, the design of the related works, such as spillways, diversion tunnels, components; and of course the costs and budgets should be considered.

When the student of Civil Engineering finishes his career he has many limitations to face this type of projects, so these shortcomings would have to be compensated through postgraduate programs; however, currently the only university offering the Master's Degree in Civil Engineering with a mention in Geotechnics is the National University of Engineering (Table 6).

In the Peruvian case it is imperative to take into account that the country is located in an area of high seismic hazard, due to the interaction of the Nazca plate and the South American plate, as well as the activity of surface geological faults, which also generate earthquakes of considerable magnitude in the interior of the country.

Table 6. Postgraduate Curriculum Plan of the National University of Engineering (UNI).

Category	Course	Credits	Weekly Hours
Obligatory	Advanced Soil Mechanics	4	4
	Foundation Design	4	4
	Rocks Mechanics	4	4
	Geology Applied to Engineering	4	4
	Seminar in Geotechnical Engineering	3	3
	TOTAL		19
Electives	Geophysics Applied to Civil Engineering	4	4
	Soil Dynamics	4	4
	Experimental Soil Mechanics	4	4
	Numerical Methods Applied to Geotechnics	4	4
	Land Dams and Castling	4	4
	Theoretical Soil Mechanics	4	4
	Special Problems in Geotechnics	4	4
	Slope Stability and Earth Push	4	4
	Design with Geosynthetics	4	4
	Foundations Design by State Limit	4	4
	TOTAL		40

The continuous presence of seismic movements has motivated that different Universities from the regions outside of Lima, led by the National University of Engineering, consider that the topics of dynamic characterization of soils should be integrated as part of the training of the students of the career of Civil Engineering not only at the theoretical level but at the experimental level. In that sense, a network of accelerographic stations, which will allow the development of research for undergraduate and postgraduate students and teachers in the area of Seismic Geotechnics, was implemented.

To continue with the advances of teaching in Geotechnical Engineering in Peru it is necessary to propose a minimum program that incorporates new topics associated with the latest advances in seismic geotechnical engineering and with basic subjects for training in Geotechnics of the future professional in Civil Engineering Undergraduate level as proposed in Table 7. Additionally, each University must consider elective Geotechnical courses according to the orientation of the student's interests.

Table 7. Basic Proposal for undergraduate courses in Geotechnics

Category	Courses	Credits	Hours		
			Theory	Practice and / or Laboratory	Sub Total
Obligatory	Geology	4	3	3	6
	Soil Mechanics	4	3	2	5
	Soil Dynamics	4	3	2	5
	Foundation Engineering	4	3	2	5
	Total		12	9	21

Another important aspect that should be considered is that professional practice in our countries should be developed in an environment of honesty and commitment to society. This commitment consists of benefiting the community, giving support to the less favored strata. Taking the words of Father Pedro Arrupe S.J., general of Jesuits to educators, "we must form men for others", which in our case would have to mean "to train civil engineers to serve society".

4. Conclusions

- In Peru, the contemporary university education in geotechnics began in 1946.
- Geotechnical professors must have certain special qualities so that the teaching of their subject matter is useful and responds to the needs of today's world.
- Courses in the area of Geotechnics and their contents should be standardized, both at the level of each country and at the regional level, to meet a basic minimum of knowledge.
- Subjects of dynamic characterization of soils should be integrated as part of the training of the students of the Civil Engineering career, not only at the theoretical level but at the experimental level.
- The deep knowledge of Geotechnics as well as its multiple applications corresponds to the postgraduate level. In Peru, the Master's programs in Geotechnics must be increased.

References

- [1] Humala G. (1987). *La Mecánica de Suelos en el Perú*. V National Congress of Soil Mechanics and Foundation Engineering. Peruvian Committee on Soil Mechanics and Foundation Engineering. Lima Peru.
- [2] Moreno Pecero G. (2005). *Academia y ejercicio Profesional en Geotecnia, experiencia en México*. Catolic University of Santiago de Guayaquil. Ecuador.
- [3] Beltrán M. (2005) .La Formación en Geotécnica del Ingeniero Civil en América Latina, una visión global. National University of Engineering.
- [4] Sánchez M. (2015). *Historia de la Geotecnia Peruana*. XIX National Congress of Civil Engineering. Huaraz, Peru.
- [5] Alcedán A. (1961). *La Ingeniería Civil y la Mecánica de Suelos*. Symposium The teaching of Civil Engineering. National University of Engineering. Lima Peru.
- [6] Wright, K. y Valencia A. (2006). *Machupicchu una maravilla de la Ingeniería Civi*. National University of Engineering. Lima Peru.
- [7] Wright, K. (2008). *Tipón – Obra maestra de la ingeniería hidráulica del imperio de los incas*. National University of Engineering. Lima Peru.
- [8] Wright, K., Wright, R., Valencia, A., McEwan, G. (2017). *Moray enigma de la Ingeniería*. National University of Engineering. Lima Peru.
- [9] Martínez A. (1976). *Responsabilidad de los Profesionales en Geotecnia y Riesgo Sísmico*. I National Congress of Civil Engineering. Lima Peru.
- [10] Alva H. (1999). *Contribuciones a la Ingeniería Geotécnica Sísmica en el Perú*. XII National Congress of Civil Engineering. Huánuco, Peru.
- [11] Alva H. (2001). Nuevas Tendencias de la Mecánica De Suelos en el Siglo XXI. National University of Engineering.

Technical Session #19 “Energy Geotechnics”



Lyesse LALOUI

Dr. Lyesse Laloui is chaired full professor and Director of the Soil Mechanics Laboratory at the Swiss Federal Institute of Technology, EPFL, Lausanne, where he developed a major research group in the area of Geomechanics for Geo-energy. He is also adjunct professor at Duke University, USA, and advisory professor at Hohai University, China. He is the recipient of an Advanced ERC (European Research Council) Grant for his project BIOGEOS (BIO-mediated GEO-material Strengthening). He wrote and edited 12 books and published over 300 peer reviewed papers. His work is cited more than 4800 times with an h-index of 34 (Scopus). He is the Editor in Chief of the International journal Geomechanics for Energy and the Environment. He is the recipient of the “Excellent Contributions Award” of the International Association for Computer Methods and Advances in Geomechanics, the “2012 Vardoulakis Lecture” from the University of Minnesota, the “12th G.A. Leonards Lecture” from the University of Purdue, the “2016 RM Quigley Award” from the Canadian Geotechnical Society and the 30th Roberval Award at the French Academy of Science in 2018. He has been involved as an expert in several international projects and acts as a consultant in civil, geotechnical and geothermal engineering, including legal and arbitration cases. He acted as the Chair of the Evaluation Panel of Civil and Geological Engineering R&D Units of Portugal in 2018. The patented “Geosynthetic element for soil bio-improvement” is currently being developed in the context of the start-up MeduSoil. He is also developing another start-up (GEOEG) in the area of Energy Geostructures.

Experimental Analyses on the Multiphysical Phenomena Governing Energy Pile Behavior

Lyesse LALOUI^{a,1} and Melis SUTMAN^b

^aProfessor, Swiss Federal Institute of Technology in Lausanne, EPFL

^bPostdoctoral Researcher, Swiss Federal Institute of Technology in Lausanne, EPFL

Abstract. Energy piles are exposed to temperature variations during their lifetime, due to their unique role combining structural support and geothermal heat exchange. Temperatures in the piles and in the surrounding soils fluctuate on a daily and seasonal basis which may cause axial displacements, additional axial stresses and changes in shaft resistance along energy piles. Furthermore, soils in the vicinity of the energy piles experience volumetric strains and changes in shear strength which may eventually have an impact on the structural behavior of energy piles. To understand the extent of temperature changes on energy piles, soils and soil-pile interfaces, various in-situ and laboratory tests have been performed. The goal of this paper is provide details regarding in-situ and laboratory tests performed on energy piles, as well as to compile an observational framework in understanding the mechanics of soils, structures and the interaction between them in consequence of thermal actions.

Keywords. Energy geostructures, energy piles, in-situ testing, laboratory testing, thermo-mechanical behavior, non-isothermal behavior

1. Introduction

In practice, energy piles can be employed only for space heating or cooling, depending on the demand of the region, or they can be used for both heating and cooling purposes. In any of the cases, as a result of their dual nature, energy piles and the surrounding soil are exposed to temperature changes during their life time.

Temperatures in the piles and in the surrounding soils fluctuate during the day in between operation and stoppage times as well as seasonally after episodes of heat injection during summer followed by heat extraction during winter. It is known that the seasonal temperature fluctuations can go up to $\pm 15\text{--}20^\circ\text{C}$ of the in-situ temperature. Furthermore, energy piles are subjected to daily temperature variations of $4\text{--}8^\circ\text{C}$, in between operation and stoppage times. These temperature changes may cause axial expansion and contraction of the energy piles which can alter resistance mobilization along their shaft. Moreover, the prevented portion of the axial elongation and contraction may cause thermally induced changes in the axial stresses.

¹ Lyesse Laloui, Laboratory of Soil Mechanics, Station 18, CH 1015, Lausanne, Switzerland; E-mail: lyesse.laloui@epfl.ch.

Due to heat exchange operations, the soil at the vicinity of energy piles is also exposed to thermal loads, which may affect soil properties such as preconsolidation pressure, shear strength and may cause excess pore water pressure generation and volumetric strains.

In this paper, details on in-situ and laboratory tests performed on energy piles, soils and soil-structure interfaces are provided along with breakthrough experimental results targeting fundamental information on mechanisms governing thermo-mechanical behavior of energy piles. First, full-scale in-situ tests investigating the thermo-mechanical behavior of energy piles are presented. Next, the response of soils subjected to monotonic and cyclic thermal loads is considered. Finally, results of laboratory tests evaluating the response of soil-concrete interfaces subject to thermal and shear cycles are presented, which is followed by discussions.

2. Full-Scale In-Situ Tests on Energy Piles

Given the great potential of energy piles on the path of less dependency on fossil fuels, various in-situ tests were performed on this topic [1-5]. The three pioneering full-scale in-situ tests on energy piles performed at Swiss Federal Institute of Technology in Lausanne (EPFL) and Virginia Tech, investigating (i) the response of a single energy pile to combinations of thermal and mechanical loads, (ii) the response of a group of closely spaced energy piles to thermo-mechanical loads and (iii) the response of a single energy pile to cyclic thermal loads are presented in this section. Compressive stresses and upward shaft resistance mobilization are considered positive, according to the adopted sign convention.

2.1. Single Energy Pile

The first in-situ test on a single energy pile [6], a pioneer in the area, was performed under a new 5-storey building, 100 m in length and 30 m in width, at EPFL campus. The building was supported by 97 bored piles, one of which was converted to an energy pile, having a diameter of 88 cm and a length of 25.8 m, with inclusion of heat exchanger tubes. A noteworthy number and type of sensors were placed along the length of the pile, which are shown in Figure 1: (i) vibrating-wire extensometers to measure vertical strain and temperature, (ii) fiber-optic extensometers, each 1 m long, to measure vertical strain, (iii) fiber-optic extensometers, each 2 m long, to measure radial strain at five depths, (iv) a load cell to measure the load at the toe of the pile and (v) extensometers at the head of the pile to measure the vertical strain in order to determine the load at the head of the pile.

To ascertain structural characteristics of the test pile, a pile integrity test was performed which showed the cross section of the pile to be considered constant. Furthermore, the Young's modulus of the concrete was evaluated with cross-hole ultrasonic transmission.

The soil profile at the field test site is shown in Figure 1, the properties of which were obtained from the boreholes, two static load tests, as well as triaxial tests on samples from layers A, B and C. The ground water table at the site is located at ground surface. Further information on soil stratigraphy and the test pile can be found in [6].

Being the first in-situ test on energy piles, the testing campaign was developed to reveal the fundamentals of an emerging field: (i) effect of temperature changes on the

structural behavior of energy piles, (ii) extent of thermally induced axial stresses and mobilized shaft resistance and (iii) influence of end-restraining conditions on the thermo-mechanical response of energy piles.

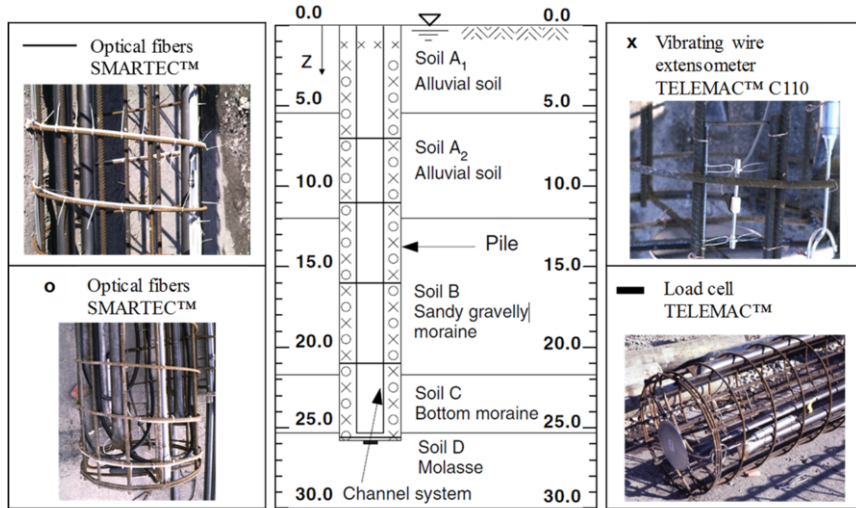


Figure 1. Soil profile at the site and sensors along the test pile (Test Site-1).

The mechanical load on the test pile was induced by the self-weight of the building. To distinguish the sole influences of mechanical and thermal loads, a heating – passive cooling cycle was applied on the test pile at the end of the construction of each storey. In total, eight tests were performed on the test pile.

The results from the last test, following the completion of the building construction, are presented in Figure 2. The mechanical load, caused by the weight of the building, decreases with depth, leaving the toe resistance not being mobilized (Figure 2a).

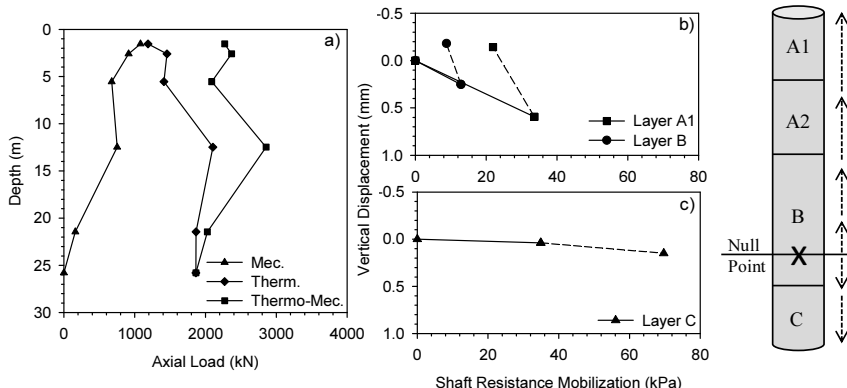


Figure 2. a) Mechanical, thermal and thermo-mechanical loads and b,c) shaft resistance mobilization along the test pile.

The subsequent heating episode ($\Delta T=13.4^{\circ}\text{C}$) results in significant mobilization of the toe (2000 kN) as well as thermally induced axial load at the pile head (1000 kN) due to restraining effect of the building and the soil on the pile thermal expansion. Figure 2b and Figure 2c presents shaft resistance mobilization at various depths along the test pile, the solid and dashed lines representing the ones due to mechanical and thermal loads, respectively. The figure highlights thermally induced shaft resistance mobilization at layer C being in opposite direction with the one along layers A and B, as a consequence of the test pile expanding in opposite directions above and below the null point.

2.2. Group of Energy Piles

A second test site was constructed at EPFL campus, 200 m away from the single energy test pile, with the purpose of investigating the thermally-induced group effects and interactions characterizing closely spaced energy pile groups. For this purpose, four out of 20 piles supporting a water retention tank within Swiss Tech Convention Center (STCC) were converted to energy piles being 0.9 m and 28 m in diameter and length, respectively.

The test piles were bored and cast onsite and were equipped with four 24 m long polyethylene U-loops connected in series, leaving the top 4 m of the piles thermally inactive. The test piles were instrumented with (i) vibrating wire strain gages at every 2 m depth to monitor temperature and axial strain, (ii) vibrating wire strain gages at the head of the piles to measure thermal strains and stresses, (iii) pressure cell at the toe of the pile to monitor mobilized toe resistance and (iv) radial optical fibers to observe radial thermal strains (Figure 3).

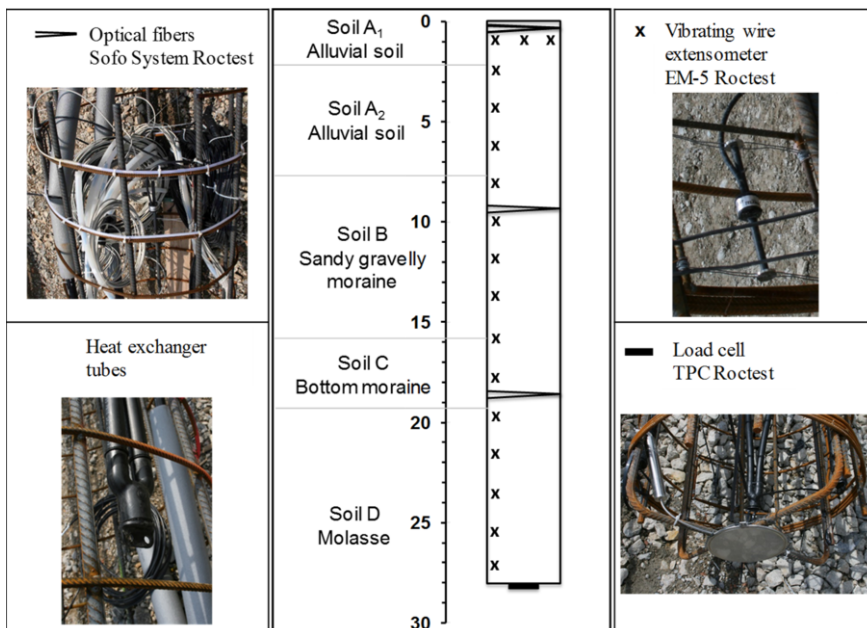


Figure 3. Soil profile at the site and sensors along the test piles.

The soil stratigraphy at the test site is similar to the one presented in Section 2.1, yet the information regarding the depth and thickness of the soil layers have been updated based on the boreholes at STCC area. Two piezometers, having the capability of temperature measurement as well, were installed along each of the two boreholes, to monitor heat propagation and excess pore water pressure generation in the soil between the piles. Furthermore, an additional thermistor was also placed in the boreholes for temperature monitoring. Detailed information on the soil stratigraphy as well as the instrumentation is presented by [7].

To investigate the thermally induced group effects on energy piles, the in-situ test involved application of heating and passive cooling cycles to a single energy pile, as well as to all four energy piles in the group [4]. This paper involves observations from the former case where EP1 corresponds to the operating pile while the other three surrounding piles (EP2, 3 and 4), 3-diameter away from EP1, act as non-operating piles.

Figure 4a shows the thermal interactions between the energy piles in the group due to the application of constant thermal power of 3 kW to EP1 for over 156 days. During the early stages of heating (i.e. 2 days), the temperature field of the non-operating energy pile, EP2, remained unchanged, while EP1 had an average temperature increase of 5°C. In the subsequent stages of heating, heat diffusion resulted in an average temperature increase of 2°C and 5°C along EP2, while the uninsulated part of EP1 was characterized by an average temperature increase of 15°C and 20°C at 35 and 156 days, respectively.

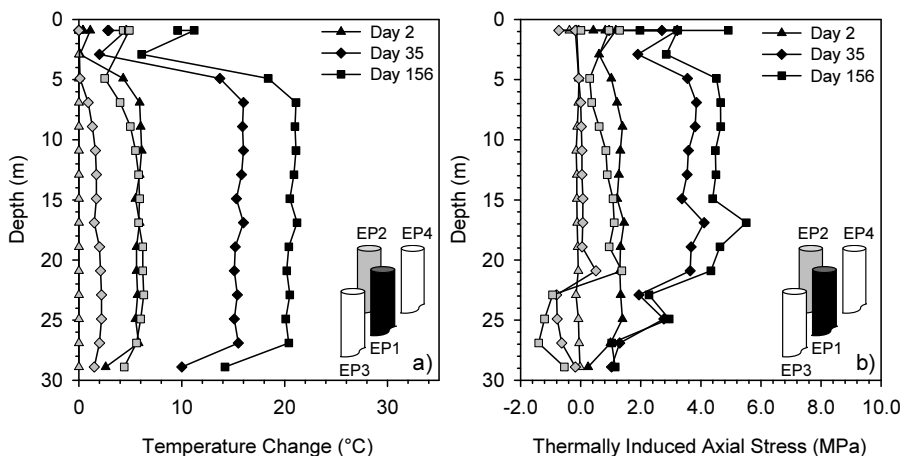


Figure 4. a) Temperature changes b) Thermally induced axial stresses along EP1 and EP2 due to geothermal operation of EP1.

Thermally induced axial stresses along the operating (EP1) and non-operating (EP2) energy piles are presented in Figure 4b. The gradual increase in the thermally induced compressive stresses along EP1 is observed in Figure 4b, which reached a maximum of 5500 kPa after 156 days of geothermal operation.

At the early stages of the field test (i.e. 2 days), temperature increase along EP1 induced axial stress changes also along the surrounding non-operating piles. The axial stresses along EP2 decreased by a magnitude of 250 kPa at the head, which were associated with the deformation field due to the heating of EP1 instead of a change in the thermal field of EP2. In other words, a change in the stress field of EP2 was observed

even though its temperature remained constant which was due to the interplay between the responses of the piles, slab and soil to temperature changes.

At later stages of geothermal operation (i.e. 35 and 156 days), maximum axial stress increase of 1370 kPa and decrease of 1419 kPa were observed at the top and bottom portions of the non-operating energy piles, respectively. The decrease in axial stresses along the bottom portion of the piles has been associated with the thermally induced deformation of the molasse layer resulting in a pull-down effect on the group of energy piles [4]. This effect was less pronounced for the operational energy pile (EP1) since the increase in axial stresses due to active heating governed the stress field along EP1.

2.3. Single Energy Pile for Cyclic Thermal Loads

A full-scale in-situ test was performed on three energy piles in Houston, Texas to evaluate the influence of cyclic thermal loads as well as of different end-restraining conditions on the thermo-mechanical behavior of energy piles. In this paper the emphasis is put on the former case by presenting the data on a single pile subjected to five active heating-cooling cycles over a period of six weeks. Figure 5 shows the test pile profile with 45.7 cm in diameter and 15.24 m in length, together with the sensors placed along its length.

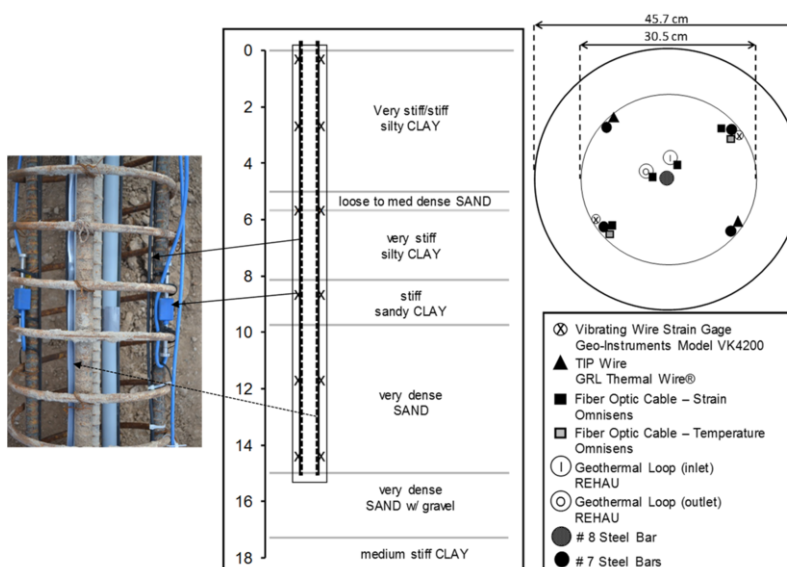


Figure 5. Soil profile at the site and sensors along the test pile.

The pile was equipped with a considerable number and type of sensors including (i) a pair of vibrating wire strain gages (VWSG) placed at 6-depths along the pile to measure strain and temperature, (ii) thermal integrity profiler wires along the full-length to measure temperature, (iii) fiber optic cables to measure strain and temperature, (iv) two linear variable differential transformers at the head of the pile to measure head displacement, and (v) two thermistors at the inlet and outlet of the geothermal loop entering and exiting the pile. To apply thermal loads, a single loop polyethylene (PEX) heat exchanger tube was placed at the center along the full-length of the pile. Finally, a

borehole was drilled 0.5 m away from the pile through which three piezometers and three thermistors were placed, at 4.3, 7 and 8.8 m, to monitor the temperature evolution and excess pore water pressure generation within the soil.

The soil stratigraphy (shown in Figure 5) was obtained from four boreholes at the test site, along with standard penetration and pocket penetrometer tests. Furthermore, thermal oedometer and soil characterization tests were performed on soil samples collected from the boreholes in the Laboratory of Soil Mechanics at EPFL. The soil stratigraphy consists of very stiff and stiff clay layers until 9.8 m depth which is followed by a very dense sand layer until 17.4 m depth. Further information on the field test setup and soil profile is presented in [8].

Five heating-cooling cycles with a maximum circulating fluid temperature of 43°C and minimum of 8°C were applied on the test pile, the measurements of which were taken by the two thermistors placed at the inlet and outlet of the heat exchanger tube (Figure 6). Unlike the former two tests, active cooling cycles, bringing the test pile below the in-situ temperature, were part of the experimental campaign. The thermal cycles were imposed without a mechanical load application at the head of the test pile.

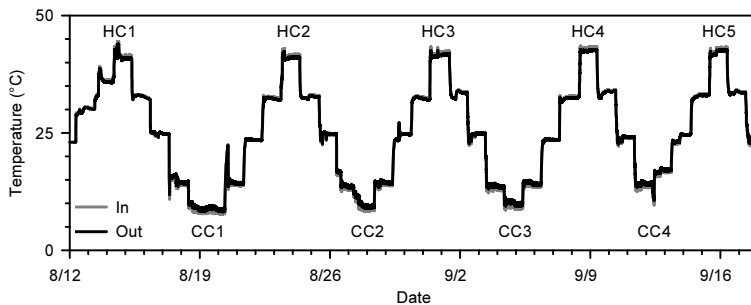


Figure 6. Circulating fluid temperature in the heat exchanger tubes embedded in the test pile.

As indicated in Section 2.1, heating of an energy pile causes an increase in compressive axial stresses as well as mobilization of downward and upward shaft resistance at the top and bottom portions of the pile, respectively, which is inverse for the case of cooling. In the case of cyclic temperature change, the pile is expected to alter between the two cases, having variations of axial stresses and mobilized shaft resistance in cyclic nature. The response of the test pile to cyclic thermal loads presented in Figure 7 confirms this expected behavior.

The thermally induced axial stresses (Figure 7a) and mobilized shaft resistance (Figure 7b) along the test pile associated with the applied thermal cycles were calculated employing the strain and temperature readings from VWSGs. The changes in axial stress, mobilized shaft resistance and temperature data are presented with respect to the in-situ state of the test pile.

Figure 7a shows the thermally induced axial stresses at the null point of the test pile, which have a transition between compressive (temperature increase) and tensile (temperature decrease) in nature, for each peak heating and cooling episode. The null point of the pile appears to be consistently at 8.7 m depth, which would be expected to change while transitioning between heating and cooling episodes, since the end-restraining conditions do not remain the same. However, although the null point depth may have changed, the change was not drastic to be detected by the VWSGs which have

almost 3 m vertical distance between each other along the test pile. Apart from that, while the thermally induced axial stresses per unit temperature change during heating are slightly higher than the ones during cooling, they remain almost unchanged in between thermal cycles, suggesting that an accumulation of thermal stresses did not occur during the field test.

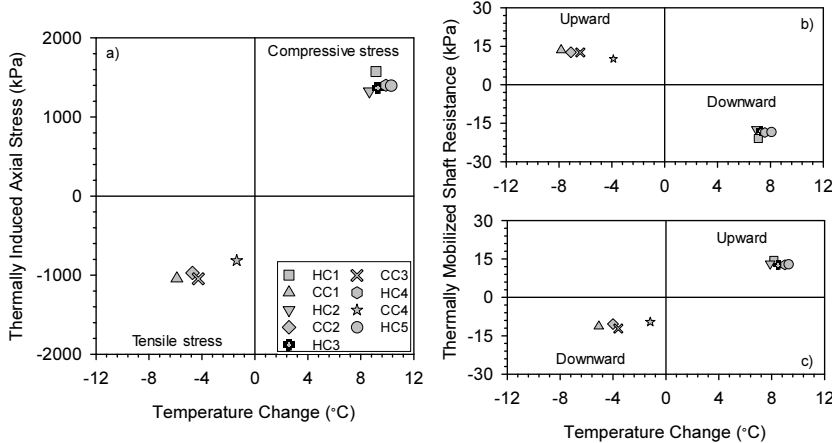


Figure 7. a) Thermally induced axial stress at null point; Mobilized shaft resistance at b) clay layer, c) sand layer due to thermal cycles.

Thermally mobilized shaft resistance imposed along the test pile are presented in Figure 7b and Figure 7c, for clay and sand layers, respectively. The two layers, being above and below the null point, show shaft resistance mobilization in opposite directions, which would be expected considering axial expansion and contraction of the test pile away from the null point, with temperature increase and decrease. Furthermore, observing the data points corresponding to each peak heating and cooling cycle, the thermal shaft resistance mobilization per unit temperature change can be considered almost unchanged, suggesting that a degradation of pile shaft resistance have not occurred. Yet, this observation cannot be generalized for energy pile applications considering the fact that the induced temperature changes on the test pile ($\Delta T \approx \pm 10^\circ\text{C}$) were lower than what would be expected from an actual geothermal operation ($\Delta T \approx \pm 15-20^\circ\text{C}$).

3. Thermo-mechanical Behavior of Soils and Soil-Concrete Interfaces

Geothermal operation of energy piles induces temperature change not only along the piles but also within the soil around them due to heat exchange phenomenon. Hence, investigating the behavior of soils and soil-concrete interfaces in non-isothermal conditions is crucial to administer a thorough knowledge on the response of energy piles to thermal and structural loads. As a consequence, three laboratory testing devices were designed and constructed at the Laboratory of Soil Mechanics at EPFL which are (i) thermal triaxial testing apparatus to evaluate the effects of temperature change on the stress-strain behavior of soils, (ii) thermal oedometer to investigate the volumetric response of soils to cyclic temperature changes and (iii) thermal direct shear device to examine the effect of cyclic thermal and mechanical loads on the soil-concrete interface.

The design of these devices are presented in this section along with a summary of the results from their employment.

3.1. Thermal Triaxial Tests

The effect of temperature change on the stress-strain behavior of clays was investigated by employing a designed, temperature-controlled triaxial testing device (Figure 8). For this purpose, an isothermal triaxial cell was modified to apply temperature changes to the soil sample with the inclusion of (i) an electric heater, which was placed in a thermal bath to serve water as circulating fluid, (ii) circulation pump, (iii) metal tube placed spirally around the sample through which heat carrier water was circulated, (iv) the insulation and (v) temperature controlling unit.

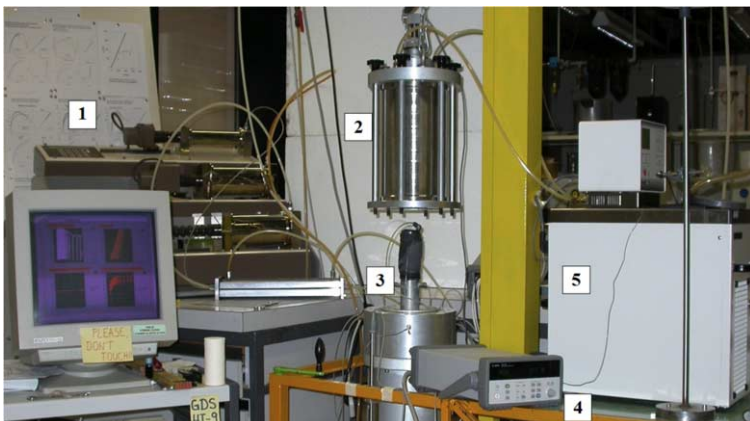


Figure 8. Thermal triaxial testing apparatus (1: GDS Controller, 2: Triaxial Cell, 3: Thermocouple, 4: Multiplexer, 5: Heating bath).

Five thermocouples were included in the setup to measure the temperature of the confining fluid (one for data acquisition and one for sending feedback to the heating bath), heating bath, room temperature and the cooling container. Finally, the standard Perspex cell was replaced with a stainless steel one to withstand high temperature and pressure, as well as corrosion. Further information on the design and calibration of the thermal triaxial apparatus can be found in [9].

The experimental campaign on Kaolin samples included (i) isotropic consolidation, which was followed by an unloading for over consolidated samples in some cases, (ii) heating from 22°C to 90°C with a rate of 10°C/3h to ensure drained conditions and finally (iii) drained shearing. To quantify the influence of temperature on shear strength, the tests performed with the same mechanical path but with different temperature history are compared in Figure 9 for normally consolidated (NC) samples as well as overconsolidated (OC) samples with an over consolidation ratio (OCR) of 2 and 6. The results demonstrate that samples tested at high temperature ($T=90^{\circ}\text{C}$) show higher shear strength compared to the ones tested at ambient temperature ($T=22^{\circ}\text{C}$). However, at large strains, the shear stresses obtained for the samples at high temperature tend to the same critical state as the samples tested at ambient temperature. Therefore, the stress path at critical state constitutes a single envelop, irrespective of the test temperature. Figure 9b presents the volumetric response of the samples sheared at different temperatures, from which no clear trend was attained.

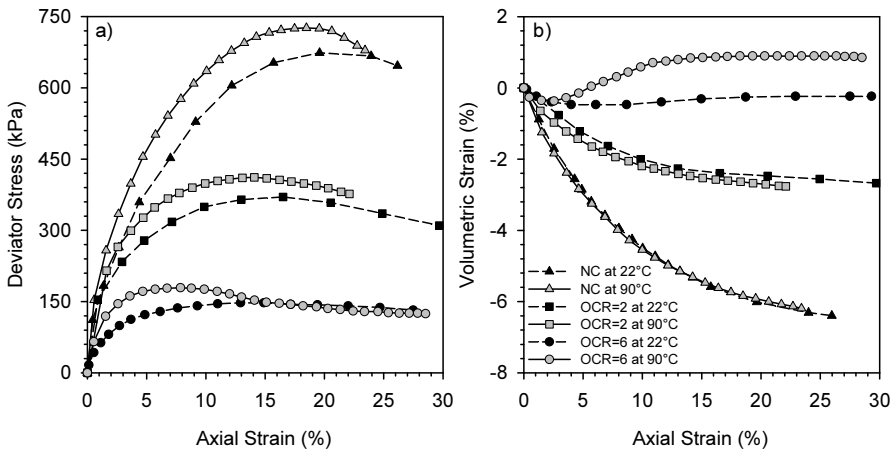


Figure 9. Drained triaxial tests at ambient (22°C) and elevated (90°C) temperatures

3.2. Thermal Oedometric Tests

The response of soils to monotonic and cyclic temperature change was investigated with the use of four oedometric devices (Figure 10). In order to adopt conventional oedometers to allow temperature control, spiral tubes were placed around the soil samples through which heat carrier water was provided with the use of a thermostat and a pump. The modified device allowed circulating water temperature of $5\text{--}60^{\circ}\text{C}$ which covers the temperature range of interest in relation to geothermal operation of energy piles. Four K-type thermocouples were placed in each oedometer cell to monitor the temperature throughout the tests. In addition to the temperature control and acquisition equipment, the cells were insulated with a polystyrene box to prevent thermal losses. Finally, water suppliers were included in the testing equipment to overcome the water evaporation during heating episodes.

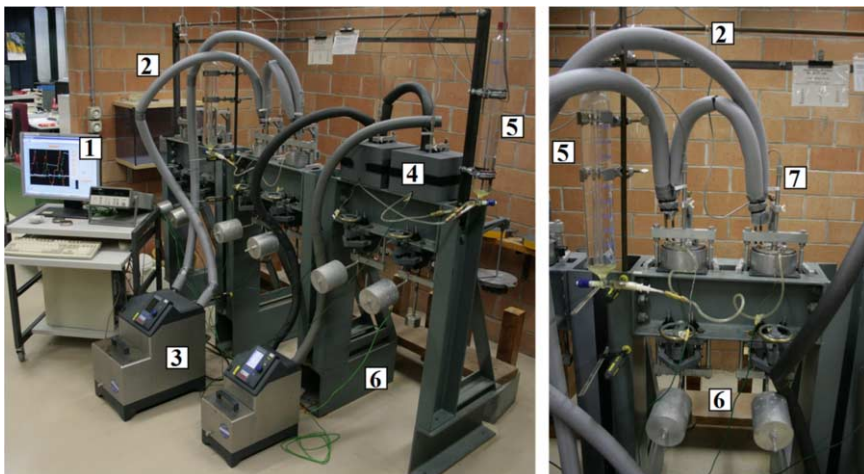


Figure 10. Thermal oedometer device (1: Acquisition system, 2: Tubes with circulating water, 3: Heater, 4: Insulation, 5: Water supplier, 6: Thermocouple, 7: LVDT).

Four soil samples collected from Geneva, Switzerland, were employed in the laboratory testing campaign. The samples were classified as silty-clay according to USGS classification and they were naturally in normally consolidated conditions. Further information on the soils samples, as well as the thermal oedometers is provided by [10].

The experimental program was designed to investigate two phenomena: (i) characterization of soil behavior in non-isothermal conditions, (ii) evaluation of soil response to thermal loads in cyclic nature. For the former aspect, oedometric tests at various constant temperatures (i.e. 20, 40, 60°C) were performed, while for the latter one thermal cycles under constant vertical effective stress were applied on soil samples to which the emphasis is put in the present paper. Within the second testing campaign, the samples were loaded to a vertical stress at normal consolidation conditions in ambient temperature (20°C), following which thermal cycles with a minimum temperature of 5°C and maximum of 60°C were imposed. Heating rate of 2°C/h and a cooling rate of 5°C/h were employed during the tests to prevent excess pore water pressure generation. Moreover, the same thermal cycles were applied to the soil samples under highly OC conditions, with an OCR of 16.

The results regarding the volumetric strain are presented in Figure 11. Thermo-elastic response corresponding to thermal expansion and compression of soil skeleton was observed for the clay sample in OC conditions. On the other hand, the NC sample showed irreversible volumetric contraction related to the thermo-plastic collapse. It is also observed that the sample accumulated irreversible contraction during the initial cycles, which becomes increasingly stabilized during the subsequent ones.

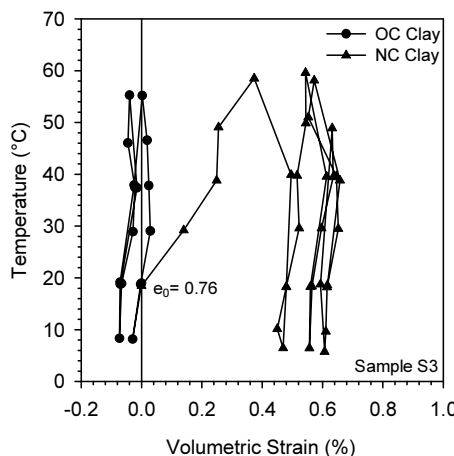


Figure 11. Volumetric response of NC and OC samples to thermal cycles.

The irreversible contractive behavior of NC clays can be mainly attributed to the particle rearrangement, which overcomes the thermo-elastic expansion of the grains and the water. For the OC clays, the particle rearrangement is limited which results in the thermo-elastic expansion of the soil constituents (water and grains) to govern. As the NC samples are continuously exposed to thermal cycles, the configuration becomes increasingly stable at each cycle, with decreasing possibility of additional collapse, suggesting a transition from an NC to OC condition [10].

To further investigate this phenomenon, the response of a clay sample mechanically loaded to a normally consolidated state and exposed to thermal cycles is presented in Figure 12. The sample was first mechanically loaded to 125 kPa (from point A to B), which was followed by four thermal cycles (between points B and C) and finally by mechanical loading up to 2000 kPa (from point C to E). It is observed in Figure 12a that during the final mechanical loading phase, the material first showed an elastic response from point C to D, which was followed by plastic response joining the normal consolidation line. Details on the volumetric response of the sample to cyclic thermal loads is shown in Figure 12b.

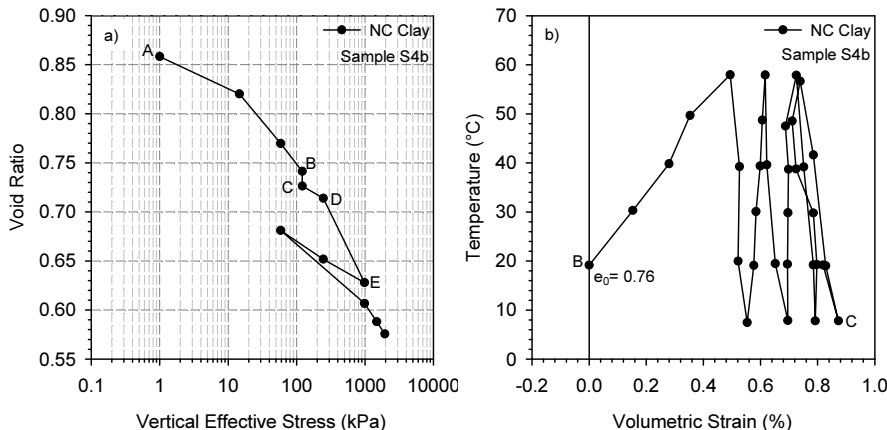


Figure 12. Effect of thermal cycles a) on the oedometric curve, b) on volumetric strain

3.3. Thermal Interface Shear Tests

The effects of cyclic temperature change on the behavior of energy piles can be considered in two main groups being; mechanical and thermal effects. The mechanical effects are the ones caused solely by the cyclic axial displacement of an energy pile due to elongation during temperature increase and contraction during temperature decrease. On the other hand, the thermal effects are due to the changes in soil behavior and soil-pile interaction caused as a consequence of temperature changes in the surrounding soil.

The second aspect, related to the response of soil-concrete interfaces to thermal variations, was investigated employing a modified direct shear device (Figure 13). Several modifications were realized on a conventional direct shear device to investigate soil-concrete interfaces in non-isothermal conditions: (i) a heating system was introduced which was composed of an electric resistance heater tissue, an electrical power supplier, an insulation and a thermocouple, (ii) the lower part of the shear box was redesigned to have a larger space with the purpose of accommodating the electrical heater as well as to have a constant contact area between the soil (60 mm x 60 mm x 10 mm) and concrete (60 mm x 105 mm x 16 mm) during shear. Regarding the placement of the samples, the heating tissue was placed first on the lower part of the shear box, which was protected by a metal plate to minimize its compression causing false normal displacement during the test. Next, the concrete sample was placed on the metal plate. Finally, the upper part of the shear box containing the soil sample was placed. Further information on the modified direct shear device is provided in [11].

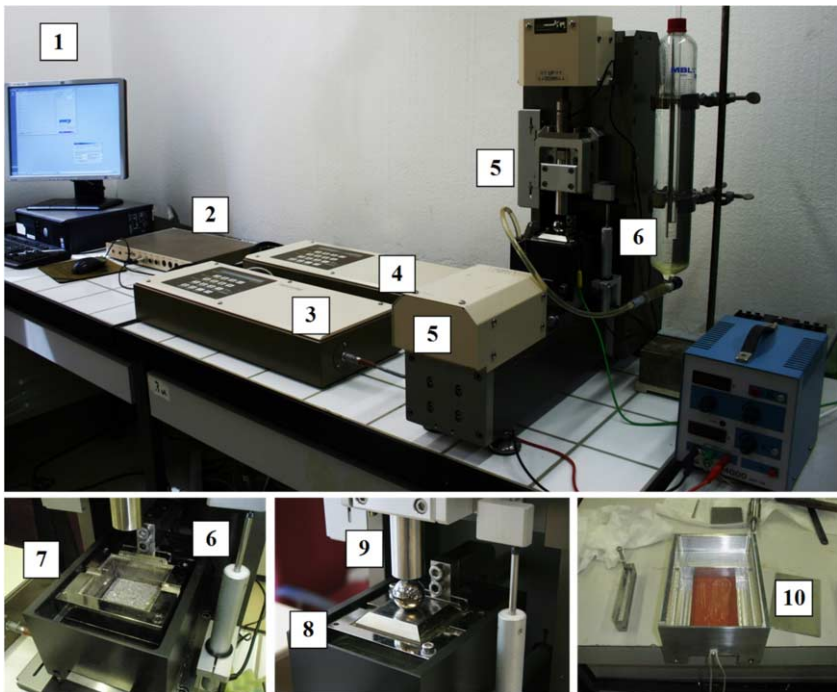


Figure 13. Thermal interface shear testing apparatus (1: GDSLAB software control, 2: LVDT Acquisition, 3: Normal actuator, 4: Horizontal actuator, 5: Load cells, 6: LVDT, 7: Specimen placement, 8: Top cap, 9: Axial piston, 10: Heating system).

The experimental campaign included tests on sand-concrete and clay-concrete interfaces at isothermal and non-isothermal conditions, under constant normal load (CNL) and constant normal stiffness (CNS). Furthermore, the effect of surface roughness on soil-concrete interaction was investigated by employing concrete samples with different degrees of roughness. CNS test results aiming attention at sand- and clay-concrete interface at different temperatures are discussed in this paper.

The CNS tests were initiated with a consolidation phase, which was followed by drained heating for the cases at high temperature. For clay-concrete interfaces, the heating was performed by increasing the temperature at a rate of $2\text{ }^{\circ}\text{C}/\text{h}$ to prevent excess pore water pressure generation. Following the drained heating, once the desired temperature and associated deformation were stabilized, the shearing phase was applied under CNS conditions where constant normal stiffness of 500 or 1000 kPa/mm for the sand-concrete samples and 200 kPa/mm for the clay-concrete samples was imposed.

The results of CNS tests performed at ambient and elevated temperature are presented in Figure 14a and Figure 14b for sand-concrete and clay-concrete interfaces, respectively. It is observed from Figure 14a that the sand-concrete interface did not show a temperature-dependent behavior, which would be expected since sandy soils are known to be indifferent to temperature change. On the other hand, the response of clay-concrete interface showed a temperature-dependent behavior during cyclic CNS tests. It is observed from Figure 14b that the interface friction angle decreased slightly at high temperatures while the adhesion at clay-concrete interface increased. This behavior was attributed to the thermal consolidation of the clay which caused an increase of contact surface between clay and concrete surfaces.

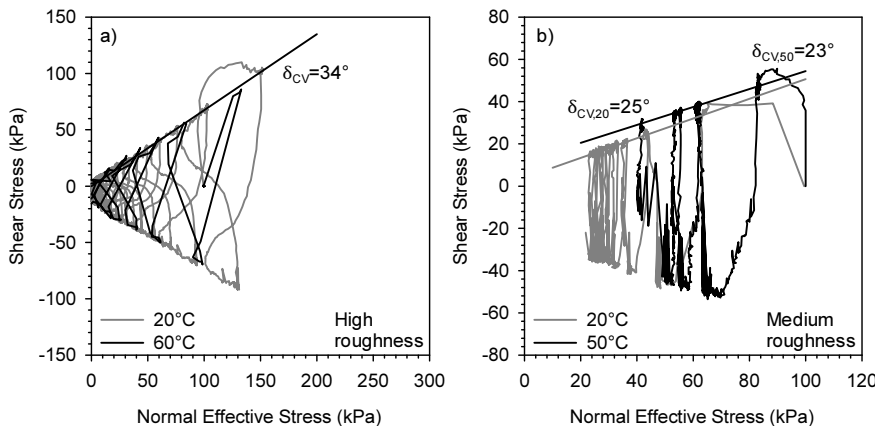


Figure 14. CNS tests on a) Sand-concrete interface (high roughness), b) Clay-concrete interface (medium roughness).

4. Summary and Discussions

Full-scale in-situ tests on energy piles, as well as laboratory test on soils and soil-concrete interfaces provided, without a doubt, insights of paramount importance on the multiphysical phenomena governing the behavior of energy piles.

The first part of this paper summarized outcomes of three full-scale in-situ tests that had diverse objectives but served the unique goal of conceiving the thermo-mechanical behavior of energy piles. The first in-situ test on a single energy pile, performed more than two decades ago at EPFL, revealed that geothermal operations cause changes in the stress state of an energy pile, the extent of which is highly governed by the end-restraining conditions. Furthermore, the null point, the depth at which no thermally induced displacement occurs, is associated with the maximum change in axial stresses and the direction of shaft resistance mobilization. The in-situ test performed on a group of closely-spaced, partially operating energy piles uncovered the interactions among active and non-operating energy piles: (i) thermally induced mechanical interactions which are governed by the changes in deformation field, due to the interplay between the pile-slab-soil responses, and (ii) thermal interactions which occur at later stages of the geothermal operation, due to the heat propagation from the active to the non-operating energy pile. The last in-situ test investigated the response of energy piles to cyclic thermal loads where cooling cycles below the in-situ temperature were applied. Concerning the outcomes of multiple heating-cooling cycles applied on the test pile, continuous thermal cycles did not cause (i) an accumulation of thermally induced axial stresses or (ii) degradation of mobilized shaft resistance with increased number of cycles. However, this outcome should not be generalized, considering the limited temperature change applied during the field test.

Design and development of non-isothermal laboratory testing devices (thermal triaxial cell, thermal oedometer and thermal direct shear device), as well as the outcomes of their employment to investigate thermo-mechanical behavior of soils and soil-concrete interfaces were presented at the second part of the paper. Since sandy soils are known to be characterized by elastic response to temperature changes, laboratory testing campaigns mainly focused on revealing the response of clayey soils to thermal loads.

The influence of temperature change on the stress-strain behavior of clayey soils was evaluated with the use of temperature-controlled triaxial testing device. The results of the test showed an increase in shear strength with temperature increase, which tend to the same critical state at large strains. Regarding the volumetric response of clayey soils, samples in OC conditions showed reversible dilative behavior while the NC ones accumulated irreversible contraction, especially during the initial cycles, which was mainly attributed to particle rearrangement. Finally, the results of soil-concrete interface shear test in non-isothermal conditions showed that sand-concrete interface was not affected by temperature changes. Contrarily, for the clay concrete interfaces, the interface friction angle decreased slightly at high temperature while the adhesion between clay and concrete increased which was attributed to the thermal consolidation of clay.

Acknowledgements

The financial supports from the Swiss National Science Foundation N. 160117 (Division III), Swiss National Science Foundation N. 200021 (Division II), Swiss Federal Office of Energy (contract Nb. 154'426) and US National Science Foundation grant CMMI-1100752 are greatly appreciated.

References

- [1] Laloui, L., Nuth, M. & Vulliet, L. (2006). "Experimental and numerical investigations of the behaviour of a heat exchanger pile", *International Journal for Numerical and Analytical Methods in Geomechanics*, 30(8), pp.763-781.
- [2] Bourne-Webb, P.J., Amatya, B., Soga, K., Amis, T., Davidson, C. & Payne, P. (2009). "Energy pile test at Lambeth College, London: geotechnical and thermodynamic aspects of pile response to heat cycles", *Géotechnique*, 59(3), pp.237-248.
- [3] You, S., Cheng, X., Guo, H. & Yao, Z. (2016). "Experimental study on structural response of CFG energy piles", *Applied Thermal Engineering*, 96, pp.640-651.
- [4] Rotta Loria, A. F. & Laloui, L. (2017). "Thermally induced group effects among energy piles", *Géotechnique*, 67(5), 374–393
- [5] Sutman, M., Brettmann, T. & Olgun, C.G. (2019). "Full-scale in-situ tests on energy piles: Head and base restraining effects on the structural behaviour of three energy piles", *Geomechanics for Energy and the Environment*, 18, pp.56-68.
- [6] Laloui, L., Moreni, M. & Vulliet, L. (2003). "Comportement d'un pieu bi-fonction, fondation et échangeur de chaleur", *Canadian Geotechnical Journal*, 40(2), pp.388-402.
- [7] Mimouni, T. & Laloui, L. (2015). "Behaviour of a group of energy piles", *Canadian Geotechnical Journal*, 52(12), pp.1913-1929.
- [8] Sutman, M., Olgun, C.G. & Laloui, L. (2018). "Cyclic Load–Transfer Approach for the Analysis of Energy Piles", *Journal of Geotechnical and Geoenvironmental Engineering*, 145(1), p.04018101.
- [9] Cekerevac, C. & Laloui, L. (2004). "Experimental study of thermal effects on the mechanical behaviour of a clay", *International journal for numerical and analytical methods in geomechanics*, 28(3), pp.209-228.
- [10] Di Donna, A. & Laloui, L. (2015). "Response of soil subjected to thermal cyclic loading: experimental and constitutive study", *Engineering Geology*, 190, pp.65-76.
- [11] Di Donna, A., Ferrari, A. & Laloui, L. (2015). "Experimental investigations of the soil–concrete interface: physical mechanisms, cyclic mobilization, and behaviour at different temperatures", *Canadian Geotechnical Journal*, 53(4), pp.659-672.

Bright Spark Lectures

This page intentionally left blank

Bright Spark Lecture



Tugce BASER

Dr. Tugce Baser is an Assistant Professor in the Department of Civil Engineering at the University of Illinois Urbana-Champaign, specializing in Geotechnical Engineering. Her research interests include unsaturated soil mechanics, energy geotechnics, permafrost mechanics, and sustainable geo-energy applications. Over the past five years, Dr. Baser has been awarded honors by international institutions and invited as a keynote speaker. She received her PhD degree in Geotechnical Engineering from University of California San Diego in 2017. Dr. Baser is a member of ISSMGE, ASCE G-I, and CGS where she is actively engaged with the student, professional, and diversity development.

Thermal Energy Storage in Borehole Arrays Installed in Unsaturated Soils

Tugce BASER^{a,1}, John S. MCCARTNEY^b and Ayse OZDOGAN-DOLCEK^c

^a*University of Illinois at Urbana-Champaign*

^b*University of California, San Diego*

^c*Balikesir University*

Abstract. In the last decades, much work has been performed to provide sustainable solutions for energy-related needs of society due to the increase in energy demands and concerns about warming of the climate. This includes using the subsurface as thermal energy sources such as in the Borehole Thermal Energy Storage (BTES) systems, an innovative approach to provide heating and cooling of the buildings through geothermal heat exchangers installed in the subsurface. This study focuses on the role of unsaturated soils on coupled thermo-hydraulic response of a BTES system, and specifically highlights how the coupled heat transfer and water flow processes and coupled thermo-hydraulic constitutive properties of soils may be exploited to optimize the performance of the BTES systems. A comprehensive study including characterization of constitutive properties of thermo-hydraulic properties and transient laboratory and field-scale responses of BTES systems, is performed. Then, the results from laboratory and full-scale field experiments are used to validate a three-dimensional finite element model to characterize heat transfer and heat storage within the BTES system. In addition, the economic and environmental impacts of the BTES systems are evaluated using a Life Cycle Assessment approach. The results indicate that the BTES systems can efficiently reduce energy consumption and CO₂ emissions that make these systems more attractive and environmentally friendly.

Keywords. BTES, heat transfer, renewable energy, unsaturated soils, LCA

1. Introduction

Borehole thermal energy storage (BTES) systems are an innovative approach, that allows to store heat collected from renewable sources in the subsurface that it can be used later for space or water heating. The BTES systems often use solar thermal panels generate heat during the day with a greater energy generation during summer months or heat recovered from waste water systems [1]. The BTES systems function in a similar way to Ground Source Heat Pumps (GSHP), where a carrier fluid is circulated through a closed-loop pipe network installed in vertical boreholes. Different from conventional GSHPs where a spacing of 2-3 m is used depending on the available space in the subsurface, the boreholes in a BTES system are spaced relatively close together (1-2 m) to concentrate heat within an array. BTES systems are proven to be an alternative to other systems as

¹ Tugce Baser, Assistant Professor, Dept. of Civil and Environmental Engineering, University of Illinois at Urbana-Champaign, 205 N. Mathews Ave, 2230C NCEL, Urbana IL 61801, USA; E-mail: tbaser@illinois.edu.

they use renewable energy resource such as solar energy rather than electricity and are space efficient as they are underground [2].

There are several successful BTES systems operating in Canada and Europe that use community-scale heat distribution systems. The Drake Landing BTES system in Canada provides 100% of the heat demand of 52 homes with an annual steady state efficiency of heat extraction over heat injection of 27% via solar thermal panels installed on garage roofs to an array of 144 boreholes in a 35 m-deep, 35-m wide grid [3]. Another successful SBTES system was installed in 2007 in Braedstrup, Denmark that supplies heat from 18,000 m² of solar thermal panels to an array of 50 boreholes having a depth of 47-50 m installed across a 15 m-wide area [4]. This system provides 20% of the heat to 14000 homes. The most recent SBTES was installed in 2008 in Crailsheim, Germany involving of a series of 55 m-deep boreholes to form a 39000 m³ subsurface storage volume. This system stores heat from 7410 m² of flat plate solar thermal collectors to provide heat for a school and 230 dwellings [5].

Although the experience from the community-scale systems at Drake Landing, Braedstrup, and Crailsheim indicates that BTES systems are functional and are sufficient to provide heating to communities at different scales, the simulation studies such as that of Catolico et al. [6] indicate that the hydrogeological setting is critical for optimizing the thermal energy storage. Therefore, this study focuses on providing a fundamental and applied understanding to the benefits of installing BTES systems in the vadose zone where the soil is unsaturated. The hypothesis of this research is based on to exploit the coupled thermal and hydraulic processes in the subsurface to take advantage of the multiple heat transfer mechanisms to increase the thermal storage capacity of the subsurface. To investigate the coupled heat transfer and water flow within borehole arrays, a full-scale BTES system was installed in University of California San Diego (UCSD) campus to monitor spatio-temporal temperature evolution during heating and cooling. The data from the experiments were used to calibrate and validate a three-dimensional finite-element-based numerical model to compare the amount of stored heat within the borehole array in different hydrological conditions.

The borehole thermal energy storage systems has become popular not only because of the increasing energy cost but also the climate change related issues such as increase in greenhouse gas (GHG) emissions with burning of fossil fuels. The BTES systems are proven to efficiently provide renewable energy and reduce the GHG emissions. However, the upfront and operational cost of these systems are still a consideration when choosing the most suitable heating and cooling system. USEIA [7] reported that the residential energy use is responsible for 30% of total annual energy consumption in the US and Heating Ventilating and Air Conditioning (HVAC) comprises 46% of the total residential energy consumption. Therefore, an efficient yet simple tool that considers cost and environmental impact can provide very useful information during the selection of the most suitable system to reduce the consumption. In this study, a life cycle analysis approach is used to perform life cycle cost and environmental impact analyses of the BTES system at UCSD using the actual data sets. The results are reported as a comparison to widely used traditional HVAC system, and GSHP system using the same assumptions and conditions.

2. Background

The major concern with BTES systems is the hydro-geological settings of the subsurface, because the soil type, amount of pore water, and in situ hydraulic gradients affect the thermo-hydraulic processes. Although the higher hydraulic gradients are favorable in GSHP systems, this is not true for BTES systems. Modeling the heat transfer in BTES systems installed in unsaturated soil profiles is complex because of the size of the system, geometry of the borehole array, and coupled constitutive relationships of thermal and hydraulic properties [8, 9]. Marcotte and Pasquier [10] numerically investigated the effect of the borehole configuration for the cases in which boreholes are connected in series, parallel, and mixed. They found that reported significantly lower inlet fluid temperatures for the parallel configuration than for the series configuration, indicating a larger heat transfer to the ground for this arrangement compared to the series configuration. Besides the geometrical configuration of the borehole heat exchangers there are other factors that affect the thermal response of a storage system, such as the subsurface temperature profile and ambient air temperature, degree of saturation profile of soil and the thermal properties. Other simulation efforts have recently been made using simplified numerical models that did not consider water vapor flow and phase change to understand the impacts of borehole array geometry, ground properties, heat injection magnitudes, and heat injection duration on the heat storage [11], characterize the behavior of borehole system behavior [12], understand the role of incorporating a thermal insulation layer [13]. Bašer et al. [13] evaluated the importance of understanding the impacts of different modes of heat transfer in SBTES systems in the vadose zone and found that it was critical to consider water vapor flow and phase change. Bašer et al. [14] investigated the effect of the ambient air temperature fluctuation on the heat storage systems and found that including ambient air temperature in the modeling efforts is worthwhile because ambient air temperature can penetrate up to 9 m from the surface. On the other hand, Nguyen et al. [15] showed that seasonal temperature variation of the subsurface increases the outlet fluid temperature causing a decrease in the heat transfer rate into the ground. Further, they found that burying boreholes at the certain depth from the surface (1-2 m) was not sufficient to hinder the ambient air temperature effects on the ground temperature near the surface. Thus, it is important to utilize validated tools to optimize these systems because of the economic concerns.

3. Field Installation

A full-scale BTES system was installed at the Englekirk Structural Engineering Center on the University of California San Diego campus. The system was sited in a 1 m of silty sand underlain by conglomerate bedrock, with a groundwater table more than 30 m deep. The BTES system consists of a network of 25 mm-diameter high density polyethylene (HDPE) U-shape heat exchanger tubing installed within 15 m deep, thirteen of boreholes in a hexagonal array with a spacing of 1.5 m as shown in Figure 1. Three additional boreholes (two within and one outside of the array) were drilled to include temperature sensors at different depths. Although the number of boreholes is much smaller than those incorporated into the district-scale heating systems mentioned above, it provides an important data point in the scaling of BTES systems for different sizes of communities. More details on the installation procedures can be found in Baser and McCartney [8].

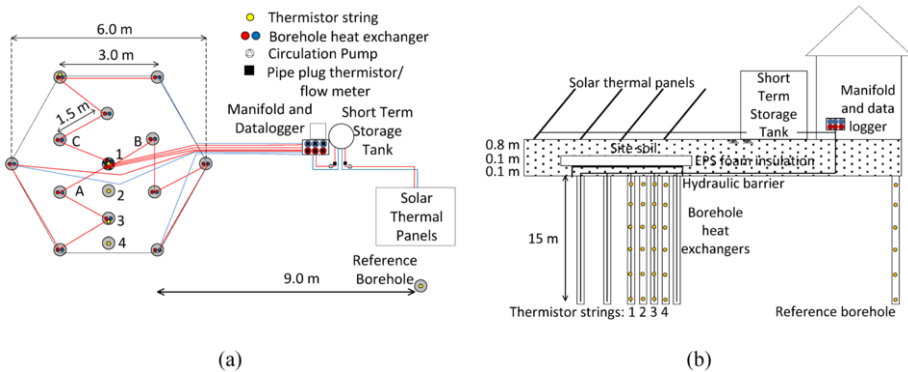


Figure 1. UCSD BTES system: (a) Plan view, (b) Elevation view of BTES system.

4. Numerical Model

Simulation of coupled heat transfer and liquid water and water vapor in unsaturated soils requires solving for four main variables: temperature, pore water pressure, pore total gas pressure, and vapor concentration using two phase flow model in which temperature and vapor pressure gradients are implemented. Governing equations for heat transfer and water flow in a continuum are presented in Table 1 (Eqs. (1) through (6)). The main assumptions of the model are: (a) soil framework is homogeneous, isotropic, and non-deformable; (b) fluid phases are immiscible; (c) hysteresis in the constitutive relationships is not considered.

Table 1. Constitutive models used in the numerical analyses.

Equation
Governing equation for liquid water flow:
$nS_{rw} \frac{\partial \rho_w}{\partial t} + n\rho_w \frac{dS_{rw}}{dP_c} \frac{\partial P_c}{\partial t} + \nabla \cdot \left[\rho_w \left(-\frac{k_{rw} \kappa}{\mu_w} \right) \nabla (P_w + \rho_w g z) \right] = -R_{gw}$ (1)
n=porosity (m^3/m^3), S_{rw} =degree of water saturation (m^3/m^3), ρ_w =temperature-dependent density of water (kg/m^3) [16], t=time(s), $P_c=P_w-P_g$ =capillary pressure (Pa), P_w =pore water pressure (Pa), P_g =pore gas pressure (Pa), k_{rw} =relative permeability function for water (m/s); κ =intrinsic permeability (m^2); μ_w =temperature-dependent water dynamic viscosity ($\text{kg}/(\text{ms})$) [17], g=acceleration due to gravity (m/s^2) R_{gw} =Phase change rate ($\text{kg}/\text{m}^2\text{s}$) [18, 19]
Governing equation for total gas flow:
$nS_{rg} \frac{\partial \rho_g}{\partial t} + n\rho_g \frac{dS_{rg}}{dP_c} \frac{\partial P_c}{\partial t} + \nabla \cdot \left[\rho_g \left(-\frac{k_{rg} \kappa}{\mu_g} \right) \nabla (P_g + \rho_g g z) \right] = R_{gw}$ (2)
S_{rg} =degree of gas saturation (m^3/m^3), ρ_g =temperature-dependent density of gas (kg/m^3) [20], k_{rg} =relative permeability function for gas (m/s); μ_g =temperature-dependent gas dynamic viscosity ($\text{kg}/(\text{ms})$) [18, 19]

Table 1. (continued) Constitutive models used in the numerical analyses.

Equation
Water vapor mass balance equation:
$n \frac{\partial (\rho_g S_{rg} w_v)}{\partial t} + \nabla \cdot (\rho_g u_g w_v - D_e \rho_g \nabla w_v) = R_{gw} \quad (3)$
D _e =D _v τ=effective diffusion coefficient (m ² /s), D _v =diffusion coefficient of water vapor in air (m ² /s) [21], w _v =mass fraction of water vapor in the gas phase (kg/kg), τ=n ^{1/3} S _{rg} ^{7/3} η=tortuosity [22, 20]
Enhancement factor for vapor diffusion, η:
$\eta = a + 3S_{rw} - (a - 1) \exp \left\{ - \left[\left(1 + \frac{2.6}{\sqrt{f_c}} \right) S_{rw} \right]^3 \right\} \quad (4)$
a=empirical fitting parameter, f _c =clay content [23]
Nonequilibrium gas phase change rate, R _{gw} :
$R_{gw} = \left(\frac{b S_{rw} RT}{M_w} \right) \left(\rho_{veq} - \rho_v \right) \quad (5)$
b=empirical fitting parameter (s/m ²), R=universal gas constant (J/molK), ρ _{veq} =equilibrium vapor density (kg/m ³) [21], T=Temperature (K), ρ _v =vapor density (kg/m ³), M _w =molecular weight of water (kg/mol) [24, 19]
Heat transfer energy balance:
$(\rho C_p) \frac{\partial T}{\partial t} + \nabla \cdot ((\rho_w C_{pw}) u_w T + (\rho_g C_{pg}) u_g T - (\lambda \nabla T)) = -L R_{gw} + Q \quad (6)$
ρ=total density of soil (kg/m ³), C _p =specific heat of soil (J/kgK), C _{pw} =specific heat capacity of water (J/kgK), C _{pg} =specific heat capacity of gas (J/kgK), λ=thermal conductivity (W/mK), L=latent heat due to phase change (J/kg), u _w =water velocity (m/s), u _g =gas velocity (m/s), Q=heat source (W/m ³) [25, 19]

As can be seen in Table 1, the governing equations don't include the constitutive relationships of thermo-hydraulic properties of unsaturated soils. To solve the sets of coupled equations, the constitutive equations were used to consider the effect of temperature on density, viscosity, surface tension, SWRC, and change in thermal conductivity and volumetric heat capacity with changing degree of saturation.

Table 2. Constitutive models used in the numerical analyses.

Equation
<i>Soil Water Retention Curve (SWRC):</i>
$S_{rw} = S_{rw,res} + (1 - S_{rw,res}) \left[\frac{1}{1 + (\alpha_{vG} P_c(T))^{N_{vG}}} \right]^{1-1/N_{vG}} \quad (7)$
where $S_{rw,res}$ is the residual degree of saturation to water, α_{vG} and N_{vG} are parameters representing the air entry pressure and the pore size distribution, respectively, and $P_c(T)$ is the temperature-corrected capillary pressure according to the model of Grant and Salehzadeh [26, 27]
<i>Hydraulic Conductivity Function (HCF):</i>
$k_{rw} = \sqrt{\left(\frac{S_{rw} - S_{rw,res}}{1 - S_{rw,res}} \right)} \left[1 - \left(1 - \left(\frac{S_{rw} - S_{rw,res}}{1 - S_{rw,res}} \right)^{1/(1-1/N_{vG})} \right)^{1-1/N_{vG}} \right]^2 \quad (8)$
where α_{vG} and N_{vG} are the same parameters as in Eq. (7) [28, 29]
<i>Thermal Conductivity Function (TCF):</i>
$\frac{\lambda - \lambda_{dry}}{\lambda_{sat} - \lambda_{dry}} = 1 - \left[1 + \left(\frac{S_e}{S_f} \right)^m \right]^{1/m-1} \quad (9)$
where λ_{dry} and λ_{sat} are the thermal conductivities of dry and saturated soil specimens, respectively, S_e is the effective saturation, S_f is the effective saturation at which the funicular regime is onset, and m is defined as the pore fluid network connectivity parameter for thermal conductivity [29]
<i>Volumetric Heat Capacity Function (VHCF):</i>
$\frac{C_v - C_{vdry}}{C_{vsat} - C_{vdry}} = 1 - \left[1 + \left(\frac{S_e}{S_f} \right)^m \right]^{1/m-1} \quad (10)$
where C_{vdry} and C_{vsat} are the volumetric heat capacities of dry and saturated soil, respectively, and are similarly treated as fitting parameters, and S_f and m are the same parameters as in Eq. (9) [14]

4.1. Calibration

To simulate the BTES system, first the numerical model needs to be calibrated for site-specific soil properties. The reconstituted site-soil was compacted to a dry density of 1650 kg/cm³ at an initial degree of saturation of 0.49. The thermo-hydraulic constitutive

relationships were determined using a transient water release and imbibition method (TRIM) of Wayllace and Lu [30] that included the measurement of the thermal conductivity and volumetric specific heat capacity described by Lu and Dong [29]. The soil water retention curve (SWRC), hydraulic conductivity function (HCF), thermal conductivity function (TCF), and volumetric heat capacity function (VHCF) were obtained using equations given in Table 2. The SWRC and HCF along with relevant parameters are shown in Figure 2(a), while the TCF and VHCF are shown in Figure 2(b).

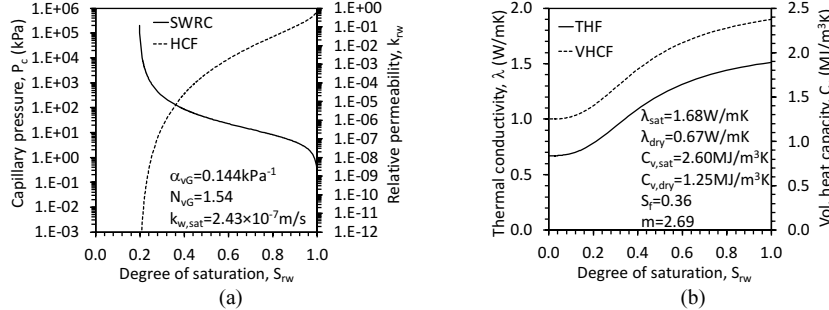


Figure 2. Coupled material properties (a) SWRC and HCF; (b) TCF and HCF.

A laboratory heating experiment was performed to characterize the thermo-hydraulic processes through site-soil as well as to provide a data set to calibrate the numerical model for empirical parameters a and b . A heating element was used to apply constant temperature for thirty-six hours at the bottom of the soil specimen that placed in a modified standard compaction mold by Iezonni and McCartney [31], which allows to include dielectric sensors in the middle of the mold. During the experiments, temporal evolution of temperature and degree of saturation were recorded. Then, the sets of coupled equations were solved using COMSOL Multiphysics v5.3 using identical initial and boundary conditions to the laboratory experiment to compare the numerical results with data collected from the experiment. The comparisons of time series are given in Figures 3(a) and 3(b). The numerical model predicted temperature and degree of saturation for a and b values of 20 and $2 \times 10^{-7} \text{ s/m}^2$, respectively.

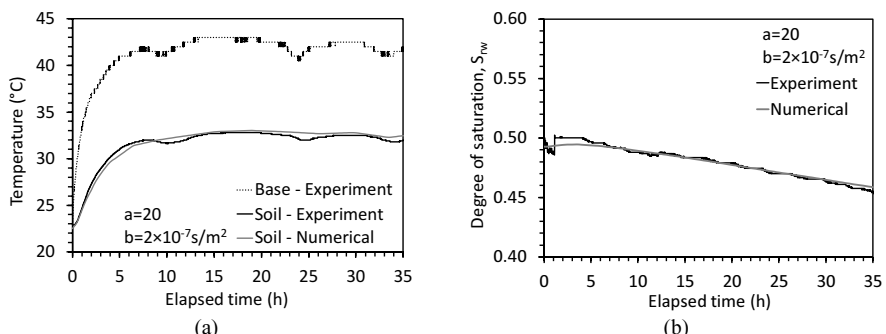


Figure 3. Comparisons of time series for experimental and numerical results: (a) Temperature; (b) Degree of saturation.

4.2. Simulations

The calibrated model was used to simulate the thermo-hydraulic response of unsaturated soils as well as the transient behavior of full-scale BTES system demonstration experiment. A plan view of the BTES system showing the connections between the borehole array, and the simulated domain are given in Figures 4(a) and 4(b). As the hexagonal borehole array is symmetrical, a quarter section was simulated as shown in Figure 4. This figure also includes the labels used to name the thirteen boreholes that include heat exchangers (boreholes A through M) and the four boreholes that include thermistor strings (T-1 to T-4). The model domain is 15 m x 15 m in plan and has a depth of 20 m and includes 5 borehole heat exchangers. The size of the domain was selected such that the heat exchangers would not affect the temperatures at the boundaries for the heat injection period under investigation. This was confirmed by ensuring that the temperature at the boundary of the array remained similar to the temperatures from the reference borehole at different depths.

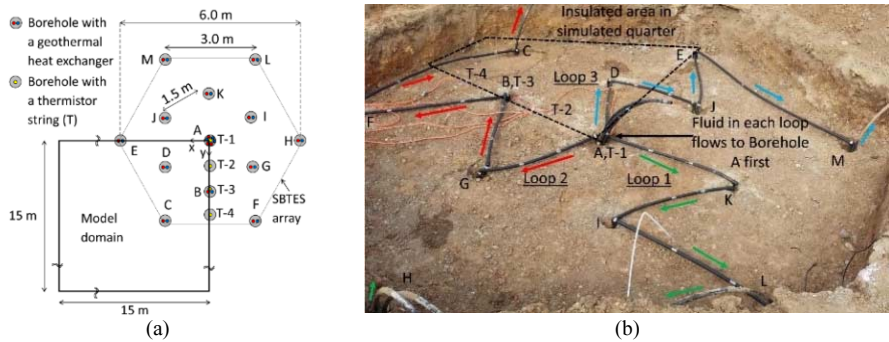


Figure 4. Simulated model domain: (a) Plan view; (b) Picture.

The plan views of the model domain shown in Figures 5(a) and 5(b) highlight the thermal and hydraulic boundary and initial conditions, respectively. The initial temperature profile was obtained from the ground temperature distribution measured by the reference borehole at the initiation of the heat injection period on April 29th, 2016. To define the initial degree of saturation profile, hydrostatic conditions were assumed. Although the water table was not encountered in the previous geotechnical site investigation which was performed in 2003, San Diego County Water Authority reported that the ground water depth ranges in depth from 14 to 24 m in the area. Accordingly, the water table was fixed at a depth of 20 m from the surface (at the base of the domain) throughout the simulations. Based on the hydrostatic profile shown in Figure 6(b), the initial degree of saturation along most of the length of the heat exchangers was approximately 0.22 which corresponds to residual saturation conditions. Near the bottom of the heat exchangers, the initial degree of saturation increases up to 0.49 due to the proximity of the water table.

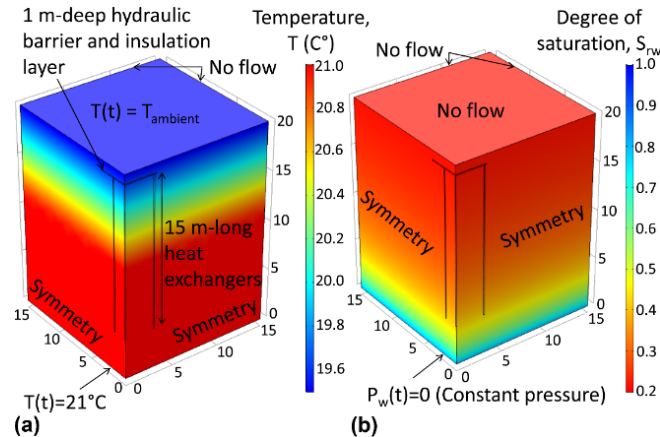


Figure 5. Initial and boundary conditions on the quarter domain model for a field-scale geothermal heat exchanger (JC is mass flux, distances in meters): (a) Thermal; (b) Hydraulic.

As could be expected from the large fluctuations in the heat transfer rate into the geothermal heat exchanger loops due to the variability in the solar thermal heat transfer rate, the temperature at the locations of the borehole heat exchangers are expected to experience significant changes in temperature each day. A comparison between the temperatures at the location of thermistor string T-2 shown in Figure 6. The temperature at the location of thermistor string T-2 depends on overlapping effects of borehole heat exchangers A and B, and heat transfer from these boreholes damps out the daily fluctuations. A good match in the trends and magnitudes at the different depths was observed during both the heat injection and ambient cooling periods, with only a slight underestimation of the temperature at depths of 16.00 m and 1.82 m. The measured temperature values during the heating injection period ranged from 29.5 °C near the bottom of the array to 34.2 °C near the top of the array. The greater increases in measured and simulated temperatures near the surface of the array may be due to greater heat transfer in initially dryer soils due to greater water vapor diffusion and latent heat transfer as well as buoyancy-driven upward movement of water vapor, both of which were observed by Baser et al. [9] in the simulation of a single geothermal heat exchanger.

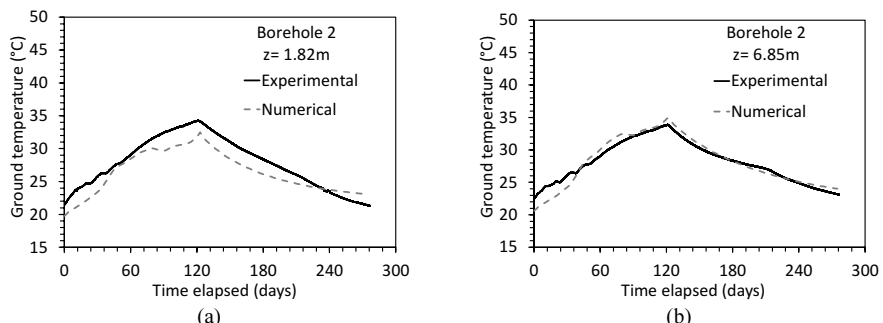


Figure 6. Predicted and measured temperature time series from thermistor string T-2 for different depths (z): (a) 16.00m; (b) 14.78m; (c) 12.95m; (d) 9.29m; (e) 6.85m; (f) 1.82m.

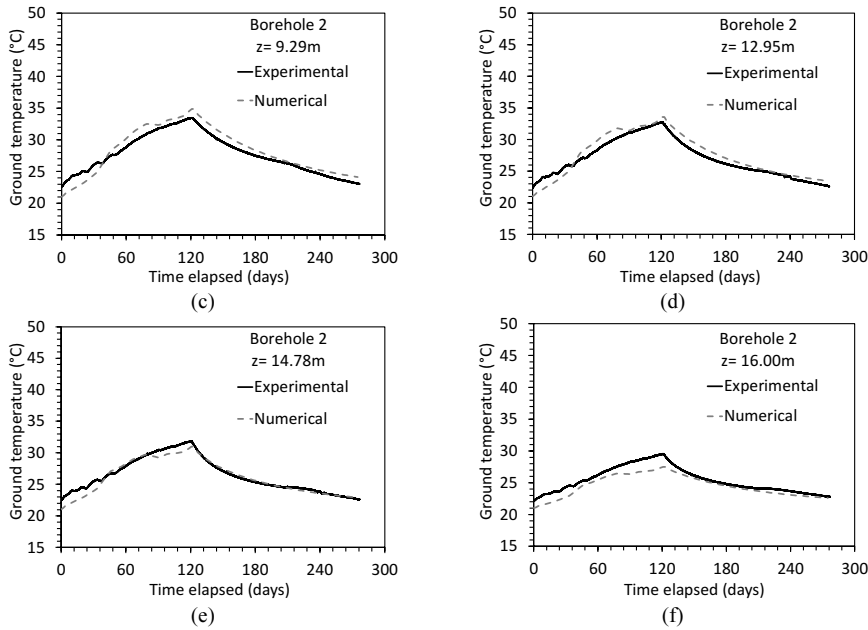


Figure 6. (continued) Predicted and measured temperature time series from thermistor string T-2 for different depths (z): (a) 16.00m; (b) 14.78m; (c) 12.95m; (d) 9.29m; (e) 6.85m; (f) 1.82m.

Radial profiles of temperatures at the end of the heat injection period from the numerical model and the field measurements are shown in Figure 7(a) for the depths that thermistors were installed. As seen in Figure 7(a), simulated temperatures were in good agreement, especially at depths of 14.78 and 1.82 m. This figure also includes the ground temperatures from the reference borehole which was at a radial distance of 10 m from the center of the borehole array to further validate the numerical model. The shapes of the radial profiles are similar to those interpreted from the field measurements, although the maximum temperatures at the locations of thermistor strings 1 and 3 due to the daily fluctuations in heat transfer rate were not captured. Radial distributions in temperature at the end of the ambient cooling period indicate that some heat (a maximum difference in temperature of 4 °C from the initial value of 21 °C) is still retained within the array after 5 months of ambient cooling as shown in Figure 7(b).

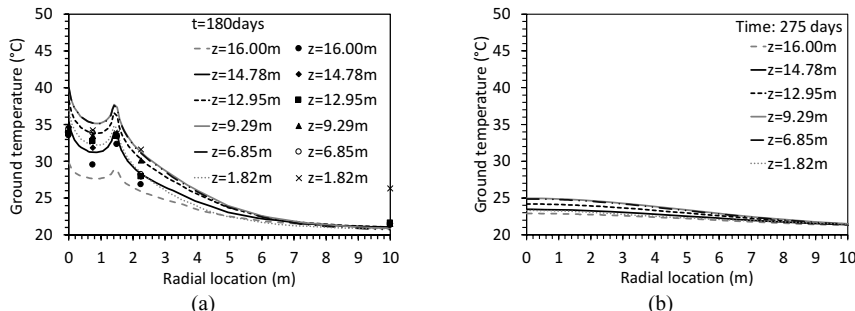


Figure 7. Radial temperature profiles at different depths (z): (a) At the end of heating; (b) After 5 months of ambient cooling.

4.3. Heat Storage

To quantify the heat stored in within the BTES system, a volume of storage is defined as the volume of borehole array assuming that any heat transferred across the outer boundaries are lost to validate hypothesis of this research. Two additional simulations were performed using the same geometry and initial and boundary conditions to compare three different hydrologic settings: (1) unsaturated, (2) saturated, and (3) dry. Then, the heat fluxes within the volume of storage were integrated over volume to calculate the power (W) and integrated over time to calculate the amount of thermal energy (GJ) retained within the same volume of storage. As seen in Figure 8, approximately 30 GJ which corresponds to the 77% of the total injected heat retained within the storage in the case of unsaturated soil while this amount was the least for saturated condition even hydrostatic conditions were assumed in the simulations. The % values in the figure indicate the heat transferred across the outer boundary of the array.

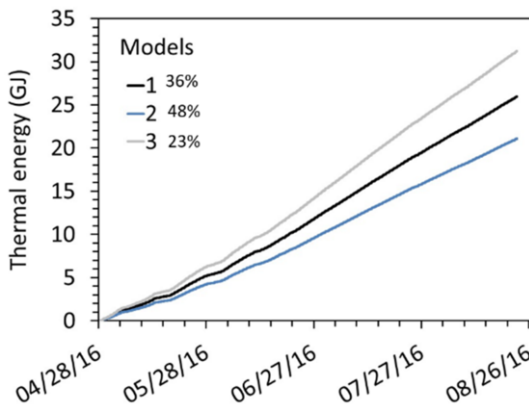


Figure 8. Comparisons of heat storage for different hydrological conditions.

5. Life Cycle Analysis of BTES

5.1. Procedure

In this study the BTES system where the heat is collected through solar panels as indicated earlier, is assessed in terms of its sustainability through its life cycle. Specifically, to investigate whether the BTES systems have more economic and environmental benefits compared to natural gas air conditioning (NGAC) and GSHP systems, a Life Cycle Assessment (LCA) approach is used to compare the life cycle cost (LLC) and environmental impact (e.g. CO₂ emission). Because the data from BTES system in San Diego, CA only includes one-year initial storage cycle, the energy cost during operation of each unit is considered for only the transient heating period.

A large data inventory is needed for a full LCA to include all the stages of a product's life from raw material extraction through materials processing, manufacture, distribution, use, repair and maintenance, and disposal/or recycling. There are various computer tools that are capable of performing the LCA of residential heating and cooling systems. Such tools include SimaPro [33, 34], Gabi5 Software [35], and RETScreen [36]. One of the

most critical implementations of LCA is the determination of the environmental impact of energy sources or life cycle energy assessment (LCEA). Considering increasing energy demand and the concern for global warming potential (GWP) is an important characterization category of LC [37]. GWP is considered a midpoint category, typically quantified by GHG emissions using units of CO₂ equivalent (CO_{2eq}). Although the predominant atmospheric GHG is CO₂ (84%), methane, nitrous oxide, carbon monoxide, and fluorinated gases contribute significantly [38]. During the analyses, the CO₂ equivalence value of each GHG can be calculated and it depends on the methods used.

In this study, present value method (PV) is used to conduct LLC analysis of BTES systems. This method was used in various projects [33, 39] and it provides relatively a quick approach that converts the future value of system into the present value by considering the discount rate and the time value as follows:

$$LCC = IC + \sum_{i=0}^n \frac{ECi}{(1+r)^i} \quad (11)$$

where IC is investment cost, EC is the annual energy, r is the real discount rate, n is the period of life-cycle analysis. IC includes purchase price of main equipment, construction, and installation cost. The discount rate, r was assumed 5% as suggested by The World Bank [40]. The rate of increase of energy cost (inflation) was set to 3%. Annual EC is calculated based on energy sources utilized in each SBTES, GSHP and NGAC heating and cooling units. Since the BTES system is operating to store heat and use it later for the heating purpose only, the energy cost used for the space heating is considered in this study.

GSHP systems require energy inputs during the use phase of electricity used by the heat exchangers and circulation pumps. For the purposes of this study, GSHP energy use is estimated with a theoretical model based on climate and building load for the state of California. This model, adapted from the study by Fredin [41], divides the building load into heating and cooling consumption. According to the model, there are two annual electricity input for a GSHP system for heating season calculated using Eqs. (12a) and (12b) as follows:

$$GSHP_{Heating[kWh]} = \frac{\text{Heating Load } \left[\frac{\text{BTU}}{\text{hr}} \right] \times \text{HDD}[\text{hr}]}{\text{COP} \times 3145 \left[\frac{\text{BTU}}{\text{kWh}} \right]} \quad (12a)$$

$$GSHP \text{ Circulating Pump}_{Heating[kWh]} = \frac{\text{Pump Power}[W] \times \text{HDD}[\text{hr}]}{\text{Motor Efficiency}[\%] \times 1000 \left[\frac{W}{kW} \right]} \quad (12b)$$

where HDD is the heating degree days and COP is the coefficient of performance that is ratio of useful energy, which is a system's output energy to its input energy use to run the GSHP system. Typical GCHPs have a COP of 3 to 4 [34], the COP for CA region is assumed as 3.5 [42]. Heating loads (26.2 kBtu/hr) and heating degree days (2948 hr) are used for a typical residential house of 2000 sq. (186 m²) from previous study done by Fredin [41]. Motor efficiency is taken as 88% [43] and combined circulating pump power is 50 W.

Another input in this approach is the energy use of a natural gas furnace during the heating season that are used as the baseline to quantify the energy savings and environmental impact. The NGAC uses natural gas for heating and electricity for both air conditioning and to run the fan in the furnace. Assuming an equal lifetime and equal heating loads for a natural gas system, the electricity and natural gas consumption are calculated using Eqs. (13a) and (13b) as follows:

$$NGAC_{\text{Heating [kWh Elec.]}} = \frac{\text{Fan Power[W]} \times \text{HDD[hr]}}{\text{Motor Efficiency[%]} \times 1000 \left[\frac{\text{W}}{\text{kW}} \right]} \quad (13a)$$

$$NGAC_{\text{Heating [kWh NG]}} = \frac{\text{Heating Load} \left[\frac{\text{BTU}}{\text{hr}} \right] \times \text{HDD[hr]}}{\text{AFUE} \times 3145 \left[\frac{\text{BTU}}{\text{kWh}} \right]} \quad (13b)$$

where EER is the energy efficient ratio taken to be 14.4, AFUE is the annual fuel utilization efficiency of natural gas assumed a mid-efficiency value of 80% [44], motor efficiency 85% and fan power $\frac{1}{3}$ HP (249 W). For BTES, energy is only consumed through operation of circulating pump, in which fluid is circulated through solar panels and array of borehole heat exchangers. Both solar and ground loops use electricity to operate the circulation pump during heat injection into the ground. Energy consumption of solar circulation pump with a power capacity of 90 W and an additional pump with a power supply of 249 W were calculated using Eq. (3).

5.2. Eco-efficiency

Solving Eq. (11) through 13, the total annual energy cost during operation is calculated and then extrapolated to a 25-year lifetime to define LCC for the operational impact of the BTES, GSHP, and NGAC systems. If energy sources for electricity use of these three systems are assumed to be natural gases, U.S. Energy Information Administration reports that the amount of CO₂ emissions is 53.07 kg/ million Btu (5.52 kg/kWh). The energy consumption of BTES, GSHP, and NGAC systems and CO₂ emissions in metric ton per kWh are calculated and the results are given in Figure 9. According to the results, the 25-year operational cost of the BTES system was only \$2,000, while this value was \$28,000 for the NGAC system. The main operational cost of the GSHP was the heat pump and the natural gas purchase for the NGAC system, respectively. The operational costs of the systems reflect to CO₂ emissions with the same trend, NGAC systems emits largest amount of CO₂ and while the BTES emits the least CO₂ with an amount of 250 ton/kWh which is 83% less than GSHP and 96% than those of NGAC system.

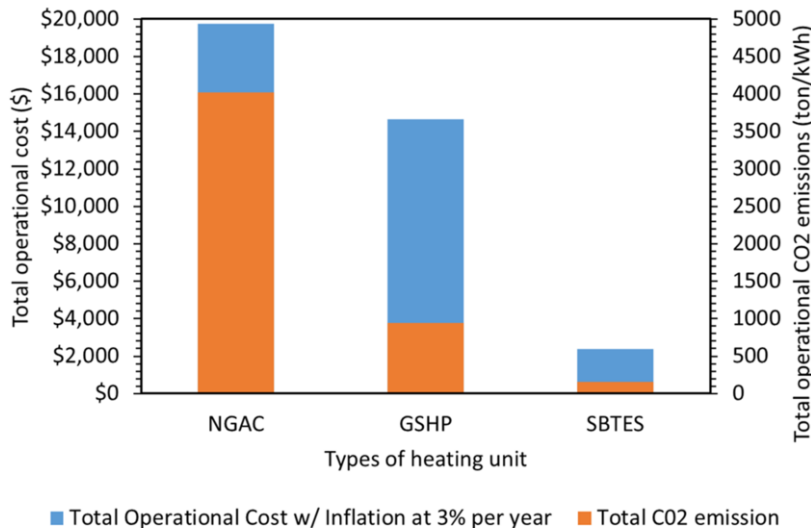


Figure 9. Life cycle cost impact of BTES, GSHP, and NGAC for 25-year of operation.

While the results from only 25-year operation was promising for BTES systems, an additional LCC analysis is needed to quantify the investment cost of all three systems. The LCC results of the BTES, GSHP, and NGAC systems are shown in Figure 10. The LCC of the BTES system was \$32,000 while this value for GSHP and NGAC systems were \$23,800 and \$24,255, respectively. One interesting observation from the Figure 10 is the similar LCC of GSHP and NGAC systems.

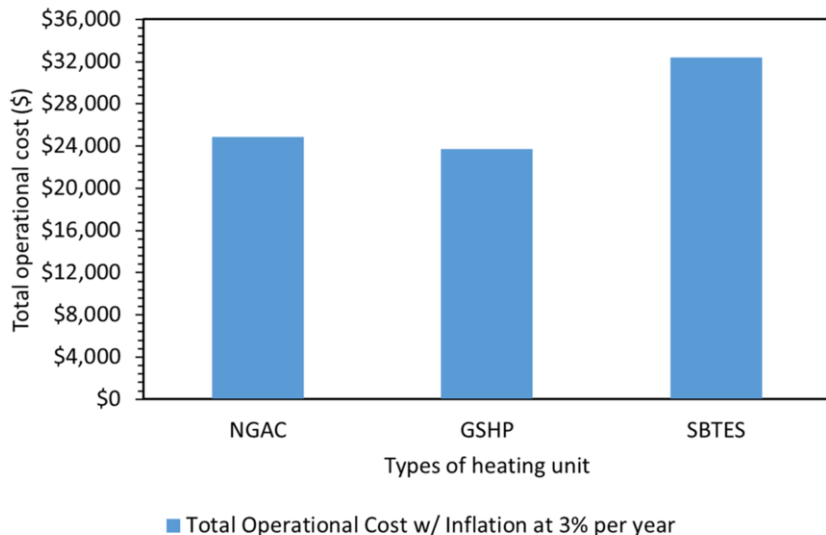


Figure 10. Life cycle cost of three different heating units (investment + operational).

6. Conclusions

This study focused on understanding the heat storage characteristics of borehole thermal energy storage (BTES) systems installed in the vadose zone. A full-scale, fully instrumented BTES system was installed in an unsaturated soil profile in San Diego, CA and subjected to a heating and cooling experiment to monitor the thermal response of the borehole array.

A calibrated and validated three-dimensional numerical model based on finite element method was used to calculate the retained heat within the borehole array to represent three different hydrologic settings: unsaturated, saturated, and dry soil profiles. It was seen that in the case of unsaturated soil, the highest amount of heat retained after the cooling period.

In addition to physics-based modeling of the BTES system, a life cycle assessment approach, eco-efficiency analysis was used to quantify the life cycle cost and environmental impact of the BTES system, and the results were compared with traditional heating and cooling systems such as ground source heat pump (GSHP) and natural gas air conditioning systems (NGAC). The results revealed that the BTES had the highest life cycle cost due to its higher investment cost compared to GSHP and NGAC, but it is more effective in terms of operational cost that will likely pay the capital cost in a short period of time. When high effective operational cost of the BTES is considered, these systems could be the best alternative in a region with moderate climate.

References

- [1] McCartney, J.S., Ge, S., Reed, A., Lu, N., and Smits, K. (2013). "Soil-borehole thermal energy storage systems for district heating." Proceedings of the European Geothermal Congress 2013. Pisa. Jun. 3-7. pp. 1-10.
- [2] Baser, T. and McCartney, J.S. (2015a). "Development of a full-scale soil-borehole thermal energy storage system." Proc. Int. Foundation Conference and Equipment Exposition (IFCEE 2015). ASCE, Reston, VA. pp. 1608-1617.
- [3] Sibbitt, B., McClenahan, D., Djebbar, R., Thornton, J., Wong, B., Carriere, J., Kokko, J. (2012). "The performance of a high solar fraction seasonal storage district heating system - Five years of operation." Energy Procedia. 30, 856-865.
- [4] Bjoern, H. (2013). "Borehole thermal energy storage in combination with district heating." EGC 2013. Pisa. June 3-7. 1-13.
- [5] Nussbicker-Lux, J. (2012). "The BTES project in Crailsheim (Germany) – Monitoring results." Proc. 12th Int. Conf. on Energy Storage – Innostock. IEA Press, Paris. 1-10.
- [6] Catolico, N., Ge, S., and McCartney, J.S. (2016). "Numerical modeling of a soil-borehole thermal energy storage system." Vadose Zone Hydrology. 1-17. doi:10.2136/vzj2015.05.0078.
- [7] U.S.EIA. (2009). Household Energy Use in California.
- [8] Baser, T. and McCartney, J.S. (2018). "Transient performance evaluation of solar thermal energy storage in a geothermal borehole array". Renewable Energy, <https://doi.org/10.1016/j.renene.2018.11.012>
- [9] Baser, T., Dong, Y., Moradi, A.M., Lu, N., Smits, K., Ge, S., Tartakovsky, D., and McCartney, J.S. (2018). "Role of water vapor diffusion and nonequilibrium phase change in thermal energy storage systems in the vadose zone." Journal of Geotechnical and Geoenvironmental Engineering. [https://doi.org/10.1061/\(ASCE\)GT.1943-5606.0001910](https://doi.org/10.1061/(ASCE)GT.1943-5606.0001910)
- [10] Marcotte, D. and Pasquier, P. (2014). "Unit-response function for ground heat exchanger with parallel, series or mixed borehole arrangement." Renewable Energy. 68, 14–24.
- [11] Baser, T. and McCartney, J.S. (2015b). "Thermal energy storage in borehole arrays." Symposium on Energy Geotechnics. Barcelona. Jun. 2-4. pp. 1-2.

- [12] Baser, T., Lu, N., and McCartney, J.S. (2016a). "Operational response of a soil-borehole thermal energy storage system." ASCE Journal of Geotechnical and Geoenvironmental Engineering. 04015097-1-12. 10.1061/(ASCE)GT.1943-5606.0001432.
- [13] Baser, T., Dong, Y., Lu, N., and McCartney, J.S. (2016d). "Role of considering non-constant soil thermal parameters in the simulation of geothermal heat storage systems in the vadose zone". Proceedings. 8th Asian Young Geotechnical Engineers Conference 2016 (AYGEC 2016). Kazakh Geotechnical Society. Astana. pp. 1-6.
- [14] Baser, T., McCartney, J.S., Moradi, A., Smits, K., and Lu, N. (2016b). "Effect of a thermo-hydraulic insulating layer on the long-term response of soil-borehole thermal energy storage systems". GeoChicago 2016: Sustainability, Energy and the Geoenvironment. Chicago. Aug. 14-18. ASCE, Reston, VA. pp. 125-134.
- [15] Nguyen, A., Pasquier, P., and Marcotte, D. (2017). "Borehole thermal energy storage systems under the influence of groundwater flow and time-varying surface temperature." Geothermics. 66, 110-118.
- [16] Hillel, D. (1980). Fundamental of Soil Physics. Academic, San Diego, CA.
- [17] Lide, D. R. (2001). Handbook of chemistry and physics. Boca Raton, FL: CRC Pres.
- [18] Bear, J. (1972). Dynamics of Fluids in Porous Media. Dover, Mineola, N.Y., 764.
- [19] Moradi, A. M., Smits, K., N. Lu, and J. S. McCartney (2016). "3-D experimental and numerical investigation of heat transfer in unsaturated soil with an application to soil borehole thermal energy storage (SBTES) systems." Vadose Zone J. 15 (10): 1-17. <https://doi.org/10.2136/vzj2016.03.0027>
- [20] Smits, K.M., Cihan, A., Sakaki, S., and Illangasekare, T.H. (2011). "Evaporation from soils under thermal boundary conditions: Experimental and modeling investigation to compare equilibrium- and nonequilibrium-based approaches." Water Resources Research. 47, W05540, doi:10.1029/2010WR009533.
- [21] Campbell, G.S. (1985). Soil Physics with BASIC: Transport Models for Soil–Plant Systems. Elsevier, New York.
- [22] Millington, R.J., and Quirk, J.M. (1961). "Permeability of porous solids." Trans. Faraday Soc. 57, 1200–1207.
- [23] Cass, A., Campbell, G.S., and Jones. T.L. (1984.) "Enhancement of thermal water vapor diffusion in soil." Soil Science Society of America. 48(1), 25–32.
- [24] Bixler, N.E. (1985). NORIA: "A Finite Element Computer Program for Analyzing Water, Vapor, Air and Energy Transport in Porous Media." SAND84-2057, Sandia National Laboratories, Albuquerque, NM.
- [25] Whitaker, S. (1977). "Simultaneous heat, mass and momentum transfer in porous media: A theory of drying porous media." Adv. Heat Transf. 13: 119–203. [https://doi.org/10.1016/S0065-2717\(08\)70223-5](https://doi.org/10.1016/S0065-2717(08)70223-5).
- [26] Grant, S.A. and Salehzadeh, A. (1996). Calculations of temperature effects on wetting coefficients of porous solids and their capillary pressure functions. Water Resources Res. 32(2), 261-279.
- [27] van Genuchten, M.T. (1980). "A closed-form equation for predicting the hydraulic conductivity of unsaturated soils." Soil Sci. Soc. Am. J. 44(5), 892–898.
- [28] Mualem, Y. (1970). The Form of the interface in steady flow in a stratified porous medium (Hebrew). Thesis for M.Sc., Technion, Israel Institute of Technology, Haifa, Israel, 1970.
- [29] Lu, N. and Dong, Y. (2015). "A closed form equation for thermal conductivity of unsaturated soils at room temperature." Journal of Geotechnical and Geoenvironmental Engineering. 141(6), 04015016.
- [30] Wayllace, A. and Lu, N. (2012). "A transient water release and imbibitions method for rapidly measuring wetting and drying soil water retention and hydraulic conductivity functions." Geotechnical Testing Journal. 35(1), 103-117.
- [31] Iezzoni, H. M. and McCartney, J.S. (2016). "Calibration of Capacitance Sensors for Compacted Silt in Non-Isothermal Applications." Geotechnical Testing Journal, Vol. 39(2), 169-180.
- [32] McCartney, J.S. and Baser, T., (2017). "Role of coupled process in thermal energy storage in the vadose zone". ISSMGE CPEG2 2017, September 6-7, Leeds, UK.
- [33] Aquino, A., Bonamente, E., Rinaldi, S., & Nicolini, A. (2017). Life cycle assessment of a ground-source heat pump including an upstream thermal storage Hydrate-based biogas upgrading and integration with other energy processes View project. Perugia, Italy April 6-7, 2017: 17th CIRIAF National Congress Sustainable Development, Human Health and Environmental Protection. Retrieved from <https://www.researchgate.net/publication/315837035>
- [34] Ozdogan-Dolcek, A. (2015). Numerical Modeling of Heat Transport for Ground-Coupled Heat Pump (GCHP) Systems and Associated Life Cycle Assessments. The University of Wisconsin - Madison, ProQuest Dissertations Publishing, 2015. 10134219, 195 p.
- [35] Li, Mo. (2013). Life Cycle Assessment of Residential Heating and Cooling Systems in Minnesota: A comprehensive analysis on life cycle greenhouse gas (GHG) emissions and cost effectiveness of ground source heat pump (GSHP) systems compared to the conventional gas furnace and air conditioner system. Retrieved from the University of Minnesota Digital Conservancy, <http://hdl.handle.net/11299/146449>.

- [36] Lee, E. J., Kang, E. C., Kim, J. Y., & Kim, Y. H. (2015). A World-wide Life Cycle Cost Analysis Tool of Ground Source Heat Pump System.
- [37] Raadal, H. L., Gagnon, L., Modahl, I. S., & Hanssen, O. J. (2011). Life cycle greenhouse gas (GHG) emissions from the generation of wind and hydro power. Renewable and Sustainable Energy Reviews, 15(7), 3417–3422. <https://doi.org/10.1016/j.rser.2011.05.001>
- [38] Desai, M., & Harvey, R. P. (2017). Inventory of U.S. Greenhouse Gas Emissions and Sinks: 1990-2015. Federal Register (Vol. 82). <https://doi.org/EPA 430-R-13-001>
- [39] Kim, J., Hong, T., Chae, M., Koo, C., & Jeong, J. (2015). An environmental and economic assessment for selecting the optimal ground heat exchanger by considering the entering water temperature. Energies, 8(8), 7752–7776. <https://doi.org/10.3390/en8087752>
- [40] TWB, 2018. The World Bank. Retrieved December 12, 2018, from <https://data.worldbank.org/indicator/FR.INR.RINR?view=chart>
- [41] Fredin, P. W. (2009). Air Force Institute of Technology. Security.
- [42] Glassley, W., Asquith, A., Lance, T., & Brown, E. (2012). Assessment of California's Low Temperature Geothermal Resources: Geothermal Heat Pump Efficiencies by Region: Evaluation of Geothermal Heat Pump System Use in California. Retrieved from <http://www.energy.ca.gov/2014publications/CEC-500-2014-060/CEC-500-2014-060.pdf>
- [43] Standards, C. A., & Verification, F. (2014). CEC. https://www.energy.ca.gov/title24/2013standards/residential_manual.html

Bright Spark Lecture



Carlos Omar VARGAS

Graduated from Technological Institute of Durango in Mexico. MSc degree obtained in 2015 from the National Autonomous University of Mexico (UNAM). Co-author of the book “Assessment of vulnerability to the liquefaction of sands” edited by the Mexican Society of Geotechnical Engineering (SMIG), for which was awarded with the “Nabor Carrillo Flores” Research Award in 2017 granted by the College of Civil Engineers of Mexico. He has published fourteen technical articles related to: soil liquefaction, site response analysis, tailings dam, numerical modeling and soft soils topics, obtained from academic work and professional practice.

He is employed of the Department of Soil Mechanics of the Federal Electricity Commission (CFE) in Mexico. Professional experience in the development of geotechnical design and analysis projects, including the following: Design of tailings dams for mining infrastructure, design of shallow and deep foundations and design of tunnels and tunnel shafts in soft soils. Currently, he is professor in the postgraduate course of National Autonomous University of Mexico (UNAM) campus Acatlán (FES-Acatlán) since 2018. Professor at the Bachelor’s Degree Program in Deep Foundations for UNAM-FES-Acatlán since 2016. He has taught the course of liquefaction analysis for SMIG and courses for a private industry in Lima, Peru. He has been part of the board of the Mexican Society for Geotechnical Engineering from the period of 2017 to 2018.

Analysis and Seismic Design of Tailings Dams and Liquefaction Assessment

Carlos Omar VARGAS^{a,1}

^a*Federal Electricity Commission, Soil Mechanics Department, Mexico.*

Abstract. The increasing of the mining industry in Latin America, combined with the high seismic conditions of some regions, represents a major challenge for geotechnical engineers in relation to the mining waste disposal design. Earthquakes are one of the principal causes of failure in this kind of structures, which are mainly attributed to liquefaction, whose consequences have been catastrophic such as cases history of Mochikoshi Tailings dams, Japan (1978); Cerro Negro and El Cobre, Chile (1965) and Amatista, Nazca, Peru (1996). Therefore, one of the main aspects in the seismic design of these structures is related to the possible liquefaction of the tailings, due to the characteristics of these materials. This paper presents the design criteria, geotechnical characterization and the seismic stability assessment of a tailings dam. This work is presented from practice approach, with emphasis on considerations that involved the dynamic analysis of a project at the design stage and the evaluation of liquefaction in this structure. The analysis results, interpretation and conclusions are presented based in local and international guidelines.

Keywords. Tailings dams, liquefaction, post-earthquake deformations, flow liquefaction.

1. Introduction

1.1. Background

Tailings dams are retention structures formed by earth materials whose main goal is the storage of mining waste resulting from the mineral benefit process in mining industry. The material stored, called “tailings”, is usually deposited in an aqueous slurry compound, generally called tailing slimes, whose solid particles are made up of silty or clayey materials produced by the crushing of rock and mineral.

Therefore, one of the main concerns in the design of these structures, are related to the possible liquefaction of the materials that make up the geotechnical structure. Therefore, it is necessary to carry out a rigorous analysis and design that guarantees the safety of the structure.

Tailings dams are structures of large dimensions and throughout history have been exposed to different types of failures related to different factors (e.g. operation, natural phenomena and construction). Earthquakes are one of the principal causes of failure in this kind of the structures, which are attributed mainly by liquefaction, whose consequences have been catastrophic such as case histories of El Cobre Old Dam and

¹ Carlos Omar Vargas; E-mail: comarvm19@gmail.com.

New Dam in Chile (1965), Mochikoshi N. 1 in Japan (1978), Cerro Negro N. 4 in Chile (1964) and Amatista Nasca in Peru (1996), among others. A typical seismic failure in tailings dams is shown in Figure 1.

In tailings dams, the seismic design starts from the conception of the construction method and type of tailings deposition, which in turn are subjected to factors related to site conditions, topography, availability of borrow materials, economics, environmental and operational factors. Therefore, geotechnical engineers must reach the best solution design that addresses these conditions as much as possible.



Figure 1. Seismic failure of Cerro Negro Tailings Dam [1].

1.2. Design considerations

The objective of tailings storage embankment design is to ensure that the structures are able to withstand the potential loading conditions that could be expected during their lifetime to the extent that the risk of failure is acceptably low [2].

The tailings dams design follows certain international and local guidelines, such as the technical bulletins of the International Commission on Large Dams (ICOLD, Bulletin 139) [3], Canadian Dam Association (CDA) [4] and Australian National Committee on Large Dams (ANCOLD) [2]; as well as compliance with local regulations.

These guidelines specify the considerations for management, tailings deposition methods, construction, characterization criteria and considerations for analysis and design. Regarding the latter and as far as seismic conditions are concerned, the guidelines provide suggestions on the target levels for earthquakes in accordance to the construction stage or phase in the life of mining dam, as well as the safety factors and deformations thresholds that guarantee the adequate behavior of the structure during an earthquake.

1.3. Construction methods

The seismic stability of tailings dams depends strongly on the construction method; within these, the main ones and of greater use in practice are the upstream, downstream, and centerline methods. In addition, there are other methods such as the upstream - downstream construction and solid waste deposition (thickened tailings).

According to the state-of-the-art and practice, the upstream construction method is vulnerable under seismic conditions, reason why, currently its use is prohibited in seismic areas. However, it is important to know and understand the conditions that have led to the vulnerability of these structures, which have been studied by different authors.

The vulnerability of these structures is governed by several factors such as the lack of rigorousness in supervision and construction process, uncertainties during mining operations, tailings deposition process and variations of source material or mineralogical composition. Furthermore, the long construction period of these structures, generally results in inadequate control and modifications of the original design conditions of the dam.

The over-elevation of the deposits for a greater storage, once the maximum elevation of design has been reached is a common practice, which affects the behavior of the structure, mainly in the vibration period, increase of stresses and pore pressure that produce deformations and possible activation of the contractive response of the soil that can trigger flow failure.

The instability of this construction method is because the retention structures are constituted by sand dykes. In addition, the stability of these dykes depends mainly on the tailing slimes for support [5], which generally become saturated and can liquefy under dynamic loading. The characteristics and configuration of the upstream method are shown in Figure 2(a).

Generally, it is known that during a severe earthquake, the material deposited will liquefy, so the principal concern is ensured that the retention dykes (sand dykes) are stable and do not liquefy. Nevertheless, the liquefaction of the tailings deposited (tailing slimes) can produce the failure, due to the saturation of the area near the contact between upstream dykes and tailing slimes. That was the case of the tailings dam of Moshicoshi in Japan, in which the 1978 Izu-Ohshima-Kinkai earthquake caused a failure due to the liquefaction of the materials behind the dam (Byrne et al. [6] and Ishihara, [7]).

The downstream construction method consists in the sequential construction of dykes using tailings sands, waste rock or borrowed fill (rockfill embankments). This option involves the use of internal drains or filters. The characteristics and configuration of this method are shown in Figure 2(b). Although this method has greater stability, it represents an expensive solution due to the volume required for the construction of retention structure.

The center-line method is a combination of upstream and downstream methods. The construction and growth of the dyke are carried out sequentially by keeping the vertical axis of the point of discharge, Figure 2(c). This method has an acceptable seismic stability in addition to a moderate cost.

Other methods of construction are deposits of solid tailings (Thickened tailings) and mixed construction methods such as the upstream-downstream method with rockfill embankment (Figure 3), the latter is specified in Mexican regulations (NOM-141-SEMARNAT-2003 [8]). The principal difference of this structure and conventional upstream method is that instead of using a starter dam, a rockfill embankment is used, which represents the principal retention structure. Currently, the use of this construction method in seismic zones in Mexico is not limited by regulations.

This type of structure must be carefully designed because the upstream dykes are supported on tailing slimes. Although the upstream dykes have a lower height than conventional upstream dams, these will be exposed to construction and operational factors that affect this kind of growth.

The disadvantages of this type of construction are the availability of materials in the area in order to build the rock fill embankment, as well as the inherent risks associated with the construction and operation of the dam, which requires a rigorous monitoring of the designer in order to evaluate the geotechnical conditions during its different stages. The adequate and rigorous design of this construction method, coupled with an

appropriate construction supervision and compliance with the operation processes, can be a feasible option in cost and security that allows a greater volume of storage.

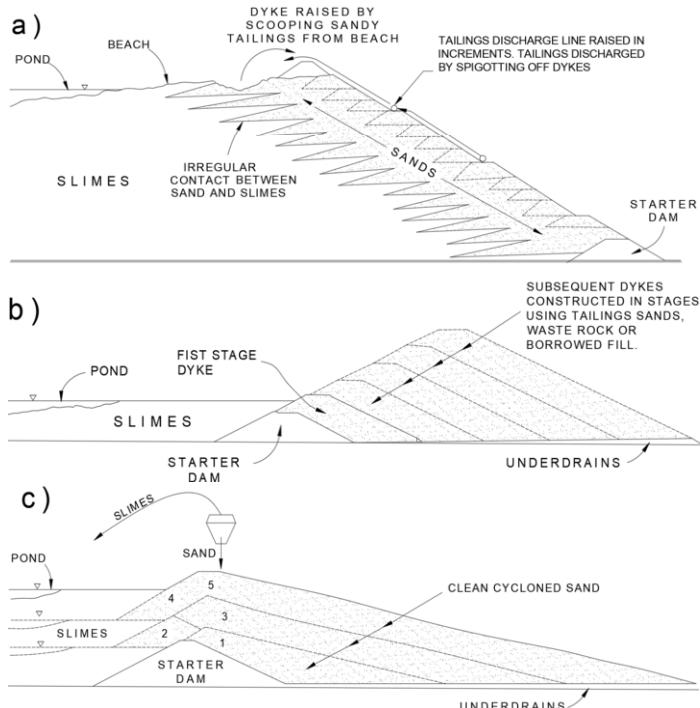


Figure 2. Methods of construction: a) Upstream, b) Downstream and c) Center-line (Figure modified from [5]).

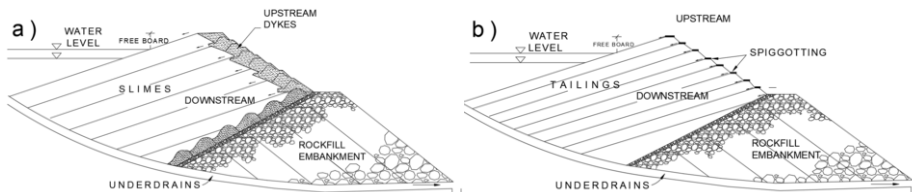


Figure 3. Scheme of upstream-downstream method with rockfill embankment: a) cyclone sand and b) spigotting (Figure modified from [8]).

1.4. Liquefaction in tailings dams

As mentioned before, an aspect of great importance to be considered in the engineering of tailings dams is related to the studies to evaluate liquefaction vulnerability. In practice, it is generally assumed that the tailings are liquefied during an earthquake; both the fine fraction of the tailings (slimes) and tailings sands (dykes) are susceptible to liquefaction. State-of-the-art and practice (Troncoso [9], Ishihara [7], Phukunhaphan *et al.* [10], Moriwaki [11], Verdugo [12] and Hu *et al.* [13]) indicate that the predominant factors in the behavior of liquefaction in mine tailings are influenced by the type of source material, grain size distribution (fine or coarse) and the materials properties (relative density and plasticity).

For the study of liquefaction, a standard has been defined in the professional practice, which includes the following stages: 1) Susceptibility and liquefaction potential, 2) Stability analysis or flow slide and 3) Displacement analysis.

Susceptibility evaluation in mine tailings is usually performed according to the criteria defined by Andrews and Martin [14] and Bray *et al.* [15], developed for soils with a significant amount of non-plastic fines. These criteria evaluate if the soil meets the physical characteristics to be liquefiable regardless of the trigger mechanism, for that purpose, the index properties of the soils are used.

Once the susceptibility of the soil to be liquefied is determined, the liquefaction potential and soil behavior (contractive or dilative response) are evaluated. The evaluation of the liquefaction potential can be carried out using semi-empirical methods based on the Seed and Idriss method [16], laboratory tests, site response analysis (time or frequency domain) or using numerical analysis with advanced constitutive models.

It is important to note that liquefaction assessment in tailings dams should not be limited to the estimation of its potential. Hence, for design purposes it is important to know the cyclic behavior of the tailings in terms of cyclic resistance, strains, generation of dynamic pore pressure and strength loss.

In geotechnical earthquake engineering the term of liquefaction can be divided into two main categories: flow liquefaction and cyclic liquefaction [17].

Both phenomena can occur in tailings deposits with different manifestations; therefore, it is important to understand and distinguish between these phenomena, as well as studying their characteristics and triggering mechanism in order to carry out a design capable of mitigating them.

According to Robertson and Wride [18] the cyclic (seismic) liquefaction is associated with the dilative response or strain hardening of the soils, generally soils of a rigid nature such as dense sands. Nevertheless, a condition of "cyclic liquefaction" or "cyclic mobility" can be reached depending on the state of shear stress reversal under cyclic loading in undrained conditions. Cyclic (seismic) liquefaction behavior is shown in Figure 4.

Cyclic liquefaction has as main characteristics, the development of shear stress reversal, which allow reaching a condition of zero effective stress, in this state the soil has very little stiffness and large deformations can occur during cyclic loading. In terms of pore pressure, it means 100% pore pressure excess ratio (r_u), frequently called "initial liquefaction". For cyclic liquefaction, the deformations stop when cyclic loading has concluded; however, flow liquefaction can active if there is a pore pressure redistribution.

In contrast to cyclic liquefaction, cyclic mobility does not present shear stress reversal, so a condition of zero effective stress will not be achieved, resulting in small deformations [18].

Casagrande [19] was the first in define the term cyclic mobility, as the progressive softening of saturated sand specimens when subjected to cyclic loading at constant water content [20]. Castro and Poulos [21] specified that cyclic mobility is distinguished from liquefaction by the fact that a liquefied soil exhibits no appreciable increase in shear resistance regardless of the magnitude of deformation. During cyclic mobility, the residual shear resistance remains greater than the driving static shear stress and deformations accumulate only during cyclic loading [22].

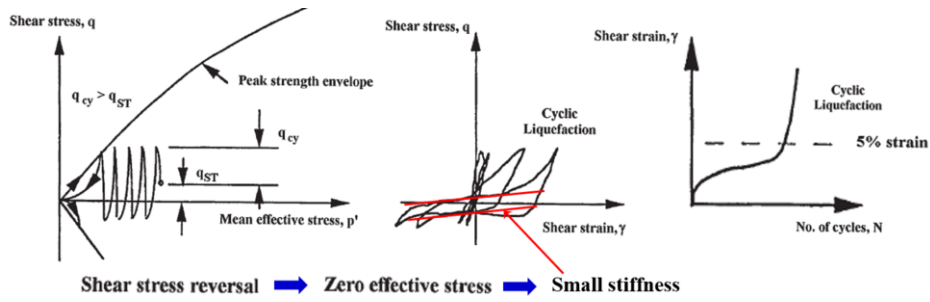


Figure 4. Cyclic (seismic) liquefaction behavior [18].

Flow liquefaction is also referred to as static liquefaction. However, the phenomenon can be triggered by either static or cyclic loading [23].

Flow liquefaction occurs when the static shear stress that maintains the static equilibrium is greater than the undrained shear strength or residual/liquefied shear strength, thus generating large deformations activated by monotonic loads. This phenomenon is related to the contractive response and strain softening behavior of the soil, such as loose sands and non-plastic silts.

Flow liquefaction is of great importance in tailings dams because the deposition of them is in a loose and saturated state, whose behavior under undrained loading conditions tends to be contractive. The risk for flow liquefaction in contractive soils depends on brittleness (sensitivity), which is the measure of the strength loss under the effect of static or seismic loading. Flow Liquefaction behavior is shown in Figure 5.

The case histories of static liquefaction in tailings dams have signified catastrophic failures as the cases of the Kolontar tailings dam failure in Hungary (Figure 6a) and Harmony, Merriespruit, South Africa (Figure 6b), as well as recently cases of failures in Brazil (Samarco dam in 2015 and Brumadinho dam in 2019).

The flow failure can occur suddenly during the earthquake or immediately after the earthquake has ceased, even at long after (few hours or up to 1 day), which is often called post-earthquake deformations, for which the estimation of residual strength is essential in order to evaluate flow liquefaction.

According to Robertson [23] the sequence to evaluate flow liquefaction is: 1. Evaluate susceptibility for strength loss, 2. Evaluate stability using post-earthquake shear strengths and 3. Evaluate trigger for strength loss.

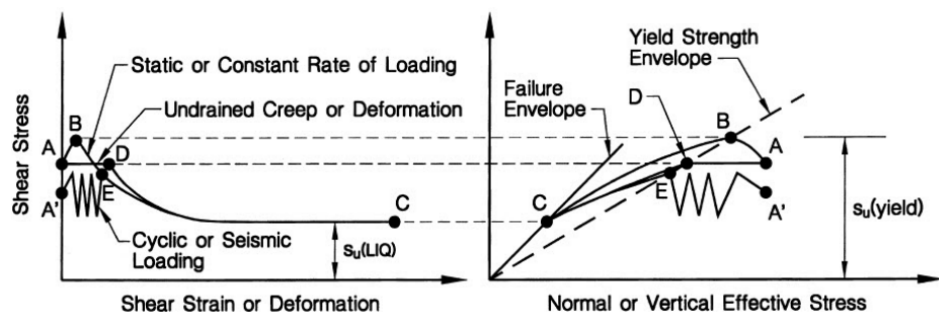


Figure 5. Flow Liquefaction behavior [23].



Figure 6. Flow liquefaction failures: a) Kolontar Tailings Dam failure in Hungary [24] and b) Harmony, Merriespruit, South Africa [25].

1.5. Analysis methods

The dynamic analysis in tailings dams aims to evaluate the response and behavior of the structure subjected to earthquake shaking. The dynamic behavior of the structure must include the estimation of permanent deformations due to the earthquake in order to evaluate the seismic stability and the service state of the dam.

There are different analytical and numerical methods for the evaluation of these aspects. Generally, the estimation of permanent deformations is carried out using semi-empirical methods (e.g. Newmark, [26], Yegian *et al.* [27] and Makdisi and Seed [28]), which have been widely accepted in practice. However, currently the dynamic analyses for tailings dams are solved using numerical methods, since it is possible to consider and integrate conditions of the dynamic behavior of the structure.

The selection of analysis methods to evaluate static and dynamic stability depends on the conditions of the problem. Therefore, in those cases, in which the estimation of deformations and generation of excess pore pressure are the principal aspects to evaluate, it is necessary to carry out a numerical analysis. Usually, the dynamic analysis in tailings dams considers the simulation of the liquefaction of the tailing slimes, which represents a conservative scenario for the design.

The main objectives in the simulation of the liquefaction are to estimate the dynamic pore-pressure generation and the prediction of deformations during and after an earthquake. For this purpose, different approaches and methods of analysis have been developed.

The finite element and finite difference methods are of great use for the solution of geotechnical problems associated to tailings dams, since these allow considering the non-linear behavior of the soil and dynamic pore pressure build up through advanced constitutive models.

The most used pore pressure generation models in numerical methods, which are incorporated in commercial codes or programs, are: Seed and Idriss Model (cyclic stress approach), Finn Model – Martin *et al.* [29] formulation, Finn Model – Byrne formulation [30], UBCTOT model, UBCSAND model and recently the PM4SAND model developed by Boulanger and Ziotopoulou [31].

In this paper a dynamic analysis is presented in order to evaluate the seismic stability of a tailings dam for a case study in the design stage. The liquefaction was simulated by Seed and Idriss model. In addition, the design criteria and the geotechnical characterization that involved the evaluation are presented for this case.

2. Case study

2.1. General and geotechnical conditions of the dam

The case study corresponds to the design of a tailings deposit located in an area of high seismicity in Mexico. The structure will be founded primarily on andesitic rock that predominates in the entire impoundment. According to the volume of storage required for the project, operation times and site restrictions, the deposit will reach a height of 80 meters on an approximate surface of 19 hectares. In addition, the design considered a length of beach of 60 meters, in order to avoid the saturation of tailings near the retention structure.

As background for this project, two construction alternatives were evaluated, which were within the local regulatory framework for the conditions of the zone. For the first alternative, a tailings dam constructed by the upstream-downstream method with rock fill embankment was considered, while the second alternative consisted in the design by the downstream method with rock fill embankment. In this article, the evaluation of the seismic stability of the first alternative is presented, given that it represents the most unfavorable condition.

Figure 7 shows the section analysis of the tailings dam, which includes a rock fill embankment (starter dam) with a height of 50 meters and 1.5:1 for upstream slope and 1.8:1 for downstream slope. The upstream dykes projected by upstream method will be constructed by borrow material (clay sand with gravel). The height of each dyke is 5 meters with 2:1 (H: V) slopes, achieving a general slope of 3:1 (H:V). The total height of the tailings dam is approximately of 80 meters in its maximum section.

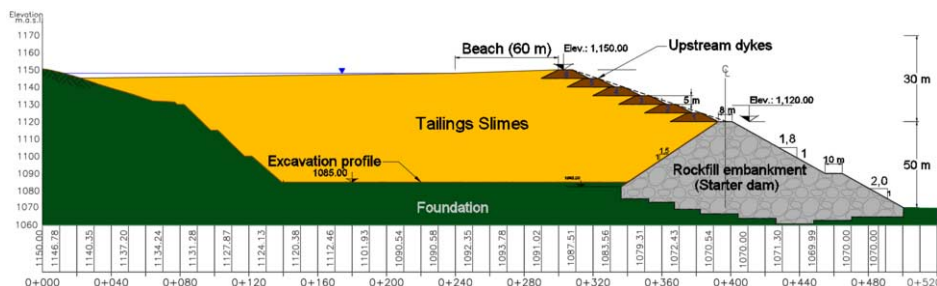


Figure 7. Cross-section of tailings dam (case study).

2.2. Seismic conditions

In order to evaluate the long-term seismic condition of the deposit, the maximum credible earthquake (MCE) was used, which was defined by a seismic hazard study that included the modeling of seismic sources close to study site. This condition was defined considering the recommendations of international guidelines (CDA [4]), which suggest the use of the MCE for a very high to extreme dam classification.

Figure 8 shows the record of maximum accelerations and response spectra associated with the designed earthquake (MCE), which will be used for the dynamic analysis. It should be noted that the earthquake was corrected by baseline.

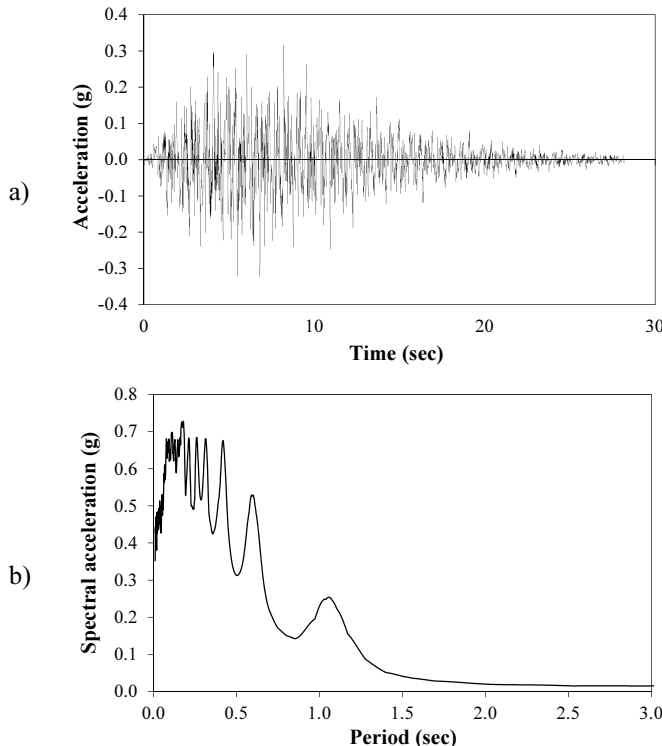


Figure 8. a) Input earthquake acceleration record and b) response spectra.

3. Geotechnical characterization

3.1. Foundation

From a geotechnical exploration campaign and geological studies, it was determined that in the study site, the predominant stratigraphy is composed of clayey sands with gravel and altered rock for the first 10 to 20 meters of depth, which is underlined by rock in a healthy state.

Simple compression tests were performed to determine the resistance parameters based on the Hoek and Brown [32] criterion, and Menard Pressuremeter tests (PMT) were performed to estimate the elastic modulus. The coefficient of permeability of the foundation was defined by in-situ tests, Nasberg tests for shallow depths (0 to 25 m) and Lugeon tests for greater depths (> 25 m).

The in-situ shear wave velocity (V_s) of foundation was defined by dispersion analysis of surface wave testing. Figure 9 shows the profiles of shear wave velocities.

3.2. Retention structures

The representative parameters for the rock fill embankment structure were taken according to the CIGB ICOLD [33]. In order to consider the stress-strain behavior of the

dam, a hyperbolic model determined from the elasticity data of the La Yesca dam published by Aleman [34] was used. Strength parameters of upstream dikes were determined from UU triaxial tests in reconstituted samples that represent the compaction conditions of the dam.

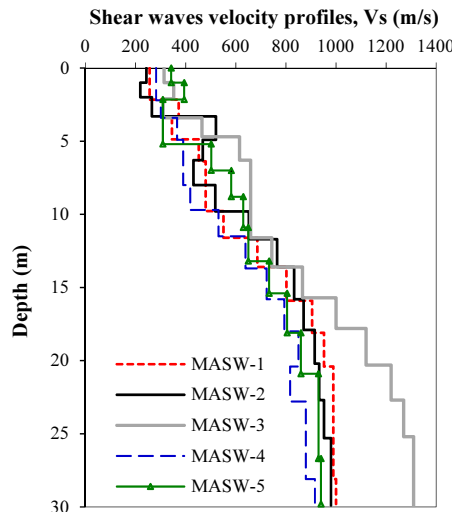


Figure 9. Shear wave velocity (V_s) profiles in foundation.

4. Tailings properties

4.1. Static properties of tailings

The mining waste material to be deposited in the impoundment is integrated of non-plastic fines with sand and minerals, mainly the result of lead and zinc recovery. On average, tailings have 45% water content, 27% of a liquid limit, and 11.9% of plasticity index.

After estimating these properties, consolidation tests were carried out simulating the process of deposition of the tailings *in situ*, under the influence of different effective confining stress (50, 100, 200, and 400 kPa) and different initial water contents (33, 43, 54, 66%). The purpose of this is to monitor the effect of the variation of water content in the dry unit weight and permeability (Figure 10). Figure 10(a) shows that water content at five meters of depth is kept below 30%, reaching 20% for a depth of 40 meters, in addition to a decrease in permeability in one order of magnitude at the depth of 10 m (Figure 10b). Figure 10(c) shows that in general, there are variations of the order of 100 kg/m³ for the different water contents. Based on these results, samples were prepared for testing and obtaining its static and dynamic mechanical parameters.

Resistance parameters were obtained from consolidated undrained triaxial test with pore water pressure measurement. Permeability was defined by variable load permeameter test, obtaining permeability values of the order of 9.8E10⁻⁸ and 8.2E10⁻⁸ cm/s. In order to represent the increase of tailings stiffness in function of depth, it was assumed that the modulus of elasticity increase with the effective vertical stress.

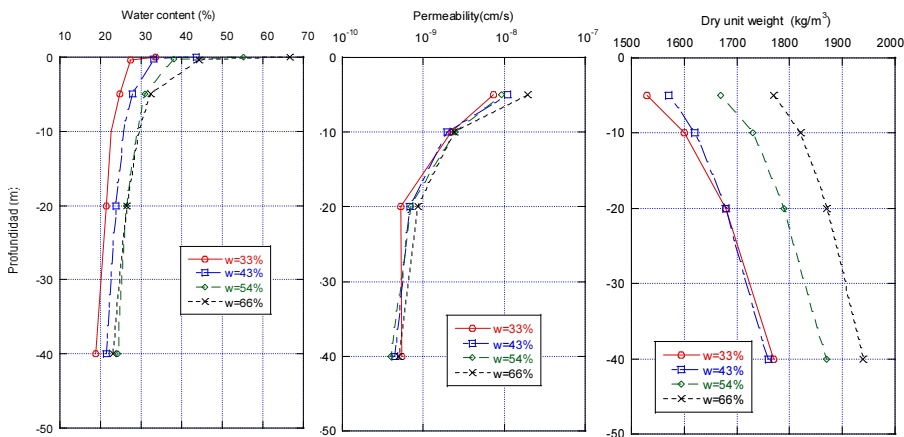


Figure 10. Simulation of the deposition process of tailings in situ: a) variation of water content, b) variation of permeability and c) variation of dry unit weight due to tailings deposition.

4.2. Dynamic properties of tailings

Dynamic behavior of the tailings was represented with curves of degradation of the shear modulus and damping curves versus shear strain amplitude. The degradation curves were obtained from dynamic laboratory test using a cyclic triaxial test and resonant column for large and low strains, respectively. Likewise, the pore pressure was measured from the cyclic triaxial test in order to evaluate the ability of the tailings to generate excess pore pressure under cyclic loading.

For cyclic triaxial test, 10 stages of constant amplitude cyclic shear stress were applied for 20 cycles under the undrained loading condition. The amplitude of shear stress was increased at each stage.

The properties of the reconstituted and tested samples were defined with the consolidation tests by simulating the in-situ tailings deposition process under different effective stresses.

Figure 11 shows the degradation curves of tailings for effective confining pressure of 50, 100, and 200 kPa and their comparison with conventional soils and other tailings. This figure shows that for these tailings at low confining pressure, the material tends to the lower limit of the sands; while at higher confining pressure, its dynamic behavior approaches the upper limit of the sands. Degradation curves of tailings are below the degradation curve for clays with a plasticity index (PI) of 11.6% determined by Dobry and Vucetic [35], which according to the Unified Soil Classification System (USCS) would correspond to tailings materials.

For the damping ratio of tested tailings, it is observed that at low strains and lower confining stresses, the material tends to behave as a fine non-plastic material (Curve of Dobry and Vucetic), but at large strains, the curves are found within the range of damping of the sands. Therefore, despite the fines content and soil classification of tailings, their dynamic behavior in terms of stiffness degradation and damping ratio tends to the behavior of the sand.

For the dynamic analysis, it was necessary to determine the shear wave velocity (V_s) values. However, given that it is a project at the design stage; dynamic properties of tailings were estimated from in situ measurements of shear-wave velocity (V_s) in a tailings dam with similar characteristics. This criterion is an adequate approximation to

represent the conditions to which the structure will be subjected during its operation phase. Nevertheless, considering that the construction is gradual, it is possible to carry out measurements of the dynamic properties in order to corroborate the design parameters. Figure 12 shows the profile of Vs for tailings.

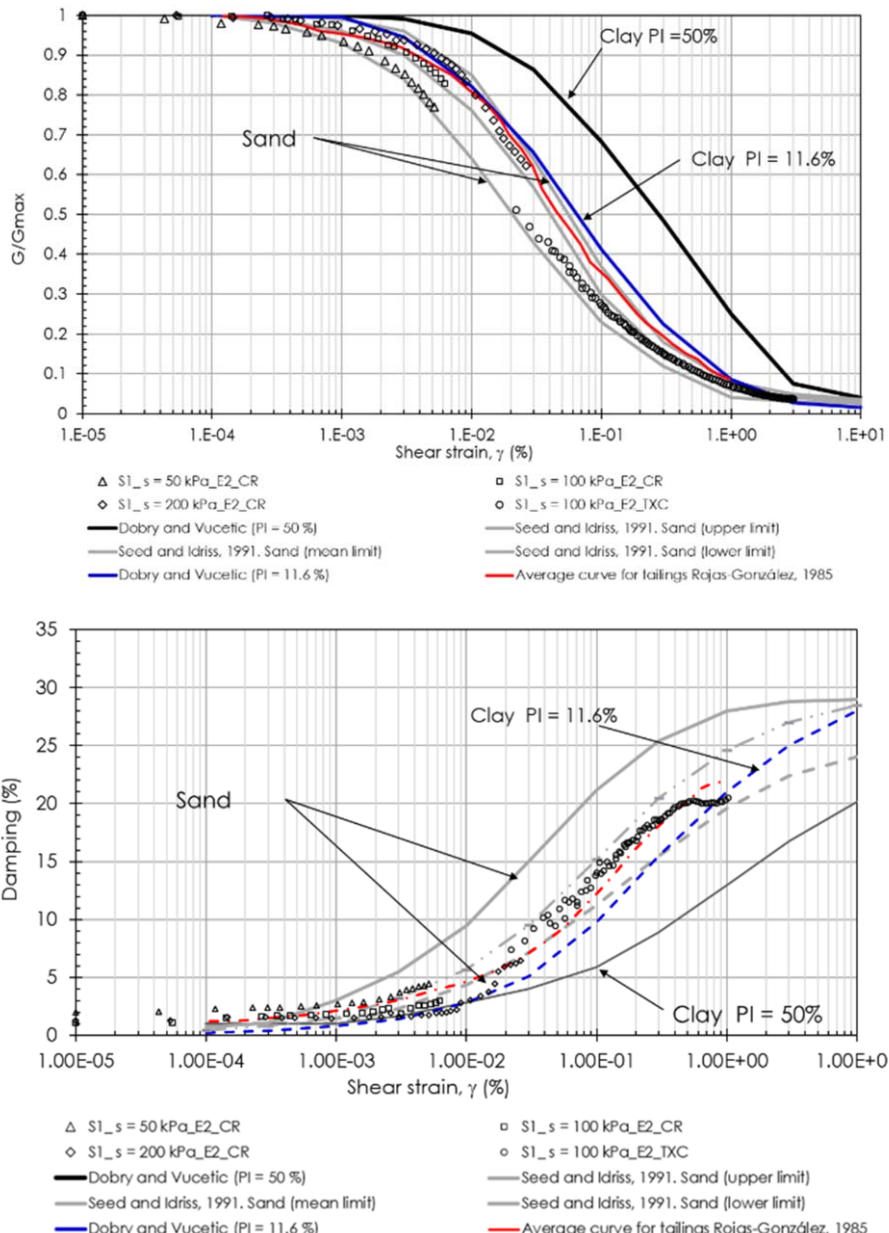


Figure 11. Curves of degradation of the shear modulus G/G_{\max} and damping curves versus shear strain amplitude under different effective confining pressure in tailings.

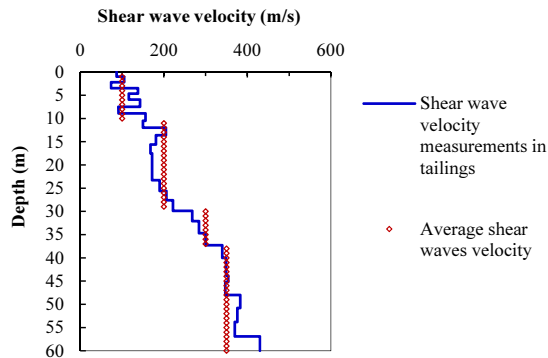


Figure 12. Shear wave velocities (V_s) profile in tailings.

5. Liquefaction

The evaluation of the tailings liquefaction consisted as a first stage in the estimation of liquefaction susceptibility and assessment of the likelihood of “triggering” or initiation of soil liquefaction, while the second stage consisted in the evaluation of flow liquefaction.

5.1. Liquefaction susceptibility assessment

Figures 13(a) and (b) show the liquefaction susceptibility assessment for four samples of tailings using the Bray *et al.* [15] and Andrews and Martin [14] criteria, the properties for this evaluation are presented in Table 1.

According to the criterion of Bray *et al.* [15], samples 2 and 4 are within the Zone A (susceptible to liquefaction), while samples 1 and 3 fall within the Zone B (water content and liquid limit ratios greater than 0.8), see Figure 13(a), so they will be materials with a moderate susceptibility or susceptible to cyclic mobility.

Figure 13(b) shows the susceptibility assessment using the Andrews and Martin criteria; the results indicate the same behavior as that defined with the criteria proposed by Bray *et al.* [15]. The results of both criteria are in the limit between susceptible to liquefaction and the zone of uncertainty; therefore, this type of material is found in the transition of clay and sandy behavior.

According to these results, it was decided to evaluate the capacity of the tailings to generate excess pore pressure from the results of the cyclic triaxial tests.

Figure 14(a) presents the results of dynamic laboratory tests in terms of excess pore pressure ratio (r_u) versus the number of cycles for confining stresses of 50 kPa, 100 kPa and 200 kPa, and maximum stress ratios of 0.25, 0.3 and 0.4, respectively.

The results of these tests indicate that tailings material reaches excess pore pressure ratios less than unit 1.0. This means that total liquefaction or “initial liquefaction” does not occur. However, the material may experience significant strength loss and shear deformations under these values of r_u . It may be noted that the results presented are associated at the last stage of cyclic triaxial tests. Likewise, Figure 14(b) shows the history of excess pore water pressure ratio and axial stress-strain hysteresis loops for cyclic triaxial test.

Table 1. Geotechnical properties of tailings.

Sample	w (%)	S (%)	F (%)	LL (%)	LP (%)	PI	Gs	USCS	Hydrometer test		
									Fine sand (%)	Silt (%)	Clay (%)
1	49.7	3.5	96.5	29	16.1	13	3.58	CL	3.5	91.2	5.3
2	44.0	5.3	94.7	25	13	12	3.58	CL	5.3	89.0	5.7
3	48.9	3.5	96.5	29	16	13	3.58	CL	3.5	88.1	8.4
4	40.5	5.5	94.5	25	14	11	3.56	CL	5.5	88.2	6.3

Water content, w. Percentage of sand, S. Percentage of fines, F. Liquid limit, LL. Plastic limit, LP. Plasticity Index, PI. Specific gravity, Gs.

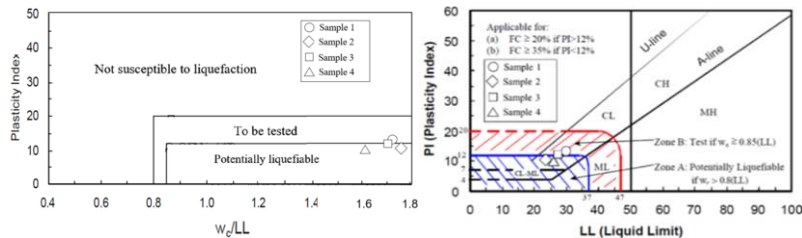


Figure 13. Assessment of the liquefaction susceptibility of the four samples of tailings: (a) Andrews and Martin criteria [14] and (b) Bray *et al.* criteria [15].

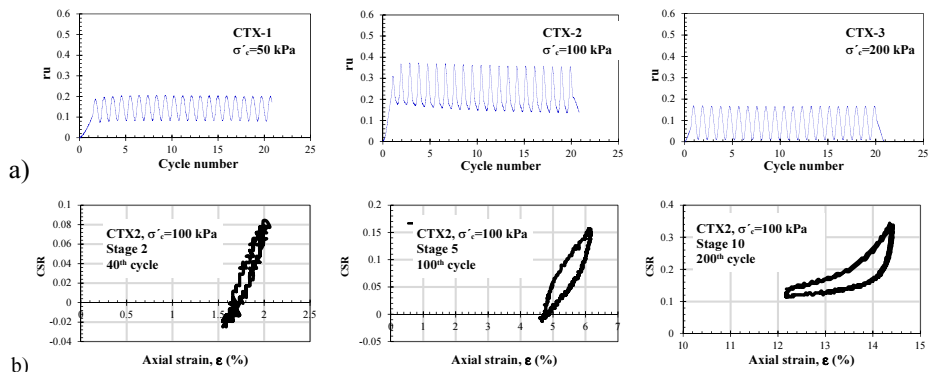


Figure 14. (a) Excess pore pressure ratio versus the number of loading cycles (10th stage) and (b) time histories of axial stress-strain hysteresis loops for different stages and cycle number from cyclic triaxial test CTX-2.

5.2. Flow liquefaction

The flow liquefaction is characteristic of steeply sloping ground, which applies to tailings structures. For the case study, and as part of the flow liquefaction evaluation process, the susceptibility for strength loss and soil behavior was evaluated using the cone penetration tests (CPT) data from a tailing deposit with similar characteristics. Figure 15 shows the results of a CPT test in tailings, which presents a predominant classification between silt mixtures – clayey silt to silty clay and sand mixtures – silty sand to sandy silt (Figure 15b).

The behavior of the soil was determined from the estimation of the concept of “clean sand equivalent” ($Q_{in,cs}$). Robertson and Wride [18] defined the value of $Q_{in,cs} = 70$ as borderline between contractive and dilative behavior, which is associated with the state parameter (ψ) of Jefferies and Been [36]. CPT results show a contractive behavior in the

superficial part from zero to five meters, as well as intercalations between the contractive and dilative behavior (Figure 15c).

Likewise, sensitivity was evaluated in these materials using CPT data. Tailings materials with a contractive response presented a medium to high sensitivity (Figure 15d). Furthermore, tailings are located within the “FC zone” of the potential liquefaction chart, which indicates a possible strength loss (Flow-liquefaction) and cyclic softening [23] (Figure 16).

According to the characteristics evaluated with CPT in tailings, the soil can strain soften in undrained shear; therefore, the post-earthquake stability and residual shear strengths will be the most relevant issue to estimate the seismic stability of the tailings dam.

The following sections present the dynamic analysis that considers the development of dynamic pore water pressure and the estimation of post-earthquake deformations.

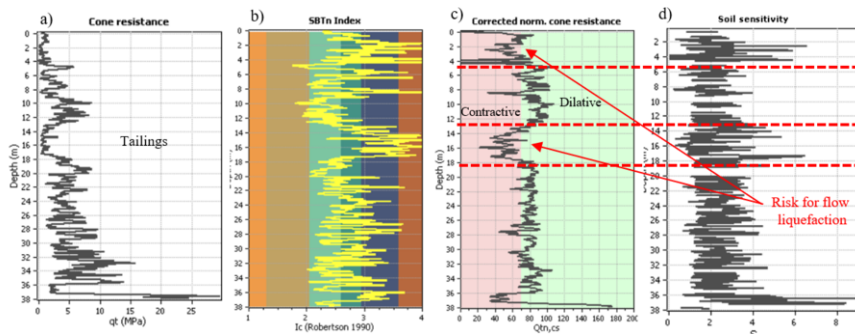


Figure 15. Cone penetration test results in tailing slimes.

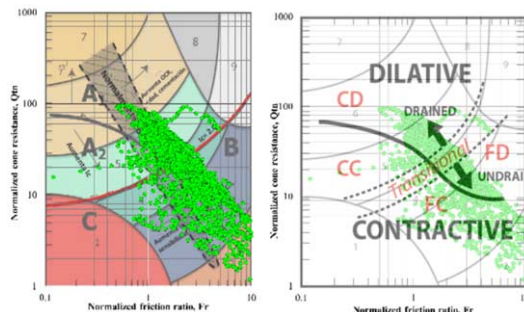


Figure 16. Evaluation of soil response in the CPT soil behavior chart.

6. Dynamic Analysis (Excess pore-pressure from CSR)

6.1. Stages of numerical modelling

The dynamic response and seismic stability of the tailings dam was computed by dynamic two-dimensional finite element analysis. The dynamic analysis considered the following stages: 1) Determination of groundwater level through the dam by transient water flow analysis, 2) Static equilibrium calculation in order to define the initial in-situ

stresses, 3) Dynamic analysis (earthquake generation of excess pore pressures in dam) and 4) Post-earthquake deformations analysis.

The numerical simulation was performed for long-term condition, in which the project has reached the maximum operation level. The parameters used for the different analysis are presented in Table 2.

Table 2. Materials properties used in the analysis.

Material	γ kN/m ³	c kPa	ϕ (°)	k m/s	v	E MPa	S_{ulq}/σ_v kPa	V _s m/s	G _{max} kPa
Tailings (Depth. 0 - 5 m)	f(z) ¹	2	30	f(z) ¹	0.33	5	0.06	100	16310
Tailings (Depth. 5- 15 m)	f(z) ¹	2	30	f(z) ¹	0.33	10	0.1	200	65240
Tailings (Depth. 15 - 30 m)	f(z) ¹	2	30	f(z) ¹	0.33	18	0.15	300	146789
Tailings (Depth. 30 - 60 m)	f(z) ¹	2	30	f(z) ¹	0.33	18	0.15	400	260958
Upstream dykes	16.4	21	23	1.00E-08	0.3	26.76	-	250	104485
Rock fill embankment	21	5	42	1.00E-06	0.28	f(σ'_e) ²	-	400	342508
Foundation (clayey sands with gravel and altered rock)	22	-	-	1.00E-07	0.3	2000	-	450	330275
Foundation (rock)	24	-	-	5.90E-08	0.25	4000	-	>620	1198777

¹ Parameters obtained from functions (Figure 10).

² Parameter obtained from function [34].

6.2. Water flow analysis

A transient water flow analysis was performed using saturated and unsaturated hydraulic properties. A total head was applied as hydraulic boundary condition at the maximum level of tailings deposit (Elevation = 1150 m.a.s.l.). The length of the beach was 60 meters (Figure 17), whose objective is to avoid the saturation of tailings close to the retention structure, this condition is essential for the seismic behavior of the structure, since it mitigates the risk of liquefaction in the tailing slimes for support. The predicted phreatic line or seepage line with numerical model is shown in Figure 17.

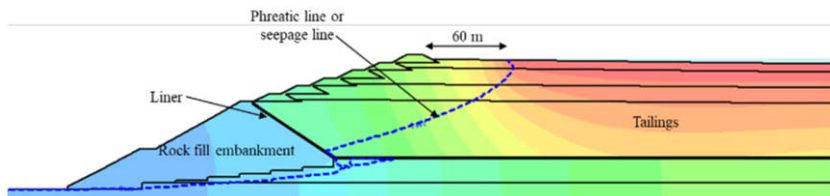


Figure 17. Seepage through the dam.

6.3. Dynamic analysis

Seismic response of the model was obtained from a 2D linear equivalent analysis using the QUAKE/W finite element program [37]. Hence, shear modulus and damping ratio curves determined in section 4.2 were used for this analysis (Figure 12). The numerical model consisted of 12191 quadrilateral elements. The boundary conditions in the model consisted in the restriction of the vertical and horizontal displacement in the base of the

model "rigid base"; while the vertical displacement for the lateral boundaries were restricted.

Since the input motion must be applied at the base of the model, a deconvolution analysis was performed through a one-dimensional site response with the code SHAKE-91 [38]. The element size was defined considering that the spatial element size (Δx), must be smaller than approximately one-tenth of the wavelength associated with the highest frequency component of the input wave [39].

$$\Delta x < \frac{\lambda}{10} \quad (1)$$

The numerical model mesh was calibrated by comparing its response against the one-dimensional site response analysis (SRA-1D). Figure 18 shows the surface acceleration records computed with site response analysis (SRA-1D) and the finite element model (FEM-2D).

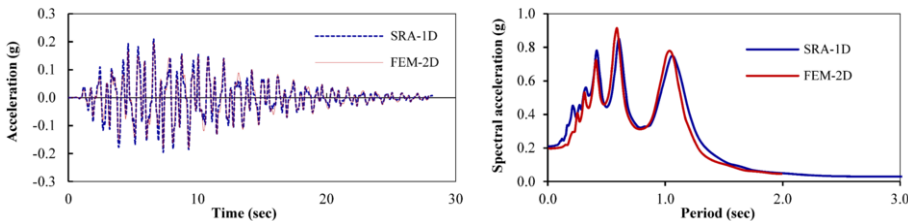


Figure 18. Comparison of acceleration record and response spectrum for SRA-1D and FEM-2D.

The liquefaction simulation was carried out using a pore pressure generation model based on the cyclic stress approach. Under this approach, the pore pressure is computed from the cyclic stresses (CSR) developed during the earthquake shaking and through the pore pressure ratio function (r_u). Therefore, it is necessary to determine the specific cyclic resistance curve and pore pressure function of materials.

The pore-pressure generated during earthquake shaking are a function of the equivalent number of uniform cycles, N , for a particular earthquake and the number of cycles, N_L , which will cause liquefaction for a particular soil under a specific set of stress conditions [37]. Liquefaction will occur once $r_u=1$ has been reached; that is, when excess pore pressure (Δu) is equal to the confining effective stress (σ_{e3}).

Lee and Albaisa [40] and DeAlba *et al.* [41] found that the pore pressure ratio, r_u , is related to the number of loading cycles by:

$$r_u = \frac{1}{2} + \frac{1}{\pi} \sin^{-1} \left[2 \left(\frac{N}{N_L} \right)^{\frac{1}{\alpha}} - 1 \right] \quad (2)$$

This function is dependent on soil properties and test conditions, in the case of tailings; its behavior is governed by grain size and mineralogical composition. The particularities of this function are important, because the amount of pore pressure determined in the simulation will have a consequence in the strength loss and post-earthquake deformations. Figure 19 presents the pore water pressure function for the numerical analysis, which are representative for fine tailings [42]; additionally, it shows the range of pore pressure behavior of tailing slimes determined by Moriwaki *et al.* [11].

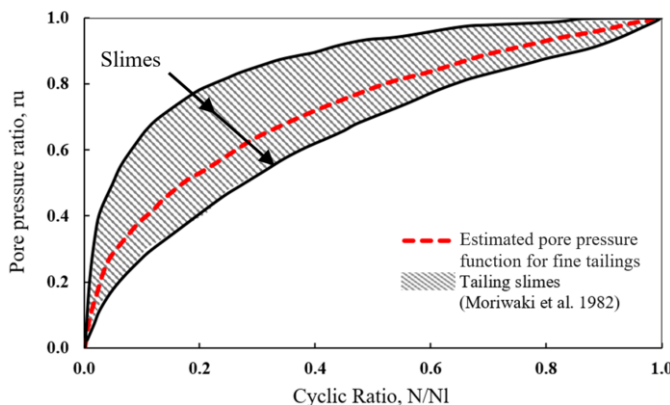


Figure 19. Pore pressure function for fine tailings.

6.4. Post-earthquake deformation analysis

One of the principal issues in the seismic stability assessment in tailings dam is to evaluate the service state of the structure during and after an earthquake. According to the international guidelines, the principal objective is that the permanent deformations generated by the earthquake are not such as to cause the loss of freeboard, that these are not greater than the total height of the structure or that are not enough to cause the failure.

Post-earthquake effects are commonly due to liquefaction phenomenon, presenting large deformations owing to softening or strength loss of soil.

The effect of delayed behavior has been associated with the fact that the soils are brought to the collapse surface by redistribution of stresses or excess pore-water pressures rather than directly by the earthquake shaking [43].

Figure 20 shows the effective stress path that illustrates the delayed behavior caused by the redistribution of stresses. As shown in this figure, during an earthquake shaking the pore pressure increases so that there will be a decrease in the effective stress, which mobilizes the ultimate shear strength or “steady state strength”. If the soil is very loose and the driving static shear stress is large enough, the soil grain structure can collapse to the steady-state and strain softening behavior occurs. This strain softening causes stress redistribution within the soil mass [43].

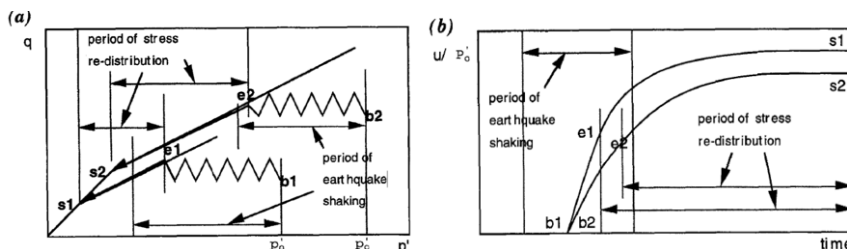


Figure 20. Delayed behavior caused by stress redistribution [43].

The Post-earthquake deformations analysis was performed using the SIGMA/W program, which uses an elastic-plastic constitutive model coupled to stress-redistribution model. Collapse surface angle and ultimate shear strength were used in the model in

order to simulate the soil behavior during the collapse. The undrained shear strength $s_{u(lq)}$ were determined using CPT's data.

7. Results of the analysis

The dynamic response of the tailings dam is presented in terms of accelerations, cyclic stresses, excess pore pressure and deformations. For this purpose, monitoring points were used in the model, which allow monitoring the results during dynamic time.

Additionally, the results are presented in the model as a shaded plot at the end of the earthquake shaking, in order to review the overall behavior of the structure.

7.1. Dynamic response

Figure 21 shows the estimated acceleration time histories at the surface of the saturated tailings and in points located at different depths. It may be seen that maximum acceleration at the surface is of the order of 0.18g. Furthermore, Figure 21 shows that there is a slight amplification of the input movement through the tailings dam; this effect may be due to the development of low excess pore pressure, since the site response is generally de-amplified when liquefaction occurs.

For the monitoring points located at the crest of the starter dam and upstream dikes, the predicted maximum accelerations were of the order of 0.28, 0.23 and 0.24g for points A, B and C, respectively (Figure 22).

The maximum acceleration at the base of the dam (Point H) was of the order of 0.16g, the comparison between this acceleration and that obtained in the crest indicates that there is an amplification level of 1.75. The natural period of the structure was of the order of 0.5 seconds, which was determined from the evaluation of the spectral ratio between seismic response at crest and base level. This period resulted independent of the seismic solicitation.

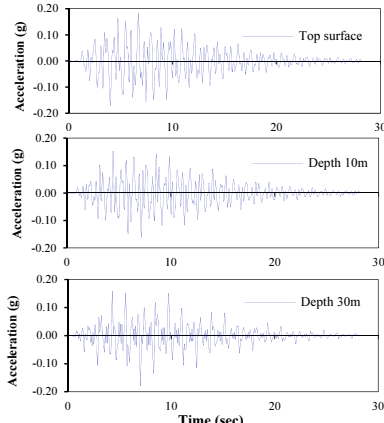


Figure 21. Acceleration time history at different depths in tailings.

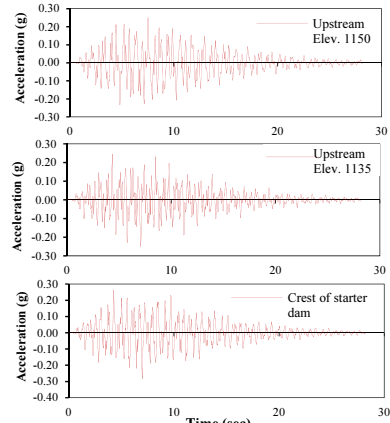


Figure 22. Acceleration time history at the crest of the starter dam and upstream dikes.

7.2. Liquefaction and cyclic stress ratio

Predicted excess pore pressures at the end of the earthquake are presented in Figure 23. It may be seen that tailings deposited superficially at 10 m of depth present low r_u values, between 0.15 to 0.35. However, there is a small zone at 5 m of depth that reach high excess pore pressures ($r_u = 0.7$). According to these results, in terms of excess pore pressure ratio, the initial liquefaction is not achieved. However, the pore pressure generated during the dynamic analysis can lead to some elements reach the collapse surface and then liquefied.

The cyclic shear stress (CSR) contours computed in the model are presented in Figure 24. It may be observed that in most of the saturated tailings show CSR values in the range of 0.1 to 0.25. Furthermore, high values of cyclic shear stress (CSR = 0.5) are observed in a small zone near the surface.

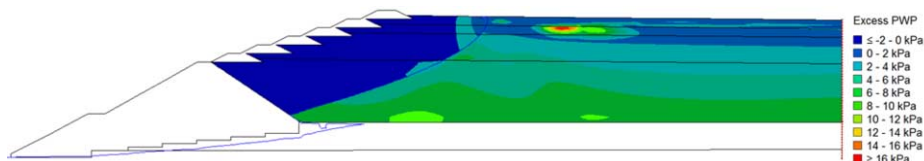


Figure 23. Excess pore pressures at the end of the earthquake.

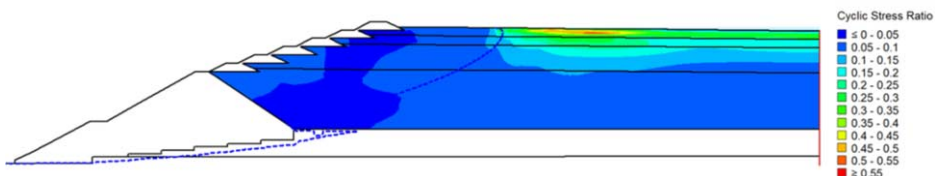


Figure 24. Cyclic stress ratio (CSR) contours computed in the numerical model.

7.3. Post-earthquake deformations

As seen in the previous sections, the post-earthquake deformation condition becomes the principal issue to evaluate in the seismic stability of the tailings dam.

The post-earthquake deformations of the dam are illustrated in Figure 25 in terms of displacement vectors and shading contours; in addition, the maximum values of permanent horizontal and vertical displacements for four monitoring points are presented. The monitoring points are located at the crest of the starter dam (Point A), the crest of the upstream dikes to the elevation of 1135 m.a.s.l (Point B), the crest of maximum elevation of upstream dikes (Elev. = 1150 m.a.s.l) (Point C) and tailings surface (Point D).

According to these results, the predicted deformation at the crest of starter dam (Point A) is less than 3% of the height of the structure, so they are considered admissible.

For point B, the predicted horizontal and vertical displacements were about of 6 and 1.5 cm, respectively. In point C, the maximum settlement computed was approximately of 6 cm and lateral displacements about of 4 cm. The predicted deformations were less than 3% of the height of the structure; in addition, the estimated vertical displacements represent a loss of free board of 2%, which is acceptable. Likewise, the vertical displacements on the crest of dikes must not be greater than 50% of the free board.

According to these results, the deformations determined in the retention structure are not significant for its global or local stability.

For point D located on the tailings surface, the permanent deformations at the end of the earthquake were of the order of 13 cm (horizontal) and 29 cm (vertical). The deformations were estimated to 60 m of distance from the dam.

The estimated results with the numerical model indicate that the maximum deformations computed are associated with tailings stored in the reservoir, also the permanent displacements induced by the earthquake are admissible for the tailings dam, considering as a threshold value of 3% of the height of the structure at different elevations.

The structure will present post-earthquake displacements, which are not enough to cause its failure or instability. Figure 25 shows that the saturated material will present considerable displacements, predominantly settlements. However, these are not of interest for the global stability of the tailings dam.

The tailings that develop high pore pressure produce significant deformations, which cause the tailings move towards the retention upstream dikes. Figure 25(b) shows that the mechanism of failure starts at the border of the beach. This indicates that despite not achieving the liquefaction during the earthquake, important deformations may occur.

Furthermore, the dynamic analysis was carried out considering the saturation in the beach zone, which resulted in important deformations that compromise the stability of the dam. Therefore, the length of the beach and the appropriate design of pumping and drainage system of the dam play an important role in the seismic behavior of the structure, in which it is pursued that the permanent deformations do not affect the serviceability of the tailing dam.

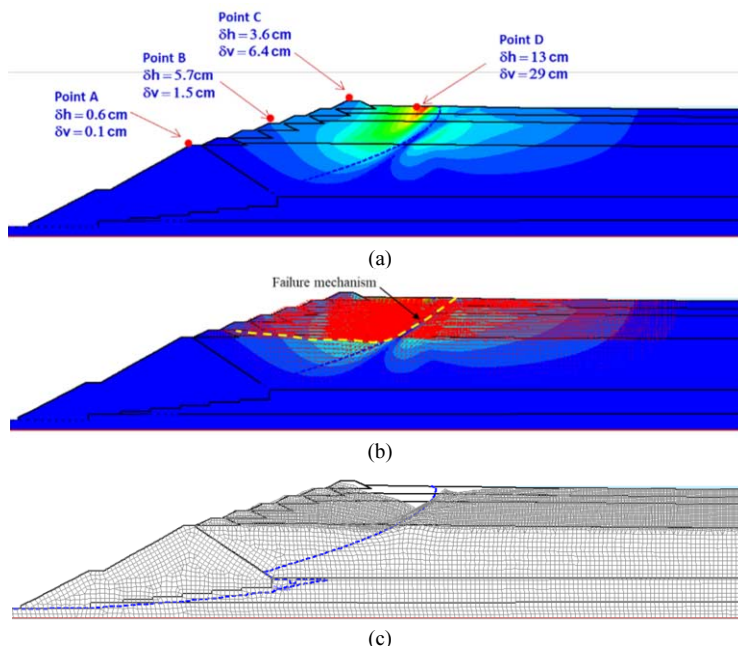


Figure 25. a) Post-earthquake deformations contours, b) Post-earthquake deformations in terms of displacement vectors b) and c) Distorted mesh of the model (50 times magnified).

8. Conclusion

The analysis and design of tailings dam signified an important challenge due to the seismic conditions of the site and project requirements, as well as compliance with local regulations. The case study allowed assessing the analysis stages that must be carried out for a tailings dam by upstream-downstream method, as well as knowing the behavior and particular properties of tailing slimes.

The following conclusions are based on the studies and analysis developed in the case study.

The project under study considered two construction alternatives, which are within the local regulatory framework for the conditions of the zone. The alternative presented in this paper involves the design of a tailings dam by the upstream-downstream method with rock fill embankment. The design of this alternative does not represent the conventional design of the upstream method; since it has a rock fill embankment (starter dam) that represents the main retaining structure of the dam; in addition, the upstream dykes are made up by borrow material.

The simulation of tailings deposition process through consolidation tests, allowed representing approximately the in situ conditions of tailings and defining the properties for the static and dynamic laboratory tests. Likewise, the use of geotechnical field tests in an active tailings deposit (young deposits) of similar characteristics allowed to determine the parameters that are sensitive to deposition conditions. This was focused on determining the shear wave velocities and behavior of tailing slimes.

The dynamic behavior of tailing slimes in terms of degradation shear modulus and damping ratio tends to the sand behavior. Tailing slimes at low confining pressure tend to the lower limit of the sands; while at higher confining pressure, their dynamic behavior approaches the upper limit of the sands.

The results of susceptibility analysis from Bray *et al.* [15] and Andrews and Martin [14] criteria indicate that tailing slimes are susceptibility to liquefaction.

The pore pressure measurements by cyclic loading show that the tailing slimes has a low pore pressure generation capacity, as well as a high cyclic resistance. These results agree with the studies that have been published by several researchers [7] [11] about the dynamic behavior of fine tailings.

According to the characteristics evaluated by CPTu, tailing slimes are in the transition between clay-like and sand-like behavior; also, these materials present a contractive response and they are susceptible to strength loss (Flow-liquefaction) and cyclic softening.

Tailing slimes can strain soften in undrained shear; therefore, the post-earthquake stability and residual shear strengths will be the most relevant issue to consider in the seismic behavior of the tailings dam.

The stability and dynamic behavior of the tailings dam in study were acceptable; also, the post-earthquake deformations do not affect the service state of the structure. For this construction method, the length of the beach and drainage system were determinant for the good seismic behavior of the structure.

However, the approach of this construction method entails inherent risks that require a rigorous monitoring of the designer and the appropriate supervision during construction and operation.

The following is a summary of comments and recommendations for the analysis and design of this kind of structures.

- The dynamic properties of soils are usually represented by curves of degradation of the shear modulus and damping ratio as a function of the shear strain, and in the particular case of tailings, these cannot be assumed depending on the type of soil, as is generally done in practice, that in many cases, predictive curves are used for sands and clays available in the literature but that do not correspond to the materials with which the tailings are constituted. Therefore, it is important to have an adequate dynamic characterization in order to obtain the specific tailings properties.
- Tailings that present an important participation in the global stability of the structure (such is the case of conventional tailings dams) are susceptible to flow liquefaction, which can be triggered by either static or cyclic loading, therefore it is important to evaluate this phenomenon. For flow liquefaction is necessary to evaluate the soil behavior, susceptibility for strength loss, stability using post-earthquake shear strengths, trigger for strength loss and deformations.
- An important aspect to consider in the dynamic analysis is to evaluate the generation of excess pore pressures during earthquake shaking, which in turn can lead to some permanent deformations that affects the behavior and seismic stability of the dam.
- The liquefaction assessment should consider the susceptibility to liquefaction analysis through their index properties. It is recommended that the liquefaction potential in tailings should be evaluated in terms of excess pore pressure.
- The upstream-downstream method with rockfill embankment may be an adequate solution in areas of high seismicity; however, it requires an appropriate supervision during its construction and operation stage.

Acknowledgments

The author would like to acknowledge the support of the Soil Mechanics Department of the Federal Electricity Commission (CFE) for allowing him to work on this project. Likewise, the author wishes to express his gratitude to the Engineers Juan de Dios Alemán, César Dumas and Oscar Luna for their contributions and valuable comments in this article.

References

- [1] Castro, G., and Troncoso, J. 1989. Effects of 1985 Chilean earthquake on three tailing dams. In Proceedings of the Fifth Chilean Conference on Seismology and Earthquake Engineering, Santiago, Chile.
- [2] ANCOLD 2012a, Guidelines on Tailings Dams-Planning, Design, Construction, Operation and Closure, Australian. National Committee on Large Dams Incorporated, May 2012.
- [3] ICOLD, Bulletin 139, 2011. Improving tailings dam safety-Critical aspects of management, design, operation and closure.
- [4] Canadian Dam Association, 2014. Application of Dam Safety Guidelines to Mining Dams. technical bulletin, ISBN 978-0-9936319-2-4A.N.
- [5] Finn, 1982. Fundamental aspects of response of tailings dams to earthquakes. Dynamic stability of tailings dams. ASCE National conventions. New Orleans, USA.
- [6] Byrne, P. M and Seid-Karbasi, 2003. Seismic Stability of Impoundments. 17th Annual Symposium, VGS.
- [7] Ishihara, K. 1984. Post-earthquake failure of a tailings dam due to liquefaction of the pond deposit. In Proc., Inter. Conf. on Case Histories in Geotechnical Engineering.

- [8] NOM -141-SEMARNAT-2003. Norma oficial Mexicana que establece el procedimiento para caracterizar los jales, así como las especificaciones y criterios para la caracterización y preparación del sitio, proyecto, construcción, operación y postoperación de presas de jales. en Diario Oficial de la Federación, 2004.
- [9] Troncoso, J. 1995. Design and Behavior of Tailings Dams Under Seismic Conditions. International Conferences on Recent Advances in Geotechnical Earthquake Engineering and Soil Dynamics.
- [10] Phukunaphan, C.F. Tsai and G.R. Thiers, 1982. Dynamic behavior of tailings materials. Dynamic stability of tailings dams. ASCE National conventions. New Orleans, USA.
- [11] Y. Moriwaki, M.R. Akky, R. Ebeling, I.M. Idriss and R.S. Ladd, 1982. Cyclic strength and properties of tailing slimes. Dynamic behavior of tailings materials. Dynamic stability of tailings dams. ASCE National conventions. New Orleans, USA.A.N.
- [12] Verdugo, R. 2009. Seismic performance based-design of large earth and tailing dams, Performance-Based Design in Earthquake Geotechnical Engineering, ICPBD Conference, Tsukuba, Japan: 41-60.
- [13] L. Hu, H. Wu, L. Zhang, P. Zhang and Q. Wen, 2017. Geotechnical Properties of Mine Tailings. Journal of Materials in Civil Engineering, ASCE, ISSN 0899-1561.
- [14] Andrews, D. C. A. and Martin, G. R. (2000). Criteria for liquefaction of silty soils. Proc., 12th World Conf. on Earthquake Engineering, Auckland, New Zealand.
- [15] Bray, J. D., Sancio, R. B., Riemer, M. F., and Durgunoglu, T. (2004). Liquefaction susceptibility of fine-grained soils. Proc., 11th Int. Conf. on Soil Dynamics and Earthquake Engineering and 3rd Int. Conf. on Earthquake Geotechnical Engineering, Stallion Press, Singapore.
- [16] Seed, H. B. and Idriss, I.M. (1971). Simplified procedure for evaluating soil liquefaction potential. Journal of the Soil Mechanics and Foundation Division, ASCE, 1971; 97(9): 1249-1273.
- [17] Kramer S. L., (1996). Geotechnical earthquake engineering. Prentice-Hall, Inc., Upper Saddle River, New Jersey.
- [18] Robertson, P.K. and Wride, C. (1998) Evaluating Cyclic Liquefaction Potential Using the Cone Penetration Test. Canadian Geotechnical Journal, 35, 442-459.
- [19] Casagrande, A. 1975. Liquefaction and Cyclic Deformation of Sands-A Critical Review. *V Panamerican Conference on Soil Mech. & Foundation Eng.* Buenos Aires, Argentina.
- [20] Castro, G. (1969). Liquefaction of Sands, PhD Thesis, Harvard University, Cambridge, MA, January.
- [21] Castro, G. and Poulos, S.J. (1977) Factors Affecting Liquefaction and Cyclic Mobility. Journal of Geotechnical Engineering, ASCE, 103, 501-516.
- [22] Rauch, 1997. EPOLLS: An Empirical Method for Predicting Surface Displacements Due to Liquefaction-Induced Lateral Spreading in Earthquakes. Doctoral Dissertations. Virginia Tech.
- [23] Robertson, P.K., 2010c. Evaluation of Flow Liquefaction and Liquefied strength Using the Cone Penetration Test. Journal of Geotechnical and Environmental Engineering, ASCE, 136(6): 842-853
- [24] Turi, David; Puszta, Jozsef; and Nyari, Istvan, 2013. Causes and Circumstances of Red Mud Reservoir Dam Failure In 2010 at MAL Zrt Factory Site in Ajka, Hungary. International Conference on Case Histories in Geotechnical Engineering. 10.
- [25] M. Davis and T. Martin, 2002. Static liquefaction of tailings-Fundamentals and case histories.
- [26] Newmark, N.M., 1965. Effects of earthquakes on dams and embankments. Geotechnique 15, 139-159.
- [27] Yegian M.K., Marcialiano E.A., Ghahraman V.G. (1991) – Earthquake-induced permanent deformations: probabilistic approach. ASCE, Journal of Geotechnical Engineering, vol. CXVII, n. 1, pp. 35- 50.
- [28] Makdisi, F.I., Seed, H.B., 1978. Simplified procedure for estimating dam and embankment earthquake-induced deformations. ASCE Journal of the Geotechnical Engineering Division 104, 849-867.
- [29] Martin G.R., Finn W.D., Liam y Seed H.B. (1975). —Fundamentals of liquefaction under cyclic loading|. Journal of the Geotechnical Engineering Division, ASCE, May 1975, Vol. 101, No GT5.
- [30] Byrne P.M. (1991). A Cyclic Shear-Volume Coupling and Pore-Pressure Model for Sand in Proceedings: Second International Conference on Recent Advances in Geotechnical Earthquake Engineering and Soil Dynamics, St. Louis, Paper No. 1.24, 47-55.
- [31] Boulanger, R. W., and Zioutopoulou, K. (2017). "PM4Sand (Version 3.1): A sand plasticity model for earthquake engineering applications." Report No. UCD/CGM-17/01, Center for Geotechnical Modeling, Department of Civil and Environmental Engineering, University of California, Davis, CA, 113 pp.
- [32] Hoek E. Brown E. T. (1968). The Hoek-Brown criterion", 1988, update, Rock Engineering for underground Excavations, Proc 15th Canadian Rock Mech. Symp. Dept. Civil Engineering, University of Toronto.
- [33] CIGB ICOLD (2010). Concrete Face Rockfill Dams: Concepts for Design and Construction. Bulletin 141.
- [34] Alemán, J.D., 2003. Diseño geotécnico de presas de gran altura de enrocamientos con cara de concreto. Academia de Ingeniería de México.
- [35] Vucetic, M. and Dobry, R. (1991) Effect of Soil Plasticity on Cyclic Response. Journal of Geotechnical Engineering, 117, 89-107.

- [36] Jefferies, M.G. and Been, K., 2006. Soil Liquefaction – A critical state approach. Taylor & Francis, ISBN 0-419-16170-8 478 pages.
- [37] Krahn John (2004). “Dynamic modelling with QUAKE/W - An Engineering Methodology”. GEO-SLOPE/W International Ltd., Alberta, Canada.
- [38] Schnabel P.B., Lysmer J.L. and Seed H.B. (1972), “SHAKE: A computer program for earthquake response analysis of horizontally layered sites”. Report No. EERC 72-12, University of California, Berkeley.
- [39] Kuhlemeyer R.L. y Lysmer J. (1973). —Finite Element Method Accuracy for Wave Propagation Problems. J. Soil Mech. & Foundations, Div. ASCE, 99(SM5), 421-427.
- [40] Lee, K.L., and Albaisa, A., 1974, Earthquake Induced Settlements In Saturated Sands, Journal of The Soil Mechanics and Foundations Division, ASCE, Vol.100, No. GT4.
- [41] DeAlba, P., Chan, C.K., and Seed, H.B., 1975, Determination of Soil Liquefaction Characteristics by Large-Scale Laboratory Tests, Report EERC 75-14, Earthquake Engineering Research Center, University of California, Berkeley.
- [42] Zhang, C., Yang, C. H., and Bai, S. W. (2006). “Experimental study on dynamic characteristics of tailings material.” Rock Soil Mech., 27(1), 0035–0040 (in Chinese).
- [43] Gu, W.H., Morgenstern, N.R., and Robertson, P.K. (1994). Post-Earthquake Deformation Analysis of Wildlife Site, ASCE Journal of Geotechnical Engineering, Vol.120, No.2, pp. 333-349

Bright Spark Lecture



Marlísio Oliveira CECÍLIO Junior

Marlísio was born and raised in São Paulo city, Brazil.

After graduating as a Civil Engineer from the Federal University of Santa Catarina - UFSC, he was granted his Master of Sciences degree on Geotechnical Engineering from the Polytechnic School of University of São Paulo - USP.

Since then, he worked for Figueiredo Ferraz, Bureau de Projetos and TÜV Süd, completing ten years of experience on design and consultancy of tunnels, retaining structures, slopes and dams. Currently, he is a PhD candidate at the University of Wollongong, Australia.

He published dozens of technical articles internationally. His awards include the best oral presentation at the 3rd Brazilian Tunnelling Congress, best technical article on the XV Panamerican Conference on Soil Mechanics and Geotechnical Engineering and finalist for the category "Young Tunneller of the Year" on the ITA-Awards.

Marlísio was the first president for the Young Members Group of the Brazilian Tunnelling Committee. He engaged in the organization and scientific committees of international conferences. As a representative member of ISSMGE's TC 204, he helped bringing their international symposium for the first time to the Americas, as the symposium vice-president.

Personal Account on Reliability Analyses, from a Young Geotechnical Engineer

Marlísio Oliveira CECÍLIO Junior^{a,1}

^a TÜV Süd - Bureau de Projetos e Consultoria Ltda., Brazil.

Abstract. The use of deterministic stability analyses for geotechnical works is still common practice. Such analyses consider a single set of input parameters and therefore a single result is taken as definitive and compared to limits established by codes. However, a deterministic stability assessment taken as satisfactory may be associated with a probability of failure considered as high. This is why one approach should not suppress the other, they should rather be complementary. A similar comment can be made for the probability of failure, while a small value may not be accepted within a densely occupied urban scenario and a high value may be considered satisfactory within an uninhabited area. This is why the risk should also be evaluated rather than solely the probability of failure. Discussions concerning the risk of failure instead of mere deterministic approaches have significant importance, bearing in mind either insurance needs or the development of projects that are both more reliable and cost-effective.

Keywords. Tunnels, Dams, Uncertainty, Probability, Risk, Bayes theorem.

1. Introduction

The present paper is a brief account on the early stages of the author's professional career and was solicited after the Pan-American Bright Spark Lecture award had been granted by the Young Member Presidential Group - YMPG from ISSMGE. This award, on its debut, is intended to acknowledge the mature research and/or practice of young geotechnical engineers.

The establishment of groups devoted to the new generation of engineers is of paramount importance. They should have full support from our societies and associations, being comprised of recently graduated professionals and undergrad students, or even teenagers willing to start a graduation course yet not utterly decided about choosing Geotechnical Engineering as a future career.

Such groups are responsible for bridging the gap between different generations and empowering the youngers with voice and space within our geotechnical society.

One should not expect academia to transmit all knowledge to their students, leaving to senior professionals the responsibility of gathering protégés and enriching their minds with past experiences, expertise, and most importantly with guidance. Conversely, senior professionals must always bear an open-mindedness to innovation, usually conveyed by the youngers. This mutual relationship is beneficial for both ends and must always be encouraged.

¹ Corresponding author, Rua Girassol n.1033, Vila Madalena, São Paulo - SP, Brazil - CEP 05433-002; e-mail: marlisiojunior@yahoo.com.br.

Fortunately, the author has been given the satisfaction of receiving a remarkable and excellence tutoring, in many diverse situations and during different extents of time, so that it would not be possible to reproduce a thorough citing. Nonetheless, bearing in mind this paper theme on Reliability Analyses, there are six names that must be praised in recognition to their contributions during the author's first twelve years of experience as a young geotechnical engineer. These outstanding Brazilian friends, inspiring mentors, are presented in Figure 1.

Arsenio Negro is a geotechnical designer and consultant who employed Marlísio with the main purpose of implementing in his company Bureau de Projetos a working group focused on non-deterministic studies. He has been successful at this hard and challenging task of gradually and continuously changing the deterministic culture a long time set in the geotechnical working practice.

Paulo Ivo B. Queiroz, kindly known as P.I. (π), is a Professor at the Aeronautical Technology Institute - ITA, expert on statistical treatment of data who has developed diverse probabilistic studies as a consultant for Bureau de Projetos, including health risk assessments of contaminated grounds. Together with Arsenio and Marlísio, he assessed probabilities of failure for several underground soil excavations.

Nelson Aoki is a Professor at the University of São Paulo - USP, specialized on foundations. He was elected to deliver the Milton Vargas Lecture 2011 titled "Probability of ruin and factor of safety for foundations" [1], as well as the Pacheco Silva Lecture 2016 titled "The factor of safety paradigm" [2], both cross-country lectures promoted by the Brazilian Association on Soil Mechanics and Geotechnical Engineering - ABMS.

Waldemar C. Hachich is a Professor at the University of São Paulo - USP, responsible for elective classes on geotechnical reliability. He is a member of ISSMGE's Technical Committee on Engineering Practice of Risk Assessment and Management (TC-304) and was elected to deliver the Milton Vargas Lecture 2018 titled "Safety, reliability and risks in geotechnical works" [3].

Tarcísio B. Celestino is a Professor at the University of São Paulo - USP, as well as the engineering manager at the company Themag. He permeates brilliantly between academia and practice, having supervised many post-graduate researches on reliability studies for the stability of underground rock excavations.

André P. Assis is a Professor at the University of Brasília - UNB, has supervised post-graduate researches and has given consultancy on reliability studies for assorted types of geotechnical works. He was elected to deliver the Pacheco Silva Lecture 2018 titled "Risk management in geotechnical works: consolidating theory into practice" [4]. Some of his works include probabilistic spatial characterization of rock masses discontinuities and risk assessments of iron ore tailing dams.



Figure 1. Inspiring mentors. From the left: Arsenio Negro, Paulo Ivo B. Queiroz, Nelson Aoki, Waldemar C. Hachich, Tarcísio B. Celestino, André P. Assis.

Evidently, many other world-wide experts could be mentioned for contributing to this paper theme. Some were pioneers on recognizing and stressing the importance of going non-deterministic, for instance, the internationally renowned late Professor Karl Terzaghi and late Brazilian Professors Milton Vargas and Victor de Mello.

Lastly, the following content shall not be taken as intended for teaching reliability methods, stating best procedures or defining state-of-art approaches. Instead, it merely stands as a humble collection of studies on reliability analyses, developed by a young engineer with the aid of brilliant senior tutors.

2. Why Going Non-deterministic?

A deterministic analysis considers a single set of input parameters and therefore yields a single result, which is taken as definitive and compared to limits established by codes or to best practice values. Normally, such parameters are mean or representative values obtained from tests, or even from previous experiences and literature.

Going non-deterministic simply means recognizing that the problem data is actually variable, thus considering at least one parameter as non-constant and analyzing all possible outcomes.

In that sense, a sensitivity analysis is often performed for its simplicity, evaluating how the change in one parameter affects the results. This is normally referred to as analyses with worst/best case scenarios.

However, a more refined analysis may be performed, which considers parameters as random variables represented by a certain probability distribution and having a possible dependency (correlation) amongst each other, the so-called probabilistic analyses.

In the case where the consequences of a certain event are also assessed, risk analyses are enabled. Such consequences are normally monetary-measured, related to the cost of repair/rebuilt, environmental damages, life losses, among others. Herein, the concept of risk is understood as the product of the probability of failure times the cost of its associated damages.

A survey carried out by ISSMGE's Technical Committee on Underground Construction in Soft Soil (TC-204) involved sending a questionnaire to practitioners dealing with the design and construction of urban tunnels in soil [5]. Based on the responses, they found that uncertainty and parameters variability are considered in tunnel projects by probabilistic analyses in only 6% of cases. Deterministic analyses with pessimistic soil parameters and adequate safety factors account for 40% of cases and deterministic analyses with averaged soil parameters and adequate safety factors predominate with 54% of cases.

It is important to point out that such responses are related exclusively to soil tunnels. For that reason, a new survey on risk assessment has been elaborated for a more comprehensive list of geotechnical works. It was created by the ABMS's Brazilian Technical Committee on Risk, a local chapter of the ISSMGE's TC-304. Although this study is unfortunately not published yet, preliminary outcomes indicate the same trend, in which practitioners still favors deterministic analysis.

Reasons for this were addressed by Ralph Peck in 1995, quoted by Whitman [6]: "Practitioners have not readily adopted reliability theory, largely because the traditional methods have been generally successful, and engineers are comfortable with them. In contrast, practitioners in environmental geotechnics require newer, more stringent assessments of reliability that call for a different approach".

Compared with other areas of knowledge, such as structural engineering, mechanics and economics, it is realized that geotechnical engineering lags behind in the use of reliability theories. It should be appraised that, apart from considering geotechnical parameters as random variables, the unpredictability of geological features and the ground spatial variability and heterogeneity should also be considered.

Then... after all, why going non-deterministic?

According to Harr [7], there is an increasing awareness that the inherent properties of geotechnical materials exhibit significant variability and that these uncertainties are not considered when value judgments concerning most likely scenarios are made.

Moreover, it is basically a matter of safety (either for ultimate limit state - ULS or serviceability limit state - SLS). A deterministic stability assessment taken as satisfactory may be associated with a probability of failure considered as high. This is the reason why one approach should not suppress the other, they should rather be complementary.

In order to ease the understanding of such a statement, different design approaches used for assessing safety should be explained:

- The Working Stress Design (WSD) approach, which is based on an overall factor of safety and has been consecrated since the beginning of geotechnical sciences.
- The Load and Resistance Factor Design (LFRD) approach, adopted mainly in North America, or the characteristic values and partial safety factor approach, widely used in Europe, which are the basis for modern design codes.
- The Reliability-based Design (RBD) approach, which considers as target a probability of failure or a reliability index.

With that in mind, Figure 2 illustrates how the use of non-deterministic analyses relates to a more proper assessment of safety. As an example, while a deterministic global factor of safety calculated by the WSD approach as $FS = 1.50$ is considered safe by different design codes, a probability of failure determined as $P_f = 10^{-2}$ may be considered inadmissible. Conversely, a deterministic $FS = 1.25$ normally not accepted by design codes may be related to a $P_f = 10^{-5}$, which might be considered as acceptable.

Therefore, it is **wrong** to make any statement towards the safety of geotechnical structures solely based on deterministic analyses (more commonly through the Global Factor of Safety). Due to the existence of uncertainties, it is not possible to assure absolute zero probability of failure, in practical and economic terms. Hence the need for evaluating safety by means of non-deterministic analyses.

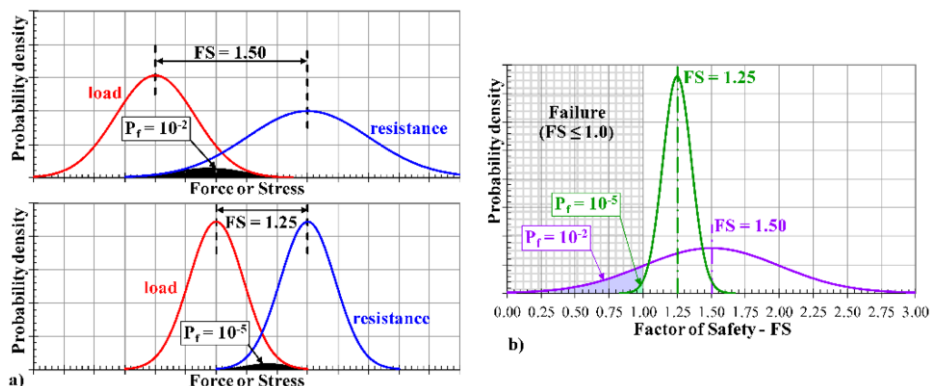


Figure 2. Non-deterministic assessment of safety, using a) LFRD approach and b) RBD approach.

Furthermore, a similar comment on “*relativeness*” can be made for the probability of failure. While a small value may not be accepted within a densely occupied urban scenario, a high value may be considered satisfactory within an uninhabited area. Therefore, the risk should also be evaluated, adding to the picture the failure consequences rather than solely the probability of failure. This may be better explained through Figure 3a, which presents a reduction of the risk by reducing the chances of failure (A), by minimizing the consequences (B), or by ideally both (C).

The monetary values in Figure 3a were deliberately not presented since the criteria for classifying the risk level is not yet common sense worldwide. Moreover, imposing a value to human life remains a very controversial topic [8].

Discussions concerning the risk of failure instead of mere deterministic approaches have significant importance, bearing in mind either insurance needs or the development of projects that are both more reliable and cost-effective.

The ideal risk-based project (design, construction, operation, etc.) should not try to eliminate risks since there is no such thing as an absolute zero probability of failure. Instead, the project should aim to minimize the expected cost (E), which is the mathematical expectation: the non-failure probability times the initial costs, plus the failure probability times the initial and the damages costs.

$$E = (1 - P_f) \cdot C_{ini} + P_f \cdot (C_{ini} + C_{dam}) = C_{ini} + P_f \cdot C_{dam} = C_{ini} + \text{Risk} \quad (1)$$

By minimizing the expected cost, an optimum condition should be found in which the project presents adequate safety without spending unnecessary costs. As an example, a soil tunnel excavated without any ground conditioning presents a lower initial cost, yet the associated risk may be high thus increasing the expected cost; whereas the excessive execution of ground conditioning reduces the risk, however, increases excessively the initial cost and thus the expected cost may remain high.

As depicted by the hypothetical example from Figure 3b, an increase in safety may reduce the project risk, however, followed by an increase in the initial costs (quantity and redundancy of equipment, change in the construction methodology, preventive measures towards consequences, among others). Such relation normally presents a minimum expected cost, which is the objective for a project optimization. Nevertheless, the respective risk level for this optimum condition still must be evaluated, in order to decide whether it is acceptable or a further increase in safety is needed.

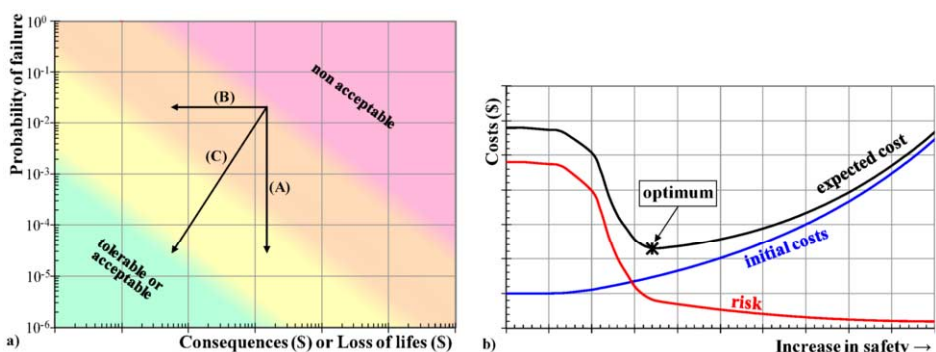


Figure 3. Illustrations for the concepts presented: a) risk as the product of the probability of failure times its consequences, and b) optimum expected cost for a risk-based project.

3. The Influence of Uncertainty

According to [9], there are basically two types of uncertainties: the intrinsic ones (natural variability) and the epistemic ones (lack of data, phenomenon comprehension or modeling ability). While the latter can be reduced by either gathering or improving information, the former must be dealt with and ideally accounted for.

It is highly intuitive the understanding that the less you know and comprehend a certain geotechnical work, the more unreliable the outcomes would be. This could also be translated as the more variable/uncertain the input parameters, or the less accurate the problem depiction, the wider the range of possible results from the analyses; therefore, the higher the number of possible undesired results and hence the higher the probability of failure.

In order to illustrate that, the author and others analyzed how the variability of geotechnical parameters affects the probability of failure of underground excavations [10], and results are following discussed. This study has been awarded the best oral presentation in the 3rd Brazilian Congress on Tunnels and Underground Structures [11].

Two soil tunnels were selected as study cases, both presented in the book "Tunnelling in Brazil" published by the Brazilian Tunneling Committee [12]: the *Alto da Boa Vista Tunnel*, a water tunnel built experimentally in 1978 in São Paulo city to link two water treatment plants [13]; and the *Paraíso Tunnel* from Line 2-Green of São Paulo metro, built in 1989 near Paulista Avenue to accommodate an additional track for maneuvering trains [14]. For both cases, the geological conditions were comprised by soils of the Neogene/Paleogene period, with groundwater level below the tunnel floor. No instability was noted during construction of both tunnels.

Two different analytical solutions were utilized to assess the underground excavations stability:

- Anagnostou and Kovári, Figure 4a.

A solution by [15] based on the limit equilibrium method, which mechanism represents a global excavation failure comprised of a wedge and a prism. Similar solutions have been presented by [16], [17], [18] and [19]. The wedge is located at the tunnel face and is limited by a plane inclined at ω degrees to the vertical and approximates the tunnel cross-section by a rectangle or a square. The prism height is equal to the tunnel cover, its width is equal to that of the tunnel and its thickness depends on the angle ω . The soil shear resistance acting on the failure surfaces are calculated considering the Mohr-Coulomb failure criteria. The Simplex optimization algorithm was used to determine the wedge angle ω , in order to minimize the Factor of Safety - FS by maximizing the acting forces and minimizing the resistant forces.

- Modified Mühlhaus, Figure 4b.

A solution by [20] based on the lower bound theorem of plasticity, modified by [21] and [22] to include gravitational forces. Its mechanism approximates the ground by a thick-walled sphere in a plastic state representing global failure, with an outer surface with radius R_e tangent to the ground surface and an inner surface with radius R_i corresponding to the unsupported excavation length. The excavation stability FS is defined from the internal limiting pressure P_{lim} that would cause collapse, the internal acting pressure P_{int} , the surface load σ_s and the octahedral stress at the tunnel crown σ_{oct} . Recently, the solution was reviewed by [23] enabling the representation of a multi-layered soil profile and accounting for seepage forces due to the groundwater flow.

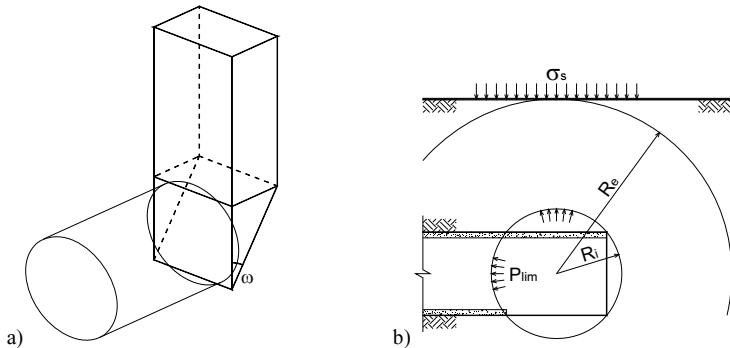


Figure 4. Failure models considered for each analytical solution: a) Anagnostou and Kovári b) Mühlhaus.

The probabilistic analyses performed for the study utilized both first-order approximations and Monte Carlo simulations, following discussed. The analyses applied the analytical solutions presented and changed the standard deviation (variability) of the geotechnical parameters.

- First-order approximation

Given a function which represents the safety (for instance the analytical solutions presented), a Taylor series expansion may be applied to the function around its mean value and approximated at its first-order term, as discussed by [24] and [25]. Thus, the mean value of the function's results is equal to the result calculated with the mean values of each random variable (i.e. the mean FS is equal to the deterministic FS); whereas the function's standard deviation is calculated from the standard deviations of each random variable. Then, the probability of failure is calculated from these two statistical moments (mean value μ , and standard deviation σ), assuming a normal probability distribution for the results.

- Monte Carlo simulations

For this approach, the function is repeatedly calculated by varying its random variables and analyzing the overall result. The technique allows any kind of problem to be approached with no restrictions on the number of variables or on the complexity of the function. The success in using it is related to the ability to perform a large number of simulations, which depends on the available computational capacity. Understandably, the simulation is known as a "brute force method", requiring a very large number of results, such that the probability to be assessed approaches the "exact value". Small probabilities of failure require a higher number of calculations. Typically, the simulation is taken as an "exact method" because, in theory, the result tends to exactness when the number of simulations tends to infinity.

After all analyses, it was observed that when considering lower standard deviations for the geotechnical parameters (less variability), the calculated results of FS - Factor of Safety presented a lower dispersion, yielding a lower probability of failure (higher reliability). Conversely, higher standard deviations for the parameters lead to higher probabilities of failure (up to $P_f = 13\%$). This is intuitively expected, as explained previously in Figure 2. However, more important and unsettling is the finding that these high probabilities of failure were associated with deterministic factors of safety (calculated with mean values parameters) that are usually considered satisfactory.

Among several results obtained, Figure 5 presents one typical example of how safety is affected by the variability of the geotechnical parameters.

After Kolmogorov-Smirnov adherence tests, the normal distribution of probabilities was chosen as the best fitted. It was noted that the analytical solution by Mühlhaus provided closer adherence to the normal distribution than the Anagnostou and Kováři solution. This can be attributed to the minimization algorithm used by the latter for obtaining FS, yielding a singularity that could be better represented by a bi-modal distribution instead ($FS \approx 1.4$ in Figure 5).

Moreover, the study also indicates that the deterministic result not necessarily is equal to the mean value of all results (in Figure 5, $FS_{\text{determ}} = 2.07$ and $\mu_{FS} = 1.66$). In such case, the use of first-order approximations may lead to probabilities of failure far from the "exact" value (in Figure 5, $P_f = 0.1\%$ for first-order and $P_f = 4.7\%$ for Monte Carlo).

Three important facts have emerged from the study [10] and [11]:

i) The geotechnical parameters variability directly affects the probability of failure. Consequently, ground investigations should not assess solely mean values of properties but also their dispersions and coefficients of correlation. The lower the parameters' standard deviations (the lower the uncertainty), the greater the project's reliability;

ii) Adequate global factors of safety might be associated with a non-negligible probability of failure. It is believed that, for future geotechnical projects, factors of safety recommended by standards and accepted in practice should be associated with acceptable levels of probability of failure, with targets also recommended by design codes;

iii) The use of first-order approximations is attractive for its simplicity; however, it should be used with caution and preference should be given to more rigorous, robust reliability-based methods.

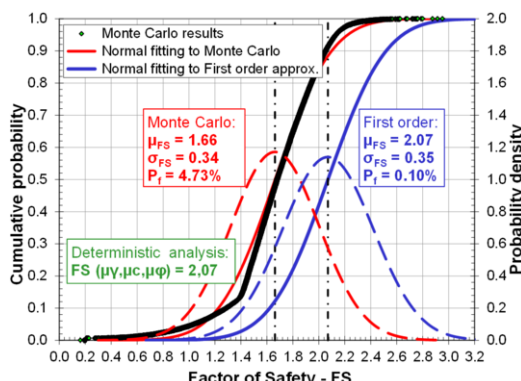


Figure 5. One of several results from the study of [10] and [11]: Alto da Boa Vista tunnel, solution by Anagnostou and Kováři, high values of standard deviation for the geotechnical parameters.

4. The Assessment of Variability

Geotechnical parameters are often characterized by mean values (μ), with no mention of their standard deviation (σ). In order to estimate their dispersion (variability) whenever data is insufficient, published values can be useful, conveniently expressed in terms of the coefficient of variation (V), which is defined as $V = \sigma / \mu$.

Values of coefficients of variation for some geotechnical parameters were compiled by [7], [9], [24], and [26], and are reproduced in Table 1 in terms of maximum and minimum bounds. The values shown cover a wide range, providing just a crude reference with which to estimate the standard deviation.

Although this stands as a possible alternative, one must bear in mind the variability effects, as previously discussed. Hence, the importance of its correct characterization or its reduction based on observations (Bayesian updating), both cases following presented.

Table 1. Values of coefficient of variation (V) for some geotechnical parameters.

γ specific weight (kN/m ³)	c' eff. cohesion (kPa)	φ' eff. friction angle (°)	Cc compression index	k coeff. conductivity (m/s)
3% to 7%	13% to 100%	7% to 12%	10% to 37%	80% to 240%

4.1. The use of available data

For cases when sufficient data is made available, the natural variability of certain property may be assessed by means of classical statistical analyses, whether or not considering its spatial and/or time dependency.

The author has performed such analysis unfortunately only during rare occasions since the availability of abundant data is not usual. For instance, the reliability assessment of an iron ore tailing dam was carried out based on the statistical analysis of some laboratory tests results [27], as presented in Figure 6.

Four different geotechnical materials were assessed: first and second stages earthfills (embankment), and residual and saprolitic soils (foundation).

The normal distribution of probabilities was chosen to represent the occurrence of the parameters specific weight (γ) and effective friction angle (φ'), while the log-normal distribution was chosen for the effective cohesion (c').

A slightly negative correlation was observed between the cohesion and the friction angle (coefficient of correlation from $\rho = -0,134$ to $\rho = -0,245$). Conservatively, both parameters were considered as independent of one another ($\rho = 0$) for the four materials.

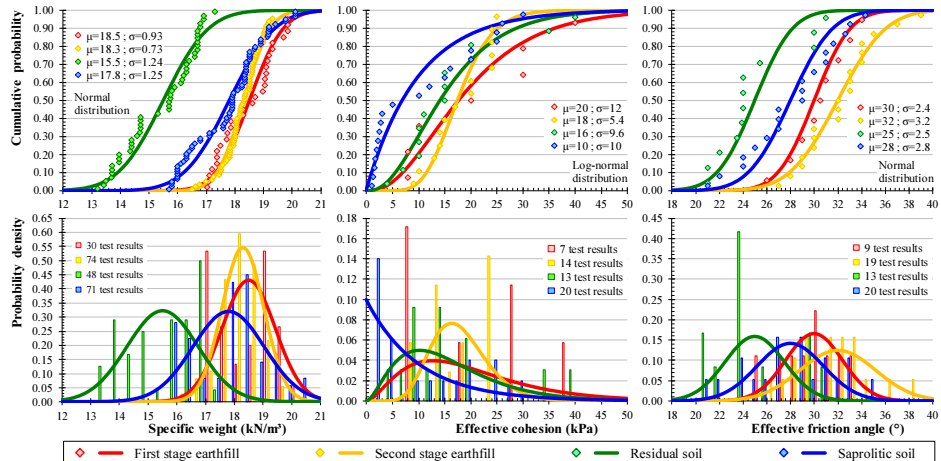


Figure 6. Statistical analysis of laboratory tests results for the assessment of parameters variability [27].

4.2. Reduction of uncertainty through observations

For those cases when properties have to be estimated due to the lack of available data, the high variability (uncertainty) associated with such properties may be reduced through the observation of some particular behavior.

Observational methods are usual for geotechnical engineers, in order to confirm or change idealized models and hypothesis made, as well as re-evaluate the parameters adopted, among other reasons, during the project execution or after its completion.

Back-analyses are the most common approach to evaluate parameters based on some performance, requiring one observation (for instance $FS = 1.0$) for each parameter to be back-analyzed. These deterministic back-analyses, however, are not capable of providing information concerning the parameters variability.

On the other hand, Bayesian probabilistic back-analyses provide the probability of occurrence of each back-analyzed parameter. Moreover, the number of performance observations does not need to be equal to the number of back-analyzed parameters, as imposed by the deterministic approach. For these reasons, the Bayesian updating poses as a powerful tool, which should be used more often.

It consists of applying the Bayes theorem of conditional probabilities, in which the likelihood of a prior event is updated given that a later event has occurred.

For instance, the probability distribution (type and moments) of geotechnical parameters may be updated conditioned to the realization of some observation, such as a collapse, a change on the expected behavior or any other type of performance measurement. Since more information is added, the updated probability relates to a more specific scenario with higher certainty associated with its occurrence and, therefore, it presents less variability than the previous one (smaller standard deviation).

The Bayesian probabilistic back-analysis methodology presented herein is based on [28] and [29] and considers a normal probability distribution for both the variables to be updated and the performance observations.

The back-analysis starts by acknowledging the parameters to be updated (initial state variables), with a vector of mean values $\{s'\}$ and a matrix of covariance $Cov[s']$. Following, the performance observations are also represented by a vector of mean values $\{P\}$ and a matrix of covariance $Cov[P]$.

The updating is based on the comparison of the performance observations and the predicted values of performance, i.e. $\{P\} - \{p\}$, where the latter is calculated using any recognized method (analytical solutions, numerical simulations, etc.).

The methodology considers a linear relationship between the initial state variables $\{s'\}$ and the predicted values of the performance $\{p\}$:

$$\{p\} = [A].\{s'\} + \{B\} + \{v\} \quad (2)$$

where $[A]$ is the linear coefficients matrix and $\{B\}$ is the independent terms vector for the hyperplane adjusted to the predicted values of performance (for instance, using least squares method). A vector of errors $\{v\}$ may also be included, related to a possible error trend from the prediction method or the observation method (systematic errors).

The updated mean values vector of the state variables $\{s''\}$ is calculated by:

$$\{s''\} = \{s'\} + Cov[s'].[A]^T.([A].Cov[s'].[A]^T + Cov[P])^{-1}.(\{P\} - \{p\}) \quad (3)$$

The updated covariance matrix of the state variables $Cov[s'']$ is attained by:

$$\text{Cov}[s''] = \text{Cov}[s'] - \text{Cov}[s'].[\mathbf{A}]^T.([\mathbf{A}].\text{Cov}[s'].[\mathbf{A}]^T + \text{Cov}[\mathbf{P}]^{-1}.[\mathbf{A}].\text{Cov}[s']) \quad (4)$$

A practical example on the use of this methodology was presented by the author and others [30], in which values of earth coefficient at rest (K_0) and of deformability modulus at 50% of failure (E_{50}) were back-analyzed for fine soils found along the tunnels from Line 3 of Santiago Metro, Chile.

The mean values and variances of the initial state variables were defined as: i) for K_0 , the lower and upper limits of 0.40 and 1.60 were considered according to previous experience, then confidence levels of 5% and of 95% were respectively adopted; ii) for E_{50} (MPa), laboratory and *in-situ* tests results were used. The initial state variables were considered independent from one another (zero covariance), resulting in:

$$\{s'\} = \begin{Bmatrix} K_0 \\ E_{50} \end{Bmatrix} = \begin{Bmatrix} 1.00 \\ 37.64 \end{Bmatrix} \quad \text{and} \quad \text{Cov}[s'] = \begin{bmatrix} 0.365 & 0 \\ 0 & 18.49 \end{bmatrix}$$

The performance observations were based on the field monitoring installed during the construction of Line 2 of Santiago Metro, whose tunnels were excavated through the same type of fine soils under study. A total of 38 monitoring sections were evaluated, using the following observations: logarithm of the surface settlement at the tunnel symmetry axis ($\ln p_{\text{sup}}$); logarithm of the calculated maximum transversal angular distortion at surface ($\ln \beta$); lining displacements in the vertical direction at the tunnel crown (δ_v) and in the horizontal direction at the tunnel springline (δ_h); and the radial ground stresses acting onto the tunnel lining at the crown (σ_v) and at the springline (σ_h). The statistical analysis of these observations yielded the following mean values and covariances (displacements in mm and stresses in MPa):

$$\{P\} = \begin{Bmatrix} \ln(p_{\text{sup}}) \\ \ln(\beta) \\ \delta_{h\text{ left}} \\ \delta_v \\ \delta_{h\text{ right}} \\ \sigma_v \\ \sigma_h \end{Bmatrix} = \begin{Bmatrix} 1.62 \\ 7.76 \\ 0.38 \\ 2.50 \\ 0.43 \\ 0.04 \\ 0.06 \end{Bmatrix} \quad \text{and} \quad \text{Cov}[P] = \begin{bmatrix} 0.25 & -0.20 & -0.07 & 0.08 & 0.36 & 0 & 0 \\ -0.20 & 0.29 & 0.50 & 0.81 & -0.63 & 0 & 0 \\ -0.07 & 0.50 & 4.44 & 0.17 & -0.38 & -0.07 & 0.04 \\ 0.08 & 0.81 & 0.17 & 6.91 & -2.02 & -0.03 & 0.01 \\ 0.36 & -0.63 & -0.38 & -2.02 & 2.81 & -0.04 & 0.02 \\ 0 & 0 & -0.07 & -0.03 & -0.04 & 0 & 0 \\ 0 & 0 & 0.04 & 0.01 & 0.02 & 0 & 0 \end{bmatrix}$$

The predicted values of the tunnel performance were obtained using a numerically derived model based on 2D and 3D finite-elements analysis [31]. A systematic error of -0.046 MPa was accounted for the pressure cells because they tend to underestimate ground stresses acting on tunnel linings. The linear relationship between the initial state variables and the predicted values of performance was found to be represented by the following linear coefficients matrix and independent terms vector:

$$[\mathbf{A}] = \begin{bmatrix} -4.00 \times 10^0 & -2.86 \times 10^{-2} \\ 5.15 \times 10^0 & 2.86 \times 10^{-2} \\ 7.72 \times 10^0 & 3.84 \times 10^{-3} \\ -5.76 \times 10^0 & -8.79 \times 10^{-3} \\ 7.72 \times 10^0 & 3.84 \times 10^{-3} \\ 1.41 \times 10^{-1} & 1.42 \times 10^{-3} \\ 7.03 \times 10^{-2} & -3.73 \times 10^{-4} \end{bmatrix} \quad \text{and} \quad [\mathbf{B}] = \begin{Bmatrix} 6.59 \times 10^0 \\ 2.06 \times 10^0 \\ -7.26 \times 10^0 \\ 7.14 \times 10^0 \\ -7.26 \times 10^0 \\ -8.51 \times 10^{-2} \\ 6.49 \times 10^{-2} \end{Bmatrix}$$

The back-analyzed parameters found for the Santiago fine soils are $K_0 = 0.84$ and $E_{50} = 40.1$ MPa, with standard deviations of 0.06 and 15.7 MPa, respectively. These

values were incorporated into the design of Line 3 of Santiago Metro, despite both being higher than what was used previously for the Line 2 design. A higher K_0 enabled the tunnel lining to be optimized, whereas a higher stiffness was favorable regarding ground settlements, reducing potential damages to nearby structures.

5. Case Study on Reliability-based Design

A reliability analysis was performed by the author and others to assess the probability of failure for the main tunnel of Universidad de Chile Station, Line 3 of Santiago Metro [32].

The excavation was completed in 2016, crossing beneath an existing track tunnel from Line 1, built in the 1970s. The surface area is densely occupied, with historical and government buildings. Two heavy traffic roads are also on site, one on the ground level parallel to the track tunnel, while the other is an underground passage parallel to the station tunnel (see Figure 7a).

Due to such complexity, Santiago Metro required during the detailed design stage that the probability of failure for the Line 3 excavations was minimized.

5.1. Site description

The ground is a thick deposit of fluvial, well graded and dense gravel with a finer cohesive matrix. As presented in Figure 7a, the stratigraphy is comprised by topsoil (1.0 m thick earthfill), over the second deposition (3.0 m thick) and the first deposition of gravels from the Mapocho River.

The cross section for the station main tunnel is presented in Figure 7b. The central pillar was chosen for the stability analyses since its excavation area (70.48 m^2) is larger than that of each side drifts.

To assess the excavation stability, the analytical solutions by Anagnostou and Kovári [15] and by Mühlhaus [20] modified by [21] and [22] were used. Both solutions were previously discussed in section 3 (see Figure 4). The tunnel cross-section presented in Figure 7b also indicates the projection of the inner surface of the thick-walled sphere for the modified Mühlhaus failure model (blue circle) and the excavation face for the Anagnostou and Kovári failure model (red rectangle).

The originally proposed soil conditioning, presented in Figure 8a, consists of forepoling in the tunnel roof (injected self-drilling bolts, Ø40/16mm, Ø70mm boring, 6m long with 3m overlapping) and soil nailing in the tunnel face (glass fiber bars injected with resin, Ø22mm, Ø123mm boring, 8m long with 4m overlapping). The reliability study led to a change in the soil conditioning design, as presented in Figure 8b: the forepoling was extended from 6 to 12m long with 8m overlapping, and the three upper layers of the frontal soil nailing were extended from 8 to 10m long with 6m overlapping.

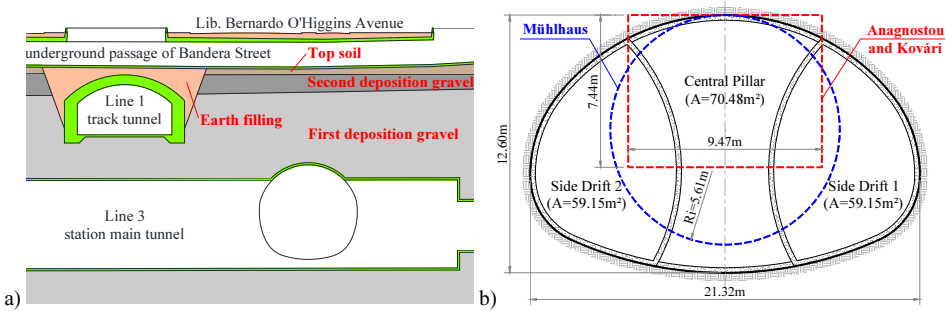


Figure 7. The main tunnel for the Universidad de Chile Station: a) longitudinal section, with soil stratigraphy and surrounding structures, b) cross-section geometry [32].

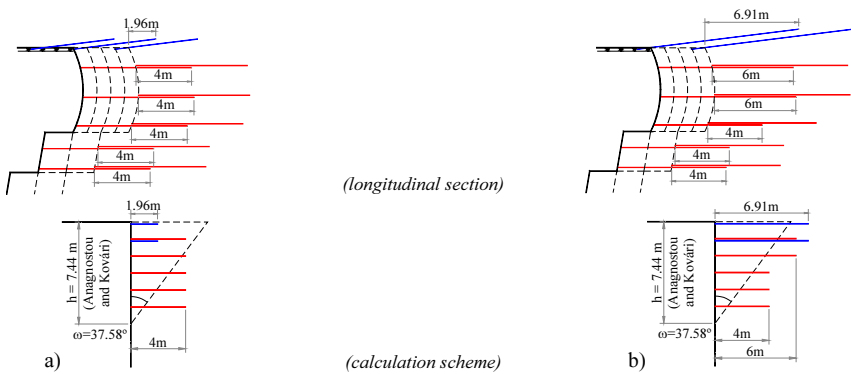


Figure 8. Soil conditioning for the station main tunnel: a) original design and b) design change [32].

5.2. Reliability analyses

The reliability analyses were carried out with Monte Carlo simulations, considering only the variability of the geotechnical parameters.

A set of different analyses was required due to the variations on the tunnel cover (15.6 m below the underground passage and 5.0 m below the existing Line 1 track tunnel), for the two analytical solutions and to represent a possible encounter of two excavation headings. This resulted in six analyses, as illustrated in Figure 9. The representation of the two headings encounter is only possible using the failure model of Anagnostou and Kováři, for the Mühlhaus failure model imposes a spherical symmetry.

The internal pressure P_{int} was determined by the mobilization of the soil conditioning (only the tension force in the bolts was considered and the shear and bending strengths were neglected), by the reaction of the open shell lining foundation (calculated according to [33]) and by the stabilizing horizontal pressure provided by the frontal core (berm).

The parameters used for the deterministic tunnel design were taken as the mean values for the probabilistic analyses. The standard deviations for γ and φ' were determined after coefficients of variation from literature; for c' laboratory test results were used; for K_0 values from a probabilistic back-analysis presented by [34] were adopted.

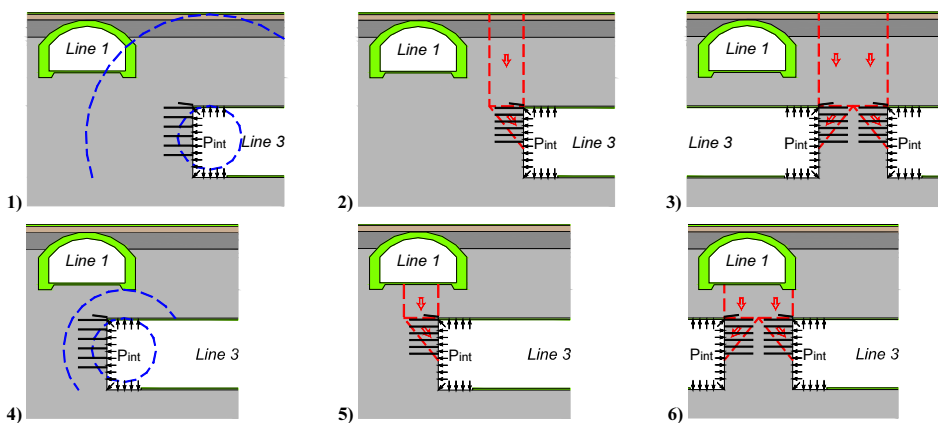


Figure 9. An illustrative summary of the analyses performed [32].

Table 2 presents the probabilities of failure calculated for each one of the reliability analyses. The results from the initial analyses, considering the originally designed soil conditioning, indicate that the excavation of the Central Pillar of the University of Chile Station main tunnel presented a probability of failure up to 6.44%. It was also noticed that the encounter of two tunnel headings increases the excavation probability of failure.

An important observation is that the modified Mühlhaus analytical solution yields higher probabilities of failure than the Anagnostou and Kovári solution, as expected. One should keep in mind that these solutions do not provide an exact value for safety. The lower bound theorem of the Mühlhaus yields safer values, whereas the Anagnostou and Kovári limit equilibrium method can roughly act as an upper bound approximation (the system energy balance and a viable kinematic motion are not ensured), what can be unsafe.

Other analyses were following performed, this time changing the soil conditioning as depicted by Figure 8, whose results are also presented in Table 2. The encounter of the two excavation headings below the existing Line 1 track tunnel presented a 0.23% probability of failure, which led to the design specification that such an encounter should be executed away from this region. For all remaining analyses, the probability of failure was considered negligible (< 0.00). This is because there was not even one case of failure observed throughout the 30,000 simulations carried out for each analysis ($P_f < 3.3 \times 10^{-5}$).

Table 2. Probabilities of failure (%) calculated for the different analyses [32].

Soil conditioning	1	2	3	4	5	6
original design	4.74	< 0.00	0.03	6.44	0.09	1.37
changed design	< 0.00	< 0.00	< 0.00	< 0.00	< 0.00	0.23

6. Case Study on Risk Assessment

A risk assessment was performed by the author and others for an iron ore tailing dam [27]. Due to restraints towards confidentiality, the object of this study shall be herein referred to as Dam X. This risk assessment has been granted the *José Machado Award* for the best Brazilian geotechnical project of the biennium 2017-2018, by ABMS.

Tailing dams are complex structures in which the material accumulated in the reservoir presents no trivial geotechnical behavior. This is an important aspect especially

when dam embankments are raised by the upstream or centerline methods, for the tailings that once acted just as a load start to act also as the embankment foundation.

Another particularity of tailing dams concerns the variation of their conditions throughout their lifespan. Typically, the dam is not built to its final height, being raised as the reservoir volume is depleted. This is especially due to fluctuations in the ore market value, which is responsible for the mine operation rhythm and for the consequent tailing disposal plan. Consequently, a single dam can be built at different times by different constructors, based on designs also elaborated by different companies.

Such complexity, translated in terms of material properties and of construction and operation histories, requires a geotechnical risk management elaborated specifically for this type of structure.

The mining company owning Dam X had the initiative of elaborating the so-called Geotechnical Risk Management project, whose purpose is to assess the safety condition of their geotechnical structures. It allows the latter to be managed, having a monetized risk as a guide for preventive or improvement actions. The methodology elaborated for this project, despite being based on consecrated theories, has pioneer application in the world, developed with the collaboration of an international consultants panel.

The Dam X was selected as a case study in order to present this risk assessment methodology. It is a compacted earthfill dam, has 71 m of height, 810 m of crest length and 130 million m³ of reservoir volume. Its design was developed to be constructed in three stages, using the downstream raising method. Currently, only the first and second stages were constructed, finished by 1981 and 2016 respectively. The tailings are disposed of in a single point at the reservoir rear end, by gravity.

Figure 10 presents the cross-section selected for analysis, which refers to the dam's maximum height. The field monitoring counts with 19 piezometers (PZs), 8 water level indicators (INAs), 6 reservoir level rulers, 2 flow meters and 21 topographical landmarks. The piezometric level acting on the cross-section was interpreted after the evaluation of the instruments installed. Distinct piezometric levels were observed for the foundation (red line) and for the embankment (blue line), justified by the different hydraulic conductivities.

The embankment (both stages) was built with a clayey earthfill extracted from the abutments, which was originally comprised of residual soils from gneiss and micaxist. The earthfill presented fines content > 50% and plasticity index > 30%.

The foundation (at the cross-section) is comprised of residual and saprolitic soils, weathered from shales. The residual soil was characterized as sandy-silt, with fines content from 30% up to 64% and plasticity index from 11% up to 37%.

The Geotechnical Risk Management methodology has five steps for each structure: i) data acquisition and consolidation; ii) probability of failure calculation; iii) hypothetical dam-break study; iv) assessment of consequences; and v) risk calculation.

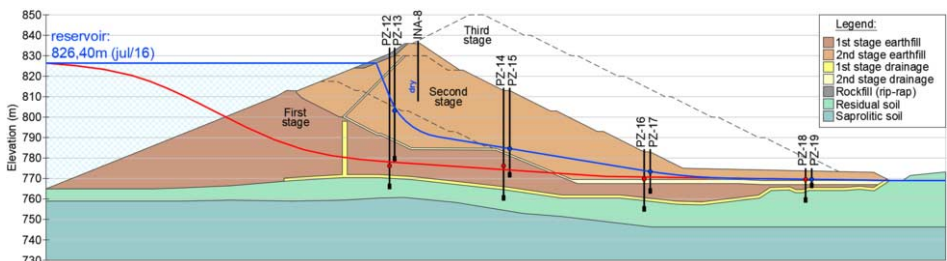


Figure 10. Cross-section with piezometric levels interpreted for the **foundation** and the **embankment** [27].

6.1. Probabilities of failure

Recent studies by [35], based on compilations from *ICOLD*, *UNEP* and *US Department of Interior*, validate the definition of four main failure modes for tailing dams: overtopping, internal erosion, embankment instability, and liquefaction.

The probability for each failure mode is calculated using quantitative approaches, which reduces the results subjectivism by minimizing the qualitative aspects along the process.

Overtopping

The analysis begins with the flood routing simulation for all existing upstream water bodies, resulting in the affluent and effluents hydrographs of the dam's reservoir. Moreover, several rainfall events are analyzed, each one associated with a certain duration and Return Period (RP). The probability of failure is then calculated as the inverse of the return period ($1/RP$) for the event that causes the overtopping.

For the Dam X, the overtopping was not verified even for the maximum flood caused by the Probable Maximum Precipitation (PMP), remaining a freeboard of 1.90 m. Therefore, the probability of overtopping was neglected.

Internal erosion

The methodology for evaluating the internal erosion potential combines Event Trees with Fault Trees and has been used since the late '90s by USACE[36], USBR [37], some Australian organizations, among others, still under development in the world. It is based mostly on [38], [39] and [40], bearing the appropriate adaptations and specificities for tailing dams. Its use has the advantage of an in-depth reflection on the failure mode progression and the factors that influence each of the phenomenon stages.

There are basically four main internal erosion mechanisms: regressive erosion with a piping formation, suffusion (internal instability), erosion due to concentrated flow and erosion on the contact between different materials. All possible initiating events likely to occur must be evaluated (piping through the dam or its foundation, erosion on the spillway concrete/soil contact, etc.).

An **Event Tree** is elaborated for each initiating event, with the nodes: (a) initiation; (b) continuation; (c) pipe formation; (d) pipe progression; (e) process detection and intervention; and (f) failure mechanism formation. The probability of occurrence of each node is determined after specific **Fault Trees**, which depend on the type of mechanism and the initiating event. The Fault Trees combine evaluations on soil properties, hydraulic gradients, the presence of filters, the ability to detect and intervene in the process, etc.

Figure 11 presents the Event Tree for the worst scenario evaluated for Dam X, piping through the left abutment, with $P_f = 1 \times 10^{-5}$. All Fault Trees were evaluated for every single node of all the analyzed Event Trees, however, they are not herein presented.

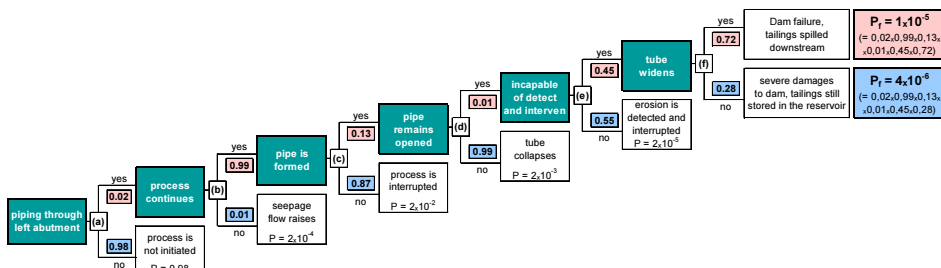


Figure 11. Event Tree for piping through the left abutment, with the nodes' probability of occurrence [27].

Embankment instability

The stability analyses were performed using the limit equilibrium method. The geotechnical parameters were considered as random variables, with probability distributions determined after statistical analyses of laboratory tests results, previously presented in Figure 6. The piezometric levels are presented in Figure 10.

The probability of failure for the embankment instability was assessed through Monte Carlo simulations. A total of 500,000 analyses were performed with non-fixed failure surfaces, i.e. a new critical surface was determined for every single analysis.

The total number of simulations was considered adequate since the mean value and the standard deviation of the Factor of Safety had converged to steady values ($\mu_{FS}=1.55$ and $\sigma_{FS}=0.11$ respectively). However, the frequentist probability of failure (number of $FS<1.0$ observations divided by the number of simulations) did not converge, what would require a greater number of simulations, but not viable in practice.

In order to avoid the influence of a limited number of analyses, the probability of failure was determined by adjusting a probability distribution to the results, according to Figure 12. After *Kolmogorov-Smirnov* adherence tests, the Beta distribution was selected as best fitted, yielding $P_f = 4.10^{-6}$.

For this assessment, the deterministic FS was found to be higher than μ_{FS} , what is the same trend discussed in section 3 with outcomes from [10] and [11].

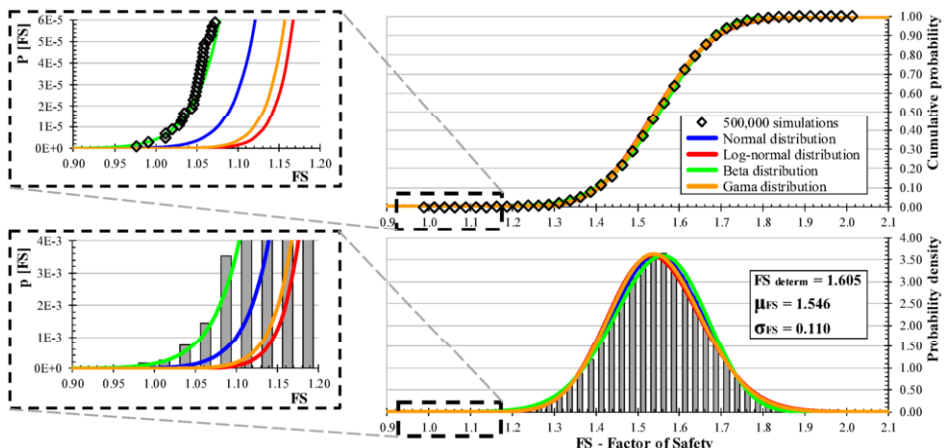


Figure 12. Results of Factor of Safety obtained from the 500,000 simulations [27].

Liquefaction

This phenomenon has been society's great concern. Its occurrence is subjected to materials being susceptible and to the deflagration of a trigger.

To be considered susceptible to liquefaction, the material must be non-cohesive, saturated, and present in-situ void ratio higher than the critical value (contractile behavior during an undrained failure).

The trigger can be associated with static or dynamic events, such as excess pore water pressure due to rapid loading (overloads, dam raising, reservoir level increasing), natural seismicity or induced vibrations (heavy equipment traffic, detonations, adjacent structures failures), as well as sudden increase of shear stresses (material removal from the dam toe, foundation differential movement), among others.

The present methodology assesses the liquefaction potential based on [41], [42] and [43], using results from CPTu and/or SPT tests. The stability is assessed using the limit equilibrium method, considering an undrained strength ratio (s_u/σ_v') for the susceptible materials and maintaining the assigned drained strength (c' and ϕ') for the remaining materials. The probability of failure is then assessed in the same way as to the embankment instability, using Monte Carlo simulations.

Liquefaction analysis is a topic that demands contributions worldwide since the geotechnical practice still relies on the limit equilibrium method. Advancements are needed towards the determination of the undrained strength (strongly dependent on the test type and on the soil in-situ state, which is difficult to characterize), as well as the approach used for the stability assessment (the analyses must be effective stresses oriented, considering the soil stress-strain behavior with post-peak softening coupled to a consolidation theory able to predict the dissipation of the excess pore water pressures).

The probability of failure due to liquefaction was neglected to the Dam X because the tailings do not act as the foundation (downstream raising) and the clayey soil used for the embankment is not susceptible.

6.2. Hypothetical Dam-break study

The dam-break study is elaborated simulating different scenarios, which include rainy or rainless day, with or without the dam failure. Its main objective is to estimate the influence of the failure, delimiting the flooded area.

The study is developed following the stages: definition of the failure hydrograph, depending on the failure mode; elaboration of the valley's geomorphological model; hydrological characterization of watercourses; flood wave propagation; flood mapping.

The dam-break study for Dam X yielded a flood damage potential up to 155 km downstream of the dam. More expressive inundations were identified along the first 50 km, striking two municipalities with houses and urban infrastructure close to the watercourse.

6.3. Assessment of consequences

The monetized values for the consequences caused by an eventual dam failure are assessed within the flood area, partitioned into six categories: i) economic; ii) health and safety; iii) social; iv) environment; v) regulatory agencies; and vi) company image.

Eight scenarios are evaluated, considering a nocturnal or diurnal failure, during a rainless or a rainy day, with an alert issued by sirens at the failure or 4 hours earlier.

The methodology details the assessment of costs for each category and scenario, with thorough procedures not presented herein. The population at risk was differentiated as diurnal or nocturnal according to the activities developed in the inventory area.

The costs of the consequences caused by the Dam X failure are summarized in Table 3, concerning the scenarios of nocturnal failure. The four remaining scenarios of diurnal failure are not presented, for their outcomes were less critical.

Table 3. Cost of consequences (BR\$) for different scenarios of nocturnal failure [27].

rainless day, no alert	rainless day, with alert	rainy day, no alert	rainy day, with alert
40,464,626,894	13,516,793,074	44,357,513,702	15,651,634,166

6.4. Risk calculation

The monetized risk for Dam X is presented in Figure 13, the so-called risk panel. Only the rainless day scenarios are presented since the failure probabilities for the rainy-day scenarios must be multiplied by the probability of a decamillennial rainfall (10^{-4}).

The risk panel allows clear visualization of the risks and facilitates decision-making actions towards their mitigation, by reducing either the probability failure or its consequences.

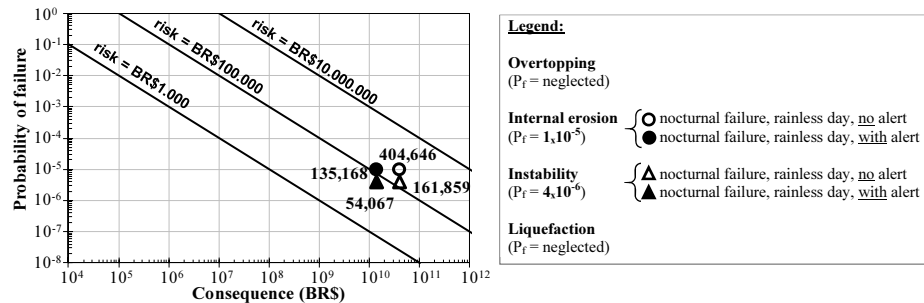


Figure 13. Risk panel for Dam X [27].

7. Final Remarks

Reliability analyses are more often recognizably needed, and it is imperative that its use becomes more common practice. Such an approach must not suppress the conventional, deterministic methods, instead, they should complement each other. As discussed, it is a matter of safety, for a deterministic outcome taken as adequate may correspond to a high probability of failure.

The quantification of the risk, besides minimizing the use of qualitative evaluations which are essentially subjective, represents a fundamental tool for the management of geotechnical structures, allowing the allocation of investments to be optimized.

Computational limitations are no longer a plausible excuse for avoiding going non-deterministic. In fact, brilliant young geotechnical engineers are out there waiting to push boundaries and introduce innovative practices, provided that they are assisted and encouraged by senior mentors.

References

- [1] Aoki, N. Probabilidade de Ruína e Fator de Segurança em Fundações: Como determinar o risco geotécnico?. *Palestra Milton Vargas*. Goiânia, Rio de Janeiro, Porto Alegre, Florianópolis, Curitiba, Recife, Salvador, Rio Grande do Norte, Belém, São Paulo: ABMS, 2011.
- [2] Aoki, N. Paradigma do Fator de Segurança. *XII Conferência Pacheco Silva*. In: XVIII Cobramseg, Belo Horizonte: ABMS, 2016.
- [3] Hachich, W.C. Segurança, Confiabilidade e Riscos em Obras Geotécnicas. *Palestra Milton Vargas*. Belém, Macapá, Goiânia, Recife, Belo Horizonte, Vitória, Porto Alegre, Curitiba, Salvador, Florianópolis, Rio de Janeiro, São Paulo: ABMS, 2018.
- [4] Assis, A.P. Gestão de Riscos em Obras Geotécnicas: Consolidando a Teoria em Prática. *XIII Conferência Pacheco Silva*. In: XIX Cobramseg, Salvador: ABMS, 2018.
- [5] Wedekin, V.M.; Kastner, R.; Bezuijen, A.; Guilloux, A.; Emeriault, F.; Standing, J. and Negro, A. Urban tunnels in soil: review of current design practice. *Proceedings of the 7th International Symposium on*

- Geotechnical Aspects of Underground Construction in Soft Ground*, Roma. Viggiani, G (editor). London: Taylor and Francis Publishers, pp.1047-1064, 2011.
- [6] Whitman, R.V. Organizing and evaluating uncertainty in geotechnical engineering. *Journal of Geotechnical and Geoenvironmental Engineering*. ASCE, 126(7), pp.583-593, 2000.
- [7] Harr, M.E. *Reliability-based design in civil engineering*. New York: McGraw-Hill. 290p, 1987.
- [8] Morgenstern, N.R. Geotechnical Risk, Regulation and Public Policy. *6th Victor de Mello Lecture*. In: 9th Portuguese-Brazilian Geotechnical Congress, Salvador: ABMS, 2018.
- [9] Baecher, G.B. and Christian, J.T. *Reliability and statistics in Geotechnical Engineering*. New York: John Wiley & Sons, 605p, 2003.
- [10] Cecilio Jr., M.O.; Queiroz, P.I.B. and Negro, A. Instability risk assessment of soil tunnel excavation based on ground properties variability. In: World Tunnel Congress. Geneva: ITA, 2013.
- [11] Cecilio Jr., M.O.; Wedekin, V.M.; Queiroz, P.I.B. and Negro, A. Avaliação de risco da estabilidade de escavações subterrâneas baseada na variabilidade de parâmetros geotécnicos. In: 3º Congresso Brasileiro de Túneis e Estruturas Subterrâneas. São Paulo: CBT/ABMS, 2012.
- [12] CBT. *Tunnelling in Brazil*. São Paulo: Dórea Books and Art, 327p, 2000.
- [13] Negro, A. and Eisenstein, Z. Ground control techniques compared in three Brazilian water tunnels. *Tunnels and Tunnelling*. Oct. pp.11-14, Nov. pp.52-54, Dec. pp.48-50, 1981.
- [14] Almeida e Sousa, J.N.V.; Negro, A.; Matos Fernandes, M. and Cardoso, A.S. Three-Dimensional Nonlinear Analyses of a Metro Tunnel in São Paulo Porous Clay, Brazil. *Journal of Geotechnical and Geoenvironmental Engineering*. ASCE, 137(4), pp.376-384, 2011.
- [15] Anagnostou, G. and Kovári, K. The Face Stability of Slurry-shield-driven Tunnels. *Tunnelling and Underground Space Technology*, 9(2), pp.165-174, 1994.
- [16] Jancsecz, S. and Steiner, W. Face support for a large mix-shield in heterogeneous ground conditions. *Tunnelling '94*, The Institution of Mining and Metallurgy and BTS, pp.531-550, 1994.
- [17] Anagnostou, G. and Kovári, K. Face Stability Conditions with Earth-Pressure-Balanced Shields. *Tunnelling and Underground Space Technology*, 11(2), pp.165-174, 1996.
- [18] Anagnostou, G. and Kovári, K. Face stability in slurry and EPB shield tunnelling. *Proceedings of the International Symposium on Geotechnical Aspects of Underground Construction in Soft Ground*. Mair, R.J. and Taylor, R.N (editors), London. Rotterdam: A.A.Balkema, pp.453-458, 1996.
- [19] Plekkenpol, J.W.; Schrier, J.S. and Hergarden, H.J.A.M. Shield tunnelling in saturated sand - face support pressure and soil deformations. *Tunnelling, a decade of progress - GeoDelft 1995-2005*. Bezuijen, A. and Lottum, H. (editors). London: Taylor and Francis, pp.133-141, 2006.
- [20] Mühlhaus, H.B. Lower bound solutions for circular tunnels in two and three dimensions. *Rock Mechanics and Rock Engineering*, 18, pp.37-52, 1985.
- [21] Sozio, L.E. NATM - Implicações do método construtivo na segurança das escavações. In: *1º Congresso Brasileiro de Túneis e Estruturas Subterrâneas*. São Paulo: ABMS/CBT, 12p, 2004.
- [22] Sozio, L.E. Analytical Stability Models for Tunnels in Soil. *Proceedings of the 5th Geotechnical Aspects of Underground Construction in Soft Ground*, Netherlands. Bakker, K.J. et al. (editors). London: Taylor and Francis Publishers, pp.299-304, 2006.
- [23] Sozio, L.E. Analytical and numerical models for evaluation of tunnel excavation stability in a multi layered soil profile with groundwater flow. *Proceedings of the 9th International Symposium on Geotechnical Aspects of Underground Construction in Soft Ground*. São Paulo: CBT/ISSMGE, 9p, 2017.
- [24] Duncan, J.M. Factors of safety and reliability in geotechnical engineering. *Journal of Geotechnical and Geoenvironmental Engineering*. ASCE, 126(4), pp.307-316, 2000; Discussions and closure 127(8), pp.700-721, 2001.
- [25] Rosenblueth, E. Point estimates for probability moments. *Proceedings of the National Academy of Sciences of USA*, 72(10), pp.3812-3814, 1975.
- [26] Assis, A.P.; Espósito, T.J.; Gardoni, M.G. and Maia, J.A.C. Métodos Estatísticos e Probabilísticos Aplicados a Geotecnia. *Publicação G.AP-002/01*, Departamento de Engenharia Civil e Ambiental, Universidade de Brasília, Brasília, 177p, 2004.
- [27] Cecilio Jr., M.O.; Namba, M.; Negro, A.; Lopes, M.; Rocha, F.F.; Penna, D.R.; Mazon, A. and Assis, A.P. O caso de estudo da Barragem X: Gestão de risco geotécnico de barragens de rejeito. In: Prêmio José Machado de melhor projeto geotécnico no biênio 2017-2018. Belo Horizonte: ABMS, 2018.
- [28] Sage, A.P. and Melsa, J.L. *Estimation theory with applications to communications and control*. New York: McGraw-Hill, 1971.
- [29] Hachich, W.C. Seepage-related reliability of embankment dams. *Thesis (PhD)*, Massachussets Institute of Technology, Cambridge, 1981.
- [30] Cecilio Jr., M.O.; Valenzuela P., L. and Negro, A. Probabilistic back-analysis of earth pressure coefficient at rest and deformability characteristics for fine soils in Line 2 of Santiago Metro. In: International Symposium on Geotechnical Aspects of Underground Construction in Soft Ground. Seoul: ISSMGE, 8p., 2014.

- [31] Negro, A. Design of shallow tunnels in soft ground. *Thesis* (PhD), University of Alberta, Edmonton, 1988.
- [32] Cecílio Jr., M.O.; Valenzuela P., L. and Negro, A. Reliability analysis for the excavation of Universidad de Chile Station, Line 3 of Santiago Metro. In: World Tunnel Congress. Iguassu Falls: CBT/ITA, 2014.
- [33] Negro, A. Soil tunnels and their supports. *Proceedings of the X Congresso Brasileiro de Mecânica dos Solos e Engenharia de Fundações*. Foz do Iguaçu. São Paulo: ABMS, pp.30-60, 1994.
- [34] Queiroz, P.I.B.; Roure, R.N and Negro, A. Bayesian updating of tunnel performance for K_0 estimate of Santiago gravel. *Proceedings of the International Symposium on Geotechnical Aspects of Underground Construction in Soft Ground*. Amsterdam: CRC Press/Balkema, pp.211-218, 2005.
- [35] Taguchi, G. Fault Tree Analysis of Slurry and Dewatered Tailings Management - A Frame Work. *Thesis* (MSC), University of British Columbia, Canada, 89p., 2014.
- [36] USACE. Reliability Analysis and Risk Assessment for Seepage and Slope Stability Failure Modes for Embankment Dams. *COE ETL 1110-2-561*, 128p., 2006.
- [37] USBR. *Best practices in dam and levee safety risk analysis*. 2015. Available at: <http://www.usbr.gov/ssle/damsafety/Risk/methodology.html>
- [38] Foster, M.A. and Fell, R. Assessing embankment dam filters which do not satisfy design criteria. *UNICIV Report No. R-376*, The University of New South Wales, Sydney, 1999.
- [39] Fell, R.; MacGregor, P.; Stapledon, D. and Bell, G. *Geotechnical Engineering of Dams*. Amsterdam: CRC Press, 1348p., 2005.
- [40] Fell, R. and Fry, J.J. *Internal erosion of dams and their foundations*. Amsterdam: CRC Press, 245p., 2007.
- [41] Fear, C.E. and Robertson, P.K. Estimating the undrained strength of sand: a theoretical framework. *Canadian Geotechnical Journal*, 32(4), pp.859-870, 1995.
- [42] Olson, S.M. Liquefaction analysis of level and sloping ground using field case histories and penetration resistance. *Thesis* (PhD) – University of Illinois at Urbana-Champaign, Urbana, 2001.
- [43] Olson, S.M. Liquefaction Analysis of Tailings Facilities. In: XVIII Cobramseg Congresso Brasileiro de Mecânica dos Solos e Engenharia Geotécnica, 2016.

Subject Index

3D slope stability	292	LCA	374
3D stability analysis	292	leaning instability	328
accelerated pavement testing	276	limit analysis	342
analysis	5	limit equilibrium	292, 342
Bayes theorem	418	liquefaction	392
BTES	374	loads	216
CAES system	342	matric suction	112
carbonate	240	monitoring	328
centrifuge testing	128	nondestructive testing	276
chemical stabilization	276	non-isothermal behavior	356
constructive methods	194	offshore installation	216
coupled model	150	offshore wind turbines	216
courses	348	pavements	276
dams	418	pile foundations	182
DCP	276	post-earthquake deformations	392
design	5, 194	probabilistic models	5
deterministic models	5	probability	418
dynamic response	216	quarry by-products	276
effective stresses	150	reliability	5
embankment	166	renewable energy	374
energy geostructures	356	risk	418
energy piles	356	rock sockets	182
expansive clays	128	rock stability	292
factor of safety	292, 342	rock-soil interface	194
field performance	276	sensitivity	240
field test	166	shear strength reduction	
finite difference method	342	technique	342
flow liquefaction	392	site investigation	240
foundation(s)	216, 240	slope stability	112
future trends	216	soft clay	166
geostatistics	5	soft soils	5
geosynthetics	166	soil bioengineering	112
geotechnical characterization	5	soil conditions	216
geotechnical seismic engineering	348	soil treatment	194
heat transfer	374	soil water retention curve	128
holding capacity	216	spatial variations	5
impedance contrast	182	stability of shallow circular	
in place behavior	216	cavities	342
in-situ testing	356	stability	292
integrity	328	stone columns	166
laboratory testing	356	suction hardening	150
landfill cover	112	sustainability	276
lateral loading	182	swell-stress curve	128

tailings dams	392	uncertainty	418
teaching	348	unsaturated flow	128
thermo-mechanical behavior	356	unsaturated soils	150, 374
tunnels	418	vegetation	112

Author Index

Almeida, M.S.S.	166	Ni, J.J.	112
Alva Hurtado, J.E.	348	O'Neill, M.	240
Auvinet, G.Y.	13	Ossa López, A.	v
Baser, T.	374	Ovando Shelley, E.	10
Bilfinger, W.	194	Ozdogan-Dolcek, A.	374
Bransby, F.	240	Ozer, H.	276
Carranza-Torres, C.	342	Paniagua Zavala, W.I.	v
Cecílio Jr., M.O.	418	Qamhia, I.	276
Cox, C.	182	Randolph, M.	240
Delimi, Z.L.	240	Rattley, M.	240
Erbrich, C.	240	Rojas, E.	150
Farrag, R.	182	Silva, M.	240
Finnie, I.	240	Sparrevik, P.	216
Fredlund, D.G.	292	Stevens, B.	240
Fredlund, M.D.	292	Sutman, M.	356
Gitirana Jr., G.d.F.N.	292	Thomas, S.	240
Hosseinpour, I.	166	Turner, B.	182
Krisdani, H.	240	Tutumluer, E.	276
Laloui, L.	356	Vargas, C.O.	392
Lemnitzer, A.	182	Viggiani, C.	328
Lima, B.	166	Watson, P.	240
López Acosta, N.P.	v	Westgate, Z.	240
McCartney, J.S.	374	Zhou, C.	112
Meecham, C.	240	Zornberg, J.	128
Ng, C.W.W.	112		

This page intentionally left blank